LBL-13366
UC-34

NUCLEAR SCIENCE

RECEIVED
LAWRENCE
BERKELEY LABORATORY
SEP 30 1982
LIBRARY AND
DOCUMENTS SECTION

ANNUAL REPORT
1980-1981

TWO-WEEK LOAN COPY

This is a Library Circulating Copy which may be borrowed for two weeks. For a personal retention copy, call Tech. Info. Division, Ext. 6782.

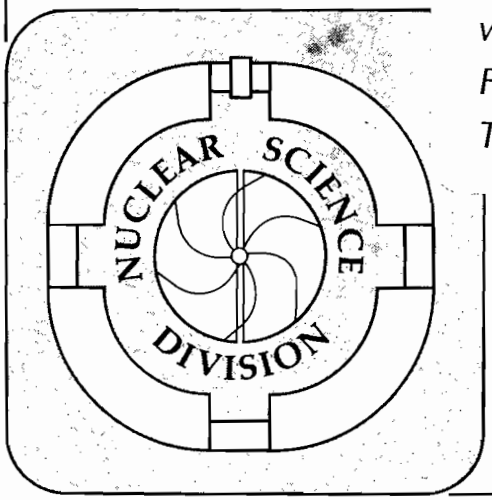

LAWRENCE BERKELEY LABORATORY
UNIVERSITY OF CALIFORNIA

Prepared for the U.S. Department of Energy under Contract DE-AC03-76SF00098

LBL-13366
c.2

LBL-13366

NUCLEAR SCIENCE

Annual Report
for the period
July 1, 1980 - June 30, 1981

J. Cerny
Division Head

E. M. Friedlander
Editor

Lawrence Berkeley Laboratory
University of California
Berkeley, California USA 94720

This work was supported by the Director, Office of Energy Research, Office of High Energy and Nuclear Physics, Division of Nuclear Physics and by the Office of Basic Energy Sciences, Division of Nuclear Sciences, of the U.S. Department of Energy under Contract No. DE-AC03-76SF00098.

Contents

Introduction
J. Cerny 1

PART 1. Research Programs

Exotic Nuclei and Nuclear Reactions
J. Cerny 5

Heavy Ion Reactions
B.G. Harvey and R.G. Stokstad 6

Nuclear Structure
R.M. Diamond, F. Stephens, and M.A. Deleplanque 8

Polarization Phenomena in Nuclear Physics
H.E. Conzett 10

Statistical Equilibrium in Deep-Inelastic Heavy Ion Reactions
L.G. Moretto 11

Heavy Element Research
A. Ghiorso and J.M. Nitschke 12

High Energy Nuclear Collisions
A.M. Poskanzer and H.H. Gutbrod 13

Relativistic Heavy Ion Physics
H.H. Heckman 15

Bevalac Research
H.G. Pugh, L.S. Schroeder, A. Sandoval, and R. Stock 17

Light Particle Emission in High Energy Nuclear Collisions
S. Nagamiya and H. Steiner 20

Heavy Ion Studies/Pion Studies
K.M. Crowe and J.O. Rasmussen 21

Nucleus-Nucleus Collisions
P.B. Price 23

Nuclear Theory
N.K. Glendenning, M. Gyulassy, W.D. Myers, J. Randrup, W.J. Swiatecki 24

Heavy Ion Superconducting Spectrometer (HISS)
D. Greiner 26

Isotopes Project
J.M. Dairiki 27

PART 2. Progress Reports

I. Experimental Research

A. NUCLEAR STRUCTURE

1. Study of Exotic Nuclei

The Decay of ^{8}He
T. Björnstad, H.Å Gustafsson, B. Jonson, P.O. Larsson, V. Lindfors, S. Mattsson, G. Nyman, A.M. Poskanzer, H.L. Ravn, and D. Schardt 31

Delayed Neutron Emission Probabilities of ^{9}Li and ^{11}Li
T. Björnstad, H.Å. Gustafsson, P.G. Hansen, B. Jonson, V. Lindfors, S. Mattsson, A.M. Poskanzer and H.L. Ravn 32

Beta-Delayed Three-Neutron Radioactivity of ^{11}Li
R.E. Azuma, T. Björnstad, H.Å. Gustafsson, P.G. Hansen, B. Jonson, S. Mattsson, G. Nyman, A.M. Poskanzer, and H.L. Ravn 34

Beta-Delayed Two-Neutron Emission from ^{30,31,32}Na
C. Detraz, M. Epherre, D. Guillemaud, P.G. Hansen, B. Jonson, R. Klapisch, M. Langevin, S. Mattsson, F. Naulin, G. Nyman, A.M. Poskanzer, H.L. Ravn, M. de Saint-Simon, K. Takahashi, C. Thibault, and F. Touchard 35

The Measurement of β-Decay Lifetimes via Projectile Fragmentation
M.J. Murphy, T.J.M. Symons, G.D. Westfall, and H.J. Crawford 37

β-Decay Energies and Masses of $^{103\text{-}105}$In
J.M. Wouters, H.M. Thierens, J. Äystö, M.D. Cable, P.E. Haustein, R.F. Parry, and Joseph Cerny 38

The $\epsilon/\beta+$ Decay of ^{145}Gd: Resolution of Decay Branching Ratio Anomalies and Evidence for Pronounced Structures in the β-Decay Strength
R.B. Firestone, R.C. Pardo, R.A. Warner, Wm.C. McHarris, and W.H. Kelly 39

Observation of Large Resonances in the β-Decay of $^{145}_{64}Gd_{81}$
R.B. Firestone 40

Determination of the Half-Life and Absolute Gamma Intensities of ^{151}Gd
K.E. Gregorich, K.J. Moody, and G.T. Seaborg 41

The Decay of the ^{155}Tb Compound Nucleus, Formed in the Reaction of ^{22}Ne with ^{133}Cs
K.J. Moody and J.J. Hogan 42

Alpha Decay of Neutron Deficient Polonium and Bismuth Isotopes
M. Leino, S. Yashita, and A. Ghiorso 44

Search For Electron Capture-Delayed Fission in the N = 126 System $^{216}_{91}$Pa EC $^{216}_{90}$Th
L.P. Somerville and M.J. Nurmia 45

Attempts to Identify the 1.5-Second Spontaneous Fission Activity Observed in the Reaction $^{18}_{8}O + ^{248}_{96}Cm$
A. Ghiorso, L.P. Somerville, R.M. McFarland, R. Lougheed, and E.K. Hulet 46

Spontaneous Fission of Rutherfordium Isotopes
L.P. Somerville, J.M. Nitschke, M.J. Nurmia, and A. Ghiorso 48

Production of Heavy Actinides from Interactions of ^{20}Ne and ^{22}Ne with ^{248}Cm
D. Lee, H.V. Gunten, M. Nurmia, Y.-F. Liu, G.T. Seaborg and D.C. Hoffman* 49

Recoil Range Experiments in the Actinide Region
R.M. McFarland, L.P. Somerville, M.J. Nurmia, and A. Ghiorso 50

A Procedure for a Fast Separation of Berkelium and Cerium
Yuan-fang Liu, Cheng Luo, Hans R. von Gunten, and Glenn T. Seaborg 52

2. High Angular Momentum

Study of High Energy Gamma Rays Emitted in the Deep-Inelastic Reactions ^{181}Ta + ^{136}Xe(1150 MeV)
J.O. Newton, J.E. Draper, K.H. Lindenberger, R.M. Diamond, C. Schück, F.S. Stephens, E.L. Dines, S. Shih, L.G. Sobotka, G.J. Wozniak, R.J. McDonald, D.J. Morrissey, A.J. Pacheco, and L.G. Moretto 53

Properties of Nuclei at Very High Spin
F.S. Stephens 54

Nuclear Structure at High Spins
F.S. Stephens 55

High-Spin Properties of ^{164}Er in the Multiple Band Crossing Region From Coulomb Excitation and In-Beam Gamma-Ray Spectroscopy
M.W. Guidry, S.W. Yates, I.Y. Lee, N.R. Johnson, E. Eichler, L.L. Riedinger, M.W. Guidry, A.C. Kahler, D. Cline, R.S. Simon, P.A. Butler, P. Colombani, F.S. Stephens, R.M. Diamond, R.M. Ronningen, R.D. Hichwa, J.H. Hamilton, and E.L. Robinson 57

Average g-Factors for High Spin States in ^{156}Dy
N. Rud, D. Ward, H.R. Andrews, O. Häusser, P. Taras, J. Keinonen, M. Neiman, R.M. Diamond, and F.S. Stephens 57

Alignment Effects in Correlation Spectra
C. Ellegaard, M.A. Deleplanque, O. Andersen, B. Herskind, F. Stephens, R.M. Diamond, H. Kluge, C. Schück, and S. Shih 59

Observation of Giant Dipole Resonances Built on States of High Energy and Spin
J.O. Newton, B. Herskind, R.M. Diamond, E.L. Dines, J.E. Draper, K.H. Lindenberger, S. Shih, C. Schück, and F.S. Stephens 61

3. Polarization Studies

Polarization
Homer E. Conzett 63

Polarization Tests of Time-Reversal Invariance: Past Failures
Homer E. Conzett 63

Deviations from the Polarization-Analyzing Power Equality and Implied Breakdown of Time-Reversal Invariance
H.E. Conzett, P. von Rossen, F. Hinterberger, R.J. Slobodrian, C. Rioux, and R. Roy 65

Time Reversal and Charge Symmetry Studies in Single Nucleon Transfer Reactions in the A = 5 System
A.L. Sagle, F.P. Brady, J.L. Romero, B.E. Bonner, N.S.P. King, M.W. McNaughton, and H.E. Conzett 66

Polarization Effects in Light Nuclei
H.E. Conzett 68

Search for Effect of Longitudinally Polarized Protons on Optically Active Amino Acids
R.M. Lemmon, H.E. Conzett, and W.A. Bonner 69

4. Nuclear Data Sheet Evaluation

Nuclear Data Sheets for A = 169 and A = 193
V.S. Shirley 71

Nuclear Data Sheets for A = 187 and A = 185
Y.A. Ellis-Akovali 71

Nuclear Data Sheets for A = 189
R.B. Firestone 72

Nuclear Data Sheets for A = 188
B. Singh and D. Viggars 72

Nuclear Data Sheets for A = 191
E. Browne 73

Evaluation of Nuclear Structure and Decay Data
C. Michael Lederer 74

B. NUCLEAR REACTION MECHANISMS WITH NONRELATIVISTIC HEAVY IONS

1. Charged Particle Emission

Alpha Particle Emission from Two Reactions Involving Very Heavy Ions
L.G. Sobotka, R.J. McDonald, G.J. Wozniak, D.J. Morrissey, A.J. Pacheco, and L.G. Moretto 76

Energy Equilibration in Composite Nuclei at High Energy and Spin: Correlations between Evaporative ^{1}H, ^{4}He and Fission
M.F. Rivet, D. Logan, J.M. Alexander, E. Duek, M.S. Zisman, and M. Kaplan 77

Direct and Evaporation-Like Emission of ^{1}H and ^{4}He in Both Fusion-Like and Inelastic Reactions of 340 MeV $^{40}Ar + ^{238}U$
D. Logan, M. Kildir, M. Kaplan, M.S. Zisman, D. Guerreau, J.M. Alexander, and L.C. Vaz 80

Prominent ^{4}He Emission from the Composite Nucleus for 480 MeV $^{56}Fe + Ag$
D. Guerreau, D. Logan, M.S. Zisman, J.M. Alexander, E. Duek, and M. Kaplan 82

Comparison of Noncompound Neutron and Proton Emission in ^{16}O Induced Reactions on ^{238}U at 310 MeV
J. Kasagi, S. Saini, T.C. Awes, A. Galonsky, C.K. Gelbke, G. Poggi, D.K. Scott, K.L. Wolf, and R.L. Legrain 84

Light Particle Correlations in 20 MeV per Nucleon ^{16}O Induced Reactions
C.K. Gelbke, W.G. Lynch, L.W. Richardson, M.B. Tsang, and R.E. Warner 87

Trends of Light Particle Spectra Observed in Nucleus-Nucleus Collisions
T.C. Awes, G. Poggi, S. Saini, C.K. Gelbke, R. Legrain, and G.D. Westfall 90

2. Angular Momentum Transfer

Q-Value and Z Dependence of Angular Momentum Transfer in Deeply Inelastic Scattering of $^{56}Fe + ^{209}Bi$
M.S. Zisman, R.J. Puigh, R. Vandenbosch, T.D. Thomas, and L. Nunnelley 93

Total γ-Ray Energy Measurements for the Reaction $^{176}Yb + ^{165}Ho$ at 8.5 MeV/A
R.J. McDonald, A.J. Pacheco, G.J. Wozniak, D.J. Morrissey, L.G. Sobotka, L.G. Moretto, H. Lindenberger, C. Schück, S. Shih, J.O. Newton, R.M. Diamond, and F.S. Stephens 94

Angular Momentum, Statistical Equilibrium and Sequential Fission in Very Asymmetric Systems
D.J. Morrissey, G.J. Wozniak, L.G. Sobotka, A.J. Pacheco, C.C. Hsu, R.J. McDonald, and L.G. Moretto 96

Fragment Spin Alignment in Deep-Inelastic Reactions
A.J. Pacheco, R.J. McDonald, G.J. Wozniak, C.C. Hsu, D.J. Morrissey, L.G. Sobotka, S. Shih, R.M. Diamond, F.S. Stephens, and L.G. Moretto 97

The $^{12}C + ^{12}C$ Reaction Cross Section Between 70 and 290 MeV Obtained from Elastic Scattering
A.J. Cole, W.D.M. Rae, M.E. Brandan, A. Dacal, B.G. Harvey, R. Legrain, M.J. Murphy, and R.G. Stokstad 99

Isomer Ratio Measurements for the Reaction $^{29}Si(^{18}O,p2n)\ ^{44}Sc^{m}\ ^{44}Sc^{g}$
H. Groening, K. Aleklett, K.J. Moody, P.L. McGaughey, W. Loveland, and G.T. Seaborg 101

Excitation Functions and Isomeric Ratio Measurements for the Reaction $^{41}K(^{6}Li,p2n)\ ^{44}Sc^{m},\ ^{44}Sc^{g}$
H.D. Nguyen, H.N. Trinh, H.D. Le, K.J. Moody, H. Groening, and G.T. Seaborg 101

3. Target and Projectile Fragmentation

Transfer Versus Fragmentation for Reactions near 15 MeV/Nucleon
M.J. Murphy, B.G. Harvey, D.L. Hendrie, J. Mahoney, W. Pang, and K. Van Bibber 103

Small Momentum Widths in Heavy Ion Fragmentation at 20 MeV/amu and Below
Bernard G. Harvey 104

Coherent and Incoherent Processes in Projectile Breakup
W.D. Rae, A.J. Cole, A. Dacal, R. Legrain, B.G. Harvey, J. Mahoney, M.J. Murphy, R.G. Stokstad, and I. Tserruya 105

Observation of Sequential Breakup in the $^{16}O + ^{197}Au$ Reaction at 218 MeV
A.N. Bice, M.D. Cable, A.C. Shotter, and Joseph Cerny 107

Observation of the Direct and Sequential Breakup of ^{7}Li from ^{12}C and ^{208}Pb Targets at 70 MeV
A.N. Bice, A.C. Shotter, J.M. Wouters, W.D. Rae, and Joseph Cerny 108

Resonant Particle Production in the 172-MeV $^{13}C + ^{208}Pb$ Reaction
A.N. Bice, M.D. Cable, A.C. Shotter, and Joseph Cerny 110

$^{12}C^{*}$ Production in the $^{12}C + ^{208}Pb$ System at 230 MeV
A.N. Bice, A.C. Shotter, and Joseph Cerny 111

Target Fragment Recoil Properties in the Reaction of 50-86 MeV/μ ^{12}C with ^{181}Ta and ^{197}Au
W. Loveland, P.L. McGaughey, K. Aleklett, K.J. Moody, P. Johnson, and G.T. Seaborg 112

Target Fragment Angular Distributions in the Reaction of 86 MeV/μ ^{12}C with ^{197}Au and ^{238}U
K. Aleklett, W. Loveland, P.L. McGaughey, R.H. Kraus, Jr., Y. Morita, G.T. Seaborg, T. Lund, D. Molzahn, E. Hagebo, and I. Haldorsen 113

Target Fragmentation from 10-2100 MeV/μ
W. Loveland, P.L. McGaughey, K. Aleklett, K.J. Moody, R.H. Kraus, Jr., R.M. McFarland, and G.T. Seaborg 114

C. RELATIVISTIC HEAVY IONS

1. Fragmentation Processes

Energy Variation of Target Fragment Mass and Charge Distributions in the Interaction of Relativistic Heavy Ions with Ta and U
W. Loveland, P.L. McGaughey, D.J. Morrissey, C. Oertel, L.L. Nunnelley, and G.T. Seaborg 116

Target Fragment Angular Distributions in the Reaction of 3.0 and 12.0 GeV ^{12}C with ^{197}Au and ^{238}U
Y. Morita, W. Loveland, P.L. McGaughey, and G.T. Seaborg 117

Fragment-Spray Correlations in High Energy Heavy Ion Collisions
A.I. Warwick, H.H. Gutbrod, S.B. Kaufman, M.R. Maier, J. Peter, H.G. Ritter, E.P. Steinberg, H. Stelzer, F. Weik, H. Wieman, and B.D. Wilkins 118

Comparative Yields of Alkali Elements and Thallium from Uranium Irradiated with GeV Protons, ^{3}He and ^{12}C
T. Björnstad, H.-Å Gustafsson, B. Jonson, O.C. Jonsson, V. Lindfors, S. Mattsson, A.M. Poskanzer, H.L. Ravn, and D. Schardt 119

A Compilation of World Data on "Anomalons"
E.M. Friedlander and Y.J. Karant 120

Further Investigation of Projectile Fragmentation: the Short Mean Free Path Effect
E.M. Friedlander, R.W. Gimpel, H.H. Heckman, Y.J. Karant, B. Judek and E. Gaussauge 121

Evidence for Two Different Reaction Mechanisms in Relativistic Heavy Ion Collisions
H.G. Baumgardt, E.M. Friedlander and E. Schopper 122

Comment on the Energy Dependence of Target Excitation in RHI Collisions
Harry H. Heckman 124

A Measurement of Deuteron-Deuteron Elastic Scattering at 5.75 GeV/c
Edgar T. Whipple, V. Perez-Mendez, A.L. Sagle, R.L. Talaga, F. Zarbakhsh, J.B. Carroll, G.J. Igo, J.B. McClelland, M. Bleszynski, and K. Ganezer 125

2. Pion Production

Production of Pions and Light Fragments at Large Angles in High-Energy Nuclear Collisions
S. Nagamiya, M.-C. Lemaire, E. Moeller, S. Schnetzer, G. Shapiro, H. Steiner, and I. Tanihata 127

Inclusive Single Negative Pion Production at Forward Angles from Collisions of Light Relativistic Nuclei
E. Moeller, W. Bruckner, L. Anderson, S. Nagamiya, S. Nissen-Meyer, L. Schroeder, G. Shapiro, and H. Steiner 127

Pion Double Charge Exchange on ^{4}He and Meson Exchange Currents
A. Stetz, L.W. Swenson, J. Davis, J. Källne, R.C. Minehart, R.R. Whitney, V. Perez-Mendez, A. Sagle, J. Carroll, J. McClelland, and J. Fawcett 129

Strong Coulomb Effects on Pions Produced in Heavy Ion Collisions
J.P. Sullivan, J.A. Bistirlich, H.R. Bowman, R. Bossingham, T. Buttke, K.M. Crowe, K.A. Frankel, C.J. Martoff, J. Miller, D.L. Murphy, J.O. Rasmussen, W.A. Zajc, O. Hashimoto, M. Koike, J. Peter, W. Benenson, G.M. Crawley, E. Kashy, and J.A. Nolen, Jr. 130

Pions Produced Near the Center-of-Mass Velocity in Heavy Ion Collisions
K.A. Frankel, J.A. Bistirlich, R. Bossingham, H.R. Bowman, K.M. Crowe, C.J. Martoff, D.L. Murphy, J.O. Rasmussen, J.P. Sullivan, W.A. Zajc, J.P. Miller, O. Hashimoto, M. Koike, J. Peter, W. Benenson, G.M. Crawley, E. Kashy, J.A. Nolen, Jr., and J. Quebert 131

π^- Temperatures, Sphericity and Thrust for Central Collisions
R. Brockmann, J.W. Harris, A. Sandoval, H. Strobele, R. Stock, M. Maier, R.E. Renfordt, J. Miller, H.G. Pugh, M. Raff, L.S. Schroeder, F. Riess, K. Wolf, A. Dacal, and M.E. Ortiz 133

Charged Particle Exclusive Analysis
R. Brockmann, J.W. Harris, A. Sandoval, H. Strobele, R. Stock, M. Maier, R.E. Renfordt, J. Miller, H.G. Pugh, M. Raff, L.S. Schroeder, F. Riess, K. Wolf, A. Dacal, and M.E. Ortiz 134

Coherence and Self-Induced Transparency in High Energy Hadronic Collisions
G.N. Fowler, E.M. Friedlander, and R.M. Weiner 137

3. Strange Particle Production

Kaon Production in Relativistic Heavy Ion Collisions
S. Schnetzer, M.-C. Lemaire, R. Lombard, E. Moeller, S. Nagamiya, G. Shapiro, H. Steiner, and I. Tanihata 139

Observation of Subthreshold K^- Production in Relativistic Nuclear Collisions
A. Shor, K. Ganezer, J. Carroll, G. Igo, J. Geaga, S. Abachi, A. Sagle, T. Mulera, V. Perez-Mendez, P. Lindstrom, F. Zarbakhsh, and D. Woodward 140

Λ Production Near Threshold in Central Nucleus-Nucleus Collisions
R. Brockmann, J.W. Harris, A. Sandoval, H. Strobele, R. Stock, M. Maier, R.E. Renfordt, J. Miller, H.G. Pugh, M.Raff, L.S. Schroeder, F. Riess, K. Wolf, A. Dacal, and M.E. Ortiz 141

4. Correlation Studies

Measurement of Two-Particle Correlations in 800 MeV pA Collisions
I. Tanihata, Y. Miake, H. Hamagaki, S. Kadota, Y. Shida, R. Lombard, E. Moeller, S. Nagamiya, S. Schnetzer, and H. Steiner 143

Few Nucleon Interactions and Correlation Studies
R.N. Treuhaft, J.M. Engelage, J.V. Geaga, J.W. Harris, P.N. Kirk, R.W. Koontz, H.G. Pugh, G.R. Roche, C.L. Ruiz, and L.S. Schroeder 144

Proton-Emitting Sources in Central Collisions of Ar + KCl at 1.8 GeV/N
A.L. Sagle, F. Zarbakhsh, F. Brochard, T.A. Mulera, V. Perez-Mendez, R. Talaga, I. Tanihata, J.B. Carroll, K.S. Ganezer, G. Igo, J. Oostens, D. Woodward, and R. Sutter 145

Two-Pion Correlations in Heavy Ion Collisions
J.A. Bistirlich, R.J. Bossingham, H.R. Bowman, C.W. Clawson, K.M. Crowe, K.A. Frankel, O. Hashimoto, J.G. Ingersoll, M. Koike, J.P. Kurck, C.J. Martoff, W.J. Macdonald, J.P. Miller, D.L. Murphy, J.O. Rasmussen, J.P. Sullivan, P. Truol, E. Yoo, and W.A. Zajc 146

Space Structure of a Fireball and the Pion Radius
T.F. Hoang, Bruce Cork, and H.J. Crawford 149

Two-Pion Correlations in Central Collisions of 1.8 GeV/u ^{40}Ar on KCl
R. Brockmann, J.W. Harris, A. Sandoval, H. Strobele, R. Stock, M. Maier, R.E. Renfordt, J. Miller, H.G. Pugh, M. Raff, L.S. Schroeder, F. Riess, K. Wolf, A. Dacal, and M.E. Ortiz 150

Correlations Between Coincident Fragments in Relativistic Heavy-Ion Reactions
E.P. Steinberg, M.S. Freedman, H.H. Gutbrod, D.J. Henderson, S.B. Kaufman, M.R. Maier, J. Peter, H.G. Ritter, H. Stelzer, A.I. Warwick, F. Weik, H. Weiman, and B.D. Wilkins 152

II. THEORETICAL RESEARCH

Nuclear Deformation Energies
W.J. Swiatecki and J. Blocki 157

The Effect of Deformation and the Neutron Skin on RMS Charge Radii
W.D. Myers and K.-H. Schmidt 158

Surface-Layer Corrections to the Level-Density Formula for a Diffuse Fermi Gas
W.J. Swiatecki and J. Toke 159

Schematic Calculation of GT Strength in N = 47,49 Isotones
S.G. Prussin, Z.M. Oliveira, and J. Randrup 160

Particle Angular Momentum Alignment Effects in Deformed Nuclei
L.K. Peker, J.O. Rasmussen, and J.H. Hamilton 161

Excitation of Shape-Vibrational Modes in Nuclei by Relativistic Heavy Ions
J.O. Rasmussen, J.S. Blair and X.J. Qiu 162

Calculation of Muon Final Probabilities after Muon-Induced Fission in Four-State Basis
Ma Zhong-yu, Wu Xi-zhen, Zhang Jing-shang, Zhuo Yi-zhong, and J.O. Rasmussen 164

Two-Nucleon Transfer Reactions in Deformed Nuclei Using Very Heavy Ions
M.W. Guidry, T.L. Nichols, R.E. Neese, J.O. Rasmussen, L.F. Oliveira and R. Donangelo 165

Ground State Properties Of Finite Nuclei In A Nonlinear Relativistic Mean Field Theory
J. Boguta 167

Relativistic Quantum Field Theory of Λ-Hypernuclei
J. Boguta and S. Bohrmann 168

Density Dependence of the Single Particle Potential in Nuclear Matter
J. Boguta 169

Dense Neutron Star Matter in the Normal and Pion Condensed State in a Relativistic Field Theory Constrained by Bulk Nuclear Properties
N.K. Glendenning, B. Banerjee and M. Gyulassy 170

The Energy-Dependent Single Nucleon Potential in a Relativistic Field Theory of Nuclear Matter
K.-H. Müller 171

A Relativistic Quantum Field Theoretical Model for Nuclear Slab Collision Dynamics
K.-H. Müller 172

Interacting Streaming Nuclear Matter Systems in a Relativistic Quantum Field Theory
K.-H. Müller and S. Bohrmann 173

Theory of Nuclear Dynamics
W.J. Swiatecki 174

The Clutching of two Colliding Nuclei
G. Fai 177

Fusion-Fission, Molecular-Capture And Symmetric Fragmentation In 3D-TDHF Calculation of the Reactions ^{238}U, ^{208}Pb (4.6-8.0 MeV/u)^{64}Ni, $^{48}Ca^{B+C}$
H. Stöcker, R.Y. Cusson, H.J. Lustig, A. Gobbi, J. Hahn, J.A. Maruhn, and W. Greiner 177

Quantum Treatment of Charge Equilibration in Fission
W.D. Myers, G. Mantzouranis, and J. Randrup 178

Correlated Mass and Charge Transport Induced by Statistical Nucleon Exchange in Damped Nuclear Reactions
W.U. Schröder, J.R. Huizenga and J. Randrup 179

Correlated Charge and Mass Distributions from Reactions of ^{56}Fe with ^{58}Ni and ^{64}Ni
H.C. Britt, B.H. Erkkila, A. Gavron, Y. Patin, R.H. Stokes, M.P. Webb, P.R. Christensen, O. Hansen, S. Pontoppidan, F. Videbaek, R.L. Ferguson, F. Plasil, G.R. Young, M. Blann, and J. Randrup 181

Transport of Angular Momentum in Damped Nuclear Reactions
Jørgen Randrup 182

Equilibrium Statistical Treatment of the Spin Fluctuations Generated in Deep-Inelastic Reactions
A.J. Pacheco, R.P. Schmitt and L.G. Moretto 183

Systematics of Angular Momentum Transfer in Intermediate Energy Heavy-Ion Reactions
C.C. Hsu, D.J. Morrissey, L.W. Richardson, G.J. Wozniak, and L.G. Moretto 184

Shell Effects on the Angular-Momentum Transfer in Heavy-Ion Reactions
L.G. Moretto and A.J. Pacheco 186

The Influence of Fluctuations on the Correlation between Exit-Channel Kinetic Energy and Entrance-Channel Angular Momentum for Heavy Ion Collisions
L.G. Moretto and L.G. Sobotka 188

On the Use of Isomer Ratios in ^{44}Sc for Predicting Spin Populations in High Energy Heavy Ion Nuclear Reactions
H. Groening, K.J. Moody and G.T. Seaborg 189

Pre-Equilibrium Nucleon Jets in TDHF Calculations of Medium-Energy, Heavy-Ion Collisions
H. Stöcker, R.Y. Cusson, J.A. Maruhn, and W. Greiner 190

Explosion-Evaporation Model for Fragment Production in Intermediate-Energy Nuclear Collisions
George Fai and Jørgen Randrup 191

Pion, Light Fragment, and Entropy Production in Nuclear Collisions
H. Stöcker 193

Pion Production from Heavy Ion Collisions at 90-380 MeV/N
P. Hecking 193

Microscopic Theory of Deuteron Formation
M. Gyulassy, E. Remler, and K. Frankel 194

Coulomb Final State Interactions
M. Gyulassy and S.K. Kauffmann 195

Formulation of the Coulomb Effects of Spectator Fragments on Pions from Heavy Ion Collisions
Hafez M.A. Radi, J.O. Rasmussen, J.P. Sullivan, K.A. Frankel, and O. Hashimoto 196

Dynamics vs Symmetrization in Hadron Interferometry
M. Gyulassy 197

The Quasi-Elastic Component in High-Energy Nuclear Collisions
Bernd Schürmann and Jørgen Randrup 198

Consequences of Impact Parameter Restrictions in Relativistic Nuclear Collisions
Steffen Bohrmann 200

Recent Results of Statistical Model Calculations for Relativistic Nuclear Collisions
Steffen Bohrmann and Jörn Knoll 201

Cascade Calculations of Relativistic Nuclear Collisions
J.D. Stevenson 201

Kaon Rescattering in Relativistic Nuclear Collisions
J. Randrup 202

Central Collisions of Heavy Ions — Indication for Fluid Dynamical Behavior?
H. Stöcker, C. Riedel, G. Buchwald, L.P. Csernai, G. Graebner, W. Greiner, J.A. Maruhn, P. Subramanian, Y. Yariv, K. Frankel, M. Gyulassy, J. Stephenson, D. Strottman, J.R. Nix, B. Schürmann 204

Two Particle Correlations Caused by Collective Fluid – Dynamical Flow
H. Stöcker, L.P. Csernai, G. Buchwald, G. Graebner, J.A. Maruhn and W. Greiner 205

Jets of Nuclear Matter from High Energy Heavy Ion Collisions
H. Stöcker, L.P. Csernai, G. Graebner, G. Buchwald, H. Kruse, R.Y. Cusson, J.A. Maruhn, and W. Greiner 206

The Bounce-Off Effect as a Barometer for Hot, Dense Matter in High Energy Nuclear Collisions
Horst Stöcker and Bernd Müller 206

Probing Dense Nuclear Matter via Nuclear Collisions
H. Stöcker, M. Gyulassy, and J. Boguta 207

Optical Model Solutions for Pions in Nuclear Matter
P. Hecking 208

Finite Temperature Pion Condensation
N.K. Glendenning and A. Lumbroso 209

Pion Condensation Threshold in Nuclear Matter and Thermal Δ-Isobars
P. Hecking 210

Test for Pion Condensation in Nuclear Collisions
M. Gyulassy 211

Significance of Temperature Measurement in Relativistic Nuclear Collisions
H. Stöcker, A.A. Ogloblin, W. Greiner 212

On the Significance of Temperature Measurements of Nuclear Fireballs
Norman K. Glendenning 213

Nuclear Physics from Subhadronic Structure—a Toy Model
Herbert M. Ruck 214

Percolation versus Gibbs Equilibrium – the Phase Transition from Hadron Matter to Quark Matter
Horst Stöcker 215

Strange Baryon Fraction from Quark-Gluon Plasma
N. K. Glendenning, M. Gyulassy, R. Anishetty, P. Koehler, and L. McLerran 215

Non-Linear Vacuum Polarization in Strong Fields
M. Gyulassy 215

III. INSTRUMENTATION

A. Spectrometers

HISS Detector Systems
Hank Crawford 219

Monitoring the HISS Magnet
F. Bieser and C. McParland 220

Program Needs for a High-B Field Facility for Visual Detectors at the Bevalac
Harry H. Heckman 220

TASS – Two-Arm Spectrometer System
G.R. Roche, J.M. Engelage, J.V. Geaga, J.W. Harris, P.N. Kirk R.W. Koontz, H.G. Pugh, C.L. Ruiz, L.S. Schroeder, and R.N. Treuhaft 221

Streamer Chamber Instrumentation
R. Brockmann, J.W. Harris, A. Sandoval, H. Strobele, R. Stock, M. Maier, R.E. Renfordt, J. Miller, H.G. Pugh, M. Raff, L.S. Schroeder, F. Riess, K. Wolf, A. Dacal, and M.E. Ortiz 223

Use of a Directly Digitized CCD Camera
R. Brockmann, J.W. Harris, A. Sandoval, H. Strobele, R. Stock, M. Maier, R.E. Renfordt, J. Miller, H.G. Pugh, M. Raff, L.S. Schroeder, F. Riess, K. Wolf, A. Dacal, and M.E. Ortiz 225

Image Intensifier Cameras for Event Recording at the Streamer Chamber
R. Brockmann, J.W. Harris, A. Sandoval, H. Strobele, R. Stock, M. Maier, R.E. Renfordt, J. Miller, H.G. Pugh, M. Raff, L.S. Schroeder, F. Riess, K. Wolf, A. Dacal, and M.E. Ortiz 227

The Plastic Ball Spectrometer
A. Baden, H.H. Gutbrod, H. Löhner, M.R. Maier, A.M. Poskanzer, H. Riedesel, H.G. Ritter, H. Spieler, A.I. Warwick, F. Weik, H. Wieman, and K.L. Wolf 228

New Developments at OASIS
J.M. Nitschke and J.D. Molitoris 229

A Versatile, High Temperature, High Efficiency Ion Source for the On-Line Isotope Separator OASIS
J.M. Nitschke 229

B. Detectors

A Glow Memory Chamber for Use in the Measurement of High Multiplicity Events
M.A. Elola, T.A. Mulera, V. Perez-Mendez, and P.E. Wiedenbeck 231

Development of a Calorimeter for Relativistic Heavy Ions
J.D. Stevenson, J. Martinis and P.B. Price 232

A Lead-Glass Gamma-Ray Detector for Relativistic Heavy Ion Collisions
M.P. Budiansky, S.P. Ahlen, and G. Tarlé 233

Response of Organic and Inorganic Scintillators to Relativistic Heavy Ions
M.H. Salamon and S.P. Ahlen 234

Calculation of the Relativistic Bloch Correlation to Stopping Power
S.P. Ahlen 235

A Search for New Nuclei Far from the Valley of Stability
J.D. Stevenson, P.B. Price and J. Musser 235

Radiation Damage in Si(Au) Surface Barrier Detectors Produced by Energetic Heavy Ions
L.G. Sobotka, G.J. Wozniak, R.J. McDonald, and L.G. Moretto 236

Development of a Beta Detector and Computer Analysis System for the On-Line Mass Separator, RAMA
J.M. Wouters, H.M. Thierens, M.D. Cable, R.F. Parry, and Joseph Cerny 237

C. Emulsions and Plastic Track Detectors

Demonstration of a Detector with Unprecedented Charge Resolution
S.P. Ahlen, P.B. Price, G. Tarlé, and M. Tincknell 239

Identification and Imaging of Nuclear Particles Using Etched Solids
S.P. Ahlen, P.B. Price, and G. Tarlé 240

Applications of Nuclear Track-Recording Solids to High-Energy Phenomena
P.B. Price 240

On the Possibility of Detecting Fractionally Charged Relativistic Projectile Fragments in Nuclear Emulsion
Harry H. Heckman 241

ICAMS: A System for Computer Assisted Nuclear Microscopy
E.M. Friedlander, H.H. Heckman, Y.J. Karant 243

Study of Highly Ionizing Particles at Mountain Altitude
K. Kinoshita and P.B. Price 243

D. Computers

The Design of MIDAS—A Modular Interactive Data Analysis System
Creve Maples, William Rathbun, Daniel Weaver, and John Meng 245

Development of a MIDAS Prototype
Creve Maples, William Rathbun, Daniel Weaver, and John Meng 247

The Utilization of Parallel Processors in a Data Analysis Environment
Creve Maples, Daniel Weaver, William Rathbun, and John Meng 249

A Fast, Time-Sliced, Multiple Data Bus Structure for Overlapping I/O and CPU Operations
W. Rathbun, C. Maples, J. Meng, and D. Weaver 251

Multidimensional Numerical Integration
R.W. Koontz 253

DATACQ, A New Data Acquisition Program
Friedemann Weik 253

An X-Y Histogramming Package Added to MULTI
Friedemann Weik 254

Data Acquisition at the HISS Facility
Charles McParland 255

Data Acquisition Setup for the Plastic Ball (488H)
Friedemann Weik 256

IV. ACCELERATORS

88-Inch Cyclotron Operation
D.J. Clark, C.M. Lyneis, D. Elo, L. Glasgow, R. Lam, T. Mast, R. Muller, P. Tans, and J. Welch 259

SuperHILAC Operations and Research
M.S. Zisman and R.M. Diamond 262

PART 3. Appendices

Thesis Abstract 267
Nuclear Science Division Seminars 267
Nuclear Theory Meetings 270
Papers Published and LBL Reports Issued 1980-81 272
Author Index 283

Introduction

This annual report describes the scientific research carried out within the Nuclear Science Division between July 1, 1980 and June 30, 1981. The principal activity of the division continues to be the experimental and theoretical investigation of the interaction of heavy ions with target nuclei. Complementary research programs in light-ion nuclear science, in nuclear data evaluations, and in the development of advanced instrumentation are also carried out.

Heavy ion research at the 88-Inch Cyclotron and the SuperHILAC focuses on spectroscopy and the properties of nuclear reactions. Currently the mechanism of nucleus-nucleus collisions (deeply inelastic scattering) and the nature of the angular momentum transfer during collision are being investigated. A 4π high-resolution γ-ray detector is being constructed to aid in the study (at both accelerators) of nuclei excited to states of extremely high angular momentum (60-70 $\hbar$). The on-line isotope separator, recently completed at the SuperHILAC, is being used in searches for new isotopes throughout the periodic table. In order to keep pace with the ever more sophisticated multiparameter data acquisition techniques, a modular system for high speed interactive data analysis is under test.

At the Bevalac, emphasis is on production of very high nuclear densities and temperatures by high-energy, head-on collisions. Recent research with relativistic heavy ions at the Bevalac has emphasized projectile and target fragmentation studies, with increasing focus on high-multiplicity events. This work is guided by close interactions with the nuclear theory group. The uranium beam capability (in FY 1982) and the recent completion of major new experimental facilities—the Heavy-Ion Spectrometer System (HISS) and the Plastic Ball/Wall detector system—will further this research. In addition, the Low Energy Beam Line is being brought into full operation to permit spectroscopic studies in the important transitional 30 to 200 MeV per nucleon energy range.

All three accelerators support strong outside user programs, including both domestic and foreign cooperative efforts. In particular, major collaborations with our German and Japanese colleagues continue to flourish at the Bevalac.

One hundred twenty six reports and journal articles were published by division members. Directly affiliated with the division throughout this period were 5 faculty senior scientists, 18 staff senior scientists, 26 staff scientists, 1 divisional fellow, 12 postdoctoral fellows, 18 graduate students, and 26 technical, administrative, and clerical support staff. Close to 50 additional graduate students from Berkeley and other universities make use of LBL's nuclear science facilities for much or all of their Ph.D. thesis work. Nearly 70 scientists from other institutions, both domestic and foreign, visited the division, bringing with them the diversity of ideas and talents upon which our research thrives.

During this period, Claude Lyneis joined the division as a staff scientist, responsible for the operation of the 88-Inch Cyclotron and for the development of cyclotron improvements. He came to LBL from the High Energy Physics Laboratory at Stanford University. Miklos Gyulassy and Jorgen Randrup were promoted to senior staff scientist positions. Both were previously Divisional Fellows; both are theoreticians and are instrumental in guiding the Bevalac research program.

Close to 1000 scientists from throughout the world gathered in Zellerbach Auditorium on the U.C. Berkeley Campus for the International Conference on Nuclear Physics, August 24-30, 1980. Conference arrangements were coordinated by members of the Nuclear Science Division: Bernard G. Harvey, program chairman, and Richard M. Diamond and John O. Rasmussen, conference secretaries. In addition to the approximately 100 invited and contributed talks, the poster sessions were extremely successful, and both types of presentations led to many stimulating discussions.

In order to meet heavy-ion physics needs beyond the 1980s, the division is collaborating with the Accelerator and Fusion Research Division to develop the concept of the Variable-Energy-Nuclear Synchrotron (VENUS). In addition to fixed-target operation at energies of up to 20 GeV/nucleon, VENUS would be capable of colliding-beam operation equivalent to that of a 1-TeV/nucleon fixed-target accelerator. It is expected that at such energy densities, new degrees of freedom of the nucleus will be excited and a quark-gluon plasma will be produced.

As part of the VENUS planning process, the 5th High Energy Heavy Ion Study was held at LBL, May 18-22, 1981. The program committee included Lee Schroeder, chairman, David Hendrie, Howel Pugh, Hans Gutbrod and Jorgen Randrup. The meeting brought together a wide spectrum of physicists ($\sim$ 150 from the U.S., Europe, and Japan) to discuss the value of heavy ion collision studies in terms of conventional nuclear physics and in the production of new and exotic states of matter. The published proceedings will serve as a valuable research document for the field in general and for the VENUS project in particular.

Joseph Cerny

PART 1. RESEARCH PROGRAMS

Exotic Nuclei and Nuclear Reactions

Joseph Cerny

A. Bice
M. Cable
R. Parry
H. Thierens
J. Wouters

This group has been actively investigating nuclei far from the valley of stability. Studies of this type yield experimental information testing various theoretical models predicting ground state mass excesses and energy level schemes. Several techniques have been developed for studying nuclei produced in low-yield reactions. Current experiments are concentrated in two regions of the chart of the nuclides, one near the double shell closure for nuclei with N = Z = 50 and the other in the mass $\simeq$ 20 region exploring nuclei which are predicted to define the proton drip line.

The experimental tool used to study isotopes near the mass 100 double shell closure has been the on-line mass separator, RAMA (an acronym for recoil atom mass analyzer) employed at the 88-Inch Cyclotron. This apparatus consists of a helium jet to transport recoil nuclei that are produced in a target chamber by both light- and heavy-ion bombardment to a hollow cathode ion source. Isotopes are then extracted from this ion source and magnetically analyzed. The mass of interest is collected on the RAMA focal plane by a tape transport system that shuttles the activity to a β-γ detection station. The decays of $^{102\text{-}105}$In have been observed following their production via 110-MeV ^{14}N bombardment of Mo targets. Knowledge of the mass excesses of the daughter Cd nuclei and the measurement of the Q_β values for the $^{103\text{-}105}$In decays have yielded mass-excess values for these indium isotopes. Comparison of these results with various theoretical predictions has produced interesting disagreements with the expected model mass surfaces. Future studies with RAMA are planned that investigate somewhat lighter isotopes (e.g., Se) at or near the N = Z line.

A recent development in this program of studying nuclei far from stability is an attempt to observe the decays of the (predicted) β-delayed proton precursors ^{22}Al (4n+2 mass series, $T_Z = -2$) and ^{23}Si (4n+3 mass series, $T_Z = -5/2$). The experimental technique employed utilizes a minimal length He-jet to transport these short lived nuclides from the target region to a collection point in front of a solid state detector telescope. Observation of the existence of these isotopes will comprise a substantial test of theoretical predictions of the stability of proton-rich nuclei in this light mass region.

In recent years, this group's research interests and efforts have also included developing techniques to detect unbound resonant states as nuclear reaction products. With these detection capabilities, it has been possible to extract valuable spectroscopic information from transfer reactions such as (^{12}C, ^{8}Be), (^{4}He,^{2}He) and [^{3}He, ^{4}He* (0^+,20.1 MeV)]. Recent studies have utilized similar techniques to investigate light heavy-ion reaction mechanisms in the range 10-20 MeV/nucleon. In particular, the importance of sequential decay processes in projectile fragmentation reactions has been under investigation with ^{7}Li, ^{12}C, ^{13}C, and ^{16}O projectiles. Such studies could prove useful in verifying theories pertaining to the mechanisms involved in fragmentation reactions and fast light-particle production.

Heavy Ion Reactions

B.G. Harvey and R.G. Stokstad

J. Mahoney
M.J. Murphy
W.D. Rae
*C. Albiston**
Lawrence Berkeley Laboratory

R. Legrain
Saclay, France

J. Cole
Grenoble, France

This group is concerned primarily with heavy ion reactions in the so-called transition region. This is a region of bombarding energy in which the phenomena characteristic of low bombarding energies, fusion and nucleon transfer, are expected to diminish as the bombarding energy increases and processes such as projectile fragmentation and nucleon-nucleon induced collisions dominate. There are several specific experiments under this umbrella which address this goal.

The most general or inclusive property of a nuclear reaction is the total cross section σ_T, which is comprised of nuclear elastic scattering and the total reaction cross section σ_R. Remarkably little was known about the behavior of σ_R and σ_T in the transition region for projectiles heavier than helium. One knew only that, at energies less than 10 MeV/nucleon (Lab), σ_R rises with E and at energies $>$ 800 MeV/nucleon σ_R is much smaller. Measurements for the $^{12}C + {}^{12}C$ system completed by this group during the past year have localized the region in which $\sigma_R(E)$ reaches a maximum at $\sim$ 15 MeV/u. This agrees rather well with the predictions of a microscopic calculation by DeVries et al. based on the known free nucleon-nucleon cross section. However, further work over a wider range of energies will be needed to understand how the respective roles of "mean field" and "nucleon-nucleon" mechanisms are exemplified in the total reaction cross section.

Peripheral reactions may be divided roughly into 1) those producing a two body final state in which the mass missing from the projectile is captured by the target, or 2) fragmentation or break-up reactions. Because of its 4π efficiency, the hybrid streamer chamber located at the 88-Inch Cyclotron makes possible the identification and separation of these two processes. Measurements of the reaction (16.5 MeV/μ) ^{16}O + CsI have recently been analyzed and, at least in terms of the relative yields of transfer reactions producing the elements N, C, and B, are explained in terms of Wilczynski's model for incomplete fusion. The next step is to compare the energy dependence of the magnitude and width of the quasi-elastic yields of these reaction products separately for transfer and fragmentation events. Because of the large amount of scanning that would be associated with a streamer chamber measurement, a 4π plastic scintillator array is being developed. The information gained from the streamer chamber is of great value in the design of the counter experiment. The ability to acquire data quickly should enable a detailed study of the projectile, target, and energy dependence of these widths, the values of which have recently been shown to approach the limiting value, $\sigma_0 \simeq 85$ MeV/c, more slowly than previously thought.

Fragmentation or break-up processes are best studied by coincidence experiments in which the relative kinetic energy of the detected particles is accurately determined. To do this requires a high angular resolution which can only be attained, without loss of solid angle, by using position sensitive detectors. Position sensitive (x-y)ΔE-E telescopes have been used to study the reactions $^{16}O + (^{12}C, ^{13}C, ^{28}Si) \rightarrow HI + \alpha$. The resolution in the spectrum of relative kinetic energy of the HI + α system was $\sim$ 130 keV. This enabled the clear identification of break-up processes proceeding through discrete states of $^{16}O^*$ (and other excited nuclei as well). By studying the particular states that were excited it was possible to identify at least two mechanisms in the breakup of ^{16}O into $^{12}C + \alpha$. The first is a coherent process that excites the projectile to states whose structure is related to that of the ground state via a multipole operator. This mechanism is important only for the lower Q values while the second mechanism, an incoherent process in which the α and ^{12}C constituents are assumed to interact independently with the target, is present for very negative Q values as well.

A part of the group's effort involves collaboration with outside users. Physicists from Michigan State University, Oak Ridge National Laboratory, the University of Mexico, and the Jagellonian University in Poland have worked with this group at the 88-Inch Cyclotron during the past year. Studies of the direct reactions, fusion-evaporation, and fusion-fission of light nuclear systems such as N + C, N + B, and Li + Ca have begun.

The instrumentation at the 88-Inch Cyclotron used by the group includes the small hybrid streamer chamber, a newly developed time of flight spectrometer with a one-meter long, position sensitive ionization chamber, and solid-state, position-sensitive ΔE-E telescopes. A most recent addition is a 60-inch diameter scattering chamber built by the Jagellonian University in Cracow, Poland. This chamber replaces the outdated 36-inch chamber and will be available to all users.

Footnote

*Graduate student

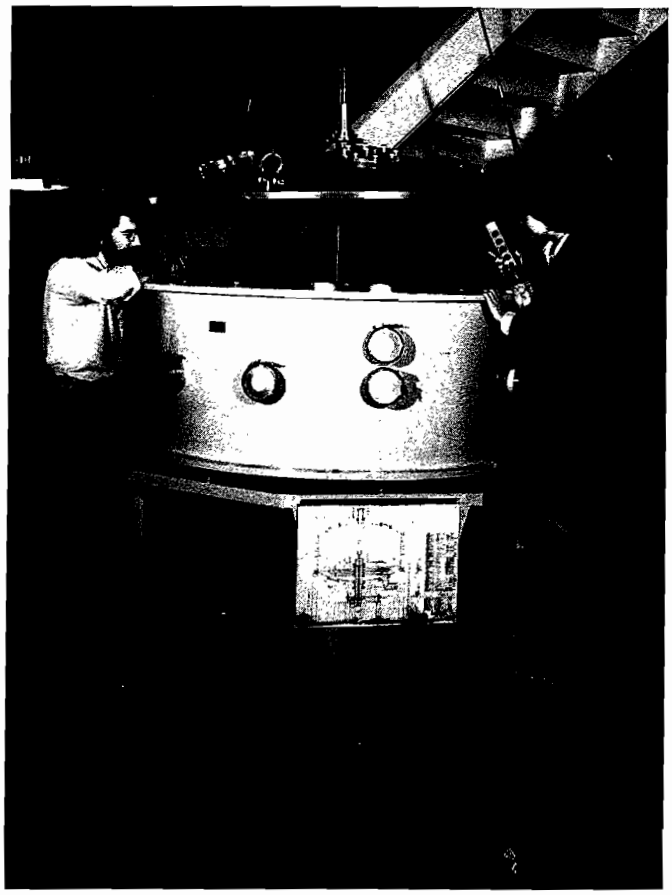

The newly acquired 60-inch diameter scattering chamber built in Poland by the Jagellonian University. Carolyn Albiston and Martin Murphy are shown inspecting the chamber. (CBB 819-8447)

Nuclear Structure

R.M. Diamond, F. Stephens, M.A. Deleplanque

J.E. Draper
E.L. Dines
U.C. Davis

K.L. Lindenberger
HMI, Berlin, West Germany

C. Schück
CSNSM, Orsay, France

J. Burde
Hebrew University, Israel

J.O. Newton
Australian National University, Canberra

S.H. Shih
Shanghai Institute of Nuclear Research
Peoples Republic of China

A. Macchiavelli
Buenos Aires, Argentina

This group is interested in studying and understanding a number of aspects of nuclear structure. For some years the principal effort has been investigation of nuclei at high angular momentum. Nuclei around the middle of the periodic table have spins near $70\hbar$ before the Coriolis and centrifugal forces disrupt them, causing fission. The chance to study nuclei under conditions where these familiar forces become major factors in determining the nuclear structure is attractive, particularly since the ^{40}Ar projectiles available from the LBL 88-Inch Cyclotron can easily bring the full $70\hbar$ into a compound nuclear system. We have learned that nuclei have both collective and single particle features at these high spins. They usually rotate in a rather classical manner; but, because the system is finite ($\sim$ 100 particles), there are strong irregularities "backbends" due to just one or two particles realigning their angular momentum. In such nuclei, a single ($i_{13/2}$ or $j_{15/2}$) particle can carry angular momentum as high as 10% of the maximum the system can hold. The interplay of these two modes of motion is one of the fascinating aspects of studies of high spin states. However, such studies are complicated by the fact that the γ-ray spectrum from states above $\sim 30\hbar$ has been thus far unresolvable. The population in this region is spread over too many levels. Several techniques have been developed to study such unresolved spectra: arrays of detectors, large (sum-energy) crystals, and currently the development of 4π detector systems.

Most recently, our group has been collaborating with Herskind et al. from Copenhagen to study the correlations of γ-ray energies in these unresolved spectra. These two-dimensional correlation spectra show structures up to the highest spins, which give information about the average behavior of both the collective and the single-particle motion. Nevertheless, it is becoming increasingly clear that the full elucidation of the physics comes only with the full resolution of the spectrum. We are now building a system consisting of an $\sim 4\pi$ bismuth germanate inner spherical shell with apertures to $\sim$ 20 Compton-suppressed intrinsic germanium detectors. This system will combine the spin selection of the inner ball with the high resolving power of Ge-Ge coincidences, and promises to give detailed information to much higher spins.

The newest study this group has undertaken, and at present one of the most exciting, is the observation of the giant dipole resonance (GDR) in the deexcitation γ-ray cascades from heavy-ion fusion and deep inelastic reaction products. States in a nucleus 15 MeV or more above the yrast line are thought to contain admixtures of the GDR based on states $\sim$ 15 MeV lower in energy (this is sometimes called Brink's hypothesis). When excited, all such states have the possibility to emit a GDR E1 γ ray in competition with the more usual neutron or particle emission. After particle evaporation down to an energy less than a neutron binding energy above the yrast line, the nucleus decays to the ground state by a cascade of up to 25-30 γ rays. In such an unresolved spectrum, the transitions above $\sim$ 2 MeV fall off exponentially in intensity with increasing γ-ray energy (the statistical region) and are very weak above 8 MeV. We have observed shoulders at 10-18 MeV in such deexcitation spectra from heavy ion fusion reaction products and have interpreted them as the GDR decays of the highly excited states above the main γ-ray cascades. The use of our total-energy γ-ray spectrometer was instrumental in eliminating γ rays of other origin, and at the moment cosmic rays are our limiting background. The information from such spectra is of a new type and potentially very interesting. It appears likely that one can measure the energy, yield, width, and shape of the GDR component of the statistical γ-ray spectrum. The strength of the resonance is related to its collectivity, and its width, to the more detailed features of the nuclear dynamics. The present measurements open the possibility of studying these as a function of excitation energy (temperature) and spin. The gross structure of the GDR is related to the shape of the nucleus; in deformed nuclei with two or three distinct radii, the GDR is split into two or three components. Thus, the observation of only the general structure of the resonance peak should provide information on the nuclear shape, again as a function of temperature and spin. Because such studies can be made on many nuclei, the observation of GDR effects in nuclear deexcitation γ-ray spectra seems likely to provide a new and general method to study nuclear dynamics far from the ground state.

In addition to these two main efforts, the group pursues its angular momentum studies to higher values than the compound system can hold by studying "deep inelastic collisions" in collaboration with the Moretto group. Here, reaction channels with angular momenta of several hundred $\hbar$ can be isolated and studied. We also study other aspects of nuclear structure and shapes in collaboration with several outside groups: Cline et al. from Rochester, Ward et al. from Chalk River, and Johnson et al. from Oak Ridge. These studies primarily concern Coulomb excitation with very heavy ions (^{136}Xe and ^{208}Pb) produced by the SuperHILAC, and currently include Coulomb excitation studies of transition nuclei such as Pt, Os, Ru, and Pd; work on deformed nuclei; Doppler-shift lifetime measurements; and g-factor measurements by means of the transient field.

Our group is also launching studies of particle transfer reactions between very heavy systems. Interesting questions arise concerning how the orientation of deformed nuclei at contact affects the transfer probabilities. One can also learn how much the pairing correlations enhance the transfer of pairs of nucleons. The only limitation of investigations such as these is the availability of accelerator time and manpower.

Polarization Phenomena in Nuclear Physics

H.E. Conzett
R.M. Larimer
Lawrence Berkeley Laboratory

E.J. Ludwig
University of North Carolina

P. von Rossen
University of Bonn, West Germany

This group's research uses the polarized beams from the 88-Inch Cyclotron and is concerned with spin-polarization effects in nuclear scattering and reactions. This research particularly addresses such fundamental questions as parity violation by the weak interaction component in pp scattering, time-reversal invariance in reactions, charge symmetry of the nucleon-nucleon interaction, and the three nucleon problem.

A most important feature of polarization effects is their ability to often display uniquely the operation of a basic symmetry property of the nuclear interaction. Our group is pursuing several fundamentally important experiments of this nature:

1. We have prepared a longitudinally polarized proton beam and the experimental apparatus for a major experiment on the basic nucleon-nucleon interaction, i.e., a determination of the weak interaction parity nonconserving part of this interaction from a measurement of the longitudinal analyzing-power component in pp scattering at 50 MeV. Calculations predict a maximum value (3×10^{-7}) at 50 MeV. The group uses one of the three existing polarized-beam facilities in the world with the capability to do the experiment at that energy.

2. We have been engaged in a collaborative experiment at TRIUMF to determine the level of validity of charge symmetry in the nucleon-nucleon interaction, which implies an equality of the neutron and proton polarizations in np scattering. The experiment is designed to check this equality to an accuracy of 10^{-3}. The one experimental run that has taken place in pp scattering, verifies that this accuracy is possible.

3. We have started a collaborative experiment with a group from Laval University to test the principle of time-reversal invariance in nuclear reactions. This principle results in the polarization-analyzing power equality, i.e., the polarization in a reaction A(a,b)B is equal to the analyzing power in the inverse reaction with polarized projectile B(b,a)A. Polarizations have been measured at Laval in several (^{3}He,p) reactions, and measurements of the analyzing powers in the corresponding (p^{3}He) inverse reactions have been made at LBL. Previous checks of time-reversal invariance in nuclear reactions have been limited to tests in elastic proton scattering.

Substantial differences between the polarization and the analyzing power have been measured. If such differences are confirmed in additional experiments underway, it would be firm evidence for the violation of the fundamental postulate of time-reversal invariance of the nuclear interaction. In view of these results, a survey of the past polarization tests of time-reversal invariance was made. Surprisingly, it was found that all such tests were inadequate, due either to lack of precision or lack of sensitivity to a violation of time-reversal invariance. Therefore, further experiments are being undertaken in order to provide significant tests of this important principle.

Polarization observables are often unique probes that can answer specific questions concerning nuclear structure. As examples, this group is planning measurements of the transfer of spin in (p,n) and (d,p) reactions. The (p,n) measurements can give explicit information on the nuclear collective modes excited, which is of great current interest, while the (d,p) measurements may provide a direct determination of a very elusive quantity, the deuteron D-state probability, which is fundamental to the most basic nuclear system.

In future work, we plan to continue to focus on experiments with polarized particles which examine the operation of the basic symmetries of the nuclear interaction, i.e., parity conservation in pp scattering, charge symmetry in np scattering, and time-reversal invariance in nuclear reactions. The increased polarized beam intensities of 2-3 microamperes, provided by our FY 1980 Accelerator Improvement Project, will be particularly important to these experiments because they require high statistical accuracy and overall precision. We will also continue studies of the consequences of particle identity and charge symmetry in nuclear reactions.

Statistical Equilibrium in Deep-Inelastic Heavy Ion Reactions

L.G. Moretto

J. Hunter
R.J. McDonald
D.J. Morrissey
*L.G. Sobotka**
*A.J. Pacheco**
G.J. Wozniak
Lawrence Berkeley Laboratory

C.C. Hsu
Beijing, Peoples Republic of China

During the last several years, this group has been investigating the short-lived dinuclear system formed in heavy ion collisions. In particular, we have been studying the transfer, alignment and partitioning of angular momentum within the dinuclear system. The experimental investigations utilize heavy ion beams of 5-50 MeV/A from the 88-Inch Cyclotron, the SuperHILAC, and the low-energy line of the Bevalac.

In a parallel effort, our group has been studying the theoretical implications of fluctuations in deep inelastic heavy ion collisions. The relevance of the statistical equilibrium limit to the description of substantially relaxed degrees of freedom has been assessed. The effects of fluctuations have been considered for (1) the correlation between the entrance-channel angular momentum and the exit-channel kinetic energy, (2) the sharing of the dissipated kinetic energy between the two fragments, and (3) the alignment of the fragment angular momentum.

Our investigations indicate that statistical fluctuations play a major role and that the statistical equilibrium limit seems to have been reached in a number of instances. For mass-symmetric and near-symmetric heavy systems, continuum γ-ray angular distributions indicate that the fragment spin alignment is destroyed at large Q-values by random spin fluctuations. In very mass-asymmetric systems, the statistical excitation of most angular momentum bearing modes is strongly suppressed; this results in a preferential dealignment of the spin creating a substantial in-plane anisotropy of sequential fission fragments. This anisotropy was observed at large Q-values for the $^{20}Ne + ^{197}Au$ and $^{20}Ne + ^{238}U$ systems. Further investigations of fluctuations are also being undertaken with a total γ-ray energy spectrometer.

An important question regarding heavy ion collisions is how the reaction mechanism evolves from the statistical equilibrium, observed in the low energy regime, to the completely nonequilibrium processes observed in the relativistic regime. In order to explore the intermediate regime, the angular momentum transferred to the heavy target-like fragment was followed in the reaction $^{20}Ne + ^{181}Ta$ in the energy range of 7.5 to 42 MeV/A. Comparisons of the measured intrinsic spin with that expected from the missing linear momentum indicate that, at bombarding energies of 17 MeV/A and above, the $^{20}Ne + ^{181}Ta$ reaction has lost its "two-body" character.

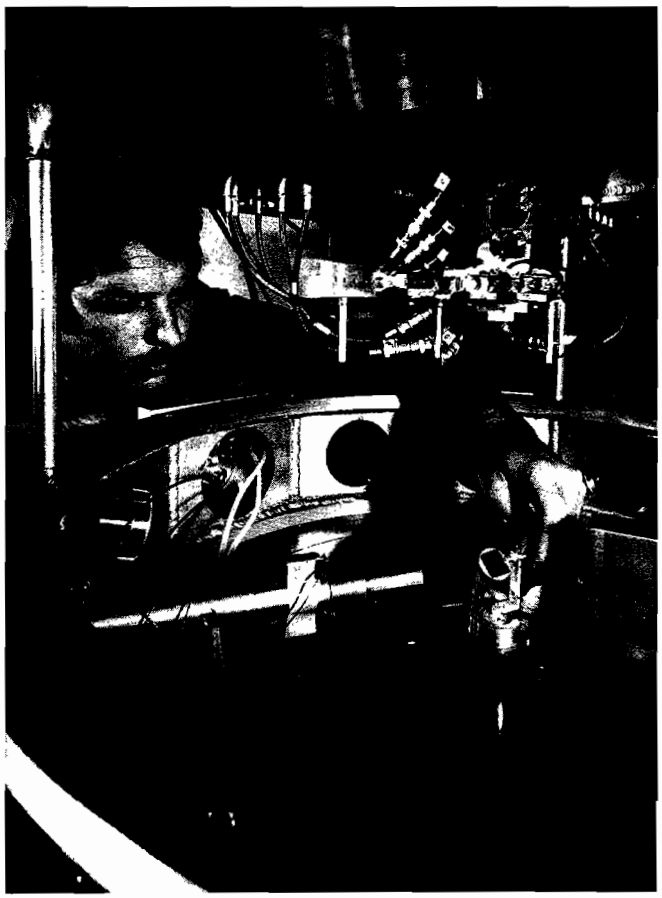

Scattering chamber and detector setup for sequential fission fragment angular distribution measurements. The beam enters the scattering chamber on the left through the brass tube and strikes a ^{197}Au target in the center. To the right of Dave Morrissey's hand is a Z-telescope that is used to detect the projectile residues and define a reaction plane. Note the raised lid and the attached array of silicon fission fragment detectors. (CBB 815-4096)

Footnote

*Graduate students

Heavy Element Research

A. Ghiorso and J.M. Nitschke

M.J. Nurmia
L.P. Somerville
S. Yashita
Lawrence Berkeley Laboratory

E.K. Hulet
R.W. Lougheed
J.F. Wild
Lawrence Livermore National Laboratory

D.C. Hoffmann
Los Alamos National Laboratory

J.D. Molitoris
Stanford University

M. Leino
University of Helsinki, Finland

The Heavy Element Research group is engaged in synthesizing new nuclides and determining the radioactive properties of known species. Important in these efforts, graduate students are trained in the advanced methods of nuclear physics. The group performs experiments, both at the 88-Inch Cyclotron and the SuperHILAC, and at times collaborates with other American laboratories in experiments at GSI, Germany.

Research at the 88-Inch Cyclotron is focused primarily on the production of neutron-rich nuclides made from various target materials from plutonium to californium with high intensity light ion beams. Three analysis methods are being employed: (1) the MG system to determine the E1 vs E2 characteristics of the fragments of short-lived spontaneous fission (SF) emitters; (2) the kilometer-long tape system to detect very short-lived SF nuclides in the presence of high intensity, longer-lived SF backgrounds; and (3) the differential range-measuring system for determination of nuclear reaction mechanisms by the direct analysis of the alpha and SF decay characteristics of recoil atoms lodged in stacks of thin foils.

The group's efforts at the SuperHILAC are centered around two large instruments: SASSY, a gas-filled magnetic spectrometer, and OASIS, the on-line isotope separator. SASSY (Small Angle Separator SYstem) is used for the analysis of fusion or near-fusion recoil products with half-lives as short as a microsecond. The system has an acceptance angle of about two degrees in the beam direction and is able to completely suppress the heavy ion beam while transmitting a very high fraction of the recoils within its acceptance angle. The heavy recoils are brought to a focus four meters downstream from the target at a focal plane where two types of detectors can be used—a solid state detector array for recoils, alphas, and SF, or a gas-filled ion chamber for recoils alone. Two avalanche counters with ultra-thin windows intercept the recoil path to provide START-STOP signals for velocity (TOF) measurements. Using the crystal detector array we have studied neutron-deficient alpha emitters in the Bi-Pa region, both to learn about the performance and limitations of SASSY, and to supplement existing information about a number of nuclides.

The on-line isotope separator at the SuperHILAC has turned out to be a viable specimen and it has therefore been given a suitable name: OASIS (On-line Apparatus for SuperHILAC Isotope Separation). It has proven its versatility with the separation of more than twenty different elements so far. On-line study of the separated isotopes has, however, been restricted to particle spectroscopy or off-line γ measurements because of the large background inside of the cave. This problem will be alleviated by an isotope transfer line which is now being built. It will guide the beam of a single separated isotope to a room on the second floor of Building 71 where it will be collected by a tape system. The radiation background in this room has been measured to be very low and will allow sensitive β-, γ-, and neutron-measurements. The tape system (based on a surplus IBM 729) facilitates the study of short-lived isotopes far from the line of β-stability in the presence of unwanted long-lived isobars of $\beta\pm$ decay chains. The range of elements which can be separated with OASIS has been greatly enlarged with improvements of the plasma ion source.

A modification of the source now permits the study of isotopes produced in deep inelastic collisions. With this reaction mechanism it is possible to reach parts of the neutron-rich side of the nuclide chart which are not easily accessible by other means. By using neutron-rich projectiles from the upgraded SuperHILAC, we will be able to complement research which has in the past been limited to fission products and high energy fragmentation. The other side of the valley of β-stability up to the proton drip line can be approached with compound nucleus reactions of neutron-deficient targets and projectiles. A special ion source has been built for this kind of reaction which also allows the use of radioactive targets.

Our collaboration with GSI was continued with a second $^{238}U + ^{248}Cm$ experiment this year. Previous experience had shown that the ^{238}U beam caused serious degradations of the metallic ^{248}Cm targets. An improvement in the target cooling, however, yielded an increase of nearly two orders of magnitude in the ^{238}U beam integral. This will push, in our present experiment, the detection limit for heavy actinides and superheavy elements well below the 10^{-33} cm^2 (1 nb) mark for half-lives between several hours and several years. The perfection of our irradiation techniques will also enable us in the future to reach shorter half-lives with chemical and physical on-line techniques.

High Energy Nuclear Collisions

A.M. Poskanzer
Lawrence Berkeley Laboratory

A. Baden[*]
J. Meneses
M. Parry[†]
T. Renner
H. Riedesel
M. White[†]
Lawrence Berkeley Laboratory

A. Wolf
Argonne National Laboratory

H.H. Gutbrod
GSI, Darmstadt, West Germany

H.G. Ritter
H. Spieler
R. Stock
F. Welk
H. Wieman
GSI, Darmstadt, West Germany

This group studies central collisions of relativistic heavy ions with the aim of learning about nuclear matter at high temperature and density. The group is a continuing collaboration between GSI and LBL.

In 1980, an experiment was performed to study the correlations between slow and fast fragments. For the slow fragments, an array of 40 detectors consisting of silicon counters, gas ΔE counters, and avalanche counters was used. For the fast fragments, the 80-counter multiplicity array and the Plastic Wall were used. The analysis focuses in one part on the ϕ correlation between the fast and slow fragments, to be used as a tool to study reaction dynamics. The correlation between two slow fragments, on the other hand, reveals novel features in the breakup of the nucleus.

The most important project this year was the construction of the Plastic Ball. This is an attempt to make a much more exclusive measurement of relativistic heavy ion interactions to search for collective phenomena.

The Plastic Ball covers 96% of 4π with 815 modules, each consisting of a CaF_2 ΔE detector and a plastic scintillator E detector. The two scintillators are observed by the same photomultiplier tube, and the signals are separated electronically by taking advantage of their different decay characteristics. In addition, positive pions are identified by their $\pi^+ \rightarrow \mu^+ \rightarrow e^+$ decay, as we have done previously. The small forward angle region is covered by the Plastic Wall placed 6 m downstream. The Wall consists of 177 plastic scintillators and identifies particles by their time of flight and energy loss. In the first experiments, the Plastic Wall provides also the trigger for the reaction. The Plastic Ball was completed in time for the very successful data-taking run in June 1981.

Footnotes

[*]Graduate student
[†]Undergraduate student

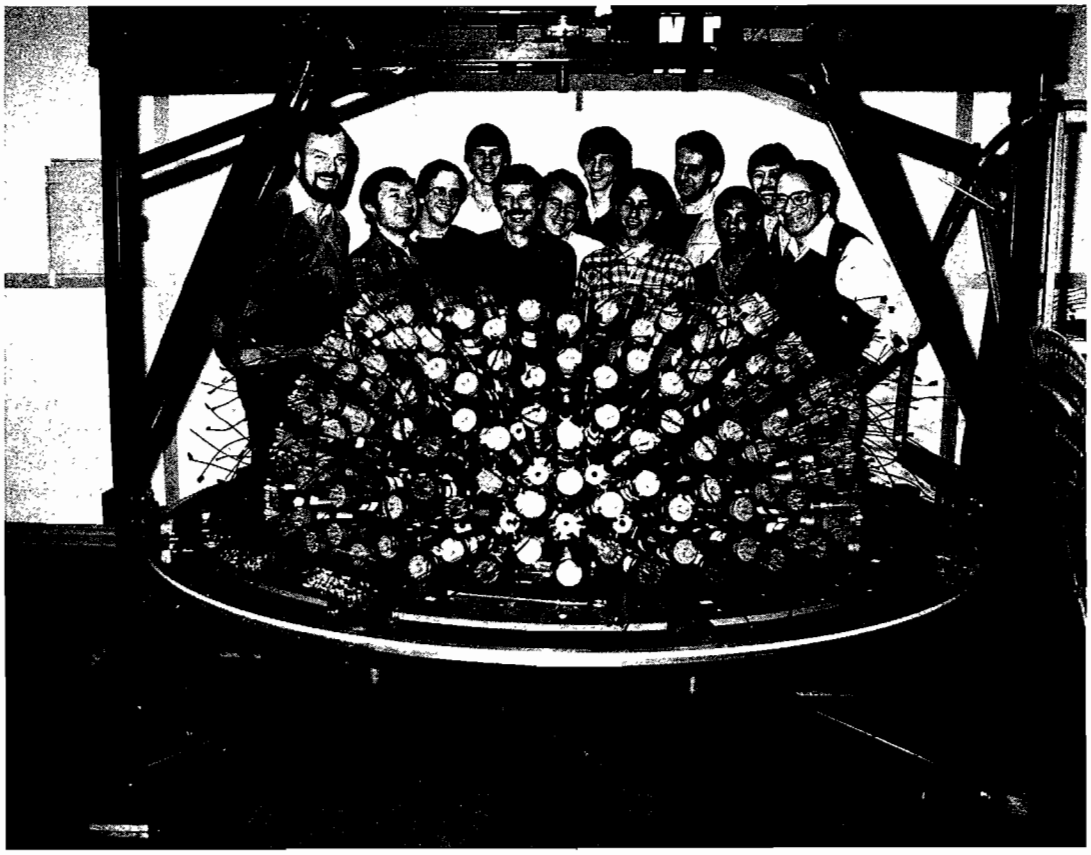

One half of the Plastic Ball in the process of being stacked. From left to right: H. Gutbrod, H. Wieman, H. Riedesel, M. Perry, H.-G. Ritter, A. Warwick, H. Loehner, A. Baden, M. Maier, M. White, J. Meneses, and A. Poskanzer.
(CBB 811-837)

Relativistic Heavy Ion Physics

H.H. Heckman

E. Friedlander
Y. Karant
M. Bloomer
J. DeLara
R. Gimpel
M. Heckman
S. Janssen
J. Sturla
H. Yee
Lawrence Berkeley Laboratory

D. Olson
Lawrence Livermore National Laboratory

E. Ganssauge
University of Marburg, West Germany

B. Judek
National Research Council, Ottawa, Canada

This group's experimental program in relativistic heavy ion physics at the Bevalac has focused on two important aspects of projectile fragmentation during FY 1981. These are, first, the interaction properties of relativistic projectile fragments of $\sim$ 2 A GeV ^{16}O and ^{56}Fe and the evidence therefrom for "anomalons." As an integral part of this particular program, we undertook the development of an interactive computer assisted measuring system (ICAMS) to improve the rate and scope of data acquisition. Second is the electromagnetic dissociation of beam nuclei by interactions with the virtual photons of the nuclear Coulomb field in high-Z targets (i.e., the Weizsäcker-Williams process), this investigation being performed with 1.7 A GeV-^{18}O.

In the field of nuclear interactions at energies comparable to those accessible in the VENUS project, a collaborative effort with the Universities of Exeter, England, and Marburg, West Germany, has produced the first direct evidence for coherent pion emission in proton-nucleus collisions along with the theoretical treatment of the suppression of nuclear cascading via self-induced transparency of nuclear matter to the coherent pulse produced in the first nucleon-nucleon encounter in the nucleus.

During collaboration with the University of Frankfurt/M (West Germany), evidence has been obtained for two kinds of reaction mechanisms in nucleus-nucleus collisions induced by Bevalac beams in nuclear emulsions. Both in the target and in the projectile frame, a subset of events could be tagged which appear to display a high-temperature ($\sim$ 40 MeV) thermodynamical behavior.

Projectile Fragmentation and the Evidence for "Anomalons"

In collaboration with B. Judek of the National Research Council of Canada, we have completed two independent nuclear emulsion experiments using Bevalac beams of ^{16}O and ^{56}Fe at $\sim$ 2 A GeV. We find, with $>$ 99.7% confidence, that the reaction mean-free paths of projectile fragments, $3 \leq Z \leq 26$, are shorter for a few centimeters after their emission than at larger distances or shorter than predicted from experiments on beam nuclei. Our results can be summarized as follows:

1. Over the first few centimeters after emerging from a nuclear interaction (or about 10^{-11} sec proper time), the projectile fragments exhibit significantly shorter mean-free paths than those derived from "normal" beams of the same charge Z,

2. At larger distances from the emission point the mean-free paths revert to "normality," and

3. The data are not compatible with a homogeneous lowering of the mean-free path and require the presence among projectile fragments of at least one component with an unexpectedly high reaction cross section.

These effects are interpretable under the simplest assumption that a small fraction ($\sim$ 6%) of the projectile fragments are anomalons with a mean free path $\lambda_a^* \simeq 2.5$ cm, independent of charge. Such a mean-free path corresponds to a cross section 5 to 10 times larger than geometric for the fragment considered. The extent of these differences between the primary, secondary, and later generation fragments have not been, and perhaps cannot be, explained within the framework of conventional nuclear physics.

Bevalac Experiment 559H. This experiment on the fragmentation reactions of ^{56}Fe at 1.8 A GeV was carried out in two run periods during this fiscal year. The experiment extends our studies on the evidences for anomalons and involved the irradiation of emulsion detectors to a variety of beams, including ^{3}He, ^{6}Li, ^{12}C, and ^{40}Ar, in addition to ^{56}Fe, the principal beam under study. Experiment 559H also included a series of emulsion exposures to measure the lifetime of the anomalon effect. All irradiations were successful and the scanning and measuring of the emulsions are in progress.

Electromagnetic Dissociation of Relativistic ^{18}O Nuclei

Bevalac Experiment 350H. This experiment, carried out in collaboration with D.L. Olson and B.L. Berman (LLNL), investigated the electromagnetic fragmentation of 1.7 A GeV ^{18}O nuclei via interactions with the nuclear Coulomb field of target nuclei. Measured in this experiment were the electromagnetic contribution to the single-

proton and the one- and two-neutron removal fragmentation cross sections for ^{18}O in a variety of targets, Be through U. It was found that the electromagnetic fragmentation cross sections deduced from the experiment for these particular reactions agree both in magnitude and Z_{target}-dependence with the predictions of the classical relativistic virtual-photon theory (the Weizsäcker and Williams process) which incorporates experimentally measured photonuclear cross sections. An important result to come from this experiment is that the factorization of the cross sections for *nuclear* processes (into beam/fragment and target dependent terms) is valid to an accuracy better than 4%, a quantity consistent with the known systematic uncertainties in the experiment.

Bevalac Experiment 517H. This experiment will use the HISS facility to investigate the electromagnetic dissociation of 2.1 A GeV ^{16}O in the reaction $^{16}O + U \rightarrow U + {}^{15}N + p$. In preparation of Experiment 514H, and as part of the overall HISS program, we have supported the following activities:

1. Specification of the technical criteria for the measurement of the magnetic field of HISS,

2. Bringing into operation of a computer code that expresses the field in parametric form, and

3. Development of a rapid computer conversion from trajectory information (i.e., drift-chamber coordinates) to the momenta and production vectors of reaction products that are transmitted through HISS.

Assistance was given to Experiment 513H, the first prototype experiment carried out with HISS, and information was gained on the problems related to the detection of $p,{}^{15}N$ coincidences and, by use of a NaI detector, the feasibility of measuring the energy of γ rays from the decay of projectile fragments.

Isotopic Measurements of Cosmic Ray Nuclei

Data from the LBL-UCSSL (HKH) instrument aboard the ISEE-3 spacecraft launched 12 August 1978 continues to be of excellent quality. The experiment continues to support systematic studies of the nuclear composition of the cosmic-ray source. Such data provide the basic input for theoretical models of stellar nucleosynthesis and the evolution of the composition of matter in the galaxy.

Future Directions

With the successful emulsion irradiations obtained from Bevalac Experiment 559H, we shall pursue a vigorous scanning/measuring program in order to improve the statistical significance of our observations on the anomalon component among relativistic projectile fragments. These measurements, and their ultimate analysis, will enable us to study with improved statistics the following aspects of the experiment: (1) the interaction properties of $Z = 2$ fragments, (2) lifetime estimates, (3) effects in higher order generations of the extranuclear cascade, (4) the semi-inclusive properties of the collision parameters, and (5) the dependence on projectile nucleus. Our aim is to enhance the subset(s) of fragmentation events responsible for the effect, which can provide insights into the pertinent production mechanisms.

A new generation of experiments in heavy ion physics will begin in 1982 when the Bevalac will initiate acceleration of all nuclei up to and including ^{238}U. With nuclear track emulsions we shall record and analyze all ionization tracks of nuclei, $Z = 1$ to 92, produced in the interactions of ^{238}U in matter. Planned experiments will be able to give information on:

1. Projectile-related phenomena
   a. Charge and multiplicity distributions of projectile fragments
   b. Angular distribution of projectile fragments; p_T of nuclei and nuclear clusters
   c. Shower production; π production
   d. Fission of U via nuclear and electromagnetic interactions
   e. Interactions of later generation projectile fragments
2. Target-related phenomena in uranium collisions
   a. Target fragmentation; charge, multiplicities and energy spectra, $E \lesssim 30$ A MeV
   b. Fragments in mid-rapidity region.

In support of our future program of research we plan to extend ICAMS to include additional measuring stations and automatic charge measurements, and to develop a 0.3-0.5 MG pulsed magnetic field to permit direct rigidity measurements in nuclear emulsion and other high-spatial-resolution visual detectors.

Bevalac Research

H.G. Pugh
L.S. Schroeder
Lawrence Berkeley Laboratory

TASS:
R. Koontz
R. Treuhaft
Lawrence Berkeley Laboratory

J.W. Harris
GSI, Darmstadt, West Germany

J. Engelage
P.N. Kirk
G. Krebs
C. Ruiz
Louisiana State University

G. Roche
Clermont-Ferrand, France

J. Geaga
U.C. Los Angeles

A. Sandoval
R. Stock
GSI, Darmstadt, West Germany

STREAMER CHAMBER:
J.P. Brannigan
E.H. McCann
I.W. Muskovich
L.M. Tinay
Lawrence Berkeley Laboratory

R. Brockmann
J.W. Harris
J. Miller (also LBL)
M. Raff (also LBL)
H. Stroebele
M. Maier (also University of Marburg)
R.E. Renfordt (also University of Marburg)
F. Reiss (also University of Munich)
GSI, Darmstadt, West Germany

K.L. Wolf
Argonne National Laboratory

M. Brandan
A. Dacal
A. Menchaca-Rocha
M. Ortiz
University of Mexico

This group operates two complementary research instruments in relativistic heavy ion research at the Bevalac. TASS is a double arm spectrometer, used in collaboration with the Louisiana State University. In contrast to this small solid angle, few-particle coordinate-measuring, fully electronic instrument, the Streamer Chamber is a 4π, charged particle exclusive, low data rate, visual data storage device. It is run in a GSI-LBL collaboration. In addition, the groups of K. Wolf at ANL and A. Dacal at the University of Mexico have made major commitments to this effort.

TASS

The Two-Arm Spectrometer System (TASS) consists of two fully rotable magnets, with accompanying wire chambers and scintillation hodoscopes for particle identification. The first run occurred in July 1980. The device has since been expanded by the addition of further wire chambers. The main activities on TASS have been:

444H. This experiment involved measuring the angular and momentum correlations between high energy particles π^+,p,d emitted in the forward and backward hemispheres. The majority of the running involved 2.1 GeV proton-carbon interactions. Particle production at backward angles is of considerable interest since it is either strictly forbidden (e.g., nucleon scattering) or severely constrained (e.g., pion production, where $P^{\pi}_{max} \lesssim 300$ MeV/c) in "free" N-N collisions. Thus, the observation of correlations between forward and backward particle emission provides a tool to probe possible exotic or cooperative production mechanisms, that is, study the short-range behavior of nucleons in nuclear matter. The data are being analyzed, with particular attention being given to that portion of the data that is sensitive to the incident proton scattering from two or more nucleon correlations in the target nucleus. The initial phase of studies was finished in early 1981.

559H. This experiment looks into the possible differences of π^- and π^+ yield distributions in the central region and up to the projectile fragmentation domain. The planned run is $^{40}Ca + {}^{40}Ca$ at 1.05 GeV/A where only Coulomb effects can be responsible for any difference observed. A multiplicity detector system was added to TASS, in order to separate peripheral and central events for the sake of a more conclusive comparison with theories of the dynamical Coulomb effects. The purposes of this experiment are to cover the full phase space at high statistics, to ascertain the possible effects of the Coulomb field on low energy pion production and to help settle controversy between other previous experiments. A parasitic run at 670 and

800 MeV/A with Ne on NaF in the spring of 1981 was successful; these data are now being analyzed.

Future research with TASS will involve measurements of $\pi\pi$ and πN correlations to ascertain the contributions of both meson and baryon resonances to the pion spectrum observed in heavy ion collisions.

Finally, we feel that a study of di-lepton production (e^+e^- or $\mu^+\mu^-$) might be a very sensitive test to determine if exotic states of nuclear matter are formed in central collisions. Being weakly interacting, the leptons will not suffer the large attenuation that pions, nucleons, and, to some extent, kaons experience in traversing the nuclear medium from their creation point in the collision process. Test runs have been made, in collaboration with J. Carroll and L. Madansky, and the group has helped organize a workshop, held at LBL on 26-27 May 1981 to study the experimental and theoretical feasibility of observing a transition to the quark-gluon plasma by this means. The primary problems are experimentally those of obtaining sufficient acceptance and theoretically those of distinguishing the effect from "uninteresting" backgrounds such as $\pi^+\pi^-$ annihilation in the nuclear environment. A further meeting of this workshop is planned prior to a final report.

Streamer Chamber

This group, with members from LBL, GSI Darmstadt, University of Marburg, ANL, and University of Mexico, is using the LBL streamer chamber, which, with its 4π charged particle exclusive information, enables one to gather simultaneously data about particle production, two particle correlations, and collective features of the reaction mechanism as reflected in the particle/momentum flux patterns of the events. Instrumentation advances have been made concerning internal metallic targets, chamber gas composition, Marx generator output, new triggering schemes, image intensifier cameras, and direct digitalization of pictures by use of CCD cameras. Data are still taken on conventional film, and measuring is done without computer automatization. We are, however, adapting a semi-automatic PEPR measuring system and considering the possibility of recording our data entirely with CCD cameras.

Recent work by the group has included the following experiments:

400H. This experiment used a proton beam to investigate the systematics of backward-going baryons. Complementing a corresponding TASS study, these streamer chamber data provide a look at other features of the events, relevant to the backward emission mechanism. The data are now being analyzed and discussed in terms of isobar excitation and absorption or decay.

401H. This experiment measured Ar + KCl reactions between 0.4 and 1.8 GeV/A, in central and minimum bias trigger configurations. From these data, a study of π^- and charged particle multiplicity systematics was first completed.[1] Analysis is under way of negative pion momentum flux and temperature distributions, of two π^- correlations (Hanbury-Brown, Twiss effect), and of global features of the full event. In order to speed up the full reconstruction of events (also applied to central Ar + Pb data at 1.0 GeV/A), the semi-automatic PEPR measuring facility at the University of Heidelberg has been adapted to 3-view, 35 mm film analysis. A further aspect of 401H data is Λ production in central Ar + KCl collisions at 1.8 GeV/A. A preliminary study of Λ $\langle p_\perp \rangle$, $\langle p_{||} \rangle$, and production cross section, as well as Λ polarization, was completed.[2]

564H. Study of ^{40}Ca reactions with KCl, ^{40}Ca and Pb at 2.1 GeV/A, in central and inelastic trigger mode. The $\sim$ 100 hour central Ca + Ca run at 2.1 GeV/A was aimed specifically at better Λ production statistics in order to investigate the spectra and, in particular, the Λ polarization. These collisions should produce the highest energy density of nuclear matter presently attainable at the Bevalac. The data will also be analyzed for all the other 401H topics, mentioned above. For example, it will be interesting to compare π^- production in Ar + KCl with that of the isospin zero system Ca + Ca. Furthermore, in Ca + Ca we should have $\langle n_{\pi^-} \rangle = \langle n_{\pi^+} \rangle$; it will thus be most appropriate in order to test our π^+ identification capabilities.

This experiment used metallic targets of Ca and Pb, replacing KCl and Pb_3O_4 targets. These targets were mounted inside SF_6-filled plastic boxes with thin Mylar windows, in order to avoid discharges across the target. In a parasitic run with a 1.05 GeV/A Ca beam, very thin (50 and 100 mg/cm^2) metallic Pb targets were employed to push down the lower proton identification limit to about 10 MeV. The CCD camera was also tested in these runs.

557H. This experiment addresses the reaction mechanism at the lowest Bevalac energies of 30-90 MeV/A, trying to cross the gap to low energy studies in Ar + BaI_2 and Ar + KCl reactions. A stack of seven thin BaI_2 targets was developed to obtain a sufficient number of event triggers while keeping the targets thin enough to let heavy recoil nuclei emerge from them. This experiment was trying to address the problem of wide range in streamer brilliance, from fast protons to slow $Z > 10$ recoil nuclei, by use of image intensifier cameras. Along with this the operating electric field strength could be lowered, thus reducing the flare and spark-breakthrough abundances in the chamber. These data are analyzed on the ALICE system at ANL, obtaining particle identification from track profile measurements.

In 1981, the group will finish the analysis of 400H, 401H, and continue on 564H, 557H. Early in 1982, the running of 564H, 557H will be finished, and a new study of reactions with heavier beams from the up-graded Bevalac, such as Xe + Xe, is planned.

The streamer chamber will be adapted to the higher multiplicities by an external 4π detector system measuring end points and dE/dx of each track. The latter will serve for p, d, t, He, and p, π^+ differentiation, a problem which must be overcome to make possible meaningful analysis of

global features of fully reconstructed events. A new on-line computer will be introduced with this 4π system. Further advances in picture storage and semi-automatic measuring will be sought.

References

1. A. Sandoval et al., Phys. Rev. Lett. **45**, 874, 1980.
2. J.W. Harris et al., Phys. Rev. Lett. **47**, 229, 1981.

Light Particle Emission in High Energy Nuclear Collisions

S. Nagamiya and H. Steiner

S. Schnetzer
Lawrence Berkeley Laboratory

H. Hamagaki
S. Kadota
I. Tanihata
INS, Japan

R. Lombard
DPhN/ME, CEN, Saclay, France

Y. Miake
Osaka University, Japan

E. Moeller
Freie Universität Berlin, West Germany

The main emphasis of our research program is the study of the reaction mechanisms involved in high-energy nuclear collisions. This experimental program includes both inclusive cross-section measurements and particle correlation studies. Most of the measurements involve the detection and identification of relatively light particles ($\pi^{\pm}$, K^{+}, p, d, α,...) over a wide kinematic domain. We are particularly interested in studying processes which are kinematically inaccessible in the collisions between two free nucleons, and thereby probing short-distance effects in nuclei. We are also searching for any unusual effects which might result when two massive nuclei interact at high energy, especially in small-impact-parameter collisions. Most of these experiments are performed under the INS (University of Tokyo)-LBL collaboration.

In Experiment 471H, kaon production has been measured with 2.1 GeV/A Ne, 2.1 GeV/N d, and 2.1 GeV proton beams on various nuclear targets. The inclusive cross section with the Ne beam shows a much stronger target-mass dependence than that with the d or p beams; this result suggests that collective effects are important in kaon production. The charged-particle multiplicity associated with kaon production has been measured as well as the multiplicities associated with producing pions and protons. The data indicate that the associated multiplicity is slightly larger when a kaon is detected than in the case of either pions or protons.

The data-taking part of Experiment 472H has been finished. In this experiment, the goal is to measure various two-particle correlations, e.g., p-p, p-d,... Measurements have been made using protons of 400 and 800 MeV and Ne of 400 and 800 MeV/A. New insight into the production mechanism responsible for backscattered protons in 800 MeV p+A collisions has been obtained by studying forward-backward correlations. The data suggest that the scattering of incident protons on a two-nucleon cluster is the dominant production mechanism for backward protons. Analysis of other data are in progress.

The analysis of experiment 205H has been completed and two papers are presently being prepared for publication. In this experiment, the inclusive spectra of pions, protons, deuterons, tritons, ^{3}He, ^{4}He, ^{6}He, and ^{8}He have been measured at small production angles ($0 \leq \theta_{L} \leq 12°$) with p, d, α and C beams at 1.05 GeV/A and 2.10 GeV/A bombarding energy on various targets. Upon comparing our pion results with various model predictions, we find that none of the existing models reproduce all of the data well in a quantitative sense and some are not even close. For light projectiles and targets, the hard scattering models (e.g., Schmidt and Blankenbecler, etc.) seem to do as well as any of the calculations and better than most.

The preparation of Experiment 512H, in which large-transverse-momentum particles near kinematical limit will be measured, has been finished. The HISS magnetic spectrometer will be used in conjunction with time-of-flight and dE/dx measurements. The detection system involves large arrays of scintillation counters, two large drift chambers, and several multiwire proportional chambers. The major data-taking is scheduled for spring of 1982.

Heavy Ion Studies/Pion Studies

K.M. Crowe and J.O. Rasmussen

J.A. Bistirlich
R. Bossingham
H.R. Bowman
K.A. Frankel
*J. Kurck**
*D.L. Murphy**
J. Ridout†
W. Schimmerling
*J.P. Sullivan**
E. Yoo†
*W.A. Zajc**
Lawrence Berkeley Laboratory

O. Hashimoto
INS, Japan

W.J. MacDonald
University of Alberta

J. Peter
Orsay, France

M. Salomon
University of British Columbia

P. Truoel
SIN, Switzerland

The Berkeley research activities of this group center mainly around the study of charged pions or correlated pairs of particles produced in high-energy heavy-ion collisions at the Bevalac. The technical approach involves a large ($\sim$ 1.5 meter long) magnetic spectrometer (JANUS) and combinations of fast scintillators and wire chambers interfaced with computer data systems. One major part of this work is the determination of the cross sections, with an exploration of the angular dependence, for pion production in heavy ion reactions. The existence of both positively and negatively charged pions facilitates determinations of simple Coulomb effects and, therefore, the charge density evolution in heavy ion collisions by observation of the π^+/π^- ratio as a function of pion energy, bombarding energy, and target-projectile charges. In fact, we have found that pions produced with low energy in the projectile frame have large π^-/π^+ ratios due to the Coulomb fields of the fragments. Systematic observations of the sharp anomaly are being made to compare with various models for production. The effects due to esoteric mechanisms, i.e., condensates, etc., are expected to modify the conventional modes; and these phenomena are being explored.

We are also studying the production cross section for low energy π^- and π^+ at 90° in the center of mass, where an enhancement in the π^+ production has been observed. We want to ascertain that this 90° peak does disappear at low energy and to attempt to measure the threshold for its appearance. The group has undertaken thick target studies in order to evaluate the practicality of heavy ion production of useful π^- beams.

The second major part of the work is an experiment to look at the Hanbury-Brown-Twiss effect for like-charged pions made by heavy ion collisions in events where many pions are produced. We look at the production of a pair of closely related pions +,+ or −,− at the Lab angle 45°. In the past ten years, such exotic phenomena as pion condensation, pionic lasing and quark matter have been predicted as possible for nuclear matter in a heavy ion collision. Gyulassy, Koonin, and others have pointed out that one possible way to see the effect of pion instabilities in heavy ion collisions is to look for the correlation of like pions in the situation when the relative momentum is extrapolated to zero.

More quantitatively, one studies the correlation function $C_2(k_1, k_2)$ for two pions. For the case of two pions, $C_2(k,k) = 0$ for coherent sources. Highly coherent pions will have a different distribution in relative momenta from that expected for chaotically produced pions, and the range of coherence depends on the size of the interaction region. This technique of pion interferometry has been employed to measure the size and lifetime of the pion source formed in the collision of 1.8 GeV/A ^{40}Ar + KCl. The values obtained provide useful constraints on models detailing the pion production mechanism. The Bose-Einstein enhancement for low relative momentum was observed.

We have also conducted measurements of neutron-proton pairs produced in the Ne + U reactions. Such measurements give information on excited (virtual) state deuteron production and on spin correlations associated with pion condensation. Preliminary results show an enhancement near zero n-p relative momentum. Future work will improve on resolution and statistics for the virtual deuterons and for wide-angle n-p correlations measuring quasi-free scattering and collective-flow processes. Cluster production provides the main information on entropy production in relativistic heavy ion collisions.

Future work will utilize the experimental techniques and apparatus we have developed. The availability of Bevalac beams of the heavier elements (Au, Pb, or U) will

Footnotes

*Graduate student
†Undergraduate student

call for new pion spectroscopic measurements to search for evidence of highly compressed nuclear matter effects, such as pion condensation, quark matter, etc. The π^+/π^- ratios will again be exploited for heavier beams to measure the dynamic charge evolution in relativistic heavy ion collisions.

The advent of Xe, Pb, U, and other heavy beams at the Bevalac provides new opportunities in atomic physics. Our earliest Bevalac work involved measuring K x-ray production cross sections. We plan not only normal survey experiments but also more exotic single-crystal experiments looking for coherence effects in x-ray emission.

Various members of the group are involved in collaborative work centered at other laboratories: pion or muon experiments at LAMPF; theoretical studies on muon fission with collaborators in China; theoretical nuclear studies by the Classical Limit S-Matrix Method with collaborators at the Universities of Tennessee, Brazil, and Kuwait; and hybrid plastic and emulsion studies of relativistic heavy ions with collaborators in Nagoya and Cairo.

Nucleus-Nucleus Collisions

P.B. Price

S.P. Ahlen
M. Budiansky[*]
K. Kinoshita[*]
S. Levin[†]
T. Liss[*]
J. Musser[*]
H. Nelson[†]
M. Salamon[*]
M. Solarz
J. Stevenson
G. Tarlé
M. Tincknell[*]
J. Zelinsky[†]
Lawrence Berkeley Laboratory

D. O'Sullivan
Dublin Institute for Advanced Studies
Ireland

F. Sauli
CERN, Geneva, Switzerland

All of this group's offices and equipment are located in Birge Hall on the UCB campus, which makes it easy to attract new students, but restricts to some extent interaction with Nuclear Science Division staff. Current research falls into the following five principal areas.

1. Relativistic heavy ion research (DOE support)
   a. Production of heavy ion fragments, including exotic neutron-rich nuclides near the dripline.
   b. Production of high-energy gamma rays.
   c. Search for Lee-Wick matter.
   d. High-order effects in electrodynamics of slowing heavy ions.
   e. Response of various detectors to heavy ions.
   f. Hadron calorimetry for nucleus-nucleus collisions.
   g. Detailed properties of secondary nuclei with anomalously short interaction lengths ("anomalons").
2. Search for highly ionizing particles in e^+e^- annihilation (PEP-2 experiment, supported by NSF)
3. Cosmic ray astrophysics (NASA support)
   a. Relative abundances of isotopes of very heavy cosmic rays.
   b. Abundances of cosmic rays in the vicinity of uranium and beyond.
   c. Design of future, large-area detectors for long-duration space exposures.
   d. Study of highly ionizing particles with anomalously long interaction lengths at mountain altitudes, including a search for grand-unification magnetic monopoles and quark globs.
   e. Design of an experiment to detect anti-iron nuclei in cosmic rays at a level $\gtrsim 3 \times 10^{-7}$ of iron.
4. New detectors (NASA and Calspace support)
   a. CR-39 with charge resolution $\sigma_Z < 0.1$ e.
   b. Streamer chamber for imaging Cerenkov light cone from heavy nucleus.
5. Neutron dosimetry (DOE support)
   a. Thin-film dosimeter for 10-200 keV neutrons.

Doctors Ahlen, Stevenson, and Tarlé play a major role in conceiving new experiments and in training students. There is much overlap among the various projects. Detectors devised to solve one problem frequently make possible the solution of all or part of another problem. A result obtained with plastic detectors may stimulate the construction of an electronic system to do a second-generation experiment. Expertise gained in resolving isotopes in a balloon-borne cosmic ray experiment may be used at PEP or the next-generation neutron-rich nuclide experiment. In all these projects, both post-graduate and undergraduate students play an active part.

Among the experiments planned for the next two years at the Bevalac are a high-energy gamma ray experiment with 10^2 times higher collecting power, detection of many new nuclides delineating the neutron dripline, hadron calorimetry with large solid angle, search for Lee-Wick matter in U-U collisions, measurement of higher-order electrodynamics in dE/dx and Cerenkov radiation by ions up to U, detailed studies of anomalons with detectors capable of resolving nonintegral charge, and determination of the response of plastic track detectors to relativistic ions up to U (the latter being of crucial importance for the proof that cosmic rays come from freshly synthesized supernova debris).

Footnotes

[*]Graduate students
[†]Undergraduate students

Nuclear Theory

N.K. Glendenning
M. Gyulassy
W.D. Myers
J. Randrup
W.J. Swiatecki
J. Boguta
G. Fai
M. Redlich
H. Ruck
V. Ruck
Lawrence Berkeley Laboratory

S. Bohrmann
MPI, Heidelberg, West Germany

P. Hecking
Regensburg, West Germany

A. Lumbroso
CEN, Saclay, France

K.H. Müller
THD, Darmstadt, West Germany

H. Stöcker
GSI, Darmstadt, West Germany

The nuclear theory program encompasses the general structure of static nuclei (including neutron stars), nuclear dynamical properties as probed in nuclear collisions at various energies, and the manifestation of the basic quark degrees of freedom.

General nuclear structure is being studied by macroscopic as well as microscopic tools. In particular, a nonlinear relativistic mean-field theory has been found to possess remarkable predictive power for a variety of nuclear properties. Due to its simplicity and consistency, this model is a versatile tool for exploring more exotic nuclear properties, e.g., the structure of hypernuclei. The good agreement with much more complicated many-body calculations suggests that the low-density properties of nuclear matter are determined by a few simple properties, such as the compressibility at saturation. The theory also implies that knowledge of the free nucleon-nucleon interaction does not suffice to understand the nuclear many-body properties. Separate studies have focused on generalizing relativistic mean-field theory to the study of time-dependent problems. While practically equivalent to time-dependent Hartree-Fock calculations at low energy, the relativistic mean field model provides a natural inclusion of the mesonic degrees of freedom which become significant at higher energies. A relativistic field theory has also been used to study dense neutron matter in the normal and pion condensed phases.

Recently, a program to apply nuclear theory to astrophysics has been initiated. For example, the role of deformations on slowing down pulsars is being studied, and beta stable neutron star masses and the temperature dependence of the equation of state has been computed.

The dynamical properties of moderately excited nuclear systems continues to be an important area of research. The general macroscopic theory of nuclear dynamics has been further developed, and favorable confrontation with experiment has been made, in particular regarding the "extra push" required to achieve the temporary coalescence of two colliding nuclei.

In the area of damped nuclear reactions, the study of the charge equilibration phenomenon has been a central theme during the past year. In particular, confrontations of a previously formulated transport theory with various sets of data have demonstrated that the observed isotopic and isobaric fragment distributions can be quantitatively well understood to result from the statistical exchange of individual nucleons between the two reacting nuclei, thus eliminating the apparent need for a collective charge-equilibration model to explain the data. In view of this success, work has been done to involve the angular-momentum carrying degrees of freedom to further test the model.

As the bombarding energy is raised, the binary idealization becomes increasingly inadequate and multi-fragment final states grow predominant. The fragment production mechanisms have been studied by various approaches. Some have focused on the production of a specific fragment type, such as nucleon jets appearing as a result of the kinematical boost of transferred nucleons due to the nuclear motion, pions resulting from nuclear collisions at a few hundred MeV/n, and the production of deuterons within the framework of the intranuclear cascade description. Other studies have attempted a comprehensive description of fragment production where all final states are treated on an equal footing. In relation to current attempts to probe the entropy production in a nuclear collision, it has been found that the eventual deexcitation of unstable ejectiles plays an important role in modifying the observed distributions relative to those immediately after the collision process.

The area of high-energy nuclear collisions is a major part of the theory program and several directions have been pursued simultaneously, e.g., the development of analytical models for elucidating the constraints of geometry and phase space on the observables, the employment of nuclear hydrodynamics for studying nuclear flow phenomena and their possible detection, and intranuclear cascade studies of the equilibration process. Special topics which have been addressed are $\pi\pi$ and pp correlations, π and K production, multiplicity distributions, composite fragment formation, and Coulomb final state interactions.

In regard to collective flow searches, an extensive comparison of model calculations with high-multiplicity triggered central data has indicated a qualitative failure in the cascade models, while, on the other hand, hydrodynamics appears to reproduce the observed forward suppression of protons. The existence of hydrodynamical phenomena would be very encouraging for our hopes to eventually deduce the high-density nuclear equation of state.

Further work has been done on various aspects of the pionic degree of freedom in nuclear matter: the propagation of the pion through matter has been studied within an optical model, pion condensation at finite temperatures has been given special attention, and a new experimental signature for pion condensation has been proposed.

An important modern frontier is associated with nuclear collisions at ultrarelativistic energies where the fields of nuclear, particle and astrophysics have common ground. We are pursuing problems in this area. In a schematic quantum chromodynamic model the properties of single hadrons, their interactions, and many-particle states have been studied, yielding insight into the occurrence of quark confinement and nuclear saturation. The phase transition from hadron to quark matter, which is expected to occur at sufficiently high energy density, has been explored: The onset of the phase transition has been studied in different models and the use of the strange baryon fraction as a signature for a quark phase has been discussed.

Heavy Ion Superconducting Spectrometer (HISS)

HISS GROUP A

E. Beleal
M. Bronson
D. Greiner
P. Lindstrom
M. Symons
R. Wada
Lawrence Berkeley Laboratory

F. Bieser
H. Crawford
I. Flores
C. McParland
U.C. Space Sciences Laboratory

G. Barsch
P. Brady
C. Castanada
M. Johnson
J. Romero
U.C. Davis

J. Carrol
U.C. Los Angeles

B. Berman
D. Olsen
Lawrence Livermore National Laboratory

H. Sann
GSI, Darmstadt, West Germany

J. Engelage
Lousiana State University

S. Kadota
INS, Japan

The HISS facility took its first data in June 1981 just before the Bevalac Improvement shutdown beginning June 29, 1981. For much of the time it appeared that it would be impossible to get data this year. Beginning in December 1980, physicists from LBL, UC Davis, the Institute for Nuclear Studies (Tokyo), and LSU overcame the budget and manpower limitations slowing detector construction and assembled the Phase I detectors. Another difficulty was a leak in the magnet vacuum system which made operations very difficult. However, we decided to attempt to run at a reduced field of 20 kG and continue with the experiments. This gamble paid off, and steady operation at 20 kG was achieved in June 1981.

The major essential detector systems were the drift chambers and the time-of-flight wall. Both these devices were brought to completion in early June 1981 with Doug Greiner leading the effort on the drift chambers and Roy Wada the-time-of-flight wall. Magnet control and testing headed by Fred Bieser achieved stable running conditions in mid-June 1981.

The magnet and detector systems would be of little use without the necessary software. In the area of magnet monitoring, Chuck McParland (SSL), and his team put together a system that collected and achieved data from the magnet sensors; this enabled diagnostic plots to be made using the MULTI programs on the VAX 11-780 computer. This tool proved essential in understanding the difficulties of running the magnet and to devising successful operating procedures.

The data was collected in the PDP 11-45 front end computer and transmitted via a shared disk to the VAX 11-780 for on-line diagnostics. Peter Lindstrom led the work on the front end computers; Chuck McParland's team did the data transmission; Hank Crawford (SSL) and a large group of physicists provided the necessary diagnostic programs in the VAX 11-780.

The payoff for all this hard work came on the last weekend of Bevalac running, when several hours of data were recorded from the first HISS experiment, which simultaneously measured all the projectile fragments from a 1.9 GeV/A ^{12}C beam and several targets. With this multiparticle data, we will be able for the first time to examine the energy and momentum transfer to the excited projectile nucleus, which will give crucial information about the reaction mechanism. The data also permit fragment spectra to be searched for resonance formation and the existence of long lived states that have been reported recently from emulsion data.

We still have many things to do this year. Data taken in June is being eagerly analyzed, and we have started to improve and document the results of the rush to get data.

In FY 1982, we will finish construction of the facility and complete the five Phase I HISS experiments. Building the Phase II detectors will also be a major task for this year. After final analysis of the performance of the Phase I detectors, the designs will be finalized and the construction begun.

Isotopes Project

J.M. Dairiki
E. Browne
R.B. Firestone
C.M. Lederer
V.S. Shirley
Lawrence Berkeley Laboratory

Y.A. Ellis-Akovali
Oak Ridge National Laboratory

The Isotopes Project compiles and evaluates nuclear structure and decay data, and develops compilation methodology. Much of the group's effort is directed to the evaluation of experimental data, based on the knowledge of experimental methods, the researchers themselves, and the relationships and constraints imposed upon the data by nuclear theory and systematics. Considerable effort is also devoted to the selection and presentation of data in formats most convenient for users.

From 1940 to 1978, the Project's main objective was the production of the *Table of Isotopes*. Since publication of the seventh (and last) edition in 1978, the group has coordinated its nuclear data evaluation effort with that of the other data centers via the national and international nuclear data networks. The group is currently responsible for the evaluation of mass chains A = 146-152 and A = 163-194. All evaluated data are entered into the international Evaluated Nuclear Structure Data File (ENSDF) and published in *Nuclear Data Sheets*.

During the past year the evaluation of nuclear structure data for all nuclei with mass A = 191 was published in *Nuclear Data Sheets*; evaluations of A = 193, A = 188, and A = 185 were accepted for publication, and the evaluations of A = 169, A = 187, A = 189, and A = 190 were completed and submitted for review. Updated evaluations of three additional mass chains (A = 181, A = 174 and A = 192) are in progress.

The Project continues to develop data handling and analysis techniques. A recent example is the restructuring of the *Table of Isotopes* level-scheme file into a computer-searchable data base. It is the most up-to-date file of nuclear structure data available and is readily accessible for horizontal compilations and systematic studies of nuclear properties.

Programming tools to aid the evaluation effort have also been developed. The physics analysis programs, written by the Nuclear Data Project (ORNL) for data in ENSDF formats, have been adapted and extended into an interactive package for use on the CDC-7600 computer. The resulting program, PACK, enables immediate calculation of such quantities as internal conversion coefficients, level energy fits, and log ft values and level feedings in radioactive decay. It also permits manipulation of the data to give, for example, energy-ordered γ-ray listings and allows on-line editing.

The *Table of Nuclear Moments*, a compilation of nuclear magnetic and quadrupole moments published by the Isotopes Project, has been the only such table maintained on a continuing basis. The most recent version was published as an appendix to the *Table of Isotopes*. User response has encouraged plans for expanding the amount of data for presentation in the next edition.

The seventh edition of the *Table of Isotopes* continues to be the most up-to-date general reference source available for nuclear data. Sales through April 1981 totaled 6,668 copies (3,269 clothbound and 3,399 paperback). Nearly all 7,000 copies of the *Nuclear Wallet Cards*, produced in 1979 by the Isotopes Project on behalf of the U.S. Nuclear Data Network have been distributed to the user community.

In addition to the evaluation effort, the Isotopes Project will produce, on behalf of the U.S. Nuclear Data Network (NDN), a *Radioactivity Handbook* for applied users. The purpose of the Handbook is to provide a compilation of recommended decay data that is detailed enough for use in sophisticated applications, but organized clearly so as to be usable in routine applications. The handbook will be produced at four-year intervals, beginning in 1983. Recommended decay data will be taken from the current version of ENSDF, without updating. Additional calculations and evaluation will be performed to provide recommended data for atomic radiations and conversion electrons. Each mass chain will be referenced to its most recent evaluation in *Nuclear Data Sheets* as the source for further details and the references to the original papers.

Nearly 6,000 copies of a Handbook sample illustrating the contents and format proposed by the group have been distributed to other data centers and members of professional societies. The suggestions and comments obtained are being considered in the development of the final format.

Work is proceeding on the computer codes needed to produce the handbook. This involves retrieval of the desired data from ENSDF and their presentation in the final publication formats. The first step is to modify the data in ENSDF so that each decay data set will contain "best" values for the γ-ray and level properties independent of the decay parent. Nonuniformities and holes in the ENSDF data are being corrected as work proceeds. The existing level-scheme graphics program (used for the *Table of Isotopes*) has been modified to handle data in ENSDF formats.

Promoting the science of nuclear data evaluation and providing assistance to the user community are important

aspects of the Project's role. With regard to the former, Project members are organizing the First Annual Conference on Nuclear Data Evaluation, to be held in conjunction with the fall meeting of the APS Division of Nuclear Physics at Asilomar (October 28-30, 1981). Periodic exchanges of both information and scientists with other data centers (both foreign and domestic) also enhance the evaluation effort. The Project continues to process approximately two user requests per month. Most require a brief data search, a letter, or a telephone response. Major requests are now referred to the National Nuclear Data Center at BNL. General use of the Project's extensive library, which contains comprehensive data files and major nuclear physics journals, is encouraged.

PART 2. PROGRESS REPORTS

I. EXPERIMENTAL RESEARCH

A. NUCLEAR STRUCTURE

1. Study of Exotic Nuclei

The Decay of ^{8}He*

T. Björnstad,† H.Å Gustafsson,† B. Jonson,† P.O. Larsson,‡ V. Lindfors,†
S. Mattsson,† G. Nyman,‡ A.M. Poskanzer, H.L. Ravn,† and D. Schardt†

The heaviest isotope of the element helium (Z = 2) has mass number 8 and is the nucleus with the highest neutron to proton ratio available. It was first definitely identified[1] with a counter telescope technique as the third fragment in ^{252}Cf fission, and the first study of its decay was made[2] in 1965. In the latter experiment the ^{8}He activity was produced by high-energy protons in a target of cotton fibers. The ^{8}He that diffused out of the target was purified by gas phase chemistry and transported to a counting chamber. By means of neutron counting the half-life was determined to be 122 ± 2 ms. The state in ^{8}Li at 981 keV with I = 1 is the only state below the neutron separation energy that could be fed in allowed beta-decay. The gamma emission from this state, observed with a NaI detector, established its parity as positive. The delayed neutron branch, P_n, was determined to be (12 ± 1)% from the ratio of the neutron to gamma count rates. Aspects of the decay have been verified but no new information has been contributed to the original decay scheme.

In this paper we report on a new series of measurements on the ^{8}He decay. The half-life and the beta-delayed neutron branch have been remeasured and energy spectra of neutrons and gamma rays were recorded. A search for the possible beta-delayed charged-particle decay mode, involving the break-up of $^{8}Li^{*}$ into α + t + n, has been made.

The ^{8}He activity was produced at the ISOLDE facility through fragmentation reactions induced either by 600 MeV proton or 910 MeV ^{3}He beams from the CERN Synchro-Cyclotron. The production target consisted of a 47.0 g/cm^2 uranium carbide matrix. A cooled transfer tube connecting the target to the plasma ion source assured chemical purity of the on-line mass separated ion beam.

The ^{8}He was directed to a low-background counting area where the 60 keV ions were deposited in an aluminized mylar tape. A beta detector, consisting of a 1 mm thick 24 × 26 mm plastic scintillator, mounted on a 30 mm diameter phototube, was placed behind the tape at the collection position. The tape was moved periodically in order to remove the daughter activity. The beta-detection efficiency was determined on-line to be (40 ± 3)% in a beta-gamma coincidence measurement on the nuclide ^{23}Ne. A coaxial Ge(Li) crystal was placed close to the collection point and a fast coincidence technique was used for the beta-gamma coincidence measurements.

For the P_n-value measurements a 4π neutron counter, consisting of twelve ^{3}He proportional counters imbedded in paraffin-wax, was slid over the beta detector so that the collection position was in the center of the counter. The neutron detection efficiency was determined to be (20 ± 1)% with a sample of uranium. A possible source of systematic error is the energy dependence of the neutron detection efficiency, which has not been determined experimentally. Since the energy spectra of ^{8}He and the fission neutron spectrum of ^{238}U are similar, the systematic error is considered to be small. The beta-neutron coincidence method used for the determination of the P_n value involved the technique[3] for measuring the time delay between the beta particle emission and the detection of a neutron.

The neutron energy spectrum was measured with a ^{3}He filled high resolution spectrometer. For the charged particle measurements the ^{8}He ions were collected in a Ni foil in front of a 100 μm thick surface-barrier Si detector.

The half-life of ^{8}He was measured with the 4π neutron counter to be 117.5 ± 1.5 ms. Combining this new value of the half-life with the one published earlier[2], we recommended a best value of 119 ± 1 ms.

The measurements of the P_n value were done both with a saturated ^{8}He source, and with periodic removal of the activity. When counting the beta activity in the saturation mode, one has to take into account the contribution from the 0.84 s ^{8}Li daughter which is in equilibrium with ^{8}He. If P_γ denotes the probability of beta decay to the 0.98 MeV state in ^{8}Li, then the beta count rate is proportional to $1 + P_\gamma$. This is equal to $2\text{-}P_n$ since one can assume that $P_n + P_\gamma = 1$. In the short collection mode, where the activity was collected and counted during a 100 ms time interval followed by an interruption of 100 ms, when the tape was moved, the beta count rate was calculated to be proportional to $1 + 0.03\ P_\gamma$.

The beta-neutron coincidence measurements gives a P_n value of (15 ± 1)%. This value is based on four measurements in saturation mode and one in the short collection mode. The error comes mainly from the uncertainty in the neutron detection efficiency. Nine sets of simultaneous beta neutron singles measurements give a somewhat larger P_n value, (18 ± 2)%, where the larger error is due to the uncertainty in the beta detection efficiency. Another method to obtain P_n is to use the ratio of neutron to gamma count rates, both normalized to their respective

beta count rates. This method again gives (18 ± 2)%, even though the beta detection efficiency cancels out of the calculation. From all these measurements we adopt a value for P_n equal to (16 ± 1)%. This is somewhat larger than the earlier published value,[2] but we believe that the present techniques, especially the β-n coincidence method, offer the best available determination of P_n.

The gamma energy spectrum showed, in addition to the 981 keV line, a broader peak at 478 keV from the deexcitation of the first excited state in ^{7}Li populated after neutron emission. The larger width of the 478 keV peak is presumably a doppler broadening caused by the neutron emission recoil. The ratio of the probability of emission of the 478 keV gamma to P_γ was found to be 0.060 ± 0.003. Using our adopted valued of P_n, this shows that the fraction of neutrons emitted to this state amounts to (32 ± 3)%.

The neutron energy spectrum showed no significant structure in the spectrum, as expected, since the known neutron emitting states in ^{8}Li are broad. The spectral shapes measured with and without lead around the source position were the same, which shows that high energy beta particles do not contribute to the spectrum.

The Q_β value of ^{8}He is 10.649 MeV and the thresholds for the break up of ^{8}Li into α + t + n and ^{5}He + t are at 4.499 and 5.39 MeV, respectively. It was therefore considered possible to detect beta feedings to states above these energies from the observation of beta-delayed triton emission. The measured charged particle spectrum was, however, severely interfered with both by alpha particles from the ^{8}Li daughters and by beta particles from ^{8}He itself. As a result only upper limits can be set at 10% per decay for charged particles with an energy below 1 MeV and 1% per decay with an energy above 1 MeV. These are not very useful limits as one expects mainly low-energy alphas and tritons from the possible ^{8}He delayed charged particle decay mode.

It has earlier been assumed that the main part of the emitted neutrons originates in the 3.21 MeV state. In order to try to detect neutron emission from higher excited states in ^{8}Li we have calculated the shape of the neutron energy spectrum and compared it with our measured spectrum. The calculated spectrum follows the main trend of the experimental spectrum but there is some additional intensity in the experimental spectrum at the lowest energy and at about 1.8 MeV which cannot be explained from neutron emission from any known state in ^{8}Li. It is interesting to speculate whether part of the intensity at the lowest energy could be due to α + t + n break-up. Assuming that all the additional intensity up to 1 MeV arises from this decay mode we get an upper limit for this decay branch of 2%. We suggest that the 3.21 MeV state, which has spin equal to 1, has positive parity, and that the 5.4 MeV state could be either 0^+ or 1^+.

Footnotes and References

*Condensed from Nucl. Phys. A **366**, 461 (1981).
†CERN-ISOLDE, Geneva, Switzerland.
‡Department of Physics, Chalmers University of Technology, Göteborg, Sweden.
1. S.W. Cosper, J. Cerny, and R.C. Gatti, Phys. Rev. Lett. **154**, 1193 (1967).
2. A.M. Poskanzer, R.A. Esterlund, and R. McPherson, Phys. Rev. Lett. **15**, 1030 (1965).
3. T. Björnstad et al., Nucl. Phys. A **359**, 1 (1981).

Delayed Neutron Emission Probabilities of ^{9}Li and ^{11}Li*

T. Björnstad,† H.Å. Gustafsson,† P.G. Hansen,‡ B. Jonson,† V. Lindfors,† S. Mattsson,† A.M. Poskanzer and H.L. Ravn†

Because of the inherent difficulty of neutron detection, the known P_n value of an accessible nucleus is often used to determine the ratio of the efficiencies of the neutron and β-detectors. For example, the P_n values for ^{11}Li, and many Na, Rb and Cs isotopes[1,2] have been deduced by using the adopted value[3] for ^{9}Li (35 ± 5)% by Chen et al.[4] Our new measurement of the ^{9}Li P_n value gives (50 ± 4)% and increases the other results correspondingly. In fact, it was the γ-measurement of ^{11}Li reported here, which proved to be inconsistent with the published P_n value and prompted us to remeasure the P_n of ^{9}Li. The P_n value of ^{11}Li is of particular interest because of the recent discoveries that it is a β-delayed two-neutron and three-neutron emitter.

The lithium isotopes were produced by the 900 MeV ^{3}He beam from the CERN SC irradiating uranium carbide or tantalum targets in combination with a thermal ion source at the ISOLDE facility. The 60 keV ion beam from the separator was deposited on a movable aluminized mylar tape. The beta detector which consisted of a 1 mm thick 24 × 16 mm plastic scintillator (NE 102) mounted on a 30-mm phototube was placed in a metal cylinder right behind the tape at the collection position.

The 4π neutron counter consisted of eight ^{3}He proportional counters imbedded in paraffin wax in concentrical geometry around the cylinder containing the beta detector. The neutron detection efficiency was determined with a sample of ^{238}U to be (14 ± 1)%. The variation of the

neutron detection efficiency with energy, which has not been measured, is in the present work the largest source of systematic error. The γ-detector was a coaxial Ge(Li) crystal.

Since the residence time of a neutron in the paraffin moderated detector is exponentially distributed with a mean lifetime of about 100 μs, the neutron-β coincidence measurements were performed by starting a clock with the β signal and stopping it with the neutron signal. The data were fitted to an exponential plus a constant value where the latter accounted for the random background at the low coincidence rates of about 10 s^{-1} used here. From β-γ coincidence measurements on ^{26}Na, the beta detection efficiency was determined to be (40 $\pm$ 3)%.

From two β-neutron coincidence measurements on ^{9}Li the P_n value was determined to be (50 $\pm$ 4)%. The statistical uncertainty is four times smaller; the error shown comes mainly from the uncertainty in the efficiency of the neutron detector. Ten other sets of singles measurements were made, which with the determined β-detection efficiency also yielded a P_n value of 50% with an equally small statistical error, but with the uncertainty in the β-detection efficiency giving a larger systematic error. Table 1 presents the P_n values measured by Roeckl et al.[1,2] renormalized to a ^{9}Li P_n value of 50% instead of 35%.

Since the ground state of ^{9}Be is the only non-neutron emitting state, the β-decay branch to the ground state is thus also (50 $\pm$ 4)%.

Table 1. Renormalized P_n values (%)

^{11}Li[a]	87 $\pm$ 10
^{27}Na[a]	0.11 $\pm$ 0.04
^{28}Na[a]	0.8 $\pm$ 0.2
^{29}Na[a]	22 $\pm$ 3
^{30}Na[a]	47 $\pm$ 5
^{31}Na[a]	43 $\pm$ 11
^{93}Rb[b]	1.8 $\pm$ 0.2
^{94}Rb[b]	12.1 $\pm$ 1.3
^{95}Rb[b]	12.2 $\pm$ 1.3
^{96}Rb[b]	19 $\pm$ 2
^{97}Rb[b]	39 $\pm$ 4
^{98}Rb[b]	19 $\pm$ 3
^{145}Cs[b]	17 $\pm$ 2
^{146}Cs[b]	20 $\pm$ 2

[a]From Ref. 1.

[b]From Ref. 2.

For ^{11}Li, the half-life was redetermined by neutron measurements to be 8.83 $\pm$ 0.12 ms. Combining this with the previous result[1] of 8.5 $\pm$ 0.2 ms, we recommend a best value of 8.7 $\pm$ 0.1 ms.

When counting the β's of ^{11}Li in the saturation mode one has to take into account the contribution from the 14 s ^{11}Be daughter in equilibrium. Assuming that the ^{11}Li decay to the ^{11}Be ground state is negligible, then all the ^{11}Be yield must come from β-decay to the 320 keV state, which is the only excited neutron bound state. If the probability of beta decay to this state is denoted P_γ, then the β count rate in the saturation should be proportional to $1 + P_\gamma$. Taking this into account the β-γ coincidence measurement gave a value for P_γ equal to (9.2 $\pm$ 0.7)%. The ^{11}Be γ-ray at 2.12 MeV was also visible. From this the ^{11}Be decays per ^{11}Li decay in saturation came to (9 $\pm$ 2)%, in agreement with P_γ. From this one can calculate that the one standard deviation upper limit on $P_{g.s.}$ is 2%. The 3.368 MeV γ-ray from the first excited state of ^{10}Be populated following neutron emission was seen with a probability of (35 $\pm$ 3)%.

For the ^{11}Li β-neutron coincidence measurement, the tape was moved every two seconds (with interruption of counting) in order to reduce the contribution of the ^{11}Be daughter to an almost negligible amount. The results gave a value for P_n equal to (96 $\pm$ 8)%, of which the statistical error was 5% and the rest of the error came from the uncertainty in the neutron detection efficiency. Six sets of singles measurements were also performed. The average value of P_n was 93% with about the same statistical error as in the coincidence measurement, but with a larger systematic error. We adopt a best P_n value of (95 $\pm$ 8)%. The renormalized value from the measurements of Roeckl et al.[1] given in Table 1 agrees with this new value.

Previously ^{11}Li had been reported[5] to be a multiple neutron emitter. The relative probabilities of two-neutron and three-neutron emission were given to be[6]

$$P_{2n}/P_{1n} = 0.048 \pm 0.005,$$
$$P_{3n}/P_{1n} = 0.022 \pm 0.002. \quad (1)$$

From this one obtains:

$$P_n/P_{1n} = 1+2P_{2n}/P_{1n}+3P_{3n}/P_{1n} = 1.16 \pm 0.01. \quad (2)$$

By assuming that the ^{8}Li + t disintegration mode as well as the ground-state β-decay are negligible one can state that:

$$1 - P_\gamma = P_{1n}+P_{2n}+P_{3n}.$$

Using the values for two- and three-neutron emission given in Eq. (1)

$$(1-P_\gamma)/P_{1n} = 1.07 \pm 0.005. \quad (3)$$

Combining this with Eq. (2) one finds that the relationship between P_n and P_γ is given by:

$$P_n/(1-P_\gamma) = 1.08 \pm 0.01. \quad (4)$$

Our results presented above give for this ratio the value 1.05 ± 0.08, which shows consistency between our neutron and γ-measurements.

With these assumptions, one may calculate a more accurate value for P_n from the measured value of P_γ by using Eq. (4). This gives a ^{11}Li P_n value of (98 ± 1)%, and by using Eqs. (2) and (1), the following multi-neutron emission probabilities are obtained:

$$P_{1n} = (85 \pm 1)\% \ ,$$

$$P_{2n} = (4.1 \pm 0.4)\%,$$

$$P_{3n} = (1.9 \pm 0.2)\%.$$

From the intensity of the 3.3 MeV γ-ray in ^{10}Be and the P_{1n} value the fraction of one neutron emission leading to excited states of ^{10}Be becomes (41 ± 4)%.

Footnotes and References

*Condensed from Nucl. Phys. A **359**, 1 (1981).

†CERN-ISOLDE, CERN, CH-1211 Geneva 23, Switzerland.

‡Institute of Physics, University of Aarhus, Denmark.

1. E. Roeckl, P.F. Dittner, C. Détraz, R. Klapisch, C. Thibault and C. Rigaud, Phys. Rev. C **10**, 1181 (1974).

2. E. Roeckl, P.F. Dittner, R. Klapisch, C. Thibault, C. Rigaud and R. Prieels, Nucl. Phys. A **222**, 621 (1974).

3. F. Ajzenberg-Selove, Nucl. Phys. A **320**, 1 (1979).

4. Y.S. Chen, T.A. Tombrello and R.W. Kavanagh, Nucl. Phys. A **146**, 136 (1970).

5. R.E. Azuma, T. Björnstad, H.Å. Gustafsson, P.G. Hansen, B. Jonson, S. Mattsson, G. Nyman, A.M. Poskanzer and H.L. Ravn, Phys. Lett. B **96**, 31 (1980).

6. Note that the probability of emission of i neutrons is denoted P_{in} so that the usual P_n value is given by $P_n = \Sigma_i i P_{in}$.

Beta-Delayed Three-Neutron Radioactivity of ^{11}Li*

R.E. Azuma,† T. Björnstad,‡ H.Å. Gustafsson,‡ P.G. Hansen,‖ B. Jonson,‡ S. Mattsson,‡ G. Nyman,§ A.M. Poskanzer, and H.L. Ravn‡

Beta-delayed emission of two neutrons has recently been observed in the decay of ^{11}Li (Ref. 1) and of the sodium isotopes $^{30\text{-}32}$Na (Ref. 2). In the present paper the extension is reported of the neutron time-correlation techniques used in the previous work. With this method a new radioactive decay mode, beta-delayed three-neutron emission, has been observed in ^{11}Li in an intensity $p_{3n} = (1.8 \pm 0.2)\%$.

The isotope ^{11}Li with a half-life of 8.6 ± 0.2 ms is ideally suited for a search for 3n emission. It has a Q_β value of 20.7 MeV (Ref. 3) and the thresholds for break-up into three neutrons lie at 8.888 MeV (residual two ^{4}He) and at 8.979 MeV (residual ^{8}Be).

The radioactivity was produced by bombarding a target of uranium carbide at 2000°C with a 0.2−2 μA proton beam of 600 MeV from the CERN synchrocyclotron. The ^{11}Li radioactivity was separated on-line in the ISOLDE facility and directed as an ion beam to the centre of a paraffin-filled 4π neutron counter.

The neutron counter[1,2] now was equipped with a total of 12 ^{3}He tubes, which increased the efficiency to (20 ± 1)% as determined with a sample of ^{238}U. (Note, however, that the neutron detection efficiency is expected to depend appreciably on the neutron energy.) The residence time in the detector, as determined from beta-neutron coincidences on ^{9}Li was exponentially distributed with a mean of 89 ± 1 μs. The neutron counters were connected in parallel and fed into a microprocessor unit that allowed the arrival times of individual neutrons to be read by a "flying clock" with a precision of 1 μs.

The rate of triple events and the histograms (Fig. 1) taken on-line with strongly reduced proton beam intensity clearly indicated the presence of true triple events. The presence of random triple correlations due to the combination of single and double events, however, necessitated a more detailed analysis.

As the evaluation is very sensitive to the precision with which the correction for randoms can be carried out, the analysis was checked in several ways. (i) Random data taken with a γ-source and with ^{9}Li neutrons were analyzed and it was found that the corrections for random events were accurate to typically (3-7)%. (ii) The neutron count rate in the ^{11}Li experiments was varied from 7.9 c/s to 202.8 c/s without any appreciable change in the results. This is a very sensitive test as the random events vary with the square or the cube of the rate. (iii) The analysis time θ was varied between 79.8 and 456 μs, again without any detectable effect. (iv) The time distributions shown in Fig. 1 were calculated from the results of the data analysis and evidently agree exactly with experiment.

From the analysis we propose as adopted values

$$p_{2n}/p_{1n} = (4.8 \pm 0.5) \times 10^{-2} \ ,$$

$$p_{3n}/p_{1n} = (2.2 \pm 0.2) \times 10^{-2} \ .$$

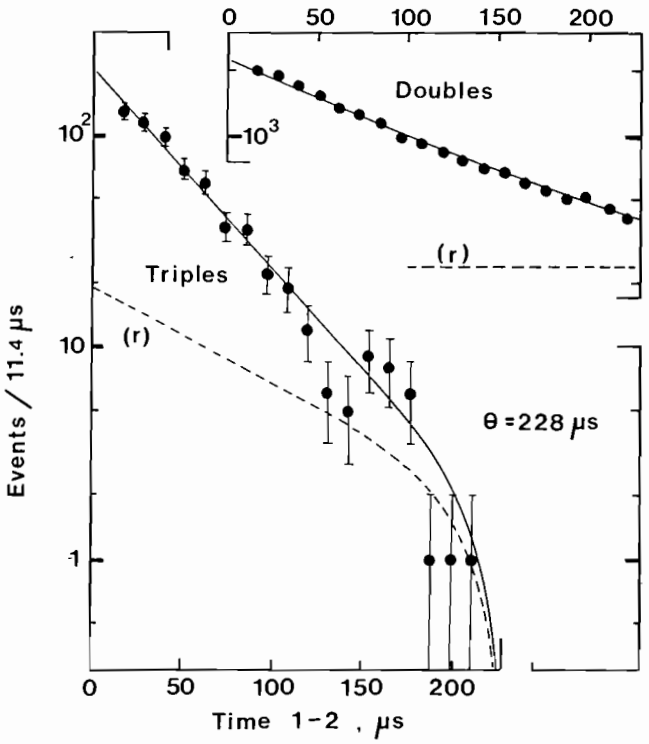

Fig. 1. Distribution of the time interval between the first and the second neutrons for events registered as doubles and triples with a correlation time $\theta = 228$ μs. The data are from a 12 h run with an average neutron count rate of 22.9 c/s. The theoretical curves showing the total number of events and the contribution from random events (r) do not represent a fit: they have been calculated on an absolute scale. Note that the triples events clearly show the $e^{-2\lambda t}$ dependence expected theoretically. (XBL 817-10857)

The p_{in} values may be put on an absolute scale by means of the total probability for neutron emission $p_n = \sum_{i=1}^{\infty} i p_{in}$. We use here the value $p_n = (95 \pm 8)\%$.[5] From this one finds for ^{11}Li

$$p_{1n} = (82 \pm 7)\%, \quad p_{2n} = (3.9 \pm 0.5)\%,$$

$$p_{3n} = (1.8 \pm 0.2)\%.$$

The experiment represents the first observation of a new radioactive decay mode: β-delayed three-neutron emission. It is furthermore noteworthy that the residual nucleus itself is unstable so that the process detected in the present work effectively is a break-up into the five nuclear particles 2α+3n.

Footnotes and References

*Condensed from Phys. Lett. B **96**, 31 (1980).

†Department of Physics, University of Toronto, Toronto, Ontario, Canada.
‡CERN-ISOLDE CERN, CH-1211 Geneva 23, Switzerland.
‖Institute of Physics, University of Aarhus, DK-8000 Aarhus, Denmark.
§Department of Physics, Chalmers Institute of Technology, S-41296 Göteborg, Sweden.

1. R.E. Azuma et al., Phys. Rev. Lett. **43**, 1652 (1979).
2. C. Détraz et al., Phys. Lett. B **94**, 307 (1980).
3. C. Thibault et al., Phys. Rev. C **12**, 644 (1975).
4. F. Ajzenberg-Selove and C.L. Busch, Nucl. Phys. A **336**, 1 (1980).
5. T. Björnstad et al., Nucl. Phys. A **359**, 1 (1981).

Beta-Delayed Two-Neutron Emission from ^{30,31,32}Na*

C. Detraz,† M. Epherre,‡ D. Guillemaud,† P.G. Hansen,§ B. Jonson,§ R. Klapisch,‡ M. Langevin,† S. Mattsson,§ F. Naulin,† G. Nyman,§ A.M. Poskanzer, H.L. Ravn,§ M. de Saint-Simon,‡ K. Takahashi,‖ C. Thibault,‡ and F. Touchard‡

Beta-delayed emission of two neutrons has recently been detected for the first time[1] in the decay of 8.6 ms ^{11}Li. This decay mode is also to be expected in the heavier elements and especially in those with odd Z, as may be seen from an inspection of theoretical mass tables. The element sodium (Z = 11) is a particularly favourable case, as its neutron-rich isotopes can be produced in high yields through mass separation of fragmentation products from reactions with high-energy protons. We report here the application of two different experimental methods, n-n time correlations with a 4π neutron counter and γ-spectroscopic identification of daughter products with mass A − 2, for demonstrating that the β^- decays of the isotopes $^{30\text{-}32}$Na are accompanied by 2n-emission.

One series of experiments was based on the n-n time correlation method, which has already been discussed in some detail in previous work.[1] The radioactivity was produced by bombarding a target of uranium-carbide at 2000°C with 600 MeV protons from the CERN synchrocyclotron. After mass separation in the ISOLDE separator, the isotope of interest was directed to the centre of a 60 cm long paraffin-filled cylinder containing eight ^{3}He proportional counters. With the detectors connected in parallel, a search was made by time correlation techniques

for pairs of neutron events with the characteristic mean time of 120 μs for residence in the detector.

The experimental time correlation spectra for ^{30,32}Na are shown in Fig. 1. The intensity of the correlated events relative to the total singles neutron counts determines the proportion of 2n-events when allowance is made for randoms, correlated background, deadtime losses and, of course, the efficiency of the neutron detector. The latter was determined with neutrons arising from ^{238}U spontaneous fission.

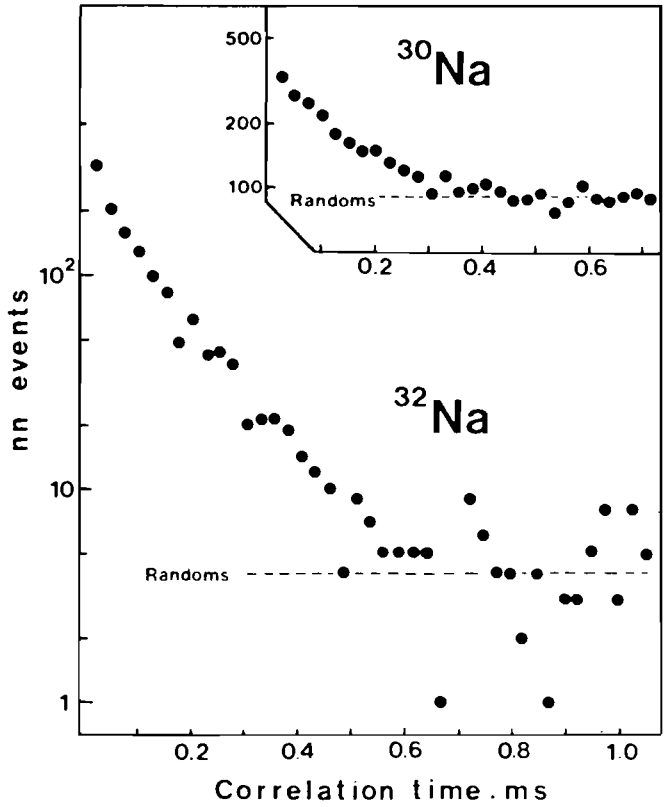

Fig. 1. Measured n-n time correlations for the isotopes ^{30}Na and ^{32}Na. The measuring time was 14.3 and 7.4h, respectively. For the ^{30}Na measurement, the initial beam intensity was reduced by a factor of about 30 in order to improve the ratio of true to random events. The dashed lines indicate the mean contributions of random n-n correlations. (XBL 817-10856)

The second series of experiments used the 24 GeV proton beam from the CERN synchrotron to bombard an iridium target at high temperature. After separation in the mass spectrometer[2], the beam of interest was directed to the end of a thin Al collecting tube viewed by a Ge(Li) detector. The presence of one- and two-neutron decay processes is revealed by the appearance of γ-rays belonging to lower mass chains than the one collected. Absolute intensities were obtained from the γ-spectra, from monitoring the β-radioactivity during the collection and from counting of the Na ions before and after the collection. The presence of mass-28 lines in the γ-spectrum of a sample produced in a long collection at mass 30 was shown.

For the case of ^{32}Na, the γ-spectra measured on-line showed contributions from the decays of ^{32}Na, ^{31}Al and ^{30}Mg, so that the relative contributions of zero-, one- and two-neutron emission could be deduced. At mass 31 no γ-rays above background were observed. $^{30\text{-}32}$Na are β-delayed two-neutron emitters and the intensities measured by the two methods agree well. The final values[3] that we have adopted for p_{2n} are ^{30}Na (1.2 $\pm$ 0.2)%, ^{31}Na (0.70 $\pm$ 0.25)% and ^{32}Na (5.1 $\pm$ 1.8)%.

The experiments demonstrate that β-delayed two-neutron emission is not a rare process far from stability; in fact, for ^{32}Na it accounts for half of all neutrons emitted. It is therefore important to take this mechanism into account in the calculation of yields in the astrophysical r-process.

Footnotes and References

*Condensed from Phys. Rev. Lett. B **94**, 307 (1980).
†Institute de Physique Nucleaire, F-91406 Orsay, France.
‡Laboratoire Rene Bernas, CSNSM, F-91406 Orsay, France.
§The ISOLDE Collaboration, CERN, CH-1211 Geneva, Switzerland.
‖Institut für Kernphysik, Technische Hochschule, D-6100 Darmstadt, Federal Republic of Germany.

1. R.E. Azuma et al., Phys. Rev. Lett. **43**, 1652 (1979).
2. C. Thibault et al., Phys. Rev. C **12**, 644 (1975).

3. The probability per β-decay for a process leading to the emission of i neutrons is denoted p_{in}, so that $\sum_{p_{in}} \equiv 1$. The usual total branching ratio for β-delayed neutron emission is $p_n = \sum i p_{in}$.

The Measurement of β-Decay Lifetimes via Projectile Fragmentation*

M.J. Murphy, T.J.M. Symons, G.D. Westfall, and H.J. Crawford†

It has recently been shown[1,2] that heavy ion projectile fragmentation produces a broad spectrum of isotopes extending far from the valley of β stability. This discovery has enabled the development of a significant new technique to measure the β-decay lifetimes of large numbers of very neutron-rich nuclei in a single experiment. The technique utilizes a multi-element position-sensitive Si(Li) telescope to stop and identify each projectile fragment; the same detector array is then used with higher electronic gain to observe the delayed electron from the embedded fragment's decay. The correlation observed between fragment and β is established by interrupting the beam upon detection of a particular isotope, and then recording the elapsed time to the first β-decay event originating at the position of the stopped fragment. Deflection of the fragments through a magnetic spectrometer greatly reduces background by selecting isotopes of a specific rigidity.

In the first application of this method, the fragmentation of ^{40}Ar at 280 MeV/n was used to measure several known and new β-decay lifetimes in the range from 40 msec to 600 msec. The half-lives are extracted by first averaging the multiple ΔE-E measurements provided by the six-element telescope to obtain mass resolution in the particle-identification spectrum for each element. An example of the resulting spectrum for aluminum isotopes of a particular rigidity is shown in Fig. 1. Gates are then set around each mass peak, and a spectrum of the elapsed time between the fragment and β^- events is made. The ^{31}Al and ^{32}Al peaks in Fig. 1 yielded the two half-life curves shown in Fig. 2. The observed ^{31}Al half-life of 620 ms agrees well with the tabulated value of 640 ms. The half-life of ^{32}Al was previously unknown; we obtain a value of 40 ms.

The success of the initial run indicates that, with the higher intensities and heavier beams which will become available from the upgraded Bevalac, this technique can make a major contribution to the study of β decay systematics, with applications to nuclear structure and to astrophysics.

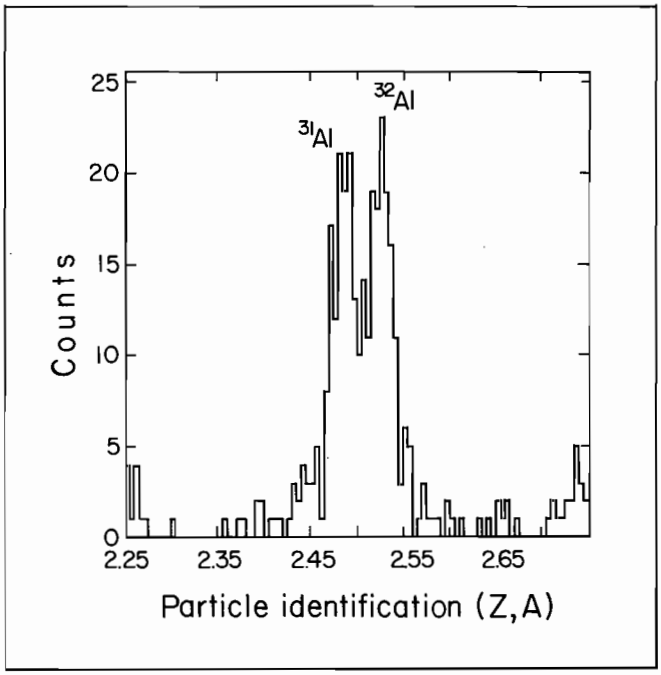

Fig. 1. Neutron-rich aluminum isotopes observed in the fragmentation of 285 MeV/n ^{40}Ar. (XBL 816-927)

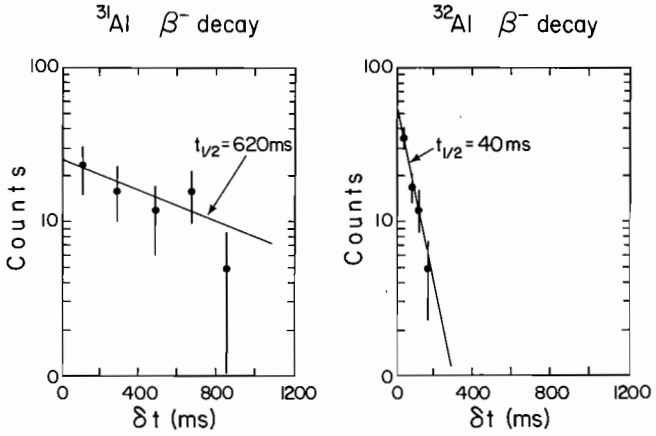

Fig. 2. β-decay lifetime curves associated with the ^{31}Al and ^{32}Al fragment peaks shown in Fig. 1. (XBL 816-926)

Footnotes and References

*Condensed from the Proceedings of the 5th High Energy Heavy Ion Study (1981).

†Space Sciences Laboratory, University of California, Berkeley, CA 94720.

1. T.J.M. Symons et al., Phys. Rev. Lett. **42**, 40 (1979).
2. G.D. Westfall et al., Phys. Rev. Lett. **43**, 1859 (1979).

β-Decay Energies and Masses of $^{103\text{-}105}$In

J.M. Wouters, H.M. Thierens, J. Äystö,† M.D. Cable, P.E. Haustein,‡ R.F. Parry, and Joseph Cerny*

The study of the nuclidic mass surface in the vicinity of the doubly magic nucleus ^{100}Sn is of fundamental interest in providing information on the strength of the shell closure when Z = N = 50. A comparison of measured mass excesses with currently available model mass predictions can determine the accuracy with which the various models include the effects resulting from shell closures. As a further step in the extension of the known mass surface we have measured the decay energies of $^{103\text{-}105}$In using β-γ coincidence spectroscopy following on-line mass separations. The decay of ^{102}In was also observed[1] but with inadequate statistics up to now to determine an accurate endpoint energy.

Heavy ion beams of ^{12}C, ^{14}N and ^{16}O from the 88-Inch Cyclotron were directed onto various targets to produce indium isotopes via (HI,xn) and (HI,pxn) reactions. The recoils were transferred via a helium-jet to the RAMA on-line mass separator, where they were mass analyzed. The mass separated recoils were collected on a mylar tape and transported to the detector station for β-γ coincidence spectroscopy. A separate contribution to this annual report gives a detailed description of the tape transport system, the detector station, and the procedure used for analyzing the β-spectra to obtain β-endpoints.

Table 1 presents a summary of the Q_{EC} determinations and Fig. 1 presents the Fermi-Kurie plot of ^{103}In as an example spectrum. Figure 2 shows a comparison of the predictions of the known indium masses with selected representatives of the different mass theories that are available. Those masses calculated according to the mass relations of the Garvey-Kelson[4] type and those calculated from the shell model formula of Liran-Zeldes[4] agree very well with the experimental results from ^{106}In to ^{125}In (Fig. 2a). For each of these mass models the root-mean-square deviation of theory from experiment for these nuclides is less than 200 keV. In the neutron-deficient side of figure 2a at ^{103}In, a strong deviation of about 1 MeV of the experimental value from the predictions of Liran-Zeldes and the

Table 1. Summary of Q_{EC} determinations.

		Q_{EC} (MeV)	
Nuclide	Gate	This work	Literature
^{103}In	188	5.38 ± 0.13	5.9 ± 0.5 (Ref. 2)
^{104}In	658,834	7.42 ± 0.14	7.1 ± 0.2 (Ref. 3)
^{105}In	131	5.14 ± 0.13	

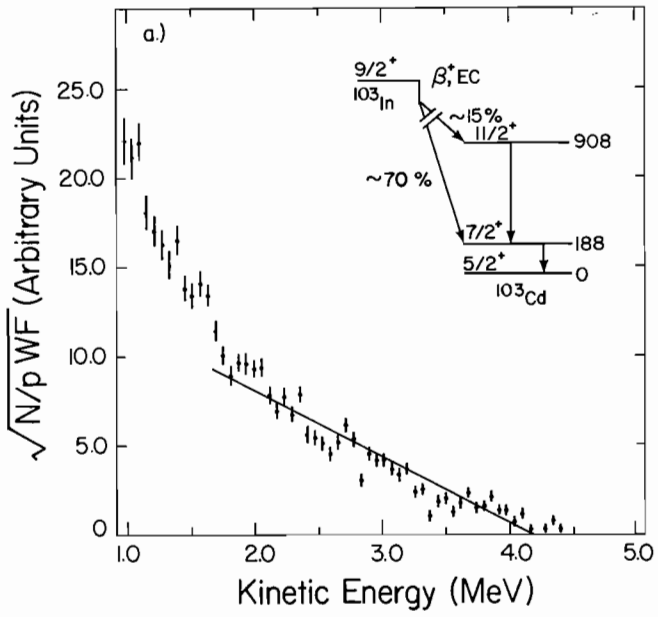

Fig. 1. Fermi-Kurie plot and partial decay scheme for ^{103}In. (XBL 8111-1592)

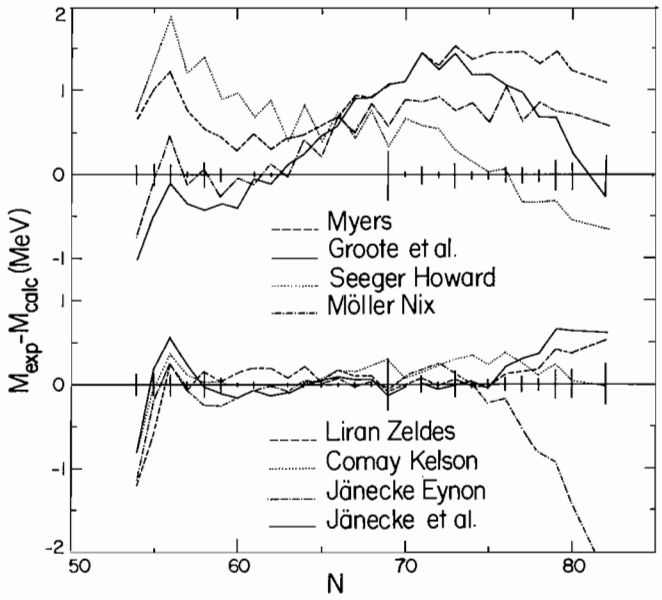

Fig. 2. A comparison of known indium masses with the predictions of some selected mass equations. (XBL 819-1350)

different Garvey-Kelson type mass formulas suddenly appears. The predictions of those liquid drop models considered here differ more from the experimentally observed mass behavior than the results of calculations based on the Garvey-Kelson relations (see Fig. 2b). For the models of Myers,[4] Groote et al.,[4] Seeger-Howard[4] and Moller-Nix,[5] the root-mean-square deviation from all the indium mass data is 1070, 830, 780 and 630 keV, respectively. As was noted for those mass models displayed in Fig. 2a, a sudden change in the systematic differences between the experimental and calculated masses also sets in for ^{103}In in the comparison with the liquid drop model predictions shown in Fig. 2b.

In conclusion, according to our results, ^{103}In is about 1 MeV more bound than predicted by the Liran-Zeldes and the different Garvey-Kelson type mass formulas. Other investigations of the mass surface near ^{100}Sn will show whether the observed deviation from the systematics for ^{103}In might have any possible relationship with the nearby double-shell closure.

Footnotes and References

*Present address: University of Gent, Belgium
†Permanent address: University of Jyväskylä, Finland
‡Permanent address: Brookhaven National Laboratory, U.S.A.

1. R. Béraud, J. Tréherne, A. Charvet, R. Duffait, J. Genevey, A. Gizon, J. Gizon and M. Meyer, Z. Physik A **299**, 279 (1981).
2. G. Lhersonneau, G. Dumont, K. Cornelis, M. Huyse, and J. Verplancke, Phys. Rev. C **18**, 2688 (1978).
3. H. Huang, B.P. Pathak and J.K.P. Lee, Can. J. Phys. **56**, 936 (1978).
4. At. Data Nucl. Data Tables **17**, 41 (1976).
5. P. Möller and J. Nix, Report LA-UR-80-1996.

The ϵ/β^+ Decay of ^{145}Gd: Resolution of Decay Branching Ratio Anomalies and Evidence for Pronounced Structures in the β-Decay Strength*

R.B. Firestone, R.C. Pardo,† R.A. Warner,†
Wm.C. McHarris,† and W.H. Kelly†

The ϵ/β^* decay of ^{145}Gd has been investigated in great detail. We have placed 136 levels deexcited by 326 γ rays in ^{145}Eu. In addition, ϵ/β^* decay branching ratios, the decay energy, and the half-life have been accurately measured by various coincidence and γ-ray singles techniques. This work is the culmination of over 10 years of experimental effort by our group.

Previously reported ϵ/β^+ decay branching ratio anomalies have been eliminated in these experiments.[1] Anomalies larger than 30% have been removed. The total ground state decay energy was measured by β-γ coincidence techniques to be 5.07 ± 0.06 MeV. A new half-life of 23.0 ± 0.4 m was determined, eliminating a preexisting discrepancy in reported values.

The decay of ^{145}Gd offers a unique opportunity to investigate the nature of beta decay to regions of high level density. Here >98% of the total decay intensity is placed and the microscopic detail of the decay is observed. Previous authors have suggested that these experiments would not be possible due to the large number of very weak transitions.[2] In fact, simple nuclear structures were observed to dominate the decay concentrating the intensity into relatively few important channels. These structures are discussed in a separate report. A part of the total ^{145}Gd level scheme is shown in Fig. 1.

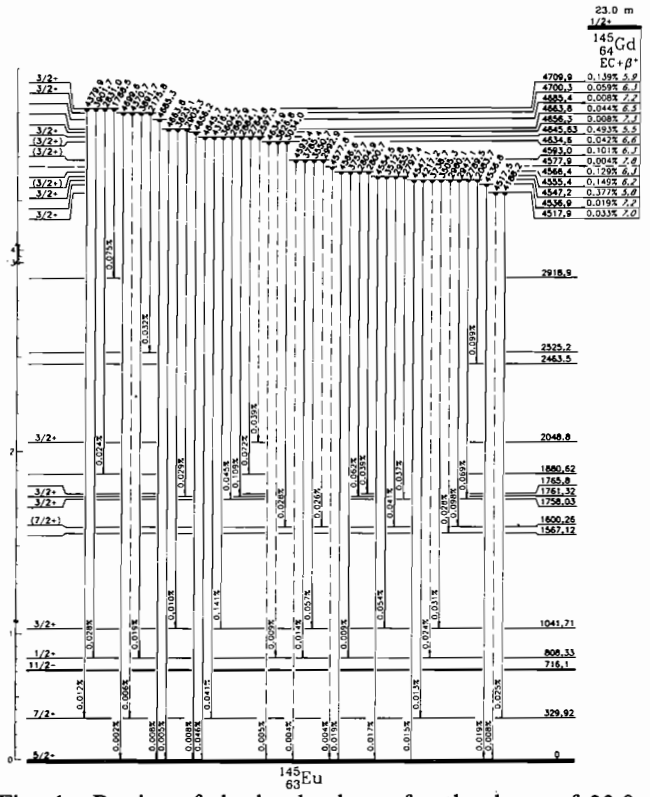

Fig. 1. Portion of the level scheme for the decay of 23.0-min ^{145}Gd to levels of high excitation in ^{145}Eu. (XBL 813-8490)

Footnotes and References

*Condensed from LBL-12424, Physical Review C **25**, (1982).

†National Superconducting Cyclotron Laboratory and Departments of Chemistry and Physics, Michigan State University, East Lansing, MI 48824

1. R.B. Firestone, R.A. Warner, Wm.C. McHarris, and W.H. Kelly, Phys. Rev. Lett. **33**, 30 (1974); **35**, 713 (1975).

2. J.C. Hardy, L.C. Carraz, B. Jonson, and P.G. Hansen, Phys. Lett. B **71**, 307 (1977).

Observation of Large Resonances in the β-Decay of $^{145}_{64}Gd_{81}$*

R.B. Firestone

The $\epsilon/\beta+$ decay of ^{145}Gd has been studied in detail and is further discussed in another report. This decay proceeds to a region of high level density in ^{145}Eu. It has been suggested that such decay should exhibit no pronounced structure and would be impossible to investigate completely.[1] That prediction was not borne out by these experiments as is indicated by the β-decay strength distribution, S_β = β-intensity/ft, which is plotted in Fig. 1. Three resonances at 1.8, 2.6, and 4.5 MeV were observed.

^{145}Gd decay is remarkable because the valence protons outside the Z = 50 closed shell occupy $\pi d_{5/2}$ and $\pi g_{7/2}$ shell model orbitals while only a $\nu s_{1/2}$ hole in the neutron core can be populated by decay. Thus no strong low-lying single particle transitions are expected or observed. The resonances at 1.8 and 2.6 MeV can be interpreted as the decay from $(\pi d_{5/2})^2$ pairs to collective $\pi d_{5/2} \times (2_1^+ + 2_2^+)$ configurations. This is confirmed by energy systematics, decay rates, and γ-ray deexcitation patterns when compared with decay of ^{144}Eu to the ^{144}Sm core (Fig. 2).

The strong resonance at 4.5 MeV probably corresponds to decay across the N = 82 shell energy gap.

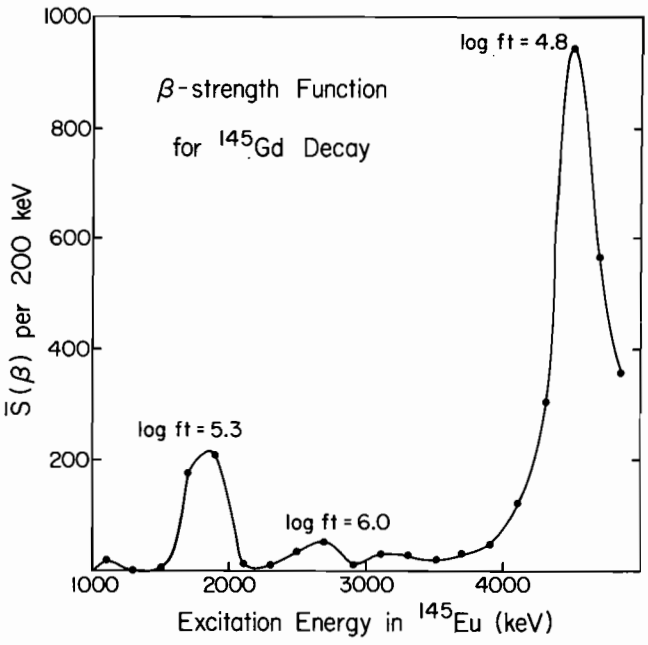

Fig. 1. The β-strength function $\bar{S}(\beta)$ (per 200 keV) plotted as a function of excitation energy in ^{145}Eu. Here we define $\bar{S}(\beta)$=b(E)/ft where b(E) is the intensity fraction per 200-keV interval of excitation and ft is the standard β decay rate to that energy domain of the daughter. Broad resonances at 1.8, 2.6, and 4.5 MeV are observed, and the effective logft's to these resonances are shown. (XBL 803-8699)

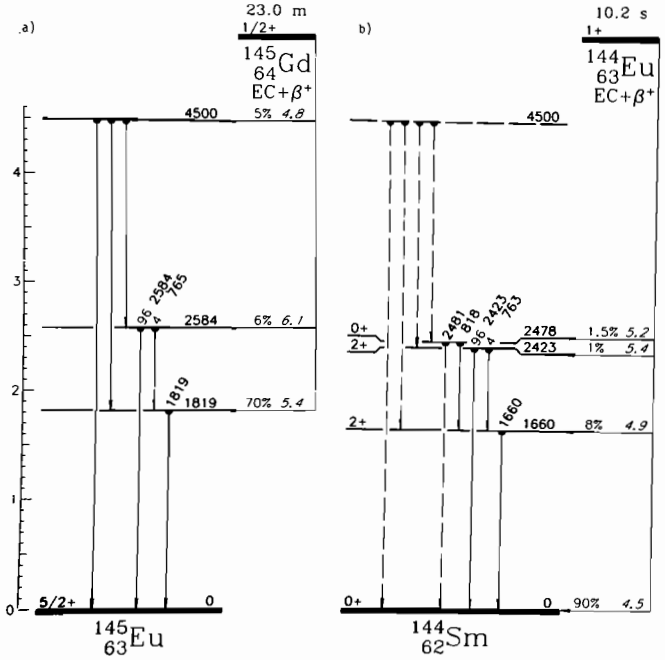

Fig. 2. Simplified decay scheme for ^{145}Gd (a) is compared with the decay of the ^{144}Eu core. Note the close agreement between the energy separation and decay intensity pattern of the 2^+ ^{144}Sm core levels and the $(\pi d_{5/2} \times 2^+)$ levels in ^{145}Eu. Although the logft's do not compare so well, additional unobserved decay to high energy states in ^{144}Sm can improve that comparison substantially. (XBL 813-8485A)

Calculations of $\nu f_{7/2}$, $\nu i_{13/2}$, and $\nu h_{9/2}$ orbitals lie at 3.9, 4.9, and 5.3 MeV, respectively. Assuming significant $(\pi h_{11/2})^2$ pair occupancy, the decay to $(\pi h_{11/2} \times \nu h_{9/2} \times \nu S_{1/2}$ 3-quasiparticle states should be very fast. The $\pi h_{11/2} \rightarrow \nu h_{9/2}$ β-decay from ^{147}Tb has been observed to proceed with a low logft. Admixtures of other orbitals with the $\pi h_{9/2}$ orbital will scatter some of its strength to lower energies and a loss of spherical symmetry will further depress that state providing reasonable agreement with the energy of the observed resonance. Indeed the increased β-strength begins at 3.9 MeV, exactly where the shell gap is predicted.

Further studies are planned to investigate the decay to higher Z, N = 82 nuclei. For ^{147}Tb, the proton becomes unbound at about 1.9 MeV so the higher energy part of the highest resonance might be observed to proton decay. Heavier nuclei should predominantly decay through this high-energy channel and can be characterized by the dominant β-delayed proton decay mode.

Footnotes and References

*See LBL-12424 and the *Proceedings of the International Conference on Nuclear Physics,* August 24-30, 1980, Berkeley, CA, p. 201.

1. J.C. Hardy, L.C. Carroz, B. Jonson, and P.G. Hansen, Phys. Lett. B **71**, 307 (1977).

Determination of the Half-Life and Absolute Gamma Intensities of ^{151}Gd

K.E. Gregorich, K.J. Moody, and G.T. Seaborg

A ^{151}Gd source was produced at the 88-Inch Cyclotron by the

$$^{133}\text{Cs}\ (^{22}\text{Ne},4\text{n})^{151}\text{Tb} \xrightarrow[17.6\text{h}]{\text{EC}} {}^{151}\text{Gd}$$

reaction at a bombarding energy of 94 MeV. The half-life of the electron capture decay of ^{151}Gd has been determined to be 129.1 ± 1.2 days, which is more accurate than the previously best known value of 120 ± 20 days.[1] The absolute intensities of the gamma rays accompanying this decay were also determined for the first time.

A target consisting of 600 μg/cm^2 layer of CsCl on a 0.10 mm thick gold backing was irradiated with 500 electrical nanoamperes of $^{22}Ne^{+4}$ for 8.5 hours. ^{151}Tb is formed in the reaction with a cross section of roughly 400 mb. Terbium was chemically separated from the target as follows: The target was dissolved in 3 ml aqua regia and the gold was extracted into diethyl ether three times. Residual gold was removed from the aqueous portion by heating it to dryness and passing through a 2 mm × 5 cm anion column filled with Dowex 1 × 8 anion resin in 2 *M* HCl. The eluant was taken to dryness and the activity was picked up in 1 drop of 0.1 *M* HNO_3. A terbium fraction, free from gadolinium was obtained by loading this on a 2 mm × 4 cm exchange column filled with Aminex Q 150-S cation resin which had been prepared with 1 *M* NH_4Cl. The terbium fraction was isolated by eluting at room temperature with 0.5 *M* α-hydroxyisobutyric acid, which had been adjusted to a pH of 3.30 with NH_4OH. The lack of any lines in the gamma-ray spectra due to a ^{153}Gd tracer indicate an upper limit on the Gd contamination in the Tb fraction to be .01%. Other nuclides present in the ^{151}Tb fraction were $^{149, 150, 152}$Tb, ^{160}Tb tracer and small amounts of some first row transition metals with +3 oxidation states.

The decay of the ^{151}Tb and the growth and decay of the ^{151}Gd daughter were measured with a 60 cm^3 Ge(Li) detector with a 4096 channel analyzer. After collecting spectra over a period of 180 days, the data were fed into the SAMPO code[2] which locates the peaks and gives them a Gaussian fit with exponential tails. SAMPO also assigns a time to each spectrum and corrects for detector efficiency. The resultant decay curves for the ^{151}Tb lines were given weighted least squares single component fits; the results are shown in Table 1, giving a half-life 17.609 ± 0.014 hours. This is an improvement on the previous best value of 17.6 ± 0.1 hours.[3] These fits, along with the known branching ratios for ^{151}Tb gamma lines, gave the ^{151}Tb decay rate at the time of chemical separation from Gd to be 6.24 ± 0.29 × 10^6 DPM.

Table 1. Half-lives of ^{151}Tb and ^{151}Gd.

E_γ(keV)	t (h)	E_γ(keV)	t (d)
108	17.599 ± 0.026	154	129.39 ± 1.99
180	17.589 ± 0.030	175	127.91 ± 2.01
252	17.600 ± 0.034	243	130.56 ± 2.45
287	17.644 ± 0.034		
444	17.639 ± 0.042		
Combined:	17.609 ± 0.014	Combined:	129.1 ± 1.2

The SAMPO results for the ^{151}Gd lines were given a weighted least squares fit for a 17.609-hour growth and subsequent decay. The half-life of the ^{151}Gd, as determined from the three most intense lines at 154, 175, and 243 keV, is 129.3 ± 1.2 days (see Table 1). These growth and decay fits for the ^{151}Gd lines also gave activities at the time of chemical separation of the Tb fraction of the "parents" of the ^{151}Gd lines. The parent activity corresponds to the activity a ^{151}Tb line would have if it had the same absolute intensity as the ^{151}Gd line in question. Since the absolute intensities of the real ^{151}Tb lines are known, the absolute intensities of the ^{151}Gd lines could now be calculated. The results are presented in Table 2.

Table 2. Relative and absolute intensities of the gamma-rays from the decay of ^{151}Gd.

E_γ	Relative intensities (Ref. 4)	Relative intensities (this work)	Absolute intensities (%)
21.5	46.2(19)		2.78(20)
106.5	1.29(6)	1.45(4)	0.087(6)
110.5	0.12(1)		0.0072(21)
153.6	100.0(30)	100.0(21)	6.01(35)
174.6	48.3(15)	49.6(29)	2.98(17)
196.5	0.48(2)		0.0288(22)
222.2	0.009(3)		0.00054(18)
239.0	2.31(11)		0.139(11)
243.2	89.9(27)	91.7(29)	5.51(33)
260.4	0.84(3)		0.0565(38)
286.0	1.35(4)	1.51(5)	0.091(6)
307.4	16.5(5)	16.7(4)	1.00(6)
328.3	1.32(5)	1.48(4)	0.088(6)
332.1	0.17(2)		0.0103(14)
353.5	2.04(6)	2.29(7)	0.138(9)
394.8	0.06(3)		0.0036(18)
416.3	0.012(3)		0.00072(18)

References

1. N.M. Anton'eva et al., Bull. Acad. Sci. USSR **22**, 135 (1958).
2. J.J. Routti, and S.G. Prussin, Nucl. Instr. Methods **72**, 125 (1960).
3. Y.Y. Chu, E.M. Franz, G. Friedlander, Phys. Rev. C **1**, 1826 (1970).
4. J.W. Ford, A.V. Ramayya, Nucl. Phys. A **146**, 397 (1970).

The Decay of the ^{155}Tb Compound Nucleus, Formed in the Reaction of ^{22}Ne with ^{133}Cs

*K.J. Moody and J.J. Hogan**

The cross sections for several evaporation products from the decay of the rotational compound nucleus ^{155}Tb have been determined as a function of projectile energy in the reaction of ^{22}Ne with ^{133}Cs. The purpose of our study is to examine the dependence of the decay of the compound nucleus on the amount of angular momentum brought in by the heavy ion. This particular reaction offers two interesting sets of evaporation products: The ^{133}Cs(^{22}Ne,xn) $^{155-x}$Tb products (for x = 3, 5, 6, 7, and 8) consist of two well-characterized isomeric states, each with known gamma abundances and long enough half-lives to make each pair useful in radiochemical studies. The ^{133}Cs (^{22}Ne,αxn) $^{151-x}$Eu products (for x = 3, 4, 5, and 6) have been studied with similar techniques in (compound nucleus, xn) studies by Hogan[1] and by Lee and Markowitz.[2]

The ^{22}Ne beams used in this study were produced at the 88-Inch Cyclotron. Intensities of as much as two electrical microamperes were delivered to our targets at six energies from 94 to 146 MeV. The targets consisted of 600 μg/cm^2 layers of CsCl vacuum-sublimated onto thick target backings. The low melting point of CsCl required that the target backings be directly cooled by water. Two irradiations were performed at each energy. In the first bombardments, targets mounted on gold were irradiated for five to ten minutes and then rapidly transported to the counting facilities in Building 70, where they were placed whole in front of a 60 cm^3 Ge(Li) detector. The time from the end of the irradiation to the beginning of the first counting interval varied between three to five minutes, enabling us to see the gamma rays from the decay of the high-spin Tb isomers with half-lives as short as 100 seconds (^{147}Tb). The second bombardments were performed with targets on nickel backings. After irradiations from two to four hours in length, the targets were dissolved in HNO_3, a rare-earth tracer was added, then LaF_3 was precipitated, which carried the activities of interest. This precipitate was filtered out on nitrocellulose paper, washed with HCl/HF and water, then was mounted for counting for the gamma-rays arising from the decay of the low-spin Tb isomers and the Eu isotopes. Cross sections were obtained from decay curve analysis and have been corrected for feeding during the bombardments.

The experimental results are shown in Figs. 1 and 2, along with a fit to the data generated by the computer code ALERT.[3] The evaporation of charged particles is strongly affected by changes in the nuclear temperature, and the best fit to the (^{22}Ne, αxn) data shown was obtained with a level density parameter of A/12. Two things are immedi-

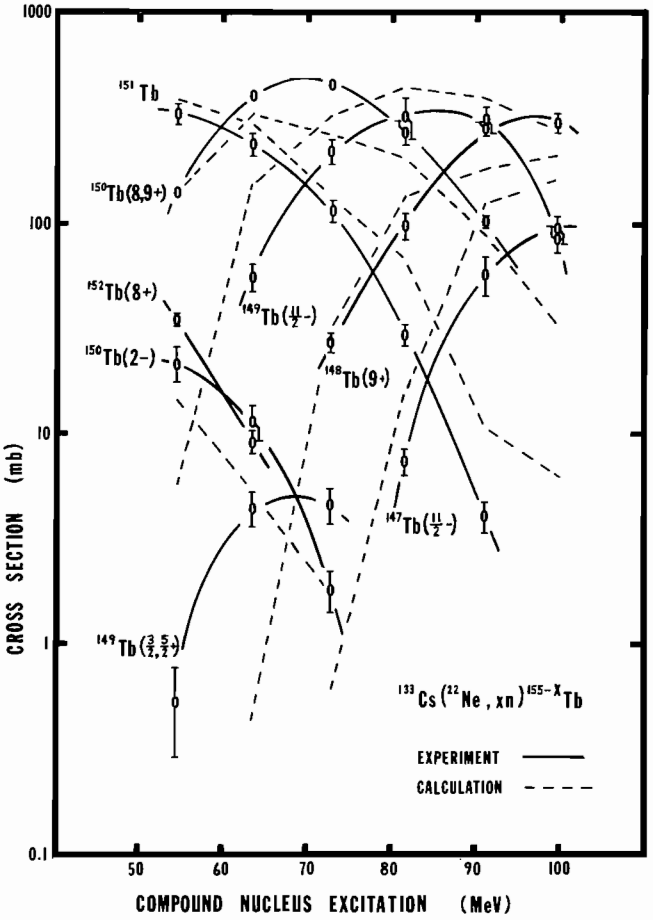

Fig. 1. Cross section distributions as a function of compound nucleus excitation energy for the $^{133}Cs(^{22}Ne,xn)^{155-x}Tb$ reaction (x = 3, 4, 5, 6, 7, and 8).

(XBL 818-11355)

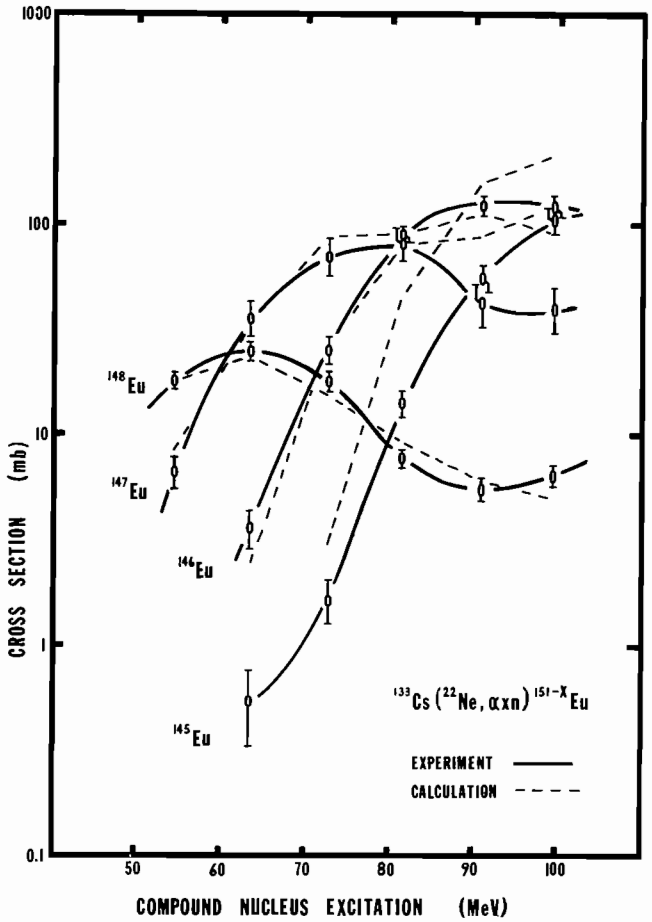

Fig. 2. Cross section distributions as a function of compound nucleus excitation energy for the $^{133}Cs(^{22}Ne,\alpha xn)^{151-x}Eu$ reaction (x = 3, 4, 5, and 6).

(XBL 818-11354)

ately striking in the data: The low-spin isomers of the Tb isotopes are populated only very weakly and the cross sections of the ($^{22}Ne,\alpha xn$) products show structure at the highest energies. The preferential population of the high-spin states in the terbiums comes about because the root-mean-square values of angular momentum in the compound nucleus vary from 28$\hbar$ to 56$\hbar$ to over the energy range studied, and the resultant yrast cascade would largely end up in the high-spin isomers. The structure in the ($^{22}Ne,\alpha xn$) product cross sections is probably due to the contribution of the evaporation of 2 protons and x + 2 neutrons.

The authors would like to acknowledge B.V. Jacak for her help with the irradiations, Dr. H. Groening for his assistance with the modeling, Dr. M. Blann for the use of his computer code and for many helpful discussions, and Dr. G.T. Seaborg for his interest and support.

Footnotes and References

*Permanent Address: Department of Chemistry, McGill University, Montreal Quebec, Canada.

1. J.J. Hogan, LBL-9711 (1980), p. 74.
2. D.M. Lee and S.S. Markowitz, LBL-2366 (1974), p. 34.
3. M. Blann, Phys. Rev. C **21**, 1770 (1980).

Alpha Decay of Neutron Deficient Polonium and Bismuth Isotopes

M. Leino, S. Yashita, and A. Ghiorso

We have been using SASSY, our gas-filled on-line mass separator, to study neutron-deficient alpha-emitting isotopes in the Pb-Ac region made in fusion reactions by heavy-ion bombardment. A number of known nuclides have been identified and a new isotope, ^{192}Po, and an isomeric state in ^{191}Bi have been found.

In SASSY, the separation of fusion products from the bombarding heavy-ion beam is achieved by a 1-torr helium-filled magnetic system consisting of a dipole followed by a quadrupole. Downstream from the quadrupole are two pentane-filled parallel-plate position-sensitive avalanche counters that provide information on the trajectories and energy losses of recoil nuclei as well as a determination of their time-of-flight between the two counters. The recoils are implanted into an array of ten 13 × 22 mm Si surface-barrier detectors to give an indication of their kinetic energy and an accurate measure of any subsequent alpha decay. An approximate mass can be determined from the recoil velocity and energy measurements but the calculation is severely limited in accuracy by the energy determination. Nuclide identification is thus determined by alpha-alpha genetic relationships where possible, by cross bombardments, and by excitation functions. Short half-lives are determined by measuring the time between arrival of an implanted recoil and subsequent alpha particle delay.

We have produced polonium isotopes in the reactions ^{nat}Ce(^{56}Fe,xn)Po and ^{141}Pr(^{56}Fe,pxn)$^{196-x}$Po, and bismuth isotopes in the reactions ^{nat}Ce(^{56}Fe,pxn)Bi and ^{141}Pr(^{56}Fe,αxn)$^{193-x}$Bi. The excitation functions for $^{192-196}$Po and $^{191-193}$Bi, including their isomers, and the half-life of ^{192}Po were determined using the ^{56}Fe + ^{nat}Ce reaction. The results of the alpha particle measurements are shown in Table 1.

In Fig. 1 we show an alpha spectrum measured in one of the detectors in the bombardment of ^{nat}Ce with 254-MeV ^{56}Fe particles. Excitation functions shown in Fig. 2 were used to make nuclide assignments. The new alpha particle activity at 7.17 MeV was found to have a half-life of 34 ± 3 ms, in good agreement with the value of 30 ms calculated from the formula of Taagepera and Nurmia.[1] Our value for the ^{192}Po alpha energy, 7.17 ± 0.02 MeV, is compatible with the systematics of Liran and Zeldes.

The bombarding energies used in these experiments were not high enough to allow the determination of the excitation functions for the 6.32-MeV, 6.63-MeV, and 6.86-MeV activities that have been assigned to ^{191}Bi in previous investigations.[2] However, the threshold energies to produce all three activities were found to be similar and the relative yields were within a factor of two from those reported in Ref. 1, so we conclude that these activities probably all belong to Bi with mass number 191. On the

Table 1. Results of alpha decay measurements

Isotope	Present Work		Ref. 2, Ref. 3	
	E_α (MeV)	$T_{1/2}$ (ms)	E_α (MeV)	$T_{1/2}$ (ms)
^{194}Po	6.84[a]	410 ± 30	6.84[b]	700 ± 100[b]
^{193}Po	6.94 ± 0.02	360 ± 50	6.94[b]	450 ± 150[b]
^{193m}Po	7.00 ± 0.02	260 ± 20	6.995[b]	420 ± 100[b]
^{192}Po	7.17 ± 0.02	34 ± 3	7.12[b]	...
^{191m}Bi	6.86 ± 0.02	150 ± 15	6.86 ± 0.02[c]	20000 ± 15000[c]

[a]Value used for internal calibration.

[b]Ref. 3.

[c]Ref. 2.

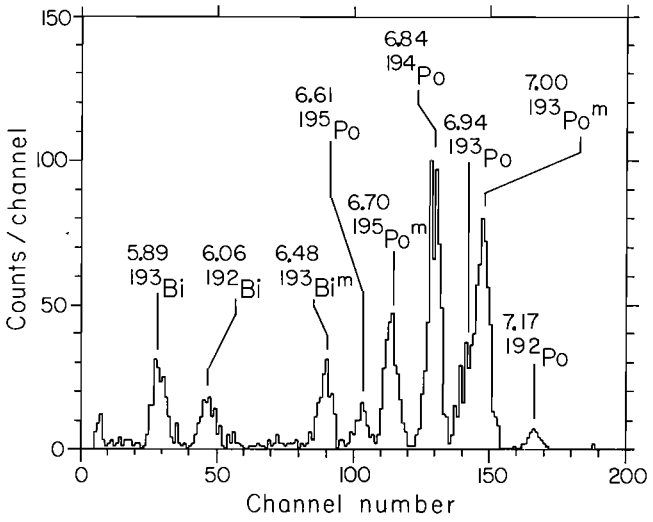

Fig. 1. Alpha particle energy spectrum of the nuclides produced in the reaction $^{56}Fe + {}^{nat}Ce$ (E_{Lab} = 254 MeV). (XBL 812-186Y)

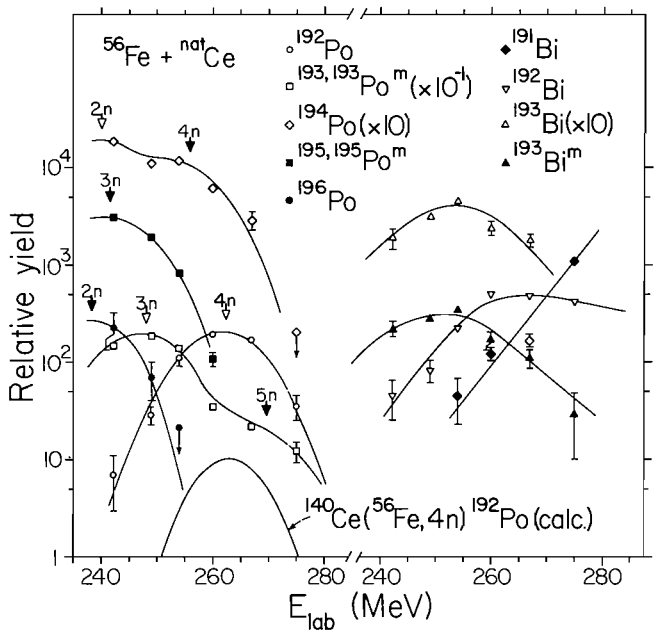

Fig. 2. Relative yields of Po and Bi isotopes produced in the reaction $^{56}Fe + {}^{nat}Ce$. The open and solid arrows show the calculated locations of the xn curves for $^{56}Fe + {}^{140}Ce$ (89%) and $^{56}Fe + {}^{142}Ce$ (11%) respectively. The calculated excitation function is not to scale.

(XBL 812-188Y)

other hand, our half-life of 150 ± 15 ms for the 6.86-MeV activity differs greatly from the value 20 ± 15 s reported in Ref. 2. Our upper limit for the intensity of the component in the 6.86-MeV peak with $T_{1/2} > 5$ s is approximately 50% of the intensity of the 6.63-MeV peak. In Ref. 2, the relative intensities of the 6.63-MeV and 6.86-MeV peaks were reported to be 30% and 70% respectively. In this work, the relative intensities were 25% and 75%. We were unable to determine the half-life of the 6.63-MeV activity accurately in this experiment, but it is on the order of seconds.

References

1. R. Taagepera and M. Nurmia, Ann. Acad. Sci. Finn. A VI No. 78 (1961).
2. Y. LeBeyec, M. Lefort, J. Livet, N.T. Porile, and A. Siivola, Phys. Rev. C **9**, 1091 (1974).
3. S. Della Negra, B. Lagarde, and Y. LeBeyec, J. Phys. **38**, L-393 (1977).

Search For Electron Capture-Delayed Fission in the N = 126 System $^{216}_{91}Pa \xrightarrow{EC} {}^{216}_{90}Th$

L.P. Somerville and M.J. Nurmia

Several neutron-deficient isotopes have been discovered with half-lives in the minute range and which give rise to spontaneous fission (SF). The hypothesis of electron capture-delayed fission has been suggested as the means of decay for these nuclides. According to this hypothesis, a nucleus, e.g., $^{234}_{95}Am$ (2.6 min), decays by electron capture to a series of levels in the daughter nucleus $^{234}_{94}Pu$, which are near the top of the fission barrier. Fission can then take place readily from these levels.

The system $^{216}_{91}Pa \xrightarrow{EC} {}^{216}_{90}Th$ appeared to be an attractive candidate for the lightest known spontaneously fissioning nucleus. Due to the 126 neutron shell in $^{216}_{90}Th$, the Q-value for electron capture was expected to be quite high, approximately 7.6 MeV.[1] A high Q-value would allow levels near the top of the fission barrier to be readily populated in some fraction of the electron capture decays, as long as the height of the fission barrier for $^{216}_{90}Th$ is less than 7.6 MeV. The half-life for $^{216}_{91}Pa$ was known to be $170\ ^{+100}_{-30}$ ms based on alpha particle decay measurements by Schmidt et al.[2] The electron capture branch for $^{216}_{91}Pa$, however, was unknown.

We searched for SF events from $^{216}_{91}Pa$ in the following reactions (Table 1). Cross-section upper limits for SF decay and upper limits for SF relative to the calculated

Table 1.

Reaction	Upper limit for SF (nb)	$\sigma^{SF}/\sigma^{calc.}$ (JORPLE)
129−137−MeV $^{24}_{12}$Mg + $^{197}_{74}$Au	≤ 0.4	$\leq 10^{-6}$
140−146−MeV	≤ 0.6	$\leq 8 \times 10^{-5}$
$\leq$ 185−MeV $^{37}_{17}$Cl + $^{183}_{74}$W	≤ 13	$\leq 5 \times 10^{-4}$
$^{182}_{74}$W	≤ 7	≤ 0.03
$^{184}_{74}$W	≤ 6	$\leq 3 \times 10^{-5}$

production cross sections using the JORPLE code are quoted. The cross sections calculated by the JORPLE code are likely to be overestimated, however.

The fission barrier for $^{216}_{90}$Th is calculated by W.D. Myers to be $\sim$ 10.5 MeV using the droplet model.[1] Since his calculation does not include shell corrections to the saddle mass, the true fission barrier might be even higher and is likely to exceed the Q-value for electron capture of ^{216}Pa (7.6 MeV). Thus, even if ^{216}Pa has a sizeable electron capture branch to excited levels in $^{216}_{90}$Th, these levels are not likely to decay by fission since they would be at least $\sim$ 2.9 MeV below the estimated fission barrier and, consequently, have a fission probability of $\sim 10^{-8}$. Although sub-barrier fission following electron capture has been suggested by Yu. Ts. Oganessian[3] for $^{230}_{95}\mathrm{Am} \xrightarrow{EC} {}^{230}_{94}\mathrm{Pu} \xrightarrow{SF}$, the high estimated fission barrier is a possible explanation for the lack of SF events from $^{216}_{91}$Pa in our experiments.

References

1. W.D. Myers, Droplet Model of Atomic Nuclei, Plenum Publishing Co. (1977).
2. K.H. Schmidt et al., Nucl. Phys. A **318**, 253 (1979).
3. Yu. Ts. Oganessian, Symposium on Classical and Quantum Mechanical Aspects of Heavy Ion Collisions, Heidelberg, p.122, Aug. 1974. Proceedings published by Springer Verlag (1975).

Attempts to Identify the 1.5-Second Spontaneous Fission Activity Observed in the Reaction $^{18}_{8}O + ^{248}_{96}Cm$

A. Ghiorso, L.P. Somerville, R.M. McFarland, R. Lougheed, and E.K. Hulet

In two previous annual reports[1,2] a 1.5-second spontaneous fission (SF) activity was reported as a product of the reaction 95 MeV $^{18}_{8}O + ^{248}_{96}Cm$ and found to have a half-life, total kinetic energy of fission, and fission mass distribution very close to some properties reported for $^{259}_{100}$Fm in the reaction 16 MeV t + $^{257}_{100}$Fm.[3] The cross section for production of the 1.5-s SF activity was measured to be 16 nb in the reaction 95-MeV $^{18}_{8}O + ^{248}_{96}Cm$. The excitation function was found to be quite broad, as expected for a noncompound nucleus product.

If our 1.5-s SF activity is indeed $^{259}_{100}$Fm, it would be produced in an exotic $^{11}_{4}$Be transfer reaction. Previous attempts to observe a $^{11}_{4}$Be transfer under more favorable conditions using ^{18}O ions bombarding targets with lower atomic number have yielded surprisingly low cross sections of $\sim$ 10 nb in the reaction 110 MeV $^{18}_{8}O + ^{208}_{82}Pb$ (Ref. 4) and $\leq 16 \pm 10$ nb in the reaction 124 MeV $^{18}_{8}O + ^{232}_{90}Th$.[5] We considered the possibility that the $^{11}_{4}$Be transfer products might be produced with excitation energies below the fission barrier, which might explain why the cross sections using targets of lower atomic number than $^{248}_{96}$Cm are not higher.

Recently we bombarded a ^{245}Cm target[6] with ^{18}O ions at 93 MeV and 99 MeV in search of the $^{11}_{4}$Be transfer

product $^{256}_{100}$Fm. The energy of 93 MeV was chosen to give the same excitation energy as in the system 95 MeV $^{18}_{8}$O + $^{248}_{96}$Cm, in which a cross section of 16 nb was measured for 1.5-s SF activity. Ten solid state detectors recorded alpha particles and SF events from a series of ten 100 $\mu g/cm^2$ aluminum catcher foils placed over the detectors after the end of the bombardment. Only upper limits of 2 nb at 93 MeV and 2 nb at 99 MeV could be established for the $^{11}_{4}$Be transfer product $^{256}_{100}$Fm in the reaction $^{18}_{8}$O + $^{245}_{96}$Cm. Table 1 shows, however, that copious quantities of other alpha particle-emitting nuclides were produced with cross sections comparable to the analogous products in the reaction $^{18}_{8}$O + $^{248}_{96}$Cm.

One possible conclusion is that the 1.5-s SF activity produced in the reaction 95 MeV $^{18}_{8}$O + $^{248}_{96}$Cm is probably *not* $^{259}_{100}$Fm. Also, either the 1.5-s SF activity is another twin nucleus to $^{259}_{100}$Fm with respect to half-life, total kinetic energy of fission, and fission mass distribution, or it is the same nucleus produced in the original reaction t + $^{257}_{00}$Fm, but different from $^{259}_{100}$Fm.

References

1. Nuclear Science Division Annual Report, 1978-79, LBL-9711 (1980), p.63.
2. Nuclear Science Divison Annual Report, 1979-80, LBL-11588 (1981), p. 85.
3. E.K. Hulet et al., Phys. Rev. C **21**, 966 (1980).
4. A. Ghiorso et al., 1979-1980 Nuclear Science Annual Report, LBL-11588, p.85.
5. R.M. McFarland et al., Second Chemical Congress of the North American Continent, Aug. 24-29, 1980, Las Vegas, Nevada.
6. The $^{245}_{96}$Cm Material was obtained by milking from ^{249}Cf that had been grown from the ultrapure $^{249}_{97}$Bk.
7. D. Lee et al., private communication (1980).

Table 1.

Pickup Particle	93 MeV $^{18}_{8}$O + $^{245}_{96}$Cm		97 MeV $^{18}_{8}$O + $^{248}_{96}$Cm[4]	
	nuclide	$\sigma(\mu b)$	$\sigma(\mu b)$	nuclide
+2p −2n	$^{245}_{98}$Cf	--	45	$^{248}_{98}$Cf
+2p −n	$^{246}_{98}$Cf	50	280	$^{249}_{98}$Cf
2p	$^{247}_{98}$Cf	--	850	$^{250}_{98}$Cf
^{3}He	$^{248}_{98}$Cf	3000	980	$^{251}_{98}$Cf
α	$^{249}_{98}$Cf	--	280	$^{252}_{98}$Cf
		σ(nb)	σ(nb)	
$^{6}_{4}$Be	$^{251}_{100}$Fm	--	2800	$^{254}_{100}$Fm
$^{7}_{4}$Be	$^{252}_{100}$Fm	1800	700	$^{255}_{100}$Fm
$^{8}_{4}$Be	$^{253}_{100}$Fm	800	300	$^{256}_{100}$Fm
$^{11}_{4}$Be	$^{256}_{100}$Fm	≤ 2	16? (95 MeV)	$^{259}_{100}$Fm

Spontaneous Fission of Rutherfordium Isotopes

L.P. Somerville, J.M. Nitschke, M.J. Nurmia, and A. Ghiorso

In previous issues of this annual report[1,2] Spontaneous Fission (SF) activities with half-lives of 21 ms, 53 ms, 1.4 s, and 4.8 s were reported in the reactions $^{16}_{8}O$ + $^{248}_{96}Cm$, $^{18}_{8}O$ + $^{248}_{96}Cm$, $^{15}_{7}N$ + $^{249}_{97}Bk$, and $^{13}_{6}C$ + $^{249}_{97}Bk$ using the recoil tape transport system. Our goal is to identify these new SF activities and, thus, gain an understanding of the SF half-life systematics for the heaviest known elements.

A possible assignment for the 21-ms SF activity is $^{260}_{104}Rf$. Half-lives determined by the maximum likelihood method and production cross sections have now been measured in the following reactions. (The errors indicated are statistical only; no estimate of possible systematic errors has been made.)

Absence of the 21-ms SF activity in the reactions $^{16}_{8}O$ + $^{244}_{94}Pu$, $^{18}_{8}O$ + $^{244}_{94}Pu$, and $^{15}_{7}N$ + $^{248}_{96}Cm$ suggests that it is probably an isotope of rutherfordium with A > 259. A 9-nb production cross section for a possible 19.3-ms $^{260}_{104}Rf$ in the reaction $^{249}_{98}Cf$($^{18}_{8}O$, α3n) $^{260}_{104}Rf$ is consistent with known cross sections of ~ 20 nb for the reaction $^{248}_{96}Cm$($^{18}_{8}O$, α3n) $^{259}_{102}No$,[3] considering the effect of fission competition, and ~ 0.5 nb for the reaction $^{249}_{98}Cf$($^{18}_{8}O$, α4n) $^{259}_{104}Rf$,[4] considering that the maximum $^{248}_{96}Cm$($^{16}_{8}O$, α3n) cross section is larger than the maximum of the $^{248}_{96}Cm$($^{16}_{8}O$, α4n) cross section.[5] In the reaction 109-MeV $^{18}_{8}O$ + $^{248}_{96}Cm$, a half-life slightly shorter than the others listed in Table 1 and a cross section of ~ 9 nb, ~ 50 times the calculated cross section to produce $^{260}_{104}Rf$, present the only possible inconsistencies for the assignment of $^{260}_{104}Rf$. The large cross section, shorter half-life, and broad excitation function for the SF activity produced in the reaction 109-MeV $^{18}_{8}O$ + $^{248}_{96}Cm$ suggest that this is a different SF activity from the one produced in the other reactions listed in Table 1. However, we cannot experimentally rule out the remote possibility that the (^{18}O,6n) reaction cross section is enhanced by some as yet unknown mechanism and that the half-life is truly 20-21 ms.

The 53-ms SF activity produced in the reactions 89- to 95-MeV $^{18}_{8}O$ + $^{248}_{96}Cm$ could be assigned to $^{262}_{104}Rf$, a deduction based on a narrow excitation function similar to the calculated one and data from other cross bombardments. In a preliminary study of the reaction 112.7-MeV $^{22}_{10}Ne$ + $^{244}_{94}Pu$ 77 SF events were observed with a half-life of 50 ± 16 ms and a production cross section of ~ 1 nb. This is close to the 1.5 nb calculated to produce $^{262}_{104}Rf$, which would be consistent with our previous assignment for this activity.

Assignments of $^{260}_{104}Rf$ to the 20- to 21-ms and $^{262}_{104}Rf$ to the 52-ms SF activities would confirm the theoretical predictions of Randrup et al.[6] which suggest a change in SF half-life systematics at Z = 104, as shown in Fig. 1, due to the disappearance of the second hump in a double-humped fission barrier.

In the reaction 93-MeV $^{18}_{8}O$ + $^{245}_{96}Cm$, a search for the 7% branching in $^{259}_{104}Rf$ ($T_{1/2}$=3 s), previously observed by Druin et al. and Bemis et al., yielded SF events with a half-life of 3.4 ± 1.7 s corresponding to 8 ± 3% of the

Table 1.

Reaction	Half-life	Cross Sections	
		Experimental	Calculated for $^{260}_{104}Rf$
80-MeV $^{15}_{7}N$ + $^{249}_{97}Bk \rightarrow$ $^{264}_{104}Rf^*$	19.8 ± 1.2 ms	14 nb	10 nb
92-MeV $^{16}_{8}O$ + $^{248}_{96}Cm \rightarrow$ $^{264}_{104}Rf^*$	21.0 ± 1.1 ms	6 nb	4.4 nb
109-MeV $^{18}_{8}O$ + $^{248}_{96}Cm \rightarrow$ $^{266}_{104}Rf^*$	17.1 ± 2.2 ms	9 nb	0.2 nb
96-MeV $^{18}_{8}O$ + $^{249}_{98}Cf \rightarrow$ $^{267}106^*$	19.3 ± 1.4 ms	9 nb	--

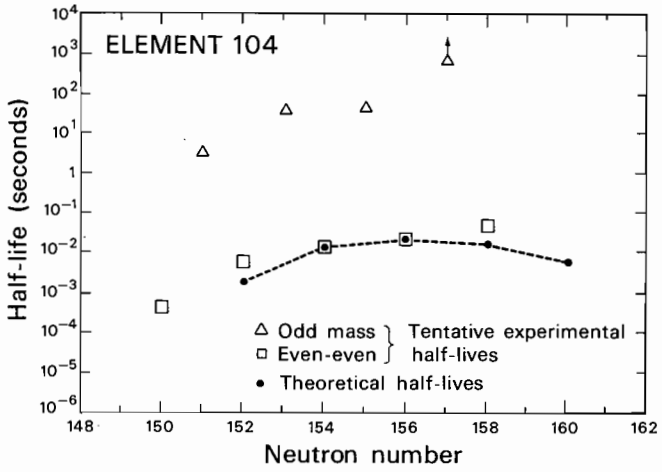

Fig. 1. Dotted lines connecting small solid circle points show the theoretically predicted partial half-lives of element 104 nuclei.[6] The experimental values correspond to Δ for odd isotopes and □ for even isotopes. None of these are known with certainty. (XBL 821-60)

3.8-nb calculated total cross section for $^{259}_{104}$Rf. SF branching ratios of possibly 7% in $^{259}_{104}$Rf (3 s) and 45 ± 20% in $^{255}_{104}$Rf (1.4 s) suggest that $^{257}_{104}$Rf (4.8 s) might also have a measurable SF branch and that the odd isotopes of element 104 may have lower hindrance factors than odd isotopes of lighter elements. This effect can also be understood in terms of a disappearance of the second barrier at element 104.[6]

References

1. Nuclear Science Division Annual Report, 1978-79, LBL-9711 (1980), p.63.
2. Nuclear Science Division Annual Report, 1979-80, LBL-11588 (1981), p.85.
3. R. Silva et al., Nucl. Phys. A **216**, 97 (1973).
4. A. Ghiorso et al., Phys. Rev. Lett. **33**, 1490 (1974).
5. A. Ghiorso, Proceedings of the Robert A. Welch Foundation Conf. on Chemical Research XIV; Houston Texas; p. 107, W.O. Milligan, editor (1970).
6. J. Randrup et al., Phys. Rev. C **13**, 299 (1976); Nucl. Phys. A **217**, 221 (1973).

Production of Heavy Actinides from Interactions of ^{20}Ne and ^{22}Ne with ^{248}Cm

D. Lee, H.V. Gunten, M. Nurmia, Y.-F. Liu,† G.T. Seaborg and D.C. Hoffman‡*

Systematic studies of the transfer of many nucleons from heavy projectiles to heavy actinide targets are continuing. Measurements for the production of heavy actinides in bombardments of ^{248}Cm with ^{20}Ne and ^{22}Ne ions at energies near the Coulomb barrier have now been completed (See Fig. 1). The experimental procedures and results for ^{16}O and ^{18}O were reported in the previous annual report.[1]

Comparisons of the maximum yields for each element are given in Table 1. In general, the maximum yield for a given element occurs about two mass units heavier for ^{18}O and ^{22}Ne than for ^{16}O and ^{20}Ne respectively, reflecting the neutron excess of the projectile.

The dependence of the yields on the energy of the projectiles is now being investigated and irradiations with ^{18}O energies on targets of 97, 103, 111, and 120 MeV have been performed. Preliminary analyses of the data show different energy dependences for production of the various actinide isotopes. These excitation functions appear to be

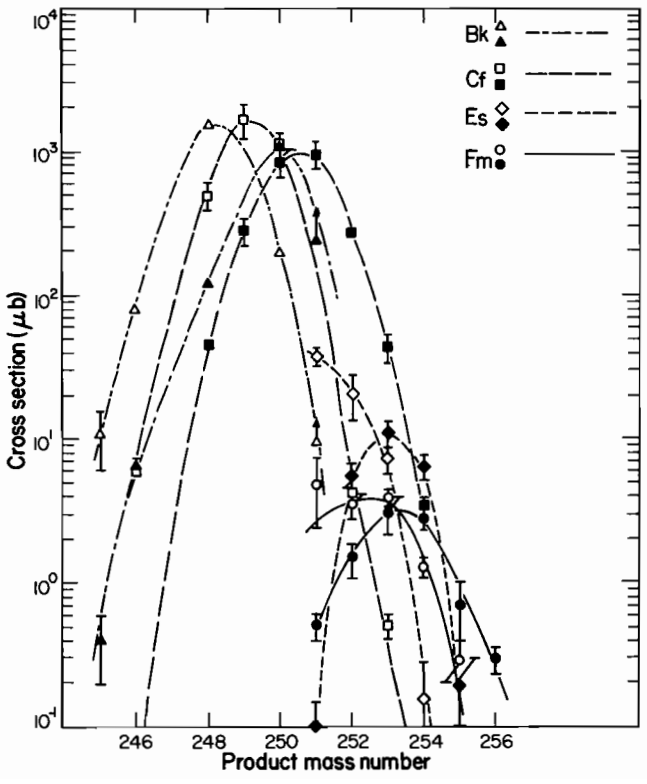

Fig. 1. Isotopic distributions measured for 115-MeV ^{20}Ne and 116-MeV ^{22}Ne bombardments of ^{248}Cm. ^{20}Ne data are open symbols; ^{22}Ne data are solid symbols. (XBL 814-644)

Table 1. Comparison of position and magnitude of maximum yields for $^{16,18}O$ and $^{20,22}Ne$ bombardments of ^{248}Cm.

	^{16}O	^{18}O	^{20}Ne	^{22}Ne
$E_{c.m.}$ (MeV)	92	90	106	106
$E_{Coulomb}$ (MeV)	89	88	108	108
Bk	248m	250	248m	~ 249
μb	1600	1100	695	~ 60
Cf	249	250.5	249	251
μb	1700	~ 1000	2670	1040
Es	251	253	251	253
μb	38	11	100	6
Fm	~ 252	253.5	252	254
μb	~ 4	3	16	3

consistent with calculations based on energy balance considerations for the appropriate transfer reactions, assuming the energy of the projectile in excess of the Coulomb barrier is apportioned to the target according to the fraction of the projectile mass transferred.

Footnotes and Reference

*University of Bern, CH-3000 Bern and Eidgenössisches Institut für Reaktorforschung, CH-5305 Würenlingen, Switzerland.

†Peking University, 100871 Beijing, The Peoples Republic of China.

‡Los Alamos Scientific Laboratory, Los Alamos, NM 87545.

1. D. Lee, et al., Nuclear Science Division Annual Report, LBL-9711 (1980).

Recoil Range Experiments in the Actinide Region

R.M. McFarland, L.P. Somerville, M.J. Nurmia, and A. Ghiorso

One of our major projects is the experimental study of the mechanism of production of nuclides of Z,A between those of the target and the compound nucleus in reactions between light heavy ions ($\sim 10 \leq A \leq 40$) and actinide targets.

One branch of this study is a series of experiments to measure the recoil range distributions and cross sections of product actinides using a variety of projectiles and targets. The angular distribution of a nuclide produced via transfer reaches a maximum at the grazing angle. Its range parallel to the beam axis is shorter than that for a compound nucleus evaporation residue. Therefore, recoil ranges can be used to differentiate between these two mechanisms. They also give rough values for the peak and width of an angular distribution.[1] The cross sections will be compared with those predicted from Wilczynski's quasi-elastic transfer model,[2] with correction for fission and particle evaporation by the primary heavy fragment.

All bombardments were done at the 88-Inch Cyclotron. Table 1 summarizes experiments done to date. Targets are actinide fluorides or oxides deposited upon 2.5 mg/cm^2 Be foil by vacuum deposition[3] or electrospraying, respectively. Beam intensities are ~ 1 to 2 electrical microamperes.

The beam traverses a 1.85 mg/cm^2 Havar window, a 0.45 mg/cm^2 N_2 cooling gas, and the Be backing before striking the target. Recoiling nuclei are caught in a stack of ten 100 μg/cm^2 Al foils. After the bombardment each foil is placed over a 1 inch diameter Si(Au) surface barrier alpha-SF detector. The detectors are interfaced with a computer. Pulse height analysis generates alpha spectra.

The decay of alpha and SF activity in each foil is followed for several months. Nuclides are identified through E_α and $t_{1/2}$. Table 2 shows decay properties of nuclides consistently produced in these bombardments.

The possibility of exotic, neutron-rich nucleon transfers from ^{18}O to an actinide nucleus has been debated since the production of an SF activity from ^{248}Cm with decay properties very like those reported for ^{259}Fm.[4] The reported cross section was 15 nb.[5] Some recoil range bombardments were designed to probe neutron-rich transfers using the 2.64 h SF decay of ^{256}Fm. In the actinide region, no such transfers have been observed with cross sections greater than a few nanobarns. The remainder of the data are now being analyzed.

References

1. R.J. Otto, G.T. Seaborg, and M.M. Fowler, Phys. Rev. C **17**, 1071 (1978).
2. J. Wilczynski, et al., Phys. Rev. Lett. **45**, 606 (1980).
3. Fluoride targets provided by E.K. Hulet and R. Lougheed of Lawrence Livermore Laboratory.
4. D.C. Hoffman, et al., Nuclear Science Division Annual Report, LBL-9711, p. 66 (1980).
5. D.C. Hoffman, "Fission Properties of Very Heavy Actinides," IAEA 4th Symp. Phys. and Chem. of Fission, Julich, Federal Republic of Germany, May, 1979; IAEA – Sm – 241/B14.

Table 1. Summary of bombardments.

Expt.	Projectile	Target	E_{Lab} (MeV) on target	Sought exotic transfer product	Nucleon transfer
M	^{18}O	^{233}U	95.7		
N	^{18}O	^{233}U	98.7		
O	^{18}O	^{244}Pu	98.7	^{256}Es (growth of ^{256}Fm)	5p7n "^{12}B"
P	^{16}O	^{233}U	96.4		
Q	^{16}O	^{244}Pu	102.1		
R	^{15}N	^{233}U	98.7		
S	^{15}N	^{244}Pu	98.7		
T	^{18}O	^{245}Cm	93.0	^{256}Fm	4p7n "^{11}Be"
U	^{18}O	^{245}Cm	99.6	^{256}Fm	4p7n "^{11}Be"
V	^{18}O	^{245}Cm	99.6	^{256}Fm	4p7n "^{11}Be"
W	^{18}O	^{245}Cm	94.0	^{256}Fm	4p7n "^{11}Be"
X	^{18}O	^{244}Pu	95.7		
Z	^{18}O	^{249}Cf	111.		
AA	^{18}O	^{246}Cm	95.7	^{256}Fm	4p6n "^{10}Be"
AC	^{18}O	^{246}Cm	87.2	^{256}Fm	4p6n "^{10}Be"

Table 2. Consistently observed actinide alpha-emitters.

Nuclide	Decay Mode	$t_{1/2}$	E_α
^{242}Cm	α	162.8 d	6.113 6.070
^{246}Cm	α	35.7 h	6.758 6.7190
^{248}Cf	α	333 d	6.26
^{252}Fm[a]	α	25.4 h	7.04
^{254}Fm	α	3.240 h	7.187 7.145
^{255}Fm[a]	α	20.1 h	7.022 6.963

[a]not well resolved.

A Procedure for a Fast Separation of Berkelium and Cerium*

Yuan-fang Liu,† Cheng Luo,‡ Hans R. von Gunten,‖ and Glenn T. Seaborg

Berkelium and cerium can be easily separated from the rest of the actinides and lanthanides using their oxidation/reduction properties. However, a separation of the two elements from each other is more difficult to achieve and generally quite time consuming. In an attempt to measure decay properties of short-lived Bk isotopes produced in heavy ion reactions, it was mandatory to develop a procedure for a fast separation of the two elements. The methods described in the literature are either too time consuming[1] or could not be reproduced in our laboratory.[2,3]

The procedure developed in our work combines the separation of Bk and Cc from other actinides, lanthanides, and fission products with a subsequent fractionation of the two elements using high pressure liquid chromatographic (HPLC) techniques.

Berkelium and cerium were oxidized with 0.1M CrO_3 in 4M HNO_3 to the 4+ state, extracted with 0.15M 2-diethylhexylorthophosphoric acid (HDEHP) in heptane, reduced to the 3+ state with H_2O_2, back-extracted into 10M HNO_3,[4] and this solution was evaporated to dryness. The residue was dissolved in 0.1 ml of 0.5M HNO_3 and was injected into the cation exchange column of an HPLC-system (ALTEX-BECKMAN, Model 110A). The precision glass column (100 × 2 mm) was filled with the resin in the Na-form (Benson Co., BC-X12, 7-10 μm) and was heated with a water jacket to a temperature of 82°C. After the injection of Bk/Ce, the elution was started using 0.5M ammonium alpha-hydroxyisobutyrate at pH 4.2 for the berkelium fraction (1-110 drops; 1 drop = 15 μl), with a change of the eluant to pH 4.4 for the cerium fraction (111-200 drops). A flow rate of 0.5 ml/min (resulting in a pressure of ~ 300 psi) was employed. A typical elution curve is shown in Fig. 1. A very good and clean separation of the two elements is obtained, the elution peaks being quite sharp and having only little tailing. The separation of Bk on the HPLC-column takes only about 4 minutes from the injection to the completion of the elution.

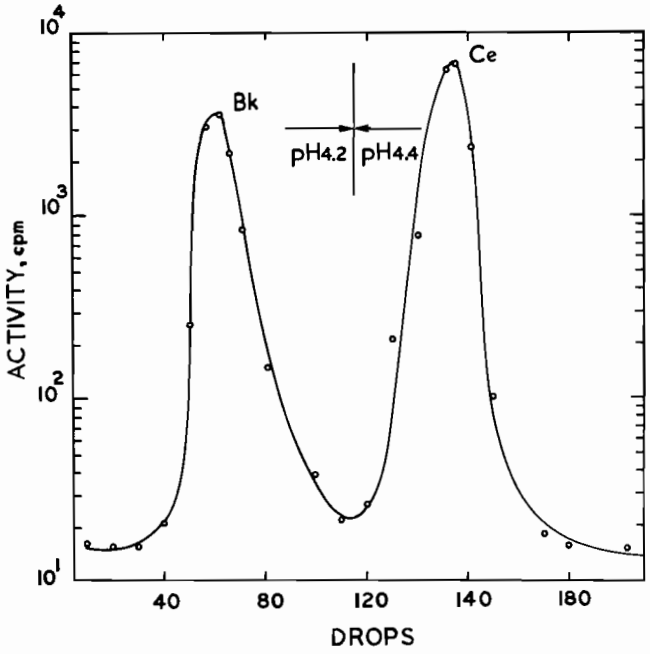

Fig. 1. Elution curve of Bk and Ce using 0.5M ammonium alpha-hydroxyisobutyrate. (XBL 814-9447)

Footnotes and References

*Condensed from LBL-12909.

†On leave from Peking University, 100871 Beijing, The People's Republic of China.

‡On leave from the Institute of Atomic Energy, P.O. Box 275, Beijing, The People's Republic of China.

‖On leave from the University of Bern, CH-3000 Bern and Eidgenössisches Institute für Reaktorforschung, CH-5305 Würenlingen, Switzerland.

1. D.C. Hoffman, et al., LA-1721, 4th Ed., 251 (1975).
2. F.L. Moore, Anal. Chem. **41**, 1658 (1969).
3. V.N. Kosyakov, E.G. Chudinov, and I.K. Shvetsov, *Proceedings of the Moscow Symposium on the Chemistry of the Transuranium Elements,* 99 (1976).
4. K.E. Williams and G.T. Seaborg, Phys. Rev. C **19**, 1794 (1979).

2. High Angular Momentum

Study of High Energy Gamma Rays Emitted in the Deep-Inelastic Reactions $^{181}Ta + ^{136}Xe(1150\ MeV)$

J.O. Newton, J.E. Draper, K.H. Lindenberger, R.M. Diamond, C. Schück, F.S. Stephens, E.L. Dines, S. Shih, L.G. Sobotka, G.J. Wozniak, R.J. McDonald, D.J. Morrissey, A.J. Pacheco, and L.G. Moretto

In a recent paper[1] we reported on the observation of gamma rays from giant dipole resonances (GDR) built on states of high energy and spin. Such measurements have the potential for providing new information on the properties of nuclei at high temperatures (T) and large angular momenta (I). For example, from observation of structure in the GDR region, one may learn about the dependence of nuclear deformation on T and I. In addition, one may be able to learn about the GDR itself by examining its energy (E_G), strength, and width as a function of T and I.

Recently, we have employed the deep inelastic reaction $^{181}Ta + ^{136}Xe$ (1150 MeV) at the SuperHILAC to explore the Q-value dependence of giant dipole transitions. The insert in Fig. 1 shows a schematic diagram of the experimental apparatus. By gating on different Q-value regions (see Fig. 1), the coincident gamma-ray spectra can be studied as a function of T. These spectra are shown in Fig. 2. A strong increase is observed in the yield of high

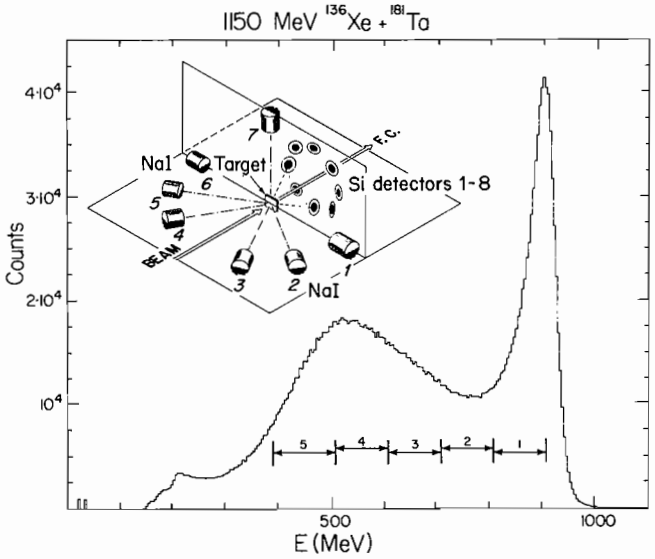

Fig. 1. The insert is a schematic of the experimental configuration, depicting the seven 5 × 6 in. NaI and eight Si solid-state detectors. The main figure shows the heavy-ion energy spectra and the five Q-value windows.
(XBL 816-1017)

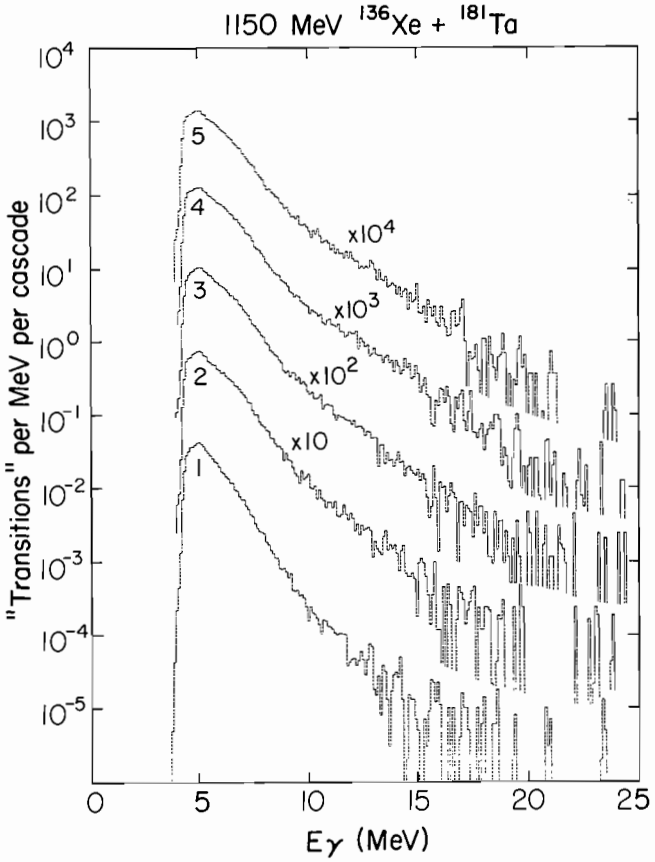

Fig. 2. Coincident gamma-ray energy spectra for the five Q-value bins shown in Fig. 1. (XBL 816-3261)

energy γ rays in the region of the GDR ($E_\gamma \simeq 14$ MeV) as one gates on more negative Q-values or higher temperatures. Most of this increase occurs between Q-value regions 1 and 3 followed by a leveling off of the yield for the largest Q-values.

Work is presently in progress to determine whether these spectra are in agreement with statistical model calculations where the GDR strength function has been included for E1 gamma decay.

Reference

1. J.O. Newton et al., Phys. Rev. Lett. **46**, 1383 (1981).

Properties of Nuclei at Very High Spin*

F.S. Stephens

Our understanding of the structure of high-spin states has developed rapidly in the last few years, and a rather satisfying perspective is now emerging. I will discuss γ-ray studies because at present they give the most detailed information about nuclear structure at these spin values.

The first question has to do with the amount of angular momentum that one can get into γ-ray cascades. By far the best method presently known to produce high-spin states is through heavy-ion fusion reactions. The maximum angular momentum resulting in γ emission following such reactions is shown in Fig. 1. Above and to the right of the curve in Fig. 1, the angular momentum is lost through fission, whereas above and to the left it is removed by particle (largely α) evaporation. Below the line, γ emission dominates, deexciting the nucleus to its ground state. It is apparent that the highest angular momentum that decays through γ emission is about $70\hbar$ for masses around 150. If these nuclei were produced cold, only about 15 to $20\hbar$ more could be retained. Thus we can study most of the possible range.

To understand the structure of nuclei at such spins, consider a classical rigid rotor. It is not clear that nuclei behave this way, though at high spins, where the pairing correlations are quenched, most people believe this is approximately true. Two limiting models for nuclear behavior suggest that this is reasonable.[1] The moment of inertia of a rigid ellipsoid (having constant volume) compared with that of a rigid sphere is shown in Fig. 2 as a function of shape (γ) for two deformation values. The value $\epsilon \simeq 0.3$ corresponds roughly to that found in deformed rare-earth nuclei, whereas $\epsilon \simeq 0.6$ corresponds to an axis ratio of about 2:1—the largest that one could hope to see in these (or probably any) nuclei. It is clear in Fig. 2 that there is a favored region of large moments of inertia, extending from an oblate shape rotating about its symmetry axis ($\gamma = 60°$) to a prolate shape rotating about a perpendicular axis ($\gamma = 0°$). To see just how significant this favoring is, I have put an energy scale on the right side of Fig. 2 for the case of mass 160 and spin $60\hbar$.

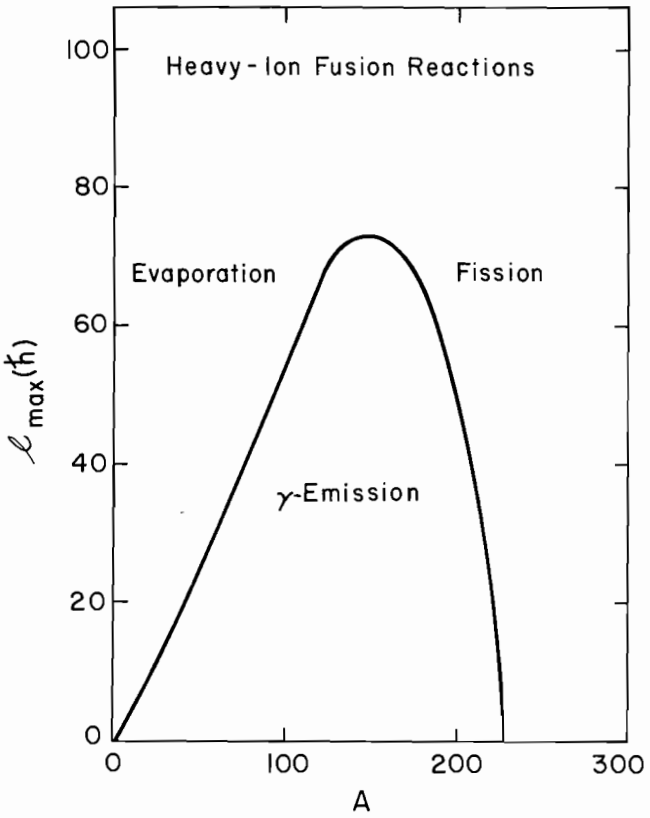

Fig. 1. The line indicates the limiting angular momentum for a nucleus (of mass A) between γ-ray emission (below) and either fission (above, right) or particle evaporation (above, left). (XBL 809-1958)

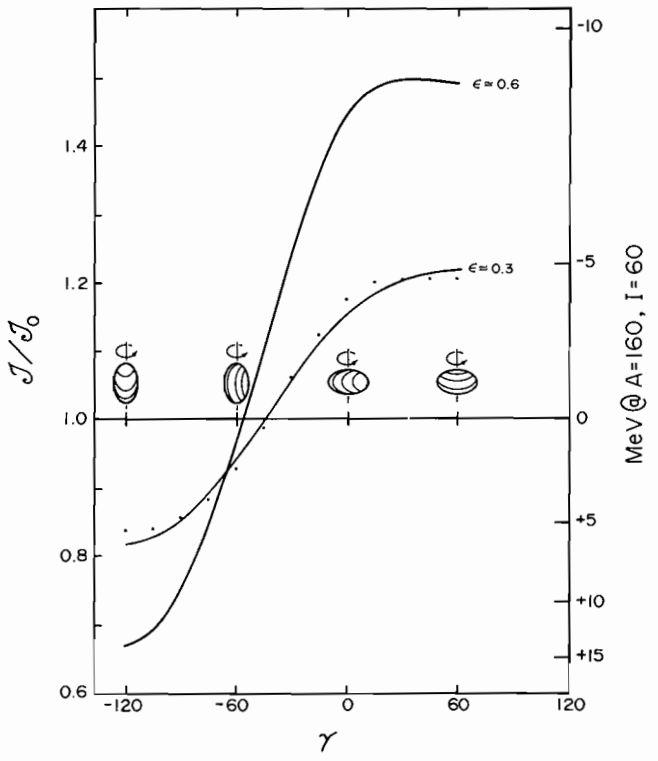

Fig. 2. Ratio of the moment of inertia of a rigid ellipsoid to that of a rigid sphere vs. the shape parameter γ for two values of the deformation $\epsilon = 0.3$ and $\epsilon = 0.6$. The right-hand scale gives the difference in rotational energy in MeV for a nucleus with A = 160 and I = 60. The dots give the differences in total liquid-drop energy (rotation + surface + Coulomb) for the nucleus. (XBL 808-11414)

These shapes are favored by about 10 MeV over the others. Since the average shell effects are only around 3 MeV, these moment-of-inertia effects should dominate at high spins and restrict the nuclei to the above shape region. It is interesting that the shape dependence of the surface and Coulomb energy terms in the liquid drop model is small, and the full LDM energy, given by the dots of Fig. 2, is remarkably near to that obtained from the moments of inertia alone—simply geometry.

There is a further aspect of these shapes that is important. The rotation of a nucleus about an axis perpendicular to the symmetry axis is a collective rotation with smooth bands and strongly enhanced E2 transitions connecting the levels. There are many beautiful examples of such rotors in the regions around mass 160 and 250. On the other hand a quantal system like the nucleus cannot rotate around a symmetry axis. This degree of freedom is contained in the single-particle motions. Thus a nucleus of $\gamma = 60°$ builds up its angular momentum by aligning one or more individual nucleons with the symmetry axis. This is completely noncollective and is much like the case of spherical closed-shell nuclei. It seems that around mass 150 some oblate nuclei exist,[2] with such noncollective states running up to around $40\hbar$. We have found that nuclei at the highest spins lie between these limits ($\gamma = 0°$ and 60°), displaying some collective and some noncollective properties.

Footnote and References

*Presented at the International Conference on Nuclear Physics, Berkeley, CA, August 1980.

1. A. Bohr and B.R. Mottelson, Nuclear Structure, vol. 2 (Benjamin, Reading, Mass., 1975).
2. T.L. Khoo, R.K. Smither, B. Haas, O. Hausser, H.R. Andrews, D. Horn, and D. Ward, Phys. Rev. Lett. **41**, 1027 (1978).

Nuclear Structure at High Spins*

F.S. Stephens

Nuclei are composed of a small (but not too small) number of nucleons. As a result they display both collective and single-particle (non-collective) features. For example, in the rare-earth and actinide regions, the low-lying rotational bands represent an almost pure collective motion, with energies following the $I(I+1)$ rotor formula to within a percent or two, and E2 transition probabilities nearly 200 times larger than a single proton would have. On the other hand, near the closed shells, the energy levels are almost completely determined by the motion of a single nucleon. Most nuclear levels display both collective and non-collective features, and high-spin states are no exception. The present objective is to understand the kinds of mixtures of collective and single particle motion that are important in nuclei at the highest spins. Our ideas about such states have undergone important developments recently that now make possible a reasonably simple description of this subject.

I will start with a collective rotational nucleus, and couple to this first one and then more single particles. The rotational angular momentum is necessarily perpendicular to the nuclear symmetry axis, and the particle angular momentum, j, can couple either along the symmetry axis or along the rotation axis. The former situation is that considered by Bohr and the projection of j along the symmetry axis, called Ω, is a constant of the motion. In this case the collective angular momentum, R, and the projection of j along the rotation axis are not constants of the motion. In the latter situation, the projection of j along the rotation axis, called j_a, is sharp, and here R and Ω are not constants of the motion. It seems rather clear that a perpendicular relationship between R and j will be much less favorable for producing low-energy high-spin states than a parallel one. This is borne out by the fact that as the nucleus rotates there is a Coriolis force which tends to align j with the rotation axis. The back-bending phenomenon, and a number of other related effects, are now known to be connected with such "rotation-aligned" states. I want to try to trace how the inclusion of such states can effect a smooth transition between fully collective and fully non-collective regions of nuclear behavior.

In the upper left portion of Fig. 1 a complete collective behavior is illustrated. The nucleus is taken to be prolate, as indicated by the small β,γ plot, and each intrinsic state (angular momentum along the symmetry axis is ignored, implying $K = 0$) has a collective rotational band corresponding to rotation about the axis perpendicular to the symmetry axis. The total angular momentum is just that of the collective motion, $\omega\Theta$. In such bands the energy is given by parabolas centered on the y-axis and displaced vertically by a band-head energy. The γ-ray energy in such a band is related to the slope of this parabola. The difference between successive γ-ray energies is related to the curvature of the parabolas, and is independent of spin for a perfect rotor.

In the upper right portion of Fig. 1, a small amount of single-particle angular momentum aligned along the rotation axis, j_a, has been added. The orbits of these particles are roughly in the plane perpendicular to the rotation axis, and will cause a bulge in the otherwise prolate nucleus. Thus the nucleus necessarily becomes slightly tri-axial as indicated in the small β,γ plot. The total angular momentum is now the sum of the collective part, $\omega\Theta_{coll}$, and a single particle part, Σj_a. The energy of the bands is given by parabolas whose horizontal displacement from the

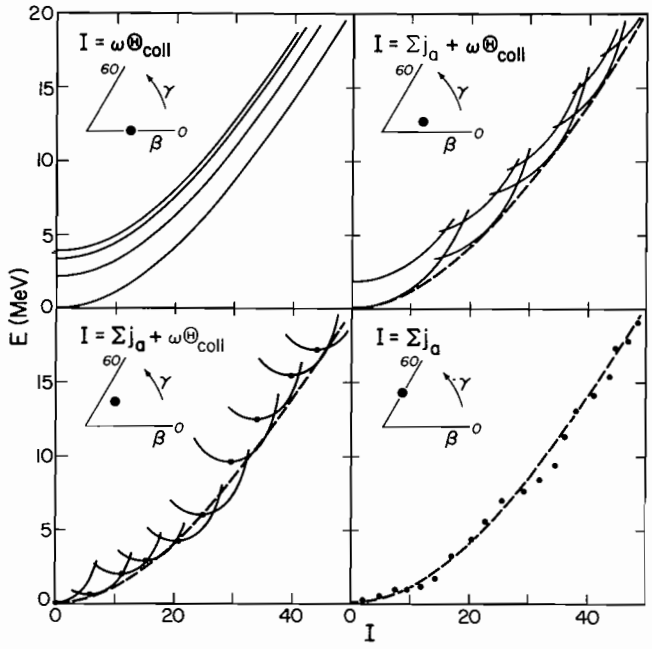

Fig. 1. Schematic excitation energy vs. spin plots for various relative amounts of collective angular momentum and single-particle rotation-aligned angular momentum. Band-head (pure single-particle) energies are shown in the lower two panels. The solid curves correspond to real bands, whereas the dashed curve is the envelope of the real bands.
(XBL 804-544)

y-axis is j_a and whose vertical displacement is still the band head energy. The solid lines in Fig. 1 represent these bands. Since the aligned angular momentum is usually not known, one generally ignores it and uses the usual rotational formula. This corresponds to the envelope curve (dashed) in Fig. 1. The average slope, and thus $E_\gamma(I)$, are the same for this envelope and for the populated portion (near the envelope) of the real bands, so that one cannot distinguish the real band structure this way. However, the curvature of the real bands in the upper right part of Fig. 1 is larger than that of the envelope. This curvature is still related to *differences* between γ-ray energies, provided they are two (correlated) γ-rays within the same band. There are now experiments sensitive to this curvature.

In the lower left part of Fig. 1, the alignment process is assumed to continue. The nucleus is moving toward an oblate shape as more particles align and thereby move in roughly circular orbits perpendicular to the rotation axis. The total angular momentum is now mostly aligned, Σj_a, with only a modest collective contribution. The band head energies are indicated as dots, and they have moved out rather close to the envelope line. As sketched (somewhat arbitrarily), there is only an average of 6 or 8$\hbar$ in the bands at the spins where they are likely to be populated (along the envelope). The band heads were not indicated in the previous panel (upper right) where they were rather far from the envelope line—15-20$\hbar$ on the average—corresponding to a considerably larger collective contribution to the total angular momentum. The curvature of the bands is much larger now since the shape is becoming more oblate, and the rotation axis will then become a symmetry axis. Another way to view this is that most of the reasonably high-j particles are aligned and thus no longer contribute to the collective moment of inertia. These bands show a much higher rate of crossing, and although the slope behaves regularly, the detailed band structure will be quite irregular. It is worth emphasizing that the γ-ray energies alone cannot distinguish among these first three panels; one must look at the γ-ray energy correlations.

Finally, in the lower right part of Fig. 1, the nucleus has acquired an axially symmetric oblate shape—the rotation axis has become the symmetry axis and collective rotations cannot exist about this axis. The band heads now scatter around the envelope line and are purely single-particle states. At $\beta = 0$ these would be the usual spherical shell-model states, but reasonably large β values may also occur. Such states are observed in several regions and will be discussed later by Khoo and others. We have thus followed the motion from collective to non-collective in a continuous way by aligning more and more particles.

There is good evidence that nuclei do exist with behavior like that shown in the first, second, and fourth panels. I believe we now have the experimental tools to determine whether nuclei at the very highest spins fall into this sequence, and if so, where. The next few years should thus be exciting ones in the study of very high-spin states.

Footnote

*Presented at the International Conference on Nuclear Behavior at High Angular Momentum, Strasbourg, France, April 22-24, 1980.

High-Spin Properties of ^{164}Er in the Multiple Band Crossing Region From Coulomb Excitation and In-Beam Gamma-Ray Spectroscopy*

*S.W. Yates,[†,‡] I.Y. Lee,[‡,§] N.R. Johnson,[‡] E. Eichler,[‡,‖] L.L. Riedinger,[‡,¶] M.W. Guidry,[‡,§,¶] A.C. Kahler,[‡,¶,**] D. Cline,[§,††] R.S. Simon,[‡‡] P.A. Butler,[§§] P. Colombani,[‖,‖] F.S. Stephens, R.M. Diamond, R.M. Ronningen,[¶¶,***] R.D. Hichwa,[¶¶,†††] J.H. Hamilton,[¶¶] and E.L. Robinson[‡‡‡]*

High-spin states in ^{164}Er have been studied by using the ^{150}Nd(^{18}O,4nγ) and ^{164}Dy(α,4nγ) reactions and by multiple Coulomb excitation with ^{136}Xe ions. Several positive-parity bands are excited, and two negative-parity bands have been identified. The previously reported backbending behavior of the yrast sequence is demonstrated to result from the intersection of the ground band (seen to spin 22^+) with an even-spin "superband" observed from spins 12^+ to 24^+. The odd-spin yrast superband and the second lowest even-spin superband also have been observed. All the superbands have moments of inertia appreciably larger than the ground band. The observed intersection of these multiple superbands with the γ band produces different backbending behavior and a staggering of the energies of the odd- and even-spin members of the γ band. B(E2) values for transitions below and through the band intersection regions of both the ground band and γ bands have been deduced from multiple Coulomb excitation yields. In addition, lifetimes have been measured for the ground band by the Doppler-broadened lineshape technique. The level energies and B(E2) values are consistent with weak interaction matrix elements ($\simeq$ 45 keV) between the intersecting bands. The B(E2) values of the unperturbed band are found to obey the simple rigid-rotor relationship. The 7^- negative-parity band exhibits a normal rotational sequence, while the 5^- band exhibits a large odd-even staggering and a larger moment of inertia. Two-quasiparticle-plus-rotor model calculations indicate strong rotation alignment and reproduce the observed properties of the high-spin states for both the positive- and negative-parity bands in ^{164}Er.

Footnotes

*Condensed from Phys. Rev. C **21**, 2366 (1980).

†University of Kentucky, Lexington, KY 40506
‡Oak Ridge National Laboratory, Oak Ridge, TN 37830
§LBL
‖Deceased
¶University of Tennessee, Knoxville, TN 37916
**Present address: Cyclotron Institute, Texas A&M University, College Station, Texas 77843.
††Nuclear Structure Research Laboratory, University of Rochester, Rochester, NY 14627
‡‡Present address: Gesellschaft für Schwerionenforschung, Darmstadt, Germany.
§§Present address: Department of Physics, University of Liverpool, P.O. Box 147, Liverpool L69 3BX, United Kingdom.
‖‖Present address: Etudes et Productions, Schlumberger, 25 Rue de la Cavée, 92142 Clamart, France.
¶¶Vanderbilt University, Nashville, TN 37235
***Present address: Cyclotron Laboratory, Michigan State University, East Lansing, Michigan 48824.
†††Present address: Department of Radiology, Medical Physics, University Hospitals, Madison, Wisconsin 53706.
‡‡‡University of Alabama in Birmingham, Birmingham, Alabama 35294

Average g-Factors for High Spin States in ^{156}Dy*

N. Rud,[†,‡] D. Ward,[†] H.R. Andrews,[†] O. Häusser,[†] P. Taras,[§] J. Keinonen,[‖,¶] M. Neiman, R.M. Diamond, and F.S. Stephens

The initial deexcitation process of nuclei formed at high spin involves a large number of possible decay paths which give rise to a quasi continuous γ-ray spectrum formed from many unresolved overlapping transitions. Nevertheless, it has been possible to determine certain average properties of the emitting states such as, average moments of inertia and collectivity. In the present experiments, we have measured average magnetic moments for states lying on and above the yrast line in the nucleus ^{156}Dy populated in the reaction ^{24}Mg(^{136},4n)^{156}Dy at various bombarding energies. The ^{156}Dy recoiled through a layer of magnetized iron during which time the aligned states precessed in the intense magnetic field experienced by ions moving rapidly in a ferromagnet. After about 1 ps the recoils left the iron and entered a copper layer, where the magnetic field was zero so that no further precession

could occur. However, the precession accumulated in the iron was passed down through further γ-ray cascades resulting in a cumulative rotation of the γ-ray angular distribution pattern for the discrete transitions at low spin. We shall refer to these low spin states as "probe" states.

The ^{136}Xe beam was obtained from the Berkeley SuperHILAC. The precession measurements were performed with two Ge(Li) detectors placed 7.5 cm from the target and set 60° on either side of the beam direction. Spectra were routed according to the field direction, which was reversed every two minutes. The effect of precession on the probe states (the 2^+, 4^+, 6^+, and 8^+ states) was derived in the usual way from appropriate ratios of their observed photopeak intensities in the two γ-ray detectors for the two field directions. The precession angles themselves were obtained by using the γ-ray angular distribution coefficients measured previously.

The centroid of the initial spin distribution, $\bar{J}$, was assumed to be $\bar{J} = 2(\langle M \rangle - 1.5)$ with a FWHM of $14\hbar$. The results are summarized in Fig. 1, where it can be seen that the centroid of the spin region contributing to the precession was appreciably lower than that of the entry distribution. This was because the higher spin states having the shortest lifetimes were not exposed to the full action time of the field, and further, there was appreciable decay during the period spent in the target and buffer layers (from t = 0 to ~ 0.5 ps).

For average entry spin $\bar{J} = 15\hbar$ there would be a strong population of the states in the vicinity of the crossing at spin 16 of the ground band by a band believed to have a neutron-aligned character, and predicted to have near zero g-factor at spin 12-16$\hbar$. In comparing our results with calculations, it must be remembered that states above the yrast line were also sampled; nevertheless, some reduction of the g-factor would be expected for this spin region from the predominance of neutron aligned states there, and this is indicated by the data. At the higher entry spins, the average g-factor has recovered to or may even exceed the 2^+ value. This behavior is expected from the breakdown of proton pairing and the occurrence of aligned proton bands which should become yrast for $\bar{J} > 26\hbar$. The present rise at spins as low as $J \simeq 20\hbar$ may result from the population of aligned proton bands lying above the (neutron aligned) yrast line.

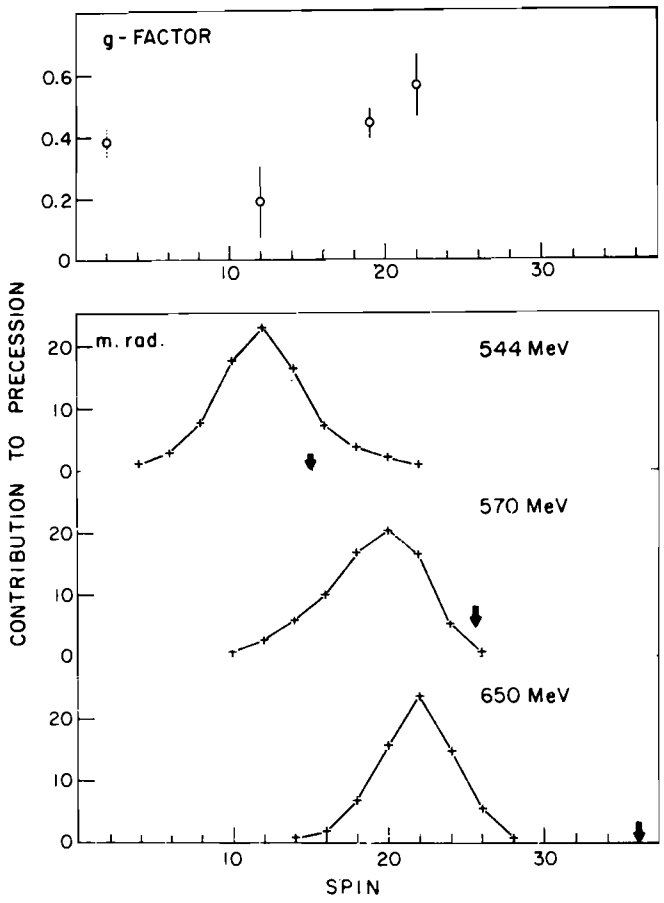

Fig. 1. Summary of average g-factors in ^{156}Dy. The top panel shows the average g-factor plotted at the centroid of states contributing to the precession. The 2^+ value was obtained from systematics of 2^+ g-factors in Dy isotopes and the N = 90 isotones. The lower panels show the contributions made by the states of spin J (not necessarily yrast) to the total precession for each entry spin distribution whose centroids are indicated by the arrows.

(XBL 819-1783)

Footnotes

*Condensed from Phys. Lett. B **101** (1,2), 35 (1981).

†Atomic Energy of Canada Limited, Chalk River Nuclear Laboratories, Chalk River, Ontario, Canada K0J1J0
‡Visiting scientist from Aarhus University, Denmark
§Laboratoire de Physique Nucléaire, Université de Montréal, Montréal, P.Q. Canada
‖Queen's University, Kingston, Ontario, Canada
¶Permanent address: University of Helsinki, Finland

Alignment Effects in Correlation Spectra*

C. Ellegaard,† M.A. Deleplanque,†,‡ O. Andersen,†
B. Herskind,† F. Stephens, R.M. Diamond, H. Kluge,§ C. Schück,‖ and S. Shih¶

In the deformed rare earth region, nuclei with spins as high as $\sim 70\hbar$ may be populated by heavy-ion fusion reactions. For the γ-ray depopulation of such nuclei, discrete-line γ-ray spectroscopy can follow the decay to spins as high as $32\hbar$. Above this limit the γ-ray spectrum is unresolved and thus appear as a continuum. Many measurements have shown that this unresolved γ-ray spectrum consists of statistical γ rays, which cool the nucleus towards the yrast line and give rise to an exponentially decreasing high-energy tail, and of a lower energy bump, which is composed of yrast-like transitions that remove spin and contain most of the nuclear structure information.

Recent experiments have shown that it is possible to observe structure in this continuum region. These experiments are based on γ-γ coincidence measurements, and the structure is brought out by measuring correlations among the γ-ray energies. These correlations arise from regularities of the γ cascades that result from certain features of the nuclear structure. The angular momentum carried by the nucleus can be generated either from the collective motion of the nucleus as a whole or from the motion of individual particles. Collective rotation of the nucleus is indicated in the two-dimensional γ-γ energy plots by a valley along the diagonal indicating an absence of two transitions of the same energy—a property of rotational bands—and by flanking ridges whose spacing is related to the band moment of inertia.[1] There is also evidence in these nuclei that angular momentum is carried by single-particle motion; specifically, bands involving unpaired high-j particles whose angular momentum becomes aligned with the rotation axis above a certain spin. Such bands generally cross other (less aligned) bands as the spin increases. These band crossings, which occur in many bands at a few specific frequencies, lead to marked deviations from the regular rotational pattern. It is important to recognize clearly the observable features associated with this latter behavior.

A backbend in a cascade is characterized by several (two, three, or even four) γ rays of roughly the same energy. An upbend is the clearest example of such behavior and seems to be common at high spins, as illustrated by the known second backbends. It has been shown,[1] that these features appear as bridges across the valley or peaks in the valley of the correlation spectra. In such cases the γ-ray transitions in coincidence with the bridge or peak transitions should also be enhanced. If there is more than one backbend in a cascade, there will be a further enhancement of the intensity at the intersection of the two backbend energies. Thus one might expect to see a "square" pattern in the correlation spectra, i.e., intersecting horizontal and vertical stripes made up of points having higher than average intensity.

In this experiment, ^{156,157,158}Er nuclei were populated at high spin with the ^{122}Sn(^{40}Ar,xn) reactions with x = 6, 5 and 4. The γ-rays were detected in five Ge(Li) detectors placed at ± 150, ± 130 and 90°. A sum spectrometer was placed around the target and Ge(Li) detectors. Since peak-to-total ratio for the Ge(Li) detectors used was only 10 to 15%, a method for subtracting uncorrelated events (Compton and background transitions) from the data was used. The method is an improvement over the one previously described.[1]

The result of this procedure is shown in Fig. 1. This plot corresponds to a high slice in the total energy spectrum of the sum spectrometer and thus populates highest spins $\gtrsim 50\hbar$, producing a spectrum which is roughly flat from about 1300 keV down. The low energy lines from the first backbend in the 4n channel are present in this spectrum, though they are weak and not so clearly seen on this low-resolution plot. The dominant feature is the strong line at 1300 keV (Ch 45). It has strong intersections with the low-energy 4n lines, the second backbend (Ch 22) and a 1060 keV line (Ch 32). Thus it definitely belongs to the 4n channel. It is impressive that the population at these spins, $\gtrsim 50\hbar$, flow strongly through the 1300 keV backbend; whereas when it is fed at lower spins this is almost completely missed. The sum-spectrometer thus provides a powerful method for studying those correlations involved in deexciting particular spin regions.

It seems clear that the enhanced rows and columns in correlation plots like Fig. 1 contain information about the single-particle aspects of nuclei at very high angular momentum. They very probably signal the alignment of the angular momentum of the major high-j orbitals. While we have not tried to make specific assignments here, the general method presented for extracting this information from correlation spectra seems clear and offers exciting possibilities for determining the important single-particle components of high-spin states throughout the periodic table.

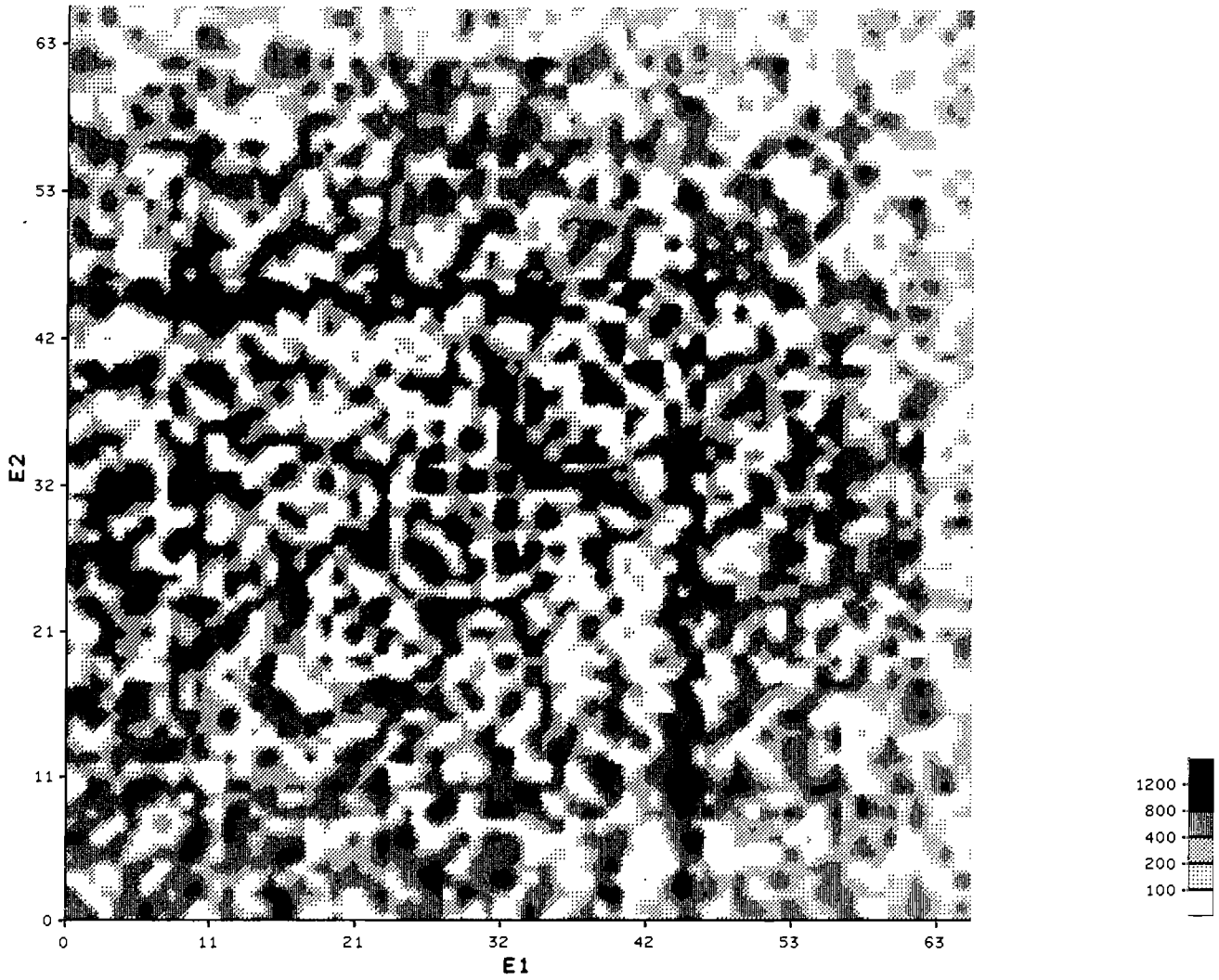

Fig. 1. Gamma-energy correlation spectra from the $^{122}Sn(^{40}Ar,xn)$ reaction after 20 iterations (see text). This corresponds to the highest-energy slice in the sum spectrometer and thus the highest spins. Channel zero of this plot is at 0.4 MeV and there are 0.020 MeV per channel.
(XBB 808-9845)

Footnotes and References

*Submitted to Phys. Rev. Lett.

†The Niels Bohr Institute, University of Copenhagen, Copenhagen, Denmark

‡Permanent address: Institut de Physique Nucléaire, B.P. no. 1, 91406 Orsay, France.

§Permanent address: Hahn-Meitner Institut, Berlin, Germany.

‖Permanent address: Centre de Spectrometrie Nucléaire et de Spectrometrie de Masse, Orsay, France.

¶Permanent address: Shanghai Institute of Nuclear Research Shanghai, People's Republic of China.

1. M.A. Deleplanque, F.S. Stephens, O. Andersen, J.D. Garrett, B. Herskind, R.M. Diamond, C. Ellegaard, D.B. Fossan, D.L. Hillis, H. Kluge, M. Neiman, C.P. Roulet, S. Shih, and R.S. Simon, Phys. Rev. Lett. **45**, 172 (1980).

Observation of Giant Dipole Resonances Built on States of High Energy and Spin*

*J.O. Newton,† B. Herskind,‡ R.M. Diamond, E.L. Dines,§ J.E. Draper,§ K.H. Lindenberger,‖ S. Shih,¶ C. Schück,** and F.S. Stephens*

Studies of the GDR have been restricted mostly to coherent excitation from nuclear ground states which excites only the giant resonances built on them. Brink,[1] however, has proposed that every state in a nucleus has a GDR associated with it. A consequence of this idea is that the strength functions for electric dipole transitions from every state would have a Lorentzian-like shape as a function of γ-ray energy E_γ, with a magnitude determined from the E1 sum rule. Such a variation of strength with E_γ would affect the shape of the spectrum of γ-rays emitted from a highly excited nucleus, particularly in the vicinity of $E_\gamma = E_G$, the energy of the GDR. We have observed this effect in the statistical γ-rays following heavy-ion fusion reactions.

The present experiments make use of a sum-spectrometer-multiplicity technique that selects the γ-rays from moderately high-spin ($\sim$ 20-65$\hbar$) states produced in heavy-ion compound nucleus reactions. The sum spectrometer consists of two 33 cm diameter by 20 cm thick NaI detectors facing the target 2.5 cm above and below the beam axis, each subdivided into four elements. Eight NaI (12.7 $\times$ 15.2 cm) detectors were placed 50 cm from the target at angles of $\pm 160°$, $\pm 100°$, $\pm 80°$, $-135°$ and $-45°$ and were shielded from each other and the beam slits by 5 cm of lead. Targets ($\sim$ 1 mg/cm^2) of ^{82}Se, ^{110}Pd, and ^{124}Sn were bombarded with $\sim$ 10 nA of 170 MeV ^{40}Ar ions from the LBL 88-Inch Cyclotron. Spectra from the eight NaI detectors, associated with three regions of sum spectrometer energy E_s with the range $\sim$ 10-40 MeV, were added. Spectra for the ^{82}Se case are shown in Fig. 1. In the energy interval from $\sim$ 2-8 MeV, the spectra show an exponentially falling tail, composed of the statistical transitions deexciting the product nuclei after neutron evaporation. All spectra rise considerably higher than this exponential at energies above $\sim$ 10 MeV, indicating a different source of γ-rays. Beyond $\sim$ 20 MeV the spectra are flat and probably due to cosmic rays.

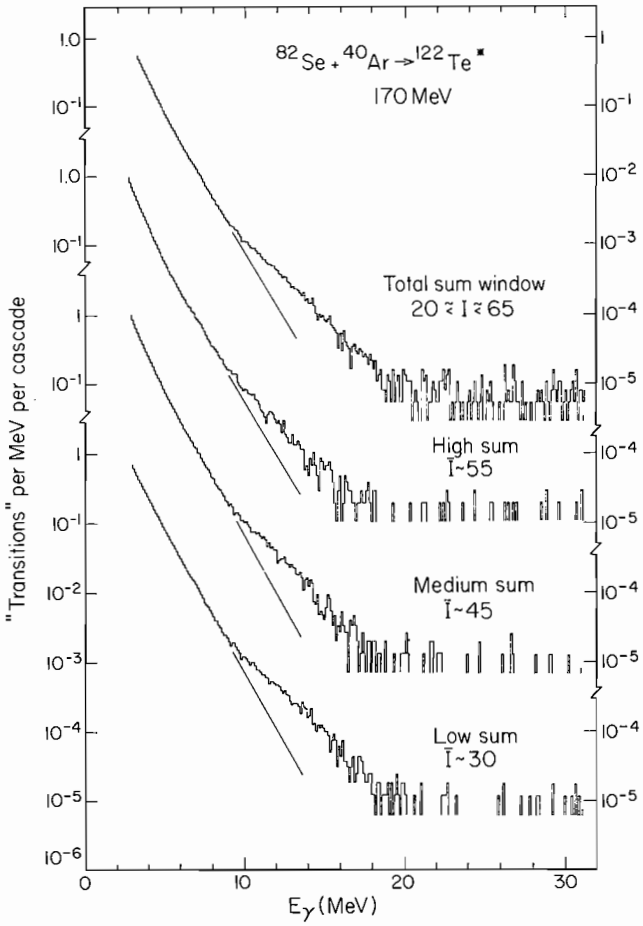

Fig. 1. NaI spectra corresponding to E_s = 10-40 MeV and three windows within this range for the ^{82}Se + ^{40}Ar system. The sloping lines show exponential extrapolations of the lower E_γ parts of the spectra. The shapes of the true γ-ray spectra are not expected to differ greatly from these, and hence the ordinate in "transitions per MeV" should be approximately correct. (XBL 812-268)

The reason for the steep slopes in Fig. 1 is that the level densities for the final states, to which the transition probabilities are proportional, vary approximately exponentially with E_x (and thus as $\exp(-E_\gamma/T)$). A rough way to see the shape of the γ-ray strength functions is to remove the level density dependence by multiplying by $\exp(E_\gamma/T_e)$, where T_e is an effective T. For the less interesting region with $E_\gamma \lesssim 8$ MeV, $T_e \simeq 1$ MeV. Above 10 MeV the curves are flatter, indicating that these γ-rays are emitted at much higher T_e. We have somewhat arbitrarily taken T_e = 1.43 MeV for ^{164}Er (^{124}Sn target), and adjusted the others for the expected mass dependence: $T \propto A^{-1/2}$. The data from the total sum window (with the flat high-energy background subtracted) multiplied by these exponentials are shown in Fig. 2. The peaked structures have maxima ($\sim$ 14 MeV) and widths similar to those for the GDR based on ground states and strongly suggest GDR strength functions. In addition, the bump becomes higher in energy as the target mass decreases, as would be expected for the GDR ($E_G \propto A^{-1/3}$). These measurements demonstrate that one can study the GDR in the γ-ray deexcitation spectra following heavy-ion fusion reactions.

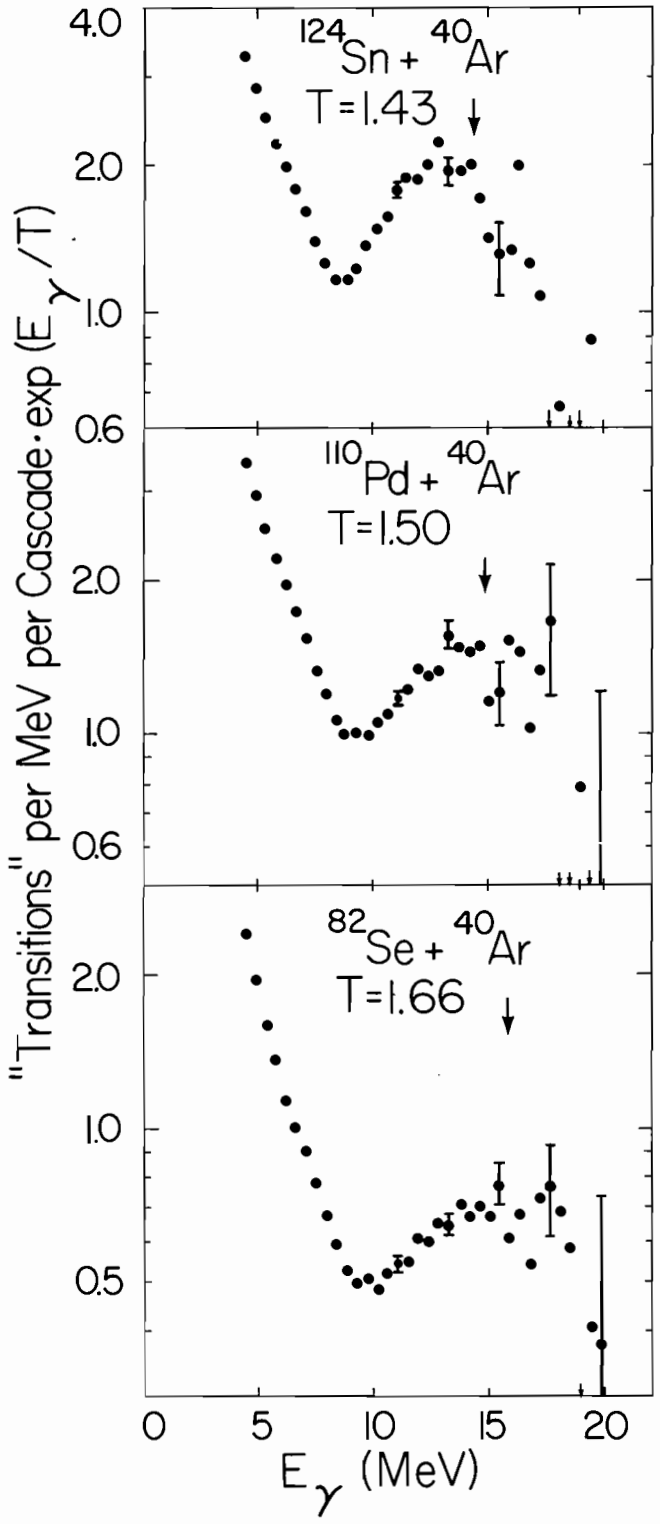

Fig. 2. Background subtracted total-window spectra multiplied by $\exp(E_\gamma/T_e)$. Arrows indicate $E_\gamma = 78/A^{1/3}$ MeV, the centroid of the ground state GDR.
(XBL 811-71)

Footnotes and Reference

*Condensed from Phys. Rev. Lett. **46**, 1383 (1981).

†Permanent address: Australian National University, Canberra, Australia.

‡Permanent address: Niels Bohr Institute, University of Copenhagen, Copenhagen, Denmark.

§Permanent address: University of California, Davis.

‖Permanent address: Hahn-Meitner Institute, Berlin, W. Germany.

¶Permanent address: Shanghai Institute of Nuclear Research, Shanghai, China.

**Permanent address: Centre de Spectrometrie Nucléaire et de Spectrometrie de Masse, Orsay, France.

1. D.M. Brink, doctoral thesis, University of Oxford (1955).

3. Polarization Studies

Polarization*

Homer E. Conzett

A polarized beam (or target) of particles is one in which the particle spins are preferentially oriented, as contrasted with the random distribution of spin directions in an unpolarized beam.

The polarization of an assembly of spin-1/2($\hbar$) particles is given by the vector p with components

$$p_i \equiv \langle\sigma_i\rangle = N_+ - N_-, \quad i = x, y, z .$$

The expectation value of the spin-1/2 operator σ is averaged over the spin states of all the particles; and for spins along (+) and opposite to (−) a specific quantization axis, N_+ and N_- are the fractional number of particles in each of the two spin states.

Preferential orientations in spin-1 assemblies are characterized by both vector, p_i, and tensor, p_{ij}, polarization components:

$$p_i \equiv \langle S_i\rangle = N_+ - N_-$$

$$i,j = x, y, z$$

$$p_{ij} \equiv 3/2\,\langle S_iS_j + S_jS_i\rangle - 2\delta_{ij} = 1-3N_o$$

S is the spin-1 operator and N_+, N_o, and N_- are the fractional magnetic substrate populations, again referred to a given quantization direction. It is seen that the less familiar tensor component is a measure of the difference of N_o from the unpolarized value 1/3. The photon carries a spin of 1, but since the electromagnetic field is transverse to the direction (z) of propagation, the photon spin substate (m_z) populations are limited to N_+ and N_-, corresponding to right and left circular polarizations, respectively. Since $N_o = 0$, photon beams are, in a strict sense, always tensor polarized.

Ion sources of polarized spin-1/2 and spin-1 nuclear particles have been developed, and this makes it possible to provide energetic polarized beams at various accelerators, principally Van de Graaff machines, cyclotrons and synchrotrons. These beams are crucial for experiments to identify spin-dependent effects in nuclear interactions.

Footnote and Bibliography

*Encyclopedia of Physics, eds. R.G. Lerner and G.L. Trigg (Addison-Wesley Publ. Co., Reading, Mass., (1981).

1. L. Wolfenstein, Ann. Rev. Nucl. Sci. **6**, 43 (1956).
2. S.E. Darden, in Polarization Phenomena in Nuclear Reactions, H.H. Barschall and W. Haeberli, eds. (University of Wisconsin Press, Madison, Wisconsin, 1971), p.39.
3. W. Haeberli, in Nuclear Spectroscopy and Reactions, Part A. J. Cerny, ed. (Academic Press, New York, 1974), p. 151.
4. G.G. Ohlsen, Rep. Prog. Phys. **35**, 717 (1972).
5. M. Simonius, Lecture Notes in Physics **30**, D. Fick, ed. (Springer Verlag, New York, 1974), p. 38.
6. B.A. Robson, *The Theory of Polarization Phenomena* (Clarendon Press, Oxford, 1974).

Polarization Tests of Time-Reversal Invariance: Past Failures

Homer E. Conzett

An important test of time-reversal invariance (TRI) is provided by the comparison of the polarization (P) and the analyzing power (A) measured in a nuclear reaction and its inverse, since the P-A equality follows directly from TRI.[1]

The most accurate of these P-A tests have been made in p + ^{3}He (Ref. 2) and p + ^{13}C (Ref. 3). It is necessary to scatter from a nonzero spin nucleus, otherwise parity conservation alone ensures that P = A. We have found that neither of these comparisons was accurate enough to provide a significant test of TRI, because the equality between P and A depends on the equality of the two possible spin-flip probabilities. And it is now known from measurements of the depolarization in p-nucleus elastic scattering that the spin-flip probabilities are very small, leading to $P - A \simeq 0$ even if the probabilities are not equal as required by TRI. Specifically, in terms of the spin-dependent cross sections,

$$P = (\sigma^{++} + \sigma^{-+} - \sigma^{+-} - \sigma^{--})/2\sigma$$

and

$$A = (\sigma^{++} + \sigma^{+-} - \sigma^{-+} - \sigma^{--})/2\sigma \ ,$$

where σ^{-+} is the cross section for the scattering of a proton from an initial negative spin-state to a final positive spin-state, and

$$\sigma = (\sigma^{++} + \sigma^{+-} + \sigma^{-+} \ \sigma^{--})/2.$$

The positive (+y) direction is along $k_i \times k_f$. Thus,

$$P - A = (\sigma^{-+} - \sigma^{+-})/\sigma, \tag{1}$$

and $\sigma^{-+} = \sigma^{+-}$ under TRI. Defining the spin-flip asymmetry as

$$\Delta S = (\sigma^{-+} - \sigma^{+-})/(\sigma^{-+} + \sigma^{+-}), \tag{2}$$

its absolute limits are $-1 \leq \Delta S \leq 1$, but TRI requires that $\Delta S = 0$. Since the depolarization parameter is given by

$$D = 1 - 2S \ , \tag{3}$$

with the (total) spin-flip probability

$$S = (\sigma^{+-} + \sigma^{-+})/2\sigma \ , \tag{4}$$

measurements of D provide determinations of S. It follows, then, from Eqs. (1)-(4) that

$$P - A = (1 - D)\Delta S. \tag{5}$$

Thus, even though ΔS, which is the real measure of time-reversal violation, may be significantly different from zero, a small value of the factor $(1 - D)$ would make the P-A comparison quite insensitive to this violation. This is, in fact, just the case in these p-^{3}He and p-^{12}C experiments. From the measurement of $1 - D = 0.05 \pm 0.03$ close to the energy and angle of the p-^{3}He experiment[4] and an estimate of $1 - D \leq 0.06 \pm 0.02$ at the energy and angle of the p-^{13}C experiment, Eq. (5) gives $(P - A) \leq 0.017$ and 0.02, respectively, for a value of the spin-flip asymmetry $\Delta S = 1/3$, which would constitute a clear and substantial violation of TRI. These P − A values are essentially as small as the experimental errors in these P-A comparisons, so no tests of TRI were really made.

It is immediately obvious from this discussion that tests of TRI in elastic scattering, using the P-A equality, should be made through measurements where the spin-flip probability is expected or known to be large. Even better, more stringent and conclusive tests are provided by P-A comparisons in a reaction and its inverse, since the testing of TRI is not then limited to the spin-flip cross sections.

Similarly, it follows that tests of TRI in the basic nucleon-nucleon interaction, via comparisons of P and A in p-p and/or n-p scattering, should be made at energies and angles for which the quantity $(1 - D)$ is maximized. Since spin-exchange forces are well-known components of the nucleon-nucleon interaction, spin-flip probabilities are generally substantial, so there should be little difficulty in satisfying this criterion. For example, in one report[5] that includes both P-A comparisons and measurements of D in p-p scattering at 142 MeV, values of $(1 - D)$ range between 0.7 and 1.2. The $(P - A)$ values are generally consistent with zero within the experimental errors of several percent, although differences of 0.04 to 0.08 are listed. However, as Bryan[6] has noted, the pp system, because of identical-particle symmetry, has reduced sensitivity for the testing of TRI. That is, T asymmetry can only show up in the coupled states of $J^P = 2^-, 4^-$, etc. Then, in a model[6] where the nucleon-nucleon T asymmetry is due to the exchange of the A_1(1070 MeV) meson and is of short range, the angular momentum barrier drastically inhibits the observable effects of TRI violation in the pp system at the energies (up to about 600 MeV) that have been investigated to date.

Now that it is realized that essentially all previous polarization tests of TRI have either been nontests or tests of very limited sensitivity, it is clear that significant tests of this important fundamental postulate should soon be pursued.

References

1. R.J. Blin-Stoyle, Proc. Phys. Soc. A **65**, 452 (1952); G.R. Satchler, Nucl. Phys. **8**, 65 (1958); L.C. Biedenharn, Nucl. Phys. **10**, 620 (1959).
2. D.G. McDonald, W. Haeberli, and L.W. Morrow, Phys. Rev. **133**, B1178 (1964).
3. E.E. Gross et al., Phys. Rev. Lett. **21**, 1476 (1968).
4. W.G. Weitkamp et al., Nucl. Phys. A **311**, 29 (1978).
5. C.F. Hwang et al., Phys. Rev. **119**, 352 (1960).
6. R.A. Bryan, Phys. Rev. C **12**, 1968 (1975).

Deviations from the Polarization-Analyzing Power Equality and Implied Breakdown of Time-Reversal Invariance*

H.E. Conzett, P. von Rossen,† F. Hinterberger,† R.J. Slobodrian,‡ C. Rioux,‡ and R. Roy‡

We are reporting on the first test that compares the polarization (P) and the analyzing power (A) from measurements in a nuclear reaction and its inverse. We find an astonishingly large P − A difference. The clear implication is that time-reversal invariance (TRI) is broken in some component of the nuclear interaction, since the polarization-analyzing power equality follows directly from TRI.[1] Thus, in view of the fundamental position that the P-A theorem has held in spin-polarization physics, both in theory and experiment, we would be very surprised if our results are not viewed with some skepticism.

The reactions chosen for the P-A comparisons were the two-nucleon transfers ^{7}Li(^{3}He,p) ^{9}Be(^{3}He,p) ^{11}B, with 14-MeV incident ^{3}He ions, and their inverses studied at the same CM energies. The Q-values are large, implying considerable mass, energy, and momentum rearrangement. The experiments were initiated by the Laval group through the measurements of the proton polarizations in the (^{3}He,$\vec{p}$) reactions, and results have already been published.[2] The analyzing powers in the inverse ($\vec{p}^{3}$He) reactions were measured at Berkeley. The (^{3}He,$\vec{p}$) proton polarizations were measured with a pair of Si polarimeters, placed at equal left-right reaction angles. The Si polarimeter combines the high scattering efficiency of a thick analyzer with the good energy resolution obtained by adding the ΔE pulse from the analyzer detector to each of the E pulses from the left and right stopping detectors.

In Fig. 1 are shown our P and A measurements in the ^{9}Be(^{3}He,$\vec{p}$) ^{11}B reaction. There is evidence for a decrease in P as the energy bite is increased, which is not unexpected. In any event, the smallest energy bite for the P measurement is nearest to the energy bite sampled in the A measurement (also indicated), and for this we find the largest P − A difference. In Fig. 2 is shown an excitation function of A at 37° lab, which is near the peak of A shown in Fig. 1. Over an energy span of some 800 keV, about 400 keV on either side of our original energy, we find a smooth variation of A. Thus, there are no sharp increases in A that could move its value closer to P with a small shift in the energy. Comparably large P − A differences were found, also, in the ^{7}Li(^{3}He,p) ^{9}Be reaction.

In summary, we have found large differences between P in the ^{7}Li(^{3}He,p) ^{9}Be and ^{9}Be(^{3}He,p) ^{11}B reactions and A in their inverse processes. Since such an inequality between P (in a reaction) and A (in its inverse) directly implies a breakdown of TRI, it follows that this is clear evidence that the interaction of nuclear particles is not time-reversal invariant. Clearly, many more experiments are necessary to explore in detail the TRI-breaking interactions.

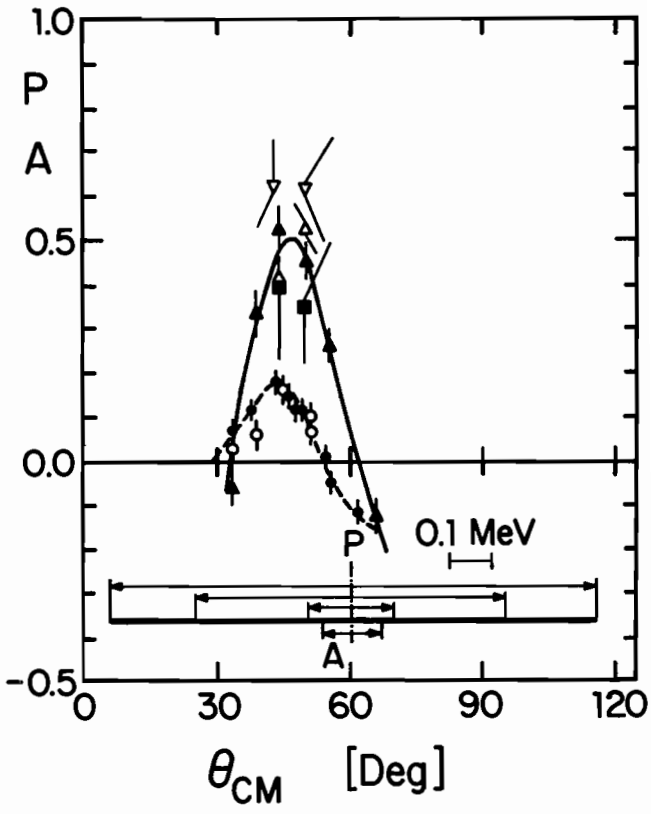

Fig. 1. The open and closed circles represent two separate measurements of A. The solid triangles are the original P results with the intermediate energy bite (due to target thickness and beam energy-width) indicated by an arrow on the energy scale near the bottom of the figure. The open triangles are later checks of the original data. The solid squares are measurements made with a completely independent polarimeter at Berkeley and with the largest energy bite indicated. The inverted open triangles are measurements with the smallest energy bite.

(XBL 807-10786)

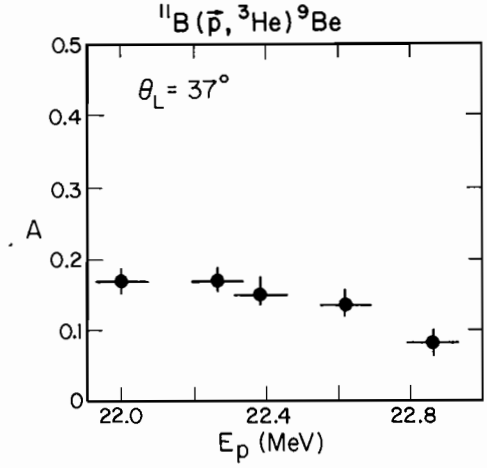

Fig. 2. Excitation function of $A(\theta_L=37°)$ in the ^{9}Be ($\vec{p}$, ^{3}He)^{11}B reaction. (XBL 809-11816)

Footnotes and References

*Condensed from LBL-11576, invited paper, High-Energy Physics with Polarized Beams and Polarized Targets, eds. C. Joseph and J. Soffer, Experientia Suppl. **38** (Birkhäuser Verlag, Basel, 1981), p. 364.

†Institut für Strahlen und Kernphysik, Universität Bonn, D-5300 Bonn, Germany.

‡Laboratoire de Physique Nucléaire, Université Laval, Québec G1K7P4, Canada.

1. R.J. Blin-Stoyle, Proc. Phys. Soc. A **65**, 452 (1952); G.R. Satchler, Nucl. Phys. **8**, 65 (1958); L.C. Biedenharn, Nucl. Phys. **10**, 620 (1959).
2. M. Irshad et al., Nucl. Phys. A **265**, 349 (1976); M. Irshad et al., Nucl. Phys. A **286**, 483 (1977).

Time Reversal and Charge Symmetry Studies in Single Nucleon Transfer Reactions in the A = 5 System*

A.L. Sagle,† F.P. Brady,† J.L. Romero,† B.E. Bonner,‡
N.S.P. King,‡ M.W. McNaughton,‡ and H.E. Conzett

Time-reversal invariance (TRI) and charge symmetry (CS) are such important fundamental postulates in the description of nuclear interactions that any significant test of their experimental consequences should be pursued. Very recent reports of spin-polarization experiments in some nuclear reactions show results which differ substantially from those expected on the basis of TRI and CS, so it is clear that additional tests of these symmetry principles are most appropriate.

Concerning TRI, Slobodrian et al.[1] reported on comparisons of the polarization (P), in the ^{7}Li(^{3}He, $\vec{p}$)^{9}Be and ^{7}Li(^{3}He,$\vec{p}$) ^{11}B reactions, with the analyzing-power (A) in the inverse reactions. Large differences between P and A were found. Since the P-A equality follows directly from TRI,[2] confirmation of this result or corroborative P − A differences in other reactions would, indeed, constitute firm evidence for violation of TRI. Additionally, Conzett[3] has examined all of the previous polarization tests of TRI in nuclear scattering and reactions, and he shows that almost all of them are really nontests of TRI and that the remaining ones are inadequate due either to lack of precision or lack of sensitivity to a violation of TRI. In view of these developments, it is now particularly important that new tests of TRI be made.

With respect to charge symmetry, a similar P_n-A_p equality, which follows from the combination of TRI and CS, has been established in (p,n) transitions between the mirror nuclear states of an isospin doublet.[4] Here, p_n is the neutron polarization in the $(p,\vec{n})$ transition and A_p is the proton analyzing power in the $(\vec{p},n)$ transition with polarized protons. This, however, is not an exact equality since the Coulomb force breaks the charge symmetry. Early $P_n - A_p$ differences were reduced to equalities by later, more precise measurements,[5,6] but surprisingly large differences were found[6] in the ^{15}N(p,n)^{15}O reaction for proton energies in the region of 5 to 9 MeV, where resonance structure is prevalent. Thus, tests of CS in nuclear reactions, as well as TRI, are now of particular interest.

We report here extensive use of the P-A equality in measurements of single nucleon transfer reactions in the mass-5 system. In one set of measurements this theorem is checked by comparing the analyzing power of ^{4}He($\vec{p}$,d)^{3}He with the polarization of ^{3}He(d,$\vec{p}$)^{4}He at equivalent center-of-mass energies and angles. In a second experiment an absolute measurement is made of the neutron polarization in a double scattering experiment with the reactions T(d,$\vec{n}$)^{4}He and ^{4}He($\vec{n}$,d)T. The analyzing powers of the charge-symmetric reactions ^{4}He($\vec{p}$,d)^{3}He and ^{4}He($\vec{n}$,d)T are then compared and found to be in agreement.

In the first experiment the analyzing powers were measured for the reaction ^{4}He($\vec{p}$,d)^{3}He at 32, 40, 50, and 52.5 MeV at the Lawrence Berkeley Laboratory using polarized protons from the 88-Inch Cyclotron. In Fig. 1

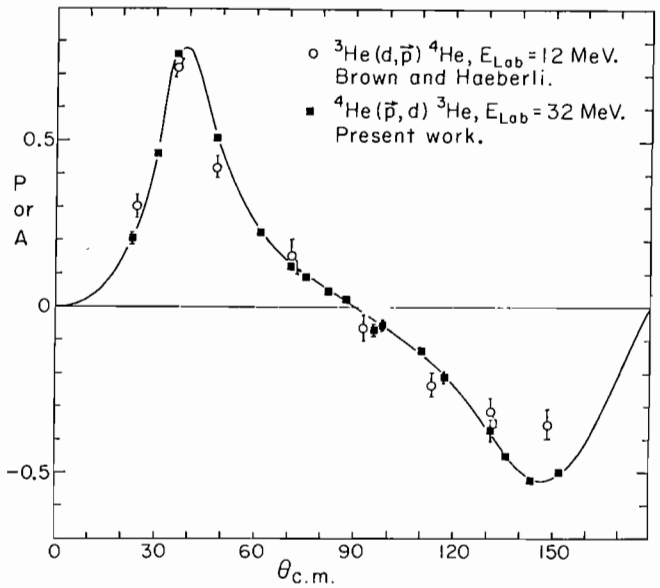

Fig. 1. Analyzing power angular distribution for the ^{4}He($\vec{p}$,d)^{3}He reaction (solid squares) compared with the polarization measurements of the ^{3}He(d,$\vec{p}$)^{4}He reaction[7] at the same (compound nucleus) center-of-mass energy. The plotted data of Ref. 7 do not include an estimated 5 to 10% uncertainty in the analyzing power of their polarimeter. The curve is a Legendre polynomial fit to the ^{4}He ($\vec{p}$,d)^{3}He data. (XBL 819-1782)

we compare the analyzing power for this reaction at E_p = 32 MeV with earlier measurements[7] of the proton polarization in the inverse reaction ^{3}He(d,$\vec{p}$)^{4}He at 12 MeV. These energies are equivalent in the center of mass because of the large reaction Q-value (18.6 MeV). Although there is general agreement between P and A, the datum for ^{3}He(d,$\vec{p}$)^{4}He at $\theta_{c.m.}$ = 140° is higher than the trend of the ^{4}He($\vec{p}$,d)^{3}He data. This disagreement, however, may not be significant because of the large uncertainty in the value of the p-^{12}C analyzing power used by Brown and Haeberli.[7]

In the second experiment an absolute measurement of the polarization was made with the 50 MeV polarized neutron facility at the Crocker Nuclear Laboratory 76-Inch Cyclotron by using a double scattering technique. The polarized neutrons produced at θ_{Lab} = 29.7° from the reaction T(d,$\vec{n}$)^{4}He impinged on a liquid-nitrogen-cooled ^{4}He gas cell. Simultaneous left-right measurements were then made of the deuterons from the reaction ^{4}He($\vec{n}$,d)T at θ_{Lab} = 25° with a pair of plastic scintillation counter telescopes. At these angles, the center-of-mass energies and angles are the same for these inverse reactions and the polarization of the neutrons produced in the first reaction is equal to the neutron analyzing power of the second reaction from the P-A equality. The measured result was $\epsilon = 0.231 \pm 0.015$, and we use this value to extract the analyzing power ($\epsilon = P^2 = A^2$) of 0.480 ± 0.016.

The datum for the analyzing power at θ_{Lab} = 25° is also a measurement of the 50 MeV neutron beam polarization if the P-A equality is valid. We have verified this equality at forward angles and at a lower energy for the charge symmetric reaction ^{3}He(d,$\vec{p}$)^{4}He and its inverse. When we use the absolute measurement of the neutron polarization, the angular distributions for ^{4}He($\vec{n}$,d)T and ^{4}He ($\vec{p}$,d) ^{3}He at 50 MeV agree quite well.

We thus conclude that our set of measurements for these (nucleon,d) reactions are all consistent (within experimental errors) with time-reversal invariance and charge symmetry.

Footnotes and References

*Condensed from LBL-13232.

†Crocker Nuclear Laboratory and Department of Physics, University of California, Davis, CA 95616.
‡Los Alamos National Laboratory, Los Alamos, NM 87545.

1. R.J. Slobodrian, C. Rioux, R. Roy, H.E. Conzett, P. Conzett, P. von Rossen, and F. Hinterberger, preprint; H.E. Conzett, *Polarization Phenomena in Nuclear Physics–1980*, AIP Conf. Proc. No. 69, ed. G.G. Ohlsen et al. (Am. Inst. of Phys., New York, 1981), p. 1422.
2. R.J. Blin-Stoyle, Proc. Phys. Soc. A **65**, 452 (1952); G.R. Satchler, Nucl. Phys. **8**, 65 (1958); L.C. Biedenharn, Nucl. Phys. **10**, 620 (1959).
3. H.E. Conzett, Ref. 1, p. 1452.
4. H.E. Conzett, Phys. Lett. B **51**, 445 (1974); L.G. Arnold, *Proceedings of the Fourth International Symposium on Polarization Phenomena in Nuclear Reactions*, eds. W. Grüebler and V. König, Experientia Suppl. **25** (Birkhäuser Verlag, Basel, 1976), p. 503; Bull. Am. Phys. Soc. **22**, 588 (1977).
5. T.R. Donoghue, et al., Phys. Rev. Lett. **37**, 981 (1976).
6. R.C. Byrd et al. Bull. Am. Phys. Soc. **22**, 587 (1977); R.L. Walter and R.C. Byrd, *The (p,n) Reaction and the Nucleon-Nucleon Force*, ed. C.G. Goodman et al. (Plenum, New York, 1980), p. 469; R.C. Byrd and R.L. Walter, *Polarization Phenomena in Nuclear Physics–1980*, AIP Conf. Proc. No. 69, ed. G.G. Ohlsen et al. (Am. Inst. of Phys., New York, 1981), p. 1475.
7. R.I. Brown and W. Haeberli, Phys. Rev. **130**, 1163 (1963).

Polarization Effects in Light Nuclei*

H.E. Conzett

This article is the rapporteur's report, prepared by the author, of the meeting on Polarization Phenomena in Nuclear Physics, August 11-15, 1980 at Santa Fe, New Mexico. The discussion during the session on Polarization Effects in Light Nuclei was limited to the following topics:

1. The deuteron D-state.
2. The three-nucleon system.
3. Polarization vs analyzing-power in the $^{15}N(p,n)^{15}O$ reaction.

Deuteron D-State

The D-state of the deuteron received the most discussion, probably because there has been a flurry of activity concerning it, both theoretical and experimental, during the past two years. In separate papers, Amado and Friar suggested that the D-state probability, P_D, is not really accessible to experimental determination. At about the same time, Amado, Locher, and Simonius showed that ρ_D, the asymptotic D to S-state ratio of the deuteron wavefunction, was experimentally determinable. This ratio is defined as:

$$\rho_D \equiv [U_2(r)/U_o(r)]_{r=\infty} ,$$

where $U_2(r)$ and $U_o(r)$ are the deuteron D and S-state radial wavefunctions, respectively. Although their first prescription for the determination of ρ_D had to be changed a bit, the method is very clear and direct. First, measure the differential cross section and the tensor analyzing-power component $T_{22}(\theta)$ in elastic $\vec{d}-p$ scattering. Then, construct the function

$$f(z) = k^2\, \sigma(z)\, T_{22}(z)\, (z-z_p)^2/(1-z^2), \qquad (1)$$

where $z = \cos\theta$. Next, extrapolate f(z) to the nucleon exchange pole at $z_p = -(5/4+9B/4E_d)$, with B and E_d the deuteron binding energy and the deuteron lab energy, respectively. Then one deduces ρ_D directly from

$$f(z_p) = -0.0542\rho_D.$$

Since ρ_D must be independent of E_d, the incident deuteron energy, it is important to do the experiment over a range of E_d in order to evaluate the consistency of the extrapolation procedure. The Zurich group reported very consistent results from measurements at ten energies between $E_d = 5$ and 45.4 MeV. Their final result is

$$\rho_D = 0.0259 \pm 0.0007, \qquad (3)$$

where the error includes both statistical and data-normalization uncertainties. This value is in excellent agreement with the earlier Berkeley result

$$\rho_D = 0.0263 \pm 0.0013. \qquad (4)$$

In a completely different experiment, the Wisconsin group have determined ρ_D from measurements of the tensor analyzing powers in the $^{208}Pb(\vec{d},p)^{209}Pb$ stripping reaction at sub-Coulomb energies. In the DWBA calculations these analyzing powers scale directly with ρ_D, and the calculated fits to these data have yielded

$$\rho_D = 0.02649 \pm 0.00043 \qquad (5)$$

at their latest value. This is some 14% larger than their original (1975) value, and I assume that data taken at lower energies and more complete DWBA calculations are responsible for the change. Clearly, Eqs. (3) (4) and (5) are in complete agreement. I would, however, caution that once the experimental uncertainties are reduced to the level of (3) and (5), one must be concerned with the "theoretical" uncertainties of the extrapolation procedure, on one hand, and of the DWBA calculation, on the other.

Three-Nucleon System

The discussion of the three-nucleon system centered on the present state of agreement or disagreement between experimental results and results calculated with the Faddeev equations (principally by Doleschall). Recent measurements of deuteron break-up cross sections in the $^2H(p,2p)n$ reaction at 26 MeV were reproduced very well by the calculations. Doleschall discussed the major outstanding disagreement in elastic nucleon-deuteron scattering. The cross sections and the nucleon and deuteron analyzing powers have been measured at several energies up to $E_N = 23$ MeV. The major discrepancy between experiment and theory is found with the nucleon analyzing power $A_y(\theta,E)$. Above $E_N = 10$ MeV there is a clear and increasing difference with increased energy, which certainly cannot be repaired by including the Coulomb interaction in the calculations. The usual concern is that not enough NN partial waves are included, but a calculation which included F-waves gave essentially the same result for $A_y(\theta)$ as the calculation which omitted them. All is not lost, however, since the $^3P_{0,1,2}$ waves and the $^3S_1$-$^3D_1$ mixing parameter ϵ_1 are still not firmly pinned down by the lower energy NN scattering data. In fact, high precision $\vec{p}p$ analyzing power data reported here are not fitted by the most up-to-date NN potentials. Some adjustment of the ^3P-waves is very likely necessary and it is known that

the $\vec{N}d$ $A_y(\theta)$ is quite sensitive to these. So, between that and ϵ_1 there may still be enough flexibility to bring experiment and calculation into agreement for the $\vec{N}d$ analyzing powers.

P-A in $^{15}N(p,n)\,^{15}O$

There was a brief discussion of the polarization vs analyzing power in the $^{15}N(p,n)^{15}0$ reaction, specifically

P_n in $^{15}N(p,\vec{n})^{15}O$

and

A_p in $^{15}N(\vec{p},n)^{15}O$.

Their difference is given by

$$P - A = (\sigma^{-+} - \sigma^{+-})/\sigma,$$

with σ^{-+} the cross section for the nucleon transverse spin flip from down to up and σ the unpolarized cross section. Since $P - A = 0$ follows from time-reversal invariance *and* charge symmetry, the large $P - A$ differences found in this reaction for $E_p \simeq 5$ to 9 MeV were quite unexpected and exciting. As was detailed in Philpott's talk earlier in this conference, these differences are very nicely explained qualitatively via microscopic shell-model calculations which include the necessary non-central nucleon-nucleon interaction and isospin mixing. It is noteworthy that almost 25 years ago Wilkinson selected this $^{15}N(p,n)^{15}O$ reaction as a prime candidate for isospin mixing at the excitation energies spanned in this experiment. Even though *either* time-reversal violation or charge-symmetry breaking could lead to $P - A \neq 0$, in view of the very satisfying explanation in terms of isospin mixing I would be the last person at this conference to even suggest that time-reversal violation might, also, be involved.

Footnote

*Condensed from Rapporteur's Report in *Polarization Phenomena in Nuclear Physics–1980*, eds. G.G. Ohlsen et al., AIP Conf. Proc. No. 69 (American Institute of Physics, New York, 1981).

Search for Effect of Longitudinally Polarized Protons on Optically Active Amino Acids*

R.M. Lemmon, H.E. Conzett, and W.A. Bonner†

Many efforts have been made[1] to find an experimental demonstration of the hypothesis of Vester and Ulbricht.[2] To explain the fact that protein amino acids are (with some minor exceptions in bacteria) entirely formed from the L-optical isomers, this hypothesis postulates that the excess of "anti-parallel" polarized beta particles from natural radionuclides, i.e., parity violation, gave a slight preference for the genesis of L-amino acids over D-amino acids on the prebiological Earth. This preference would arise from the betas' interactions in such a way as to selectively favor the formation of L-amino and/or promote the selective decomposition of D-amino acid.

Experimental work on the Vester-Ulbricht (V-U) hypothesis has included studies on a great variety of optically active organic compounds that have been irradiated with betas[3] and positrons[4] from radionuclides and with accelerated, polarized electrons[5] and muons.[6] The results have been mixed, but it can be said at once that no report of a claimed selective optical isomer-polarized particle interaction has been successfully duplicated in another laboratory. The V-U hypothesis is still considered a reasonable one, but, without doubt, it still lacks reproducible experimental confirmation.

Another promising approach to test the V-U hypothesis is through the use of polarized protons. Such protons are available with the equipment recently installed on the Lawrence Berkeley Laboratory's sector-focused 88-Inch Cyclotron. The polarized beam from the cyclotron has its spin-polarization axis aligned along the cyclotron magnetic field direction (vertical). The external beam first passes along the axis of a solenoid magnetic field, which precesses the spin direction through 90° into the horizontal plane, although still transverse to the beam direction. A dipole magnet than bends the beam through an angle of 47.7°, and, at the same time, precesses the spin axis into the beam direction. Thus, the vertical polarization (up or down) of the proton beam from the cyclotron is converted to longitudinal polarization (positive is in the direction of the beam's propagation, and negative is in the reverse direction). The beams incident upon the samples were typically of about 10 MeV and were limited to 10-14 nanoamps. The degree of polarization for both proton spin directions was approximately 80%.

We have carried out six irradiations with polarized protons. Each irradiation was done on a pair of DL-leucine disks, each about 1 cm in diameter, about 0.1 cm thick, and weighing 110-130 mg. Leucine was the amino acid of choice because it gives an excellent separation of its D- and L-optical isomers on the optically active gas chromatographic column. The analyses of the irradiated samples are shown in Table 1.

Table 1. Percent of optical isomers remaining in DL-leucine irradiated with longitudinally polarized protons.

Expt.	Beam[a]	% D	% L	(+)[f]
1	A	50.12	49.88	--
	PT	49.99	50.01	--
2	A	50.14[b]	49.86[b]	0.04
	PT	50.01[c]	49.99[c]	0.13
3	A	50.11	49.89	--
	PT	50.12	49.88	--
4	A	50.20[b]	49.80[b]	0.11
	PT	50.20[d]	49.80[d]	0.14
5	A	49.98[d]	50.02[d]	0.11
	PT	49.96[d]	50.04[d]	0.15
6	A	50.23[e]	49.77[e]	0.19
	PT	50.12[d]	49.88[d]	0.06

[a]A=beam absorbed in sample;
PT=beam passed through sample.
[b]Average of 2 GLC analyses.
[c]Average of 4 GLC analyses.
[d]Average of 3 GLC analyses.
[e]Average of 7 GLC analyses.
[f]Standard deviation of replicate analyses.

It is apparent from Table 1 that we have not detected any asymmetric degradation of DL-leucine with longitudinally polarized protons, even at 50% gross degradation.

Footnotes and References

*Condensed from LBL-12243; Origins of Life, in press.
†Department of Chemistry, Stanford University, Stanford, CA 94305.

1. D.C. Walker, ed., Origins of Optical Activity in Nature. Elsevier, Amsterdam, 1979.
2. T.L.V. Ulbricht and F. Vester, Tet. **18**, 629 (1962).
3. W.A. Bonner and R.M. Lemmon, Bioorg. Chem. **7**, 175-187 (1978).
4. Y.C. Jean and H.J. Ache, J. Phys. Chem. **81**, 1157 (1977).
5. W.A. Bonner et al., Israel J. Chem. **15**, 89 (1976/77); L.A. Hodge et al., Nature **280**, 250 (1979).
6. R.M. Lemmon et al. Nature **252**, 692 (1974).

4. Nuclear Data Sheet Evaluation

Nuclear Data Sheets for A = 169 and A = 193

V.S. Shirley

Data pertaining to the levels of all nuclei with mass A = 169, as populated both by radioactive decay and in nuclear reactions, were evaluated for publication.[1] First, individual level schemes were compiled for each decay mode or reaction for each nucleus. Then a summary set of "adopted" level properties, including best energies, half-life values, nuclear moments, spin-parity assignments, modes of deexcitation, and relationships to expectations from theory, was derived for each nucleus.

The evaluation/compilation process was straightforward and manageable for all of the A = 169 nuclei except for ^{169}Yb. With 60 levels and 400 γ rays involved in the ^{169}Yb levels populated in ^{169}Lu decay, and slightly fewer, but many overlapping, levels and γ rays involved in the population by thermal neutron capture, the ^{169}Yb evaluation process was overwhelmingly complex. Physics and mathematics computer programs, designed to aid in the evaluation process, made it possible to sort out the data and arrive at a more complete level scheme for each mode of population than was possible in a study of either mode alone. For example, γ-ray branchings from levels weakly populated in ^{169}Lu decay could be deduced from the data for the same, more strongly populated levels in thermal neutron capture, and vice versa. The resulting level properties summarized in the "adopted" levels for ^{169}Yb were as consistent and complete as the data allowed.

Data for A = 193 were similarly evaluated and prepared for publication.[2] Unlike the case with A = 169, though, the evaluation of the A = 193 data was straightforward for every A = 193 nucleus.

References

1. V.S. Shirley, Nuclear Data Sheets, submitted for publication, 1981.
2. V.S. Shirley, Nuclear Data Sheets, accepted for publication, 1981.

Nuclear Data Sheets for A = 187 and A = 185

*Y.A. Ellis-Akovali**

The available experimental data pertaining to the structure of nuclei with mass numbers A = 187 and A = 185 (Refs. 1 and 2 respectively) have been evaluated. The best data for decays and reactions, as well as the adopted properties of levels and gammas deexciting the levels in each nucleus are presented. Inconsistencies, discrepancies, and areas which need further study are noted. Arguments for adopted spin, parity and configuration assignments are also included.

Footnote and References

*Nuclear Data Project, Oak Ridge National Laboratory, Oak Ridge, TN 37830.

1. Y.A. Ellis-Akovali, Nuclear Data Sheets, submitted for publication, 1981.
2. Y.A. Ellis-Akovali, Nuclear Data Sheets, accepted for publication, 1981.

Nuclear Data Sheets for A = 189

R.B. Firestone

Radioactive decay and reaction data for nuclei with mass A = 189 have been evaluated. All data published through September 1980 were covered. Some outstanding discrepancies in the literature were resolved, and new information has been inferred.

For ^{189}W β^--decay, the available γ-ray data were combined with ^{189}Re reaction data to produce the first partial level scheme from that decay. Data for ^{189}Os levels were compiled with only minor revisions, except for the level at 233.53 keV; this level was previously assigned spin 5/2− but is more consistent with spin 3/2− due to an apparent M1 + E2 γ-ray feeding a level of known spin 1/2−. The levels of ^{189}Ir still suffer from considerable ambiguity due to conflicting results in the literature, especially for reaction γ-ray data. Some γ rays were placed without proper regard for intensity balances. The level at 2332.3 keV was originally suggested as 25/2+ and 27/2− by separate authors.[1,2] Re-analysis of the delayed γ-ray intensity data[1] in this evaluation allowed unambiguous determination of the critical conversion coefficients for γ rays deexciting that level. Transitions from the 2332.3-keV level were determined to feed levels of 23/2+ by E1, 23/2− by M1, and 21/2+ by M2 multipolarity. Thus, a new spin 25/2− was adopted in disagreement with the previous authors (Refs. 1 and 2).

Decay data for ^{189}Pt were less ambiguous but incomplete. It was necessary to estimate some γ-ray intensities on the basis of published spectra because values were not reported. Also, numerous multiple γ-ray assignments in the decay data were eliminated. ^{189}Au decay data were too incomplete to calculate logft values for the decay scheme. The reaction γ-ray data were not entirely consistent between authors, and discrepancies in the ordering of a rotational band built on the 440 ns isomer at 2678.1 keV could not be resolved. The relative intensities of a critical unresolved γ-ray doublet at 198.6 keV were determined in this evaluation from the associated γ-ray intensity balances from the level scheme. Only minimal data exist for levels in ^{189}Hg, ^{189}Tl, ^{189}Pb, and ^{189}Bi.

The status of data for mass A = 189 remains inadequate. Insufficient and conflicting results abound for these data, and most A = 189 nuclei are still poorly characterized. The unavailability of convenient targets for production of most of these nuclei has retarded interest in producing them by light-ion reactions, but with heavier beams becoming available, mass A = 189 should deserve further interest.

References

1. P. Kemnitz et al., Nucl. Phys. A **245**, 221 (1975).
2. S. Andre et al., Nucl. Phys. A **243**, 229 (1975).

Nuclear Data Sheets for A = 188*

B. Singh† and D. Viggars‡

Experimental data pertaining to the nuclear structure and decay of all nuclei with mass number A = 188 have been evaluated. Level schemes from radioactive decay and reaction studies are presented for each nucleus. An adopted level scheme is also included for each nucleus; it contains both adopted level and gamma properties.

Footnotes

*B. Singh and D. Viggars, Nuclear Data Sheets, accepted for publication, 1981.

†Kuwait Institute for Scientific Research, Shuwaik, Kuwait.
‡Physics Department, Kuwait University, Shuwaik, Kuwait.

Nuclear Data Sheets for A = 191

E. Browne

Experimental data for all nuclei with mass number A = 191 have been compiled and evaluated from over 170 reference papers. Level schemes from radioactive decay and reaction work, as well as other adopted nuclear properties, have been included. The literature cut-off date is September 1979.[1]

A serious inconsistency in the level scheme of ^{191}Pt from the electron-capture decay of ^{191}Au led the evaluator to reinterpret the experimental data given in Ref. 2. Figure 1 shows some low-lying levels and connecting transitions in ^{191}Pt from Ref. 3. The predominantly E1 multipolarity assigned to the 24.39 keV transition in Ref. 2 on the basis of the conversion-electron subshell ratios $L_1/L_2 = 1.7 \pm 0.4$ and $L_2/L_3 = 0.65 \pm 0.15$ is not consistent with the placement of this transition between two even-parity states as suggested in Ref. 3. However, it is evident that, because of the extremely large values for the E2 conversion coefficients $\alpha(L_2)$ and $\alpha(L_3)$ (1390 and 1630 respectively) compared to M1 (5.4 and 0.59 respectively), the subshell ratio L_2/L_3 for an M1 + E2 transition is not sensitive to the amount of E2 (above 2%) mixed with M1. The experimental subshell ratio $L_2/L_3 = 0.65 \pm 0.15$ is essentially consistent within two standard deviations with the value of 1.0 expected from the L_1/L_2 experimental subshell ratio for an M1 + 2%E2 transition. This multipolarity is consistent with the placement of the 24.39 keV transition on the level scheme given in Ref. 3.

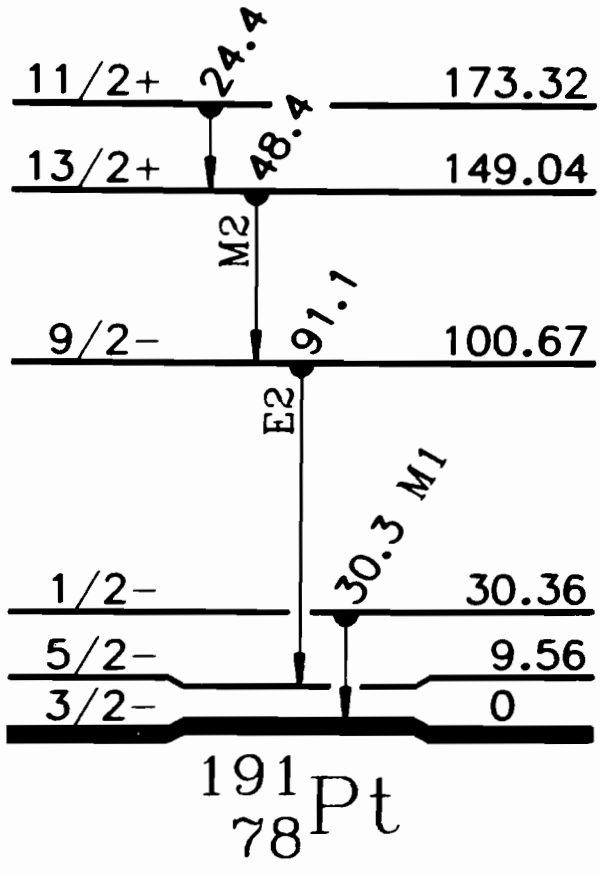

Fig. 1. Some low-lying ^{191}Pt levels from level scheme reported in Ref. 3. (XBL 818-11273)

Another inconsistency is shown in Table 1, where the experimental conversion coefficients of the 30.27- and 87.55-keV transitions in Ref. 3 are in total disagreement with the theoretical ones[4] calculated on the basis of the assigned multipolarities. Either the photon intensities or the conversion-electron intensities, or both, are incorrect for these transitions. The intensity balance through the 149 keV ($J\pi = 13/2+$) level calculated using the electron intensities given in Ref. 2 for the 24.27- and 48.37-keV transitions shows essentially no electron-capture population to this level. This indicates that the electron intensities for these low-energy transitions are correct. Therefore, the electron intensities of the 30.27- and 87.5-keV transitions were assumed to be correct, and their photon intensities recalculated using theoretical conversion coefficients.[4] A new measurement of these photon intensities to confirm this interpretation would be very useful.

Table 1. Comparison of Experimental and Theoretical L-Conversion Coefficients in ^{191}Pt.

Energy[a] (keV)	Exp. L-conv.[a] coeff.	Theor. L-conv.[b] coeff.	Multipolarity assigned in Ref. 3
30.27	1.7	31(M1)	M1
87.55	0.52	1.4(M1) 5.9(E2)	M1/E2

[a]From Ref. 3.

[b]From Ref. 4.

References

1. E. Browne, Nucl. Data Sheets **30**, 653 (1980).
2. A. Johansson et al., Nucl. Phys. A **98**, 278 (1967).
3. M. Piiparinen et al., Nucl. Phys. A **265**, 253 (1976).
4. R.S. Hager and E.C. Seltzer, Nucl. Data A **4**, 1 (1968).

Evaluation of Nuclear Structure and Decay Data

C. Michael Lederer

^{190}Os has been restudied recently via the reaction ^{189}Os(n,γ)[1] and by Coulomb excitation with heavy ions.[2] A summary diagram for this much-studied nucleus is shown as Fig. 1. The format of this diagram, prepared for use by the author, has several advantages over the ladder diagrams used for publication in the Nuclear Data Sheets. It shows explicitly which adopted level or levels correspond to a level observed in a particular reaction or decay scheme. It also shows the known γ-decay branches of the levels in an abbreviated form.

A recent finding[3] of some interest is the small magnitude and negative sign of the g-factor of the 24.1-ns isomer in ^{190}Hg (Fig. 2). The measured value, $g = -0.21 \pm 0.02$, supports the assignment of the isomer as a member of the $(\nu i_{13/2})^2$ band, whereas the 2596.8-keV (10^+) state, previously assumed to be the isomeric state, had been assigned the configuration $(\pi h_{11/2})^2$ in order to explain its hindered γ decay.[4,5] An $h_{11/2}$ assignment for the isomer is inconsistent with the measured g-factor. It is thought that the isomer lies above the 10^+ state and decays to it by a low-energy, unobserved transition; further measurements to confirm and clarify this point are recommended.

Footnote and References

*To be published in Nuclear Data Sheets (1981).

1. R.F. Casten et al., Nucl. Phys. A **316**, 61 (1979).
2. Douglas Cline, private communication (October 1980); C.Y. Wu et al. Bull. Am. Phys. Soc. **25**, 605, KF12 (1980).
3. S.A. Hjorth et al., Phys. Rev. Lett. **45**, 878 (1980).
4. R.M. Lieder et al., Nucl. Phys. A **248**, 317 (1975).
5. T. Inamura et al., J. Phys. Soc. (Japan) **32**, 1163 (1972).

Level energies are adopted values that take into account measurements of the decay of the ^{190}Tl isomers also. It is not known whether the 3015.8-keV state decays to the 2596.8 keV state (as shown), or to the 24.1-ns isomeric state.

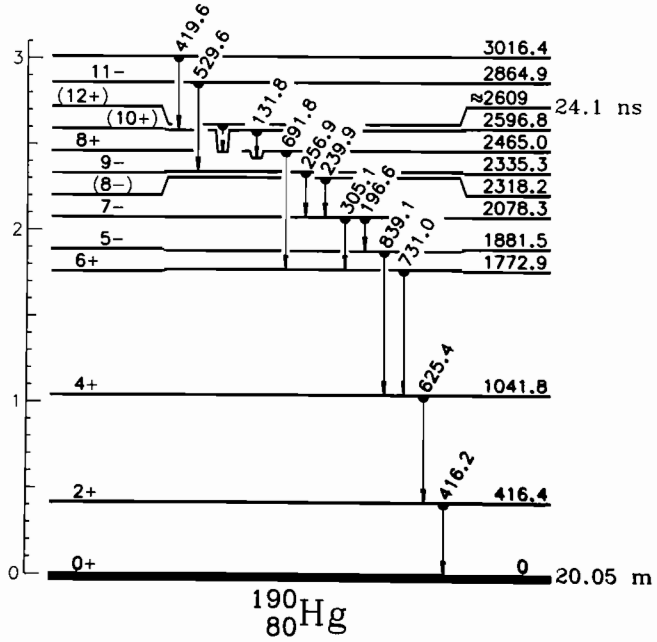

Fig. 2. Levels of ^{190}Hg observed in (heavy ion, xnγ) reactions. A recent measurement of the g-factor of the 24.1-ns state supports the assignment of a $(\nu i_{13/2})^2$ configuration to the isomer, in contrast to previous interpretations, and requires the assumption of a low-energy, unobserved transition from the isomer. (XBL 827-888)

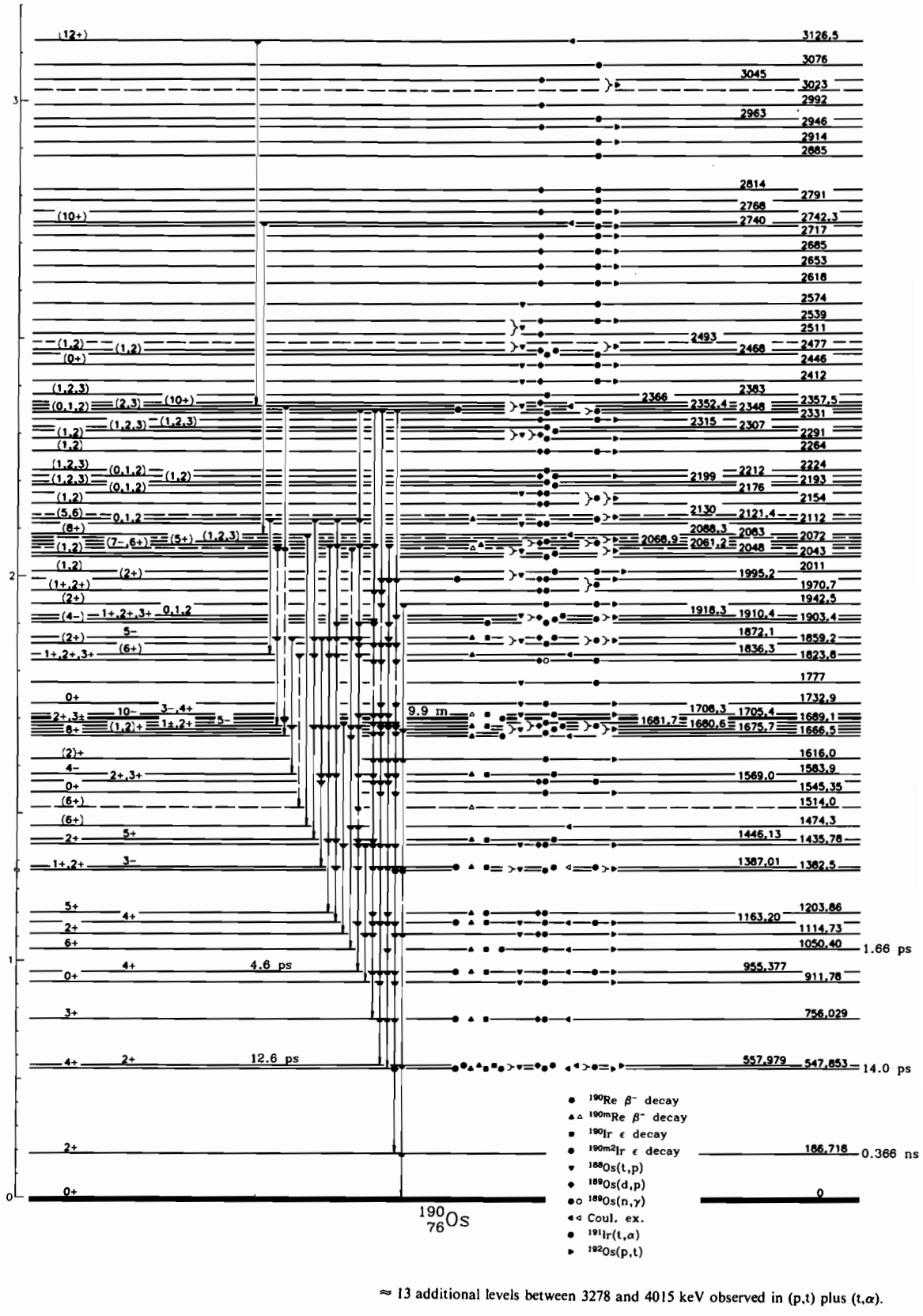

Fig. 1. Adopted levels of ^{190}Os, showing which decay parents and nuclear reactions populate each of the levels. (All parents and reactions also populate the ground and first excited states.)

(XBL 8111-12546)

B. NUCLEAR REACTION MECHANISMS WITH NONRELATIVISTIC HEAVY IONS

1. Charged Particle Emission

Alpha Particle Emission from Two Reactions Involving Very Heavy Ions

L.G. Sobotka, R.J. McDonald, G.J. Wozniak, D.J. Morrissey, A.J. Pacheco, and L.G. Moretto

There is some question as to whether light particle emission associated with deep inelastic processes in heavy ion reactions can be explained by evaporation from the fully accelerated fragments[1,2] or if some pre-scission[3] or nonevaporative mechanism is present. We have attempted to answer this question for two near symmetric heavy systems: $^{nat}Ag + {}^{84}Kr$ (664 MeV) and $^{181}Ta + {}^{165}Ho$ (1354 MeV). By using coincidence techniques (heavy ion-light particle) involving five light-particle telescopes, we have measured coincidence light particle energy spectra over a large range of angles.

In order to address the question stated above, one can plot a vector diagram for the reaction and superimpose the extracted root mean square velocity, $\langle V^2\rangle^{1/2}$, for the α-particles. This has been done in Figs. 1 and 2 where we have plotted the $\langle V^2\rangle^{1/2}$ for the detected projectile-like fragment (gated on the DI events), the calculated velocity of the undetected fragment, and the measured velocity of the α-particles. The full rings indicate the loci of expected α-particle velocities from three different rest frames.

One can clearly see from Fig. 1 that the trend in the data does not agree with evaporation from a source moving with the system center-of-mass velocity. On the other hand, the data follow the prediction for evaporation from the target-like fragment quite well. The systematic overprediction of $\langle V^2\rangle^{1/2}$ is probably due to an overestimate of the Coulomb barrier. Additional support for fragment emission is seen in the energy spectra at the most forward angles, which show two distinct peaks. The associated $\langle V^2\rangle^{1/2}$ for both peaks clearly show that the lower energy peak corresponds to evaporation from the projectile-like fragment, while the higher energy peak is due to evaporation from the target-like fragment.

The same conclusion—that the bulk of the α-particles can be explained by evaporation from the target-like fragment—is reached after examining the data for the

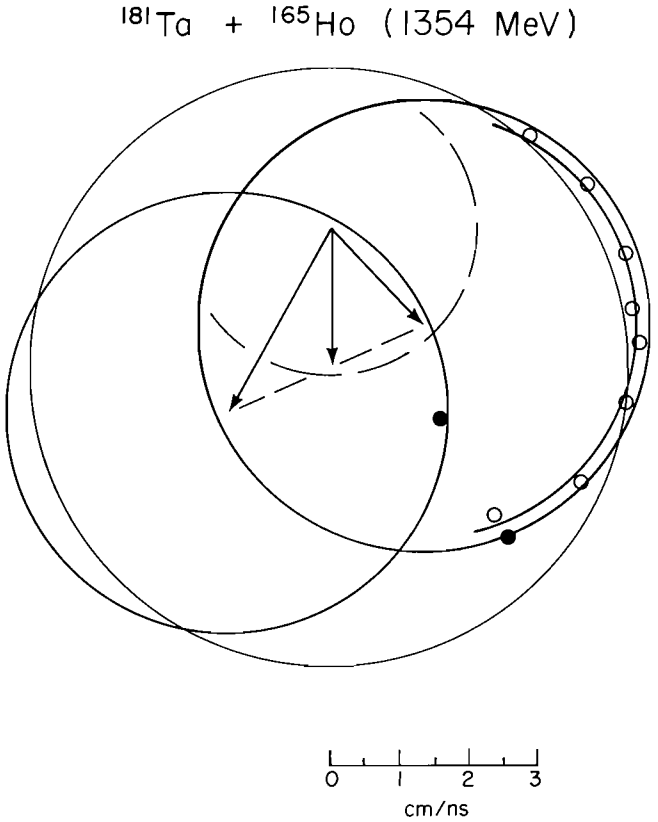

Fig. 1. Velocity diagram for the $^{181}Ta + {}^{165}Ho$ (1354 MeV) system. Open circles are velocities extracted from α-particle energy spectra. Solid circles indicate velocities of the two separate peaks in the most forward data. Large full rings indicate loci of expected α-particle velocities from the three different rest frames. For target-like fragment, locus of velocities for a 10% reduction in expected average emission energy is indicated by a partial ring. Detection threshold is shown as a dashed arc.

(XBL 818-2452)

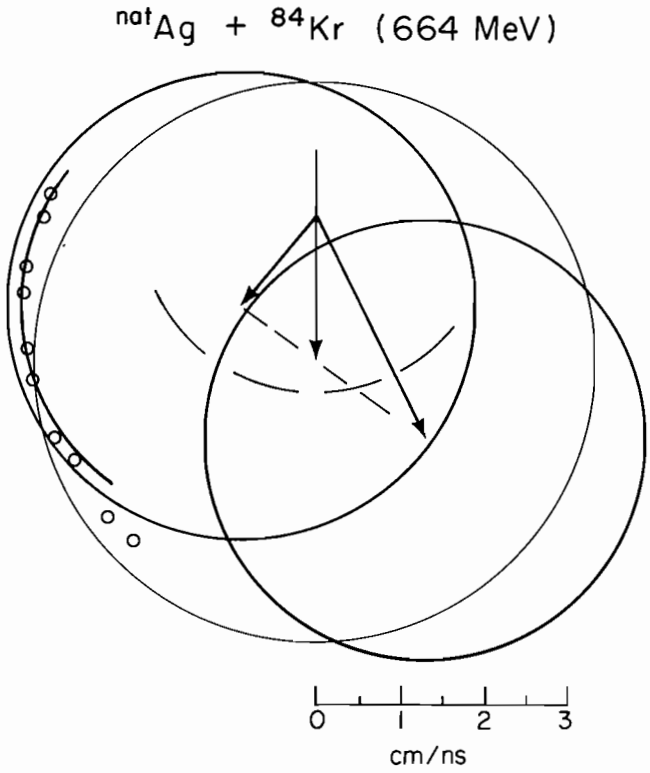

Fig. 2. Velocity diagram for the $^{nat}Ag + ^{84}Kr$ (664 MeV) system; symbols same as Fig. 1.
(XBL 818-2451)

$^{nat}Ag + ^{84}Kr$ system shown in Fig. 2. Again, the trend of the data, except for the two most forward points, agrees with expectations for evaporation from the target-like fragment. The energy spectra for these angles exhibit a high-energy component that is not explained by evaporation from either fragment. The claim of fragment evaporation is further supported by the lack of an angular dependence of the spectral shape when examined in the rest frame of the target recoil.

References

1. R. Babinet et al., Z. Physik A **295**, 153 (1980).
2. L.G. Sobotka et al., Phys. Rev. Lett. **46**, 887 (1981).
3. D. Logan et al., Phys. Rev. C **22**, 1080 (1980).

Energy Equilibration in Composite Nuclei at High Energy and Spin: Correlations between Evaporative ^{1}H, ^{4}He and Fission

M.F. Rivet, D. Logan,† J.M. Alexander,* E. Duek,* M.S. Zisman, and M. Kaplan†*

Studies[1] have recently indicated that the dominant emission source of light charged particles in 200 to 340 MeV ^{40}Ar induced reactions with ^{116}Sn, ^{164}Dy, and ^{197}Au is from the composites prior to scission. The arguments that led to this conclusion were based on the following observations:

1. The measured singles spectra were much narrower than those expected of evaporation from the thermally equilibrated fission fragments.

2. Similarly, the measured coincidence spectra for both in- and out-of-plane correlations with fission were quite different in shape, and moreover did not follow the trend in angular distribution expected for fission parentage. Here, as in the above case, the comparisons were made with simulated spectra generated by Monte Carlo calculations.

3. The observed ratio of proton to alpha multiplicities suggested much larger than expected spins for fission parentage. (The measured values of ℓ_{crit} along with the sticking model allow a first-order estimation of the maximum spin for fission.)

4. The backward angle singles energy spectra in the center-of-mass system indicated emission barriers and temperatures consistent with evaporation from a thermally equilibrated composite.

In the present work, we have extended these measurements by recording the backward angle out-of-plane correlations between fission and ^{1}H and ^{4}He for the systems of 340 MeV Ar + Sn, Sm and Au. It has been shown[2] that these correlations may be expected to follow a distribution that goes as $\exp(\beta_2 \sin^2\phi^*_{cm})$ where ϕ^*_{cm} is the angle with respect to the spin vector of the emitter. For our systems, we have assumed emission from the composites and also that their spin vectors are well approximated by the normal to the plane determined by the fission detector and the beam axis.

The above formalism has been extended[3] to allow an iterative procedure between the back angle singles spectra and the measured β_2 parameter to infer some properties of the composites. However, this procedure has merit only to the extent that the out-of-plane correlations, when integrated over light-particle and heavy-particle space, agree with the measured singles symmetric cross sections. This comparison is indicated in Fig. 1 for alphas in the systems of Ar + Sm and Ar + Au. On the top are shown the center-of-mass singles angular distributions, the fits to the component symmetric about 90° c.m. (solid lines), and the inferred cross sections σ_{evap}. The out-of-plane correlations are shown on the bottom for each system, with the two coincidence geometries shown as insets. Indicated are the appropriate β_2 values as well as the predicted total cross sections in coincidence with fission, σ_{coinc}. As may be evident, σ_{coinc} agrees very well with σ_{evap} for the Au system and is approximately 80% for the Sm system. For the latter case, the small discrepancy is apparently due to evaporation from the composites that survive fission. Thus, for the Au system and, with slightly less confidence, the Sm system, the procedure alluded to above may be used to infer some properties of the composites. This was not the case for the Sn system, where only 20% of the singles events were found to be in coincidence with fission.

The results of this analysis allow first-order estimates of the barrier to emission B, the temperature T', the level parameter A/a, and the root mean square spin J_{rms}. These are shown in Table 1 for alphas and protons for the indicated systems. Also entered in this table are the average center-of-mass energy in singles $<<\epsilon>>$, the expected emission barriers from fusion systematics,[4] and the measured singles cross sections, $\sigma_{singles}$, for the symmetric (about 90° c.m.) components. The sharp cutoff angular momenta implied by the measured cross sections for evaporation residues and fusion are shown as ℓ_{ER} and ℓ_{crit}

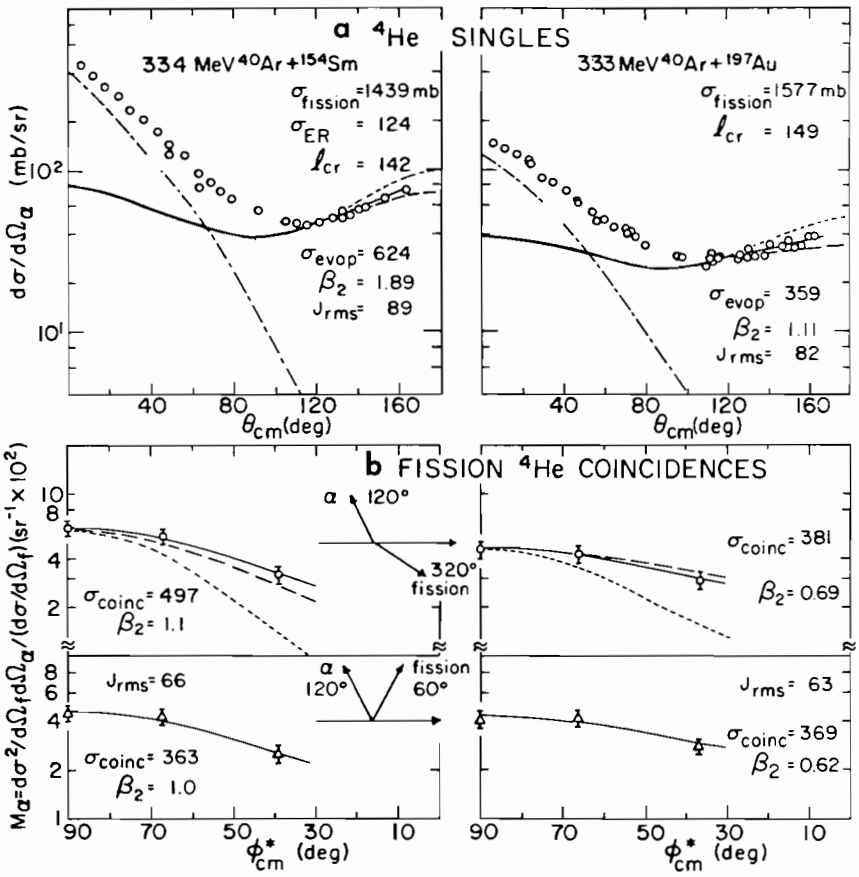

Fig. 1. (a) Measured angular distributions for ^{4}He (points) in the singles mode from Ref. 1. The decomposition into evaporative and direct components is shown: solid line shows least squares fit of Eq. (12) of Ref. 3; dot-dash line shows difference between data points and solid line. Also given are the related cross sections, ℓ_{crit}, β_2 and J_{rms} values as taken from the singles data (see Ref. 1). Long and short dashed curves were drawn from Eq. (12) of Ref. 3 to indicate minimum and maximum acceptable anisotropies. (b) Out-of-plane correlations are shown from this work with solid lines indicating least-squares fits to Eq. (6) of Ref. 3. Also shown are the resulting values of β_2 and the corresponding integrated coincidence cross sections σ_{coinc}. Long and short dashed curves were drawn from Eq. (6) of Ref. 3 with minimum and maximum values of β_2 considered acceptable for the singles data as shown above. (XBL 818-11284)

Table 1. Quantities derived from singles and coincidence data for reactions of 333 MeV ^{40}Ar + X.

	^{197}Au		^{154}Sm		^{116}Sn	
	^{4}He	^{1}H	^{4}He	^{1}H	^{4}He	^{1}H
Results from studies in singles mode						
T (MeV)[a]	2.54(+-.1	2.06±0.1	2.63±0.10	2.30±0.15	3.22±0.15	2.44±0.08
A/a (MeV)[b]	9.75	6.4	7.1	5.4	8.7	5.0
$<<\epsilon>>$ (MeV)	24.0±0.3	12.3±0.3	22.1±0.1	11.8±0.1	21.4±0.3	10.8±0.1
B (MeV)[c]	17.4±0.4	7.3±0.2	14.7±0.1	6.2±0.3	11.1±1.3	5.4±0.1
B_{fusion} (MeV)[d]	22.35	12.0	19.2	10.4	17.14	9.35
β_2[e]	1.11±0.58	0.98±0.69	1.89±0.55	0.78±0.39	1.70±0.70	0.95±0.82
J_{rms}[f,g]	82	140	89	115	66	100
σ_{coinc}(mb)[f,g]	252	145	287	348	232	356
$\sigma_{singles}$(mb)[g]	359±54	386±58	624±94	703±106	1158±174	1697±254
ℓ_{ER}[g]	0		39		68	
ℓ_{crit}[g]	149		142		112	
Results from coincidence studies						
$\theta_G = 60°$ $\theta_S = 120°$						
β_2[h]	0.62±0.11	0.09±0.07	1.0±0.1	0.26±0.13	0.6±0.6	0.57±0.16
J_{rms}[i]	61	42	65	66	39	77
σ_{coinc}[i]	369	351	363	400	117	368
$\theta_G = 320°$ $\theta_S = 120°$						
β_2[h]	0.69±0.07	0.11±0.11	1.1±0.1	0.22±0.12	2.3±0.2	0.30±0.15
J_{rms}[i]	65	47	68	61	77	56
σ_{coinc}[i]	381	363	497	447	194	393

[a]From Eq. 1 of Ref. 3.

[b]From Eqs. 13, 14 of Ref. 3.

[c]From $<<\epsilon>>$, Eqs. 9-11 and β_2 from fits of Eq. 6 (see Ref. 3) to the coincidence data.

[d]From Ref. 4.

[e]From fit of Eq. 12 (Ref. 3) to singles data.

[f]From β_2 for singles data (e above).

[g]From Ref. 1.

[h]From fits of Eq. 6 (Ref. 3) to the coincidence data.

[i]From β_2 for coincidence data (h above).

respectively. Under the section labeled coincidence studies are shown the measured β_2 values, the portion of the singles cross sections in coincidence with fission, σ_{coinc}, and the inferred values of J_{rms}.

The values of the temperatures and the level density parameters are in agreement with those found in lighter, less energetic systems. However, the inferred emission barriers we find are of the order of 20-30% lower than expected from fusion systematics,[4] implying that some deformation may exist for these composites prior to emission. The values of J_{rms} deduced are of the order of 60-70 $\hbar$. This is surprising in that, for composites of such high excitation energy and spin, models such as the rotating liquid drop[5] suggest that first step de-excitation should be dominated by fission because of the near-zero fission barriers. Overall, we are led to conclude that these composites are characterized by quite large multiplicities for equilibrated alpha and proton emission. We further conclude that the competition between light charged particle emission and fission is not completely governed by the phase space equilibrium statistical mode.

Footnotes and References

*State University of New York at Stony Brook, Stony Brook, NY 11794.
†Carnegie-Mellon University, Pittsburgh, PA 15213.

1. D. Logan et al., Phys. Rev. C **22**, 1080 (1980).
2. T. Doessing (unpublished).
3. M.F. Rivet, D. Logan, J.M. Alexander, E. Duek, M.S. Zisman, and M. Kaplan (submitted to Phys. Rev.).
4. M.A. McMahan and J.M. Alexander, Phys. Rev. C **21**, 1261 (1980).
5. S. Cohen, F. Plasil and W. Swiatecki, Ann. Phys. (N.Y.) **82**, 557 (1974).

Direct and Evaporation-Like Emission of ^{1}H and ^{4}He in Both Fusion-Like and Inelastic Reactions of 340 MeV ^{40}Ar + ^{238}U

D. Logan, M. Kildir,† M. Kaplan,* M.S. Zisman,*
D. Guerreau,‡ J.M. Alexander,§ and L.C. Vaz§

Reactions between complex nuclei generally lead to substantial emission of H and He. Evaporative emission has been observed from compound or composite nuclei[1] as well as from strongly damped reaction products after scission.[2] Pre-equilibrium emission has also been reported, but its nature cannot yet be said to be well understood.[3]

A simple and powerful technique for associating H/He emission with a fusion-like reaction is provided by a triple-coincidence requirement[4] between two fission fragments and the H or He. A small folding angle (θ_f) between fission fragments provides a clear signature for the large momentum transfer of a fusion-like collision.[4] A quasi-elastic or deeply inelastic collision will generally impart a much smaller momentum to the target, but still enough excitation energy for it to sequentially undergo fission. This smaller velocity leads to a distinctly larger folding angle.[5] We have measured coincident fission-fragment pairs, produced in the 340 MeV ^{40}Ar + ^{238}U reaction, by means of a gas ionization telescope (GT) and a two-dimensional, position-sensitive avalanche detector (PSAD) with full apertures of 2° and 25°, respectively.[6] Two GT's were used simultaneously so that a range of 118° $< \theta_f <$ 168° was observed, sufficient to separate the deeply inelastic and fusion-like events. A second coincidence was required between one of the GT's and any of four three-element Si solid state telescopes (SST) that identified H or He.

The angular dependences of the differential multiplicities for ^{1}H and ^{4}He are shown in Fig. 1. Each has a nearly isotropic component (in- and out-of-plane) aft of $\simeq$ 100° and a significant forward-peaked component. The angle-integrated multiplicities, M, for the isotropic components are also indicated in Fig. 1. Typical energy distributions for ^{4}He at $\theta_{c.m.} \simeq 110°$ (coincident with fusion-like collisions) show evaporative behavior and the spectra are very similar in- and out-of-plane. At $\theta_{c.m.} \simeq 28°$, again in coincidence with fusion collisions, an additional high-energy component is abundantly present in-plane but more weakly out-of-plane; at the same angle, alphas coincident with sequential fission show a dominant high-energy component which again exhibits a decrease as one moves out-of-plane.

A simple test for the dominant source of emission can be obtained from the angular dependence of the observed mean velocities as shown for ^{4}He in Fig. 2. The vector diagram shows mean velocities for the detected fission fragments as arrows and those expected for evaporative ^{4}He as circles, dashed for the fragments and solid for the composite nucleus. Points indicating measured mean velocities are most consistent with the solid circle representing evaporation from the composite system, and do not follow the trends of the dashed circles. We find similar behavior for the ^{1}H emission as well. Therefore, we conclude that the composite nucleus is the dominant emission source for the

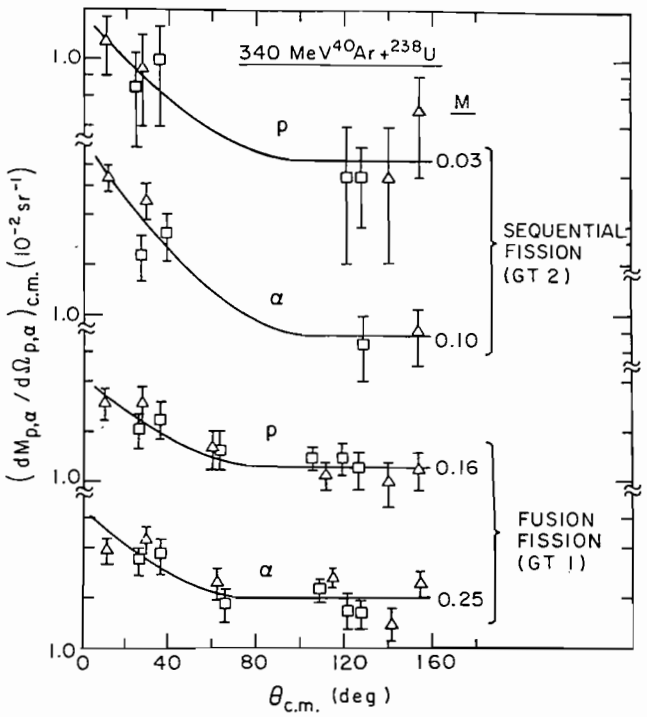

Fig. 1. Differential multiplicities $(dM_{p,\alpha}/d\Omega_{p,\alpha})_{c.m.}$ vs center-of-mass angle $\Theta_{c.m.}$ for ^1H and ^4He in triple coincidence with fission-fragment pairs registered in the PSAD and GT 1 or GT 2. Triangles represent measurements in the reaction plane, and squares correspond to out-of-plane detectors (ϕ_{Lab} = 21° at the more forward angles and ϕ_{Lab} = 55° at the more backward angles). Angle-integrated multiplicities M are indicated for the isotropic component of each curve. (XBL 818-11285)

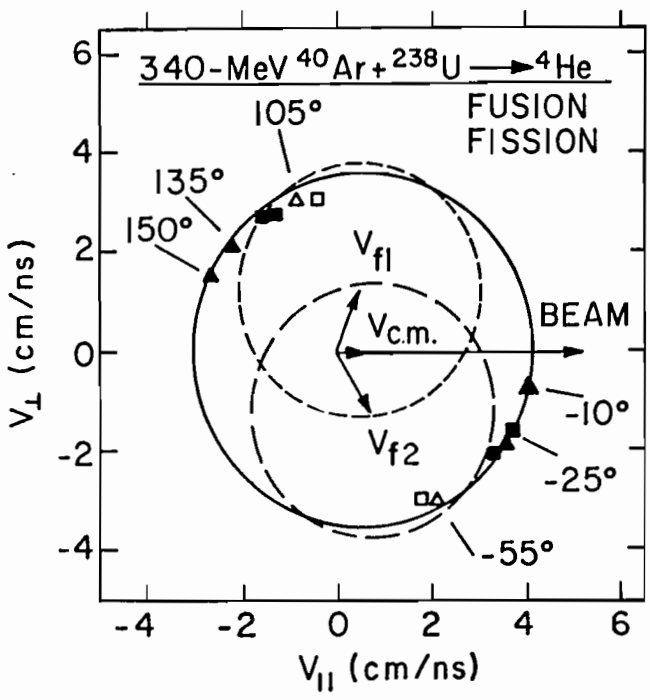

Fig. 2. Vector diagram for ^4He emitted in fusion-fission. Mean ^4He velocities observed in-plane are given by triangles and out-of-plane by squares. Short and long dashed circles correspond to expected mean velocities for evaporation from the fully accelerated fission fragments (for GT 1 or V_{fl} at 70°). Large solid circle is for evaporation from the composite system. Open points at about −55° and 105° were measured in coincidence with GT 1 or V_{fl} at 40° rather than at 70° as shown here. (XBL 818-11286)

low energy components of both ^4He and ^1H. For H/He in coincidence with sequential fission, the number of events recorded is more limited, and the vector diagram is more complicated. Here, we must also consider the projectile-like and target-like fragments as potential sources of evaporative emission. As in the fusion-fission case, the measured mean velocities for H/He do not follow the trends expected for evaporation from fission fragments. Furthermore, although it cannot be completely excluded, evaporation from projectile-like fragments is not a dominant emission source.

In summary, our data show evidence for forward angle emissions, characterized by strong forward peaking and higher than evaporative velocities with a preference for the reaction plane. This direct emission appears to be more abundant for the deeply inelastic than for the fusion-like collisions. These features, along with the sizeable multiplicities for ^4He as well as ^1H emission, seem to be evidence for angular momentum as a primary driving force. The nearly isotropic components have all the appearances of a classic evaporation mechanism. Those from fusion-like collisions must arise from a composite system of $Z \simeq 110$, and are expected to have spins up to $\ell = 130$ but no barrier to fission (for $J \geq 50$).[7] The integrated multiplicities for ^1H and ^4He evaporation for these fusion collisions are rather high, $\simeq 0.2$, and are comparable to those from the much lighter systems[1] $^{237}_{97}Bk$, $^{204}_{84}Po$, and $^{194}_{80}Hg$. The lack of a strong Z dependence for this H/He evaporation clearly indicates that dynamics rather than phase space must be controlling the choice of exit channel.[1] These emission processes are particularly exciting because they may provide the most direct view yet available of a composite system predicted not to have an equilibrium shape.

Footnotes and References

*Carnegie-Mellon University, Pittsburgh, Pennsylvania 15213.
†Department of Chemistry, Middle East Technical University, Ankara, Turkey.
‡Laboratoire de Chimie Nucléaire, B.P. No. 1, 91406 Orsay, France.
§State University of New York at Stony Brook, Stony Brook, New York 11794.

1. D. Logan et al., Phys. Rev. C **22**, 104 (1980) and Phys. Rev. C **22**, 1080 (1980); M.F. Rivet et al. (submitted to Phys. Rev. C.).
2. See, for example, R. Babinet et al., Z. Phys. A **295**, 1953 (1980).

3. *Proceedings of the International Symposium on Continuum Spectra of Heavy Ion Reactions,* San Antonio, Texas (1979), Harwood Academic Publishers (New York).
4. B.B. Back et al., Phys. Rev. C **22**, 1927 (1980) and references therein.
5. T. Sikkeland, Phys. Lett. B **27**, 277 (1968).
6. M.M. Fowler and R.C. Jared, Nucl. Instruments and Methods **24**, 341 (1975); Y. Eyal and H. Stelzer, Ibid. **155**, 157 (1978).
7. S. Cohen et al., Ann. Phys. (N.Y.) **82**, 557 (1974).

Prominent ^{4}He Emission from the Composite Nucleus for 480 MeV ^{56}Fe + Ag

D. Guerreau, D. Logan,† M.S. Zisman, J.M. Alexander,‡*
E. Duek,‡ and M. Kaplan†

Recently, various studies of heavy ion reactions have identified an evaporative component for ^{4}He emission and have used it to determine the root mean square spin of the emitters.[1] To search for the process of emission of evaporation-like α particles from a very short-lived composite nucleus, we have chosen the reaction 480 MeV ^{56}Fe + Ag. We have measured α particles in coincidence with heavy fragments in a geometrical configuration selected to test for evaporative emission from all three sources, the composite system, fission fragments, or deeply inelastic fragments. Four three-member Si solid-state detector telescopes (SST) were used to identify the ^{4}He particles, and a gas ionization telescope (GT) was used to measure Z and energy of the lighter of the two heavy fragments. A GT was placed at 50° or 30° ($\theta_{c.m.} = 95°$) to emphasize detection of fission-like and strongly-damped reaction products well aft of the grazing angle, 25°. The natural Ag target (670 μg/cm^2) was irradiated with ^{56}Fe from the SuperHILAC. Details of the experimental techniques have been described elsewhere.[2]

Measured coincidence spectra are most readily discussed in terms of invariant cross sections[1,3] ($d^3\sigma/p_\alpha c\, d\Omega_f d\Omega_\alpha\, dE_\alpha$); these are plotted vs the velocity in the frames of the average moving fragments in Fig. 1. Dashed curves are drawn with empirically estimated shapes for evaporation from these fragments.[3,4] As these evaporative components must be essentially isotropic (in-plane),[5] we have set their upper limits by reference to the SST at 75° (emphasizing emission from the lighter of the two heavy fragments) and 15° and −15° (emphasizing emission from the complimentary heavy fragments). From this analysis, we estimate multiplicities of 0.09 and 0.2 (upper limits) for emission from light and heavy fragments respectively. It is clear from Fig. 1 that the bulk of α-particle emission (in the coincidence mode) cannot be described by evaporation from the fragments. This result is in strong contrast to the results from Ref. 6 for ^{84}Kr + Ag; possibly the angular range explored in that study did not allow the measurement of emission characteristics from the composite system.

To what extent can the additional α emission be ascribed to "quasi-evaporation" from the composite nucleus? The average ^{4}He velocities and energies are rather close to those expected for such evaporation, and the observed c.m. spectra for $V_\alpha \geq 3$ cm/ns (see Fig. 2a) are very similar to the shape expected for evaporation from a nucleus of Z = 73. However, the differences in the spectra for +15° and −15° (for $V_\alpha < 3$ cm/ns) indicate significant emission from the fragments. In Fig. 2b and 2c, we compare the laboratory spectra to the sum of the evaporation components calculated with multiplicities taken from Figs. 1 and 2a. We can see the necessity to include prominent emission from the composite nucleus itself in addition to that from the fully accelerated fragments. We note that, even for the composite system, there seems to be a rough conformity of the spectra to evaporative behavior. Angular integration for such an evaporative component gives a multiplicity of 0.44.

Integrated cross sections are listed in Table 1 and compared with corresponding quantities from the reaction 340 MeV ^{40}Ar + Ag. For the ^{56}Fe reaction, more α particles are emitted both from the fragments and from the composite nucleus. The former enhancement is surely expected with increasing fragment spin,[1] but the latter enhancement is less obvious. Whereas the composite system was a negligible source of ^{4}He emission for 280 MeV ^{40}Ar + ^{58}Ni,[1] it is roughly comparable to the fragments in the reaction Ar + Ag (see Table 1); and, finally, it is the dominant source for the present Fe + Ag system. It seems likely that the entrance channel spin provides the driving force for this increase. However, one expects the lifetime of the composite system to decrease with increasing spin, and therefore it is amazing to find so much evaporation-like emission from composite systems with such high spins. Whether or not emission from the tips of a strongly deformed system can account for this α-particle emission remains an open question at present.

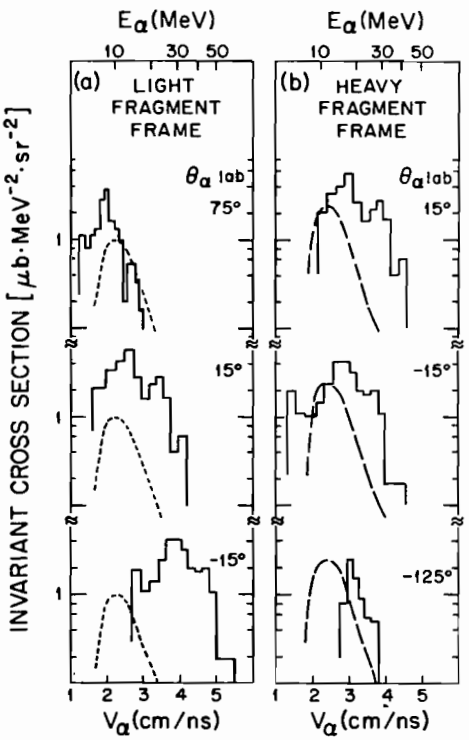

Fig. 1. The invariant cross section ($d^3\sigma/d\Omega_f d\Omega_\alpha dE_\alpha p_\alpha c$) vs mean velocity in the detected light fragment frame (a) and in that of its heavy complement (b). Histograms show the experimental data; dashed lines give empirically estimated shapes for evaporation spectra. These shapes are normalized to maximum allowable magnitude (for the light fragment at 75° and the heavy fragment at 15° and −15°).
(XBL 818-11282)

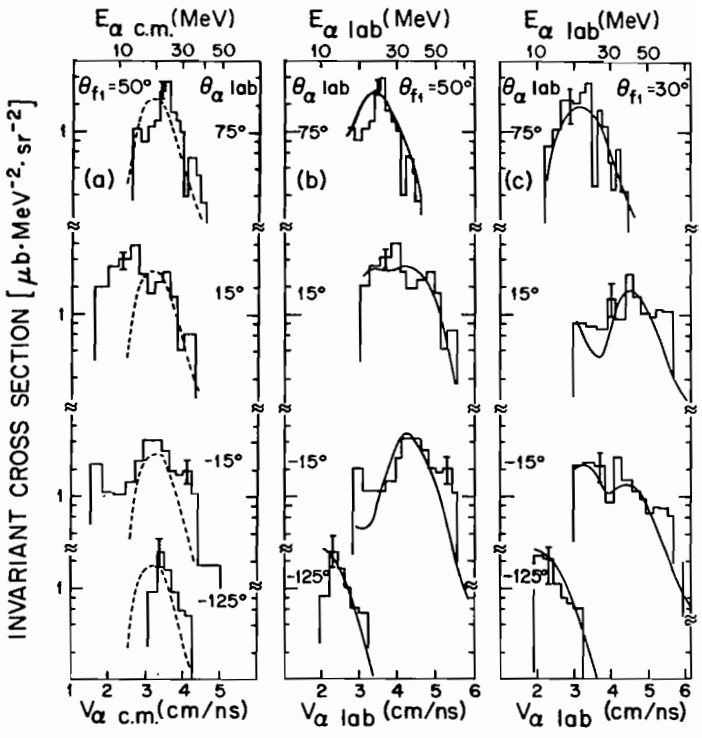

Fig. 2. Invariant cross section vs (a) c.m. velocity and (b) and (c) laboratory velocity for the GT angles 50° and 30°. The dot-dashed curves were drawn in (a) for the composite system. The solid curves in (b) and (c) represent the sum of all three evaporative components. (XBL 818-11283)

Table 1. Cross sections (mb) and ℓ values for two reactions Ag (natural) + X (8.5 MeV/u).

	^{40}Ar	^{56}Fe
E* (MeV)	195	205
σ_{ER} (mb)	455 ± 50[a]	~290[b]
ℓ_{ER} ($\hbar$)	(71)[a]	(71)[b]
"Fission-like"	800 ± 80[c]	1480 ± 170[d,e]
σ_{sum} (ℓ_{sum})	1255 (118)	~1770 (~175)
σ_R (ℓ_{max})	2704[b] (172)	2694[b] (217)
Symmetric α's from the composite in coincidence with fragments (their multiplicity)	125 ± 35[f] (0.16)	650 ± 100[d] (0.44)
α's evaporated from fragments (their multiplicity)	155 ± 40[f] (0.2)	430 ± 65[d] (0.29)

[a]H.C. Britt et al., Phys. Rev. C **13**, 1483 (1976).

[b]Estimated from systematics.

[c]Ref. 2.

[d]Determined in this work.

[e]$d\sigma/d\Omega$ for $18 < Z < 38$ at 50° integrated by assuming $1/\sin\theta$ angular distribution.

[f]Fragment detector at $\theta_{c.m.} \simeq 90°$ where only fission-like fragments were observed; values from Ref. 2.

Footnotes and References

*Laboratoire de Chimie Nucléaire, Institut de Physique Nucléaire, B.P. No. 1, 91406, Orsay, France.
†Carnegie-Mellon University, Pittsburgh, Pennsylvania 15213.
‡State University of New York at Stony Brook, Stony Brook, NY 11794.

1. D. Guerreau and R. Babinet, J. de Physique (Paris) C **10**, 217 (1980) and references therein.
2. D. Logan et al., Phys. Rev. C **22**, 1080 (1980); G. Catchen et al., Phys. Rev. C **21**, 940 (1980); M.F. Rivet et al. (submitted to Phys. Rev. C, 1981); D. Guerreau et al. (to be published).
3. R. Babinet et al., Z. Phys. A **295**, 153 (1980).
4. Systematic studies of evaporation spectra show that spectral shapes can be approximated by the standard formula $P(E_\alpha) \propto (E_\alpha - B) \exp -[E_\alpha/T]$. The empirical parameters (B and T) have been taken from the data given in Refs. 1 and 5. Mean evaporation velocities can be estimated with relative uncertainties of less than 3%.
5. W. Kuhn et al., Z. Phys. A **298**, 95 (1980).
6. L.G. Sobotka et al., Phys. Rev. Lett. **46**, 887 (1981), and LBL-11840 (1981).

Comparison of Noncompound Neutron and Proton Emission in ^{16}O Induced Reactions on ^{238}U at 310 MeV

J. Kasagi, S. Saini,* T.C. Awes,* A. Galonsky,* C.K. Gelbke,* G. Poggi,* D.K. Scott,* K.L. Wolf,† and R.L. Legrain*

In the last few years, it has been established that collisions between complex nuclei at non-relativistic energies may lead to the emission of energetic light particles which cannot be explained in terms of evaporation from completely equilibrated nuclei. Assuming that protons and neutrons have similar spectral shapes, it has been shown[1,2] that the energy spectra of deuterons and tritons may be related to the energy spectra of protons by a simple coalescence relation. However, a direct comparison of noncompound proton and neutron cross sections has not yet been performed. To make such a comparison, we used the LBL 88-Inch Cyclotron to investigate the reaction ^{238}U(^{16}O,pf) and ^{238}U(^{16}O,nf) at 310 MeV incident energy.

The differential neutron multiplicities per fission event, $d^2N/N_f dE d\Omega$, are shown in Fig. 1. At low energies, the spectra are dominated by a low temperature component that is consistent with the statistical evaporation of neutrons from equilibrated target residues and fission fragments. The high energy regions of the neutron spectra exhibit characteristics that are qualitatively similar to those observed for the emission of energetic charged particles: with increasing scattering angle the cross sections decrease and the energy spectra become steeper.

To facilitate the comparison of proton and neutron cross sections, we have decomposed each neutron spectrum into two components by fitting the energy spectra with the following function:

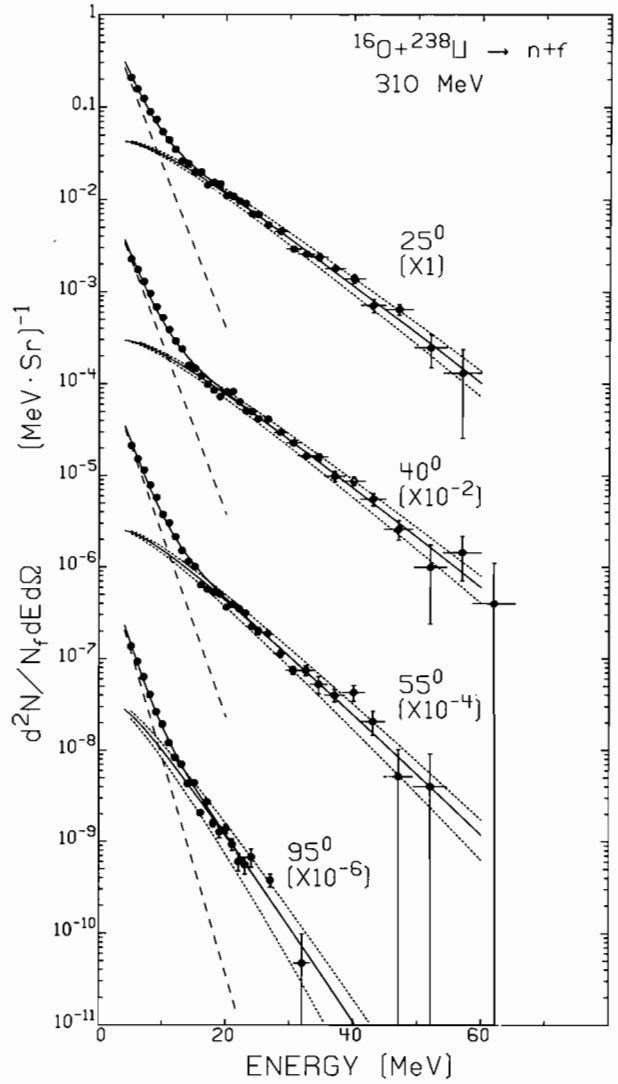

Fig. 1. Differential neutron multiplicities per fission event measured for the reaction $^{238}U(^{16}O,nf)$ at 310 MeV. Solid and dashed lines show the decomposition into equilibrium and non-equilibrium components, respectively. Dotted lines indicate the estimated errors within which the high energy regions of the neutron spectra are established. These limits are used for the comparison with the proton spectra in Fig. 2. (XBL 8111-12352)

$$\frac{d^2N(E)}{N_f dE d\Omega} = N_0\, e^{-E/T_0} + N_1 \sqrt{E}\, e^{-E/T_1} \quad . \tag{1}$$

The first term, which omits an energy factor, adequately represents the low energy component, and the second term describes the high energy component which we associate with preequilibrium processes; N_0, T_0, N_1, T_1 are adjustable parameters. This decomposition is shown in Fig. 1 for the parameters given in Table 1.

The proton cross sections measured in this experiment are compared to the corresponding neutron cross sections in Fig. 2. The shapes of the proton and neutron spectra exhibit significant differences. At lower energies ($E \lesssim 30$ MeV) the neutron cross sections exceed the proton cross sections. However, the neutron cross section drops below the proton cross section at higher energies ($E \gtrsim 30$ MeV), a result which conflicts with the simple expectation[3] that the neutron-to-proton cross section ratio should scale with the neutron-to-proton ratio of the emitting system (be it projectile, target, or the composite system).

The differences between the low energy part of the proton and neutron spectra are most likely due to barrier penetration effects. To illustrate this point, we have transformed the neutron spectra of Fig. 2a according to the relation

$$\frac{d^2N^{(p)}(E)}{N_f dE d\Omega} = \frac{\sigma_R^{(p)}(E)}{\sigma_R^{(n)}(E)} \frac{d^2N^{(n)}(E)}{N_f dE d\Omega} \quad . \tag{2}$$

In Eq. (2), the inverse reaction cross sections are calculated from the optical model by using the potentials of Ref. 4. The resulting cross sections are shown by the shaded areas in Fig. 2(b). Reasonable agreement with the proton cross sections is obtained in the low energy region. The high energy part of the spectrum is, however, only slightly modified ($\sigma_R^{(p)} \simeq \sigma_R^{(n)}$ at high energies) and, as a consequence, the proton-to-neutron ratio at high energies is not affected by this procedure.

The coalescence relation referred to above was derived[2] by making the simplifying assumption that the cross sections for preequilibrium proton and neutron emission are related by[2,5]

Table 1. Parameters of Eq. (1) used for the decomposition of equilibrium and nonequilibrium components shown in Fig. 1.

θ_n	N_0 (MeV·sr)$^{-1}$	T_0 (MeV)	N_1 (MeV$^{3/2}$·sr)$^{-1}$	T_1 (MeV)
25°	1.35	2.45	0.036	7.60
40°	1.85	2.35	0.025	7.4
55°	2.00	2.20	0.024	6.2
95°	1.78	1.85	0.038	4.0

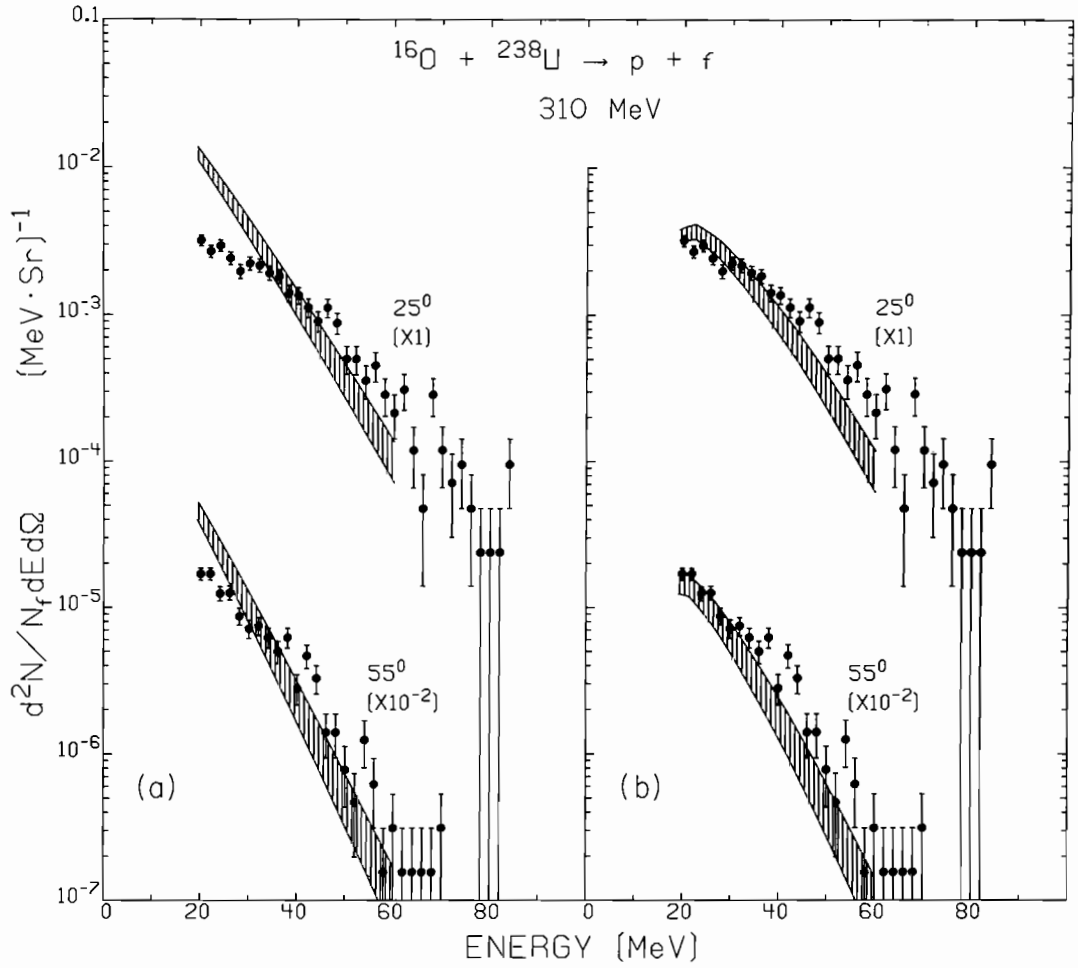

Fig. 2. Differential proton multiplicities per fission event measured for the reaction $^{238}U(^{16}O,nf)$ at 310 MeV. (solid points) Shaded areas represent the measured preequilibrium neutron multiplicities (part a) and their predicted transformation into proton multiplicities according to Eq. (2) of the text (part b). (XBL 8111-12353)

$$\frac{d^2\sigma_n(E)}{dEd\Omega} = \frac{N}{Z}\,\frac{d^2\sigma_p(E+E_c)}{dEd\Omega} \quad . \tag{3}$$

In Eq. (3), N/Z is the neutron-to-proton ratio of the compound nucleus. The energy shift E_c was introduced to correct for the final state Coulomb repulsion from the target nucleus. The physical picture behind Eq. (3) is that protons and neutrons have identical kinetic energy distributions at the nuclear surface, where the observed complex particles are most likely to originate. The Coulomb field of the target nucleus merely displaces the energy spectrum of charged particles by the amount E_c. It is clear from Fig. 2(a) that Eq. (3) is inconsistent with our observations. The shapes of the neutron spectra predicted from the proton cross sections would differ significantly from the measured neutron spectra. The coalescence calculations are quite sensitive to this low energy region; as a consequence, the deuteron cross sections are not given by the product of proton and neutron cross sections as determined in this experiment. Possible alternative explanations[6] for the formation of composite light particles remain an interesting subject for future investigations.

Footnotes and References

*Michigan State University.
†Argonne National Laboratory.

1. T.C. Awes et al., Phys. Rev. Lett. **45**, 513 (1980).
2. T.C. Awes et al., Phys. Rev. C **24**, 89 (1981).
3. W.W. Morison et al. Phys. Lett. B **93**, 379 (1980).
4. F.D. Becchetti, Jr., and G.W. Greenlees, Phys. Rev. **182**, 1190 (1969).
5. M. Gyulassy and S.K. Kauffmann, Nucl. Phys. A **362**, 503 (1981).
6. E. Hachenberg, H.C. Chiang and J. Hufner, Phys. Lett. B **97**, 183 (1980).

Light Particle Correlations in 20 MeV per Nucleon ^{16}O Induced Reactions

C.K. Gelbke, W.G. Lynch,* L.W. Richardson,* M.B. Tsang,* and R.E. Warner†*

The attainment of local thermal equilibrium in heavy ion induced reactions is an important assumption underlying many theoretical models. Until now, light particle correlations testing the thermalization assumption have been measured only at relativistic energies (E/A=400 and 800 MeV) where the existence of a non-thermal knockout component was demonstrated. In this article, we discuss the first such measurement at non-relativistic energies.

Aluminum and gold targets of 1.6 and 10 mg/cm^2 thickness were bombarded with 310 MeV $^{16}O^{6+}$ ions from the LBL 88-Inch Cyclotron. Single and coincident protons and deuterons were detected with four ΔE-E telescopes consisting of solid state silicon-ΔE and NaI (Tl)-E detectors. The telescopes were mounted in a plane at the angles of −110°, −30°, +30°, and +75° with respect to the beam axis, subtending solid angles of 62, 49, 49, and 62 msr, respectively.

We present our results in terms of the correlation function $\sigma_{12}/(\sigma_1\sigma_2)$ where

$$\sigma_{12} = \sigma_0 \int_{\Delta E_1} dE_1 \int_{\Delta E_2} dE_2 \frac{d^4\sigma(\theta_1,E_1,\theta_2,E_2)}{dE_1 dE_2 d\Omega_1 d\Omega_2} \quad , \qquad (1)$$

and

$$\sigma_k = \int_{\Delta E_k} dE_k \; \frac{d^2\sigma(\theta_k,E_k)}{dE_k d\Omega_k} \; ; \; k = 1,2. \qquad (2)$$

The constant σ_0 was arbitrarily fixed by requiring $\sigma_{12}/(\sigma_1\sigma_2) = 1$ for the proton-proton correlation corresponding to the variables $\theta_1 = -30°$, $\theta_2 = +30°$, $\Delta E_1 = 20-40$ MeV, and $\Delta E_2 = 20-100$ MeV.

Our experimental results are shown in Fig. 1. The first light particle is defined to be the one detected at $\theta_1 = -30°$. The range of energy integration for the second particle was fixed at $\Delta E_2 = 20-100$ MeV for $\theta_2 = +30°$ and $\Delta E_2 = 10-100$ MeV for $\theta_2 = \pm 110°, \pm 75°$. The error bars shown in the figure are purely statistical; systematic errors are believed to be on the order of 5%.

The correlation function exhibits sizable variations which are more pronounced for the Al target than for the Au target. It usually has a minimum value for the forward emission of the second light particle. For the Al target, a pronounced left-right asymmetry is observed, corresponding to an enhanced probability for coincident emission of the two light particles on opposite sides of the beam.

For the case of thermal emission from an infinite ensemble, the correlation function is constant. However, for nuclear reactions, finite particle number effects might not be negligible and variations in the correlation function could be imposed by conservation laws. We have performed simple calculations to investigate the correlations that might be imposed by energy and momentum conservation for a source of A nucleons that emits light particles with a Gaussian momentum distribution. The Galilean-invariant cross section is then given by

$$\frac{d^3\sigma}{dp^3}(\vec{p},\vec{v}_0,T,m) = C(2\pi mT)^{-3/2} \exp\left[-\frac{(\vec{p}-m\vec{v}_0)^2}{2mT}\right] \qquad (3)$$

where C is a normalization constant, m is the mass of the emitted particle, T is the temperature parameter and $\vec{v}_0$ is the velocity of the source in the laboratory.

The detection of a light particle of laboratory momentum $\vec{p}_1$ and mass m_1 changes the values of both the temperature and the velocity of the remaining ensemble. Denoting $\vec{v}'_0$ and T′ as the new source velocity and temperature respectively, the coincidence cross section for the emission of particle 1 of momentum $\vec{p}_1$ followed by the emission of particle 2 of momentum $\vec{p}_2$ is then proportional to the product

$$P(\vec{p}_1,\vec{p}_2) = \frac{d^3\sigma}{dp_1^3}(\vec{p}_1,\vec{v}_0,T,m_1) \times \frac{d^3\sigma}{dp_2{}^3}(\vec{p}_2,\vec{v}'_0,T',m_2) \; . \qquad (4)$$

Since, experimentally, we cannot distinguish the reverse time sequence, the cross section for the emission of particles 1 and 2 is given by

$$\frac{d^6\sigma}{dp_1^3 dp_2^3} = C_0[P(\vec{p}_2,\vec{p}_1) + P(\vec{p}_1,\vec{p}_2)] \quad , \qquad (5)$$

where C_0 is a normalization constant.

The results of these calculations are compared to the experimental proton-proton correlations for the Al target in Fig. 2. The source parameters of $v_0 = 0.085c$ and T = 6.25 MeV for the Al target were obtained from fits to the singles cross sections. The calculations were arbitrarily normalized to the data at a point which is obvious in the figures. To exhibit the effect of the number of source nucleons on the predicted correlation several values of A have been used for the calculations. In addition, one calculation is shown for the case of T=T′=T″ (which violates energy conservation for the ensemble but still exhibits the constraints due to momentum conservation).

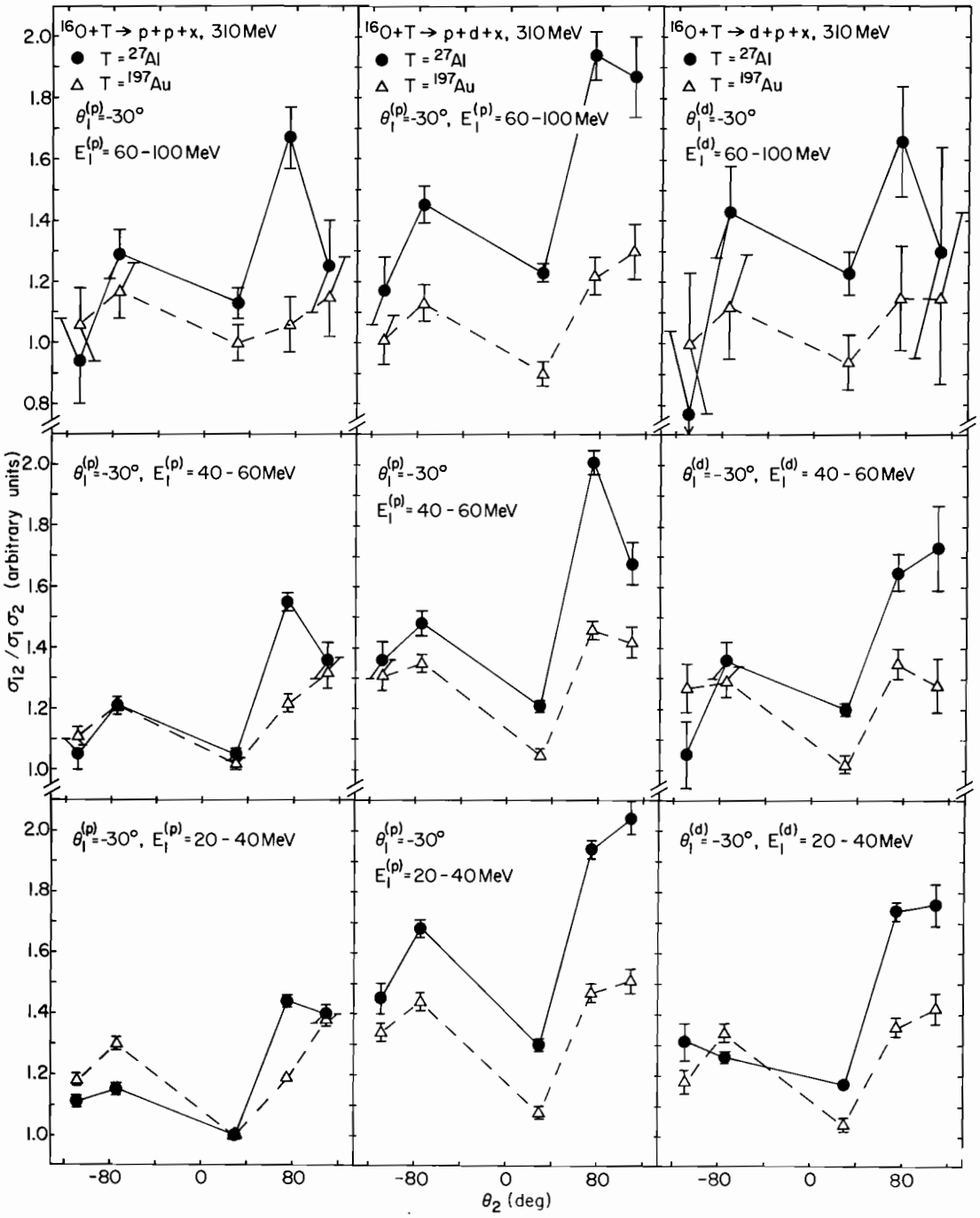

Fig. 1. Experimental light particle correlations for 20 MeV/A ^{16}O ions incident on Al and Au targets. (XBL 8111-12327)

For the Al target (Fig. 2) the magnitude of the observed left-right asymmetries are comparable to those already predicted for the maximum number of participating nucleons, A=43. This comparison of calculation with experiment cannot quantitatively determine A since neither the small values of the correlation at $\theta_2 = +30°$ nor the large values at $\theta_2 = +75°$ can be explained by the calculations in a consistent way.

These discrepancies are interesting subjects for future studies with more refined models. Of particular interest is the determination of the influence of impact parameter averaging on the correlation function, and whether the small values of the correlation function at $\theta_2 = +30°$ can be caused by the presence of low multiplicity peripheral collisions in the singles spectrum at forward angles. Of comparable importance is the calculation of the direct

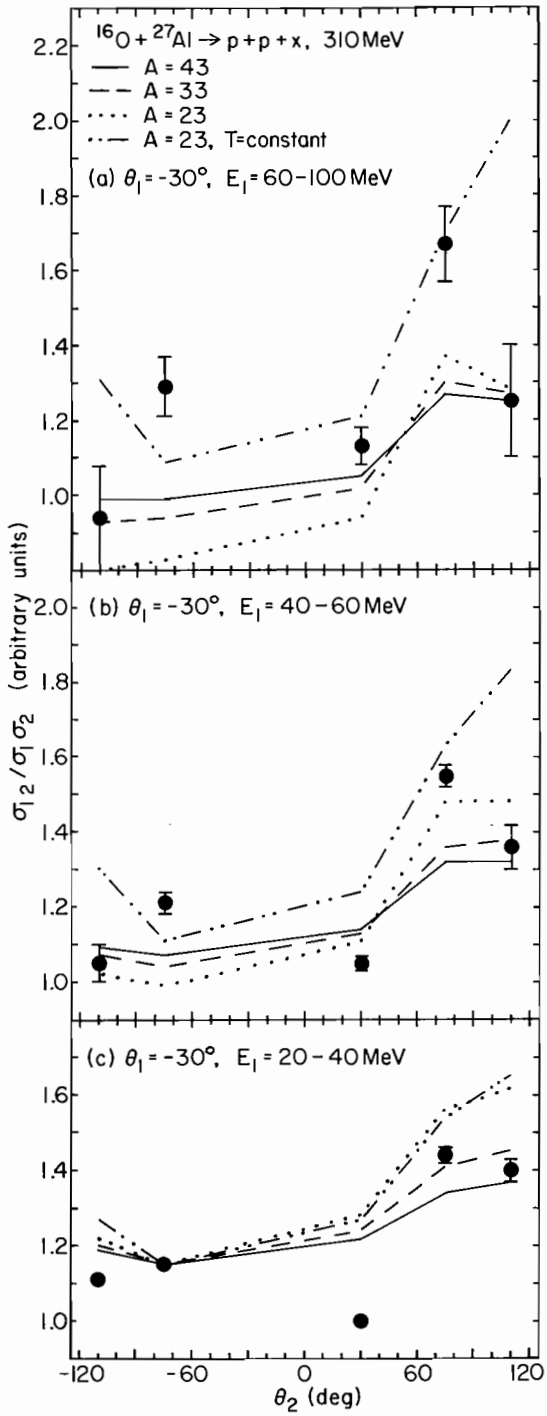

Fig. 2. Comparisons of measured proton-proton correlations with the predictions of the simple thermal model described in the text. (XBL 8111-12328)

knockout contribution to the correlation as a function of the target mass. Such a component, if present, would be expected to be more important for lighter target projectile combinations and for relative proton laboratory angles close to 90°. This could possibly be related to the enhancement in the correlation at $\theta_2 = +75\%$ for the Al target. Moreover, rescattering and absorptive effects (shadowing), especially for heavy target projectile combinations, and possible hydrodynamic effects are of potential interest.

Footnotes

*National Superconducting Cyclotron Laboratory, Michigan State University, East Lansing, MI 48824.
†Oberlin College, Oberlin, OH 44074 and National Superconducting Cyclotron Laboratory.

Trends of Light Particle Spectra Observed in Nucleus-Nucleus Collisions

T.C. Awes, G Poggi,* S. Saini,* C.K. Gelbke,* R. Legrain, and G.D. Westfall*

Information about the early stages of heavy-ion induced reactions may be obtained from the detection of energetic light particles which cannot be associated with evaporation from the compound nucleus. At low energies (E/A $\leq$ 20 MeV), recent experiments have mainly used coincidence techniques to study detailed aspects of the reaction mechanisms producing energetic light particles. However, few single particle inclusive measurements have been published in this energy domain, and little information is available about the dependence of non-compound light particle emission on projectile, target, and beam energy. We report here some of the results obtained from a survey of reactions on Al, Zr, and Au targets using beams of 140, 215, and 310 MeV energy from the LBL 88-Inch Cyclotron.

As an example of the general features of the energy spectra that were observed in the present experiment, Fig. 1 shows the results for the ^{197}Au(^{16}O,p) reaction for three incident energies. The energy spectra are smooth structureless distributions which, at forward angles, extend to about four times the incident energy per nucleon. With increasing detection angle, the cross sections decrease, and the slopes of the energy spectra become steeper.

The cross sections can be described in terms of a Maxwellian distribution observed in a rest frame that moves with a velocity intermediate between target and projectile (see solid curves in Fig. 1.) Correcting for the Coulomb repulsion from the target nucleus, one obtains non-relativistically[1,2]

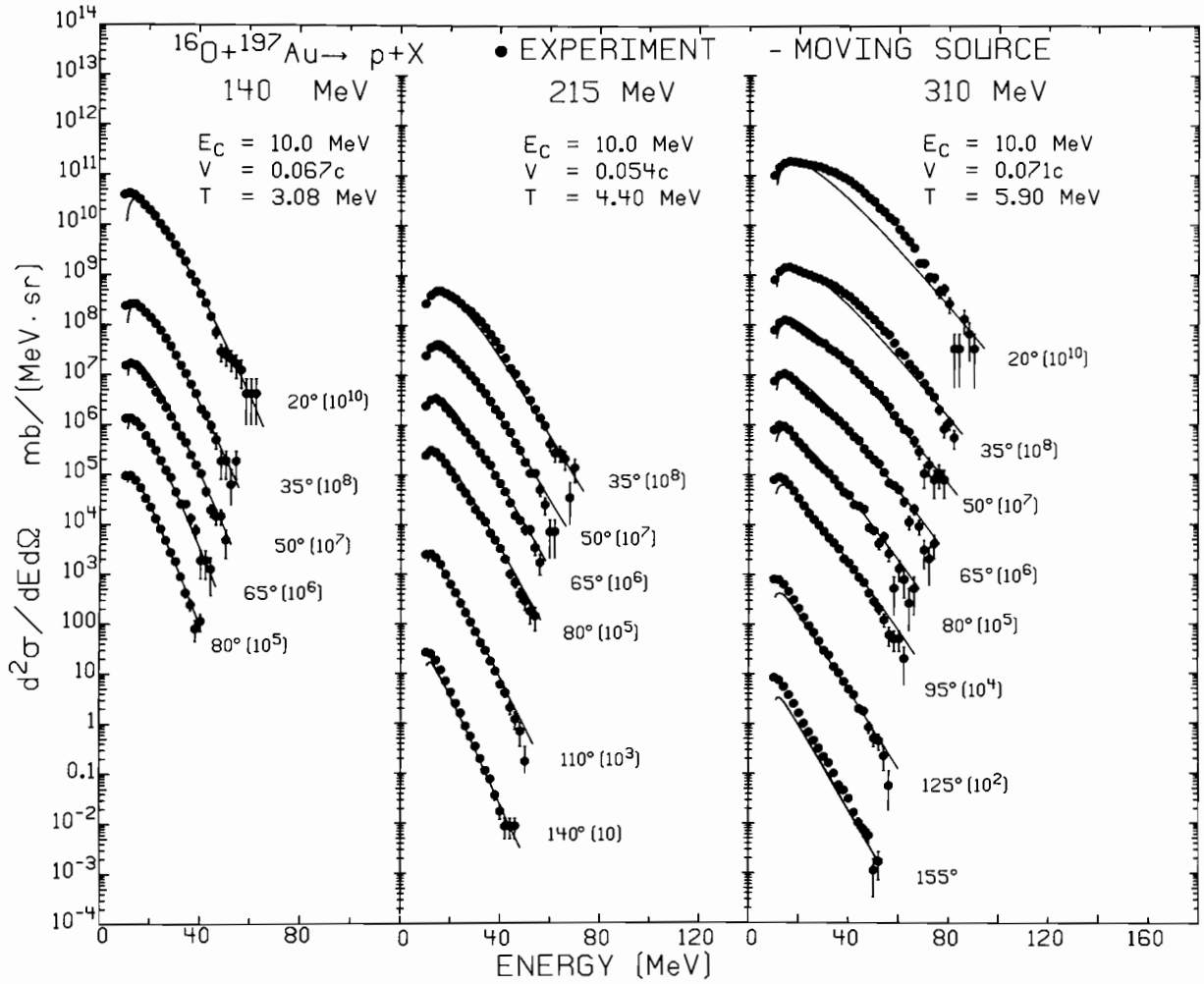

Fig. 1. Energy spectra of protons detected in the reaction ^{197}Au(^{16}O,p) at incident energies of 140, 215, and 310 MeV. The curves have been calculated with Eq. (1) of the text.

(XBL 8111-12354)

$$\frac{d^2\sigma}{dEd\Omega} = N_0 (E-E_c)^{1/2}$$

$$\exp\{-[E-E_c + E_1 - 2E^{1/2}(E-E_c)^{1/2}\cos\theta]/T\} \quad . \qquad (1)$$

Here, E_c is the kinetic energy gained by the Coulomb repulsion from the target, $E_1 = 1/2mv^2$ is the kinetic energy of a particle at rest in the moving frame, T is the temperature, and N_0 is a normalization constant. The successful application of this parameterization should not be interpreted as evidence for a hot gas of nucleons separated from the target nucleus.[1,2] Instead, it indicates the randomization of light particle velocities in a rest frame that is different from the compound nucleus rest frame. In the present analysis, the values of E_c = 0, 5, and 10 MeV were used for the Al, Zr, and Au targets, respectively.

The temperature parameters determined in this experiment are shown in Fig. 2, where they are plotted as a function of $(E\text{-}V_c)/A$, the beam energy per nucleon above the Coulomb barrier. For a given type of light particle, the apparent temperatures are approximately proportional to $[(E-V_c)/A]^{1/2}$ or, equivalently, to the relative velocity of projectile and target at the point of contact (see insert, Fig. 2). Such a dependence is not expected from compound nucleus emission. It rather suggests more rapid processes such as knockout or, perhaps, the formation of a thermalized subset of nucleons consisting of about equal numbers of target and projectile nucleons. The deduced values of T are systematically larger for deuterons and tritons than for protons. At present, it is not clear whether this effect could be due to different contributions to the spectra from more equilibrated processes such as compound nucleus evaporation.

The parameterization used to describe our data is similar to the thermal models[3,4] that have been used to describe light particle spectra from relativistic heavy-ion collisions. In order to compare the trends observed at low energies to the ones at relativistic energies, we have determined the temperature parameters for the reaction ^{20}Ne + NaF → p at energies of E/A=400 and 800 MeV[5] by using the relativistic generalization of Eq. (1):

$$\frac{Ed^2\sigma}{p^2dpd\Omega} = N_0\gamma(E-\beta p\cos\theta)$$

$$\exp(-\gamma(E-\beta p\cos\theta)/T) \quad , \qquad (2)$$

where β is the velocity of the source (c = 1), $\gamma = (1-\beta^2)^{-1/2}$, and $E = (p^2 + m^2)^{1/2}$. To minimize the contribution from projectile fragmentation and knockout,[5] we have restricted the data to large transverse momenta ($\Theta \geq 45°$) for the determination of T. Despite the simplicity of the parameterization, the fits are of acceptable quality. The resulting temperature parameters are included in Fig. 2.

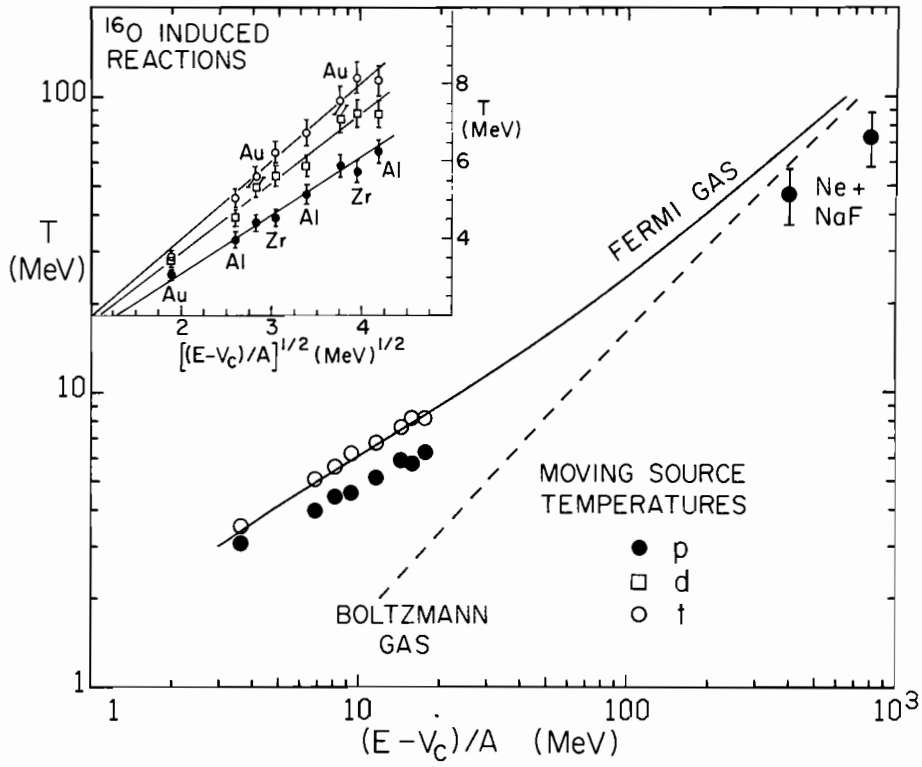

Fig. 2. Temperature parameters for the proton, deuteron, and triton spectra in ^{16}O induced reactions on targets of Al, Zr, and Au at incident energies of 140, 215, and 310 MeV and for the reaction Ne+NaF→p at 400 and 800 MeV/A. The solid and dashed curves are explained in the text.

(XBL 8111-12355)

As is obvious from Fig. 2, the trends observed at low energies can be connected smoothly to the observations at high energies. For orientation, the solid and dashed curves have been calculated for relativistic Fermi and Boltzmann gases consisting of equal nucleon contributions from target and projectile.

The general trend of the experimental temperature parameters is seen to follow the one depicted by the Fermi gas curve. Although the observed trends suggest the thermalization of a subset of nucleons, investigations should be made to determine if alternative approaches such as single or multiple nucleon scattering models or hydrodynamical models would predict similar trends.

Footnote and References

*Michigan State University.

1. T.C. Awes et al., Phys. Rev. Lett. **45**, 513 (1980).
2. T.C. Awes et al., Phys. Rev. C **24**, 89 (1981).
3. G.D. Westfall et al., Phys. Rev. Lett. **37**, 1202 (1976).
4. J. Gosset, J.I. Kapusta, and G.D. Westfall, Phys. Rev. C **18**, 844 (1978).
5. S. Nagamiya et al., LBL-12123, to be published; and private communication.

2. Angular Momentum Transfer

Q-Value and Z Dependence of Angular Momentum Transfer in Deeply Inelastic Scattering of $^{56}Fe + ^{209}Bi$

M.S. Zisman, R.J. Puigh, R. Vandenbosch,* T.D. Thomas,† and L. Nunnelley‡*

In the last several years our group at the SuperHILAC has been interested in studying the angular momentum transfer, and its alignment, in the deeply inelastic scattering (DIS) process.[1-4] The technique we have developed to accomplish our goal is described in detail in Ref. 2; it involves measurement of the in-plane and out-of-plane sequential fission angular correlations of a heavy target which is excited by a DIS process.

Subsequent to the publication[1] of our $^{86}Kr + ^{209}Bi$ data a similar experiment was performed by Specht,[5] but using reverse kinematics, i.e., a ^{208}Pb beam bombarded targets of ^{90}Zr and ^{58}Ni. In contrast to our results, however, they reported that there was *no* evidence for an in-plane anisotropy in their data. Given this discrepancy, we have re-examined some of the techniques used to analyze our (kinematically incomplete) experiments.[1-3]

First of all, we have looked into the approximation, made in previous analyses, that the laboratory to center-of-mass Jacobians can be properly estimated by using "average" values corresponding to a symmetric mass split of the fissioning ^{209}Bi system. We have done this by carrying out Monte Carlo calculations of the fission decay using a code provided by M.F. Rivet.[6] The code allows us to investigate the effects of a (presumed) symmetric mass split having a standard deviation of 25% and an energy spread of 8%. After first ensuring that the code properly reproduced our "analytic" Jacobians in the limit of zero mass and energy widths, we find corrections of the magnitude shown in Fig. 1 for the $^{56}Fe + ^{209}Bi$ case. These corrections do not appear to be of primary concern for the Fe + Bi system, since they are quite small over the angular range for which we have data. We note, however, that the corrections are in such a direction as to *reduce* the anisotropy compared with that obtained using the analytic Jacobians, that is, the forward angle cross sections are reduced somewhat while those at more backward angles are increased compared with the average.

It turns out, however, that the size of this correction depends strongly on the velocity of the recoiling target-like nucleus. Thus, for the $^{86}Kr + ^{209}Bi$ system studied earlier, the corrections are larger. Fortunately, however, our Kr + Bi data were measured at fairly forward angles ($< 61°$) so the corrections will not be more than about 15-20%. (Again, the sense of the correction is to reduce, but not eliminate, the reported[1,2] anisotropy.) Because of the experimental technique employed, the Specht data[5] require no such correction.

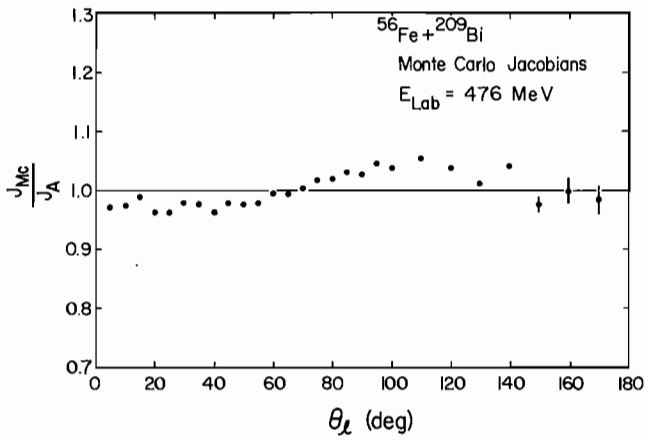

Fig. 1. Ratio of Monte Carlo Jacobians (including the finite mass distribution) to analytic Jacobians (assuming emission of two equal mass fragments) for $^{56}Fe + ^{209}Bi$. (XBL 813-472)

Another aspect of the data analysis has to do with the location of the symmetry axis. Based on the observed peaking along the recoil direction, Vandenbosch[7] has developed a model in which the Fermi motion of the transferred nucleons generates a random component of angular momentum in the plane perpendicular to the line of centers between the collision partners. This leads to a symmetry axis along the recoil direction, i.e., 0° in our coordinate system. In fact, however, the correspondence between the recoil axis and the symmetry axis is strictly true only for the elastic scattering case. A shift in the symmetry axis will influence (but probably only slightly) our determination of the random component J_2. More importantly, it could modify to some extent the angular distribution reported by Specht[5] since their data were reflected around $\theta_{c.m.} = 0°$; reflection around a displaced axis will tend to reduce the apparent anisotropy in the data.

On the assumption that the random component of angular momentum is indeed generated in the plane perpendicular to the line of centers, we have estimated the location of the symmetry axis by making use of a trajectory calculation code, due to Randrup,[8] which employs a one-body dissipation mechanism including a neck degree of freedom. By following the trajectory corresponding to a particular energy loss, we determine the location of the line of centers between the interacting nuclei at the point when

half of the total number of exchanges has taken place. In our picture, this direction corresponds to the (laboratory) symmetry axis for that energy loss. For both the Fe + Bi and Kr + Bi systems of interest here, we get results very nearly identical to what one would predict from the simple picture in which the overall trajectory is viewed as a single coulomb orbit. In this latter case the normal to the line of centers at the halfway point in the orbit is at $\theta_{c.m.}/2$ and the laboratory symmetry angle is given by

$$\theta_{sym} = \frac{\theta_{c.m.} - \pi}{2} .$$

Although we have not yet incorporated this refinement into our fitting code, the predicted location of the symmetry axis generally seems to agree well with the data points.

If we compare our results for Fe + Bi with the Pb + Ni in-plane correlation of Specht,[5] we see (Fig. 2) that the shapes of the two data sets agree reasonably well except for the normalization. Interestingly, a French group[9] has recently repeated the experiment on the $^{58}Ni + ^{208}Pb$ system at 7.5 MeV/A, but without using "reverse" kinematics. In agreement with our results, their preliminary data indicate a rather large in-plane anisotropy, peaked more-or-less along the recoil direction. Thus, the discrepancy still appears not to be completely understood.

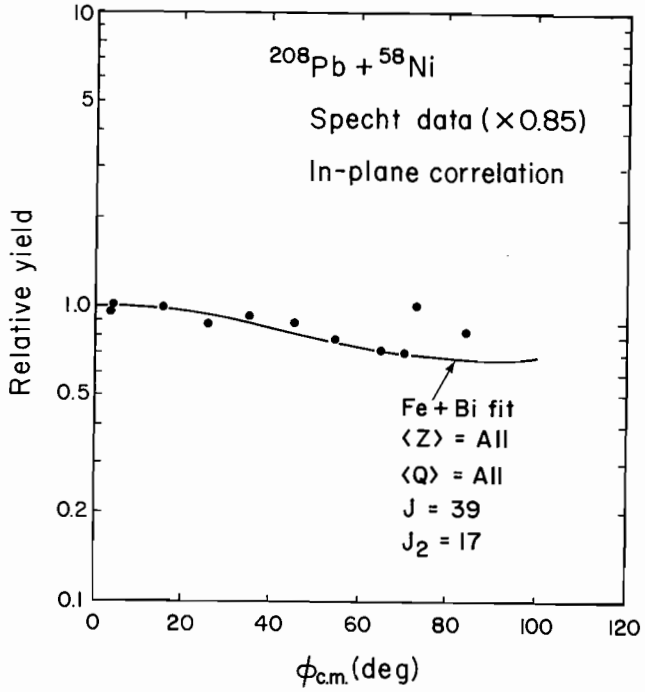

Fig. 2. Renormalized in-plane angular correlation from the $^{208}Pb + ^{58}Ni$ reaction (Ref. 5) compared with the best fit curve for our $^{56}Fe + ^{209}Bi$ data. (XBL 813-474)

Footnotes and References

*University of Washington, Seattle, WA 98195.
†Oregon State University, Corvallis, OR 97331.
‡Chemeketa Community College, Salem, OR 97308.

1. P. Dyer et al., Phys. Rev. Lett. **39**, 392 (1977).
2. P. Dyer et al., Nucl. Phys. A **322**, 205 (1979).
3. R.J. Puigh et al., Phys. Lett. B **86**, 24 (1979).
4. R.J. Puigh et al., Nucl. Phys. A **336**, 279 (1980).
5. H.J. Specht, Invited Talk at Int. Conf. on Nucl. Interactions, Canberra, Australia, 1978; D.V. Harrach et al., Phys. Rev. Lett. **42**, 1728 (1979).
6. M.F. Rivet, private communication.
7. R. Vandenbosch, Phys. Rev. C **20**, 171 (1979).
8. J. Randrup, (unpublished).
9. C. Le Brun et al., preprint, 1980.

Total γ-Ray Energy Measurements for the Reaction $^{176}Yb + ^{165}Ho$ at 8.5 MeV/A

R.J. McDonald, A.J. Pacheco, G.J. Wozniak, D.J. Morrissey, L.G. Sobotka, L.G. Moretto, H. Lindenberger,† C. Schück,‡ S. Shih,§ J.O. Newton,‖ R.M. Diamond, and F.S. Stephens*

The correlation between fragment spin and γ-ray multiplicity has been used extensively to investigate angular momentum transfer in both compound-nucleus and deep-inelastic reactions. Since rotational energy is proportional to spin, a similar correlation should exist between the total γ-ray energy emitted from the reaction products and the transferred nuclear spin. This latter technique has been used to investigate high-spin states formed by compound-nucleus reactions. In this paper, we report the first measurement of total γ-ray energy for a deep-inelastic reaction. The reaction $^{176}Yb + ^{165}Ho$ was chosen since it had previously been studied via continuum γ-ray multiplicity and anisotropy techniques.

The rationale behind the sum-crystal technique is that nuclear rotational energy is given by $E_r = I(I + 1)/2\mathcal{I}$ where I is the nuclear spin and $\mathcal{I}$ is the moment of inertia. In reality, this picture is complicated by the emission of statistical γ-rays and neutrons which deposit energy in the sum crystal along with the "rotational" γ-rays. Fluctuations plus the < 100% efficiency of the sum crystal also

increases the width of the distribution above that expected from the distribution of spins alone.

Two particle detectors were placed at 28° to the beam direction. Scattering into either of these detectors defined a reaction plane. A 5 × 6 inch NaI detector was placed in this reaction plane at 90° to the beam. An identical detector was placed perpendicular to this direction, also at 90° to the beam. This detector looked through a hole in the sum crystal. The upper and lower halves of the sum crystal were separated by 2 inches.

The 5 × 6 inch NaI detectors were used to measure the γ-ray multiplicity and anisotropy for the reaction ^{176}Yb + ^{165}Ho at 8.5 MeV/A over the range of Q-values from 0 to −400 MeV. Almost all of these particle-γ coincidence events were accompanied by sum-energy data.

Figure 1 shows the resulting data for the average γ-ray energy and the standard deviation of its distribution as a function of Q-value. Only "arbitrary energy units" are used in Fig. 1 due to difficulties in calibrating the sum spectrometer.[1] Note how the total energy increases with increasing Q-value, similar to the well known increase of the γ-ray multiplicity with energy damping. Besides uncertainties in the energy calibration, the sum energy contains significant energy due to neutrons (up to 30 neutrons are emitted per reaction) and statistical γ-rays.

Figure 2a shows the γ-ray multiplicity both with and without gates on the sum energy. Similarly, Fig. 2(b) shows the continuum γ-ray anisotropy both with and without sum-energy gates.

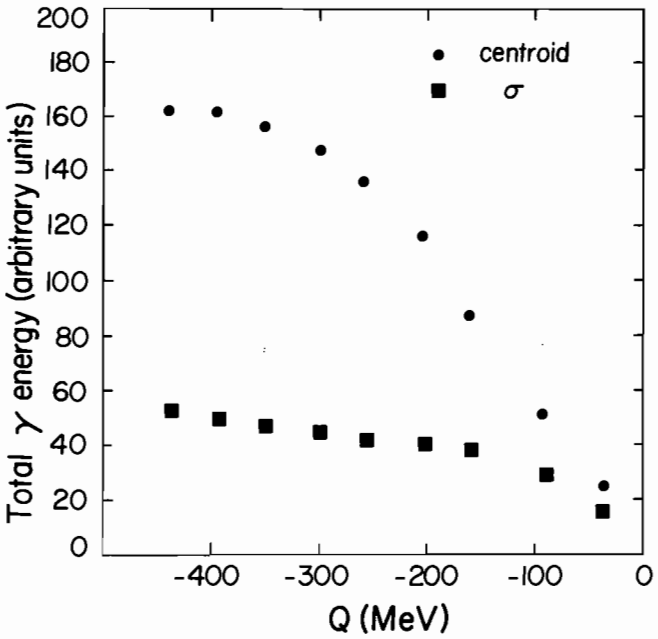

Fig. 1. Centroid and standard deviation of the sum-energy distribution. (XBL 818-2444)

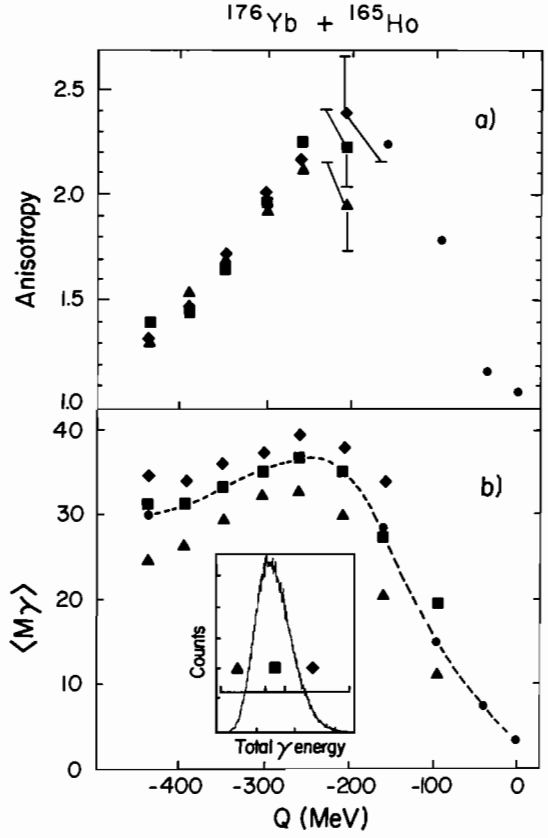

Fig. 2. (a) Continuum γ-ray anisotropy and (b) γ-ray multiplicity with and without gates on sum-E shown as an insert. (XBL 818-2443)

At present, significant uncertainties are associated with a quantitative interpretation of the sum-energy data. However, the trends in multiplicity and anisotropy are as expected from the simple theory given above. A gate on higher than average sum energy is associated with larger than average $<M_\gamma>$ (and therefore spin) and higher-than-average spin events tend to exhibit a slightly higher anisotropy.

Footnotes and References

*Comisión Nacional de Energía Atómica, Argentina.
†Hahn-Meitner Institute, Berlin, Germany.
‡C.S.N.S.M, Orsay, France.
§Shanghai Institute of Nuclear Research, People's Republic of China.
‖Australian National University, Canberra.

1. F. Folkmann et al., Nucl. Phys. A **361**, 242 (1981).

Angular Momentum, Statistical Equilibrium and Sequential Fission in Very Asymmetric Systems*

D.J. Morrissey,† G.J. Wozniak, L.G. Sobotka, A.J. Pacheco,‡
C.C. Hsu,§ R.J. McDonald, and L.G. Moretto

The measurement of the internal spin and its alignment for reaction partners from deep-inelastic heavy-ion collisions (DIC) has become an important tool for studying the process of angular momentum transfer. The measurement of fluctuations in the spin components provides a test of whether statistical equilibrium of angular momentum bearing modes of the dinuclear complex is achieved in a DIC.[1] Evidence for statistical equilibrium has been observed in symmetric reactions which have been studied by means of γ-ray angular distributions. In the very asymmetric ^{20}Ne + ^{197}Au and ^{238}U systems the statistical excitation of a number of angular momentum bearing modes is strongly suppressed. In particular, a large difference in the moments of inertia of the two reaction partners will increase the amount of energy necessary to excite any mode in which the small fragment is forced to rotate (wriggling, bending and twisting).[1] Excitation of the only surviving mode (tilting) predicts a minimum in the angular distribution of sequential fission fragments along the line-of-centers.[2] Thus very asymmetric reaction systems should provide an excellent test of the excitation of selected normal modes and of the statistical model in general.

A beam of 252-MeV ^{20}Ne from the 88-Inch Cyclotron was incident on targets of either 915 μg/cm^2 ^{197}Au or 922 μg/cm^2 $^{238}UF_4$. Projectile-like products were detected in a solid state telescope (11 μm ΔE, 300 μm E, dΩ = 3 msr) fixed at $-30°$. This angle is slightly behind or right at the classical grazing angles (26° and 30°, respectively). Fission fragments were detected in coincidence on the opposite side of the beam in an array of ten single element surface-barrier detectors (dΩ = 9 msr/detector), five in-plane and five out-of-plane. This array was moved to cover the angular region between $+30°$ and $+160°$ in-plane as well as between 0° and 75° out-of-plane along and perpendicular to the laboratory recoil axis. Fission fragments were unambiguously identified in a two-dimensional map of fission fragment energy vs time. The data were transformed event by event into the rest frame of the recoiling target nucleus using the energy, charge and angle of the light product and the energy and angles (Θ,Φ) of the fission fragment. The measured angular distributions are presented in Figs. 1 and 2 for the ^{20}Ne + ^{238}U and ^{197}Au systems as a function of Q-value. The data have been integrated over the fission fragment energy and the atomic number of projectile residues ($6 \leq Z \leq 14$). The direction $\Phi^H = 0$ was arbitrarily chosen to coincide with the laboratory recoil angle calculated as a function of Q (negative angles lie between the recoil direction and the beam). In order to ensure that evaporation was not biasing the kinematics, the data was also gated on $9 \leq Z \leq 10$. This gating does not alter the results, it only decreases the

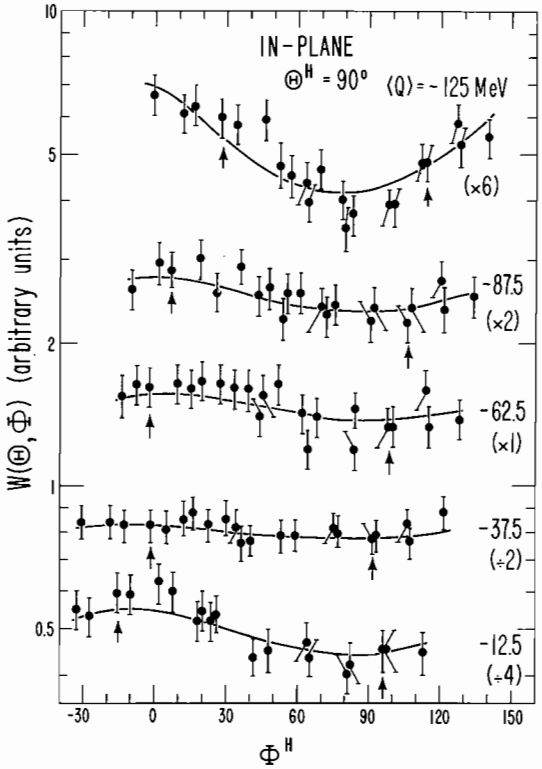

Fig. 1. The in-plane angular distributions of sequential fission fragments in the rest frame of the heavy fragment (H) are shown as a function of reaction Q-value for the ^{20}Ne + ^{238}U system. The arrows indicate the in-plane angles at which out-of-plane measurements were made.
(XBL 813-2180)

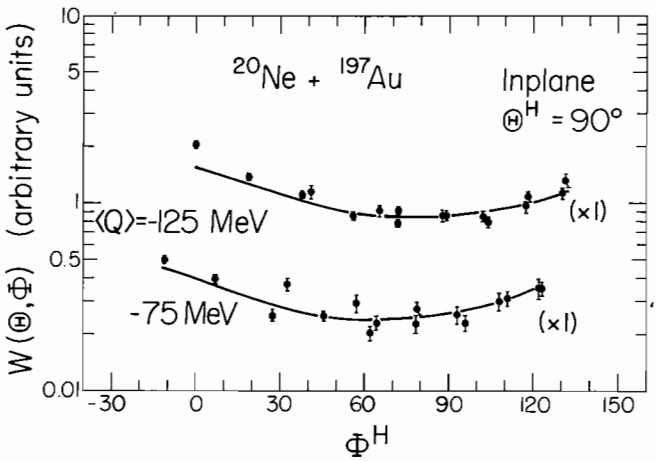

Fig. 2. Similar to Fig. 1, except for the ^{20}Ne + ^{197}Au system.
(XBL 817-2365)

statistical accuracy.

In order to extract quantitative values for the spin polarization of the heavy fragment we have fit the angular distribution data to the generalized function of the statistical model of Broglia et al.[3] In this description the three cartesian widths σ_x, σ_y and σ_z (defined such that x lies along the line-of-centers) appear explicitly along with the projection of the spin on the alignment axis, I_z, and the projection of I on the fission separation axis, K_o. Finally, one must determine the direction of the line-of-centers of the intermediate complex with respect to the traditional reference direction, the laboratory recoil angle. The appropriate choice for the line-of-centers in a equilibrium statistical model is the line connecting the centers of the two fragments at scission when the directions and magnitudes of thermally induced spin components are frozen in. An estimate of the direction of the line-of-centers can be made by tracing the projectile-like product backward along the coulomb trajectory that corresponds to the average orbital angular momentum, L_{out}, for each bin. These estimates are consistent with the shift in the positions of the minima seen in Figs. 1 and 2. The results of reduced chi-squared fitting of the function to the data are shown by the solid curves in Figs. 1 and 2.

From the results of the fitting we find that the statistical model predictions are in good agreement with all of the out-of-plane angular distributions. For the more stringent test afforded by the in-plane angular distributions, this model overpredicts the anisotropy, except for the most negative Q-value where the agreement is good. These trends agree with our expectations that the statistical model represents the long-time limit which is attained in collisions with the largest energy-losses.

Footnotes and References

*Condensed from LBL-12181, submitted to Z. Phys.

†Permanent address: Department of Chemistry, Michigan State University, East Lansing, Michigan 48824.

‡Permanent address: Comisión Nacional de Energía Atómica, Buenos Aires, Argentina.

§Permanent address: Institute of Atomic Energy, Beijing, People's Republic of China.

1. L.G. Moretto and R.P. Schmitt, Phys. Rev. C **21**, 204 (1980).

2. R.P. Schmitt and A.J. Pacheco, to be published. See also contribution to this annual report.

3. R.A. Broglia et al., Phys. Rev. Lett. **43**, 1649 (1979).

Fragment Spin Alignment in Deep-Inelastic Reactions

A.J. Pacheco, R.J. McDonald, G.J. Wozniak, C.C. Hsu,† D.J. Morrissey, L.G. Sobotka, S. Shih,‡ R.M. Diamond, F.S. Stephens, and L.G. Moretto*

Recently, the magnitude and alignment of the spin transferred to the fragments in the system ^{165}Ho + ^{165}Ho at 8.5 MeV/amu were studied using continuum γ-ray multiplicity and anisotropy techniques.[1] Results were in substantial agreement with the predictions of an equilibrium statistical model.[2] In the present work we report preliminary results from a similar investigation carried out in three different reactions: ^{176}Yb + ^{165}Ho, ^{148}Sm + ^{165}Ho and ^{nat}Ag + ^{165}Ho, all at 8.5 MeV/amu.

The purpose of the experiment was to investigate the extent to which the measurement of continuum γ-rays in different systems represents a useful technique in the study of angular-momentum transfer processes. The targets used cover a wide region of the chart of nuclides and therefore exhibit well differentiated nuclear properties. The neutron-rich ^{176}Yb nucleus lies in the region of the good rotors, and the expected evaporation of a large number of neutrons per fragment in these reactions still leaves the residual fragments in the rotational region. On the other hand all the isotopes in ^{nat}Ag are well removed from this region of good rotors. Finally, the ^{148}Sm nucleus, only 4 neutrons away from the N = 82 closed shell, represents an intermediate situation between these two regimes. It is also our purpose to utilize the data from the various systems to further test the validity of the equilibrium model.

The experimental set-up was similar to that used in Ref. 1. Three surface-barrier Si detectors were used for heavy-particle detection. These counters together with the beam direction determined two mutually perpendicular reaction planes. Three 5 × 6 inch NaI crystals for γ-ray detection were arranged so that each of them gave at least one in-plane and one 90°-out-of-plane measurement when observed in coincidence with the various Si detectors. This arrangement provided a high redundancy that helped in the identification and correction of possible systematic errors. In addition an array of eight 3 × 3 inch NaI detectors (multiplicity filter) was used, and the number of detectors firing per event was recorded.

For each of the three targets average multiplicities and anisotropies were calculated as a function of Q-value. The average "in-plane" and "out-of-plane" multiplicity was calculated as proportional to the ratio between particle-γ coincidences and particle singles, using all the combinations between each 5 × 6 inch NaI detector and each Si detector. Corrections for angular distributions were made in order to calculate the average multiplicity

$<M_\gamma>$. The anisotropies were calculated as the ratio between in-plane and out-of-plane multiplicities.

Figure 1 shows the dependence of $<M_\gamma>$ (90°) on Q for the three systems. There is a characteristic rise in the quasi-elastic region followed by a saturation or even a slight decrease at the most inelastic events. The maximum value reached steadily decreases when going from the ^{176}Yb to the ^{nat}Ag target. This trend is expected from changes in both the maximum total angular momentum in the system and the moments of inertia of the fragments. In all three targets the selection on 2-and-higher-fold coincidences in the multiplicity array produces a systematic increase of $<M_\gamma>$ throughout the whole Q-value range. This effect illustrates the correspondence between the independent measurements of high-fold γ-ray coincidences and $<M_\gamma>$.

Figure 2 shows γ-ray anisotropies as a function of Q-value. For the three targets one observes a rise at the quasielastic and a fall throughout the deep-inelastic region.

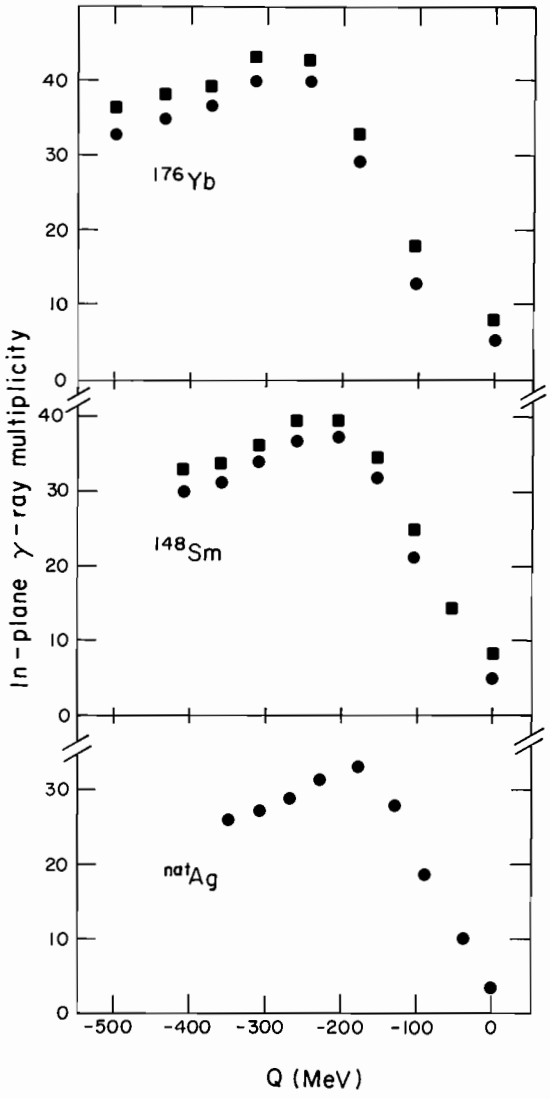

Fig. 1. In-plane multiplicity as a function of Q-value with (squares) and without (circles) gates on high-fold coincidences. (XBL 818-2448)

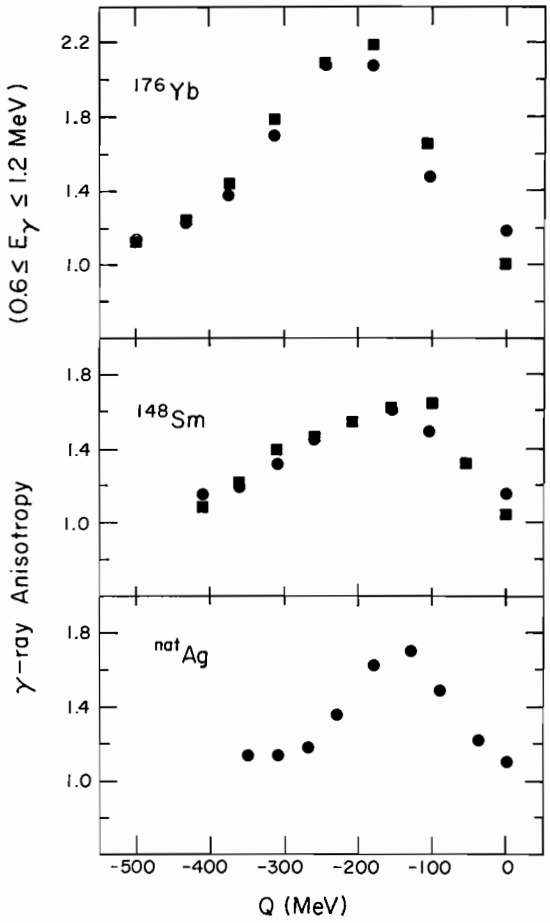

Fig. 2. Anisotropy as a function of Q-value with (squares) and without (circles) gates on high-fold coincidences. (XBL 818-2449)

There is a noticeable difference in the maximum value reached when the ^{176}Yb data are compared to those of the other two targets. However one can tentatively conclude that even in the ^{nat}Ag + ^{165}Ho reaction the predominant γ-decay occur via stretched E2 transitions, and therefore the observed anisotropies are correlated to the spin alignment. Finally one observes that gating on 2-and-higher-fold coincidences does not alter substantially the anisotropies. This result may be ascribed to the fact that the geometrical arrangement of the multiplicity filter was not optimized to detect the in-plane-peaked quadrupole radiation.

A more quantitative interpretation of these data in terms of the angular-momentum-transfer mechanism and the comparison with the equilibrium model are underway.

Footnotes and References

*Comisión Nacional de Energía Atómica, Buenos Aires, Argentina.
†Institute of Atomic Energy, Beijing, People's Republic of China.
‡Shanghai Institute of Nuclear Research, People's Republic of China.

1. G.J. Wozniak et al., Phys. Rev. Lett. **45**, 1080 (1980).
2. L.G. Moretto and R.P. Schmitt, Phys. Rev. **C21**, 204 (1980).

The $^{12}C + ^{12}C$ Reaction Cross Section Between 70 and 290 MeV Obtained From Elastic Scattering*

A.J. Cole, W.D.M. Rae, M.E. Brandan,† A. Dacal,† B.G. Harvey, R. Legrain,‡ M.J. Murphy, and R.G. Stokstad

The variation of the nuclear reaction cross section $\sigma_R(E)$ has been investigated recently by DeVries and collaborators.[1,2] They suggest that the nuclear transparency increases quite rapidly at energies above 10 MeV/A even for strongly absorbed projectiles such as α particles and that this increase seems to correlate with the known fall-off of the nucleon-nucleon cross section[3,4] suggesting the dominance of the latter in determining σ_R. In particular their calculations predict that for $^{12}C + ^{12}C$ scattering σ_R and σ_T reach a maximum at $E_{cm} \simeq 100$ MeV.

Although some data for $^{12}C + ^{12}C$ exist at higher[5,6] and lower[7,8] energies, there is a serious lack of experimental data on σ_R for heavy ions in this energy region. Thus measurements of the elastic scattering of $^{12}C + ^{12}C$ were undertaken between 120 and 290 MeV.

The experiments were carried out using 4^+ and 5^+ beams of ^{12}C from the LBL 88-Inch Cyclotron. Measurements were made in 0.25° steps in the forward angle region (2°-15° lab) which is of critical importance in the determination of σ_R and σ_T. Since an accurate knowledge of the scattering angle is essential for the accurate determination of σ_R and σ_T, two sets of four lithium-drifted silicon detectors of 3 mm thickness were located on moveable arms at angles to the left and right of the beam direction. The targets were made of natural carbon of thicknesses between 275 and 1000 $\mu g/cm^2$ determined to ± 5% by α energy loss measurements. Data were taken at 10 energies between 121.6 MeV and 287.8 MeV.

Final differential cross sections were obtained by averaging results from left and right detectors, thereby eliminating to first order effects of beam movement and misalignment. The angular error of the data was essentially due to the precision with which the angles of the detectors could be set and was estimated to be 0.125°. An additional measurement at 289 MeV was carried out using two position-sensitive detectors and a strip target. The angular accuracy in this case was ± 0.07°.

Several of the resultant differential cross sections are shown in Fig. 1. The results are plotted against momentum transfer rather than c.m. angle to emphasize that the positions of the most forward angle minima are almost energy independent and that the depths of the minima evolve smoothly over the energy range investigated.

A phase shift parameterization was used in a computer program that optimized the parameters using a nonlinear least squares fitting procedure. The ability of this parameterization to reproduce known values of σ_R and σ_T was determined by fitting theoretical "data" between 5° and 25° (cm) generated from an optical model calculation. Values of σ_R and σ_T so deduced agreed to within 1.5% with the optical model values. Values obtained from the analysis of the experimental data are displayed in Fig. 2. The above analysis was also applied to published data[8] between 70 and 127 MeV (Lab) and the results are included in Fig. 2.

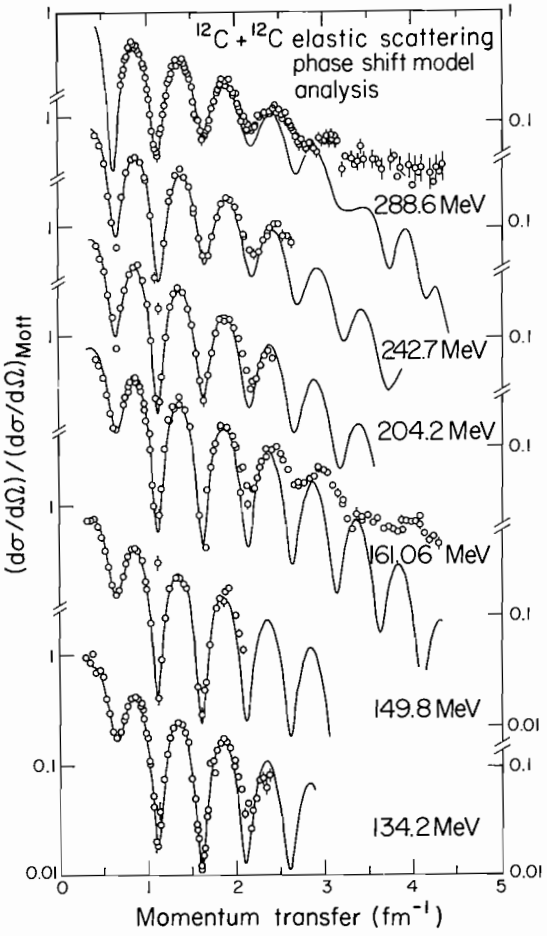

Fig. 1. Elastic scattering cross sections as a function of momentum transfer. The smooth lines are the results of calculations using the parameterized phase shift model.
(XBL 817-2416A)

To investigate the model dependence of the deduced values of σ_R and σ_T, our data were also fitted using the standard 6 parameter optical model. It should be made clear that in these fits emphasis was placed on obtaining the best description of the forward angle diffraction structure and not on the determination of a smoothly energy-dependent optical model parameter set. The deduced

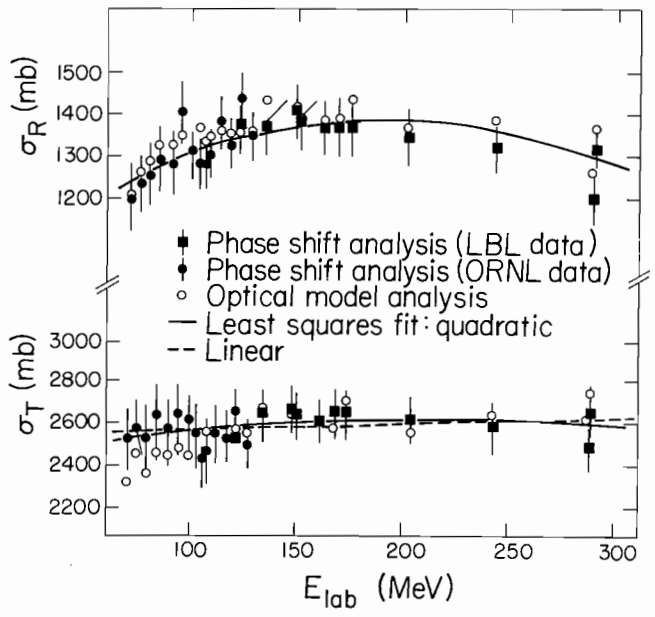

Fig. 2. Deduced values of σ_R and σ_T from parameterized phase shift analysis shown with least squares quadratic fit for $\sigma_R(E)$ and least squares linear and quadratic fits for $\sigma_T(E)$. Results of optical model fits are also given. (XBL 817-2417)

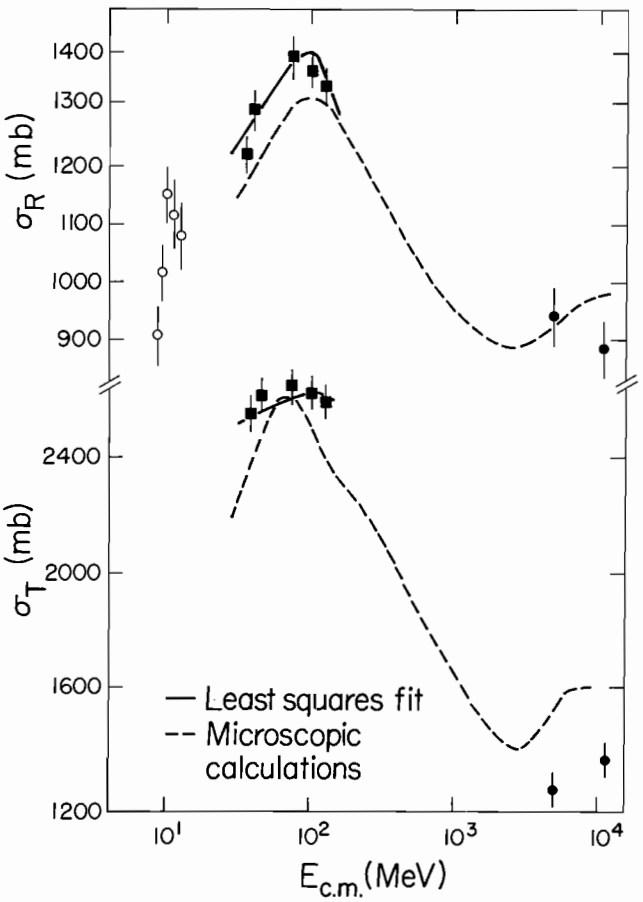

Fig. 3. Least squares quadratic fits from Fig. 2 shown with microscopic calculations for σ_R (Ref. 2) and σ_T (Ref. 4). Representative data points from the present work (squares) as well as low energy data taken from Ref. 7 (open circles) and high energy data from Ref. 6 (filled circles) are given in the figure. (XBL 817-2418)

values of σ_R, although slightly higher (see Fig. 2), exhibit the same trend with energy as those obtained from the phase shift model. The values of σ_T are also very similar for the two models except at the lowest energies.

In Fig. 3 our results for σ_R are compared with the calculations of DiGiacomo et al.[2] and those for σ_T with that of Peng et al.[4] The calculation for σ_T disagrees somewhat with our data, which do not exhibit the sharp rise and fall of the predicted values. In fact our data are consistent with a constant value (σ_T = 2570 mb) over the energy range studies. The agreement for σ_R is more satisfactory. In particular it does appear that the reaction cross section reaches a maximum at $E_{cm} \simeq 100$ MeV.

In conclusion our experiments indicate a maximum in $\sigma_R(E)$ at $E_{cm} \simeq 100$ MeV as predicted in Refs. 1 and 2. However, the role of the energy dependence of the nucleon-nucleon force in producing such a maximum remains uncertain. Accurate measurements of σ_R and σ_T over a wider range of energies will undoubtedly be of use in understanding the respective roles of "mean field" and "nucleon-nucleon" aspects of the problem. Further theoretical work in the low and medium energy region near the maximum of $\sigma_R(E)$ would also be valuable.

Footnotes and References

*Condensed from LBL-13011.

†Permanent address: Instituto de Fisíca, Universidad National Autonoma de Mexico, Mexico 20 DF.

‡Permanent address: DPhN-BE, CEN-Saclay, PB no. 2, 91190 Gif-sur-Yvett, France.

1. R.M. DeVries and J.C. Peng, Phys. Rev. Lett. **43**, 1373 (1979); R.M. DeVries and J.C. Peng, Phys. Rev. C **22**, 1055 (1980).
2. N.J. DiGiacomo, private communication.
3. N.J. DiGiacomo et al. Phys. Lett. B **101**, 383 (1981).
4. J.C. Peng, et al., Phys. Lett. B **98**, 244 (1981).
5. M. Buenerd et al., Phys. Lett. B **102**, 242 (1981).
6. T. Jaros et al., Phys. Rev. C **18**, 2273 (1978).
7. W. Treu et al., Phys. Rev. C **22**, 2462 (1980).
8. R.G. Stokstad et al., Phys. Rev. C **20**, 655 (1979).

Isomer Ratio Measurements for the Reaction $^{29}Si(^{18}O,p2n)\ ^{44}Sc^{m},\ ^{44}Sc^{g}$

H. Groening, K. Aleklett,† K.J. Moody, P.L. McGaughey, W. Loveland,‡ and G.T. Seaborg*

The isomeric ratio dependence on projectile kinetic energy for the reaction $^{29}Si(^{18}O,p2n)\ ^{44}Sc^{m},\ ^{44}Sc^{g}$ was previously reported in the 1978-1979 LBL Nuclear Science Annual Report.[1] We have attempted to fit the experimental data with essentially one parameter, that is, the ratio of dipole to quadrupole gamma ray strengths. Our calculations were divided into two parts. In the first part, we have used M. Blann's evaporation code "ALERT"[2] to calculate population distributions in the E-J plane for $^{44}Sc^{*}$. In the second part, we have taken the portion of the $^{44}Sc^{*}$ population lying between the yrast line and a line roughly one neutron binding energy above it and calculated the fractions of such populations decaying to the isomeric and ground states, respectively. The best fit obtained in the calculation was for a quadrupole to dipole gamma ray strengths ratio $|M_{if}(E2)|^2/\ |M_{if}(E1,M1)|^2 = 0.03$, where $M_{if}(\sigma\lambda)$ is the reduced matrix element for radiation of multipolarity λ; σ represents the nature of the radiation, magnetic or electric; and $|M_{if}(E1,M1)|^2$ is the sum of $|M_{if}(E1)|^2$ and $|M_{if}(M1)|^2$. Figure 1 shows some of the fits to the experimental data. The gamma ray strengths ratio deduced in this work agrees substantially well with the one estimated from measured gamma ray strength averages in the literature[3] ($\sim$ 0.02). Reducing the number of discrete levels results in an increase of the isomeric ratio.

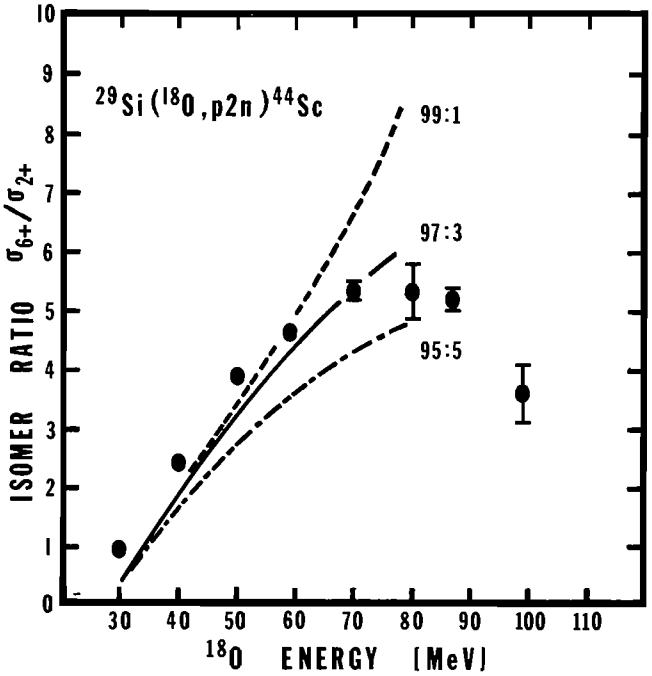

Fig. 1. Isomer ratios and calculated fits for the reaction $^{29}Si(^{18}O,p2n)\ ^{44}Sc^{m},\ ^{44}Sc^{g}$, using different values of dipole to quadrupole gamma-ray strengths ratio.

(XBL 818-11296)

Footnotes and References

*On leave from Universidad Simón Bolívar, Caracas, Venezuela.

†Present address: Studsvik Science Res. Lab. S-611 82, Nyköping, Sweden.

‡Present address: Radiation Center, Oregon State Univ., Corvallis, OR 97330.

1. K. Aleklett et al., Lawrence Berkeley Laboratory Report LBL-9711, p. 77 (1980).

2. M. Blann, Phys. Rev. C **21**, 1770 (1980).

3. P.M. Endt, Atomic Data and Nuclear Data Tables **23**, 3 (1979).

Excitation Functions and Isomeric Ratio Measurements for the Reaction $^{41}K(^{6}Li,p2n)\ ^{44}Sc^{m},\ ^{44}Sc^{g}$

H.D. Nguyen, H.N. Trinh, H.D. Le, K.J. Moody, H. Groening, and G.T. Seaborg*

In a previous report,[1] isomeric ratios in ^{44}Sc resulting from the $^{41}K(\alpha,n)$ and $^{29}Si(^{18}O,p2n)$ reactions were related to specific patterns in the average spins and energies of $^{44}Sc^{*}$ previous to most of its gamma ray deexcitation. The purpose of this work is to determine additional points in the $\langle E\rangle - \langle J\rangle$ plane for low values of the average angular momentum in $^{45}Sc^{*}$ that will result in corresponding ^{44}Sc isomer ratios. With this in mind, we have measured excitation functions and isomeric ratios of the reaction $^{41}K(^{6}Li,p2n)\ ^{44}Sc^{m},\ ^{44}Sc^{g}$. The excitation function has been determined for ^{6}Li energies of 14.4, 23.4, 32.0, and 41.5 MeV, while the isomeric ratios have

been deduced for energies of 14.4, 23.4, 32.0, 37.0, 41.5, and 50.0 MeV.

Targets consisting of a 500 $\mu g/cm^2$ layer of enriched (99%) ^{41}KCl on a backing of 0.25-mm Ta were irradiated with as much as a particle-micro-ampere of ^{6}Li at the 88-Inch Cyclotron. With ^{6}Li at higher energies, activation of the Ta backing was severe, and chemistry was performed to separate scandium from the other reaction products. Figure 1 shows the isomeric ratio as a function of ^{6}Li kinetic energy for the reaction $^{41}K(^{6}Li,p2n)\ ^{44}Sc^{m}, ^{44}Sc^{g}$. The increase in isomeric ratio with ^{6}Li energy cannot be explained through compound nucleus theory. As Fig. 1 shows, experimental ratios increase much slower than predicted by this mechanism. We hope to infer the initial $<E> - <J>$ distributions in $^{44}Sc^{*}$ and $^{45}Sc^{*}$ by accounting properly for the direct component in this reaction.

Footnote and Reference

*On leave from Universidad Simón Bolívar, Caracas, Venezuela.

1. H. Groening, K.J. Moody and G.T. Seaborg, in this Annual Report.

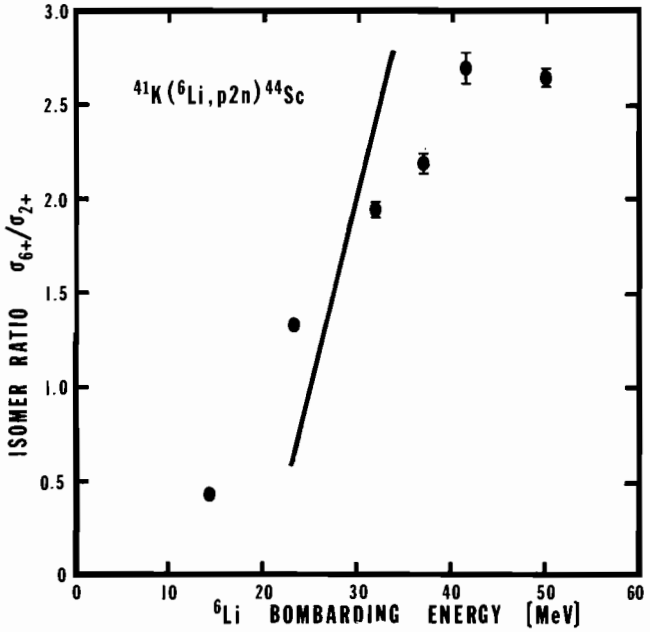

Fig. 1. Isomeric ratio as a function of projectile kinetic energy for the reaction $^{41}K(^{6}Li,p2n)\ ^{44}Sc^{m}, ^{44}Sc^{g}$. Solid line is calculated isomeric ratio, assuming that the reaction proceeds only through compound nucleus formation.

(XBL 818-11295)

3. Target and Projectile Fragmentation

Transfer Versus Fragmentation for Reactions Near 15 MeV/Nucleon*

M.J. Murphy, B.G. Harvey, D.L. Hendrie, J. Mahoney, W. Pang, and K. Van Bibber†

Somewhere between 10 and 100 MeV/Nucleon, peripheral heavy ion reactions change from being mainly transfer-like events to being mainly fragmentation-like events. In the same energy range, the intrinsic momentum width σ_0 of the inclusive heavy ion spectra for peripheral reactions changes from a characteristic low energy value to a limiting high energy width.[1] It appears that these transitions are well underway at 15 MeV/nucleon.[2]

In an effort to find the explanation for the transition from transfer to fragmentation and its (possible) connection with the change in inclusive momentum widths, we have been studying the spectra of heavy ion ejectiles as a function of charged particle multiplicity for the reaction of 16.5 MeV/nucleon ^{16}O + CsI. The first measurements have been made at the 88-Inch Cyclotron using a streamer chamber triggered by forward-angle Si(Li) particle telescopes. The telescopes identify the charge, mass, and energy of a particular heavy ion ejectile, and the streamer chamber records the total charged-particle multiplicity of the event. This enables a separation of complete transfer-like events from higher multiplicity (fragmentation and incomplete transfer) events.

Our first results show two important features. First, the relative probability of transferring a cluster of mass A decreases as A increases, in a way closely consistent with Wilczynski's model of transfer[3] (Fig. 1). Second, as the ejectile mass decreases, the relative probability of higher multiplicity events increases, i.e., there is a trade-off between transfer and fragmentation (Fig. 2).

The next research step is an analysis of the ejectile momentum widths as a function of final state multiplicity. This will show if the change in intrinsic widths with increasing energy is due to a basic difference in the characteristic widths for transfer and for fragmentation. The streamer chamber system places rather too severe a limit on the statistics for a definitive study of the reaction widths (this will be made using solid state detectors), but it is an invaluable device for studying the basic multiplicities and topology of reactions in this energy range.

Footnotes and References

*Condensed from the Proceedings of the 5th High Energy Heavy Ion Study, Lawrence Berkeley Laboratory Report, LBL-12652 (1981).

†Stanford University.

1. D.K. Scott, The Current Experimental Situation in Heavy-Ion Reactions. Lawrence Berkeley Laboratory Report LBL-7727 (1978).

2. M.J. Murphy et al., *Proceedings of the 5th High Energy Heavy Ion Study*, Lawrence Berkeley Laboratory Report LBL-12652 (1981).

3. J. Wilczynski et al., Phys. Rev. Lett. **45**, 606 (1980).

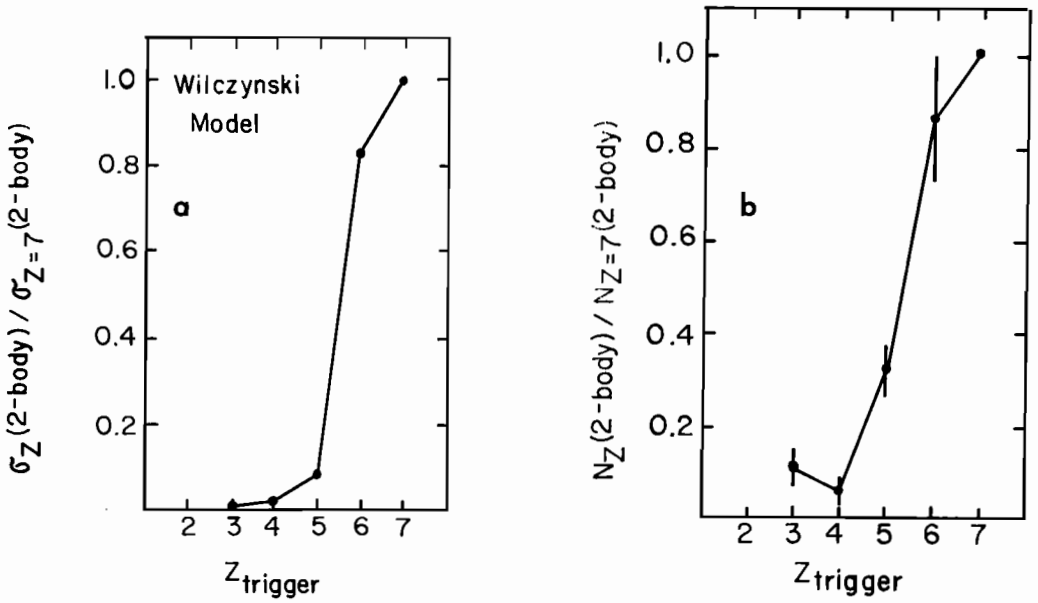

Fig. 1. A comparison of calculated (a) and observed (b) cross sections for transfer in the reaction ^{60}O + CsI at 16.5 MeV/n, as a function of cluster charge and normalized to z = 1 clusters. [(a) XBL 819-1278; (b) XBL 819-1277]

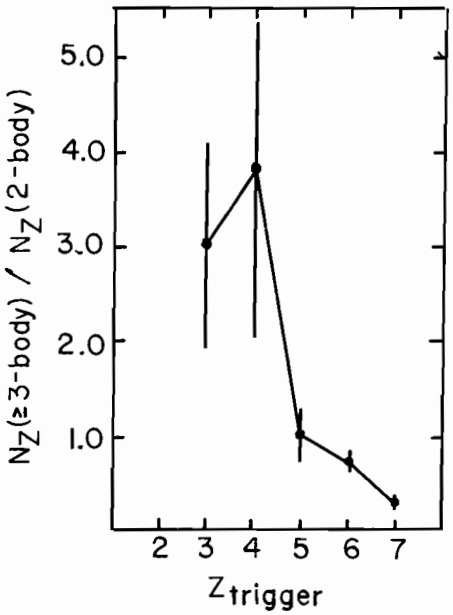

Fig. 2. The relative probability of transfer-like and fragmentation-like events for ^{16}O + CsI, as a function of ejectile charge. (XBL 819-1279)

Small Momentum Widths in Heavy Ion Fragmentation at 20 MeV/amu and Below*

Bernard G. Harvey

Egelhaaf et al.[1] have reported that the momentum widths of ^{16}O and ^{12}C produced by the fragmentation of ^{20}Ne on a ^{197}Au target are substantially smaller than the value published by Gelbke et al.[2] for the fragmentation of ^{16}O by a Pb target. In Ref. 1, several reasons for the apparent discrepancy are given, one of them being that Gelbke et al. measured the momentum spectra for elements whereas Egelhaaf et al. measured them for individual isotopes. Moreover, Egelhaaf et al. extracted the momentum width by fitting a Gaussian only to the high-momentum side of each peak. The peak shapes in both experiments are approximately Gaussian on the high-momentum side and down to half-maximum on the low-momentum side.

In reality, the momentum width reported by Gelbke et al.[2] is not a fit to the spectrum of any single element. It was adjusted to make an approximate fit to *all* the elements from Li to N that were observed in the experiment. A Gaussian least squares fit just to the C peak in fact yields a width that is substantially smaller than the global value for all observed elements.

Scott et al.[3] have used the data of Ref. 2 and additional data to measure the spectra of individual isotopes produced by the fragmentation or incomplete fusion of ^{16}O at several energies on Pb and Au targets. Making a least squares fit to these unpublished data yields a width σ which can be related to the reduced width σ_0 by:

$$\sigma^2 = \sigma_0^2 m_f(m_p - m_f)/(m_p - 1) \ ,$$

where m_p and m_f are the projectile and observed fragment masses.[4,5] The results for ^{12}C are shown in Table 1 and compared with the results of Ref. 1.

Table 1 shows that the reduced widths for $^{16}O \rightarrow {}^{12}C$ are much smaller than the "global fit" value of 80 MeV/c of Ref. 2. There is no serious discrepancy between the two experiments.

Scott[6] used the results of Ref. 2 to suggest that σ_0 attains a limiting value of about 86 MeV/c at a beam energy of only 10 MeV/amu above the Coulomb barrier. The results of Egelhaaf et al. and the present reanalysis of the unpublished data of Scott et al.[3] show that, at least for the reactions $^{16}O \rightarrow {}^{12}C$ and $^{20}Ne \rightarrow {}^{16}O, {}^{12}C$ the limiting value is approached much more slowly than was previously thought. In the fragmentation of 92.5 MeV/amu ^{16}O by ^{197}Au, though, σ_0 averaged 80 MeV/c for all observed fragments.[7] The evolution of σ_0 for beam energies between 20 MeV/amu and 90 MeV/amu remains to be explored.

Table 1. Reduced widths of fragmentation spectra.

Projectile	$^{16}O \rightarrow {}^{12}C$		$^{20}Ne \rightarrow {}^{16}O$	$^{20}Ne \rightarrow {}^{12}C$
Energy	σ_0[a]	σ_0[b]	σ_0[c]	σ_0[c]
(MeV/amu)	(MeV/c)	(MeV/c)	(MeV/c)	(MeV/c)
19.7	50	58	35	42
15.6	43	50	35	41
13.6	33	40	34	40
8.75	32	34	21	31

[a] σ_0 obtained from fit to high-momentum side of peak. Data of Ref. 3.

[b] σ_0 obtained from fit to all data down to one-half maximum on low-momentum side of peak. Data of Ref. 3.

[c] σ_0 from Fig. 2 of Ref. 1.

Footnote and References

*Condensed from LBL-12787.

1. Ch. Egelhaaf et al., Phys. Rev. Lett. **46**, 813 (1981).
2. C.K. Gelbke et al., Phys. Lett. B **70**, 415 (1977).
3. D.K. Scott et al., LBL-7729 (June 1978), unpublished.
4. A.S. Goldhaber, Phys. Lett. B **53**, 306 (1974).
5. D.E. Greiner et al., Phys. Rev. Lett. **35**, 152 (1975).
6. D.K. Scott, *Proceedings of the International Conference on Nuclear Physics*, Berkeley, Aug. 1980, **Vol. 2**, p. 375c.
7. K. Van Bibber et al., Phys. Rev. Lett. **43**, 840 (1979).

Coherent and Incoherent Processes In Projectile Breakup*

W.D. Rae, A.J. Cole, A. Dacal,† R. Legrain,‡ B.G. Harvey, J. Mahoney, M.J. Murphy, R.G. Stokstad, and I. Tserruya§

There has been much interest recently in the field of heavy ion breakup and fragmentation reactions. The simplest case that can be studied is binary breakup where only two projectile fragments are produced. Binary breakup has been classified as either sequential or direct.[1] Sequential breakup is associated with decay from excited states of the projectile, while direct breakup describes those events for which the relative kinetic energy of the two fragments is not necessarily correlated with an excited state of the projectile.

Our recent analysis[2] of the ground state ($Q = -7.16$ MeV) breakup of 140 MeV $^{16}O \rightarrow {}^{12}C + \alpha$ on a ^{12}C target revealed only sequential processes. We have continued these studies, and our new data suggest a classification different from that implied by the terms "sequential" and "direct" because we observe at least two mechanisms leading to sharp states in ^{16}O which decay sequentially.

Although the experiment and analysis were similar in principle to those described in Ref. 2, the introduction of position-sensitive detectors made possible the use of large solid angles without loss of angular resolution ($\lesssim 0.2°$ Lab). In the analysis of the data for each coincident event, two quantities were determined: the sum $E_T = E_\alpha + E_{12c}$, which is related to the reaction Q_3-value, and E_{real}, the relative kinetic energy of the α and the ^{12}C in their center-of-mass system.

The spectrum of E_T and the spectra of E_{real} for different values of E_T are shown in Figs. 1 and 2. For the highest E_T bin, which corresponds to $Q_3 = -7.16$ MeV, states at the following energies in ^{16}O are clearly observed: 9.88 (2^+), 10.36 (4^+), 11.06 (4^+), 11.52 (2^+), 12.41 (1^-), 13.10 (2^+), 14.00 (0^+), and 15.60 MeV (3^-). For $Q_3 = -11.60$ MeV, an additional strong peak is observed which probably corresponds to a state at 17.14 MeV (2^+) which decayed to $\alpha + {}^{12}C$ (4.44 MeV).

There is a marked qualitative change in the spectra of E_{rel} for values of $Q_3 < -11.6$ MeV: only the states at 9.85, 10.35, and 11.10 MeV and a broad background extending beyond $E_{rel} = 14$ MeV are observed. Significantly, these three states are the only states consistently observed in our data which are populated in α-transfer reactions on ^{12}C.[3] Furthermore, with the exception of the state at 15.60 MeV, all other strong states observed for low $|Q_3|$-values are excited strongly in $^{16}O(\alpha,\alpha')$, $^{16}O(e,e')$, or $^{15}N(p,\gamma)$ reactions.

The mechanisms which excite the background and the states at 9.85, 10.35, and 11.10 MeV appear to be different from that which excites the collective states. Collective excitation of the projectile involves the coherent response of the whole projectile to the field of the target nucleus; thus, we term the excitation and decay of these states "coherent breakup."

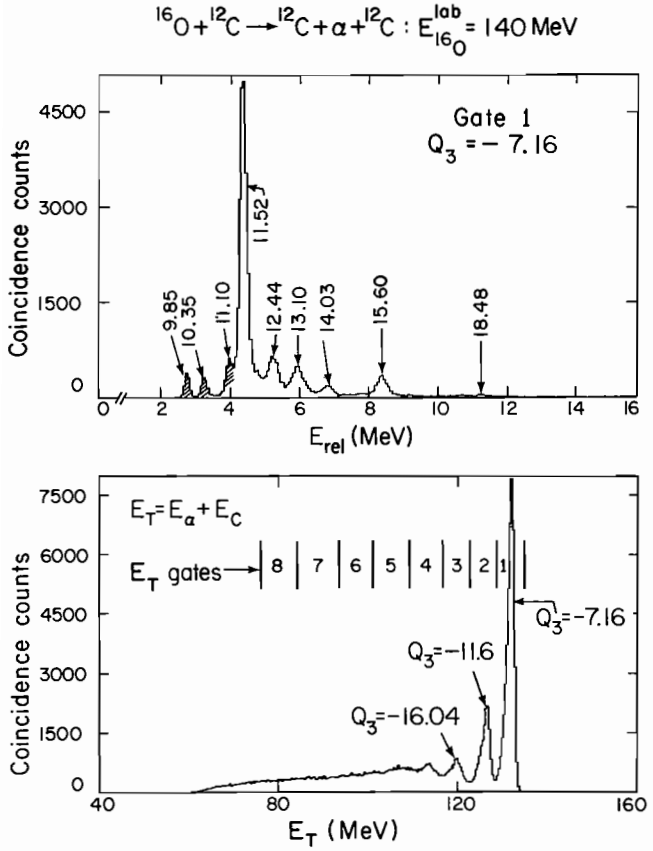

Fig. 1. $E_T = E_\alpha + E_{12_C}$ and E_{rel} spectra (as defined in text) for Q = −7.16 MeV. Excitation energies refer to ^{16}O and are in MeV. (XBL 814-655)

On the other hand, the three states which are also observed in α-transfer reactions are those which might be expected to be observed in a quasi-free scattering of the α and ^{12}C constituents of ^{16}O to the continuum via the individual interaction of either constituent with the target. Since the α and ^{12}C constituents are assumed to interact independently with the target, we can class this mechanism as an incoherent breakup process.

In conclusion, our experimental data reveals the presence of at least two mechanisms in the breakup of ^{16}O and $^{12}C + \alpha$: (1) a coherent process which excites the projectile to states whose structure is related to that of the ground state via multipole operator, and (2) incoherent processes. The incoherent amplitudes contain resonant contributions at relative energies corresponding to specific excited states of the projectile, as well as possible non-resonant contribution. We speculate that the dominant incoherent process is the quasi-free scattering of the α or ^{12}C constituents of the projectile by the target, viz, the direct breakup of the ^{16}O projectile.

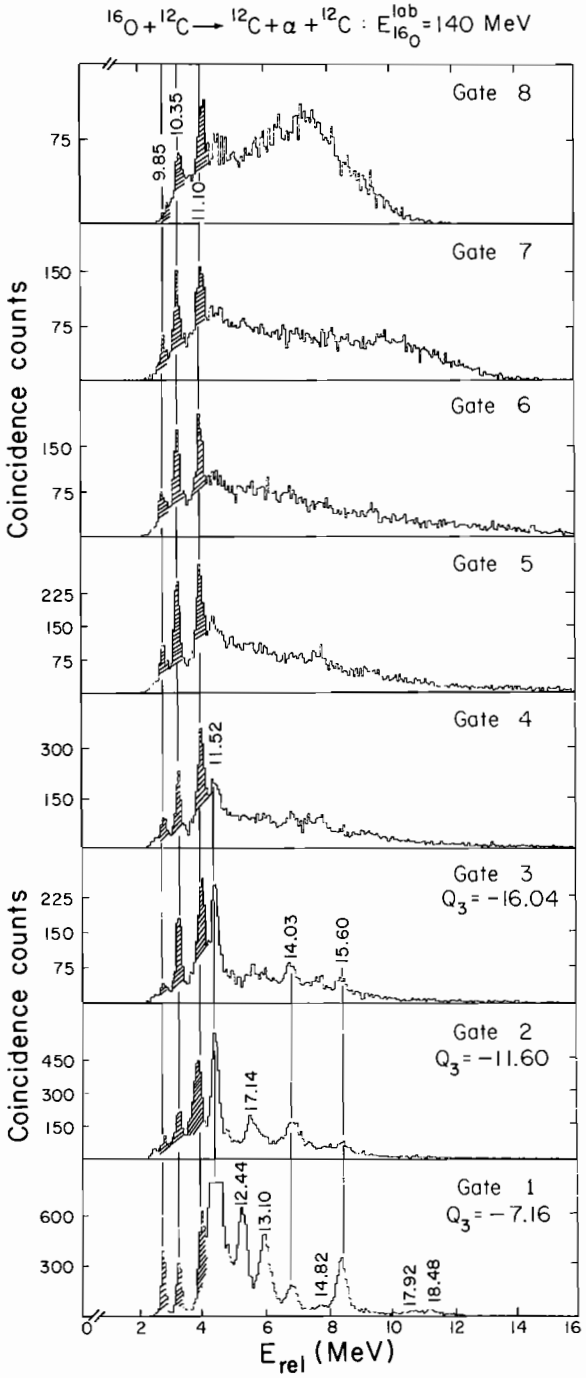

Fig. 2. E_{rel} spectra for various E_T gates. There is a detection threshold at $E_{rel} \simeq 2.5$ MeV. The data have not been adjusted for coincidence efficiency which is a strong function of E_{rel} but depends weakly on E_T. (XBL 814-654)

Footnotes and References

*Condensed from Lawrence Berkeley Laboratory Report LBL-12568 (1981).

†Universidad Nacional Autonoma de Instituto de Física, México 20, D. F.

‡Département de Physique Nucléaire/Basses Energies, Centre d'Etudes Nucleaires de Saclay, F-91190 Gif-sur-Yvette, France.

§Department of Physics, Weizman Institute of Sciences, Rehovot, Israel.

1. A.C. Shotter et al., Phys. Rev. Lett. **46**, 12 (1981).
2. W.D. Rae et al., Phys. Rev. Lett. **45**, 884 (1980).
3. P.T. Debevec et al., Phys. Rev. C **9**, 2451 (1974).

Observation of Sequential Breakup in the ^{16}O + ^{197}Au Reaction at 218 MeV

A.N. Bice, M.D. Cable, A.C. Shotter, and Joseph Cerny*

Angular correlations between fast α-particles and outgoing heavy reaction products for the system ^{16}O + ^{197}Au and ^{16}O + ^{208}Pb have previously been studied at the bombarding energies of 140 MeV and 310 MeV.[1] Although a detailed understanding of the reaction mechanism responsible for the observed fast α-particle production was not achieved, Gelbke et al.[1] inferred that the α-particles could not originate from the sequential decay of an ejectile. In contrast, our simple Monte Carlo simulations indicated that the data of Gelbke et al. were consistent with a sequential decay process and, hence, that this type of reaction mechanism should be considered further. Therefore, an initial investigative study of the ^{16}O + ^{197}Au system at 218 MeV was performed. It should be noted that Bini et al.[2] recently reported that most of the α-particles observed in the ^{16}O + ^{197}Au system at 310 MeV were emitted from projectile-like fragments. Also Rae et al.[3] reported a strong $^{16}O^*$ sequential decay channel in the ^{16}O + ^{12}C system at 140 MeV.

A 218 MeV ^{16}O beam produced by the 88-Inch Cyclotron was used to bombard targets of ^{197}Au and ^{208}Pb. The data taken with each target are qualitatively the same. A triple telescope system (as described in the contribution "$^{12}C^*$ production in the ^{12}C + ^{208}Pb system at 230 MeV," Bice et al., in this Annual Report) was used to record particle-particle coincidences. Since the three particle telescopes are located in close proximity, the observation of the decay of ^{16}O states near the breakup threshold is facilitated. Figure 1(a) shows a summed energy spectrum of α + ^{12}C coincidences taken at 19° in the laboratory with the closest spaced two counter configuration (center-to-center counter separation of 5.9°). Strong transitions to the ground state and low-lying states of ^{197}Au are evident as well as a significant number of α + ^{12}C events with more negative production Q-values. Figures 1(b) and 1(c) show projected spectra onto the ^{12}C energy axis of α + ^{12}C coincident events that summed to an energy falling within the gates indicated in Fig. 1(a). The peaks in Fig. 1(b) are representative of $^{16}O^*$ sequential decay into the α + ^{12}C channel and resemble the data observed by Rae et al.[3] for the ^{16}O + ^{12}C system. The projected spectrum (Fig. 1(c)) that results from α + ^{12}C events with more negative Q-values does not display any clear peaks in the "relative energy" spectrum and suggests that other processes than sequential decay are involved in this reaction. Taken together, Figs. 1(b) and 1(c) indicate the need for further consideration and measurement of the relative contributions of sequential and nonsequential processes to fast α-particle production and α-heavy ion correlation measurements.

In addition to the observation of the α + ^{12}C channel, other particle-particle coincidences were investigated

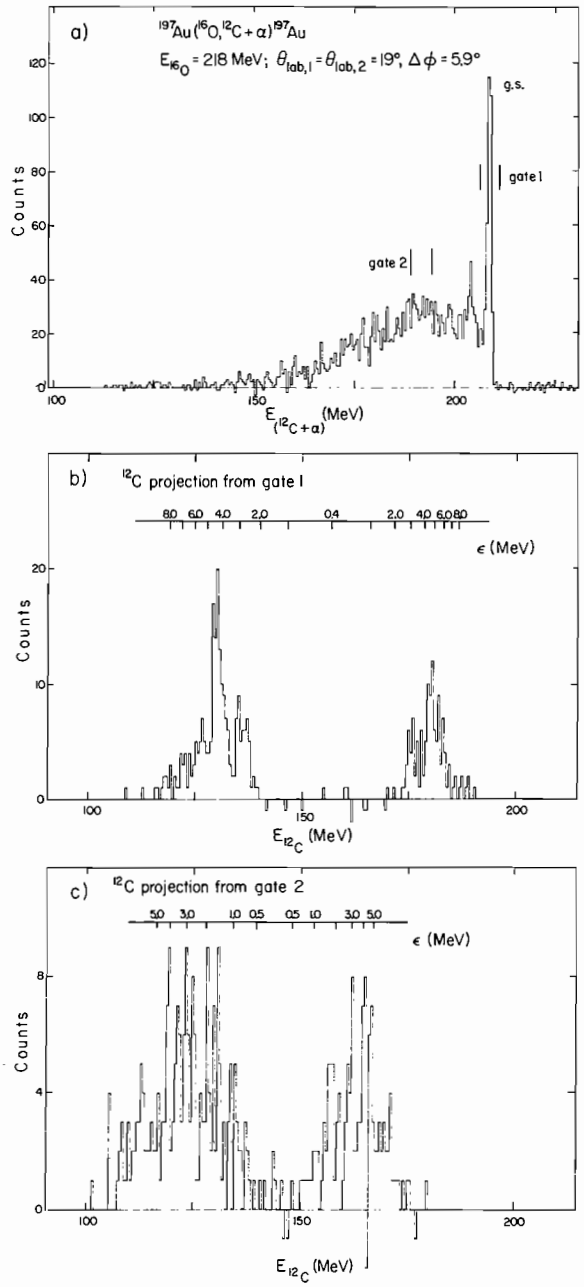

Fig. 1. (a) Energy spectrum obtained from the $^{197}Au(^{16}O,^{12}C + \alpha)$ reaction at θ_{Lab} = 19° with an ^{16}O bombarding energy of 218 MeV. The two particle telescopes were separated center-to-center by 5.9°. (b) Projected energy spectrum of ^{12}C nuclei in one telescope in coincidence with ^{4}He nuclei such that their summed energy is located within the gate 1 indicated in (a). (c) Same as (b) but for gate 2. (XBL 816-944)

for this system. The overwhelming majority of all particle-particle coincidences consisted of α-α events. Closer examination indicated most α-α coincidences were due to the decay of a ^{8}Be(g.s.) or an excited ^{8}Be(2.94 MeV) nucleus. The mechanism for the large production of ^{8}Be is not known and would provide an interesting area of study for the future. Indeed, it is of interest to see if the singles fast α-particles and ^{8}Be nuclei produced in the ^{16}O + ^{197}Au system at 218 MeV are explainable in terms of current incomplete fusion models.

Footnote and References

*Physics Department, University of Edinburgh, Edinburgh EH93JZ, United Kingdom.

1. C.K. Gelbke et al., Phys. Lett. B **71**, 83 (1977).
2. M. Bini et al., Phys. Rev. C **22**, 1945 (1980).
3. W.D. Rae et al., Phys. Rev. Lett. **45**, 884 (1980).

Observation of the Direct and Sequential Breakup of ^{7}Li from ^{12}C and ^{208}Pb Targets at 70 MeV*

A.N. Bice, A.C. Shotter,† J.M. Wouters, W.D. Rae, and Joseph Cerny

The reaction mechanisms involved in projectile dissociation in the field of a target nucleus are currently attracting substantial interest. For projectile energies below the Coulomb barrier, the projectile may be excited by the electromagnetic field between the incident channel nuclei. If the excited states are above the threshold for particle emission and have small energy widths, the projectile will in most instances sequentially break up beyond the influence of the target's nuclear field. In contrast, at high energies ($\sim$ 100 MeV/A) a projectile incident on the peripheral region of the target nucleus might be expected to undergo a rapid fragmentation in the surface field of the nucleus.[1]

For a projectile with an intermediate energy, it should be possible to identify a transition from a sequential to a rapid nonsequential process. A suitable projectile is ^{7}Li, in which the first α decaying state is at 4.63 MeV, 2.16 MeV above the α + t breakup threshold. Thus, direct ^{7}Li breakup events with α − t relative energies less than $\sim$ 2.1 MeV can clearly be distinguished from all possible sequential breakup events.

Presented briefly here are results of an investigation of 70 MeV ^{7}Li $\rightarrow$ α + t breakup on ^{12}C and ^{208}Pb targets. The breakup fragments were detected by two particle telescopes in close vertical geometry. Summed energy spectra of α + t coincidence events obtained with this system from a ^{12}C target yielded three peaks, corresponding to those breakup events which leave the ^{12}C target in the g.s. or excited to the 4.4 MeV, 2+ or 9.6 MeV, 3− states. For the ^{208}Pb target the majority of breakup events into the α + t channel left the target in its ground state.

Further interpretation of the character of these breakup events was obtained from the t projected spectra. Figure 1(a) shows such a spectrum corresponding to the ^{12}C(g.s.) transition. The two peaks of Fig. 1(a) correspond to the two kinematically allowed t energies (as indicated by the arrows) from the sequential breakup of ^{7}Li*(4.63 MeV). If direct breakup had occurred in the field of the target nucleus, the relative energy, ϵ, between the α and t would no longer be restricted to a definite value corresponding to ^{7}Li* sequential decay; but, instead, the value of ϵ could vary over some continuous distribution related to the momentum distribution of the fragments in the projectile ground state.[2] In Fig. 1(a), there is little or no evidence of such a distribution of ϵ.

Two projected spectra corresponding to the ^{208}Pb(g.s.) transition for the lab angles of 32° and 18° are shown in Figs. 1(b) and 1(c), respectively. The arrows again indicate the triton energy limits for the sequential breakup of ^{7}Li*(4.63 MeV). It is apparent that Figs. 1(a) and 1(b) are similar, showing little evidence for direct breakup. However, data taken at more forward angles (Fig. 1(c)) include events with a continuous distribution of ϵ that cannot arise from discrete states of ^{7}Li. This is taken as evidence of direct breakup.

Angular distributions for the sequential and the direct components were measured and showed distinct differences. At this time, however, it is only possible to speculate as to the mechanisms involved in direct projectile breakup. Whatever the precise mechanisms are, it will be of great interest to determine how the direct and sequential breakup components vary with incident energy, especially in the region 10-100 MeV/A, because this could lead to a much greater understanding of fragmentation processes in general.

Footnotes and References

*Condensed from Lawrence Berkeley Laboratory Report LBL-11458, Phys. Rev. Lett. **46**, 12 (1981).

†Physics Department, University of Edinburgh EH93JZ, United Kingdom.

1. A.S. Goldhaber and H.H. Heckman, Ann. Rev. Nucl. Sci. **28**, 161 (1978).
2. R. Shyam, G. Baur, F. Rösel and D. Trautman, Phys. Rev. C **19**, 1246 (1979).

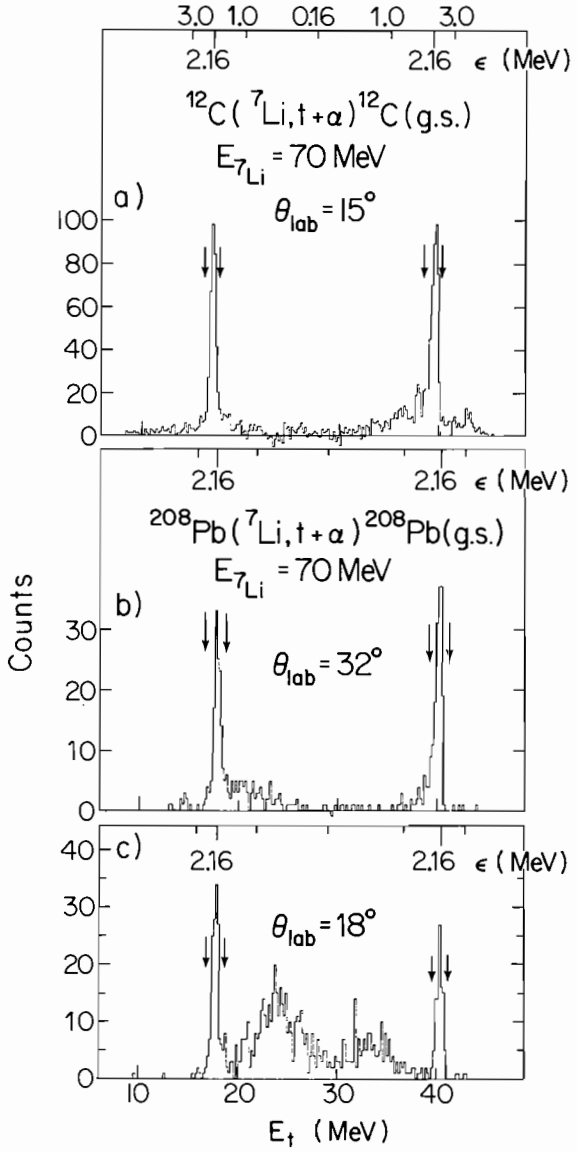

Fig. 1. (a) The triton energy spectrum for coincident α + t events in which the residual ^{12}C nucleus remained in its ground state. The detector system was located at $\theta_{Lab} = 15°$. (b) The triton energy spectrum for coincident α + t events in which the residual ^{208}Pb nucleus remained in its ground state. The detector system was located at $\theta_{Lab} = 32°$. (c) As for (b) but with the detector system at $\theta_{Lab} = 18°$. (XBL 809-1881)

Resonant Particle Production in the 172-MeV $^{13}C + ^{208}Pb$ Reaction

A.N. Bice, M.D. Cable, A.C. Shotter, and Joseph Cerny*

In a previous breakup reaction study of the $^{12}C + ^{208}Pb$ system at 187 MeV bombarding energy, it was noted[1] that there was a relatively strong neutron pickup channel, which yielded ^{13}C states unbound with respect to alpha decay. Two possible reaction mechanisms for the production of $^{13}C^*$ are: (1) a direct neutron transfer to unbound levels in ^{13}C and (2) a two-step process such as $^{208}Pb[^{12}C,^{13}C(g.s.)]$ $[^{13}C,^{13}C^*]^{208}Pb(g.s.)$. If this latter process [involving the $^{13}C(g.s.)$] were dominant, then one might expect that the reaction $^{208}Pb(^{13}C,\ ^{13}C^* \rightarrow \alpha + ^{9}Be)^{208}Pb(g.s.)$ would exhibit a relatively large yield in reactions conducted at a similar bombarding energy. To investigate this mechanism as well as to provide an interesting comparison to the $^{12}C + ^{208}Pb$ system, an initial survey was made of the $^{208}Pb(^{13}C,^{13}C^*)$ reactions at 172 MeV.

A 1.5 mg/cm^2 ^{208}Pb target was bombarded with a 172 MeV ^{13}C beam from the 88-Inch Cyclotron. The production of resonant unbound reaction products was observed by detecting the decay products in coincidence with a "piggyback" telescope system. This system was comprised of three particle telescopes stacked vertically with respect to the scattering plane (which bisected the post separating two of the telescopes). This system allowed three combinations of particle-particle coincidences to be observed at each laboratory scattering angle.

The yield of $\alpha + ^{9}Be$ coincidences between 15° and 25° in the laboratory system was observed to be small, a factor of 15-20 less than that observed in the $^{208}Pb(^{12}C,\ ^{13}C^*)$ reaction at 187 MeV. Indeed, only two strong reaction channels were observed for this system—$(^{13}C,\alpha)$ and $(^{13}C,\alpha + \alpha)$. Figure 1(a) shows a $^{208}Pb(^{13}C,\alpha + \alpha)$ coincidence spectrum obtained by the two telescope combination, which has an average angular separation of $\Delta\psi = 5.9°$. A rather broad peak near beam velocity is seen in the coincident spectrum as was observed in the $^{12}C + ^{208}Pb$ system. Figure 1(b) shows a projected spectrum of the ^{4}He energy in one telescope from $\alpha + \alpha$ coincident events located within the gate indicated in Fig. 1(a). The majority of $\alpha_1 + \alpha_2$ events have $E_{\alpha_1} \simeq E_{\alpha_2}$ as expected from the decay of a $^{8}Be(g.s.)$. The other two detector combinations for particle-particle coincidences, which are separated by angles larger than a $^{8}Be(g.s.)$ decay cone width, recorded very few $\alpha + \alpha$ events. Evidently most $\alpha + \alpha$ coincidences do arise from the decay of a ^{8}Be.

Given the large production cross section of ^{8}Be (at $\theta_{Lab} = 15°$, $d\sigma/d\Omega \simeq 360$ mb/sr), it is interesting to deduce what fraction of the singles alpha spectrum arises from decaying ^{8}Be nuclei. Integrating over Fig. 1(a) and folding in the ^{8}Be detection efficiency, it is found that approximately 55% of the singles alphas at 15° must arise from the decay of ^{8}Be nuclei.

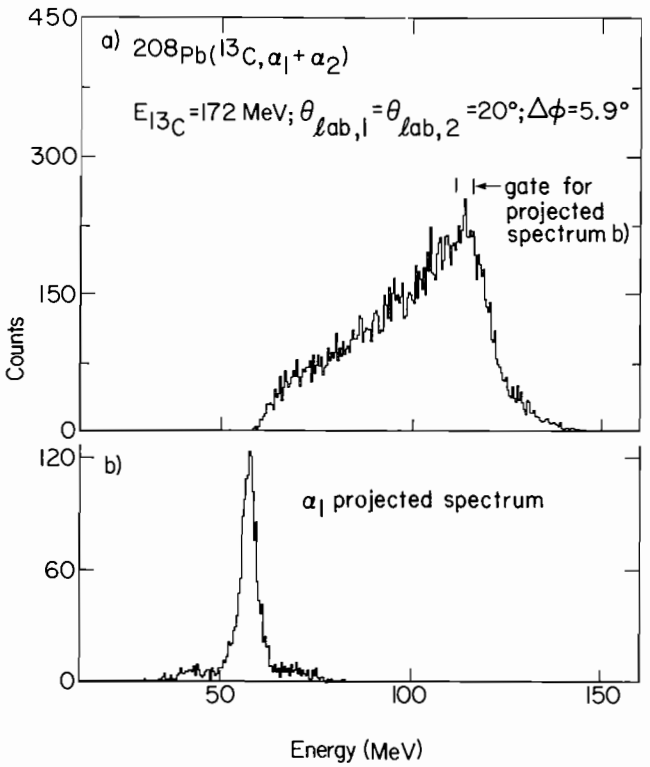

Fig. 1. (a) Energy spectrum obtained from the $^{208}Pb(^{13}C,\alpha+\alpha)$ reaction at $\theta_{Lab} = 20°$. The two particle telescopes were separated center-to-center by 5.9°. (b) Projected energy spectrum of ^{4}He nuclei in one telescope in coincidence with ^{4}He nuclei in the other telescope such that their summed energy is located within the gate indicated in (a). (XBL 818-11233)

Of future interest is the determination of the mechanism responsible for the copious α and ^{8}Be production in this reaction. The similarity between the $^{13}C + ^{208}Pb$ and $^{12}C + ^{208}Pb$ systems suggests that it also would be interesting to extend this comparison to a variety of other bombarding energies.

Footnote and Reference

*Physics Department, University of Edinburgh, Edinburgh EH93JZ, United Kingdom.

1. A.N. Bice, A.C. Shotter, and J. Cerny, Lawrence Berkeley Laboratory Nuclear Science Division Annual Report 1979-1980, LBL-11588, p. 69.

$^{12}C^*$ Production in the $^{12}C + ^{208}Pb$ System at 230 MeV

A.N. Bice, A.C. Shotter, and Joseph Cerny*

The reaction mechanism involved in the production of fast α-particles in heavy-ion collisions is a subject of study that has only recently been under intense investigation. Interestingly, the observation of such fast α-particles was made as early as 1961 by Britt and Quinton[1] from heavy-ion reactions at energies of about 10 MeV/A. Recent studies have concentrated in part on whether such fast alpha particles are produced when a massive fragment of the projectile is transferred to and retained by the target nucleus. Recently, Siwek-Wilczynska et al.[2] proposed a model of incomplete fusion reactions based partially on their study of the $^{12}C + ^{160}Gd$ system at bombarding energies of 90-200 MeV. Their measurements and incomplete fusion model calculations suggest that, for the $^{12}C + ^{160}Gd$ system, $\sim$ 40% of the observed singles α-particles result from the massive transfer reactions ($^{12}C,\alpha$) and ($^{12}C,2\alpha$). The remaining $\sim$ 60% or more of the singles α-particle cross section, which amounts to several hundred millibarns, is suggested to arise from 3α-particle breakup. However, direct measurement of the 3α-particle breakup cross section, which includes the sequential processes $^{12}C^* \rightarrow 3\alpha$, were not performed by Siwek-Wilczynska et al.

We have previously reported[3] measurements of ^{12}C breakup for a very similar system, the $^{12}C + ^{208}Pb$ system, at 132 and 187 MeV. Our measurements have recently been extended to a bombarding energy of 230 MeV with a beam produced at the 88-Inch Cyclotron. As before, two counter telescopes, arranged in a close vertical geometry with respect to the normal scattering plane, were employed to detect 3α events. In addition, for this experiment, a third telescope was located above the other two particle telescopes, thereby providing three possible telescope-telescope coincidences and vertical angular separations at each laboratory angle. For this triple telescope system, the minimum vertical angular separation of two telescopes was 1.5° and the maximum was 20°.

Similar to the results of the 132 MeV and 187 MeV bombarding energy measurements, little evidence for direct 3α-particle breakup was obtained at 230 MeV with this detector configuration. The majority of the $\alpha + 2\alpha$ coincident events resulted from the sequential decay of ^{12}C, primarily from its 7.6 MeV, 0^+ state. The angular distributions for the sequential breakup of ^{12}C into the $\alpha + ^8Be$ channel, where the target remains unexcited, is shown in Fig. 1(a) for the three ^{12}C bombarding energies. The total cross sections, obtained by integrating the angular distributions in Fig. 1(a), are shown in Fig. 1(b).

From the data displayed in Fig. 1(b) and estimates of $^{12}C^*$ production for more negative Q-values, it is possible to conclude that $^{12}C^*$ production and subsequent decay is not a significant source of fast alpha particles for this system. Furthermore, if the 3α production is as likely as

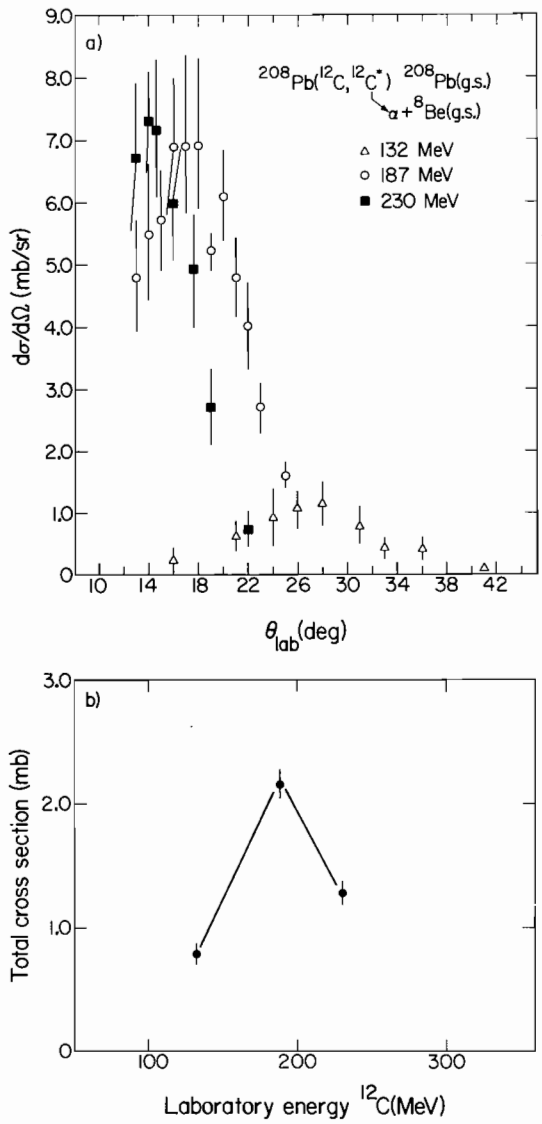

Fig. 1. (a) The measured differential cross section for the $^{208}Pb(^{12}C,\alpha^8Be)^{208}Pb(g.s.)$ reaction at 132, 187 and 230 MeV. (b) The total cross section for the reaction $^{208}Pb(^{12}C, \alpha^8Be)^{208}Pb(g.s.)$. (XBL 818-1158)

Wilczynska et al. suggest, we can conclude that the three breakup α's are not focused in as narrow a cone as they would be, for instance, if they originated from a sequential $^{12}C^*$ decay. Clearly, more detailed knowledge of the laboratory distribution of α's from the proposed $^{12}C \rightarrow 3\alpha$ breakup reaction is needed.

Footnote and References

*Physics Department, University of Edinburgh, Edinburgh EH93JZ, United Kingdom.

1. H.C. Britt and A.R. Quinton, Phys. Rev. **124**, 877 (1961).

2. K. Siwek-Wilczynska et al., Phys. Rev. Lett. **42**, 1599 (1979) K. Siwek-Wilczynska et al., Nucl. Phys. A **330**, 150 (1979).

3. A.C. Shotter, A.N. Bice, and Joseph Cerny, Nuclear Science Division Annual Report for 1979-1980, LBL-11588, p. 73.

Target Fragment Recoil Properties in the Reaction of 50-86 MeV/μ ^{12}C with ^{181}Ta and ^{197}Au

W. Loveland, P.L. McGaughey, K. Aleklett,† K.J. Moody, P. Johnson,* and G.T. Seaborg*

As a guide to assist in the understanding of the changes that occur in nucleus-nucleus collisions as the projectile energy increases from the low energy ($\leq$ 10 MeV/μ) to the high energy regimes (250 MeV/μ), we have undertaken a program of measurement of the target fragmentation systematics throughout this energy range. Earlier, we reported the results of such measurements for the interaction of 7.4, 13.0, 17.1, and 19.7 MeV/μ ^{16}O with ^{197}Au.[1] More recently, we have made measurements of the average target fragment momenta and energies using the thick-target thick-catcher recoil technique, which has been described previously,[2] for the reactions of 50 and 86 MeV/μ ^{12}C with ^{197}Au, and for 75, 80 and 86 MeV/μ ^{12}C with ^{181}Ta. These experiments were performed using the 86 MeV/μ ^{12}C provided by the CERN SC synchrocyclotron. The beam energy was degraded using Al absorbers to supply the three lower energies.

A range-weighted measure of the extent of forward peaking of the fragment angular distributions is the F/B ratio, the ratio of the fraction of target fragments recoiling forward (F) from a thick target to the fraction of fragments recoiling backward (B). The variation of this F/B ratio with target fragment mass number A, shown in Fig. 1, behaves similarly for the interaction of 86 MeV/μ ^{12}C with both ^{181}Ta and ^{197}Au. The magnitude of the F/B ratios is extremely large and far exceeds any values obtained from proton induced reactions using similar targets. Furthermore, the observed F/B values greatly exceed those seen for similar products produced in the interaction of 7.4-19.7 MeV/μ ^{16}O with ^{197}Au. The changes in the recoil properties in the projectile energy range of 50 to 86 MeV/μ are modest and dependent on the atomic number and mass of the target fragment. The interpretation of these data in terms of the two step vector model to deduce average fragment energies and momenta is discussed in the report entitled "Target Fragmentation from 10-2100 MeV/μ" by Loveland et al. in this Annual Report.

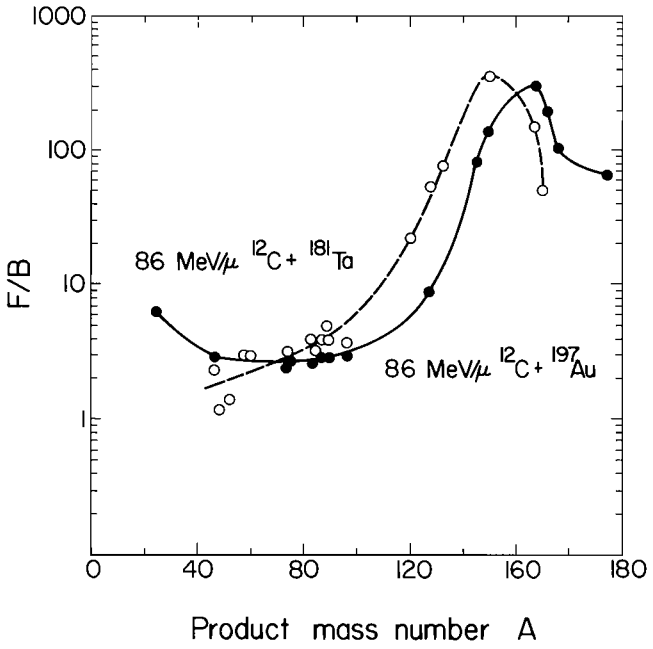

Fig. 1. Variation of the F/B ratio as a function of target fragment mass number A for the interaction of 86 MeV/μ ^{12}C with ^{181}Ta and ^{197}Au. (XBL 818-1125)

Footnotes and References

*Radiation Center, Oregon State University, Corvallis, OR 97331.

†Studsvik Science Research Laboratory, S-611 82 Nyköping, Sweden.

1. W. Loveland et al., Oregon State University Report DOE/ER/70035-1, September 1980.

2. W. Loveland et al., Phys. Rev. C **23**, 253 (1981).

Target Fragment Angular Distributions in the Reaction of 86 MeV/μ ^{12}C with ^{197}Au and ^{238}U

K. Aleklett, W. Loveland,† P.L. McGaughey, R.H. Kraus, Jr.,†*
Y. Morita, G.T. Seaborg, T. Lund,‡ D. Molzahn,‡ E. Hagebo,§ and I. Haldorsen§

The direct measurement of target fragment angular distributions and energy spectra enables one to experimentally characterize in a model independent manner the kinematics of the nucleus-nucleus collision that produced the fragments. The availability of high intensity energetic heavy ion beams from the CERN SC synchrocyclotron has made it possible for the first time to measure these quantities for intermediate energy nucleus-nucleus collisions. We report herein the preliminary results of the first measurements of target fragment angular distributions from the interaction of 86 MeV/μ ^{12}C with ^{197}Au and ^{238}U.

Thin targets of ^{197}Au and ^{238}U ($\sim$ 750 μg/cm^2 UF_4, $\sim$ 300 μg/cm^2 Au) were placed at the center of cylindrical scattering chambers and were irradiated separately with an 86 MeV/μ ^{12}C beam from the CERN SC synchrocyclotron. The irradiations lasted $\sim$ 15 hours with an average beam flux of 3 to 5 $\times$ 10^{11} ^{12}C ions per second. The beam spot diameter was less than 10 mm^2. Fragments emerging from the targets were stopped in catcher foils that were later cut into nine or ten sections corresponding to particular angular intervals. The radionuclides present in each foil were assayed by off-line gamma-ray spectroscopy. The solid angle subtended by each catcher foil was calculated analytically.

In Fig. 1, we show the angular distributions of typical fragments from the 86 MeV/μ ^{12}C reaction with ^{197}Au. Note the enormous magnitude of the forward peaking of the heaviest fragments and the initial tendency for the degree of forward peaking to increase as the target fragment mass decreases. Further decreases in fragment mass result in less forward peaking of the angular distributions, while the lightest fragments show more forward peaking.

For the reaction of 86 MeV/μ ^{12}C with ^{238}U, the thirty fragments whose angular distributions were measured can be placed into four representative classes. In Fig. 2, the distributions for one fragment from each of the four classes are given. The neutron-rich fission fragments have isotropic angular distributions indicating that little or no momentum transfer occurred before fission. The neutron-deficient products of similar mass are more forward peaked, as are the light fragments. The greatest degree of forward peaking occurs for the heavy fragments. This pattern is similar to that observed for the interaction of 4.8 GeV ^{12}C with ^{238}U.[1] Fragments from the ^{238}U target have a much smaller degree of peaking compared to the corresponding ^{197}Au fragments.

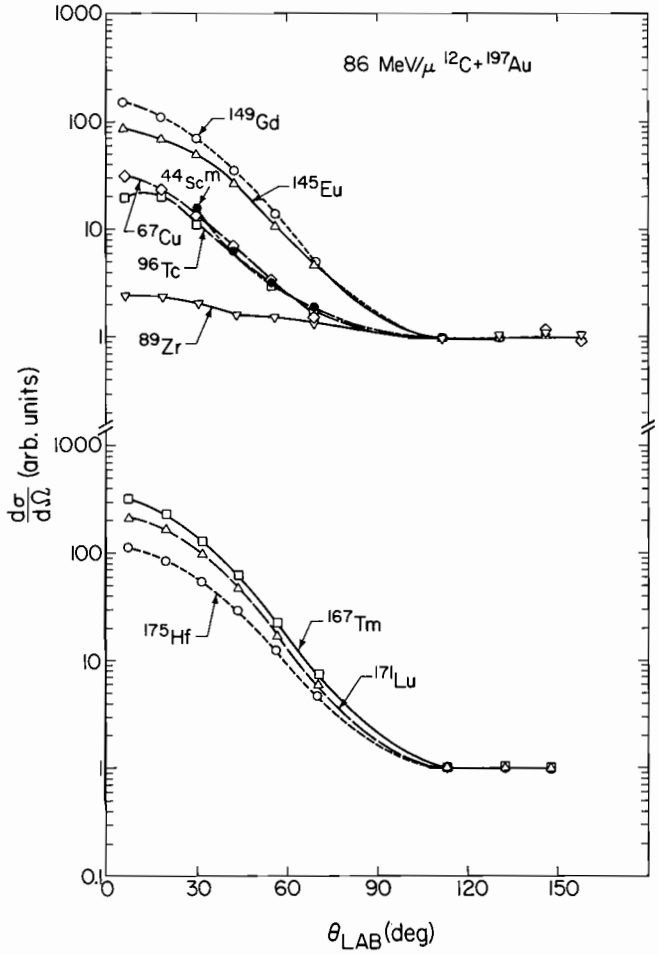

Fig. 1. Selected target fragment angular distributions from the interaction of 86 MeV/μ ^{12}C with ^{197}Au.
(XBL 818-1122)

Comparisons of these results with one another and with current models of high energy nucleus-nucleus collisions are in progress and should yield interesting results. We hope to complement these experimental measurements by determining the target fragment energy spectra using differential range techniques at the CERN SC synchrocyclotron.

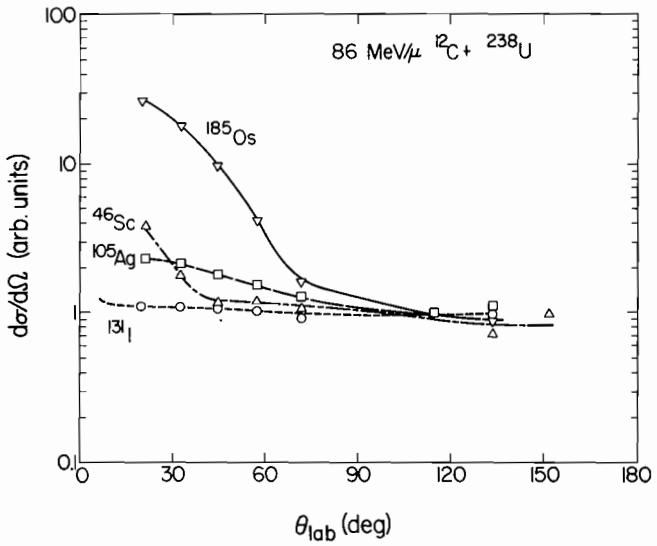

Fig. 2. Representative target fragment angular distributions for a typical neutron-rich fission fragment (^{131}I), a neutron deficient fragment (^{105}Ag), a light fragment (^{46}Sc), and a heavy fragment (^{185}Os) from the interaction of 86 MeV/μ ^{12}C with ^{238}U. (XBL 818-1121)

Footnotes and Reference

*Studsvik Science Research Laboratory, S-611 82 Nyköping, Sweden.
†Radiation Center, Oregon State University, Corvallis, OR 97331.
‡Phillips-Universität F.B. 14, Auf den Lahnbergen, D-355 Marburg/Lahn, West Germany.
§Department of Nuclear Chemistry, University of Oslo, Oslo, Norway.

1. W. Loveland et al., Lawrence Berkeley Laboratory Report LBL-11658 (1980).

Target Fragmentation from 10-2100 MeV/μ

W. Loveland, P.L. McGaughey, K. Aleklett,† K.J. Moody, R.H. Kraus, Jr.,* R.M. McFarland, and G.T. Seaborg*

In recent years, there has been increasing interest in studying how the mechanisms in nuclear heavy-ion reactions change as the projectile energy increases from low energies ($\sim$ 10 MeV/μ) to relativistic energies (2100 MeV/μ). We thought that it would be valuable to make radiochemical measurements of target fragment average energies and momenta to help characterize the changes in target fragmentation over this projectile energy regime. Accordingly, in this paper we compare the results of studies of target fragmentation in the reaction of ^{12}C, ^{16}O, and ^{20}Ne at seven different projectile energies from 13-2100 MeV/μ. We report new data from studies of reactions induced by projectiles whose energies ranged from 13-86 MeV/μ, showing unusually large momentum transfers to the target fragments. It is interesting to compare our data with that of Kaufman et al., who studied the interaction of 400-2100 MeV/μ ^{12}C with ^{197}Au.[1] The overall thrust of the data requires significant revision of our ideas concerning the energy evolution of nuclear heavy ion reactions.

We studied the interaction of 13 and 19 MeV/μ ^{16}O with ^{197}Au, using the LBL 88-Inch Cyclotron, and the interaction of 50 and 86 MeV/μ ^{12}C with ^{197}Au, using the CERN SC synchrocyclotron. The 50 MeV/μ beam was obtained by degrading the primary 86 MeV/μ beam with an aluminum absorber. The thick-target thick-catcher recoil properties of the fragments were measured, from which we deduced the average fragment momenta. The experimental techniques have been described previously.[2]

A range-weighted measure of the extent of forward peaking of the fragment angular distributions is the F/B ratio, the ratio of the fraction of fragments recoiling forward (F) from a thick target to the fraction recoiling backward (B). The F/B ratios for four typical target fragments produced by the reaction of energetic heavy ions with ^{197}Au, shown in Fig. 1, increase with total projectile kinetic energy until $\sim$ 1 GeV and then decrease with further increases in projectile energy. This behavior is quantitatively similar to that observed in the interaction of energetic protons with ^{197}Au[3] and has been qualitatively explained as a consequence of time dilation.[4] If similar mechanism(s) are operating in both heavy-ion and proton induced reactions, this explanation must be incorrect since at these energies (50-86 MeV/μ) time dilation effects are negligible for heavy ions.

The two step vector model[5] was used to deduce values for P_{11}, the longitudinal component of the momentum transferred to the target fragment precursor during the initial projectile-target interaction. As an aid to understanding the variation of P_{11} with fragment mass and projectile energy, we have defined a parameter called "inelasticity" as the ratio of the measured P_{11} value for a given fragment

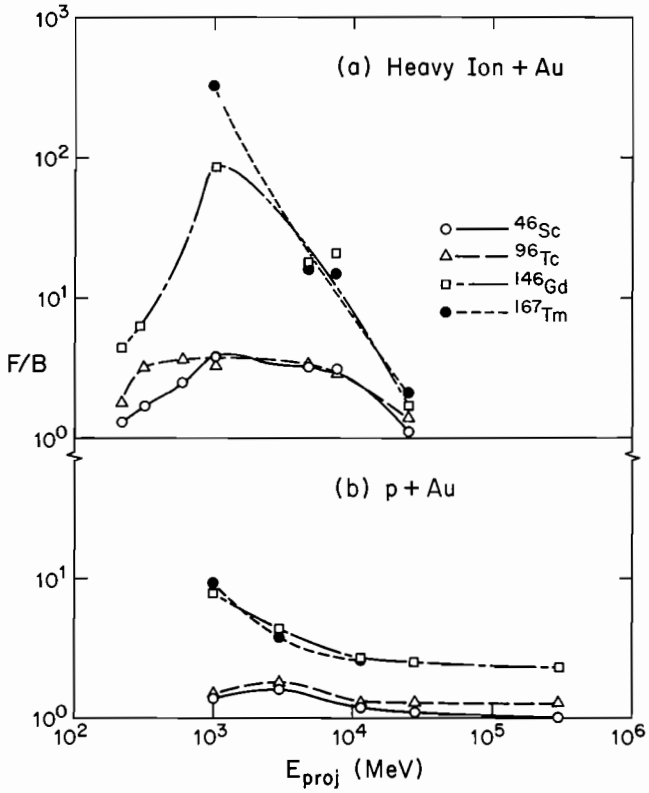

Fig. 1. The variation of F/B for selected products from the reaction of (a) heavy ions with ^{197}Au; (b) protons with ^{197}Au (Ref. 3). The data for heavy ion projectile energies ≥ 4.8 GeV are from Ref. 1. (XBL 818-1118)

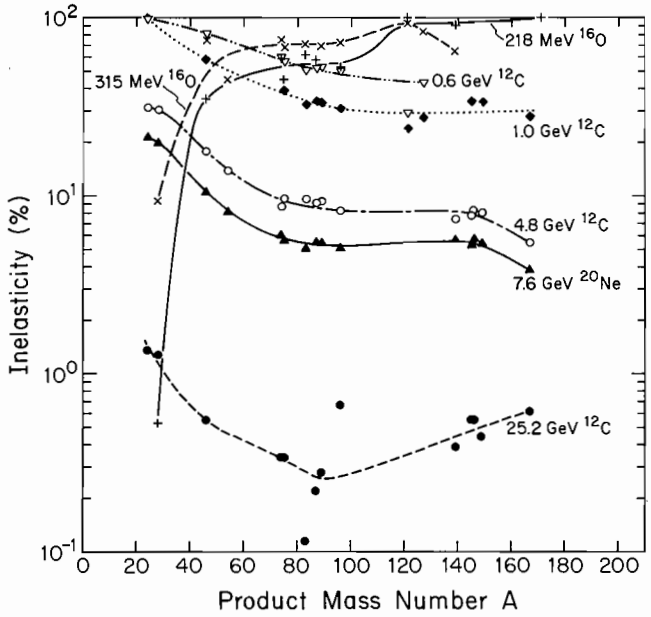

Fig. 2. The variation of inelasticity with product mass number for the reactions of various heavy ions with ^{197}Au. The data for the three highest energies are from Ref. 1. (XBL 818-1120)

to the maximum momentum that could be imparted to that fragment. The variation of inelasticity with product mass number for various heavy ion reactions with ^{197}Au is given in Fig. 2. One is immediately struck by the large fractional momentum transfer occurring in the 0.6 and 1.0 GeV (50 and 86 MeV/μ) ^{12}C induced reactions. The magnitude of these momentum transfers indicates that the generalized critical angular momentum model[6] does not correctly describe incomplete fusion at these energies because it predicts no significant momentum transfer can occur at energies greater than $\sim$ 20 MeV/μ. The variation of inelasticity with product mass number appears to be different below 50 MeV/μ, as compared to the higher energies. The fragment inelasticities decrease smoothly with projectile energies above $\sim$ 50 MeV/μ, indicating a continuous evolution of reaction mechanism(s).

If one examines the variation of the absolute value of P_{11} with projectile energy, one finds that P_{11} increases from $\sim$ 10 MeV/μ to 20 MeV/μ and decreases at higher energies. The decrease in P_{11} from 50 MeV/μ to 2100 MeV/μ is described by a remarkably simple relationship:

$$P_{11} = a + b\sqrt{1 - \beta^2} \ ,$$

where a and b are constants and β is the projectile velocity in units of c. This relationship is valid for all fragments where data are available at the five projectile energies. The constants a and b smoothly increase and decrease, respectively, with increasing fragment mass. The reasons for the validity of this simple correlation, which encompasses such a wide range of projectile energies and fragment masses, are not clear at this time.

Footnotes and References

*Radiation Center, Oregon State University, Corvallis, OR 97331.
†Studsvik Science Research Laboratory, S-611 82 Nyköping, Sweden.

1. S.B. Kaufman et al., Phys. Rev. C **22**, 1897 (1980).
2. W. Loveland et al., Phys. Rev. C **23**, 253 (1981).
3. S.B. Kaufman, E.P. Steinberg, and M.W. Weisfield, Phys. Rev. C **18**, 1349 (1978).
4. See, for example, H. Feshbach, First Workshop on Ultra-Relativistic Nuclear Collisions, Lawrence Berkeley Laboratory Report LBL-8957, (1979), p. 261.
5. See, for example, J.M. Alexander in *Nuclear Chemistry*, L. Yaffe, Ed. (Academic, New York, 1968), p. 273.
6. K. Siwek-Wilczynski et al., Phys. Rev. Lett. **42**, 1599 (1979).

C. RELATIVISTIC HEAVY IONS

1. Fragmentation Processes

Energy Variation of Target Fragment Mass and Charge Distributions in the Interaction of Relativistic Heavy Ions with Ta and U

W. Loveland, P.L. McGaughey, D.J. Morrissey, C. Oertel,**
L.L. Nunnelley, and G.T. Seaborg*

The yields of various target fragments of differing atomic mass number produced in relativistic nuclear collisions are measures of some of the details of the projectile-target interaction. As the velocity of the incident projectile approaches the speed of light, the projectile-target nucleus interaction time approaches a constant value, and experimental product distributions are not expected to change with further increases in projectile energy. This behavior, commonly termed "limiting fragmentation," appears to dominate the yield distributions observed in the interaction of relativistic heavy ions (RHIs) with low mass targets (e.g., Cu) for projectile energies larger than ~4 GeV.[1] To determine if this effect was predominant with heavy targets, we initiated a program to systematically survey the changes in product yield distributions as a function of projectile energy for Ta and U targets. The use of these targets should make possible the occurrence of more collisions in which the central densities of the two nuclei overlap considerably compared with the light targets.

To date, we have performed experiments to measure these target fragment yield distributions in the reactions of 3.0 GeV ^{12}C, 5.0 GeV ^{20}Ne, 8.0 GeV ^{20}Ne, 25 GeV ^{12}C, 28 GeV p and 42 GeV ^{20}Ne with ^{181}Ta and 3.0 GeV ^{12}C, 4.8 GeV ^{12}C, 5.0 GeV ^{20}Ne, 8.0 GeV ^{20}Ne, 12 GeV ^{12}C, 21 GeV ^{20}Ne, 25 GeV ^{12}C, 28 GeV p, and 42 GeV ^{20}Ne with ^{238}U. Although the analysis is complete for only a fraction of these experiments, we can discuss some of the trends observed in the data. In general, the fragment yields from the interaction of a variety of projectiles of differing energy with ^{181}Ta are similar in magnitude and in variation with fragment mass number, as demonstrated in Fig. 1. The fragment yield distribution from the reaction of 28 GeV protons with ^{181}Ta shows a similar shape to those measured in RHI-induced reactions, but it differs in the magnitude of the yields. The ratio of the total reaction cross sections (as measured by summing the total residue cross sections from A = 40 to A = 180 and correcting for binary fission) for the 25 GeV ^{12}C induced reaction relative to the 28 GeV proton induced reaction was 1.7 ± 0.3, which is in moderate agreement with the geometric cross-section ratio of 1.42. With uranium targets the situation is quite different, as is apparent from an inspection of Fig. 2. In RHI interactions with this target, one notices a dramatic increase in heavy residue yields as the incident projectile energy increases from 8 to 25 GeV. Also, the shape of the yield distribution resulting from the 28 GeV proton induced reaction is quite different from similar distributions in RHI-induced reactions.

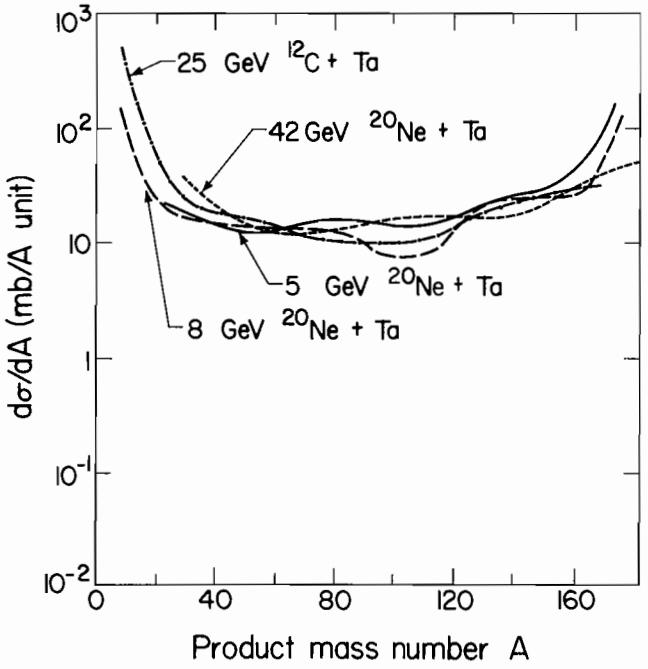

Fig. 1. Target fragment yield distributions for the interaction of 5 GeV ^{20}Ne, 8 GeV ^{20}Ne, 25 GeV ^{12}C, and 42 GeV ^{20}Ne with ^{181}Ta. (XBL 818-1124)

We have attempted to compare these experimental product yield distributions with the prediction of two current models of relativistic nuclear collisions, the intranuclear cascade model[2] and the nuclear firestreak model.[3] In general, both models are able to predict the approximate shapes and magnitudes of the mass yield distributions and the centers of the isotopic distributions for target fragments heavier than A = 60. The formation of fragments lighter than this cannot be predicted by conventional statistical de-excitation models; instead, they may require the existence of an "explosion" type mechanism in which the highly excited targets fragment initially into many smaller pieces. Neither model predicts the dramatic increase in heavy fragment production observed in the reaction of 25 GeV ^{12}C with ^{238}U. From the observed invariance of

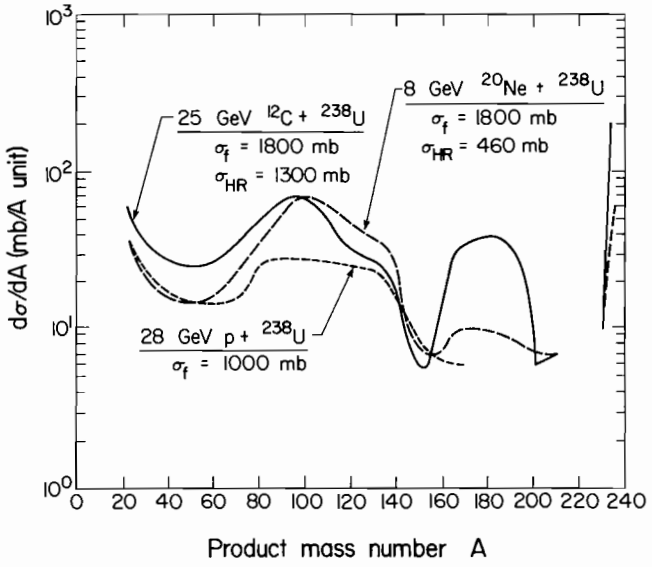

Fig. 2. Target fragment yield distributions for the interaction of 25 GeV ^{12}C, 8 GeV ^{20}Ne, and 28 GeV proton with ^{238}U. (XBL 818-1123)

the total experimental reaction cross-sections resulting from the interaction of ^{20}Ne with ^{181}Ta at various energies, we conclude that the nucleus-nucleus reaction cross-section is nearly a constant over this energy range. This implies that the free nucleon-nucleon scattering cross-sections, which vary strongly with energy in this energy range, may not have a pronounced effect on the total reaction cross-sections for RHI reactions with heavy targets, where simple geometry seems to have the predominant effect.

Footnote and References

*Radiation Center, Oregon State University, Corvallis, OR 97331.

1. J.B. Cumming, P.E. Haustein, and R.W. Stoenner, Phys. Rev. C **10**, 739 (1974); J.B. Cumming, P.E. Haustein, T.J. Ruth, and G.J. Virtes, Phys. Rev. C **17**, 1632 (1978).

2. Y. Yariv and Z. Fraenkel, Phys. Rev. C **20**, 2227 (1979).

3. P.L. McGaughey, D.J. Morrissey, and G.T. Seaborg, Nuclear Science Div. Annual Report 1979-1980, LBL-11588, 159 (1981).

Target Fragment Angular Distributions in the Reaction of 3.0 and 12.0 GeV ^{12}C with ^{197}Au and ^{238}U

Y. Morita, W. Loveland, P.L. McGaughey, and G.T. Seaborg*

Fragment angular distributions are useful tools to aid in the understanding of high energy fragmentation reaction mechanisms. Unfortunately, previous experimental studies of heavy-ion induced target fragmentation have only involved measurements of F/B ratios[1,2] which are range-weighted measures of the extent of forward peaking of the angular distributions. Therefore, we have undertaken the direct determination of target fragment angular distributions for relativistic heavy-ion reactions. Specifically, we thought it of interest to compare distributions resulting from the interaction of a sub-relativistic heavy ion, 3.0 GeV ^{12}C, and a relativistic one, 12.0 GeV ^{12}C, with a very fissionable ^{238}U target and the less fissionable ^{197}Au.

The major difficulty in the determination of these angular distributions is the relatively low ^{12}C particle intensity provided by the LBL Bevalac; typical intensities are less than 10^{10} particles per minute. To overcome this problem, special target-catcher assemblies were employed. Each assembly consisted of 17 identical target foils, each backed with a conical-catcher foil assembly in which the fragments recoiling from the target were stopped. After irradiation, each conical-catcher foil was cut into four pieces, corresponding to the approximate angular ranges of 0-30°, 30-50°, 50-70°, and 70-90°, with respect to the incident beam direction. Then, the foils belonging to the same angular ranges were all combined to form single samples. Gamma-ray spectroscopic techniques were used to assay the relative amounts of different radionuclides present in each sample.[3]

The determination of the effective solid angle subtended by each catcher foil, the corrections for fragment scattering and absorption, and for widely differing counting efficiencies for the extended sources were a complex matter. A semi-empirical approach to the problem was chosen. First, the relative solid angles subtended by the various conic catcher sections, with respect to extended-area circular targets, were calculated numerically. Using the same method, the average scattering angle of a fragment stopping in each catcher section was evaluated. The next step involved the use of a single ^{238}U target-catcher assembly to measure the fission fragment angular distribution produced by 43 MeV alpha particle induced fission. During this experiment, the alpha particle beam provided by the LBL 88-Inch Cyclotron was defocused to provide the same beam profile used in the Bevalac experiments. The relative activities of the four catcher sections were assayed using the same counting geometry and techniques as employed previously. Relative values of the differential cross-section $d\sigma/d\Omega$ (θ) were computed for the typical fission products using the measured activities and numerically calculated

solid angles. The values of $d\sigma/d\Omega$ (θ) for the observed nuclides were averaged and compared to the known gross fission fragment angular distributions.[4] This comparison was used to generate a set of correction factors, ranging from 10 to 50% to correct for the effects of extended counting sources and fragment absorption and scattering.

Despite the measures used to overcome the problem of low beam intensity, only 6 to 8 nuclides were reliably identified in the preliminary analysis of each experimental set of data, and these all contain appreciable uncertainties. Nevertheless, some useful information may be extracted from trends in the data. In general, roughly isotropic angular distributions are observed for neutron-rich ^{238}U fission products such as ^{97}Zr, ^{99}Mo, and ^{133}I at both beam energies. This is in good agreement with previous determinations which indicated that the low excitation energy fission of ^{238}U induced by relativistic heavy ions results from peripheral collisions with little momentum transfer. Those fragments not normally considered to be ^{238}U fission fragments, such as ^{43}K, ^{72}As, ^{149}Gd, all show forward peaked distributions with the greatest degree of peaking being observed in the ^{149}Gd angular distribution. This is in qualitative agreement with the trends of the F/B ratios.[1] For the fragmentation of ^{197}Au, all the observed distributions are forward peaked, with maximum peaking observed for fragments with mass number A such that $145 \leq A \leq 155$, which agrees with general trends in their F/B ratios.[5]

It is interesting to compare the fragment angular distributions measured for this work with similar data measured for the interaction of high energy protons with ^{238}U.[6] The most dramatic difference between these sets of data is the absence of a sidewise peaked ^{44}Sc fragment distribution in the ^{12}C induced reactions, whereas such a distribution is observed in the interaction of 11.5 GeV protons with ^{238}U. If this sidewise peaked light fragment angular distribution seen in proton induced reactions is due to collective effects such as compression of nuclear matter or a shock wave, it is surprising that the effect is not enhanced or even apparent with relativistic heavy ions.

Reference and Footnotes

*Radiation Center, Oregon State University, Corvallis, OR 97331.

1. W. Loveland et al., LBL-11658, (1980).
2. W. Loveland et al., Phys. Rev. C **23**, 253 (1981).
3. D.J. Morrissey et al., Nucl. Instrum. Meth. **158**, 499 (1979).
4. R. Vandenbosch, H. Warhanek, and J.R. Huizenga, Phys. Rev. **124**, 846 (1961).
5. S.B. Kaufmann, E.P. Setinberg, B.D. Wilkins, and D.J. Henderson, Phys. Rev. C **22**, 1897 (1980).
6. D.R. Fortney and N.T. Porile, Phys. Lett. B **76**, 55 (1978).

Fragment-Spray Correlations in High Energy Heavy Ion Collisions

A.I. Warwick, H.H. Gutbrod, S.B. Kaufman, M.R. Maier, J. Peter, H.G. Ritter, E.P. Steinberg,* H. Stelzer, F. Weik, H. Wieman, and B.D. Wilkins**

We report here the partially analyzed results of an experiment performed at the Bevalac last year, which focused on heavy ion collisions leading to final states with heavy target fragments moving slowly in the laboratory frame. Experimental details were described in last year's annual report.[1] Typically, fragment energies are in the range 0.3 MeV/n to 3 MeV/n. Fragments across the entire mass range are measured.

We particularly wish to investigate the reaction mechanism, looking beyond the late stage evaporation kinematics to see features of the fast energy deposition stage.

One of the models to be considered is a hydrodynamic description of such collisions. This model predicts distinctive "bounce-off" features in which the transverse momentum transfer to the heavy fragment is accomplished through the expansion of a pressure zone.[2] A more traditional approach has been to consider the Coulomb force as the origin of the kinetic energy of the heavy fragment, which, in this model, emerges as an evaporation product or fission fragment. We do observe events for which such a Coulomb description is appropriate; there is a wealth of experimental studies of such data.[3] However, we also observe, due to the exclusive nature of our experiment, a direct correlation between the fast stage of the collision and the fragment emission, in the form of an angular correlation between the numerous fast light charged particles emitted and the fragment itself. This correlation is omnipresent but seems to be strongest for the heaviest fragments, which are considered to be residues of an evaporating system. Thus, by studying the heaviest fragments and their correlation we are looking at the effects of the initial collision, smeared by the random walk of evaporation recoil. The properties of the lighter fragments are considered to be dominated by the late-stage evaporation mechanism, although a spray-fragment correlation is observed here too.

A further observation to be understood within the various models is the fact that the data are dominated by the total incident kinetic energy, independent of projectile mass.[4]

Figure 1 shows the azimuthal correlation between the heavy fragments $M > 50$ and the spray of fast charged particles in the paddle array.[1] The reaction is 400 MeV/n Ne + Au and the fragments are detected at $\theta \simeq 90°$, $\psi = 0°$. There is a strong azimuthal correlation between the spray and the fragment. Thus, the fast spray plays a role in balancing the transverse momentum of the heavy target remnant. This coupling of the fragment emission to the fast stage of the reaction is in direct contradiction to the two-step interpretation and furthermore is an effect explicitly predicted by the hydrodynamic models. This experimental correlation has been called "bounce-off" but has not been explicitly shown to originate with an expanding pressure zone.

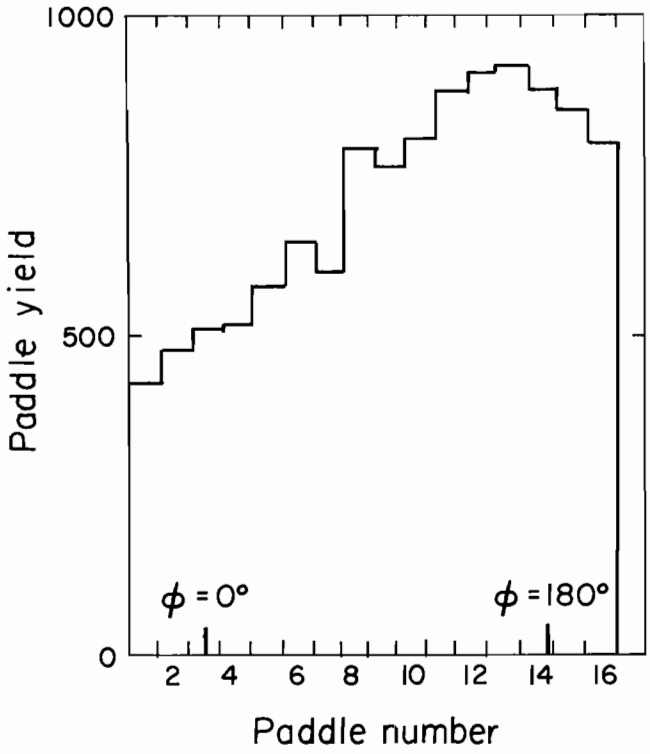

Fig. 1. Yield of fast charged particles in paddle ring A as a function of azimuthal angle, observed in coincidence with a heavy fragment ($M > 50$) at $\theta = 90°$, $\psi = 0°$.
(XBL 818-1155)

Footnote and References

*Argonne National Laboratory, Gesellschaft für Schwerionenforschung, and LBL.

1. Nuclear Science Division Annual Report, LBL-11588 (1981).
2. H. Stöcker and B. Müller, GSI Preprint 80-4 (1980).
3. G.D. Westfall et al., Phys. Rev. C **17**, 1368 (1978), and references therein.
4. A. Sandoval et al., Phys. Rev. C **21**, 1321 (1980). W.G. Meyer et al., Phys. Rev. C **22**, 179 (1980).

Comparative Yields of Alkali Elements and Thallium from Uranium Irradiated with GeV Protons, ^{3}He and ^{12}C*

T. Björnstad,† H.-Å Gustafsson,§ B. Jonson,§ O.C. Jonsson,§ V. Lindfors,‡ S. Mattsson,§ A.M. Poskanzer, H.L. Ravn,§ and D. Schardt§

Mass-separated ion beams of the alkali elements Na, K, and Fr, and of the element Tl, were produced by bombarding a uranium target with 600 MeV protons, 890 MeV $^3He^{2+}$, and 936 MeV $^{12}C^{4+}$. Isotopic production yields were measured. In the case of the ^{12}C beam, these are thick target yields. Absolute cross-sections for the proton beam data were deduced by normalizing the delay-time corrected yield curves to measured cross-sections. For products farthest away from stability, the $^3He^{2+}$ beam generally gives the highest yields.

Footnotes

*Greatly condensed from Z. Phys. A **303**, 227 (1981).
†Department of Nuclear Chemistry, University of Oslo, N-1000 Oslo 3, Norway.
‡Department of Physics, University of Helsinki, SF-00170 Helsinki 17, Finland.
§The ISOLDE Collaboration, CERN, Geneva, Switzerland.

A Compilation of World Data on "Anomalons"

E.M. Friedlander and Y.J. Karant

We present a compilation of world data referring to the observation of relativistic projectile fragments from high energy heavy ion collisions that exhibit an anomalously short mean free path for nuclear interaction ("anomalons"), which were first noticed (1954) by Milone.[1]

We use as quantitative measures for this effect either (1) the ratio R_1 for the mean free path (MFP) observed on projectile fragments to the MFP observed on "primary" nuclei which can be considered "normal," or (2) the ratio R_2 of the MFPs of projectile fragments measured at different distances from their points of emission (e.g., close to the origin and far from it).

R_1 implies "external" calibration (or theoretical evaluation of the normal MFP, while R_2 is an "internal standard" comparison and is therefore free of many real or suspected systematic effects.

To assess the statistical significance of deviations of R_1 or R_2 from unity (the null hypothesis), we note that $2nR_1$ is distributed like χ^2 with 2n degrees of freedom (DOF), where n is the number of nuclear interactions observed. The quantity R_2 obeys a Fisher variance ratio (or F−) distribution with n_1 and n_2 DOF, where n_1 and n_2 are the numbers of collisions observed at the two different distances from the origin. The integral probabilities $p_1(<R_1)$ and $p_2(<R_2)$ are uniformly distributed between 0 and 1.

The latter property is useful in combining the results of different experiments to obtain a global level of significance. Indeed, given any set of independent p_i values, (i=1,2,n) the quantity $-2\Sigma\ln P_i$ is distributed like χ^2 with 2n DOF. The integral of this χ^2 distribution can be used to reduce the confidence level to the more familiar number of equivalent standard deviations (ESD) by which the "effect" deviates from "normalcy."

Table 1 shows the results of this kind of analysis performed on

(1) Two cosmic ray emulsion experiments measuring R_1.[2,3]

(2) Three emulsion experiments measuring R_2 (Refs. 4 and 5 on 2 AGeV Bevalac beams, Ref. 6 on cosmic rays at higher energies), and

(3) A propane bubble chamber (PBC) experiment[7] using 4 AGeV beams from the Dubna synchrophasotron, measuring R_1.

While the emulsion experiments are directly comparable, the PBC experiment[7] (as stated by the authors themselves) lacks the spatial resolution necessary to measure R_2, i.e., to measure the MFP close to the origin of the projectile fragments.

While all emulsion experiments had this ability (the R_1 values reflected the inclusion of the region where most of the effect is located) the PBC experiment excluded this region; in spite of this systematic weakening of any possible effect, their R_1 value is systematically lower than unity (for four different charges of projectile fragments by (globally) 2.1 EDS.

Thus, all data available in the world literature consistently show that the MFP of relativistic projectile fragments are anomalously short immediately after emission (be it by reason of time elapsed or of amount of matter traversed).

Note that all the deviations in Table 1 are in the same direction (i.e., all MFPs are shorter than normal or shorter close to the point of emission). For the three emulsion experiments (group 2 in Table 1), the overall probability that this deviation is due to a statistical fluctuation is $\lesssim 10^{-7}$.

If the results of all the independent experiments mentioned in Table 1 are taken together, the level of discrepancy goes up to $>$ 6 SED, or, in other words, a probability of 10^{-10} for a chance fluctuation!

Table 1. Our statistical evaluation of world data.

Group	Primary beam	Ratio measured	ESD	Global ESD	Ref.
1	Cosmic rays	R_1	2.8[a]	2	
	Cosmic rays	R_1	3.1		3
2	2 AGeV Fe, O	R_2	3.4		4
	2 AGeV Fe, Ar	R_2	3.2	5.1	5
	Cosmic rays	R_2	2.8[a]		6
3	4 AGeV C	R_1[b]	2.1		7

[a]These experiments share, in part, a common data base.

[b]Excluding the first 7 cm of track after collision.

References

1. A. Milone, Nuovo Cimento Supple. **12**, 353 (1954).
2. T.F. Cleghorn, P.S. Freier, and C.J. Waddington, Can. J. Phys. Suppl. **46**, 572 (1968).
3. B. Judek, Can. J. Phys. **50**, 2082 (1972).
4. E.M. Friedlander et al., Phys. Rev. Lett. **45**, 1084 (1980).
5. P.L. Jain and G. Das, presented at the 5th High Energy Heavy Ion Summer Study, LBL-12652 (1981).
6. H.B. Barber, P.S. Freier, and C.J. Waddington, contribution HE 3.1-6, 16th Cosmic Ray Conference, Versailles, France.
7. G.M. Agakishyer et al., Dubna preprint P1-81-79.

Further Investigation of Projectile Fragmentation: the Short Mean Free Path Effect

E.M. Friedlander, R.W. Gimpel, H.H. Heckman, Y.J. Karant, B. Judek and E. Gaussauget*

Two independent experiments using nuclear emulsion were conducted to examine the interaction characteristics of relativistic projectile fragments (PF), $3 \leq Z \leq 26$.[1] One experiment, scanned and measured at the NRC, Ottawa, used 2.1 A GeV ^{16}O as the incident beam; the other, at LBL, used 1.88 A GeV ^{56}Fe.

The principal interaction characteristic examined in these data was the inclusive reaction mean free path (MFP), symbolized by "λ." We have measured the MFPs of primary beams, and fit to these primary results a power law, $\lambda = \Lambda Z^{-b}$, where "Λ" is a parameter which is independent of the charge Z. For primary beams, $\Lambda = 30.4$ cm and $b = -0.44$. We have also measured the MFP parameter on PFs as a function of distance after emission (Fig. 1). As is readily observable, the MFP parameter Λ does vary as a function of distance after emission. The solid line in Fig. 1 is the result of a fit with 0.06 of the PFs having a constant MFP of 2.5 cm, independent of Z (which is a MFP for a nucleus on the order of Pb), and the rest of the PFs have the MFP values obtained from the primary beam fit. This hypothesis of a 6% admixture gives a reasonable fit to our observations. The ratio of any two measured values of the MFP (for particles of the same intrinsic MFP) obeys the Fisher F-variance ratio distribution. The probability of obtaining this ratio or a larger one from a pair of measurements should obey the uniform distribution U(0,1).

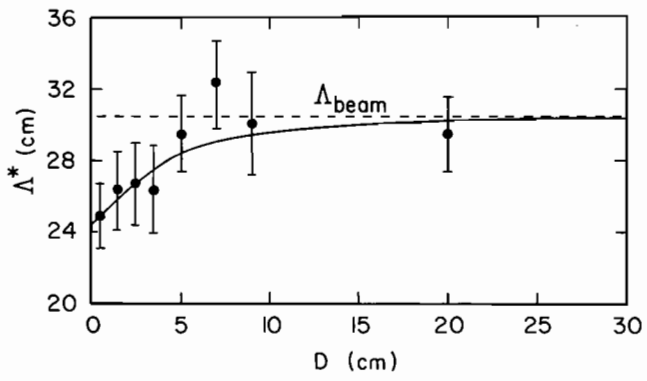

Fig. 1. Estimates of Λ^* for the parameter Λ at different distances D from the origins of PFs: full circles, experiment; dashed line, prediction from Λ as fit to primary beams; solid line, fit assuming a 6% admixture of PFs with a constant 2.5 cm MFP. (XBL 808-11485)

In addition to examining the MFP as a function of distance after emission, we also consider the MFP as a function of the generation of the PF; we regard the incident beam nuclei as "primaries," their immediate PFs as "secondaries," the immediate PFs from secondaries as "tertiaries," etc. Proceeding via the F-test by generation (secondaries versus tertiaries and later generations), we obtain the mean P value, which is only about 2.1 SD from its expectation. However, the largest P value recorded was only 0.778, and the binomial probability of observing 0 events in the uniform distribution out of 29 attempts with $P \geq 0.778$ is $7(10^{-4})$. We would expect about 6 events in this P region.

In the above discussion, we have considered total track length S_N observed for N interactions, whether or not all particles interacted. We may also limit consideration to those particles which did interact, neglecting those which did not. To investigate further the apparent shortening of the MFP from one generation to the next, we consider the topology in which a secondary interacted and emitted a tertiary that also interacted. Taking into account the expected MFP from the primary beam fit and the distance over which a particle could in fact have been observed to interact within our detectors (the potential path), one may calculate probability values $P_2(X)$ and $P_2(Y)$ for the secondary and tertiary particles respectively to have interacted within the observed distances X, Y, or shorter. These probabilities are independent because of the way in which we have calculated them. Thus, a scatter plot of $P_2(X)$ vs $P_2(Y)$ should populate uniformly the unit plane. Dividing each axis into two a priori equiprobable bins, we obtain the scatter plot, Fig. 2. We define a quantity C equal to the number of counts in quadrant III minus the number in

Comment on the Energy Dependence of Target Excitation in RHI Collisions*

Harry H. Heckman

Over the past several years, there have been a variety of radiochemical experiments on the cross sections and recoil properties of target fragmentation products (radionuclides) formed by the reactions of RHI and protons with various target nuclei. Such studies have been found to be particularly sensitive tests of limiting fragmentation as it applies to the asymptotic kinematic limits of the target recoil velocities.

By assuming that the recoil fragments result from a two-step (fast-flow) process, the observations can be interpreted in terms of the mean forward-directed velocity $\langle\beta_{||}\rangle$ of the prefragment produced in the primary projectile-target interaction and the mean Maxwellian-distributed velocity $\langle\beta\rangle$ that arises from the de-excitation of the prefragment to produce the observed residue. Figure 1 summarizes the dependence of the mean longitudinal recoil velocity of the first step, $\langle\beta_{||}\rangle$, on the mass number of the detected fragment. These data were collected from the works of Loveland and Kaufman[1,3] and coworkers.[2,4]

A most interesting feature of Fig. 1 is that the recoil velocities $\langle\beta_{||}\rangle$ are inversely proportional to the mass of the fragment, A_F, particularly for $A_F \leq 100$. This leads

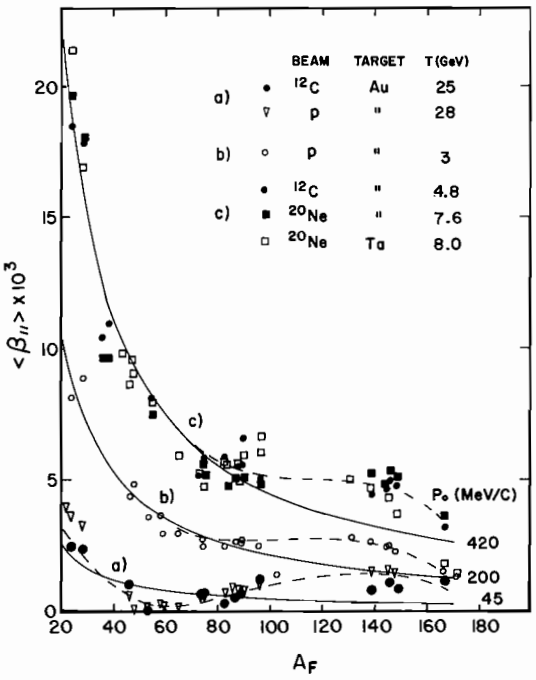

Fig. 1. Longitudinal recoil velocity of fragment of mass number A_F as a function of beam and beam energy. Solid curves are $\langle\beta_{||}\rangle = P_o/931\ A_F$ for the values of P_o indicated. Dashed lines delineate data points. (XBL 815-9830)

to the suggestion that the loci of data points can be expressed rather well in terms of a characteristic mean momentum $P_o = 971\ A_F\ \langle\beta_{||}\rangle$ MeV associated with each plot of $\langle\beta_{||}\rangle$ vs A_F. For the data shown, I have evaluated P_o from the unweighted data for $\langle\beta_{||}\rangle$, with $A_F \leq 100$, and have drawn the resultant curves of the expression $\langle\beta_{||}\rangle = P_o/971\ A_F$, where the values of P_o corresponding to curves a), b), and c) in Fig. 1 are 420 ± 7 MeV/c, 200 ± 6 MeV/c, and 45 ± 6 MeV/c, respectively. The data are compatible with $A_F\langle\beta_{||}\rangle$ = constant over most of the range of fragment mass, with the largest deviations occurring at high beam energies (curve c) and, in all cases, for $A_F \simeq 140$.

An interesting consequence of this observation comes from considering the two-step kinematic model proposed by Masuda and Uchiyama,[5] which describes target fragmentation by the sequence of reactions, i) $B + T \rightarrow B^* + T^*$ and ii) $T^* \rightarrow F + X$, whereby the target (projectile) nucleus T(B) is excited to the state $T^*(B^*)$, the decay of which leads to the detected target (projectile) fragment F. Given the approximations that the recoil << excitation << nuclear rest energies and that the excitation energies of the target and beam nuclei are, on the average, equal (considering pionic degrees of freedom, this approximation is applicable to proton beams), the conservation of energy and momentum leads to the following expression for the recoil velocity $\langle\beta_{||}\rangle$ of the target system[6]:

$$\langle\beta_{||}\rangle = \frac{E^*}{M_T}\sqrt{\frac{\gamma+1}{\gamma-1}}\ , \qquad (1)$$

where E^* is the excitation energy of the target (projectile), M_T is the mass of the target, and γ is the Lorentz factor of the beam nucleus. Given the approximate constancy of the mean momentum $P_o = M_F\langle\beta_{||}\rangle$ of the fragments at beam energy $M_B(\gamma-1)$ as depicted in Fig. 1, the following reaction holds:

$$M_F E^* = P_o M_T \sqrt{\frac{\gamma-1}{\gamma+1}}\ . \qquad (2)$$

Simple kinematics of the two-step model, incorporating the observation $P_o = M_F\langle\beta_{||}\rangle$, thus indicates that the quantity $M_F E^*$ is a constant for a given beam energy and that E^* is linearly related to the mean recoil velocity $\langle\beta_{||}\rangle$ of the fragment F, Eq. (1).

In Fig. 2, I have plotted $M_F E^*$ (Eq. (2)) versus beam kinetic energy for a variety of beam and target nuclei, using the values of P_o extracted from published $\langle\beta_{||}\rangle$ vs A_F data.[1,2,3,4] The data are ordered by the kinetic energy of the beam and show that E^* associated with each fragment mass attains a maximum near 5 GeV, decreasing

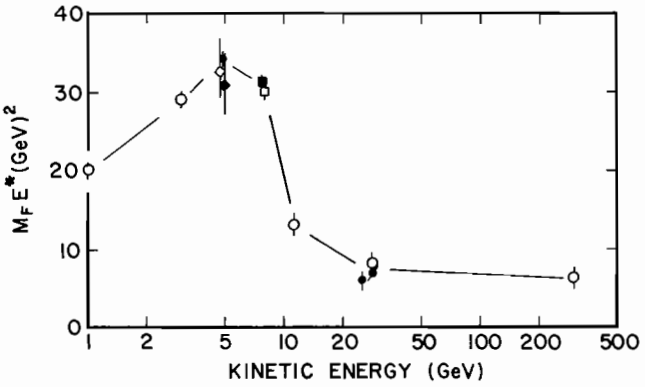

Fig. 2. The product of fragment mass and excitation energy as a function of beam energy and mass. Symbols are: for Au target, o protons, ● ^{12}C, ■ ^{20}Ne; for Ta target, □ ^{20}Ne, and for U target, ◇^{12}C and ◆^{20}Ne. Data are compiled from Refs. 1-4. (XBL 815-9832)

thereafter with increasing beam energy, approaching an asymptotic value for energies > 25 GeV. Within experimental errors $E^*(25\ GeV) \equiv E^*(300\ GeV)$. Limiting fragmentation is thus satisfied for the variable $M_F E^*$ for beam energies > 25 GeV. Because $\langle\beta_{||}\rangle \propto E^*$ [(Eq. (1)], the recoil velocity $\langle\beta_{||}\rangle$ which is the kinematic quantity that controls the forward/backward ratio of fragments, also attains a limiting value at beam energies > 25 GeV. Other obvious conclusions from Fig. 2 are: (1) the fragment angular distributions in the laboratory, because of their dependence on $\langle\beta_{||}\rangle$, will exhibit maximum asymmetries in the laboratory at beam energies 5 GeV; (2) limiting fragmentation is clearly not met for energies < 10 GeV; (3) the scaling factor that "universally" interrelates $\langle\beta_{||}\rangle$ and E^* for beam nuclei $1 \leq A_B \leq 20$ for which data are available, is the total kinetic energy of the beam; and (4) the excitation energies, hence $\langle\beta_{||}\rangle$, are independent of the projectile mass, i.e., factorization is valid, as indicated by Eq. 1.

Footnote and References

*Based on LBL-12656, May 1981.

1. W. Loveland et al., Phys. Rev. C **23**, 253 (1981).
2. S.B. Kaufman et al., Phys. Rev. C **22**, 1897 (1980).
3. W. Loveland et al., Phys. Rev. C (in press); also LBL-11658 (1980), 38 p.
4. S.B. Kaufman, E.P. Steinberg and M.W. Weisfield, Phys. Rev. C **18**, 1349 (1978).
5. N. Masuda and F. Uchiyama, Phys. Rev. C **15**, 1598 (1977).
6. Derived from relativistic energy conservation with the approximation that neglects all quadratic terms of the recoil momentum and excitation energies. The nonrelativistic expression for the recoil momentum is also used.

A Measurement of Deuteron-Deuteron Elastic Scattering at 5.75 GeV/c*

Edgar T. Whipple, V. Perez-Mendez, A.L. Sagle, R.L. Talaga,† F. Zarbakhsh, J.B. Carroll,‡ G.J. Igo,‡ J.B. McClelland,† M. Bleszynski,‡ and K. Ganezer‡

The multiple diffraction model of Glauber[1] successfully explains many of the major features of elastic hadron-deuteron scattering. The model has been extended to systems in which both target and projectile are composite and in which simultaneous multiple collisions can occur in addition to the normal, sequential collisions.[2] These extra processes introduce more structure into the differential cross section and thus permit new tests of the parameterizations which enter the model. Deuteron-deuteron scattering is the simplest system in which such effects can be studied.

This experiment was performed at the LBL Bevatron. A 5.75 GeV/c deuteron beam was extracted and focused onto a deuterated (about 97%) polyethylene target. The three-momentum and time of flight of the forward scattered particle were measured in a magnetic spectrometer. A wire chamber and scintillator determined the position and time of flight of the recoil particle. The elastic signal was identified by selecting events for which the measured variables satisfied the four kinematic equations of elastic scattering. A 5.75 GeV/c proton beam incident on a normal polyethylene target provided p-p elastic scattering signal which was used to check the apparatus and analysis procedure.

The results of the experiment are shown in Fig. 1, where only statistical errors are indicated. The t-resolution is always less than the indicated bin width, and the error in the absolute normalization is estimated to be 10%. We observe a narrow minimum at $-t = 0.18\ (GeV/c)^2$ and a significant departure from a simple exponential behavior in the double scattering region. This latter effect has not been mentioned explicitly in the literature, although it is implicitly contained in the Glauber model.

At the second maximum [$-t \sim 0.3\ (GeV/c)^2$], the cross section is dominated by three roughly equal amplitudes, simultaneous and sequential double scattering, and triple scattering. The slope of the sequential double scattering is significantly larger than the almost equal slopes of the other two terms. The phases are such that the

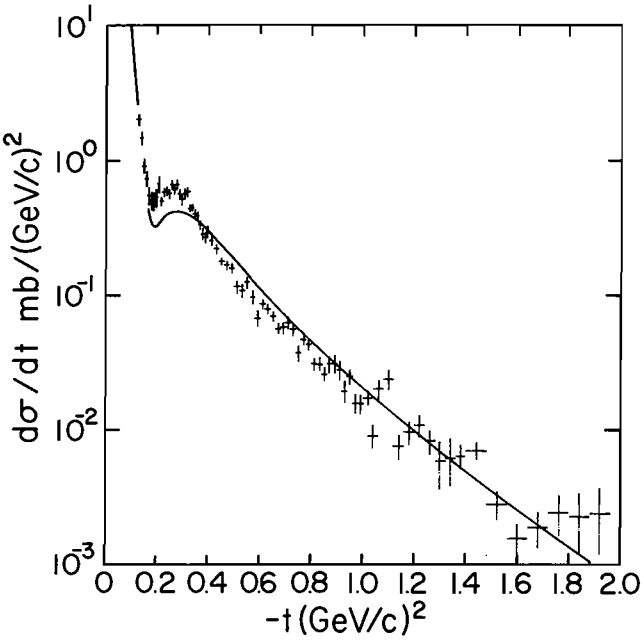

Fig. 1. (XBL 818-11304)

sequential term is approximately parallel to the resultant of the remaining terms. The net effect of the rapidly decreasing sequential amplitude is simply a corresponding rapid decrease in the cross section. When the sequential term becomes smaller than the sum of the other two terms, the cross section assumes the more slowly varying behavior of the simultaneous double and triple amplitudes.

Figure 1 also shows the result of a calculation[3] in which the d-state of the deuteron was taken into account by considering terms in the amplitude proportional both to the square of the quadrupole deformation and to the product of the spin-1 operators of the two deuterons.

In conclusion, we have produced the first high-statistics, high-resolution data on deuteron-deuteron scattering in the intermediate energy range. We have observed a well-defined minimum and a hitherto unremarked complex behavior in the double scattering region. We believe that this reflects the constructive interference of the simultaneous and sequential double scattering region.

Footnotes and References

*Condensed from LBL-11966.

†Los Alamos Scientific Laboratory, Los Alamos, NM.
‡Department of Physics, UCLA

1. R.J. Glauber, in *Lectures in Theoretical Physics*, W.E. Brittin et al., eds., Interscience Publishers, Inc., New York (1959), Vol. I, p. 315.
2. V. Franco, Phys. Rev. **175**, 1376 (1968).
3. M. Bleszynski and K. Ganezer, to be published.

2. Pion Production

Production of Pions and Light Fragments at Large Angles in High-Energy Nuclear Collisions*

S. Nagamiya, M.-C. Lemaire,† E. Moeller,‡ S. Schnetzer, G. Shapiro, H. Steiner, and I. Tanihata§

Inclusive cross sections for production of π^+, π^-, p, d, ^{3}H, ^{3}He, and ^{4}He have been measured at laboratory angles from 10° to 145° in nuclear collisions of Ne + NaF, Ne + Cu and Ne + Pb at 400 MeV/nucleon, C + C, C + Pb, Ne + NaF, Ne + Cu, Ne + Pb, Ar + KCl and Ar + Pb at 800 MeV/nucleon, and Ne + NaF and Ne + Pb at 2.1 GeV/nucleon. The production of light fragments in proton-induced collisions at beam energies of 800 MeV and 2.1 GeV has also been measured in order to allow us to compare these processes.

For equal-mass nuclear collisions the total integrated yields of nuclear charges are well explained by a simple participant-spectator model. For 800 MeV/nucleon beams the energy spectra of protons at c.m. 90° are characterized by a "shoulder-arm" type spectrum shape with an exponential fall-off at high energies, while those of pions are of a simple exponential type. The inverse of the exponential slope, E_0, for protons is systematically larger than that for pions. This E_0 is larger for heavier-mass projectiles and targets. It also increases monotonically with the beam energy. The angular anisotropy of protons is larger than that of pions. The yield ratio of π^- to total nuclear charge goes up with the beam energy, while the yields of composite fragments decreases. The ratio of low-energy π^- to π^+ as well as that of ^{3}H to ^{3}He are larger than the neutron to proton ratio of the system. The spectrum shape of the composite fragments with mass number A is explained very well by the A^{th} power of the observed proton spectra. The sizes of the interaction region are evaluated from the observed coalescence coefficients to 3-4 fm. The yield ratio of composite fragments to protons strongly depends on the projectile and target masses and the beam energy, but not on the emission angle of the fragments.

These results have been compared with currently available theoretical models.

Footnotes

*Condensed from LBL-12123.

†Present address: DPhN/ME, CEN de Saclay, 91190 Gif-sur-Yvette, France.

‡Present address: Institüt für Theoretische Physik, Freie Universität Berlin, 1000 Berlin 33, West Germany.

§On leave from Institute for Nuclear Study, University of Tokyo, Tanashishi, Tokyo, Japan.

Inclusive Single Negative Pion Production at Forward Angles from Collisions of Light Relativistic Nuclei

E. Moeller,† W. Bruckner, L. Anderson, S. Nagamiya, S. Nissen-Meyer,‡ L. Schroeder, G. Shapiro, and H. Steiner

We have measured single particle inclusive spectra of negative pions produced at angles from 0° to 12° (lab) in collisions of 1.05 and 2.1 GeV/N protons, deuterons, alpha particles, and carbon nuclei with targets of C, Cu, Pb, and H (from a CH_2-C subtraction). The detected pions have momenta from 0.25 GeV/c to 4.25 GeV/c in the lab frame.

Figure 1 shows the 0° negative pion spectra for 2.88 GeV/c/N p, d, α and carbon projectiles on a carbon target. The spectra are seen to fall steeply as a function of momentum. The proton projectile data show a clear cut-off at the kinematic limit; for pion production from free nucleons, this limit is indicated in Fig. 1 by an arrow. The d, α, and C projectiles show considerable production beyond this limit, and it is these fast pions which interest us most. The fact that we see pions at up to twice the kinetic energy per nucleon of the projectile is a clear indication that effects of a nuclear origin are involved. For example, such energetic pions could be produced if the nucleons in the nucleus have sufficiently high momentum or if these are processes involving more than two colliding nucleons.

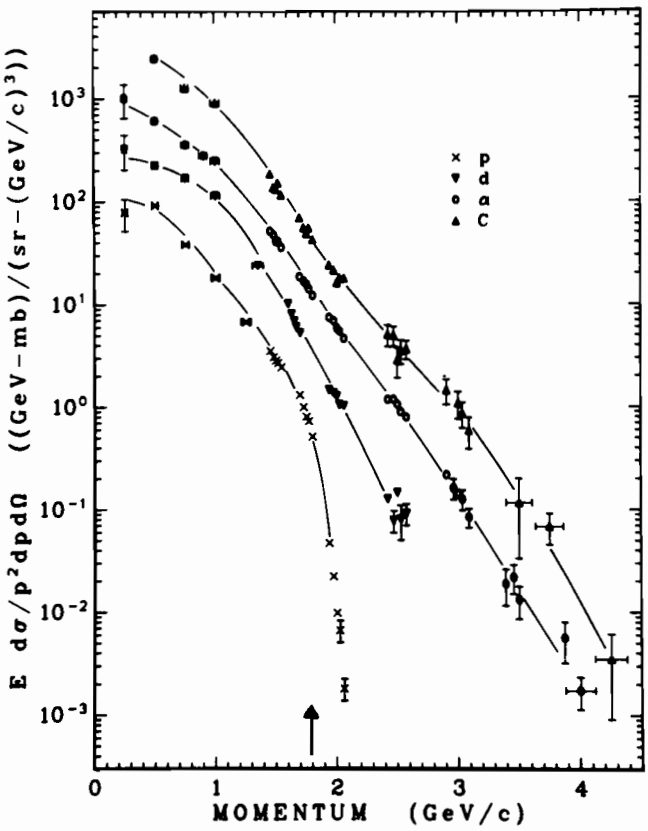

Fig. 1. Lorentz invariant negative pion inclusive cross section vs the (lab) momentum at 0° for 2.88 GeV/c/N protons (x), deuterons (▽), alphas (○), and carbon nuclei (△) interacting with a carbon target. Arrow indicates the kinematical limit for pion production from free nucleons. The curves are drawn to guide the eye. (XBL 818-11274)

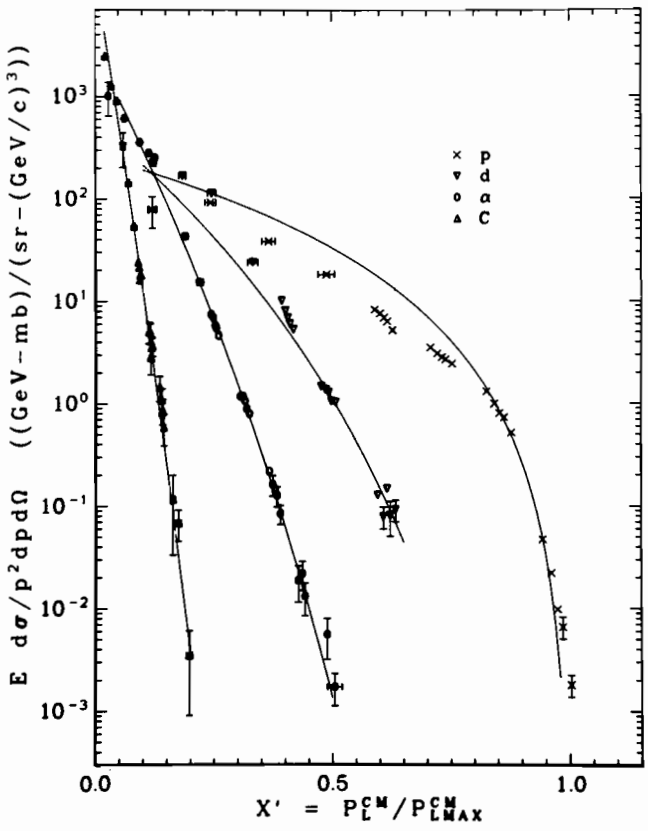

Fig. 2. Comparison of our 2.88 GeV/c/N data with the hard scattering model[1] (see text). (XBL 818-11275)

Figure 2 shows the x′ distribution at 0° for 2.88 GeV/c/N p, d, α and C projectiles on a C target. Here $x' = p_{||}^*/(p_{||}^*)_{max}$ is the Feynman scaling variable, where $p_{||}^*$ is the pion longitudinal momentum in the center of mass and $(p_{||}^*)^{max}$ is its maximum kinematically allowed value. We see that the fall-off of these distributions with x′ becomes steeper as the mass of the projectile increases, indicating that complex nuclei tend not to transfer a large fraction of their kinetic energy to individual pions. The curves in Fig. 2 represent the functional form $(1 - x')^n$ with the values n = 3, 9, 21, and 69 for p, d, α, and carbon projectiles, respectively, predicted by the hard scattering model of Schmidt and Blankenbecler.[1] This model reproduces the general trend of the data; however, we see deviations from scaling which increase as the mass of the projectile increases.

The dependence of the cross sections on the mass of the target is approximately $A_T^{0.4}$ whereas the projectile mass dependence ranges from $A_p^{1.2}$ to $A_p^{1.7}$ depending on the energy of the pion.

Footnotes and Reference

*Now at CERN, Geneva, Switzerland.
†On leave from Freie Universität, Berlin, West Germany.
‡Now at Simens, Munich, West Germany.

1. I.A. Schmidt and R. Blankenbecler, Phys. Rev. D **15**, 3321 (1977).

Pion Double Charge Exchange on ^{4}He and Meson Exchange Currents

A. Stetz, L.W. Swenson,* J. Davis,† J. Källne,† R.C. Minehart,†*
R.R. Whitney,† V. Perez-Mendez, A. Sagle, J. Carroll,‡
J. McClelland,‡ and J. Fawcett§

One promising class of reactions for studying meson exchange effects is pion double charge exchange (DCX). Conservation of charge automatically rules out the "first order" processes that usually mask the weaker exchange effects. However, there are some DCX transitions between light nuclei and *continuum* states, which are simple enough for a detailed study of the reaction mechanism as proposed by Germond and Wilkin.[1]

We have completed an experiment on DCX on ^{3}He and ^{4}He using the EPICS pion spectrometer at LAMPF, which can be compared directly with the work of Germond and Wilkin as well as with other theoretical reaction mechanisms.[2,3]

A substantial number of the low momentum pions decay in the spectrometer. We used two criteria for discriminating between pions and muons, based on trajectory reconstruction and on time of flight.

A typical spectrum is shown in Fig. 1. Here we have plotted the differential cross section $d^2\sigma/d\Omega\, dT$ vs T at fixed scattering angle. The energy variable T is the "missing mass"; this is equivalent to the total kinetic energy of the protons in their own center-of-mass coordinate system. The data in Fig. 1 include seven overlapping spectrometer settings; to obtain $d\sigma/d\Omega$ we integrated the spectra over T.

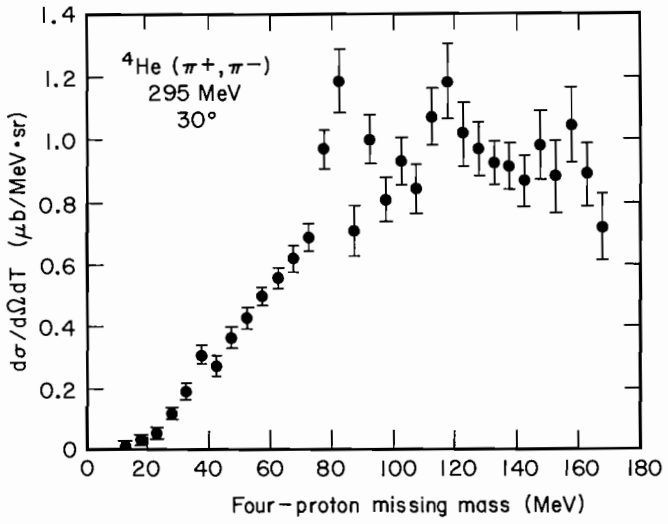

Fig. 1. (XBL 8111-1607)

In order to obtain the total cross section we fitted the experimentally determined values of $d\sigma/d\Omega$ with the integrated phase space to obtain σ_T. The fits are shown in Fig. 2. Our cross sections are consistent with the earlier data of Falomkin[4] and Carayannopoulos.[5]

There are two important mechanisms to consider in calculating double charge exchange at low energies, namely, two successive single charge exchange interactions, and scattering from meson exchange currents. The first reaction mechanism has been discussed by Becker and Schmit[2] and by Gibbs et al.;[3] these two calculations, while superficially similar, predict total cross sections which differ by three orders of magnitude.

A simple calculation based on pion exchange scattering done by Germond and Wilkin predicts total cross sections that are intermediate between those of Gibbs et al. and Becker and Schmit, and achieves the best overall agreement with experiments.

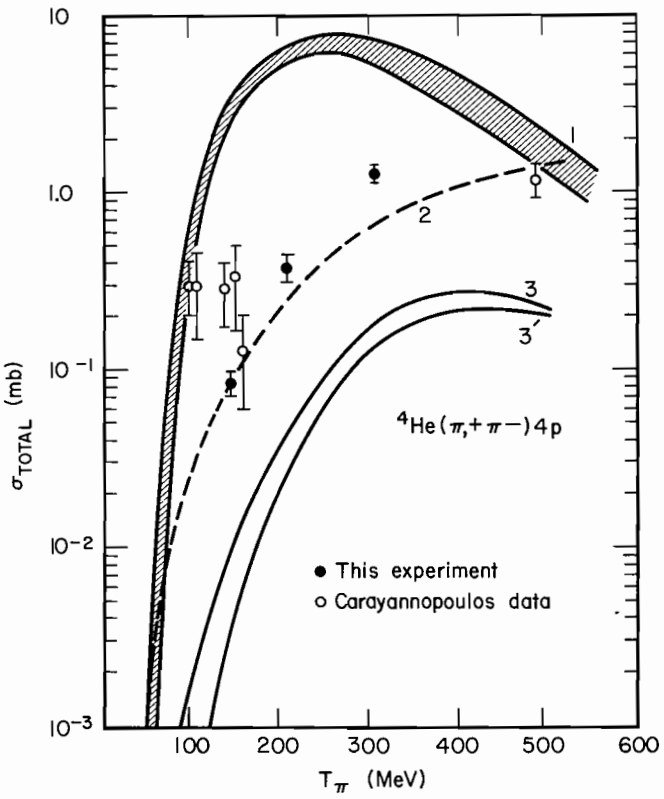

Fig. 2. Experiment σ_t compared to the theoretical curves of: (1) Becker, Schmidt; (2) Germond, Wilkins; (3,3′) Gibbs et al. (XBL 8111-1604)

If these calculations confirm that sequential single charge exchange contributes a relatively small fraction of the observed cross sections, then double charge exchange could become an important probe of mesonic effects within the nucleus.

Footnotes and References

*Oregon State University.
†University of Virginia.
‡University of California at Los Angeles.
§University of Oregon.

1. J.F. Germond and C. Wilkin, Lett. Nuovo Cimento **13**, 605 (1975).
2. F. Becker and C. Schmit, Nucl. Phys. **B 18**, 607 (1970).
3. W.R. Gibbs et al., Phys. Rev. C **15**, 1384 (1977).
4. I.V. Falomkin et al., Nuovo Cimento A **22**, 333 (1974).
5. N. Carayannopoulos et al., Phys. Rev. Lett. **20**, 1215 (1968).

Strong Coulomb Effects on Pions Produced in Heavy Ion Collisions*

J.P. Sullivan, J.A. Bistirlich, H.R. Bowman, R. Bossingham, T. Buttke, K.M. Crowe, K.A. Frankel, C.J. Martoff,† J. Miller,‡ D.L. Murphy, J.O. Rasmussen, W.A. Zajc, O. Hashimoto,§ M. Koike,§ J. Péter‖ W. Benenson,¶ G.M. Crawley,¶ E. Kashy,¶ and J.A. Nolen, Jr.¶

Doubly differential cross sections for the production of π^+ and π^- near the velocity of the incident beam for pion lab angles from 0° to 20° were measured. Beams of ^{20}Ne with E/A = 280, 380, and 480 MeV and ^{40}Ar with E/A = 535 MeV incident on C, NaF, KCl, Cu and U target were used. A sharp peak in the π^- spectrum and a depression in the π^+ spectrum is observed at 0° near the incident projectile velocity. The effect is explained in terms of Coulomb interactions between pions and fragments of the incident beam. Least squares fits to the data using the Coulomb correction formulas of Gyulassy and Kauffmann[1] and an effective projectile fragment charge have been made.

A sample of the data and the fits is shown in Fig. 1 which shows the Lorentz invariant cross section cuts for Ne + NaF → $\pi^{\pm}$ at E/A = 380 MeV. The left side of the graph shows the cross section vs momentum at 0° in the lab for π^- (top) and π^+ (bottom). The right side shows the cross section vs lab angle at a fixed lab momentum near the peak in the π^- spectrum. The solid line is from a least squares fit of a function based on the Coulomb correction equations of Gyulassy and Kauffmann.[1] This solid line has the experimental resolution folded into it. The dashed line is the same function before folding with the resolution. The dotted line shows the cross section predicted by the uncharged pion source function to which the Coulomb corrections were applied. The arrows on the left-hand graphs mark the velocity of the incident beam. The peak in the π^- spectrum and the hole in the π^+ spectrum at a pion velocity slightly below the beam velocity are clearly seen.

For light target-projectile combinations, these Coulomb effects can be explained quantitatively in terms of Coulomb interactions between the pions and cold projectile fragments using Gyulassy and Kauffmann's[1] Coulomb correction formulas. Our treatment of the Coulomb effects differs from that of Gyulassy and Kauffmann in that a different expression has been used for the uncharged pion source function. We also reinterpret their formulas for thermal averaging in terms of an average over the velocity dispersion of the projectile fragments. The shift of the peak in the π^- spectra from the incident beam velocity and the approximate width of these peaks are consistent with previously measured projectile fragmentation data.[2-4] We have also seen that the effective charge of the projectile fragment is less for π^+ near beam velocity than for π^-. This difference is consistent with our expectation that positive pions near beam velocity tend to come from more central collisions. Using the same methods, qualitative agreement is achieved for heavier targets and projectiles. The differences between our fitting function and the data are due, at least in part, to an incomplete treatment of impact parameter averaging.

Footnotes and References

*Condensed from LBL-11971, submitted to Phys. Rev. C.
†Boston University, Boston, MA 02215.
‡Physik-Institüt der Universität Zürich, Schönberggasse 9, 8001, Zürich, Switzerland.
§Institute for Nuclear Study, University of Tokyo, Tanashi, Tokyo 188, Japan; and LBL.
‖Institut de Physique Nucléaire, B.P. no. 1, 91406, Orsay, CEDEX, France.
¶Michigan State University, East Lansing, MI 48824.

1. M. Gyulassy and S.K. Kauffmann, Nucl. Phys. A **362**, 503 (1981).
2. K. Van Bibber et al., Phys. Rev. Lett. **43**, 840 (1979); and references therein.
3. D.E. Greiner et al., Phys. Rev. Lett. **35**, 152 (1975).
4. Y.P. Viyogi et al., Phys. Rev. Lett. **42**, 33 (1979).

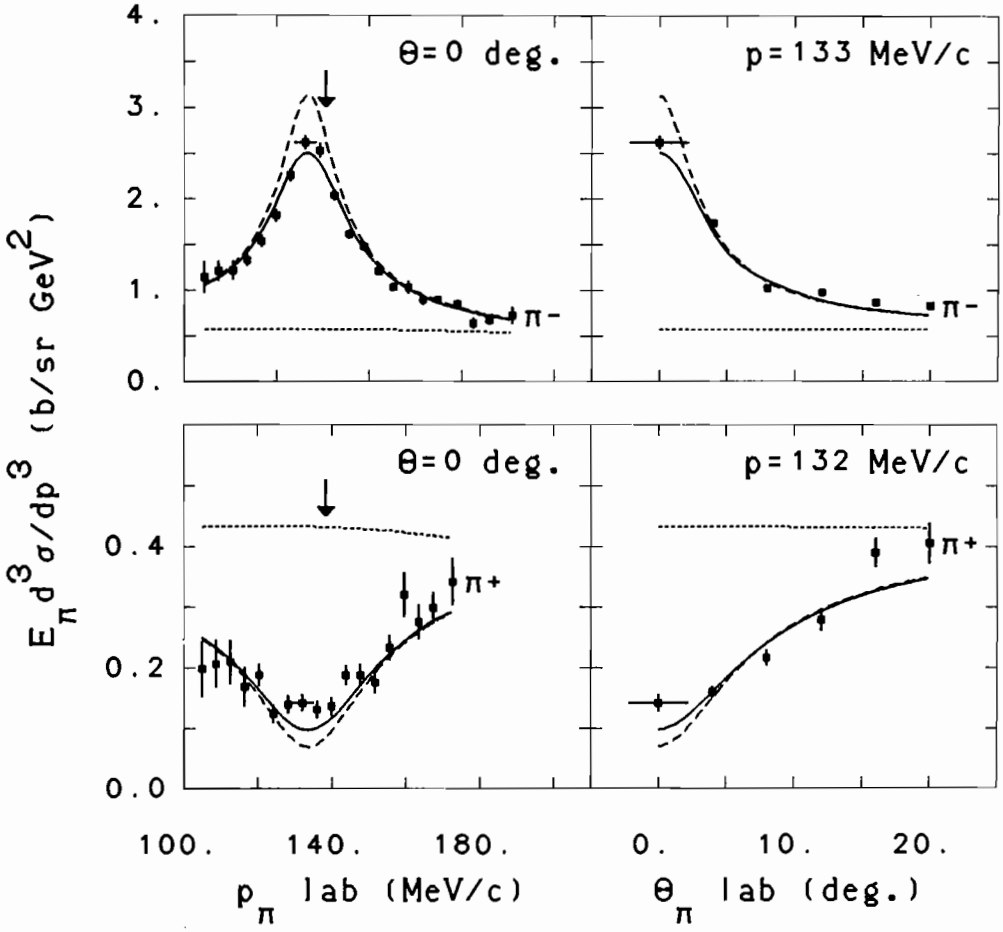

Fig. 1. Differential cross section vs pion momentum (left side) and vs pion angle (right side) for Ne + NaF → π^- (top) and π^+ (bottom) at E/A = 380 MeV. See text for details. (XBL 816-10183)

Pions Produced near the Center-of-Mass Velocity in Heavy Ion Collisions*

K.A. Frankel, J.A. Bistirlich, R. Bossingham, H.R. Bowman, K.M. Crowe, C.J. Martoff,† D.L. Murphy, J.O. Rasmussen, J.P. Sullivan, W.A. Zajc, J.P. Miller,† O. Hashimoto, M. Koike,‡ J. Peter,§ W. Benenson,‖ G.M. Crawley,‖ E. Kashy,‖ J.A. Nolen, Jr.,‖ and J. Quebert¶

In a recent experiment by Wolf et al.[1] a difference between pion production by nucleus-nucleus collisions and production by nucleon-nucleon collisions was noted. The contour plots for the cross section of E/A = 1.05 GeV ^{40}Ar on ^{40}Ca showed a ridge near $P_\perp = 0.5\ m_\pi c$ and $P_{||}^{cm} = 0$. Theories by Libbrecht and Koonin,[2] Gyulassy and Kauffmann,[3] and Cugnon and Koonin[4] claim that pions near 90° c.m. would feel significant Coulomb effects of both target and projectile and particularly of the hot nuclear matter which has been postulated to exist in the $P_{||}^{cm} = 0$ frame.[5] The present experiment was undertaken to observe the π^-/π^+ ratio R in the center-of-mass region extending from $P_\perp = 0$ through the ridge observed by Wolf et al.[1] A magnetic spectrometer with a 30° angular range was set at 15° with respect to the beam. The target was 2.0 g/cm^2 of Ca, giving an overall energy resolution of about 2 MeV. A comparison in the right half of Fig. 1 with the data of Wolf et al. for π^+ at 30° gives good agreement, except for the cases in which the present data were reflected about $P_{||}^{cm} = 0$. The data points given by

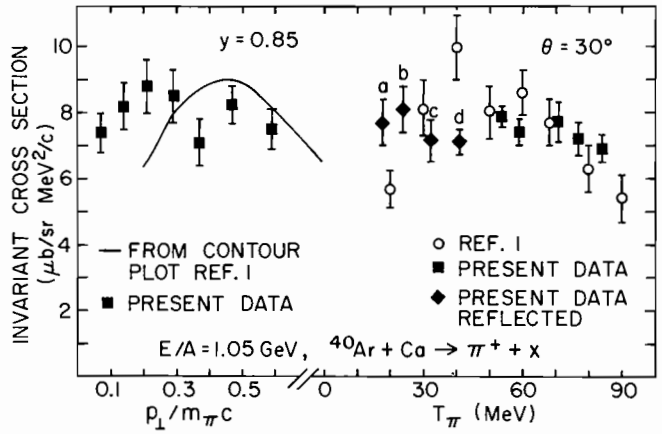

Fig. 1. Comparison of the Wolf et al. data with the present results. In the right side of the figure, the diamonds are reflections of present data about the $y_{c.m.} = 0$ axis. In the left side of the figure, our data for $y = 0.85$ are compared to such a cut through the contour plot of Wolf et al.

(XBL 815-9920)

closed diamonds in Fig. 1 are calculated under the assumption of symmetry of the invariant cross section about the $P_{||}^{cm} = 0$ axis and were taken at the angles and energies in the caption. In the left half of Fig. 1 we compare our direct data at $y = 0.85$ with a cut through their contour plot at the same rapidity. Our data do not show the rise given in their contour plot from $P_{\perp} = 0.2$ to 0.6 $m_{\pi}c$ at $y = 0.85$. This comparison is made on the left half of Fig. 1. In this case the plotted points are taken directly from the present data but the curve is from their contour plot, which includes reflections of data about $P^{cm} = 0$. Since $^{40}Ar + ^{40}Ca$ is only approximately a symmetric system, caution is in order regarding reflection of data points through the center of mass.

The π^-/π^+ ratio for Ar + Ca is 1.5 ± 0.2 for data taken nearly at rest in the center of mass. Calculations by Cugnon and Koonin[4] predict the ratio R to be about 5.5 for Ar + Ca at this point. On the other hand, if they assume complete transparency, Libbrecht and Koonin obtain a π^-/π^+ ratio at c.m. of $R \simeq 1.7$, very close to our experimental results.

Calculations with Gyulassy-Kauffmann formulas given $R \simeq 1.6$ for the complete transparency case,[6] $R \simeq 2.7$ using an impact parameter averaged fireball model, and a high degree of transparency at 1 GeV per nucleon. We believe the apparent agreement with the complete transparency limit is fortuitous. Our preliminary calculations show that the Coulomb effects on π^-/π^+ ratios near the center of mass are small if one does not treat pions as propagating through nuclear matter only under the influence of the Coulomb forces and neglecting charge exchange with nuclear matter. We note that there is a neutron excess in ^{40}Ar, so simple counting on nn to np to pp collision ratios and decay modes of the Δ intermediate leads to $R \simeq 1.15$. Stöcker points out[7] that thermodynamic considerations in hot nuclear matter allowing for condensation into clusters, such as alpha particles, leads to a primitive π^-/π^+ ratio (1.35) for the ^{40}Ar plus ^{40}Ca system.

Footnotes and References

*Partially condensed from LBL-12585.

†Department of Physics, Boston University, Boston, MA 02215.
‡Institute for Nuclear Science, Tokyo, Japan; and LBL.
§Institut de Physique Nucléaire, Orsay, France.
‖Michigan State University, East Lansing, MI 48824.
¶Université de Bordeaux, Le Haut-Vigneau, 33170 Gradignan, France.

1. K.L. Wolf et al., Phys. Rev. Lett. **42**, 1448 (1979).
2. K.G. Libbrecht and S.E. Koonin, Phys. Rev. Lett. **43**, 1581 (1979).
3. M. Gyulassy and S.K. Kauffmann, Nucl. Phys. A **362**, 503 (1981).
4. J. Cugnon and S.E. Koonin, Nucl. Phys. A **355**, 477 (1981).
5. G.D. Westfall et al., Phys. Rev. Lett. **37**, 1202 (1976).
6. M. Gyulassy, private communication (1981).
7. H. Stöcker, private communication (1981).

π^- Temperatures, Sphericity and Thrust for Central Collisions

R. Brockmann, J.W. Harris,* A. Sandoval,* H. Strobele,* R. Stock,* M. Maier,† R.E. Renfordt,† J. Miller,‡ H.G. Pugh,‡ M. Raff,‡ L.S. Schroeder,‡ F. Riess,§ K. Wolf,‖ A. Dacal,¶ and M.E. Ortiz¶*

Temperature

Inclusive negative pion spectra from Streamer Chamber data of central collisions of ^{40}Ar + KCl at 1.8 GeV/u were transformed into the c.m. frame of the colliding nuclei. The energy spectra

$$\frac{1}{P_{cm}} \frac{d\sigma(E_{c.m.},\theta \pm \Delta\theta)}{dE_{c.m.}d_\theta}$$

were fitted to an exponential distribution e^{-E/E_o} for every 10° $\theta_{c.m.}$ − interval.

In Fig. 1 the obtained slope parameter E_0 is plotted as a function of the pion c.m. angle $\theta_{c.m.}$. One observes a drop in E_0 of 20 MeV between 20° and 90°, reflecting a nonthermal distribution. The forward-backward asymmetry of the slope parameter is mainly due to detector inefficiencies for low energy π in the backward direction in the lab frame.

The data are compared with recent calculations of a statistical model.[1] The slope parameter E_0 of these calculations is roughly 35% larger than the data; that means the model gives a relatively larger pion yield at high energies but reproduces the angular dependence of the slope parameter.

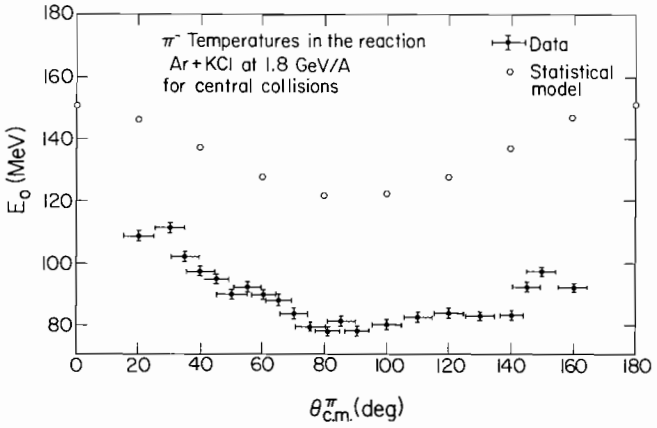

Fig. 1. Slope parameter E_0 (see text) as a function of the emission angle θ of the negative pions in the NN-c.m.-system in the reaction ^{40}Ar + KCl → $n\pi^-$ + X for central collisions at 1.8 GeV/u. (XBL 818-1151)

Sphericity and Thrust

To investigate the question whether the spatial momentum distribution of the negative pions is spherical or exhibits, for example, a jet-like structure, the variables sphericity and thrust[2] were calculated in the c.m. frame of the colliding nuclei, in an event-by-event analysis. Figure 2(a) shows the sphericity distribution, and Fig. 3 the frequency distribution of the polar angle of the main sphericity axis (Q3-axis) relative to the beam axis. A clear forward-backward peak is seen in this distribution.

The sphericity distribution (Fig. 2(a)) was compared with a Monte Carlo calculation. The events in the Monte Carlo calculations were generated by randomly selecting a

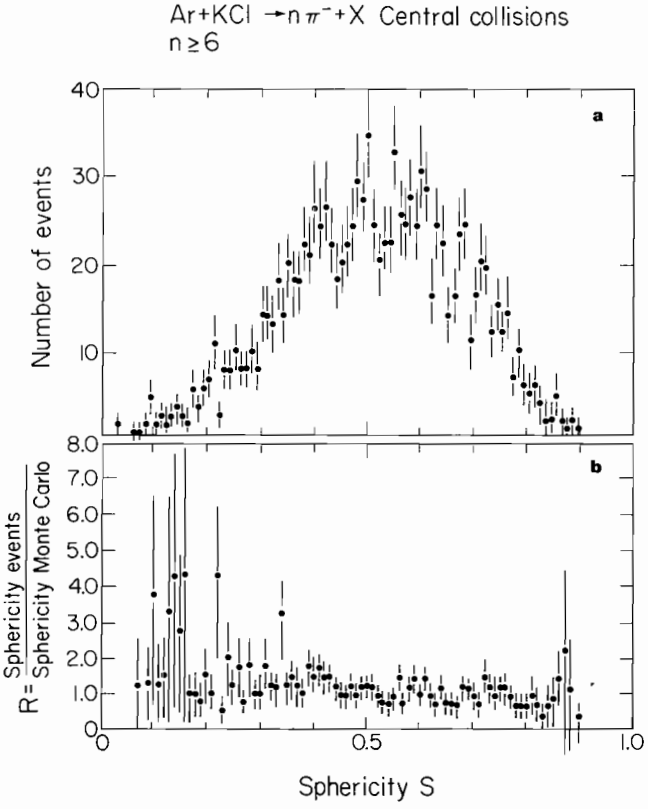

Fig. 2. (a) Frequency distribution of the sphericity S in the reaction ^{40}Ar + KCl → $n\pi^-$ + X for central collisions with $n_\pi \geq 6$ at 1.8 GeV/u. (b) Ratio R = sphericity of the events/sphericity of a Monte Carlo calculation as a function of sphericity. (XBL 818-1152)

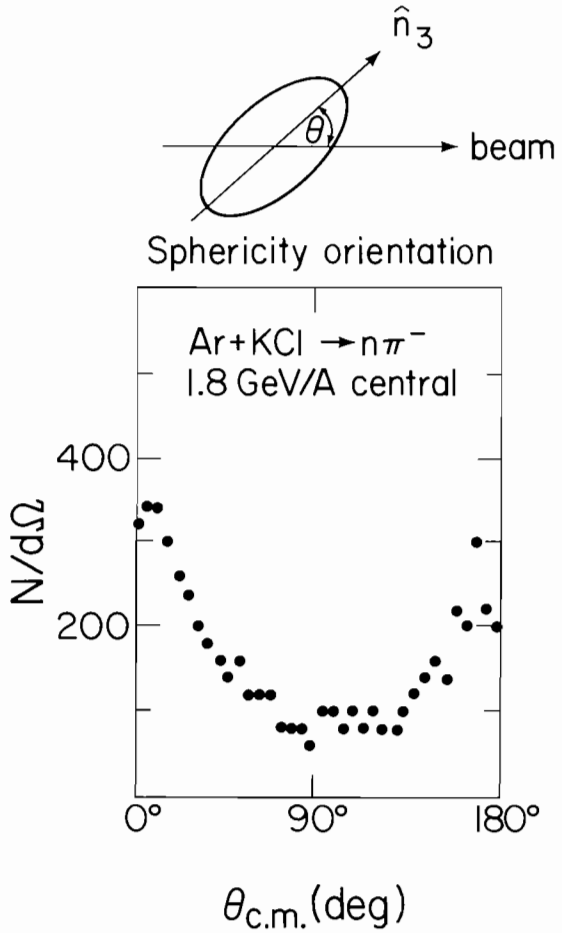

Fig. 3. Frequency distribution of the polar angle θ of the sphericity axis (Q3 axis) per solid angle interval.
(XBL 818-1153)

new direction for the pion momenta within a uniform distribution in the unit sphere. The multiplicity distribution and the distribution of the pion c.m.-momenta remained the same as in the real events. The streamer chamber efficiencies were taken into account. In the case of spherical events one would expect a mean sphericity $\langle S \rangle$ close to 1, but the Monte Carlo calculation gives a value comparable with experimental data, $\langle S \rangle_{MC} = 0.53$, $\langle S \rangle_{exp} = 0.51$. The small $\langle S \rangle_{MC}$ value is due to a finite particle number effect being the π^- multiplicity of $\langle n_\pi \rangle \simeq 8$ is not high enough to define the shape. Figure 2(b) shows the ratio R = sphericity of the events/sphericity of a Monte Carlo calculation. No clear signal is seen above the statistically distributed events. The same kind of analysis has been carried out for the variable thrust; again the results are governed by finite particle number effects.

The event shape analysis will be more reasonable when all charged particles are included.

Footnotes and References

*GSI, Darmstadt, West Germany.
†Universität Marburg, West Germany.
‡LBL, Berkeley.
§Universität München, West Germany.
‖Argonne National Laboratory.
¶IFUNAM, Mexico.

1. S. Bohrmann and J. Knoll, Nucl. Phys. A **356**, 498 (1981).
2. S. Brandt and H.D. Dahmen, Z. Phys. C **1**, 61 (1979); L. Wu and J. Zobernig, Z. Phys. C **2**, 107 (1979).

Charged Particle Exclusive Analysis

R. Brockmann, J.W. Harris,* A. Sandoval,* H. Strobele,* R. Stock,* M. Maier,†*
R.E. Renfordt,† J. Miller,‡ H.G. Pugh,‡ M. Raff,‡ L.S. Schroeder,‡ F. Riess,§
K. Wolf,‖ A. Dacal,¶ and M.E. Ortiz¶

The full event analysis of streamer chamber pictures has been started at the Institute for High Energy Physics in Heidelberg using a Frankenstein digitizer and the TVGP reconstruction program. High multiplicity events have been selected for this first analysis.

Figure 1 shows the particle trajectories as measured in one of the three views of a 1.8 GeV/u ^{40}Ar + KCl interaction. By matching the tracks in the three views, one can reconstruct the trajectory in space and from this its rigidity and emission angle. With mass and charge identification (see below) one obtains the momentum $\vec{p}$ of each particle in the center-of-mass system. Figure 2 shows the event of Fig. 1 in the center-of-mass momentum space. Shown here are the momentum per nucleon vectors.

A total of 20 events of the reaction Ar + KCl at 1.8 GeV/u and 38 events of the reaction Ar on Pb at 0.8 GeV/u have been measured and analyzed. The negative tracks have been identified as π^-. For the positive tracks a rough particle identification was performed on a kinematic basis, since identification from track density has not yet been implemented. Protons, deuterons, and tritons have been assigned by making cuts in the lab and c.m. momenta corresponding to the maximum momentum a particle with a given mass would have in an elastic scattering taking 200 MeV/c Fermi motion into account. All particles beyond this limit are tested with the next higher mass assignment.

The positive pions could be partially identified by

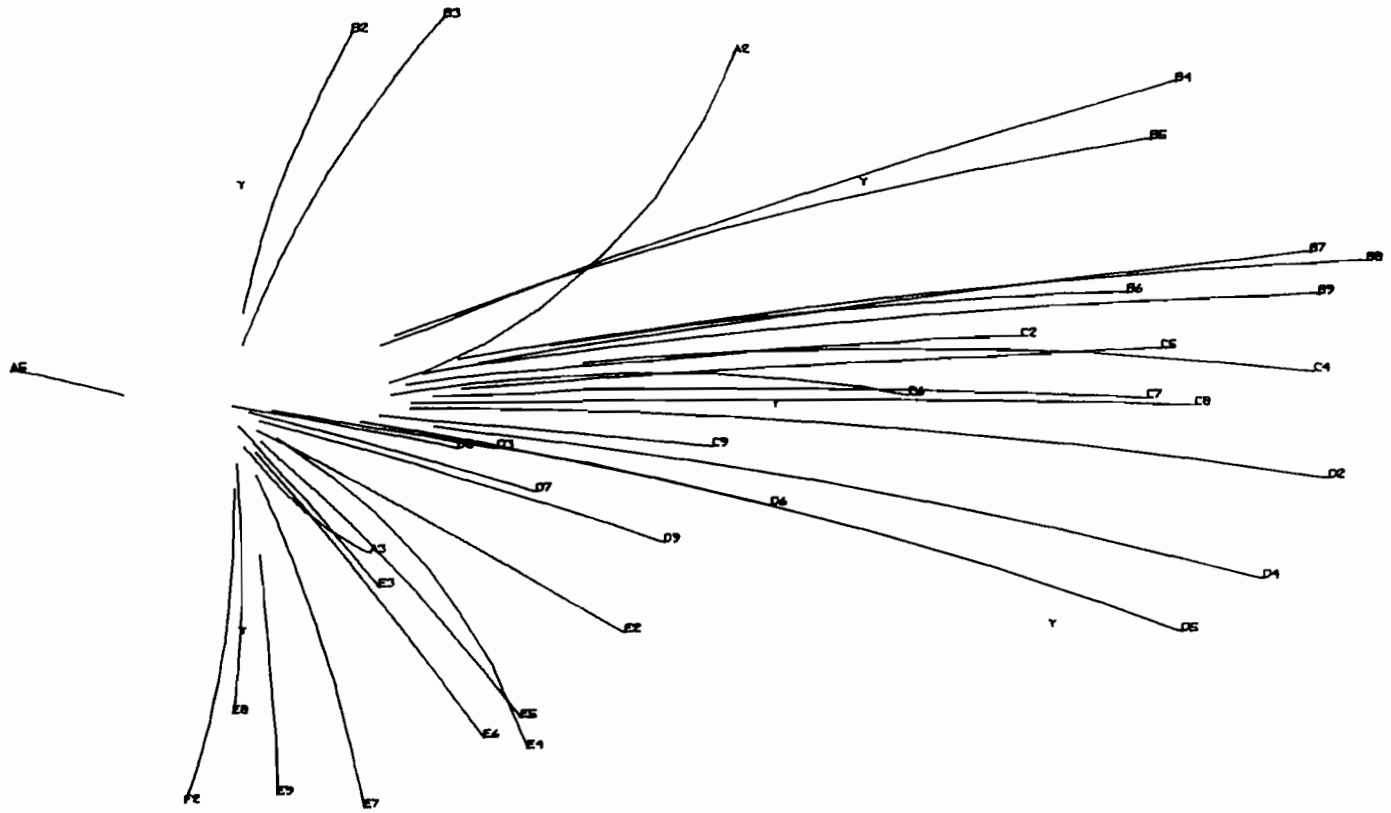

6052702.

Fig. 1. Projection of particle trajectories produced in the central interaction of ^{40}Ar + KCl at 1.8 GeV/u as measured from a streamer chamber picture. (XBL 816-10164)

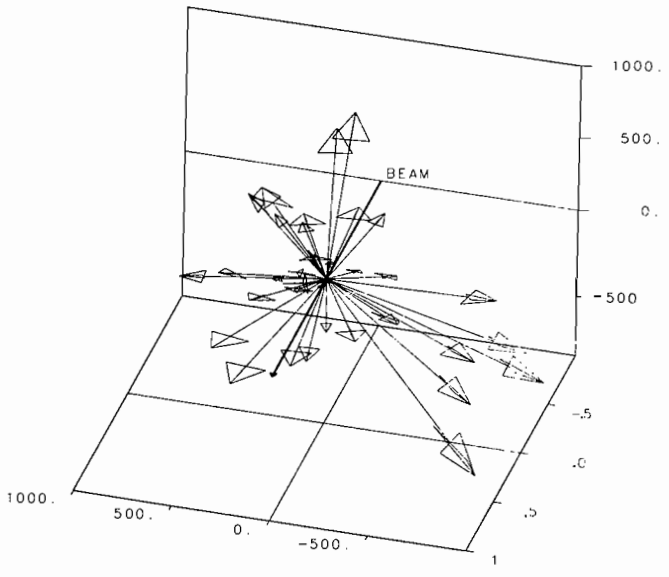

Fig. 2. Center-of-mass momentum vectors corresponding to the same interaction as shown in Fig. 1. In this event 35 charged particles were observed. (XBL 818-11281)

comparing the phase space of the π^- in the lab with that of the c.m. system and selecting the regions where they dominate over the protons. This provides a zero order characterization of the charged particle final state in central collisions. The mean multiplicities so extracted are shown in Table 1 together with their estimated uncertainties.

Mean longitudinal and transverse momenta per nucleon per interaction have been extracted. Figure 3 shows a scatter plot of the $\langle p_\perp \rangle$ vs $\langle p_{||} \rangle$ per event for both reactions.

Footnotes

*GSI, Darmstadt, West Germany.
†Universität Marburg, West Germany.
‡LBL, Berkeley.
§Universität München, West Germany.
‖Argonne National Laboratory.
¶IFUNAM, Mexico.

Table 1. Charged particle exclusive event characterization of the central collisions of ^{40}Ar + KCl at 1.8 GeV/u and ^{40}Ar + Pb at 800 MeV/u.

System	$\langle n_{charge} \rangle$	$\langle n_{\pi^-} \rangle$	$\langle n_{\pi^+} \rangle$	$\langle n_p \rangle$	$\langle n_d \rangle$	$\langle n_t' \rangle$
Ar + KCl	41 ± 2	5.9 ± 0.5	5 ± 2	24 ± 4	5 ± 3	1 ± 1
Ar + Pb	45 ± 2	2.6 ± 0.3	2.5 ± 1.5	34 ± 4	5 ± 3	1 ± 1

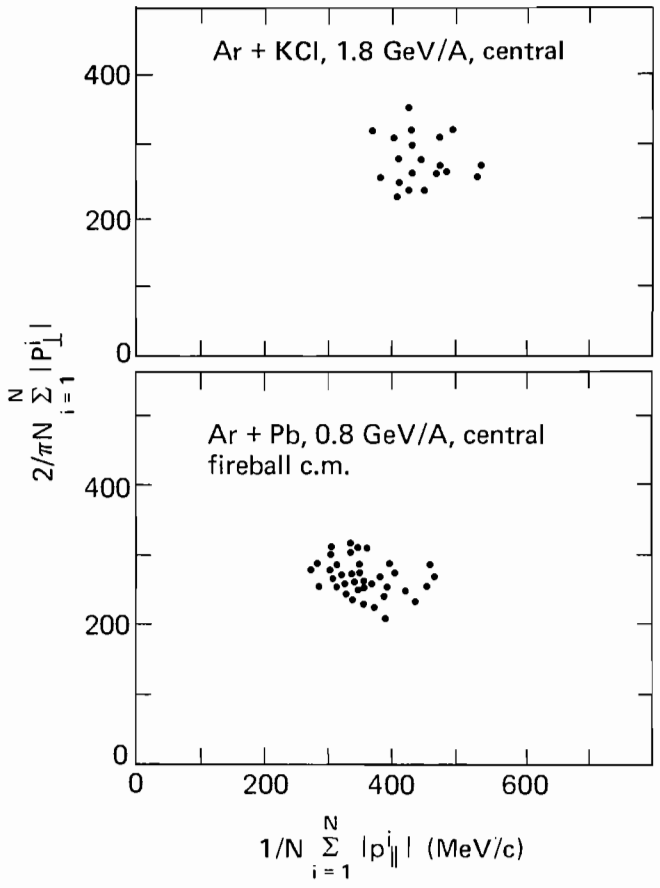

Fig. 3. Scatter plots of the $\langle p_\perp \rangle$ vs $\langle |p_\parallel| \rangle$ for the central collisions of ^{40}Ar + KCl at 1.8 GeV/u and ^{40}Ar + Pb at 800 MeV/u. The ordinate has been multiplied by $2/\pi$ since $\langle |p_\parallel| \rangle = 2/\pi \langle p \rangle$ for an isotropic source. (XBL 818-1254)

Coherence and Self-Induced Transparency in High Energy Hadronic Collisions*

G.N. Fowler,† E.M. Friedlander, and R.M. Weiner‡

The suppression of cascading in very high energy collisions of hadrons with nuclei was interpreted by Landau and Belenkii[1] within a hydrodynamical model as a consequence of the formation of a tube in nuclear matter. Although the idea of a "coherent" tube has been considered by many workers[2] up to the present, no explanation or direct experimental confirmation for this "coherent" property was given. With the advent of high-energy accelerator beams the suppression of cascading was confirmed[2] in the energy range 50-400 GeV. Moreover, it was found that the increase of multiplicity with target size is localized in the backward hemisphere and the name "transparency" was coined[3] for this effect.

In this article:

1. We introduce a different (quantum-optical) concept of coherence in the physics of proton-nucleus scattering.
2. We show how this leads to self-induced transparency (SIT) in nuclear matter in close analogy to the same effect discovered in optics in 1967 by McCall and Hahn.[4]
3. We present the first direct experimental evidence for the coherence of meson (pion) fields.
4. We show that in the forward cone a coherent part of the mesonic field is filtered out.

We start with the observation that in a hadron-hadron collision a partially coherent mesonic field is created. By coherent field we understand a field the state of which is an eigenstate of the annihilation operator.[5] So far the existence of this coherent field was "derived"[6] from theoretical arguments (spontaneous breakdown of symmetries, classical solutions in field theory, etc.) and from experimental indications in the Bose-Einstein correlations. In a proton-nucleus collision such a partially coherent field is created in the first encounter of the projectile with a constituent of the target.

The following conditions are sufficient for SIT:

(1) The coherent pulse is broad enough in the direction of propagation to overlap many scattering centers which remain to be identified.

(2) There exist (at least two) energy levels of the scattering centers in the medium such that the excited levels have lifetimes comparable to or longer than that of the coherent pulse.

(3) The intensity of the pulse is high.

If conditions (1)-(3) are met, the front of the coherent pulse produced in the first collision will excite the scattering centers as it encounters them, and the rear of the (same) pulse will then de-excite them by stimulated emission. This process will continue so that the pulse will eventually leave the medium without cascading.

Possible evidence for coherence was reported[6] so far only through the HBT effect, and there the situation is complicated mainly because the second-order correlations are rather insensitive to even large admixtures of coherence. There exists, however, another way to look for coherence, i.e., through the shape of the multiplicity distributions: when the fields are completely coherent the multiplicity distributions have Poisson form.[5]

We now present experimental evidence for "Poissonicity" of the particles emitted into the forward cone of high-energy proton-nucleus collisions. The data come from nuclear emulsion exposures to high-energy proton beams, viz., 69 GeV (IHEP-Serpukhov) and 200 and 300 GeV (FNAL-Batavia)

For the purpose of this analysis each event was divided into several pseudorapidity ($\eta = -\ell n \tan\theta/2$) bins. Each such bin was treated as a "ministar" of multiplicity n_i, where i denotes the η-bin. The "local" multiplicity distribution of these ministars was recorded for each primary energy and N_h combination (N_h is the number of target-related heavy prongs, a good measure of target size and/or involvement).

Whereas at low η (backward in c.m.s.) the "local" multiplicity distributions are close to chaotic, in the forward direction they become purely Poisson, as expected for coherent emission. To illustrate this behavior we define the following measure for the deviation of each local multiplicity distribution from the Poisson law. Since for a Poisson distribution

$$P_i(0) = \exp(-\langle n_i \rangle) \tag{1}$$

the quantity

$$\Delta_i = |\,|(\ell n\, P_i(0)| - \langle n_i \rangle| \tag{2}$$

should vanish.

In Fig. 1 we plot estimates for the Δ_i (i = 1-12) against pseudorapidity. It is obvious that in the "forward" η-bins the Δ-values are well compatible with zero, while highly significant deviations occur in the low-η bins; this effect increases strongly with N_h, i.e., with nuclear size.

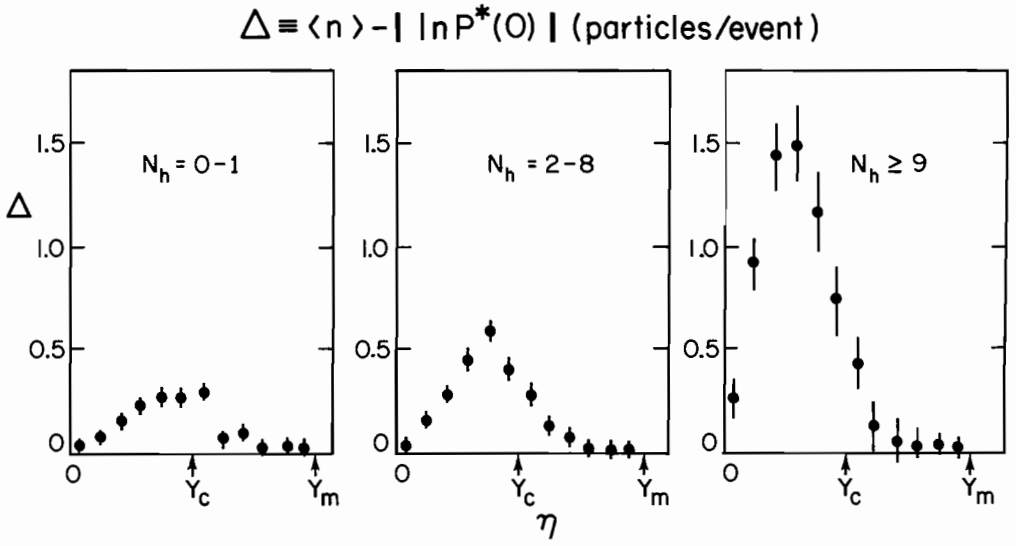

Fig. 1. (XBL 816-935)

Footnotes and References

*Condensed from LBL-12279, Phys. Lett. B **104** (1981).

†Physics Department, University of Exeter, England.

‡Physics Department, University of Marburg, Germany.

1. S.Z. Belenkii and L.D. Landau, Usp. Fiz. Nauk **56**, 309 (1955).

2. For a review of this subject, see L. Bergström, et al., to appear in Phys. Reports.

3. J. Cohen et al., Lett. Nuovo Cimento **9**, 337 (1974).

4. S.L. McCall and E.L. Hahn, Phys. Rev. Lett. **18**, 908 (1967).

5. R. Glauber, Optique et electronique quantique, in Les Houches Lectures, 1964 (Gordon and Breach, New York).

6. G. Fowler and R. Weiner, Phys. Lett. B **70**, 201 (1977).

3. Strange Particle Production

Kaon Production in Relativistic Heavy Ion Collisions

S. Schnetzer, M.-C. Lemaire, R. Lombard,† E. Moeller,‡ S. Nagamiya, G. Shapiro, H. Steiner, and I. Tanihata§*

The inclusive spectra of K^+ mesons in collisions of 2.1 GeV/amu nuclei with various targets were measured by means of magnetic spectrometer. The laboratory angles covered were from 15° to 80°, and the momentum range of the K^+'s extended from 350 to 750 MeV/c.

The triple differential cross section, $d^3\sigma/d^3p$, falls off exponentially with center-of-mass energy in the nucleon-nucleon center-of-mass frame. As an example, we show the K^+ c.m. energy distribution for Ne + NaF in Fig. 1. In addition, the angular distribution of the kaons is nearly isotropic in this frame even for p + NaF and Ne + Pb collisions.

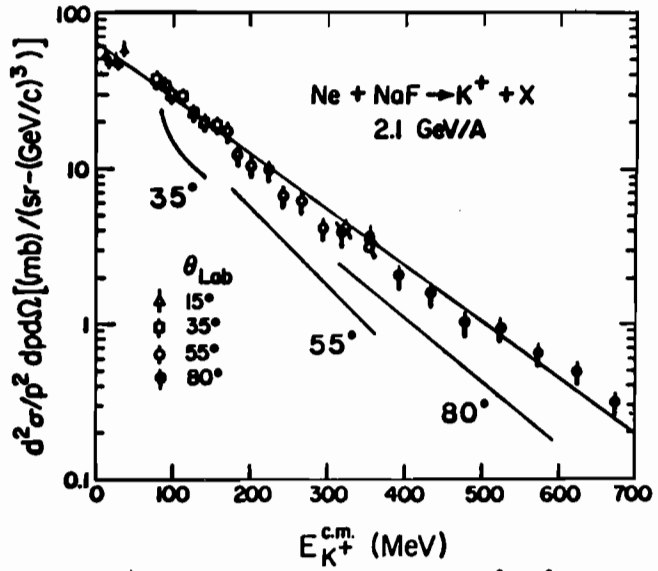

Fig. 1. K^+ inclusive c.m. cross section $d^3\sigma/d^3p$ vs the kinetic energy of the K^+ in the c.m. for 2.1 GeV/A Ne + NaF. Also shown are the row-on-row model predictions for θ_{lab} = 35°, 55°, and 80°. (XBL 818-11276)

The data has been compared with a row-on-row model[1,2] and a thermal model.[3] Neither are able to explain all features of the data. The row-on-row does not reproduce the near-isotropy in the NN frame as can be seen in Fig. 1, where the curves represent these predictions for θ_{lab} = 35°, 55°, and 80°. The thermal model overpredicts the kaon yield by a factor of ~ 20.

We have also observed an interesting A-dependence effect. The kaon yield increases by a larger factor when going from Ne + NaF to Ne + Pb collision than when going from d + NaF to d + Pb collisions. This is suggestive of some form of collective behavior.

Footnotes and References

*Now at DPhN/ME, CEN Saclay, France.
†On leave from DPhN/ME, CEN Saclay, France.
‡On leave from Freie Universität Berlin, Berlin, West Germany.
§On leave from INS, University of Tokyo, Tokyo, Japan.

1. J. Randrup and C.M. Ko, Nucl. Phys. A **343**, 519 (1980).
2. J. Randrup, Phys. Lett. B **76**, 547 (1978).
3. F. Asai, H. Sato, and M. Sano, Phys. Lett. B **98**, 19 (1981).

Observation of Subthreshold K^- Production in Relativistic Nuclear Collisions

A. Shor, K. Ganezer, J. Carroll,* G. Igo,* J. Geaga,* S. Abachi,**
A. Sagle, T. Mulera, V. Perez-Mendez, P. Lindstrom,
F. Zarbakhsh, and D. Woodward†

The possible occurrence of exotic nuclear phenomena in relativistic nuclear collisions necessitates some degreé of thermalization or collective interactions among the colliding nucleons. A clear signature for collective or thermal effects is the production of particles which require significantly more energy than is available in individual nucleon-nucleon collisions. At 2.1 GeV/nucleon, the threshold for K^- production is 140 MeV above the available N+N center of mass energy, while antiproton production requires 1 GeV above the available energy.

We have recently conducted a search for K^- and $\bar{P}$ production in the reaction $^{28}Si + {}^{28}Si$ at 2.1 GeV/nucleon. Negative secondaries (with $P = \beta_{cm}\gamma_{cm} M_{\bar{p}}$) produced in the collision were transported through a magnetic beam line with detectors at appropriate locations for TOF measurements and pion rejection. The resulting TOF spectrum (Fig. 1) contains a distinct kaon peak. Our measured differential cross section for K^- produced at 0° and 1 GeV/c is $d^2\sigma/dpd\Omega = 1.3$ mb/sr − GeV/c (error $\simeq$ 50%). To compare this result with above threshold K^- production, we have also measured the K^- rate in the reaction p-Cu at 4.8 GeV, where for K^- under identical conditions, $d^2\sigma/dpd\Omega = 0.9$ mb/sr − GeV/c.

The significance of the subthreshold K^- yield is evaluated by comparing the experimental ratio $R = d\sigma(N + N(2.1\ GeV/n) \rightarrow K^-)/d\sigma(p + Cu(4.8\ GeV) \rightarrow K^-)$ with calculations incorporating nuclear Fermi momentum of the projectile and target nucleons to allow for subthreshold particle production. For the Fermi momentum distribution, we applied the double Gaussian reported by Geaga et al.,[1] which also results in a good fit for subthreshold antiproton production in p - N collisions, as shown in Fig. 2. These calculations are found to underpredict our subthreshold K^- yield by about *two orders of magnitude.*

We do not feel we have yet attained the sensitivity required for meaningful antiproton measurement. However, the large K^- rate we have observed is an indication of some interesting phenomena taking place in relativistic nuclear collisions. We plan to pursue the study of subthreshold particle production as a probe of matter at high energies and densities.

Footnotes and References

*University of California, Los Angeles, CA.
†California State University, Hayward, CA.

1. J.V. Geaga et al., Phys. Rev. Lett. **45**, 1993 (1980).
2. D.E. Dorfan et al., Phys. Rev. Lett. **14**, 995 (1965).

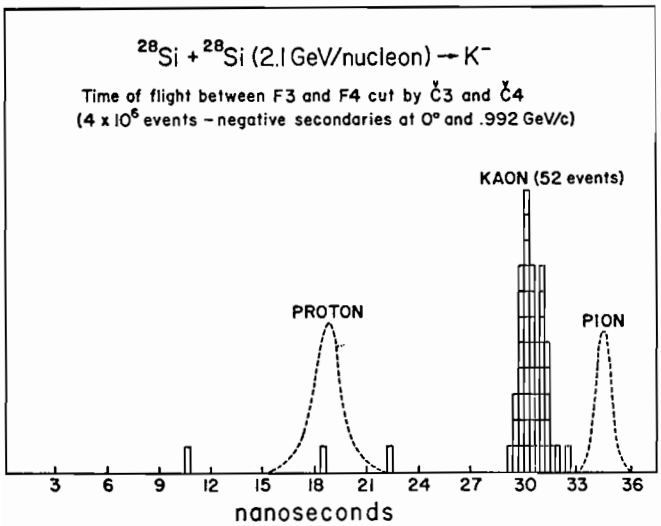

Fig. 1. (XBL 8111-12545)

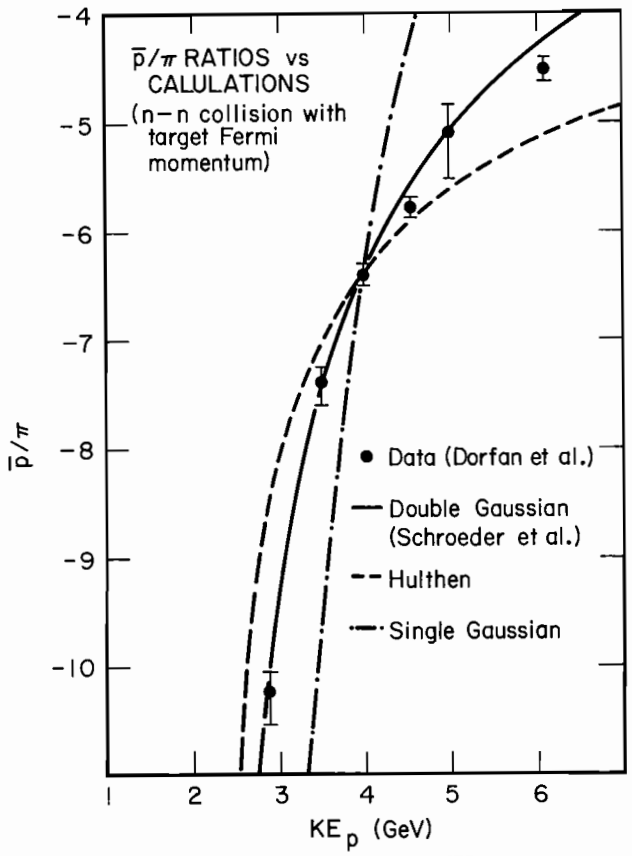

Fig. 2. (XBL 8111-1603)

Λ Production Near Threshold in Central Nucleus-Nucleus Collisions

R. Brockmann, J.W. Harris,* A. Sandoval,* H. Strobele,* R. Stock,* M. Maier,† R.E. Renfordt,† J. Miller,‡ H.G. Pugh,‡ M.Raff,‡ L.S. Schroeder,‡ F. Riess,§ K. Wolf,‖ A. Dacal,¶ and M.E. Ortiz¶*

Λ production was studied in central ^{40}Ar + KCl collisions at 1.8 GeV/u incident energy using the Streamer Chamber facility at the Bevalac. The streamer chamber, with its 4π solid angle capability, was operated in both inelastic and central trigger modes. The central trigger selects events with small total charge in projectile fragments. This trigger, which corresponds to 10% of the reaction cross section (σ_R = 1.8b), is associated with impact parameters b < 2.4 fm in a geometric model. The open channels for production of strange particles in this energy regime are NN → ΛKN (1.58 GeV), → ΣKN (1.79 GeV), and → ΛKNπ (1.96 GeV). Neutral strange particles were detected by their charged-particle decay in the active volume of the chamber. In order to derive Λ production cross sections and momentum spectra, detection and scanning efficiencies were determined. The neutral strange particles were identified by a kinematical fit of the decays Λ → $p\pi^-$ and K → $\pi^+\pi^-$.

The identified Λs are displayed in Fig. 1a as a function of $p_\perp$ and $p_{||}$ in the nucleus-nucleus c.m. system. The solid curve in Fig. 1a represents the kinematic limit for Λ momenta produced in the elementary NN → ΛKN reaction at 1.8 GeV. Most of the Λs are observed beyond the limit indicating the necessity to include Fermi motion and/or collective multi-particle interactions. To investigate further the origin of the observed high Λ momenta, a Monte Carlo phase space calculation incorporating Fermi motion was performed. The results after folding in the detection efficiencies are shown in Fig. 1b. The distribution, which peaks at p = 0, is broadened in phase space but still does not adequately describe the observed spectrum.

Inclusion of Λ rescattering in the nuclear medium was next considered. Rescattering from the thermal "fireball" distribution (RsI) has little effect on the Λ spectrum. However, rescattering from a superposition of the colliding initial distributions (RsII) shown in Fig. 1c depletes events from the central peak and creates peaks near $p_{||}$ = ± 0.8 GeV/c. The backward peak at $p_{||}$ = −0.8 GeV/c is suppressed by the detection efficiency which is included in the calculation. In addition, the $p_\perp$ is boosted in qualitative agreement with the observations.

A quantitative comparison of the data with results of the Monte Carlo calculations can be found in Table 1 where the mean and rms values of $p_\perp$ and $|p_{||}^{cm}|$ for the invariant $(E/2\pi p_\perp)(d^2\sigma/dp_\perp dp_{||})$ distributions are presented. The data exhibit a much higher $<p_\perp>$ than predicted by any of the calculations.

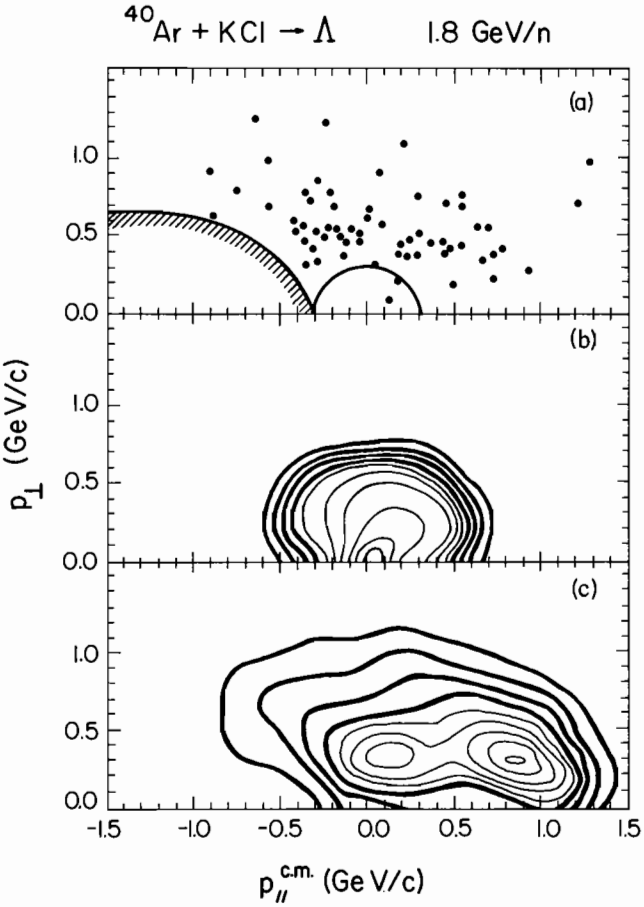

Fig. 1. ^{40}Ar + KCl → Λ events as a function of $p_\perp$ and $p_{||}$ in the nucleus-nucleus c.m. at 1.8 GeV/u. (a) Scatterplot of the data. The hatched curve shows the region where events were excluded due to inefficiencies. The solid curve corresponds to the NN → ΛKN kinematic limit. (b) Linear contour plot of the results for the Monte Carlo calculation AA (Fermi motion only). (c) Linear contour plot of the calculation RsII with subsequent Λ rescattering (see text). (XBL 813-437)

Table 1. Quantitative comparison of data with results of Monte Carlo calculations.

	$\langle p_\perp \rangle$ (GeV/c)	$\sigma_{rms}(p_\perp)$ (GeV/c)	$\langle \lvert p_{\parallel}^{c.m.} \rvert \rangle$ (GeV/c)	$\sigma_{rms}(\lvert p_{\parallel}^{c.m.} \rvert)$ (GeV/c)
Data	0.493	0.243	0.429	0.264
NN	0.122	0.077	0.117	0.077
AA	0.207	0.150	0.212	0.154
RsI	0.220	0.180	0.229	0.184
RsII	0.276	0.233	0.641	0.380

The mean Λ multiplicity was found to be $\langle n_\Lambda \rangle = 0.04$ for the central trigger. Using the measured cross section for central trigger events, $\sigma = 180$ mb, the Λ cross section in central collisions of $^{40}Ar + KCl$ at 1.8 GeV/u is $\sigma_\Lambda = 7.6 \pm 2.2$ mb.

Since Λ decay is self-analyzing for polarization in the decay process $\Lambda \rightarrow p\pi^-$, the distribution of decay protons in the Λ decay frame relative to the Λ spin direction is $dW/d\theta = (1 + \alpha P\cos\theta)/4\pi$, where P is the Λ polarization, $\alpha = -0.642$ and θ is the angle between the decay proton and the unit vector normal to the plane. Using the relation $\alpha P = \langle\cos\theta\rangle/\langle\cos^2\theta\rangle$, the polarization extracted from the present experiment was found to be $P = -0.10 \pm 0.05$.

Footnotes and References

*GSI, Darmstadt, West Germany.
†Universität Marburg, West Germany.
‡LBL, Berkeley.
§Universität München, West Germany.
‖Argonne National Laboratory.
¶IFUNAM, Mexico.

1. S. Bohrmann and J. Knoll, Nucl. Phys. A **356**, 498 (1981).
2. S. Brandt and H.D. Dahmen, Z. Phys. C **1**, 61 (1979); L. Wu and J. Zobernig, Z. Phys. C **2**, 107 (1979).

4. Correlation Studies

Measurement of Two-Particle Correlations in 800 MeV pA Collisions*

I. Tanihata, Y. Miake, H. Hamagaki, S. Kadota, Y. Shida, R. Lombard, E. Moeller, S. Nagamiya, S. Schnetzer, and H. Steiner

Two-particle (p-p, p-d) coincidences have been measured in p + A collisions. The production mechanism of backscattered protons has been studied by forward-backward coincidence events. These coincidence spectra are measured in two modes: in-plane coincidence (IPC), ($\theta_1 = 15°$, $\theta_2 = 118°$, $\Delta\phi = 180°$) and out-of-plane coincidence (OPC), ($\theta_1 = 15°$, $\theta_2 = 118°$, $\Delta\phi = 90°$).

Figures 1(a),(b) show scatter plots of p-p and d-p IPC events in p + C reactions. Solid curves in the figures show the kinematics of p-p and d-p quasi-elastic scatterings (QES). The kinematic loci of the breakup of two and three nucleon clusters with zero excitation energy are represented by broken lines. The numbers along the curves indicate the initial momenta of the p, d, or clusters inside the target nucleus. The IPC events show the clear existence of the p-p and p-d QES which are not seen in OPC. Besides the p-p QES, a broad but definite population is seen in the region of 2N-cluster breakup. In spite of the large excitation (300-400 MeV) of the remaining system, which includes all the particles other than those detected, the number of IPC events is still larger than that of OPC. Figure 2 shows the spectra of the backscattered proton associated with the different components, namely, QES, non-QES IPC, and OPC. All of the spectra, except d-p QES are fitted well by a function Ae^{-P/P_0}, as in the case of the inclusive spectra. The slope factors, P_0 of the p-p QES and OPC are smaller than those of the inclusive spectra. Because of the fast fall-off of the spectra, these two components cannot contribute significantly to the backscattered high-energy protons. The slope factors P_0 of in-plane p-p and d-p non-QES are similar to the P_0 of the inclusive spectra and, therefore, suggest that there is a close relationship between these spectra. The similarity of the backscattered proton spectrum of d-p events and the difference spectrum between in-plane and out-of-plane coincidence events on correlated 2N-clusters. However, incoherent multiple scattering processes involving a few nucleons cannot be rejected at this stage of analysis. We need further analysis including angular distributions and also better theoretical calculations to distinguish these components.

Footnote

*Condensed from LBL-12978.

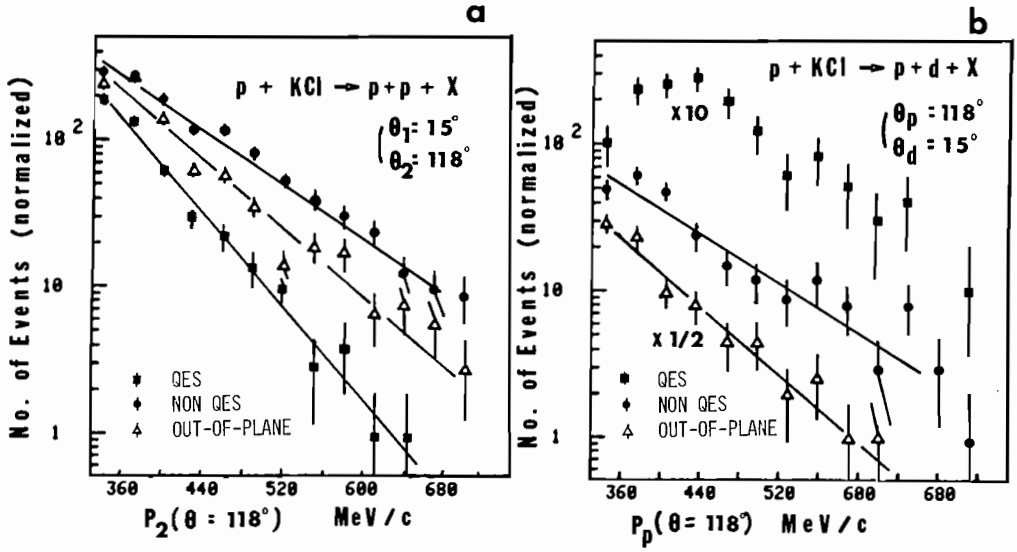

Fig. 1. Momentum-momentum scatter plots of the p-p (a) and p-d (b) events for the in-plane-coincidence mode. The area of circle in the figure is roughly proportional to the number of events. (XBL 817-10846)

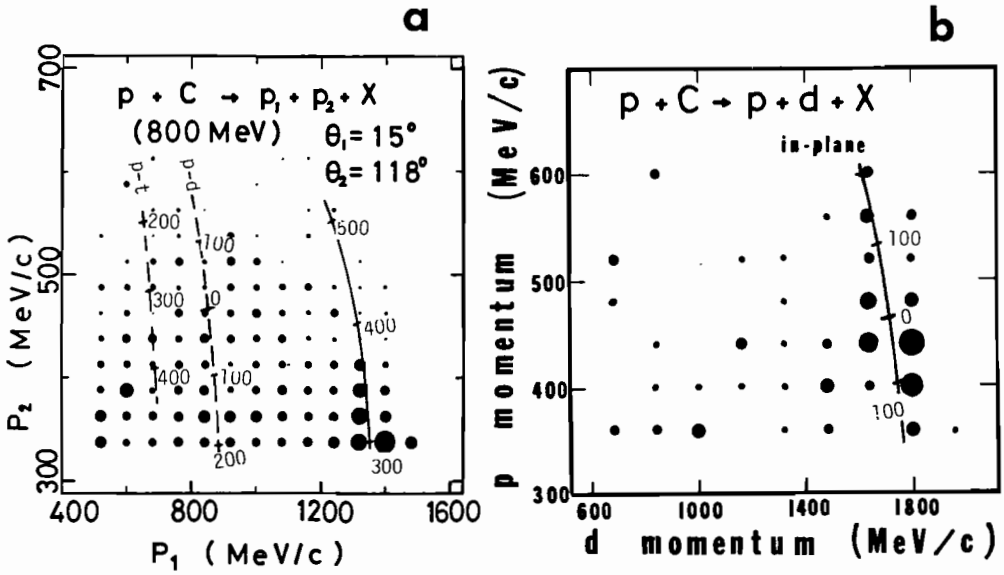

Fig. 2. Spectra of the backscattered protons for different components. Solid lines are exponential fits to the data. (XBL 817-10847)

Few Nucleon Interactions and Correlation Studies

R. N. Treuhaft, J.M. Engelage, J.V. Geaga,† J.W. Harris,‡*
P.N. Kirk, R.W. Koontz, H.G. Pugh, G.R. Roche,§ C.L. Ruiz,* and L.S. Schroeder*

A principal aim of our research has been to uncover the characteristics of elementary or few-body reactions as they take place in the nuclear medium. In the study of proton-nucleus collisions, we pose two questions: (1) Can any of the high momentum back-scattering of protons on nuclei[1,2] be attributed to scattering off a small number of correlated nucleons? And if so, (2) can one discover the properties of the proton-correlated group scattering?

In a (p,2p) experiment recently done with TASS,[3] we concentrated on the possibility of scattering 2.1 GeV incident protons from correlated groups of two nucleons in carbon. The two arms of the spectrometer were set to encompass part of the phase space available to the two outgoing protons in the reaction pd → ppn. For example, if the rear arm, which was at 120° to the beam throughout the experiment, accepted protons in the momentum range 400 to 600 MeV/c, the front arm set at 10.4° would detect protons from the p-d reaction in two momentum ranges: 400 to 960 MeV/c, and 2170 to 2720 MeV/c. It is expected that Fermi momentum of the two nucleon object in carbon would smear these ranges somewhat.

Figure 1 shows

$$\frac{d^6\sigma}{(d\Omega dp)_f(d\Omega dp)_r}$$

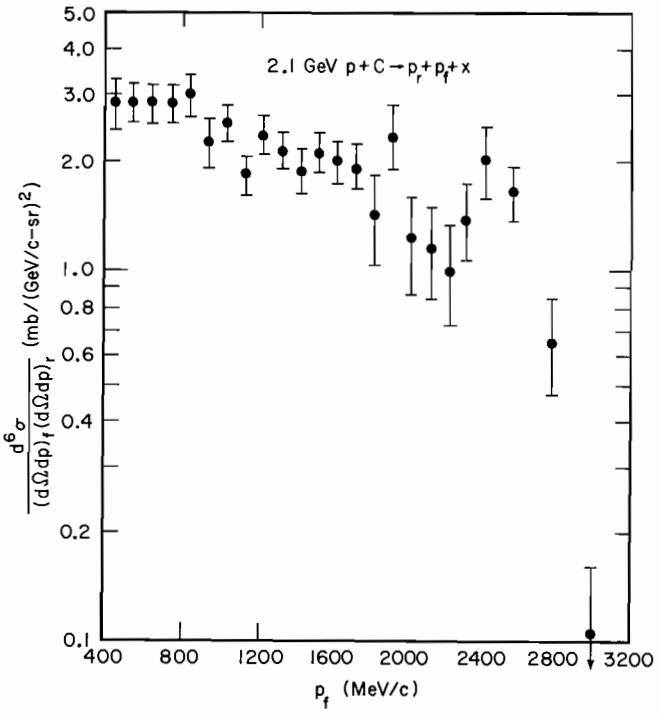

Fig. 1. Preliminary results from 2.1 GeV p + C → p + p + X with θ_f = 10.4°, θ_r = 120°, p_4 = 400–600 MeV/c (coincidence spectrum). (XBL 8111-1606)

vs p_f, the forward proton's momentum for the p-carbon reaction in the kinematics described above. In contrast to our coincidence data, Fig. 2 shows the singles spectrum for protons taken by Tanihata et al. at 10°.[2] The shapes of the two spectra are *different*. If the protons observed in the coincidence measurement were uncorrelated, we would expect to find that a cut on the backward momentum vector changed only the scale of the front momentum spectrum

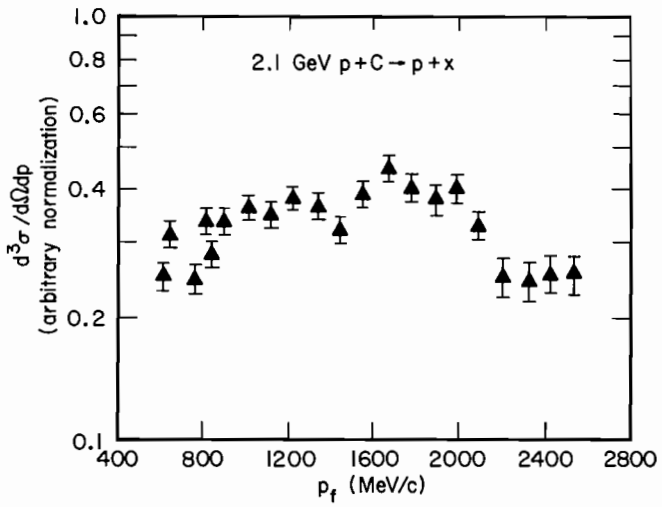

Fig. 2. The 2.1 GeV p + C → p + X with $\theta_f = 10°$ (single spectrum). (XBL 8111-1608)

and not the shape. After further reduction of the data, we will be able to relate the observed correlation to the number of participants in the reaction and make stronger conclusions about the scattering from the two nucleon cluster. We also have data for the same backward kinematics with the forward going proton at 45° to the beam. In early 1982, we expect to obtain more statistics on a carbon target. Also, for a definitive comparison, we will perform the same set of measurements on a liquid deuterium target.

Viewing the nucleus as an alternative setting for elementary interactions is a useful perspective for understanding the behavior of the nuclear participants. This experiment will contribute to the description of the nuclear deuteron.

Footnotes and References

*Department of Physics and Astronomy, Louisiana State University.
†Department of Physics, University of California, Los Angeles.
‡GSI, Darmstadt, West Germany.
§On leave from University of Clermont-Ferrand II, France.
Supported in part by a NATO grant.
1. J.V. Geaga et al., Phys. Rev. Lett. **45**, 1993 (1980).
2. I. Tanihata et al., Lawrence Berkeley Laboratory Report LBL-12978 (1981).
3. See description of TASS by G.R. Roche et al. in this annual report.

Proton-Emitting Sources in Central Collisions of Ar + KCl at 1.8 GeV/N

A.L. Sagle, F. Zarbakhsh, F. Brochard, T.A. Mulera, V. Perez-Mendez, R. Talaga, I. Tanihata, J.B. Carroll, K.S. Ganezer,* G. Igo,* J. Oostens,* D. Woodward,† and R. Sutter‡*

We have measured the single proton inclusive cross sections, the two-proton correlation function, and the associated multiplicity of high P_T fragments in collisions of Ar + KCl at 1.8 GeV/n. With these measurements, we hope to see if dense nuclear matter can be formed in central relativistic nucleus-nucleus collisions. In particular, we wish to determine if there are enough interactions to slow down and quasi-equilibrate at least some of the nucleons while the nuclei are interpenetrating.

Measurements were made at two different spectrometer settings, S_1 and S_2, corresponding to the beam rapidity Y_B and to $Y_B/2$, respectively. For projectiles and targets of equal mass, $Y_B/2$ corresponds to the velocity of the nucleus-nucleus center of mass.

We show in Table 1 the invariant single particle inclusive cross sections f in arbitrary units for settings S1 and S2. The column labeled $M \geq 0$ shows the invariant cross section with no multiplicity requirements. The column labeled $M > 4$ shows the cross section when 5 or more particles are detected by the multiplicity counters. The quantity C (defined as the ratio of f for $M > 4$ to f for $M \geq 0$) is larger at $Y_B/2$ than Y_B. The larger value of C at $Y_B/2$ indicates that this multiplicity requirement is selecting more central collisions since this selection tends to decrease the emission of particles at Y_B more than at $Y_B/2$. On the other hand, f is larger for the data at Y_B than at $Y_B/2$ even when the high multiplicity requirement is imposed. This implies that even for smaller impact parameter central collisions, most of the nucleons are not thermalized in the Ar-KCl center of mass.

We now turn to the results for the correlation function R. Details about its definition and experimental determination are given elsewhere.[1] In Fig. 1 we show R for data at Y_B and $Y_B/2$ when $M \geq 4$. Koonin[2] has shown that the

Table 1. Invariant cross sections $E/P^2\ d\sigma/dpd\Omega$ (arbitrary units) for different multiplicity requirements M.

Setting	P (lab)	(Lab)	M≥0	M>4	C=M>4/M≥0
S1, (Y_B)	2.4	6	548	37.8	0.069
S2, ($Y_B/2$)	1.0	13.5	100	9.4	0.096

peak in R at $\Delta P \simeq 20$ MeV/c decreases with the average separation $<\Delta r>$ between the two protons at the time of their emission. The $<\Delta r>$ for data at Y_B is larger than for data at $Y_B/2$. This again supports the idea that most of the projectile and target nucleons are not equilibrated in the Ar-KCl center of mass.

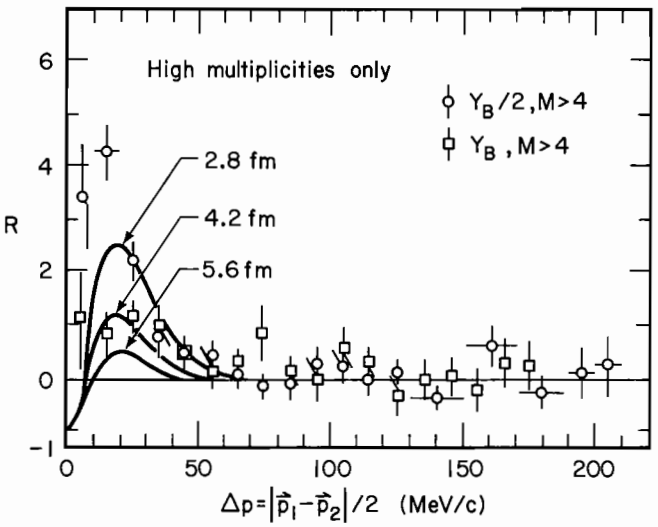

Fig. 1. The correlation function, R, for Ar + KCl → p + p + X at 1.8 GeV/n. (XBL 8111-1605)

The $Y_B/2$ data do, however, indicate that a significant number of interactions occur while the projectile and target are interpenetrating. The small $<\Delta r>$ with M > 4 excludes the possibility that these mid-rapidity protons are emitted from projectile and target remnants after the colliding nuclei have passed through each other. If such a process were significant, we would measure a large separation along the beam direction (a large $<\Delta r>$) since, for equal mass colliding nuclei, any given $Y_B/2$ proton could come with equal probability from either the projectile remnant or the target remnant.

The small $<\Delta r>$ is, however, consistent with two other possibilities. The $Y_B/2$ protons may come from an isolated low density source at late stages of the collision after most of the projectile and target nucleons have passed through each other. On the other hand, these mid-rapidity protons may be emitted from a dense non-equilibrated system while the nuclei are still interpenetrating. We plan to better determine the properties of the mid-rapidity proton source by measuring a larger part of the phase space with the new Hiss facility.

Footnotes and References

*University of California, Los Angeles, CA.
†California State University, Hayward, CA.
‡Brookhaven National Laboratory, Upton, L.I., NY.

1. F. Zarbakhsh et al., Phys. Rev. Lett. **48**, 1268 (1981).
2. S. Koonin, Phys. Lett. B **70**, 43 (1977).

Two-Pion Correlations in Heavy Ion Collisions*

J.A. Bistirlich, R.J. Bossingham, H.R. Bowman, C.W. Clawson, K.M. Crowe, K.A. Frankel, O. Hashimoto,† J.G. Ingersoll, M. Koike,† J.P. Kurck, C.J. Martoff,‡ W.J. Macdonald,§ J.P. Miller, D.L. Murphy, J.O. Rasmussen, J.P. Sullivan, P. Truol,‖ E. Yoo, and W.A. Zajc

The technique of pion interferometry has been applied to study the reaction 1.8 GeV/A ^{40}Ar + KCl → $2\pi^{\pm}$ + X. In particular, pion interferometry has been proposed as a tool for measuring the radius and lifetime of the pion source.[1] This sensitivity to the source size has recently been verified in streamer chamber measurements.[2] In addition, Gyulassy et al.[3] have emphasized that the pion-pair correlation function also contains information related to the degree of coherence of the pion field.

Approximately 5500 $2\pi^+$ pairs and 4500 $2\pi^-$ pairs with laboratory momentum between 200 and 1000 MeV/c were analyzed with a magnetic spectrometer system

situated at 45° to the beam axis. The measured momenta spectra are in good agreement with the predictions of a Monte Carlo program, which has also been used to calculate the momentum resolution. The Monte Carlo results indicate that the momentum resolution is $\lesssim 4\%$ for $p \lesssim 250$ MeV/c and falls rapidly to $\sim 2\%$ for $p \gtrsim 300$ MeV/c.

The measured pion momenta are transformed to the center of mass, where the relative momentum and energy of each pair are calculated, and then used to determine the correlation function

$$C_2(q,q_0) = N(q,q_0)/B(q,q_0) \quad . \tag{1}$$

Here $q = |\vec{p}_2 - \vec{p}_1|$, $q_0 = |E_2 - E_1|$, $N(q,q_0)$ is the number of pions observed with q and q_0. $B(q,q_0)$, the expected background in the absence of Bose-Einstein correlations, is generated by mixing pion momenta from different events. (See Ref. 4 for further details.) The resulting correlation function is then fit to the expression

$$C_2(q,q_0) = 1 + \lambda \exp(-\frac{1}{2} q^2R^2 - \frac{1}{2} q_0^2T^2) \quad . \tag{2}$$

In this expression, R and T are the radius and lifetime of the corresponding spatial distribution function $\rho(r,t) \simeq \exp(-r^2/R^2 - t^2/T^2)$. The parameter λ is expected to be 1 for a maximally chaotic pion source. If, however, the pion's wave functions are not mutually incoherent, substantial deviations from 1 may occur.

The results of performing such fits may be found in Table 1. In most cases, T has been fixed to 1.5 fm/c, the same value assumed in the analysis of Ref. 2. This is necessary in most cases because the small number of events, combined with the strong correlation between q and q_0, often does not permit separate extraction of R and T. In the first fit, λ is also fixed to the value of one, and no Coulomb corrections have been applied to the data.

This data and the corresponding fit, assumed over q_0, are shown in Fig. 1a. The summation over q_0 defines a spectrometer-averaged correlation function

$$\langle C_2(q) \rangle = \frac{\sum_{q_0} N(q,q_0)}{\sum_{q_0} B(q,q_0)} \quad . \tag{3}$$

While no longer a true correlation function, this form is chosen to provide a convenient one-dimensional presentation of the data and the fitted function.

The small value of R implied by the raw data ($R = 1.84 \pm 0.27$ fm) results from the suppression of the like charge correlation by the Coulomb interaction between the two pions. An event-by-event correction for this effect (Fig. 1(b)) leads to $R = 2.98 \pm 0.30$ fm, again with $\lambda = 1$. R is largely unchanged when λ is left as a free parameter (Fig. 1(c)): $R = 3.18 \pm 0.33$ fm, with $\lambda = 0.86 \pm 0.07$. The R value obtained from the corresponding $2\pi^+$ fit (Fig. 1(d)), 3.92 ± 0.43 fm, is somewhat larger, while $\lambda = 0.78 \pm 0.07$ is smaller.

It would be premature to conclude that these values of λ indicate appreciable source coherence. Aside from the question of statistical significance, λ is also affected by factors such as the event geometry, the construction of the background, spatial correlations within the source, etc.

Finally, allowing T to vary in the case of the $2\pi^+$, we obtain $T = 1.34^{+1.31}_{-1.34}$ fm/c, consistent with our fixed value of 1.5 fm/c. At present, the $2\pi^-$ data set does not allow separate extraction of R and T. However, analysis of added data should produce similar results for these events.

Footnotes and References

*Condensed from LBL-12652.

†Institute for Nuclear Studies, University of Tokyo, Tanashi, Japan.
‡Present address: Swiss Institute for Nuclear Research (SIN), Villigen, Switzerland.
§The University of Alberta, Edmonton, Canada.
Boston University, Boston, MA.
‖University of Zurich, Zurich, Switzerland.

1. F.B. Yano and S.E. Koonin, Phys. Lett. **41**, 1592 (1978).
2. J.J. Lu et al., Phys. Rev. Lett. **46**, 898 (1981).
3. M. Gyulassy et al., Phys. Rev. C **20**, 2267 (1979).
4. J.A. Bistirlich et al., in "High Energy Nuclear Interactions and Properties of Dense Nuclear Matter," Proceedings of the Hakone Seminar, K. Nakai and A. Goldhaber, eds., Vol. 1, 393 (1980).

Table 1. Results from fits to the function $C_2(q,q_o) = 1 + \lambda \exp(-q^2R^2/2 - q_o^2 T^2/2)$.

Description	λ	R(fm)	χ^2/NDF
$2\pi^-$, raw	1	1.84 ± 0.27	114/113
$2\pi^-$, Coulomb Corrected	1	2.98 ± 0.30	120/113
$2\pi^-$, Coulomb Corrected	0.86 ± 0.07	3.12 ± 0.33	116/113
$2\pi^+$, Coulomb Corrected	0.78 ± 0.07	3.92 ± 0.43	89/109

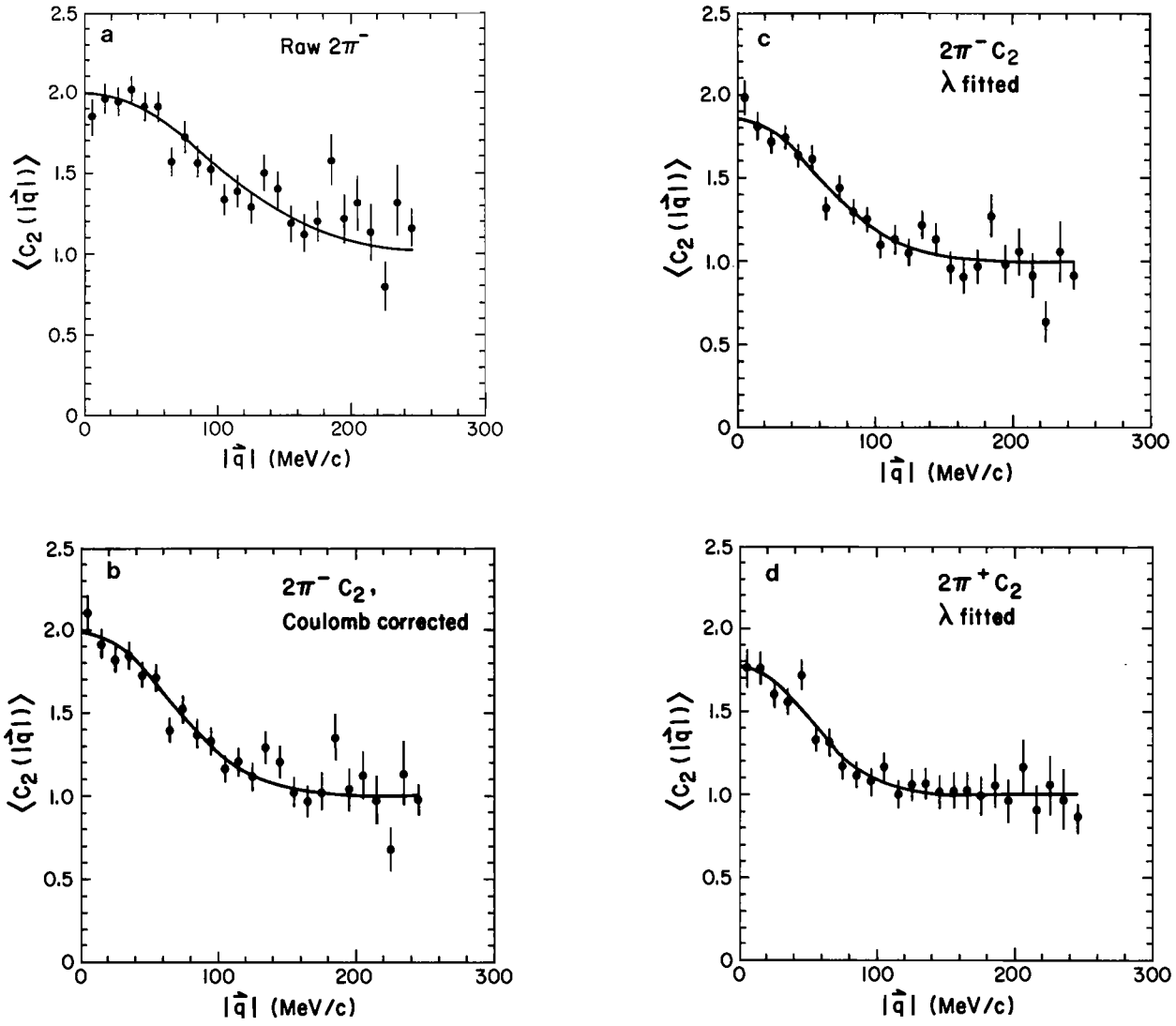

Fig. 1. Correlation functions generated from data and fits as described in text.
[(a) XBL 816-3218; (b) 816-3219; (c) 816-3220; (d) 816-3221]

Space Structure of a Fireball and the Pion Radius*

T.F. Hoang, Bruce Cork, and H.J. Crawford

One of the fundamental problems concerning Landau's hydrodynamical model of meson production[1] is the space-time structure of the fireball. That this property can actually be investigated by means of the Hanbury-Brown and Twiss (HBT) effect[2] has been suggested by several authors. Its application was first made to investigate the diameter of a radiostar and now is used to study the π-π correlation of multiparticle production in high energy physics. There exists a wealth of data on the measurements of the fireball dimensions for a variety of reactions covering a wide range of energies, measurements made on the basis of the HBT effect. In this paper, we interpret these measurements in terms of Landau's model and describe a method to estimate the pion radius from the fireball radius.

Our idea is based on the assumption that the fireballs (albeit prematter) produced in, say, high energy collisions undergo a stage of expansion and then break up and that this last stage takes place when the volume of a fireball becomes equal to that constituted by the mesons it emits. According to this view, the radius R of a fireball is related to the pion radius r_π by the simple geometrical relation:

$$R = n^{1/3} r_\pi \ , \qquad (1)$$

n being the number of the emitted mesons, charged as well as neutral.

We have estimated the pion radius using available data on the fireball radius. As our method of estimating r_π is different, it is interesting to compare those measurements with our results. For this purpose, we have plotted in Fig. 1 our values of r_π. The overall average

$$r_\pi = 0.76 \pm 0.20 \text{ fm}$$

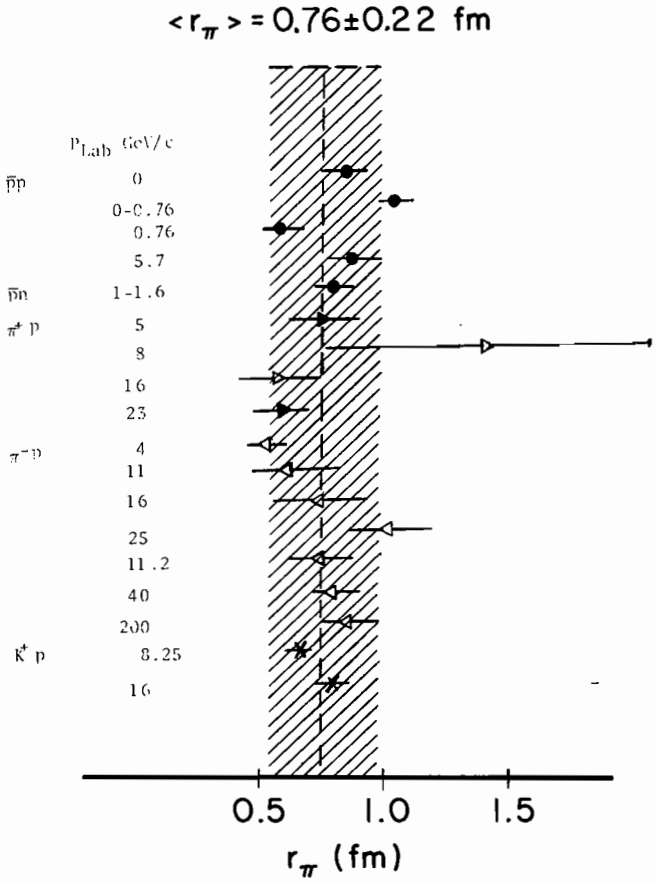

Fig. 1. (XBL 817-10572)

is consistent with previous results, within large statistical errors of our estimates. In this regard, it should be mentioned that all the data used in the present analysis, except the case of pp at 28.5 GeV/c, came from bubble chamber experiments. It would be interesting to have high statistics data in the future so that we can attempt to compare more accurate estimates of r_π with values determined by other methods, and to investigate if there is actually any disparity of results from different methods as pointed out by Chou.[3]

Bearing in mind that we have applied the method in its simplest form, we mention further refinements to be made, for instance, by taking properly into account the decoherence factor. Furthermore, if events from different channels are used for measuring R, account should be taken of appropriate weights of these channels in order to estimate the correct number of πs involved in the fireball.

Footnote and References

*Condensed from LBL-12362.

1. L.D. Landau, Izv. Akad. Nauk. SSSR, ser. fiz. **17**, 51 (1953).

2. R. Hanbury-Brown and R.O. Twiss, Phil. Mag. **45**, 663 (1954).

3. See, e.g., T.T. Chou, Phys. Rev. D **19**, 3327 (1979), $r_K = 0.54 \pm 0.14$ fm and $r_\pi = 0.61 \pm 0.03$ fm.

Two-Pion Correlations in Central Collisions of 1.8 GeV/u ^{40}Ar on KCl

R. Brockmann,[*] J.W. Harris,[*] A. Sandoval,[*] H. Strobele,[*] R. Stock,[*] M. Maier,[†] R.E. Renfordt,[†] J. Miller,[‡] H.G. Pugh,[‡] M. Raff,[‡] L.S. Schroeder,[‡] F. Riess,[§] K. Wolf,[‖] A. Dacal,[¶] and M.E. Ortiz[¶]

We have analyzed part of our data of 1.8 GeV/u ^{40}Ar on KCl taken at the streamer chamber in terms of intensity interferometry of the Hanbury-Brown-Twiss type (Ref. 1 and literature therein).

The experimental correlation function used is defined as

$$C_2(q,\Delta E) = \frac{\rho_2(q,\Delta E)}{\rho_1(\vec{p}_1,E_1)\ \rho_2(\vec{p}_2,E_2)}$$

with $q = |\vec{p}_1 - \vec{p}_2|$, $\Delta E = |E_1 - E_2|$. The correlated pion pair density $\rho_2(q,\Delta E)$ is directly available from the data, whereas the background of uncorrelated pairs (i.e., the product of single particle pion densities) has been constructed by mixing pions from different events with the same multiplicity, then calculating $\rho_2^{back}(q,\Delta E)$. Only events with π^- multiplicities $n_- \geq 4$ have been used in the analysis. The momenta of the correlated pairs have been corrected for their mutual Coulomb repulsion. Figure 1 shows the two-dimensional correlation function; one sees the enhancement towards q and $\Delta E \rightarrow 0$.

Under the assumption of a Gaussian density distribution in space and time of the pion source, the correlation function can be parameterized as

$$C_2(q,\Delta E) = 1 + \beta\exp(q^2R^2/2 - \Delta E^2T^2/2)$$

with R giving the space, T the time dimensions, and β the degree of coherence of the source. This function has been fitted to the experimental correlation function in the range $0 \leq q \leq 150$ MeV/c and $0 \leq \Delta E \leq 150$ MeV. A projection of the data and the best fit is shown in Fig. 2. Since half of the q-ΔE space is kinematically forbidden, i.e., $q = 0$ implies $\Delta E = 0$, the correlation function is very insensitive to the T parameter. The values obtained from the fit are

$$R = 6.7 \pm 1.5 \text{ fm}$$

$$T \leq 4 \text{ fm/c}$$

$$\beta = 1.6 \pm 0.3$$

For comparison the radius of a fused ^{40}Ca + K system at normal density is 5.6 fm in the liquid drop model. The intercept $I = 1 + \beta$ is higher than the value expected for Boston emission by an incoherent source ($I = 2$). However, the present preliminary data are still affected by a systematical error caused by a mismatch of the tracks in the different views, an effect that specifically occurs with close tracks (small Δp) and may account for a 10% overestimate of β. We are now systematically eliminating this error and measuring the pairs of another 3000 events to check conclusively whether or not I exceeds two, a possibility that was recently discussed by Gyulassy.[2]

Footnotes and References

[*]GSI, Darmstadt, West Germany.
[†]Universität Marburg, West Germany.
[‡]LBL, Berkeley.
[§]Universität München, West Germany.
[‖]Argonne National Laboratory.
[¶]IFUNAM, Mexico.

1. J.A. Bistirlich et al., Proceedings of the Hakone School, Vol. 1, 343 (1980).
2. M. Gyulassy, LBL-12389 (1981).

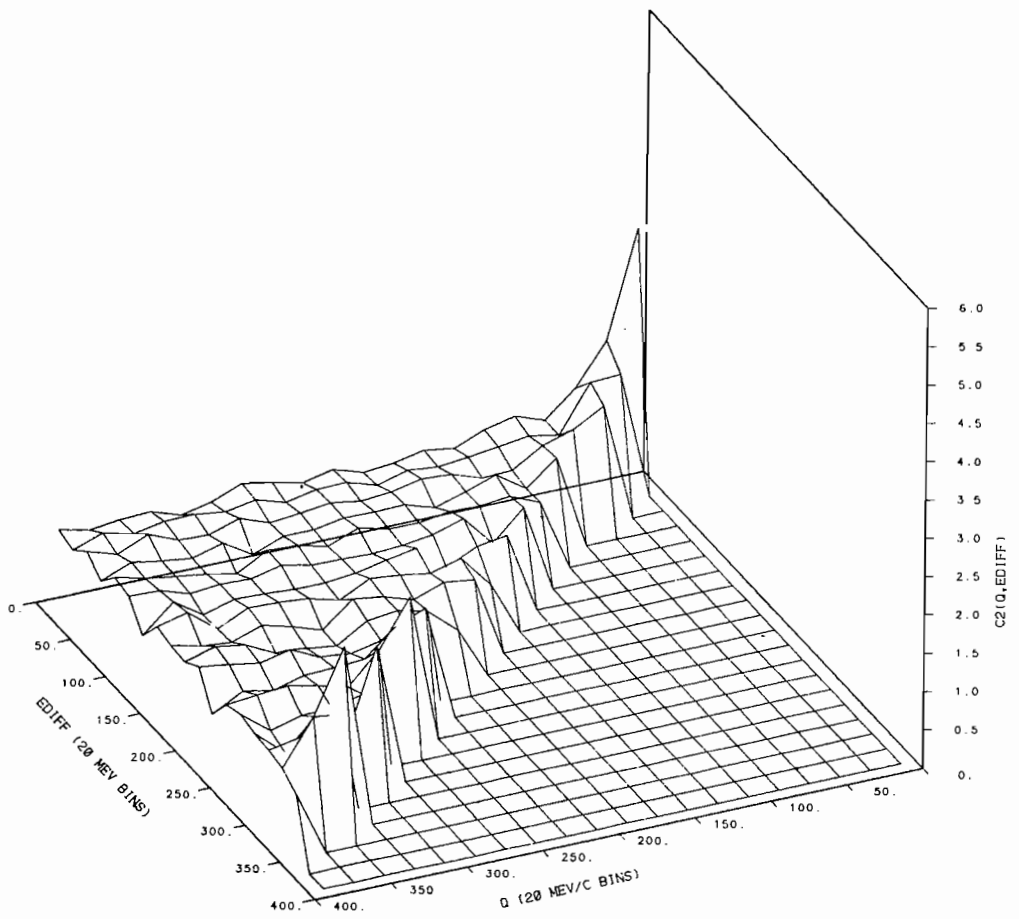

Fig. 1. Two-dimensional correlation function $C_2(q,\Delta E) = \rho_2^{corr}(q,\Delta E)\rho_2^{back}(q,\Delta E)$. (XBL 818-11280)

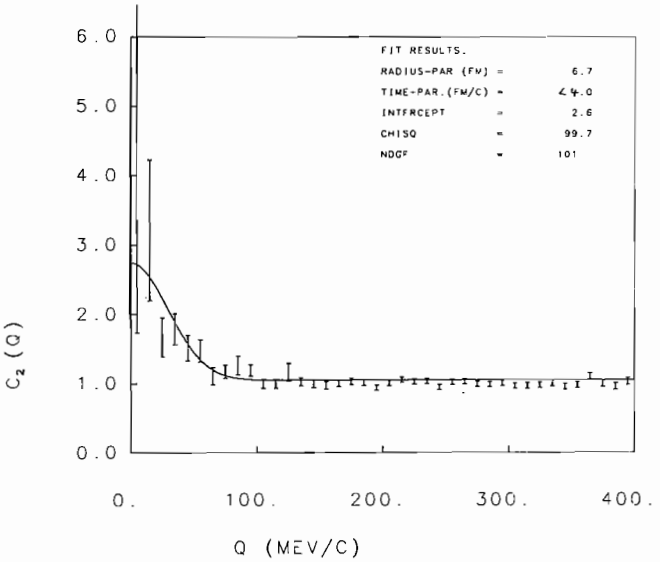

Fig. 2. Projection of C_2 $(q,\Delta E)$ on the q axis with the maximum likelihood fit. The fit parameters are shown in the insert. (NDGF = number of degrees of freedom.)
(XBL 818-11278)

Correlations Between Coincident Fragments in Relativistic Heavy-Ion Reactions

E.P. Steinberg, M.S. Freedman,* H.H. Gutbrod,† D.J. Henderson,* S.B. Kaufman,* M.R. Maier,† J. Péter, H.G. Ritter,† H. Stelzer,† A.I. Warwick, F. Weik,† H. Weiman,† and B.D. Wilkins**

The interactions of 5 GeV protons and ^{4}He ions, and 5-42 GeV ^{20}Ne ions with ^{197}Au have been investigated in experiments at the LBL Bevalac. Masses, kinetic energies, and angular correlations between coincident heavy ($A > 12$) fragments were measured along with the associated multiplicity of fast charged particles.

Two arrays of silicon surface-barrier detectors, one of 12 detectors, the other of 16 detectors, were mounted on either side of the beam to measure the kinetic energies and masses of coincident fragments by time of flight. The start signal was provided by two gas avalanche counters. The number and angular distribution of energetic, light charged particles (e.g., $\pi^{\pm}$, H^+, He^{++}) emitted at angles greater than 9° to the beam were measured in coincidence by an array of 80 plastic scintillators outside a thin-walled, 1-meter diameter, spherical chamber. Particles emitted at smaller angles were measured by a 2m × 2m plastic wall of 60 pairs of scintillators located about 6 meters downstream of the chamber. Although the analysis of the extensive data obtained in these experiments is not yet complete, the results to date provide further evidence and details of an unusual nuclear breakup mechanism first observed with protons at the Argonne ZGS[1] and the importance of the total projectile energy, rather than the energy per nucleon, in determining the reaction mechanisms.[2]

The geometrical arrangement of the two arrays of fragment detectors used for mass measurement covered the region around a correlation angle of 180°, thus emphasizing events with low momentum transfer from the beam. The sum of the two fragment masses, $M_t = M_1 + M_2$, is a measure of the extent of disruption of the target. The distributions in M_t for projectiles of protons, ^{4}He, and ^{20}Ne, all of 5 GeV kinetic energy, show a peak at M_t = 160-180°, with a broad distribution down to low masses (Fig. 1). The peak is due to binary fission of the near-target residues which result primarily from peripheral collisions in which little energy and momentum are transferred. The events of much lower total mass probably arise from more nearly central collisions in which extensive disruption of the target occurs.

The angular correlation between these fragments provides another way to characterize different kinds of nuclear breakup. As shown in Fig. 2, the correlation is relatively narrow for events with $M_t > 160°$, with a most probable angle a few degrees forward of 180°, as expected for the binary fission mechanism. The distribution broadens for lower values of M_t and is essentially flat for $M_t < 100$.

For $M_t < \sim 150$, a large fraction of the events occur with a total fragment kinetic energy considerably greater

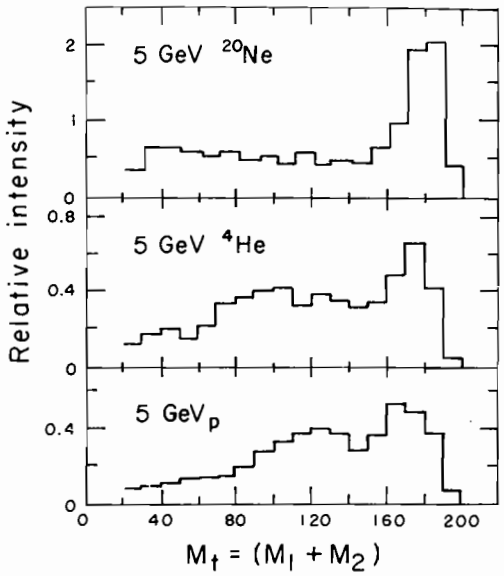

Fig. 1. Coincident fragment mass distribution.
(XBL 818-1154A)

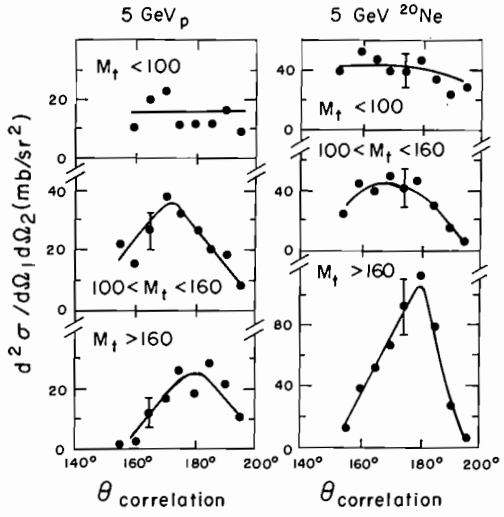

Fig. 2. Angular correlation of coincident fragments.
(XBL 818-1154B)

than that expected for a fission mechanism. This suggests that the nascent fragments were closer together at the time of breakup than in a normal, deformed fission configuration.

Correlated light charged particle multiplicity distributions depend on the total mass of the coincident fragment pairs. For total fragment masses > 160, the distribution peaks at low multiplicity, consistent with a fission mechanism. For lower M_t, the distributions show an increasing probability of high multiplicity associated with the binary events. The distributions scale with the total projectile energy rather than the energy per nucleon, a feature common to a number of aspects of these reactions.[2]

These studies have demonstrated the complexity of the breakup of a heavy nucleus by relativistic projectiles. The features of binary events suggest a new mechanism distinct from fission, but further analysis of the data and further studies are required to establish a detailed interpretation.

Footnotes and References

*Argonne National Laboratory, Argonne IL 60439.
†Gesellschaft für Schwerionenforschung, Darmstadt, West Germany.

1. B.D. Wilkins et al., Phys. Rev. Lett. **43**, 1080 (1979).
2. J.B. Cumming et al., Phys. Rev. C **10**, 739 (1974), Phys. Rev. C **14**, 1554 (1976), Phys. Rev. C **17**, 1632 (1978); D.J. Morrissey, W. Loveland, and G.T. Seaborg, Z. Phys. Z **289**, 123 (1978); S.B. Kaufman, E.P. Steinberg and B.D. Wilkins, Phys. Rev. Lett. **41**, 1359 (1978); W.G. Meyer et al., Phys. Rev. C **22**, 179 (1980); S.B. Kaufman et al., Phys. Rev. C **22**, 1897 (1980).

II. THEORETICAL RESEARCH

THEORETICAL RESEARCH

Nuclear Deformation Energies

*W.J. Swiatecki and J. Blocki**

The binding energy (or mass) of an atomic nucleus may be considered as made up of a "local" part, akin to the energy of a drop endowed with a surface tension, and a "nonlocal" part (Coulomb energy, proximity energy and shell effects—see Ref. 1). The two leading terms in the local (liquid-drop) part are a shape-independent volume energy and a surface energy proportional to the surface area of the shape in question. Together with the electrostatic energy of a uniform distribution of electric charge, these contributions represent the major part of the potential energy of a nuclear system.

Even though some of the most important features of the deformation energy of a charged drop have been adequately studied and tabulated, there are others that are still not well understood—more than forty years since the introduction of the deformable liquid-drop model in connection with nuclear fission. The need for a better understanding and a quantitative tabulation of nuclear deformation energies becomes more acute with the increased interest in the physics of nucleus-nucleus collisions, in which a variety of configurations, not encountered in fission, make their appearance. The present work aims at alleviating this need by presenting what amounts to three-dimensional tabulations (deformation-energy maps) based on a careful choice of three deformation degrees of freedom (corresponding to a mass asymmetry variable, and elongation or fragment-distance variable, and a necking or fragment-deformation variable).

We have finished the production of 665 computer-drawn potential-energy maps together with 150 maps of other nuclear properties of interest. Each map refers to a fixed mass asymmetry and displays the property of interest as a function of the elongation/distance and the neck/fragment deformation variables. The maps span the range of virtually all possible systems accessible through the collision of any two nuclei in the periodic table.

Figure 1 is one of these maps. Contours of equal deformation energy are plotted against the distance or

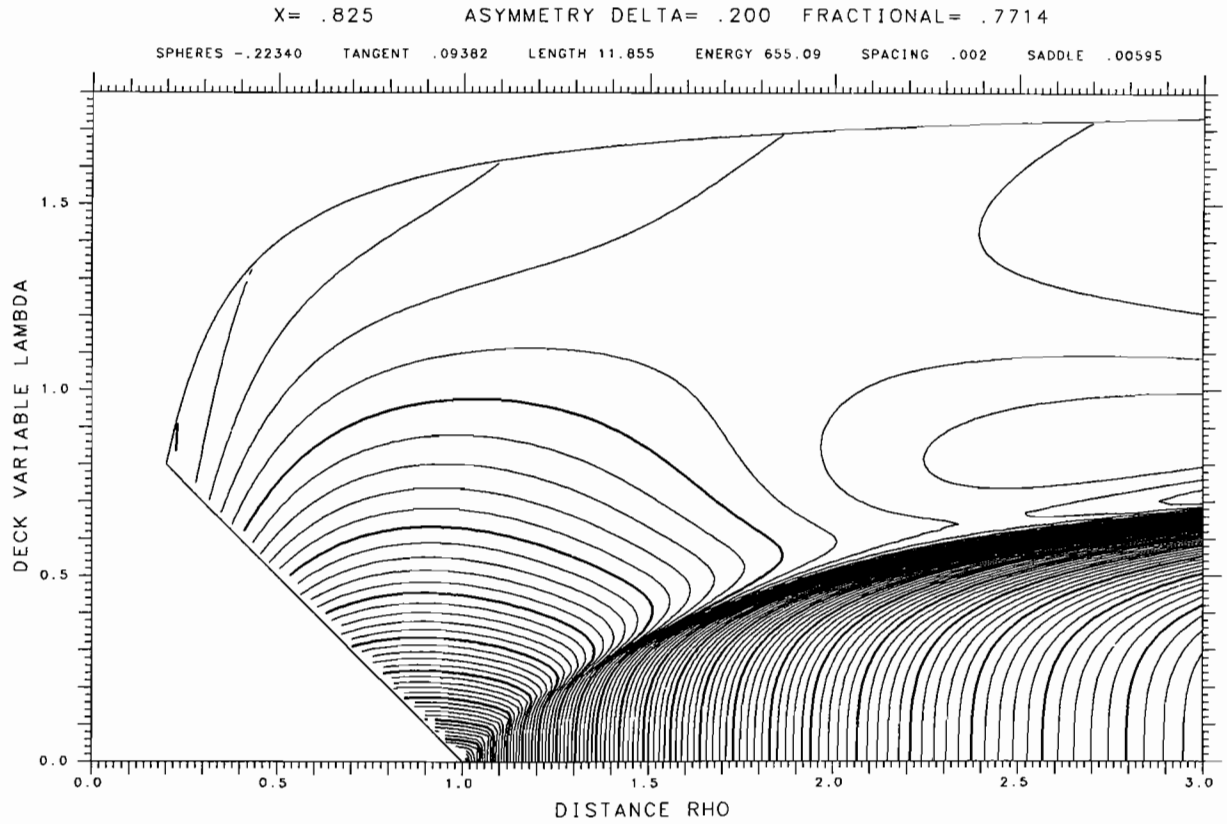

Fig. 1. One of 815 maps of nuclear properties displayed, at fixed asymmetry, as function of a distance variable RHO and a neck variable DECK. See text for a description.

separation variable "RHO" and the fragment-*de*formation or ne*ck* variable "DECK." The contours are spaced at 0.002 of the surface energy of the sphere (655.09 MeV in this case). The map refers to a mass asymmetry corresponding to the heavier fragment having a fraction 0.7714 of the total mass. The total system has a fissility parameter x = 0.825, corresponding to a nucleus close to ^{252}Cf. Configurations of approaching spheres are along the abscissa. The spheres touch at RHO = 1. Shapes formed by portions of intersecting spheres are along the edge sloping up at 45° and end up as a single sphere at the left-hand tip of the map, where the larger sphere has swallowed up the smaller one. The upper curved boundary of the map corresponds to an elongating spheroid with one tip blunted by a portion of a sphere. Scission configurations (in the form of two tear-drop fragments with tips in contact) are just below the ridge running from the configuration of tangent spheres at RHO = 1 to the right-hand edge at DECK $\simeq$ 0.7.

An interesting feature of this map is the existence of a conditional minimum in the potential-energy landscape near RHO = 2.7, DECK = 0.85, where the (strongly deformed) nucleus would be in equilibrium if the asymmetry were frozen. The unfreezing of the asymmetry destroys the equilibrium but, even so, if a nuclear system could be coaxed to run into the neighborhood of this conditional equilibrium, its dynamical disintegration time might exceed 10^{-20} sec – perhaps substantially. Dynamical trajectory calculations are planned which, among other things, should help to optimize the reaction parameters in a nucleus-nucleus collision designed to produce relatively long-lived composite systems.

Footnote and Reference

*Institute of Nuclear Research, Swierk, Poland.

1. W.J. Swiatecki, Prog. Particle and Nucl. Phys. **4**, 383 (1980); Lawrence Berkeley Laboratory preprint LBL-8950, March 1979.

The Effect of Deformation and the Neutron Skin on RMS Charge Radii*

W.D. Myers and K.-H. Schmidt†

In 1977, Angeli and Csatlos compiled all the data on nuclear RMS charge radii that were available at that time.[1] They presented these data in a particularly interesting way that seemed to show that there were substantial shell effects in the measured quantities.

Our analysis of these data shows that most (if not all) of the apparent shell effects are due to deformations rather than actual variations in the spatial extent of the nuclear charge distribution.[2] In order to establish this conjecture we have compared the measured nuclear RMS charge radii with droplet model predictions,[3] after first making an approximate correction using calculated values for the nuclear deformation.[4] We have also compared the corrected RMS radii with liquid drop model predictions. Rather large systematic deviations remain in this case, because the model contains no provision for the influence of the neutron skin on the charge radius.

In Fig. 1 we have plotted the difference between the measured RMS radii and the predictions of the droplet model. Most of the plotted points lie near, but slightly below, the zero line, suggesting that the droplet model nuclear radius constant r_0 should probably be reduced by about one-half percent. At this stage it is not possible to determine whether the remaining structure is evidence for shell effects or merely due to the approximate nature of the calculated deformation corrections.

In Fig. 2 the same comparison is made, but without the corrections for deformation or for the central depression. The larger mid-shell RMS radius values associated with deformations can be clearly seen. The general upward slope of the points toward heavier nuclei is expected because of the charge redistribution associated with the Coulomb repulsion that creates the central depression.

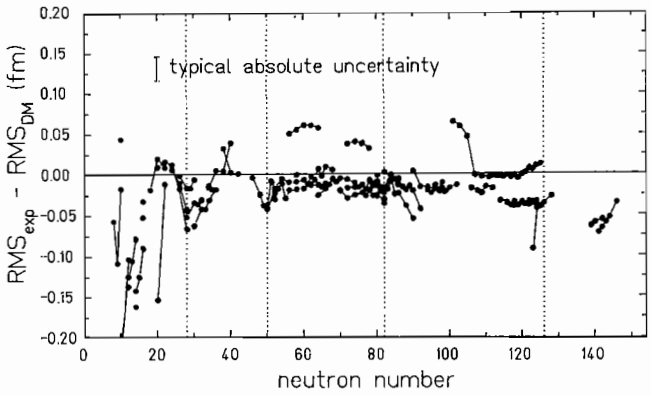

Fig. 1. The difference between measured RMS radii and the droplet model predictions. (XBL 815-9566)

Figure 3 is a comparison of measured and calculated RMS radii similar to Fig. 1, except that the liquid drop

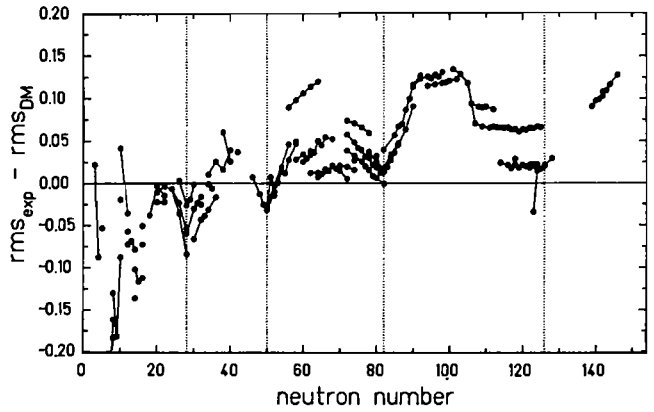

Fig. 2. The same as Fig. 1 but without the corrections for deformation and redistribution. (XBL 815-9567)

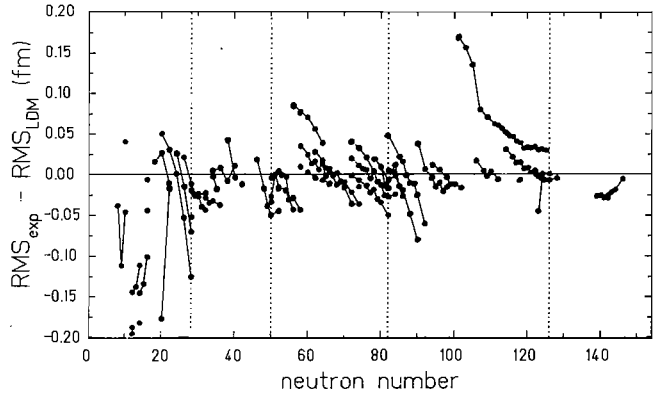

Fig. 3. The same as Fig. 1 but using the liquid model. (XBL 815-9565)

model has been used instead of the droplet model. In almost every isotopic sequence the differences plotted slope steeply downward to the right because the effect of the neutron skin thickness is not included in the liquid drop model.

The three figures above serve to illustrate the importance of deformations and the neutron skin in the calculation of RMS charge radii. Meticulous care will have to be taken to assess the accuracy of the measured values and the values of the deformations that are used in the calculations before it will be possible to determine whether or not there are volume shell effects. At present, most of remaining differences lie within the experimental uncertainty.

Footnotes and References

*Condensed from LBL-12790.

†Gesellschaft für Schwerionenforschung D-6300 Darmstadt 11, W. Germany

1. I. Angeli and M. Csatlos, Nucl. Phys. A **288**, 480 (1977).

2. W.D. Myers, contribution to the "XIX International Winter Meeting on Nuclear Physics," Bormio, Italy, Jan. 1980.

3. W.D. Myers and W.J. Swiatecki, Nucl. Phys. A **336**, 267 (1980).

4. P. Möller and J.R. Nix, to be published in Nucl. Phys. A **363**.

Surface-Layer Corrections to the Level-Density Formula for a Diffuse Fermi Gas*

W.J. Swiatecki and J. Toke†

Using the Thomas-Fermi treatment and the leptodermous expansion in powers of $A^{-1/3}$, a formula was derived for the nuclear level-density parameter a, which corrects the conventional expression for the presence of a diffuse surface region. This appears to remove the discrepancy (of about a factor of 1.7) between the empirical values of a/A and those that would follow from considering the nucleus to be a simple Fermi gas at constant (bulk) density. The formula for a has an appearance quite analogous to the nuclear binding-energy formula: a volume term, a surface-area term, and a curvature correction, with a modification for the neutron excess, analogous to the symmetry energy. Thus

$$a = \frac{A}{14.61\ \text{MeV}}\left(1 + 3.114\,A^{-1/3}\,F_2 + 5.626\,A^{-2/3}\,F_3 \ldots\right)\left[1 - \frac{1}{9}\left(\frac{N-Z}{A}\right)^2\right], \quad (1)$$

where F_2 is the area of the nuclear shape in question in units of the area of the sphere ($4\pi R^2$), and F_3 is the integrated curvature, in units of its value for the sphere ($8\pi R$). All numerical coefficients follow from known or estimated nuclear properties, and agreement with the empirical trend represented by $a \simeq A/(8.5\ \text{MeV})$ follows without arbitrary adjustments. Without the surface and

curvature corrections, the volume term alone would underestimate the values of a by a factor of 1.7. A pocket formula which mocks up the curvature term by a slight increase in the surface term (and disregards the small neutron-excess correction) is

$$a \simeq \frac{A}{14.61\ \mathrm{MeV}} (1 + 4\, A^{-1/3} F_2) \quad . \qquad (2)$$

Footnote

*GSI-24-81 preprint, July 1981, Nucl. Phys. A **372** (1981) 141.

†GSI, Darmstadt, West Germany.

Schematic Calculation of GT Strength in N = 47,49 Isotones

S.G. Prussin,,† Z.M. Oliveira,† and J. Randrup*

Recent measurements of Gamow-Teller (GT) strength distributions via charge exchange reactions on ^{90,91,92,94}Zr have suggested that an important fraction of the total strength lies well below the structureless giant resonance hypothesized by Ikeda, Fujii and Fujita.[1] This low-lying strength will effect substantial modifications to the decay properties of far unstable neutron-rich nuclei as calculated with the gross theory of β-decay.[2]

The most striking feature of the strength distributions found from the charge exchange reactions is that the envelope of the strength appears to be divided into two rather distinct peaks. For ^{90}Nb, data from both (p,n) and (^{3}He,t) reactions locate one peak near 8.4 MeV where the GT giant resonance is expected. The other peak, centered somewhat below 2 MeV and containing 20-25% of the observed strength, is found in the energy range where calculations based on the simple shell model with pairing locate low-lying configurations that would be populated by GT decay of ^{90}Zr if it were energetically allowed. Qualitatively similar results were obtained from the ^{92,94}Zr(p,n) reactions. For both cases, the separation in energy of the two peaks was found to be roughly the same as seen in the ^{90}Zr reaction data.

In a previous publication[3] we showed that these features are well reproduced by schematic RPA calculations using as residual interaction the isospin-flip part of $\chi\vec{\sigma}\cdot\vec{\sigma}\ \vec{\tau}\cdot\vec{\tau}$ to which the GT strength distribution is especially sensitive.[4] The latter, the so-called GT force, induces correlations amongst configurations formed in various n$\rightleftarrows$p transitions and for neutron rich nuclei it has the main effect of shifting the β^--strength to higher energies. From the calculations of GT strength in ^{90,92,94}Nb, we found that in all cases about 25% of the sum rule strength was located in the lower peak and a principal effect of addition of neutron pairs was to increase the dispersion of strength at lower energies without much effect on the splitting between the peak centroids.

Since, to a first approximation, ^{90}Zr can be considered as a doubly magic nucleus, the insensitivity of the GT strength distribution to addition of neutron pairs beyond the N = 50 shell leads naturally to the question of the effects produced by removal of neutron pairs as well as those due to addition or removal of proton pairs from the Z = 40 core. To examine such effects, in part, we have calculated the GT strength distributions in the N = 47,49 isotones of Rb, Y and Nb that would be probed in charge exchange reactions on the respective Kr, Sr and Zr targets. The calculation is based on the model developed in Ref. 4.

All of the distributions are remarkably similar and qualitatively the same as found for the heavier Nb isotopes.[3] The highest-energy transitions are all located near the strength centroid predicted by the gross theory and are well separated from the remaining strength.

The main part of β-strength with magnitude corresponding to $g_{9/2}$ neutron decay resides in the high-energy peak, as expected, whereas the fraction of strength in the low-energy peak is roughly that associated with 2p neutron decay. This feature can be understood qualitatively from the form of the reduced matrix elements of the GT residual interaction between the neutron-proton states $|(\pi\nu)1^+>$ and $|(\pi'\nu')1^+>$ corresponding to configurations formed in GT decay:

$$<(\pi\nu)1^+ \| V_{GT} \| (\pi'\nu')1^+> =$$

$$2\chi(v_\pi u_\nu v_{\pi'} u_{\nu'} + u_\pi v_\nu u_{\pi'} v_{\nu'}) \frac{1}{\sqrt{3}} <\pi\|\sigma\|\nu><\pi'\|\sigma\|\nu'> \quad .$$

The pairing factors u and v account for the reduction of specific $\pi \leftrightarrow \nu$ transitions relative to the pure shell model. The reduced single-particle matrix elements of the spin operator are roughly proportional to the square root of the orbital angular momentum ℓ of the nucleons involved, $<\pi\|\sigma\|\nu> \sim \ell^{1/2}$. Consequently, the GT mixing will tend to be strongest between those configurations which contain nucleons with high angular momentum, as long as the pairing factors are not too small. In the shell-model-plus-pairing limit, about 85% of the sum rule strength in ^{90}Nb is due to the transitions $\nu g_{9/2} \rightarrow \pi g_{9/2}$ and $\nu g_{9/2} \rightarrow \pi g_{7/2}$ while the remainder arises from the decay of 2p neutrons. In this approximation all transitions lead to β-strength in the low-lying peak except for the $\nu g_{9/2} \rightarrow \pi g_{7/2}$ decay which would correspond to the GT resonance. As a result

of the residual interaction, the strength in the low-lying peak is substantially reduced and the remainder has a magnitude equivalent to that from pair scattering plus about 1/4 of that from the $\nu g_{9/2} \rightarrow \pi g_{9/2}$ transition. The increase in the low-lying strength as proton pairs are removed from the Z = 40 core can thus be traced to the relatively weak interaction between the states formed by p-neutron decay and that corresponding to the GT resonance. On the other hand, the increased total β-strength as neutron pairs are added to the $d_{5/2}$ orbitals in ^{92,94,96}Zr is more strongly affected by the residual interaction and leads to the constancy of the fraction of strength seen in the low-lying peak.

Notwithstanding the schematic nature of the calculations, it is expected that the main effects of residual interactions on the β-strength functions are contained in the GT interaction as the remainder is expected to produce rather uncorrelated effects. Thus, apart from the extent of dispersion about centroids, the calculations reported here and in Ref. 3 suggest that the relative weakness of the spin-isospin part of the residual nuclear interaction and the strong spin-orbit splitting of the 1g proton orbitals conspire to produce an overall distribution with much more strength in the important low energy region than expected from the simple giant resonance idealization.

Footnotes and References

*Institut für Kernchemie, Universität Mainz, D-6500 Mainz, West Germany.
†Department of Nuclear Engineering, University of California, Berkeley.

1. K. Ikeda, S. Fujii and J.I. Fujita, Phys. Lett. **3**, 271 (1963).
2. K. Takahashi, M. Yamada and T. Kondoh, Atomic Data and Nucl. Data Tables **12**, 101 (1973).
3. S.G. Prussin and Z.M. Oliveira, Nucl. Phys. A **339**, 503 (1980).
4. J. Randrup, Nucl. Phys. A **207**, 209 (1973).

Particle Angular Momentum Alignment Effects in Deformed Nuclei*

L.K. Peker,† J.O. Rasmussen,‡ and J.H. Hamilton§

Systematic examinations of the angular momentum generated by particle alignment were made for Dy and Er isotopes. Marked deviations are observed from the aligned spin values expected for full alignment of $i_{13/2}$ (odd A) and $(i_{13/2})^2$ (even A) particles.

The sudden changes in the momentum of inertia, back-bending in yrast cascades in even-even rare earth nuclei, are now generally understood in terms of the crossing of the ground-rotational band (GRB) with a rotational aligned band built on a $(j \geq 9/2)^2$ configuration Stockholm band (SB). One of the more important characteristics of this band is the magnitude of the alignment I_0—the projection of the intrinsic angular momentum of both unpaired aligned particles on the axis of rotation.[1] Recently Bohr and Mottelson[2] proposed a way to extract the information on I_0 from an analysis of experimental data on the function $I = I(\omega)$, where the angular frequency $\hbar\omega = \partial E(I)/\partial I \simeq 1/2\, E_\gamma(I + 1 \rightarrow I - 1)$.

Because of the importance of the effect of Coriolis alignment for the understanding of the nature of high spin collective states, we analyze the proposed Bohr and Mottelson[2] interpretation of the quantity $i_\alpha(\omega) = I_{SB}(\omega) - I_{GRB}(\omega)$ in more detail. The function $i_\alpha(\omega)$ depends not only on the properties of the SB (including alignment) reflected in the function $I_{SB}(\omega)$, but by definition depends on the properties of the GRB reflected in the function $I_{GRB}(\omega)$ and as well on the strength of coupling of these two bands, $\simeq h/\Delta E(I)$. In this paper we consider the possible effects on these last two factors on the magnitude of $i_\alpha(\omega)$.

First of all the GRB and the SB have a very different dependence on I. For a more clear qualitative illustration of these differences, we consider another simplified approximation of the expansion,[3]

$$E_{rot} = \sum_i A_i[R(R+1)]^i \qquad (1)$$

where $R = I - I_0^i$, and I is the total angular momentum of the rotational state; which is

$$E_{rot} = A_1[R(R+1)] - A_2[R(R+1)]^2 \quad , \qquad (2)$$

where A_2 characterizes the softness of a nucleus. From Eq. (2) it follows that the two leading terms of $E_\gamma(I)$ are

$$E_\gamma(I) = 4A_1R - 8A_2R^3 + \ldots \quad .$$

Usually $A_2/A_1 \simeq 10^{-2} - 10^{-3}$ (Ref. 3) and at low R the influence of the first term is dominant. But with the increasing of R, the influence of the second term on E_γ increases very fast. For the rotational states with the same I, $R_{GRB} >> R_{SB}$ since $R_{GRB} = I$ and $R_{SB} = I - I_0$ ($I_0 \simeq 12$ for $i = 13/2$). Therefore, the energies of the GRB at a given I are much more strongly affected by the second and higher order terms in Eqs. (1) and (2) than are the energies in the SB at the same I. Thus, we can expect that in the GRB as I increases, E_γ increases not as fast as

in the SB, and the $I = I_{GRB}(\omega)$ curve up bends faster than the $I = I_{SB}(\omega)$ curve.

Detailed examination of some Dy and Er isotopes shows that the magnitude of the "aligned angular momentum," $i_\alpha^{e\text{-}e}(\omega)$, introduced by Bohr and Mottelson[2] reflects not only the real alignment in SB_1 but also the properties of the GRB and the strength of the mixing of the GRB and SB_1. Thus, i_α is not a measure of the real alignment of the SB.

Footnotes and References

*Condensed from Phys. Lett. B **91**, 365 (1980).

†NDDC, Brookhaven National Laboratory, Upton, LI, NY, USA.

‡Chemistry Department, University of California.

§Physics Department, Vanderbilt University, Nashville, TN, USA.

1. F.S. Stephens and R. Simon, Nucl. Phys. A **183**, 257 (1972).
2. A. Bohr and B.R. Mottelson, Suppl. J. Phys. Soc. Japan **44**, 157 (1978).
3. A. Bohr and B. Mottelson, Nuclear Structure, Vol. 2 (Benjamin, New York, 1975).

Excitation of Shape-Vibrational Modes in Nuclei by Relativistic Heavy Ions*

J.O. Rasmussen, J.S. Blair† and X.J. Qiu‡

Overview

Data on excitation of collective 2^+ and 3^- states in relativistic ($\geq$ 250 MeV/N) heavy-ion collisions are reviewed. Our theoretical approach uses the diffuse-edge diffraction model. We use a microscopic model to relate the elemental nucleon-nucleon total cross section to the nuclear transparency parameters for the diffraction model. The integrated inelastic cross sections are approximately inversely proportional to the thickness of the diffuse partial transmission region. Coulomb excitation of giant quadrupole states in the projectile appears to be negligible in comparison to the excitation produced by nuclear interactions.

Diffraction Model

Let us now apply the shadow diffraction scattering model of Refs. 1 and 2. In this model inelastic scattering to isoscalar shape vibrational states increases with the strength function δ_L^2 (the square of the nuclear radius times the zero-point amplitude β_L of the 2^L pole vibration). The differential cross section is expressible in terms of Bessel functions, the period of the diffraction oscillations being inversely proportional to the product of wave number and nuclear radius. The fall-off of the envelope with angle is slow for a sharp absorption shadow surface and more rapid the more diffuse the shadow.

$$\frac{d\sigma_{0\to L}}{d\Omega} = (kR)^2 \frac{\delta_L^2}{4\pi} \sum_{-L\leq M\leq L} [L{:}M]^2 J_M^2(kR\theta)\, F^2(y) \qquad (1)$$

In this formula, δ_L ($\equiv\beta_L R$) is the familiar deformation length, k is the wave number for the relative motion of the projectile and the target, R is the strong absorption radius, and

$$[L{:}M] = \qquad (2a)$$

$$\begin{cases} i^L \dfrac{[(L+M)!\,(L-M)!]^{1/2}}{(L+M)!!\,(L-M)!!} & , \text{ for } (L+M) \text{ even} \\ 0 & , \text{ for } (L+M) \text{ odd} \end{cases}$$

For a partial survival amplitude $\eta(b)$ of the Fermi form,

$$\eta_F(b) = \left[1 + \exp\left(\frac{R-b}{d}\right)\right]^{-1} \qquad (2b)$$

so that d parameterizes the diffuseness of the shadow, the damping factor F(y) has the form

$$F(y) = \frac{\pi y}{\sinh \pi y} \qquad (2c)$$

with $y = kd\theta$.

This differential cross section can be integrated numerically over angle to obtain the total inelastic cross section, σ_L, for the transition in question. Alternatively, an approximate analytic expression has been found[3] for σ_L when the Bessel functions are approximated by their (sinusoidal) asymptotic forms,

$$\sigma_L \simeq \frac{\delta_L^2}{12}\frac{R}{d} \qquad (3)$$

Comparison to values obtained by numerical integration shows that this formula is amazingly accurate. The exact values can be written as the product of the cross section given by Eq. (3) times a factor G_L which is a slowly varying function of the ratio d/R and L. For d/R = 0.05, a

value typical of low energy α scattering, G_L drops from unity to 0.9 as L varies from 0 to 5. For the more diffuse shadows, d/R = 0.10 and 0.15, G_L varies from unity to 0.7 and 0.5, respectively, for the same range of L. In subsequent numerical work, the factor $G_L(d/R)$ is taken to account.

Let us examine diffuseness values from various inelastic scattering data such as for ^{12}C-^{40}Ca collisions at 0.4 GeV/N. The inputs to this latter estimate have been the observed[4] cross section, 14.4 ± 4.4 mb, for producing the 3.73-MeV γ rays which result from decay of the first 3^- state of ^{40}Ca, values of deformation lengths for the particle-stable states in ^{40}Ca obtained from analysis of low-energy scattering experiments, and the γ-ray branching ratios of the particle-stable states. When the diffraction model is used for the angle-integrated cross sections to the particle stable states, one finds the ratio, d/R = 0.10 ± 0.02. With a guessed value for the radius parameter, R = 6.0 fm, one has d ≃ 0.6 fm. Perhaps more meaningful is the quantity 3.69 d, the distance over which the transparency changes from 0.1 to 0.9, which is here estimated to be 2.2 fm. A similar analysis of the γ-ray cross section[4] for 0.4 GeV/N α particles on ^{40}Ca yields a value for the ratio, d/R = 0.16 ± 0.03.

There are also available differential cross section data[5] from the Saturne facility for 0.34 GeV/N α particles scattered from ^{40}Ca. The elastic cross sections are adequately fitted[3] by the diffraction model with the parameters R = 4.72 fm and d/R = 0.135 so that d = 0.64 fm. Similarly, the elastic differential cross sections to the lowest 3^- and 5^- levels are fitted rather well by Eq. (1) with the same values for R and d and with the deformation lengths, δ_3 = 1.14 fm and δ_5 = 0.68 fm, respectively. Table 1 summarizes the determination of (d/R) and d.

The derived diffuseness parameters are generally consistent.

Microscopic Soft-Sphere Model

Can we estimate by model calculations how the sharpness of the absorption shadow might change with bombarding energy? Certainly the elemental nucleon-nucleon total cross section changes over the energy range of Table 1. The σ_{tot}(pp) reaches a minimum of 24 mb near 180 MeV and σ_{tot}(np) has a minimum of ~ 33 mb near 390 MeV. Both cross sections rapidly rise beyond this energy, reaching a ~ 40 mb plateau around 1.0 GeV.

It is appealing now to make comparison with a microscopic model based on experimental pp and np scattering cross sections. Karol[6] has used Gaussian forms to approximate nuclear density distributions in the surface and has derived simple analytical expressions for the nuclear transparency T(b) as a function of impact parameter b. Karol's equation (16) has an apparent misprint in that the left hand side T(b) should actually be −ln T(b) and read as follows:

$$-\ln T(b) = \pi^2 \bar{\sigma}(E)\, \rho_T(0)\, \rho_P(0)\, a_T^3 a_P^3 (a_T^2 + a_P^2)^{-1} \cdot \exp[-b^2/(a_T^2 + a_P^2)] \quad (4)$$

where target (T) and projectile (P) nuclei have densities of

$$\rho_i(r) = \rho_i(0)\, \exp[-(r/a_i)^2] \quad (5)$$

The parameter $\bar{\sigma}(E)$ is a weighted average of pp and np cross sections (his Eq. (4)). Karol integrated to get the corresponding reaction cross section in terms of an exponential integral. (Note that factors of ten appear in his equations because cross sections are given in millibarns. We use fm^2 for cross sections.)

From the above equations we derive an expression for the diffuseness d of the transmission profile.

$$d = \frac{a^2}{R}\ \frac{1}{4 \ln 2} = 0.3607\ \frac{a^2}{R} \quad (6)$$

In terms of the newly defined parameters, R and d, $\eta(b)$ can be written.

The parameters R, d, and d/R given by the "soft-sphere" model for the heavy ion systems being studied are listed in Table 2. In obtaining these an unnormalized Gaussian density has been adopted for ^{40}Ca which gives a reasonable fit in the surface region to the matter density inferred from elastic electron scattering.[16] Normalized Gaussian densities are chosen for ^4He, and ^{12}C which give the measured values[7] of the rms radius of the proton density.

Table 1. Shadow diffuseness parameters (d/R) and d derived for the diffuse-edge shadow diffraction model.

Beam Energy (GeV/N)	System Excited	Collision Partner	Excited State E (MeV)	I_π	σ(exp) (mb)	d/R	Diffuseness Parameter d(fm)	Refs.
0.40	^{40}Ca	^{12}C	3.736	3^-	14.4 ± 4.4	0.10 ± 0.2	0.6	4
0.40	^{40}Ca	α	3.736	3^-	7.2 ± 2.4	0.16 ± 0.03	0.76	4
0.34	^{40}Ca	α	3.736	3^-	$d\sigma/d\Omega$	0.135	0.64	5
0.34	^{40}Ca	α	4.4915	5^-		0.135	0.64	5

Table 2. Microscopic model values of diffraction model parameters.

E_{Lab} (GeV/N)	A_P	A_T	a_P (fm)	a_T (fm)	a^2	$\rho_P(0)$ (fm^{-3})	$\rho_T(0)$ (fm^{-3})	$\sigma(E)$ (mb)	χ	R (fm)	d (fm)	d/R
0.40	12	40	1.884	2.520	9.900	0.322	0.658	30	67.8	6.21	0.575	0.093
0.34 − 0.40	4	40	1.187	2.520	7.759	0.430	0.658	30	28.9	5.45	0.576	0.119

Comparing the "experimental" d/R values of Table 1 to the microscopic "soft-sphere" model values of Table 2, we see that the "soft-sphere" values for collisions with ^{40}Ca are of the order of the "experimental" values, though systematically smaller. The narrower transition regions of the "soft-sphere" model may be attributed to two over simplifications of this model: (a) The unrenormalized Gaussian density adopted for ^{40}Ca is considerably more dense in the interior than that deduced from the scattering of electrons and protons. (b) The "soft-sphere" model may be viewed as a version of the "optical limit" to the Glauber multiple scattering theory.[8] As such it bears the deficiency of all optical limit treatments of nucleus-nucleus collisions, that no account is taken of shadowing corrections. Both oversimplifications result in greater attenuation for decreasing impact parameter than is predicted by more sophisticated theories.[9]

Footnotes and References

*Condensed from Proceedings of Nuclear Physics Workshop, Drexel University, September 1980.

†Physics Department, University of Washington.

‡On leave from Nuclear Research Institute, Shanghai, People's Republic of China.

1. J.S. Blair, Lectures in Theoretical Physics, Vol. VIIIc, eds. P.D. Kunz, D.A. Lind, and W.E. Britten (University of Colorado Press, Boulder, 1966), p. 343.
2. N. Austern and J.S. Blair, Annals of Physics (N.Y.) **33**, 15 (1965).
3. J.S. Blair, Bull. Am. Phys. Soc. **23**, 932 (1978).
4. T. Shibata et al., Nucl. Phys. A **308**, 513 (1978).
5. G.D. Alkhazov et al., Nucl. Phys. A **280**, 365 (1977).
6. P.J. Karol, Phys. Rev. **11**, 1203 (1975).
7. R.C. Barrett and D.F. Jackson, Nuclear Sizes and Structure, (Clarendon Press, Oxford, 1977).
8. W. Czyz, and L.C. Maximon, Ann. Phys. (N.Y.) **52**, 59 (1969).
9. G. Fäldt and I. Hulthage, Nucl. Phys. A **316**, 253 (1979).

Calculation of Muon Final Probabilities after Muon-Induced Fission in Four-State Basis*

Ma Zhong-yu,† Wu Xi-zhen,† Zhang Jing-shang,†
Zhuo Yi-zhong,† and J.O. Rasmussen

Our earlier theoretical work on the relative muon capture between heavy and light fission fragments is extended by including $2p\sigma$ states as well as $1s\sigma$. We calculate about 0.8% population of the 2p state in the heavy fragment, with negligible change from our earlier two-state basis regarding the 1s population of light and heavy fragments.

Earlier calculations[1,2] were made with two basis states, using linear combinations of the 1s atomic orbitals (LCAO) on the two fragments. In a recent study Maruhn et al.[3] have made large numerical integrations of the muon wave function in the Coulomb field of spherical uniformly charged fragments. They have expanded their wave functions to extract p-state as well as s-state probabilities.

We have thought it worthwhile to expand the two-state basis to a four-state basis by including two $2p_z$ states. We have investigated the muon dynamics problem in the Coulomb field of two separate exponential charges by the same method as in Ref. 2. The four eigenvalues of the stationary Schroedinger equation at each instant of time are obtained by the LCAO method, and the time-dependent Schroedinger equation is solved by the PSS method (perturbed stationary states).

We first solve the stationary problem of a muon in the Coulomb field of two centers by the LCAO method. We have chosen four nonorthogonal basis functions, i.e., the wave functions of 1s and $2p_z$ states for light and heavy fragments. The Hamiltonian matrix in this basis set can be obtained analytically. Then the generalized eigenvalue problem is solved numerically.

The time-dependent solution for the muon can be expressed by

$$\Psi = \sum_{\alpha=1}^{4} a_\alpha(t)\, \psi_\zeta e^{-\frac{i}{\hbar}\int^t E_\alpha dt'} \qquad (1)$$

Substitution of Eq. (1) into the time-dependent Schroedinger equation gives the coupled equations,

$$a_\alpha(t) = -\sum_{\beta=1}^{4} a_\beta < \psi_\alpha \left| \frac{\partial}{\partial t} \right| \psi_\beta > e^{-\frac{i}{\hbar}\int^t (E_\beta - E_\alpha)\, dt'}$$

$$\alpha = 1,2,3,4 \quad . \qquad (2)$$

The time differential can be expressed as $d/dt = \dot{R}\frac{d}{dR}$, where R is fragment separation speed.

The results for the most probable asymmetric case are shown in Fig. 1. The solid line represents the final occupation probability of the muon on the light fragment; the dash-dot line is for the case of the 2-state basis. The lowest line shows the probability of the muon lying in the 2p state of the heavy fragment. It shows that the final occupation probability of the muon on the light fragment is about 3.5% and the probability for the 2p state of the heavy fragment is about 0.8%. The population of the 2p level in the light fragment is negligibly small, and the dominant ls_h population can be determined by difference.

The results show that the inclusion of the two 2p orbitals along with the ls did not make much change for final ls population of fission fragments, compared with the case of two ls states as basis.[2]

We should comment about the oscillation on the $2p_h$ probability of large separation distance. This oscillation is not physical and represents a small numerical instability in the calculations giving transitions between ls and 2p states in the separated fragment.

Our result of 0.8% for the heavy fragment 2p final state probability is a bit lower than that of Maruhn et al.,[3] who found 1.7-2% probability. Given the many different assumptions and methods in our and their calculations, the agreement seems satisfactory. The percentage of p state unfortunately seems so low as to make experimental detection unlikely.

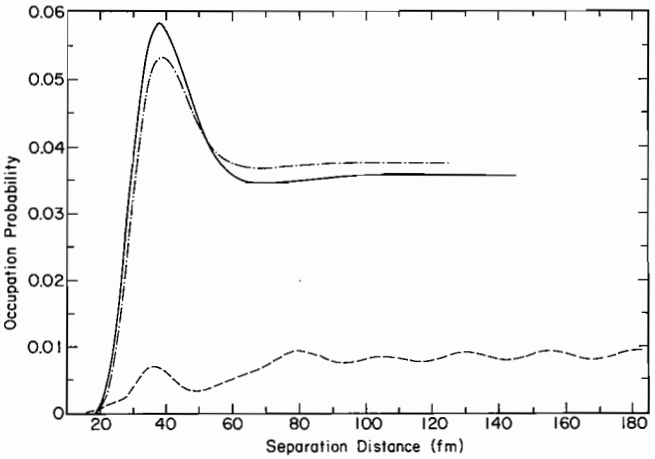

Fig. 1. Calculated muon orbital occupation probabilities as a function of fission fragment separation energies. The upper curves refer to the ls level of the light fragment, the solid curve being present results for the 4-state basis and the dash-dot line for the 2-state basis. The lowest (dashed) line is the probability for being in the state that correlates with the 2p level of the heavy fragment. The system shown is $^{98}Zr + ^{140}Te$. (XBL 8012-13579)

This work was partially supported by the Chinese Academy of Science.

Footnotes and References

*Condensed from Phys. Lett. B **106**, 159 (1981).

†Institute of Atomic Energy, Academia Sinica, P.O. Box 275, Beijing, People's Republic of China.

1. P. Olanders, et al., Phys. Lett. B **90**, 193 (1980).
2. J.O. Rasmussen, et al., Chinese Journal of Nucl. Phys. **2** (1980)(in Chinese); Z.Y. Ma, et al., Nucl. Phys. A **348**, 446 (1980).
3. J.A. Maruhn, V.E. Oberacker, and V. Maruhn-Rezwani, Phys. Rev. Lett. **44**, 1576 (1980).

Two-Nucleon Transfer Reactions in Deformed Nuclei Using Very Heavy Ions*

M.W. Guidry,† T.L. Nichols,† R.E. Neese,† J.O. Rasmussen, L.F. Oliveira‡ and R. Donangelo‡

Semiclassical methods found to be highly accurate for inelastic scattering are applied to the calculation of rotational population signatures in heavy-ion two-neutron transfer reactions involving highly deformed targets. Basic features to be expected for such reactions are predicted and are shown to have straightforward semiclassical interpretations. The rotational population signatures for 2-neutron transfer are shown to be quite different from those expected for the analogous inelastic scattering case. Several calculations were made for Xe projectiles on rare-earth targets,

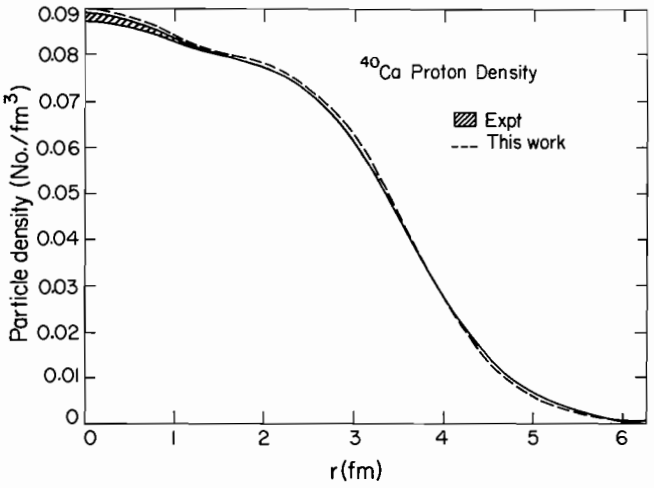

Fig. 1. XBL 816-1016

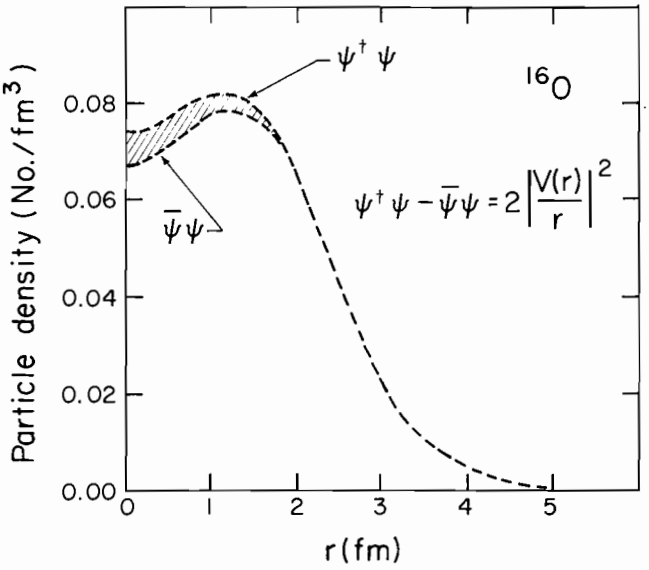

Fig. 2. XBL 811-25

Relativistic Quantum Field Theory of Λ-Hypernuclei*

J. Boguta and S. Bohrmann

That a relativistic model can account for the small spin-orbit splitting in Λ hypernuclei was first shown by Brockmann and Weise.[1] Our approach, though relativistic, is essentially different from the above work. The model that we deal with is a field theory model of nuclear interactions. This means that the motion of the Λ inside a nucleus will be completely determined by the existing fields $\sigma(r)$ and $\omega_0(r)$ inside the nucleus and the coupling, $g_{\Lambda\Lambda\sigma}$, $g_{\Lambda\Lambda\omega}$, to these fields. The fields $\sigma(r)$ and $\omega_0(r)$ are determined in the Hartree approximation. While Brockmann and Weise had to consider a number of complicated intermediate states in the NΛ interaction, we describe the Λ interaction through the fields.

The relativistic quantum field theory of nuclear matter as proposed by Walecka[2] and extended by Boguta and Bodmer[3] assumes that the nuclear interactions are mediated by a scalar σ and vector meson fields ω_μ and that these mesonic degrees of freedom are essential ingredients in the study of nuclear matter. In the Boguta and Bodmer model, the mesonic degrees of freedom cannot be eliminated in favor of nucleon degrees of freedom, and in general they are necessary to define a systematic program to compute higher order corrections. In the mean field approximation, $\sigma \to \langle\sigma\rangle$, $\omega_\mu \to \delta_{\mu 0}\langle\omega_0\rangle$, these fields can saturate nuclear matter because of relativistic kinematics. Infinite nuclear matter problem reduces to a simple set of algebraic equations in terms of g_s/m_s, g_v/m_v (where g_v, g_s are the coupling constants of the σ and ω_μ to the nucleon, and m_s, m_v are the masses). Since m_v is known and m_σ can be determined by fitting to the surface thickness of a finite nucleus (m_σ = 500 MeV), all parameters of the model are determined by the gross properties of nuclear matter. We apply this method to the study of Λ hypernuclei. On the basis of the quark model we will argue that $g_s/g_{\Lambda\Lambda\sigma} = g_v/g_{\Lambda\Lambda\omega} = x$, which has to be determined. We need one piece of information about Λ hypernuclei or Λ in nuclear matter to determine the model completely. We fit to one known neutron-lambda single particle energy difference.[4]

The hypernucleus is assumed to consist of a Λ moving in the mean fields that are created by all the baryons inside the nucleus. The motion of the Λ is given by the Dirac equation

$$[-i\vec{\alpha}\cdot\vec{\nabla} + \beta(m_\Lambda + g_{\Lambda\Lambda\sigma}\sigma)]\,\psi_\Lambda = (E - g_{\Lambda\Lambda\omega}\omega_o)\,\psi_\Lambda \quad . \quad (1)$$

The field σ and ω are obtained from the properties of closed shell nuclei in relativistic mean field theory.[5] In Table 1 we show the predicted energy level differences in Ca^{40} and O^{16}. The experimental data is also shown. We see that a

Table 1.

	${}_{\Lambda}Ca^{40}$	
	Theory (MeV)	Exp (MeV)
$(1d_{5/2}^{-1}, 1d_{5/2})$	19.6	20
$(1d_{3/2}^{-1}, 1d_{3/2})$	12.0	15
$(1d_{5/2}^{-1}, 1p_{3/2})$	12.2	10
$(1d_{3/2}^{-1}, 1p_{1/2})$	4.7	5
	${}_{\Lambda}O^{16}$	
$(p_{3/2}^{-1}, p_{3/2})$	17.6	18
$(p_{1/2}^{-1}, p_{1/2})$	9.9	12
$(p_{3/2}^{-1}, s_{1/2})$	8.9	8
$(p_{1/2}^{-1}, s_{1/2})$	0.6	2

field theoretic approach to the study of hypernuclei can be very successful.

Footnote and References

*Condensed from LBL-11670.

1. R. Brockmann and W. Weise, Phys. Lett. B **69**, 167 (1977).
2. J.P. Walecka, Ann. Phys. **83**, 491 (1979).
3. J. Boguta and A.R. Bodmer, Nucl. Phys. A **292**, 413 (1977).
4. B. Povh, Nucl. Phys. A **335**, 233 (1980).
5. J. Boguta, "Ground State Properties of O^{16}, Ca^{40} and Ca^{48} in a Relativistic Hartree Theory of Nuclear Matter," to be published, LBL-11894.

Density Dependence of the Single Particle Potential in Nuclear Matter*

J. Boguta

A relativistic quantum field approach to the study of infinite nuclear matter and finite nuclei is a natural idea to pursue. On the basis of such an approach Teller, Duerr and Johnson[1] were able to make reasonable predictions for spin-orbit splitting in finite nuclei, the well depth of the real part of the optical potential, and its energy dependence. These seemingly unrelated quantities are in fact simple consequences of the Dirac equation for the nucleons, solved in the presence of nuclear interactions of colossal strength. The underlying picture of the model is naively simple. It classifies nuclear interactions according to the irreducible representations of the Lorentz group. Nuclear attraction is generated by a Lorentz scalar meson σ through the interaction $g_s \bar{\psi}\psi\sigma$, while the repulsion is given by a Lorentz vector meson ω_μ through an interaction $g_v \bar{\psi} \gamma_\mu \psi \omega_\mu$.[2] This distinction plays a fundamental role in the theory. It was shown by Schiff[3] that this distinction between interactions is sufficient to obtain nuclear matter saturation without introducing hard core repulsion. In the relativistic field approach, nuclear matter saturation is a consequence of the apparent Lorentz covariance of the theory. Nuclear attraction is determined by a Lorentz scalar source term ρ_s and repulsion by a Lorentz vector source function $(\vec{J}, i\rho_v)$.

Recently it was shown that a relativistic mean field model reproduces reasonably well the real part of the optical potential.[4] The density dependence of this potential has not been investigated. The purpose of this work is to make such an investigation in a variety of relativistic mean field models. We investigate the Walecka model (W-model),[2] the Boguta and Bodmer model (BB-model),[5] and a recent model proposed by the author (B-model).[6] We show that all these models satisfy the Hugenholtz-van Hove theorem for an interacting Fermi gas.[7] A comparison of the predicted single particle potentials at various nuclear densities is made with those of Friedman and Pandharipande (FP-model), who use Fermi-hypernetted and single-operator-chain summation techniques with a realistic nuclear Hamiltonian.[8]

In Fig. 1 we show the energy dependence of the optical potential, together with a compendium of the available

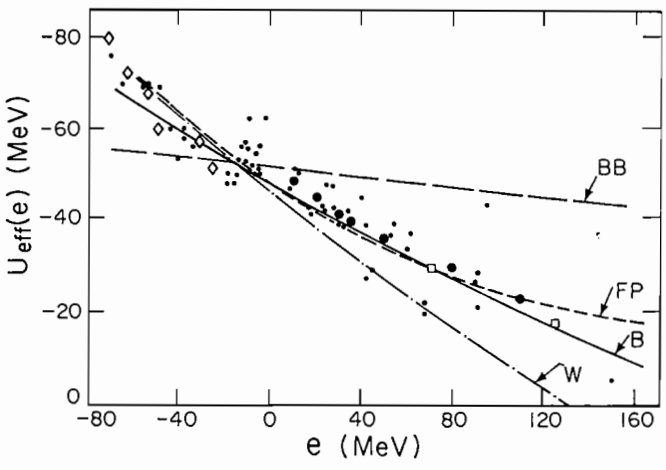

Fig. 1. (XBL 815-798)

data. Clearly the B-model gives a much better description of the data than the Walecka or the Boguta and Bodmer model. In Fig. 2 we show the density dependence and the energy dependence of the optical potential. What is strikingly surprising is that a simple relativistic mean field approach to the study of nuclear matter can reproduce reasonably well the variational calculation predictions.

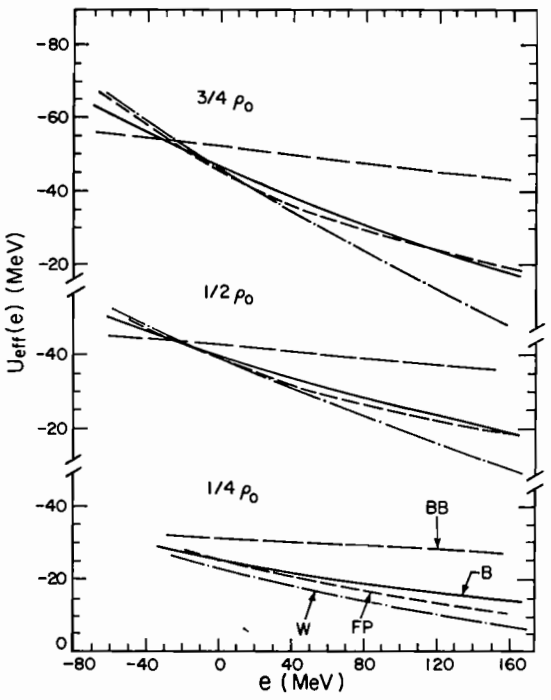

Fig. 2. (XBL 815-797)

Footnote and References

*Condensed from LBL-12628.

1. M.H. Johnson and E. Teller, Phys. Rev. **98**, 783 (1955). H.-P. Duerr, Phys. Rev. **103**, 496 (1956).
2. H. Gaus, Zeitschrift für Naturforschung **4a**, 721 (1949), J.D. Walecka, Ann. Phys. **83**, 491 (1974).
3. L.I. Schiff, Phys. Rev. **84**, 1 (1951); **84**, 10 (1951).
4. J. Boguta, "Nucleon-Nucleus Optical Potential in a Relativistic Theory of Nuclear Matter," Lawrence Berkeley Laboratory Report, LBL-11466 (to be published); L.G. Arnold, B.C. Clark and R.L. Mercer, Phys. Rev. C **19**, 917 (1979); M. Jaminon, C. Mahaux and P. Rochus, Phys. Rev. Lett. **43**, 1097 (1979); L.G. Arnold, B.C. Clark, R.L. Mercer and P. Schwandt, "Dirac Optical Model Analysis of p-Ca^{40} Elastic Scattering at 180 MeV and the Wine-Bottle-Bottom Shape," OSU-TR-80-351; M. Jaminon, C. Mahaux and P. Rochus, Phys. Rev. C **22**, 2027 (1980).
5. J. Boguta and A.R. Bodmer, Nucl. Phys. A **292**, 413 (1977).
6. J. Boguta, "A New Mechanism Leading to Density Isomers," Lawrence Berkeley Laboratory Report LBL-12333.
7. N.M. Hugenholtz and L. Van Hove, Physica XXIV, 363 (1958).
8. B. Friedman and V.R. Pandharipande, "The Single Particle Potential in Nuclear Matter," ILL-(NU)-80-48.

Dense Neutron Star Matter in the Normal and Pion Condensed State in a Relativistic Field Theory Constrained by Bulk Nuclear Properties

N.K. Glendenning, B. Banerjee and M. Gyulassy

This article formulates a theory of dense neutron star matter in a relativistic field theory solved in the mean field approximation. Its special contribution is that the theory is by construction sufficiently rich that it can be constrained to be consistent with the bulk properties of nuclear matter. These important constraints are 1) saturation binding, 2) saturation density of symmetric nucleon matter, 3) compressibility of nuclear matter, and 4) the symmetry energy. In addition the conditions of charge neutrality and β-stability are imposed. These constraints have never before been imposed on a field theoretic model of neutron star matter.

In this theory we study the pion condensate solution as well as the normal solution to the field equations. Our goal in this article is to lay the theoretical framework on which more reliable estimates of neutron star properties can be made.

At, and up to a few times normal nuclear density, and below the threshold for quark matter, nuclear forces can be

described through the exchange of various mesons, the lightest of which are

$$\sigma\ ,\ \omega_\mu\ ,\ \underset{\sim}{\pi}\ ,\ \underset{\sim}{\rho_\mu}$$

They are Yukawa-coupled to the nucleons through the interaction Lagrangian density

$$\mathcal{L}_{\text{int}} = \bar{\psi}_N \left(g_\sigma \sigma - g_\omega \not{\omega} - g_\pi \gamma_5 \underset{\sim}{\tau} \cdot (\not{\partial} \underset{\sim}{\pi}) \right.$$

$$\left. - \frac{1}{2} g_\rho \not{\underset{\sim}{\rho}}_\mu \cdot \underset{\sim}{\tau}^\mu \right) \psi_N - g_\rho \underset{\sim}{\rho^\mu} \cdot \pi x \partial_\mu \underset{\sim}{\pi}$$

The pion mean field is assumed to be

$$\pi_\pm(x) = \frac{1}{\sqrt{2}} \bar{\pi} e^{\pm ikx}$$

which is shown to be a self-consistent solution in the mean field approximation. We are free to choose the direction of k, viz $k_\mu = (k_o,0,0,k)$. Then it can be shown that the Lorentz and isospin structure of the ρ_M and ω_μ fields is

$$\rho_\mu = (\rho_o,0,0,\rho) x (0,0,1) \quad , \quad \omega_\mu = (\omega_o,0,0,\omega)$$

The eight field quantities σ, $\bar{\pi}$, ρ_o, ρ, ω_o, ω, k_o, k are solutions to the coupled non-linear field equations.

$$m_\sigma^2 \sigma = g_\sigma \langle \bar{\psi}\psi \rangle - \langle dV/d\sigma \rangle$$

$$m_\omega^2 \omega_\mu = g_\omega \langle \bar{\psi} \gamma_\mu \psi \rangle$$

$$[m_\rho^2 + (g_\rho \bar{\pi})^2] \rho^\mu = g_\rho \tau_3^\mu$$

$$(-K_\mu K^\mu - g_\rho^2 \rho_\mu \rho^\mu + m_\pi^2) \bar{\pi} = -g_\pi \langle \bar{\psi} \gamma_5 \not{K} \tau_2 \psi \rangle$$

where the nucleon quasiparticle field

$$\psi = e^{\frac{i}{2} k x \tau_3} \psi_N$$

satisfies

$$(\not{p} - g_\omega \not{\omega} - m + g_\sigma \sigma + \not{K}(\frac{1}{2} \tau_3 + g_\pi \bar{\pi} \gamma_5 \tau_2) \psi = 0$$

and

$$K_\mu = k_\mu - g_\rho \rho_\mu .$$

The nucleon quasiparticle propagator and eigenvalue equation and explicit forms for the source currents are derived.

The Energy-Dependent Single Nucleon Potential in a Relativistic Field Theory of Nuclear Matter*

K.-H. Müller

In an attempt to develop a full relativistic description of the many-particle nuclear matter system and to allow explicitly for the mesonic degree of freedom, Walecka[1] has proposed a model quantum field theory in which baryons interact with each other via a scalar and vector meson exchange. The single nucleon spectrum that results from this model determines a momentum K dependent single nucleon mean potential U_R, which is given in terms of the effective nucleon mass and the repulsive vector meson field. Using the parameters as given by Walecka[1] the agreement of U_R with experiment is excellent as shown in Fig. 1.

At nuclear matter densities of $\rho_o/2$ and $\rho_o/4$ a comparison of U_R is made with results from the nonrelativistic mass-operator theory. Here in the Brückner-Hartree-Fock approach[2] the real part of the mean potential U_M is determined by a complex effective nucleon-nucleon interaction. The momentum dependence of U_R in the Walecka model is similar to U_M as shown in Fig. 2.

A correction to the mean field approximation is the inclusion of the scalar and vector meson exchange contributions,[3] which lead to additional momentum dependent terms in the single nucleon mean potential U_{RE}. As we show in Fig. 1, the momentum dependence of the potential for bound states is only slightly changed by the meson exchange terms.

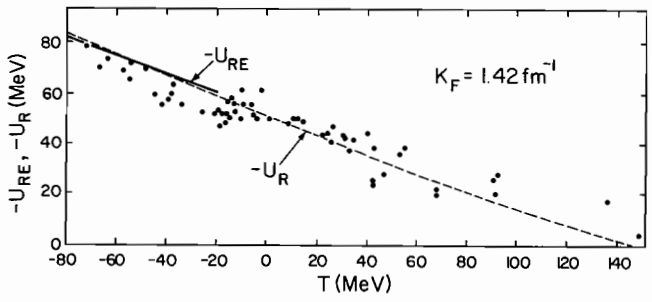

Fig. 1. The single nucleon potential U_R without exchange and U_{RE} with meson exchange corrections versus the nucleon energy T. (XBL 815-808)

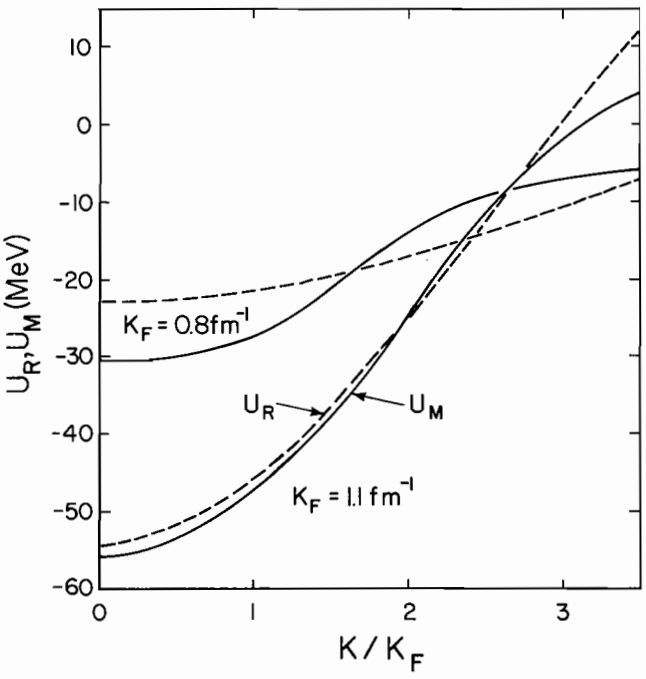

Fig. 2. The single nucleon potential U_R and the Brückner-Hartree-Fock potential U_M versus the momentum ratio K/K_F. (XBL 815-806)

Footnotes and References

*Condensed from LBL-12684. This work was partially supported by the Deutsche Forschungsgemeinschaft, West Germany.

1. J.D. Walecka, Ann. Phys. **83**, 491 (1974).
2. J.P. Jeukenne, A. Lejeune and C. Mahaux, Phys. Rev. C **10**, 1391 (1974).
3. S.A. Chin, Ann. Phys. **108**, 301 (1977).

A Relativistic Quantum Field Theoretical Model for Nuclear Slab Collision Dynamics*

K.-H. Müller

The relativistic mean field model proposed by J.D. Walecka[1] was recently used with great success to describe the properties of nuclear matter as well as the structure of the finite static nuclei. Starting from Walecka's Lagrangian the nucleons are represented by single particle spinors, which are determined by a Dirac equation containing a repulsive mean neutral vector meson field and an attractive mean isoscalar meson field. Both fields satisfy Klein-Gordon equations whose source terms are again determined by the spinors.

We applied this relativistic mean field model to the dynamics of two colliding nuclear slabs. The slabs are translationally invariant in two transverse dimensions and consist of spin and isospin symmetric nuclear matter. The appropriate initial conditions for the approaching slabs are constructed by applying inhomogeneous Lorentz transformations to the static relativistic nucleon wave functions, which correspond to the ground state of a single slab at rest.

We solved numerically the coupled system of differential equations of Dirac- and Klein-Gordon-Type for different bombarding energies. With the constraint of 1.4 nucleons per unit area for each slab, self-consistency leads to a slab thickness that corresponds to a $A \simeq 35$ nucleus.

Figure 1 shows the resulting density ρ_v during the slab collision at $E_{c.m.}/A = 100$ MeV. The maximum density reached is less than $2\rho_0$. The dashed curves show the result taking retardation effects into account. The rapidly increasing repulsive vector meson field leads to one body energy dissipation and slows down the colliding slabs.[2] At low bombarding energies the results are like those from a corresponding TDHF calculation.[3]

Footnotes and References

*Condensed from LBL-12667. This work was partially supported by the Deutsche Forschungsgemeinschaft, West Germany.

1. J.D. Walecka, Ann. Phys. **83**, 491 (1974).
2. K.-H. Müller and S. Bohrmann, Lawrence Berkeley Laboratory Report LBL-12663.
3. P. Bonche, S. Koonin and J.W. Negele, Phys. Rev. C **13**, 1226 (1976).

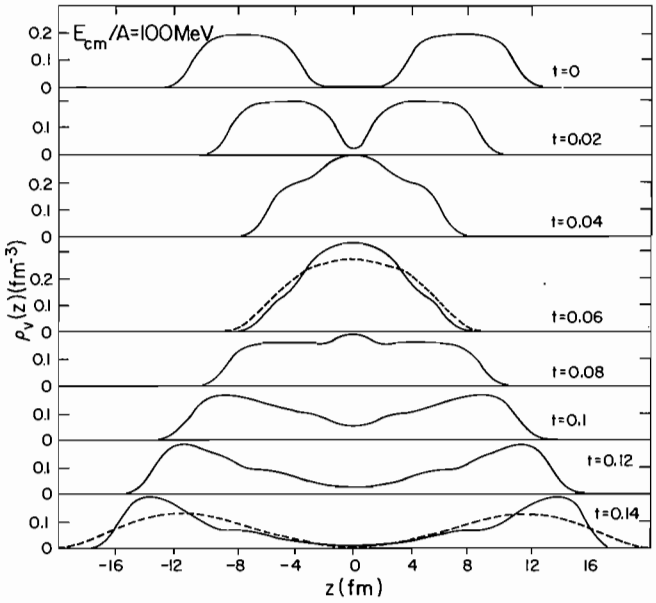

Fig. 1. Density profiles for the $E_{c.m.}/A = 100$ MeV slab collision. The time t is in units of 10^{-21} sec.
(XBL 814-4570A)

Interacting Streaming Nuclear Matter Systems in a Relativistic Quantum Field Theory*

K.-H. Müller and S. Bohrmann†

We study the energetical behavior of two mutually interacting streaming systems of spin and isospin symmetric nuclear matter in a relativistic quantum field model proposed by J.D. Walecka.[1] Both matter systems are of infinite size, overlap completely in coordinate space, and stream in z-direction with velocities V and -V, respectively. The interaction between the baryons is mediated by an attractive scalar and a repulsive vector-meson field. Because of the symmetry in our problem, there is no net baryon current in z-direction and therefore all space components of the vector-meson field vanish.

The relativistic many-body baryon state is assumed to be a product of plane wave spinors. The plane wave quantum numbers occupy a Fermi sphere in each respective rest frame. For small flow velocities the Fermi spheres overlap leading to doubly occupied single baryon states. To avoid this, we rearrange the doubly occupied cells.[2]

In order to present the behavior of streaming matter systems transparently and in a way comparable to nonrelativistic many-body theories, we split the total energy into a kinetic part T and a potential part. This is accomplished by identifying each system with a free nucleon gas in an effective spatially constant potential. We assume that before the two systems flowed through each other, both systems existed without any spatial overlap in their ground states and approached each other with c.m. energy $T_{c.m.}$. Total energy conservation then relates the kinetic energy T of the interacting system with $T_{c.m.}$. Figure 1 shows the ratio $R = T/T_{c.m.}$ and the change in flow velocity $\bar{R} = V_i/V_n$, where V_i and V_n are the flow velocities for the interacting and noninteracting systems, respectively.

The conclusion of our investigation is that for high flow velocities the vector meson field evokes a strong repulsion between the streaming systems that slows down the systems strongly.[3]

Footnotes and References

*Condensed from LBL-12663. This work was partially supported by the DFG, West Germany, by NATO fellowship, DAAD, West Germany, and by BMFT, West Germany.

†Inst. f. Theor. Phys., Philosophenweg 19, 6900 Heidelberg, West Germany.

1. J.D. Walecka, Ann. Phys. **83**, 491 (1974).
2. F. Beck, K.-H. Müller and H.S. Köhler, Phys. Rev. Lett. **40**, 837 (1978).
3. K.-H. Müller, Lawrence Berkeley Laboratory Report LBL-12667 (submitted to Nucl. Phys.).

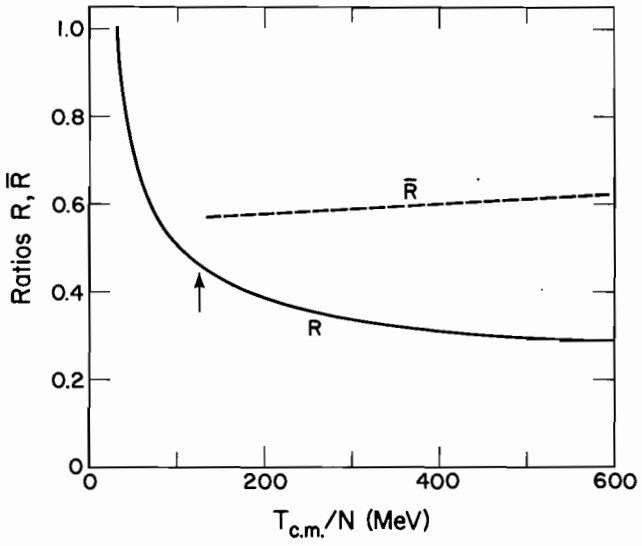

Fig. 1. The relative change R of the kinetic energy and the relative change $\bar{R}$ of the flow velocity for systems of normal nuclear matter density. (XBL 818-1109)

Theory of Nuclear Dynamics

W.J. Swiatecki

The theory of macroscopic nuclear dynamics, based on the concept of a nucleus as a visco-elastic system[1,2] has made appreciable progress in the past year. As is the case with statics, the nature of nuclear dynamics is profoundly affected by symmetries, associated also with shell effects. There are two limiting cases that are particularly simple. On the one hand, when the system is away from symmetries, the static potential energy is described accurately by a leptodermous (liquid-drop) type of expression and the dynamics of shape changes is expected to follow a simple equation of motion, based on the one-body dissipation concept.[3,4] The resulting motion is predicted to be severely overdamped: the nucleus should behave like a *viscous fluid,* with a novel type of viscosity. On the other hand, when the system is close to symmetrical configurations (in the first place a sphere but, to a lesser degree, most ground-state configurations) the single-particle level structure acquires special features (crossings and near-crossings of levels) and the nucleus becomes more like a visco-elastic *solid,*[2] in some cases actually dominated by elasticity (e.g., the giant quadrupole resonances.[5])

The theoretical exploration of the dissipation-dominated regime, initiated half a dozen years ago,[3,4] has made striking contact with recent experiments at GSI, Darmstadt. These confrontations of theory and experiment center around the prediction of an "extra push" necessary to make two sufficiently heavy nuclei fuse, and an "extra-extra push" to make a compound nucleus.[6-12] Merely from the conservation of energy and angular momentum it is possible to derive the following extra push theorem, relating the fusion cross section σ to the center-of-mass energy E:

"When an extra radial injection energy over the interaction barrier B is needed to initiate fusion, the square root of the cross-section defect Δ should be approximately linear in the energy-weighted reduced cross-section Σ, viz:

$$\sqrt{\Delta} = c_1 + c_2\Sigma + \ldots \text{"} \qquad (1)$$

In the above

$$\Sigma \equiv E\sigma/\pi r^2$$

$$\Delta \equiv E - B - E\sigma/\pi r^2$$

r = center-to-center distance at contact.

The parameters c_1,c_2 are constants for a given target-projectile pair. On dimensional grounds (together with a small neck approximation) the one-body dissipation theory predicts the following dependences of these parameters on the atomic and mass numbers Z_1, Z_2, A_1, A_2 of the colliding nuclei:

$$c_1 = \sqrt{K}[(Z^2/A)_{eff} - (Z^2/A)_{thr}] \ , \qquad (2)$$

$$c_2 = \frac{\sqrt{K}}{e^2/r_o} \quad \frac{8f^2}{A_1^{1/3}A_2^{1/3}} \quad , \tag{3}$$

where

$$K = \frac{32}{2025}\left(\frac{3}{\pi}\right)^{2/3}\left(\frac{e^2}{\hbar c}\right)^2 \times mc^2 \frac{A_1^{1/3}A_2^{1/3}\left(A_1^{1/3}+A_2^{1/3}\right)^2}{A_1+A_2}\, a^2 \tag{4}$$

r_o = nuclear radius constant
m = atomic mass unit = 931.5 MeV/c^2.

The effective fissility, defined by

$$(Z^2/A)_{eff} \equiv \frac{4Z_1Z_2}{A_1^{1/3}A_2^{1/3}\left(A_1^{1/3}+A_2^{1/3}\right)} \tag{5}$$

appears as a fundamental scaling parameter of fusion dynamics in the regime of necked-in configurations.

There are three parameters (pure numbers) in Eqs. (2-4): the threshold fissility $(Z^2/A)_{thr}$, the "thud wall slope coefficient" *a* and the "effective angular momentum fraction" f (see Refs. 9,10). They have to be estimated from dynamical model calculations or deduced from fits to experiments. The schematic model of Refs. 8-10 suggested $(Z^2/A)_{thr}$ somewhat greater than 27 and *a* considerably greater than 5. The parameter f should be somewhat less than 1.

Figure 1 shows a comparison of the recent GSI experiments[11] with the above theory. The deduced values of the parameters are: $(Z^2/A)_{th} \simeq 33 \pm 1$, $a \simeq 12 \pm 2$, $f \simeq 3/4 \pm 10\%$.

A recent application of the schematic model of Refs. 8-10 to the clutching stage of nuclear collisions suggests $f \simeq 0.85$. (See contribution of G. Fai to this annual report.)

Current dynamical calculations done in collaboration with J. Blocki and others (at the Institute of Nuclear Research, Swierk, Poland, and the Technische Hochschule and GSI, Darmstadt), using the model underlying the potential-energy maps described elsewhere in this report, gave $(Z^2/A)_{thr} = 33.3$, in agreement with experiment. On the other hand, the same calculations seem to overestimate substantially the value of *a*.

Joint work with S. Bjørnholm (Niels Bohr Institute, Copenhagen), initiated very recently, extends the above considerations to the extra-extra push necessary to make a compound nucleus. This leads to a semi-quantitative survey of nuclear reactions, classified as (a) elastic (plus quasi-elastic), (b) deep-inelastic, (c) fast-fission and (d) compound-nucleus. It should be possible to provide simple estimates of the associated cross sections. A crucial element in this treatment is the discovery of a promising candidate for a scaling parameter for fast-fission and compound nucleus reactions, namely the (geometric) mean fissility, defined by

$$(Z^2/A)_{mean} \equiv \sqrt{(Z^2/A)_{eff}\,(Z^2/A)}\ , \tag{6}$$

where Z^2/A is the ordinary fissility of the whole system.

References

1. D.L. Hill and J.A. Wheeler, Phys. Rev. **89**, 1102 (1953).
2. W. Nörenberg, "Memory Effects in the Energy Dissipation for Slow Collective Nuclear Motion," Preprint GSI-81-14, May 1981.
3. J. Blocki et al., Annals of Phys. **113**, 338 (1978).
4. J. Randrup and W.J. Swiatecki, Annals of Phys. **124**, 193 (1980).
5. G.F. Bertsch, Nucl. Phys. A **249**, 253 (1975); J.R. Nix and J. Sierk, Phys. Rev. C **21**, 396 (1980).
6. J.R. Nix and A.J. Sierk, Phys. Rev. C **15**, 2072 (1977).
7. W.J. Swiatecki, Prog. Particle and Nucl. Phys. **4**, 383 (1980); Lawrence Berkeley Laboratory Report LBL-8950 (1979).
8. W.J. Swiatecki, "The Dynamics of Nuclear Coalescence of Reseparation," talk presented at the Nobel Symposium on High Spin States, Orenäs, Sweden, June 22-25, 1980, to be published in Physics Scripta, 1981; Lawrence Berkeley Laboratory Report LBL-10911.
9. W.J. Swiatecki, "Fusion Cross-Sections and the New Dynamics," Lawrence Berkeley Laboratory Report LBL-12708 (1981).
10. W.J. Swiatecki, "The Dynamics of the Fusion of Two Nuclei," Lawrence Berkeley Laboratory Report LBL-12642 (1981), to appear in Nucl. Phys. A.
11. H. Sann et al., "Fusion Reaction Studies of Transuranic Elements," Proc. Int. Conf. on Nucl. Physics, Aug. 24-30, 1980, Berkeley, California, Lawrence Berkeley Laboratory Report LBL-11118; A. Gobbi, Contribution to "GSI Nahrichten" 1-81, p. 4, 1981; H. Sann et al., "Deformability as a Critical Factor in Initiating Fusion between Very High Ions," GSI-Preprint 81-6, Feb. 1981; submitted to Phys. Rev. Letters.
12. B. Sikora et al., "Parameter Scaling Test of a Dynamic Nucleus-Nucleus Collision Theory," Lawrence Livermore Laboratory Report UCRL-86277 (1981); submitted to Phys. Rev. Letters.

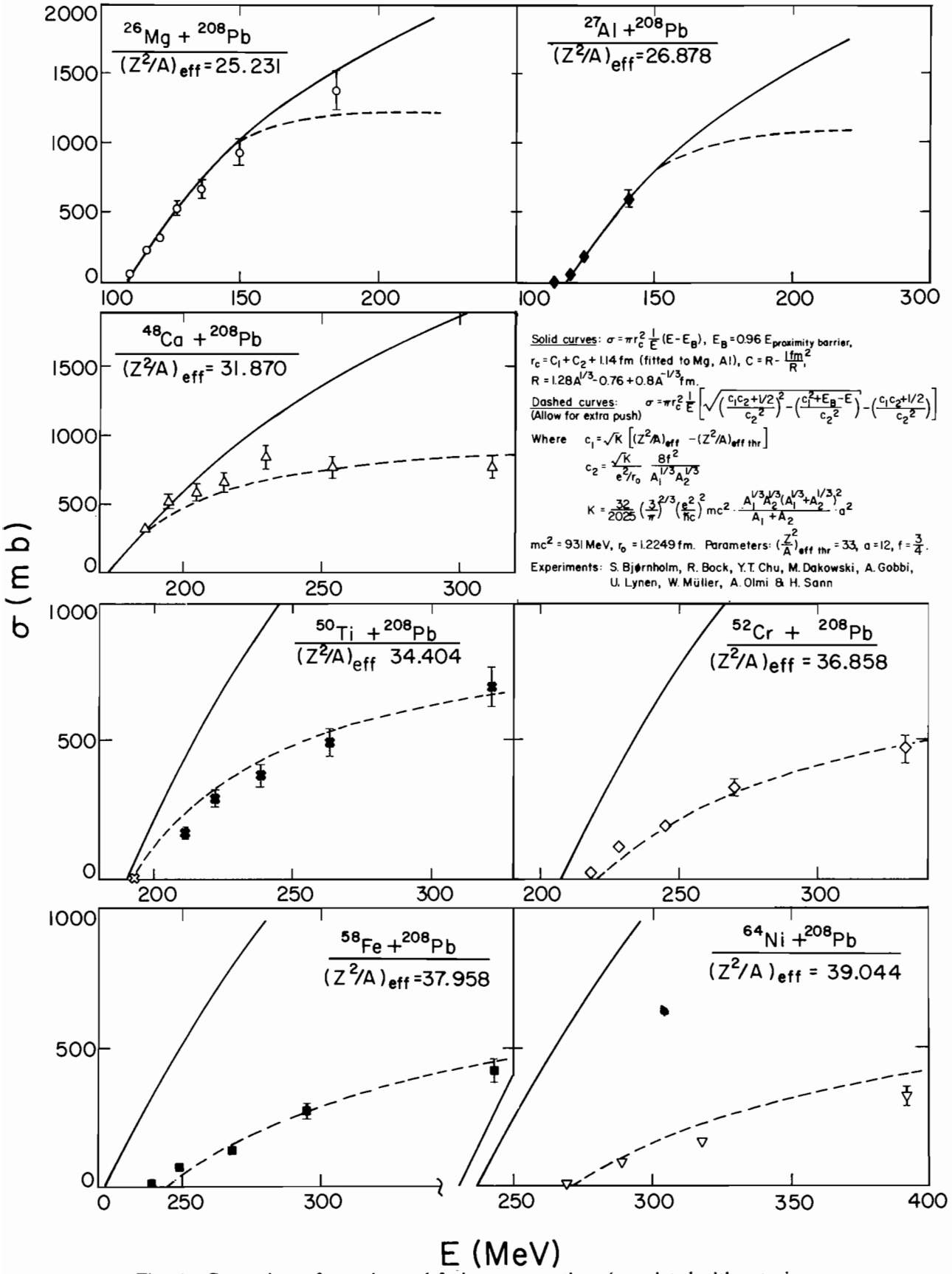

Fig. 1. Comparison of experimental fusion cross-sections (associated with outgoing fragment masses centered around symmetry) with theory. The solid curves are conventional reaction cross-section predictions, and the dashed curves incorporate the requirement of an extra push in the approach degree of freedom. The data are from Ref. 9. (XBL 815-829)

The Clutching of Two Colliding Nuclei

G. Fai

The existing macroscopic model of nuclear coalescence or reseparation[1] describes head-on collisions. In the present work the treatment is extended to noncentral collisions by taking into account the relative angular momentum and the rotation of the individual nuclei. The relevant degrees of freedom are the following: asymmetry, fragment separation, neck size, and the total amount of sliding that has taken place until the two nuclei "clutched." Rolling friction is neglected.

The equations of motion are sufficiently simple that approximate solutions in closed form may be found in several cases of interest. In particular, the theory provides the normal modes of motion around the saddle points of the potential energy surface. For not too light systems the characteristic time of the transition from sliding to rolling appears to be shorter than the characteristic time of any other mode (fission, damping, and oscillation). This can be interpreted as a fast clutching of the colliding nuclei.

The dynamics of the collision as described by the present model suggests that centrifugal force to a good approximation can be traded for electric repulsion via an "angular momentum fraction" as has been done to fit recent experimental data.[2] The model also yields a theoretical prediction for the value of the angular momentum fraction f, which turns out to be $f \simeq 0.8$, while the best fit to experiments has been obtained using $f = 3/4 \pm 10\%$. Both of these values are notably far from $f = 1$, corresponding to a "mass-points" moment of inertia on one hand, and from $f = 0.54$, corresponding to a limit of rigidly stuck spheres with a ratio of masses of about 208:50 on the other.

A numerical study of the dynamics of the clutching of two colliding nuclei is under way.

References

1. W.J. Swiatecki, Lawrence Berkeley Laboratory Report LBL-10911 (1980).
2. W.J. Swiatecki, Lawrence Berkeley Laboratory Report LBL-12642 (1981).

Fusion-Fission, Molecular-Capture And Symmetric Fragmentation In 3D-TDHF Calculation of the Reactions ^{238}U, ^{208}Pb (4.6-8.0 MeV/u) ^{64}Ni, ^{48}Ca B+G

H. Stöcker,† R.Y. Cusson,†‡ H.J. Lustig,† A. Gobbi,†*
J. Hahn,§ J.A. Maruhn,§ and W. Greiner§

Beams of ^{208}Pb and ^{238}U between 4.6 and 8.0 MeV/u from the GSI UNILAC have been used recently to bombard light targets such as ^{48}Ca and ^{64}Ni. These data show in addition to ordinary deep inelastic processes some broad fusion-fission type mass distributions[1] centered around $(A_T + A_P)/2$; these new effects are the subject of our present study using the 3-dimensional time-dependent Hartree-Fock model calculation.[2]

Four distinct reaction types are found in our calculations (see Fig. 1): For impact parameters b < b grazing, the nuclei develop a neck and the single particle viscosity present in TDHF causes large angular momentum and kinetic energy losses but the reaction time is too short to cause an appreciable change in fragment mass. Besides these well known deep inelastic collisions, we distinguish the following: 1) Capture events with subsequent symmetric fragmentation; the time for mass asymmetry equilibration is approximately $\gtrsim 3\times10^{-21}$ s, while energy and

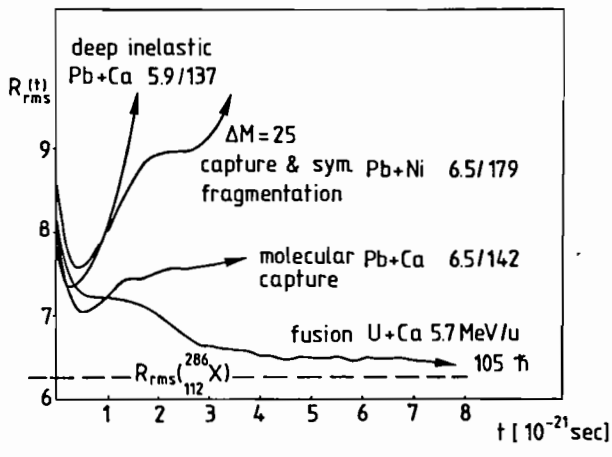

Fig. 1. The rms-radius in fm vs time. (XBL 8110-12112)

angular momentum loss is much faster with $\tau \simeq$ 1-1.5 10^{-21} s. 2) The formation of long-lived very heavy nuclear molecules with two-centered shapes, the molecular capture being characterized by nearly stationary, large rms-radii (see Fig. 1). These rotate for $\tau \gtrsim 10^{-21}$ s without appreciably changing its shape. 3) Fusion, characterized by an rms-radius of the compound system approaching that of the ground state spherical nucleus after $\tau \gtrsim 10^{-20}$ s. The very heavy composites formed in processes 2 and 3 are likely to fission. Their fission mass distribution can hardly be distinguished from those of process 1, capture and symmetric fragmentation.

In order to obtain a rough comparison of our results with the symmetric fragmentation component extracted from the experimental data,[1] we computed the sum of the capture cross sections (processes 1, 2, and 3) with a minimum mass drift of 15 mass units, and calculated the capture excitation functions for the system

$$^{238}U + {}^{48}Ca \rightarrow (^{286}_{112}X,SF)$$

and

$$^{208}Pb + {}^{48}Ca \rightarrow (^{256}_{102}X,SF)$$

(see Fig. 2). Considering the fact that the theory includes events which are not completely equilibrated in mass asymmetry we find reasonable agreement with the experimental data.

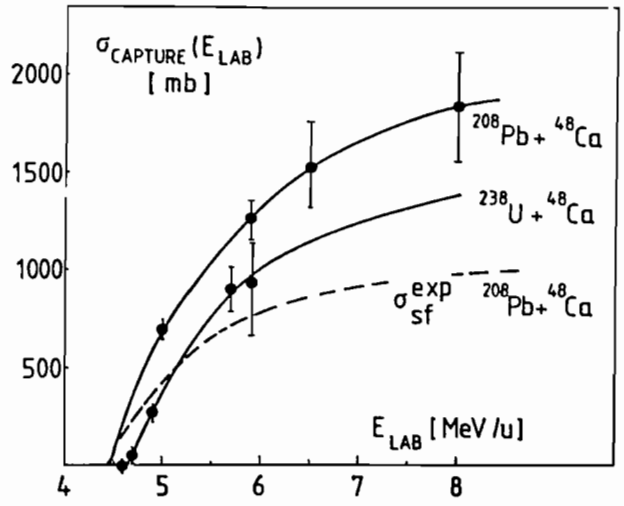

Fig. 2. Excitation function of the calculated capture cross reactions vs E_{Lab} compared to the recent GSI data (Ref. 1, dashed line). The bars denote the upper and lower limit for capture, reflecting the fact that only a few impact parameters for each bombarding energy can be computed. The solid lines are to guide the eyes.

(XBL 8110-12211)

Footnotes and References

*Presently at LBL.

†GSI, Darmstadt, West Germany.

‡Permanent address: Physics Department, Duke University, Durham, NC 27706.

§Institut für Theoretische Physik, Universität Frankfurt, West Germany.

1. A. Olmi et al., "15th Bormio Winter Meeting on Nuclear Physics," Bormio, Italy (1978), p. 724. Also H. Sann et al., to be published.

2. H. Stöcker et al., GSI-preprint 81-3. R.Y. Cusson, J.A. Maruhn, and H. Stöcker, Z. Physik A **294**, 257 (1980).

Quantum Treatment of Charge Equilibration in Fission*

W.D. Myers, G. Mantzouranis,† and J. Randrup

The prospect that originally motivated this investigation was the hope that the width of the charge distribution in fission would provide a key to differentiating between two substantially different proposals for the path of a fissioning nucleus on its way from saddle to scission. In Ref. 1 two different dynamical paths are determined for fission that both give the correct value for the asymptotic kinetic energy release. One trajectory is quite rapid and is only weakly damped by an ordinary hydrodynamic viscosity. The final velocity comes from the relative motion at scission and the Coulomb acceleration of the separating fragments. The other trajectory is based on the one-body damping mechanism and is much slower. The resulting scission shape is more compact and the relative motion is slower. However, the increased Coulomb acceleration after scission results in a final kinetic energy that is nearly the same as for the trajectory based on viscous damping.

The final width of the fragment charge distributions depends on the rate at which the neck between the two nuclei closes off at scission. In Fig. 1 the inverse mass b (in the charge equilibration degree of freedom) is plotted as a function of time for the two different fission trajectories. (See Ref. 2 for details of the calculation.) Since the rate at which b decreases is quite different, we expected that the predicted charge dispersions would also be quite different.

Unfortunately, the freeze-out of the charge dispersion occurs so late in the process (see Fig. 2) that there is

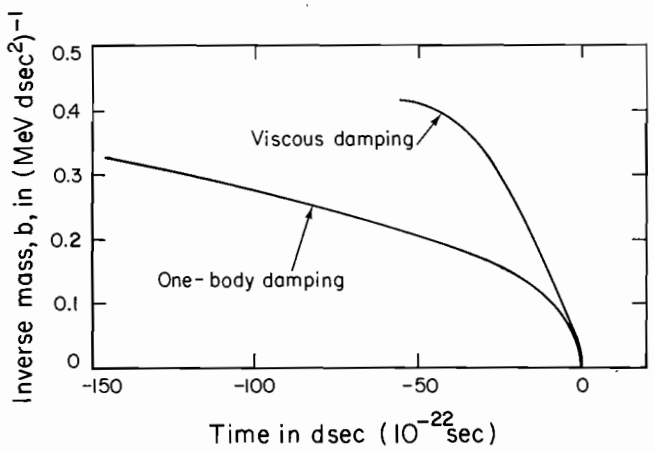

Fig. 1. The inverse mass b associated with the flow of neutrons and protons back and forth through the neck connecting the two halves of the fissioning nucleus ^{236}U is plotted against time. (XBL 809-1915)

almost no difference between the two predictions. In Fig. 2 the last part of Fig. 1 is shown on an expanded scale. In the lower half of the figure the quantity C, an adiabaticity variable developed in Ref. 2, is plotted for the case where the fission trajectory was calculated using viscous damping. C attains the critical value of 1.108 at $t_c = -1.11 \times 10^{-22}$ sec. This corresponds to a predicted charge dispersion of $\Gamma_f = 1.38$ which is somewhat smaller than the experimental value of 1.50. The quantity C for the case of the trajectory associated with one-body damping is not plotted since it lies nearly on top of the curve for viscous damping. Since the curves for b are so similar when freeze-out occurs, the predicted charge widths are nearly the same in the two cases. Consequently, we are forced to conclude that these considerations do not provide a means for choosing between the two fission trajectories.

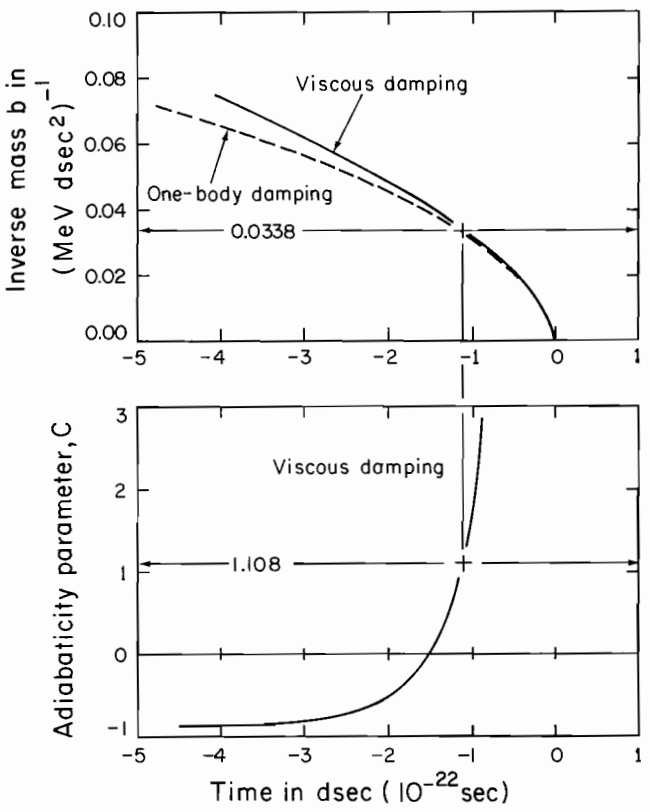

Fig. 2. The same two curves as appear in Fig. 1 are shown here on a greatly expanded scale. In addition the adiabaticity parameter is shown in the lower part of the figure for the viscous damping case. (XBL 809-1914)

Footnotes and References

*Condensed from Ref. 2.

†Max Planck Institut für Kernphysik, D-6900 Heidelberg, West Germany.

1. A.J. Sierk and J.R. Nix, Phys. Rev. C **21**, 982 (1980).
2. W.D. Myers, G. Mantzouranis and J. Randrup, Phys. Lett. B **98**, 1 (1981).

Correlated Mass and Charge Transport Induced by Statistical Nucleon Exchange in Damped Nuclear Reactions*

W.U. Schröder†, J.R. Huizenga† and J. Randrup

Extensive studies of damped nuclear reactions at energies a few MeV/u above the barrier have revealed a reaction mechanism intermediate between those of direct and compound-nucleus processes. Although not all degrees of freedom may reach statistical equilibrium in the course of a damped collision, many reaction features such as fragment distributions in A, Z and energy loss (E_{loss}) have been successfully interpreted in terms of classical or quantal transport models. Recently, however, narrow fragment isotopic mass and isobaric charge distributions have been observed, whose variances σ_A^2 (Z = const) and σ_Z^2 (A = const), respectively, saturate after an initial increase with E_{Loss}. This feature has been claimed[1] to be inconsistent with the picture of statistical exchange of individual

nucleons and has induced speculations about the existence of a fast collective mode of charge equilibration described in terms of a quantal harmonic oscillator coupled to thermal degrees of freedom.

The dominance of such a dinuclear quantal collective mode would call for a significant revision of the interpretation of damped reaction phenomena previously understood to be due to statistical processes. However, as shown in this work, the observed isobaric and isotopic fragment distributions can actually be quite well accounted for by an independent-particle transport mechanism. There appears to be no need to involve a collective mode of charge equilibration. To demonstrate this important fact, predictions are presented, for the first time, for isobaric and isotopic fragment distributions that are based on a model[2] of stochastic exchange of individual nucleons between the two collision partners.

In a transport approach, a two-dimensional Fokker-Planck equation is expected to govern the dynamical evolution of the probability P(N,Z;t) for finding N neutrons and Z protons in the projectile-like reaction partner. The physical information on the microscopic transition probabilities at each time t is contained in the transport coefficients V(N,Z;t) and D(N,Z;t). Average neutron and proton numbers are predicted to change with rates determined only by the drift coefficients only by the drift coefficients, according to $\partial\bar{N}/\partial t \simeq V_N$ and $\partial\bar{Z}/\partial t \simeq V_Z$, whereas the growth of the corresponding covariances of the probability distribution depends on diffusion and drift coefficients, as well as on the covariances already accumulated. Evaluated along the mean trajectory $[\bar{N}(t),\bar{Z}(t)]$, these growth rates can be written as:

$$\frac{\partial\sigma_N^2}{\partial t} \simeq 2\left(D_{NN} + \sigma_N^2\frac{\partial V_N}{\partial N} + \sigma_{NZ}\frac{\partial V_N}{\partial Z}\right) ,$$

$$\frac{\partial\sigma_N^2}{\partial t} \simeq 2\left(D_{ZZ} + \sigma_N^2\frac{\partial V_Z}{\partial Z} + \sigma_{NZ}\frac{\partial V_N}{\partial Z}\right) ,$$

$$\frac{\partial\sigma_{NZ}}{\partial t} \simeq 2D_{NZ} + \sigma_N^2\frac{\partial V_Z}{\partial N} + \sigma_Z^2\frac{\partial V_N}{\partial Z} + \sigma_{NZ}\left(\frac{\partial V_N}{\partial N} + \frac{\partial V_Z}{\partial Z}\right) . \quad (1)$$

The dispersion σ_A^2 of the mass number A = N + Z of the projectile-like fragment can subsequently be obtained from the relation $\sigma_A^2 = \sigma_N^2 + \sigma_Z^2 + 2\sigma_{ZN}$. In the derivation of Eqs. (1) from the Fokker-Planck equation, account is given of the confinements imposed on the transport processes by the variation of the drift coefficients with N and Z. These constraints, mainly due to curvature and alignment of the underlying time-dependent potential energy surface, are more respective for larger variances and enforce the proper equilibrium variances.

In order to arrive at quantitative predictions for mass and charge distributions of fragments from damped reactions and their variation with E_{loss}, the theory of Randrup[2] is employed in this study. In this model, transport of mass, charge, energy, linear and angular momentum in a damped reaction is attributed to the stochastic exchange of individual nucleons between the reaction partners, taking proper account of the Pauli exclusion principle.

The dynamical calculations of mean collision trajectories in the multidimensional coordinate space were performed by solving numerically the Lagrange-Rayleigh equations of motion for two spherical nuclei joined by a small cylindrical neck.

The predictions of the transport model[2] based on statistical exchange of individual nucleons are found to be in agreement with experimental fragment A and Z distributions. They also give a satisfactory account of data on other reaction properties such as energy losses and deflection functions. The observed variations of $\bar{A}/\bar{Z}$ and σ_A^2/σ_Z^2 ratios with E_{loss} are understood to reflect the strong interdependence between neutron and proton exchange processes imposed by the dynamical driving forces. Consistently, after an initial increase with E_{loss}, predicted isotopic mass and isobaric charge variances exhibit a saturation behavior in the E_{loss} range where this correlation is observed to be important for the ratios σ_A^2/σ_Z^2. The predicted drop in the variances for larger values of E_{loss} may not lend itself to a test by the data, before deexcitation processes of the primary fragments are more fully understood. The success of the model employed lends strong support to the predominance of incoherent nucleon exchange in the dynamics of incoherent nucleon exchange in the dynamics of damped nuclear reactions. Although the presence of collective charge equilibration and dissipation mechanisms cannot be excluded on grounds of the present study, no positive evidence in their support is seen in the data.

Footnotes and References

*Condensed from Phys. Lett. B **98**, 355 (1981).

†Departments of Chemistry and Physics and NSRL, University of Rochester, NY 14627.

1. M. Berlanger et al., Z. Phys. A **291**, 133 (1979).
2. J. Randrup, Nucl. Phys. A **307**, 319 (1978); A **327**, 490 (1979).

Correlated Charge And Mass Distributions From Reactions Of ^{56}Fe With ^{58}Ni And ^{64}Ni

H.C. Britt,[*] B.H. Erkkila,[*] A. Gavron, Y. Patin,[*] R.H. Stokes,[*] M.P. Webb,[*] P.R. Christensen,[†] O. Hansen,[†] S. Pontoppidan,[†] F. Videbaek,[†] R.L. Ferguson,[‡] F. Plasil,[‡] G.R. Young,[‡] M. Blann,[§] and J. Randrup

One of the primary subjects in the study of heavy ion reaction properties has been the attempt to understand the fundamental nature of the energy loss process in deep inelastic collisions. In the past several years a large number of macroscopic and microscopic models have been developed emphasizing radically different physical processes which may be important in various stages of the energy loss process. At the extreme of the current microscopic models are those based on transport theories that consider primarily the effects of the exchange of single nucleons between the two heavy ions during the collision process and theories that deal primarily with the damping of energy via an irreversible excitation of various collective surface vibrations or giant resonance modes in the two impinging nuclei. A priori it might be expected that the excitation of collective modes is most important in the early stages of the collision or in the very fast grazing collisions, whereas the nucleon exchange processes would become important at later times in more central collisions. The relative importance of these two energy damping modes has been a subject of considerable debate, but until recently, most theoretical-experimental comparisons had been of a qualitative nature and yielded ambiguous conclusions on the fundamental nature of the energy damping process.

Following the original attempts by Nörenberg to apply transport theory to the problem of heavy ion collisions, Randrup[1] has recently developed a more realistic transport theory that incorporates energy damping nucleon exchanges in a one-body dissipation approximation. An important feature of this model is that it incorporates effects due to the blocking of transfers to states below the Fermi sea because of the Pauli principle. This model has been compared to experimental mass and charge variances[2-4] and yielded good qualitative agreement for relatively heavy systems. In addition, it has given qualitative predictions for average deflection functions and properties of angular momentum transfer to the outgoing particles.[5] In all cases a reasonably good qualitative agreement was obtained between the experimental data and theoretical predictions of average properties of the outgoing particles. In most cases deviations could be at least partially ascribed to the neglect of the deexcitation process for the excited fragments.

We have made a detailed comparison of calculations using this transport theory with experiment for the systems ^{56}Fe + ^{56,64}Ni at bombarding energies of 315 MeV and 464 MeV. Moments of the neutron-proton distributions in the projectile-like fragment are compared as functions of kinetic energy loss. Quantitative comparisons are obtained by using theoretical final fragment distributions determined from the initial theoretical distribution by means of a Monte Carlo evaporation cascade. For energy losses greater than 10 MeV up to the beginning of the completely damped region the theoretical calculations, with no adjusted parameters, reproduce the measured first and second moments of the projectile-like NZ distributions almost exactly. This comparison suggests that the single-nucleon exchange mechanism provides an adequate framework for describing the damping of kinetic energy in the region between quasielastic and completely damped nuclear reactions. From these results, there seems to be no indication of other important energy damping mechanisms such as the excitation of collective modes. If there were an important mode that involved irreversible energy loss without particle exchange then we would have expected the experimental σ_A values to be less than the theoretical transport model predictions in some energy loss region. If the transfer of large chunks of nuclear matter were important we might have expected the experimental σ_A values to be larger.

The excellent agreement between theory and experiment also demonstrates that it is possible to make realistic evaporation corrections even for relatively light highly excited nuclei. However, it is necessary to generate theoretical final fragment distributions from calculated initial distributions rather than trying to recreate an initial experimental distribution from the measured final distribution.

Footnotes and References

[*]Los Alamos National Laboratory, Los Alamos, NM 87545.
[†]Niels Bohr Institute, University of Copenhagen, DK-2100 Copenhagen, Denmark.
[‡]Oak Ridge National Laboratory, Oak Ridge, TN 37830.
[§]Lawrence Livermore Laboratory, Livermore, CA 94550.

1. J. Randrup, Nucl. Phys. A **327**, 490 (1979).
2. W.U. Schröder, J.R. Birkelund, J.R. Huizenga, W.W. Wilcke and J. Randrup, Phys. Rev. Lett. **44**, 308 (1980).
3. P. Dyer, M.P. Webb, R.J. Puigh, and R. Vandenbosch, Phys. Rev. C **22**, 1509 (1980).
4. W.U. Schröder, J.R. Huizenga and J. Randrup, Phys. Lett. B **98**, 355 (1981).
5. A. Lazzarini, V. Metag, A.G. Seamster, R. Vandenbosch, and R. Loveman, Phys. Rev. Lett. **46**, 988 (1981).

Transport of Angular Momentum in Damped Nuclear Reactions*

Jørgen Randrup

During the last decade our understanding of damped nuclear reactions has increased steadily. Many of the characteristic features, such as the deflection function, the energy loss, and the angular momentum gain, can be understood by considering the classical motion of two idealized macroscopic nuclei interacting via conservative and dissipative forces. Furthermore, the accumulation of appreciable dispersions in the various macroscopic observables, such as the binary partition of the total mass and charge and the energies and spins of the emerging fragments, can be described as a transport process. Within such a framework the dissipative properties of the system are contained in the coefficients entering in the transport equation. While these transport coefficients can, to a large degree, be determined phenomenologically from data, their qualitative origin as well as their quantitative calculation still presents a major challenge in nuclear theory.

It is an outstanding feature of damped nuclear reactions that many nucleons are exchanged between the two interacting nucleides in the course of the collision process. (The large dispersions in the mass and charge of the final fragments testify to this fact.) Elementary kinematical considerations indicate that exchange of nucleons has a substantial effect on the dynamical state of the dinucleus. It is therefore essential to take account of this mechanism in the theoretical description of damped nuclear reactions.

Indeed, our estimates indicate that nucleon exchange plays a major, possibly dominant, role as a dissipative mechanism in damped nuclear reactions. Therefore, we have found it important to explore a model in which the only dissipative coupling between the two interacting nucleides is the exchange of nucleons. This idealization permits us to go far without introducing arbitrary assumptions and, in fact, enables us to calculate and interrelate a wealth of observables. In consequence, the subsequent comparison with data may lead to relatively unambiguous conclusions concerning the dissipation mechanism.

Towards this end, a general theory was developed for transport induced by nucleon exchange.[1] Subsequently, it was demonstrated that the theory provides a good understanding of the relation between energy loss and particle-number dispersion[2] as well as of the interrelation between charge and mass exchange.[3] In view of this success, it is important to broaden the confrontation with experiment by considering other observables as well. Therefore, we focus on the angular-momentum related observables, which are more complicated but also encompass a richer variety of physical phenomena.

At first, after outlining the description of nuclear dynamics within the framework of transport theory in general terms, we consider the dynamics of the rotational degrees of freedom in the dinucleus and derive and discuss the appropriate equations of motion. Subsequently some illustrative applications of the theory are made to cases of experimental interest. The characteristic features observed for the spin distributions of the fragments are well reproduced by the model calculations, although a precise comparison must await the proper inclusion of the deexcitation processes.

The model, being fully dynamical, permits detailed studies of the relaxation phenomena and, in fact, it predicts significant nonequilibrium behavior, particularly for partially damped reactions.

The only dissipative mechanism considered is the exchange of nucleons. In consequence, several observables are fundamentally related. To gain more definite insight into the reaction mechanisms, it is likely that one must consider several observables simultaneously. Therefore, more refined experiments are called for. As a specific example, it is suggested that attempts be made to measure the degree of mutual alignment of the two reaction products. Such an experiment would provide novel information which would help discriminate between different models and thus improve our understanding of the reaction mechanism.

Footnotes and References

*Condensed from LBL-12676; Nucl. Phys. A in press.

1. J. Randrup, Nucl. Phys. A **327**, 990 (1979).
2. W.U. Schröder et al., Phys. Rev. Lett. **44**, 308 (1980).
3. W.U. Schröder, J.R. Huizenga and J. Randrup, Phys. Lett. B **98**, 355 (1981).

Equilibrium Statistical Treatment of the Spin Fluctuations Generated in Deep-Inelastic Reactions

A.J. Pacheco, R.P. Schmitt† and L.G. Moretto*

One of the distinctive features of heavy-ion collisions is a large angular-momentum transfer from relative motion to intrinsic degrees of freedom.[1] It has been found experimentally that in many reactions the rotational degrees of freedom reach complete relaxation, i.e., the dinuclear complex rotates rigidly about an axis perpendicular to the line between centers. Recent experiments have also shown that the rigid-rotation limit is but an average regime about which large fluctuations occur, and as a consequence, one observes in the exit channel a probability distribution for both the magnitude and orientation of the spins of the outgoing fragments. In a recent work Moretto and Schmitt[2] have proposed an equilibrium statistical model to account for the production of random spin components in a system of two equal rigid spheres in contact. The purpose of the present work is to extend this equilibrium statistical treatment to systems of arbitrary mass asymmetry.

The most general configuration of the system is completely determined by the spins of the heavy and light fragments ($\vec{S}_H$ and $\vec{S}_L$) and by the orbital angular momentum ($\vec{\ell}$). In order to describe the normal modes, it is convenient to define a set of "spin-excess" variables $\Delta\vec{S}_H$ and $\Delta\vec{S}_L$ by means of the equations:

$$\vec{S}_{H(L)} = \vec{R}_{R(L)} + \Delta\vec{S}_{H(L)} \ , \qquad (1)$$

where $\vec{R}_H$ and $\vec{R}_L$ are the spins of the fragments arising from rigid rotation about an axis perpendicular to the line of centers and with a total angular momentum $\vec{I} = \vec{S}_H + \vec{S}_L + \vec{\ell}$. The normal coordinates (two for each cartesian axis) are constructed as suitable linear combinations of $\Delta\vec{S}_H$ and $\Delta\vec{S}_L$. Two of these normal modes (tilting and twisting) generate spin components along the direction of symmetry (y-axis). The other four modes (two wriggling and two bending) produce spin components on a plane perpendicular to it (x-z plane).

The physical interpretation of the modes is given in Fig. 1. Curve a) shows the dependence of the ratio

$$\frac{\Delta\vec{S}_H)_{xz}}{\Delta\vec{S}_L)_{xz}}$$

as a function of mass asymmetry for the wriggling mode. In this case both fragments have their spin vectors pointing in the same direction, and as the asymmetry increases the heavy fragment carries an increasing fraction of the angular momentum. The opposite behavior is predicted for bending as indicated by the fact that the same curve a) represents the ratio

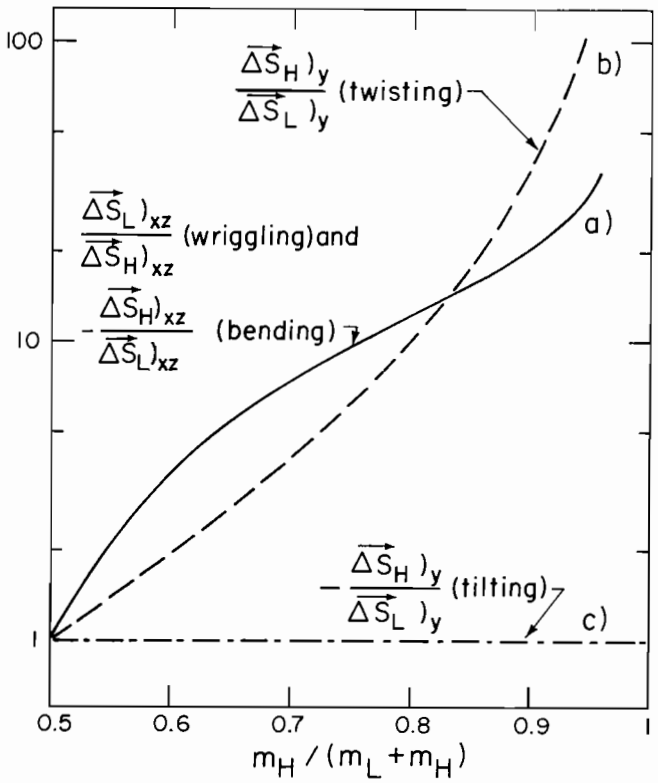

Fig. 1. Illustration of the normal modes as a function of mass asymmetry, based on the relative amounts of spin going into the heavy and light fragments. (XBL 818-2423)

$$-\frac{\Delta\vec{S}_L)_{xz}}{\Delta\vec{S}_H)_{xz}}$$

for this mode. The interpretation of the twisting and tilting modes does not differ from that given in Ref. 1 for a symmetric system.

The dependence of the reduced variances of the spin distribution as mass asymmetry is shown, for each mode, in Fig. 2. The overall variances for each cartesian coordinate have simple analytical expressions in terms of the relevant moments of inertia of the system:

$$\sigma^2_{H(L)} \equiv \sigma^2_{WR} + \sigma^2_{BE} = \frac{\vartheta_{H(L)}[\vartheta_{L(H)} + \mu R^2]}{\vartheta_L + \vartheta_H + \mu R^2}$$

for the x and z directions , (2)

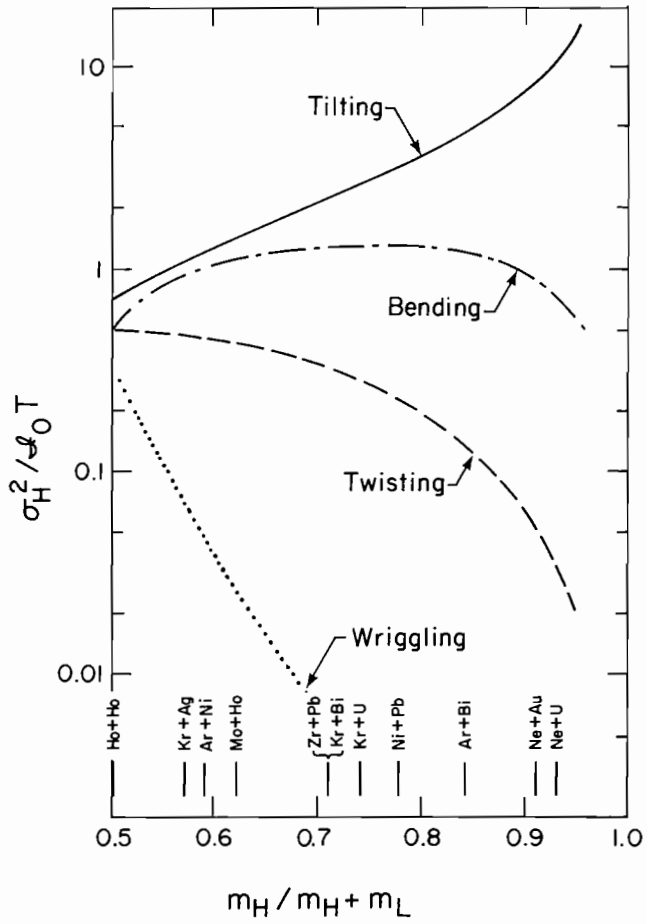

Fig. 2. Contribution from each mode to the reduced variances of the spin distribution in the heavy fragment (ϑ_0: moment of inertia of a sphere of mass $(m_H + m_L)/2$, T: nuclear temperature). (XBL 812-2114A)

$$\sigma^2_{H(L)} \equiv \sigma^2_{TW} + \sigma^2_{TI} = \frac{\vartheta_{H(L)}[\vartheta_{H(L)} + \mu R^2]}{\mu R^2}$$

for the y direction . (3)

Equations (2) and (3) and Fig. 2 indicate that at very large asymmetries the spin fluctuations in the heavy fragment occur mainly along the symmetry axis. Such effect should be detectable by measuring in-plane angular distribution of the sequential-fission fragments.

Footnotes and References

*Permanent address: Comisión Nacional de Energía Atómica, Buenos Aires, Argentina.

†Present address: Cyclotron Institute and Department of Chemistry, Texas A&M University, College Station, TX 78843.

1. M. Lefort and C. Ngô, Riv. Nuovo Cimento **2**, 12 (1979) and references therein.

2. L. G. Moretto and R.P. Schmitt, Phys. Rev. C **21** (1980).

Systematics of Angular Momentum Transfer in Intermediate Energy Heavy-Ion Reactions*

C.C. Hsu,† D.J. Morrissey,‡ L.W. Richardson, G.J. Wozniak, and L.G. Moretto

An important question regarding heavy-ion collisions is how the reaction mechanism evolves from the statistical equilibrium observed in the low energy regime to the completely nonequilibrium processes observed in the relativistic regime. At bombarding energies of a few MeV/A over the Coulomb barrier, the two heavy-ions undergo a gentle collision. As the bombarding energy increases, the collision becomes harder. At intermediate velocities, new reaction processes may occur which should be amenable to kinematic analysis if the collisions are not too violent.

A detailed study[1] of the linear momentum transfer has demonstrated that the $^{16}O + ^{238}U$ reaction deviates from two-body kinematics at a bombarding energy of 20 MeV/A. It would be interesting to determine whether similar deviations exist for other reaction systems and the bombarding energy dependence of any deviation. In this article, we present a complementary technique for studying the two-body character of a heavy-ion reaction with nonfissioning products. In this technique we indirectly determine the linear momentum transferred to the product nucleus by measuring the angular momentum converted into intrinsic spin via γ-ray multiplicity (M_γ) techniques. The connection between the linear and angular momenta transferred in peripheral reactions is straight forward because a localized linear impulse on the periphery of the target nucleus gives rise to a torque which causes the target nucleus to spin.

The intrinsic spin can be calculated in a simple model as a function of the detected fragment's mass and energy. This simple model assumes a two-body reaction, a tangential collision, an average impact parameter, and no radial damping. The intrinsic spin, I, that would be created by a highly localized tangential force at the nuclear surface can be estimated rather simply: the torque, τ, is equal to the time integral of the force, F(t) crossed into the radius at which it acts:

$$\tau = \int R(t) \times F(t)\, dt \quad . \qquad (1)$$

If the force is tangential and sharply peaked at some radius, $\bar{R}$, then the integral can be replaced by: $\tau = \bar{F}\, t\, \bar{R}$, where $\bar{F}$ is an average force. The connection to linear momentum balance is now obvious because the linear impulse, Δp, can be written as:

$$\Delta p = \int F(t)\, dt \quad . \qquad (2)$$

For a localized force, $\Delta p = \bar{F}t$, the angular momentum is the change in linear momentum times the average radius at which is it created, $I = \Delta p\, \bar{R}$. A similar analysis with the explicit matching of the entrance channel orbital angular momentum to that in the exit channel has been suggested as a tool for the analysis of light-ion reactions.[2] Assuming that the orbital angular momentum is completely aligned in the entrance and exit channels, we can write a classical expression for the transferred spin: $L_i = L_f + \langle I_{TOTAL} \rangle$ in terms of the orbital angular momenta in the entrance and exit channels, L_i and L_f, respectively. These orbital angular momenta are calculated from the kinetic energies.

The strong as well as the weak points of our picture of the spin transfer can be seen in Fig. 1 where the observed value of the total intrinsic spin is plotted against the calculated value. The spin transfer is nearly equal to the simple estimate at low bombarding energies and roughly only half that at higher energies. Perfect agreement between theory and experiment would, of course, yield a straight line with a slope equal to one and an intercept of (0,0). However, the discrepancies may be more apparent than significant in light of the simplicity of the model. At the lowest energies Fig. 1 shows a small discrepancy between the model and the data, the slope is $\sim$ 0.8 rather than 1. There is a dramatic decrease in the slope at 17 MeV/nucleon which is also observed at higher bombarding energies. At 17 MeV/A and above, the spin transfer is less than half that observed at lower energies for producing the same product at the same energy loss at the grazing angle. The

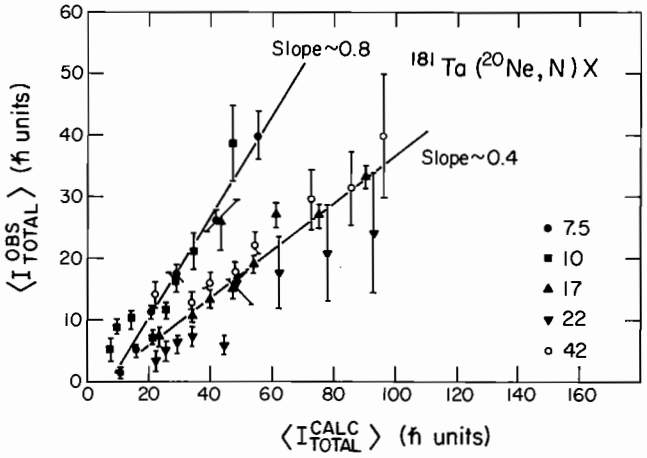

Fig. 1. The calculated total spin $\langle I_{TOTAL}^{CALC} \rangle$ is plotted against the observed total spin. Perfect agreement between model and experiment would give a slope of 1, the grouping of the data by the bombarding energy is discussed in the text. (XBL 818-2426)

simple model that we have used is based on momentum balance between the entrance and exit channels where both channels were assumed to have only "two bodies." However, if an excited projectile residue breaks up into two or more bodies then this simple model will overestimate the spin transfer, because it assumes all missing momentum has been captured by the target nucleus. The explanation of the decrease in the observed spin transfer at high bombarding energies requires a breakdown of the assumption that the exit channel is two body. This is in agreement with the results of Back et al. on linear momentum transfer at 20 MeV/A. However, it is somewhat surprising that at 17 MeV/nucleon projectile breakup seems to be the predominent process.

Footnotes and References

*Condensed from LBL-12519, submitted to Nuclear Physics A.

†Permanent address: Institute of Atomic Energy, Beijing, People's Republic of China.

‡Permanent address: Department of Chemistry, Michigan State University, East Lansing, MI 48824

1. B.B. Back et al., Phys. Rev. C **22**, 1927 (1980).
2. D.M. Brink, Phys. Lett. B **40**, 37 (1972).

Shell Effects on the Angular-Momentum Transfer in Heavy-Ion Reactions

*L.G. Moretto and A.J. Pacheco**

The measurement of γ-ray multiplicities in heavy-ion reactions provides information on the sum of the spins generated in both fragments. The dependence of this quantity upon the total kinetic energy loss reflects the interplay between the relaxation time of the rotational degrees of freedom and the interaction time associated with a given entrance-channel angular momentum. We present here a very simple model of this process and we use it to calculate the effects that are expected in reactions in which one of the partners is a closed-shell nucleus.

In our model we describe the dinuclear complex by means of two touching spheres with spins S_1, S_2, and orbital angular momentum L. The relaxation of the rotational modes of the system as a function of interaction time is expressed by:[1]

$$S_1 + S_2 = \frac{\vartheta_1 + \vartheta_2}{\vartheta_1 + \vartheta_1 + \mu R^2} \left(1 - e^{-t/\tau_R}\right) I \qquad (1)$$

where ϑ_1 and ϑ_2 are the moments of inertia of the nuclei, μ is the reduced mass of the system, R is the distance between centers, τ_R is the relaxation time constant, and I is the total angular momentum. For the dependence of the interaction time on I, we assume the following analytical expression:

$$t = \tau_I \ell n \left(\frac{I_{MAX}}{I}\right) \qquad (2)$$

where I_{MAX} is the maximum angular momentum corresponding to a grazing collision and τ_I is a constant time. From Eqs. (1) and (2) the spin transferred to the fragments can be related to the total angular momentum:

$$\frac{I}{I_{MAX}} = 1 - \frac{\vartheta_1 + \vartheta_2 + \mu R^2}{\vartheta_1 + \vartheta_2} \frac{S_1 + S_2}{I} \tau_R/\tau_I \qquad (3)$$

If we restrict ourselves to the case of short-lived peripheral collisions

$$\frac{S_1 + S_2}{I} \ll \frac{\vartheta_1 + \vartheta_2}{\mu R^2 + \vartheta_1 + \vartheta_2}$$

we can find an analytical solution for I, which may in turn be used in the expression of the orbital kinetic energy:

$$\frac{E}{E_{MAX}} =$$

$$\frac{1}{4}\left[1 + \sqrt{1 - \frac{4\left(\vartheta_1+\vartheta_2+\mu R^2\right)}{\vartheta_1+\vartheta_2} \frac{\tau_R}{\tau_1} \frac{S_1+S_2}{I_{MAX}} - \frac{2\left(S_1+S_2\right)}{I_{MAX}}}\right]^2$$

where $E_{MAX} = I^2_{MAX} / 2\mu R^2$. The exact solution for the reduced orbital energy $\epsilon = E/E_{MAX}$ as a function of the reduced total spin

$$S = \frac{7}{2} \frac{(S_1 + S_2)}{I_{MAX}}$$

is shown in Fig. 1a for a mass-symmetric system and four different values of the ratio τ_R/τ_I. Figure 1b illustrates the prediction of the model for the case in which one of the two fragments is magic and has zero angular momentum (this is of course an extreme approximation).

We shall now discuss another aspect of the same problem, namely the extent to which shell effects are present in the second moments of the spin distribution.[2] The dependence of the fluctuations induced in one fragment upon the moment of inertia of the other is shown in Fig. 2. The reduced variance along the symmetry axis is constant as a consequence of an exact cancellation between a stiffer twisting mode and a softer tilting mode as one approaches the closed-shell limit

$$\left(\frac{\vartheta_2}{\vartheta_1} = 0\right) .$$

Due to a similar effect the fluctuations on a plane perpendicular to the symmetry axis, although not constant, are also very insensitive to variations of the ratio $_1/\ _2$.

Footnote and References

*Permanent address: Comision Nacional de Energía Atómica, Buenos Aires, Argentina.

1. S. Ayik, G. Wolschin and W. Nöremberg, Z. Phys. A **286**, 271 (1978).
2. A.J. Pacheco, R.P. Schmitt, and L.G. Moretto, in this annual report.

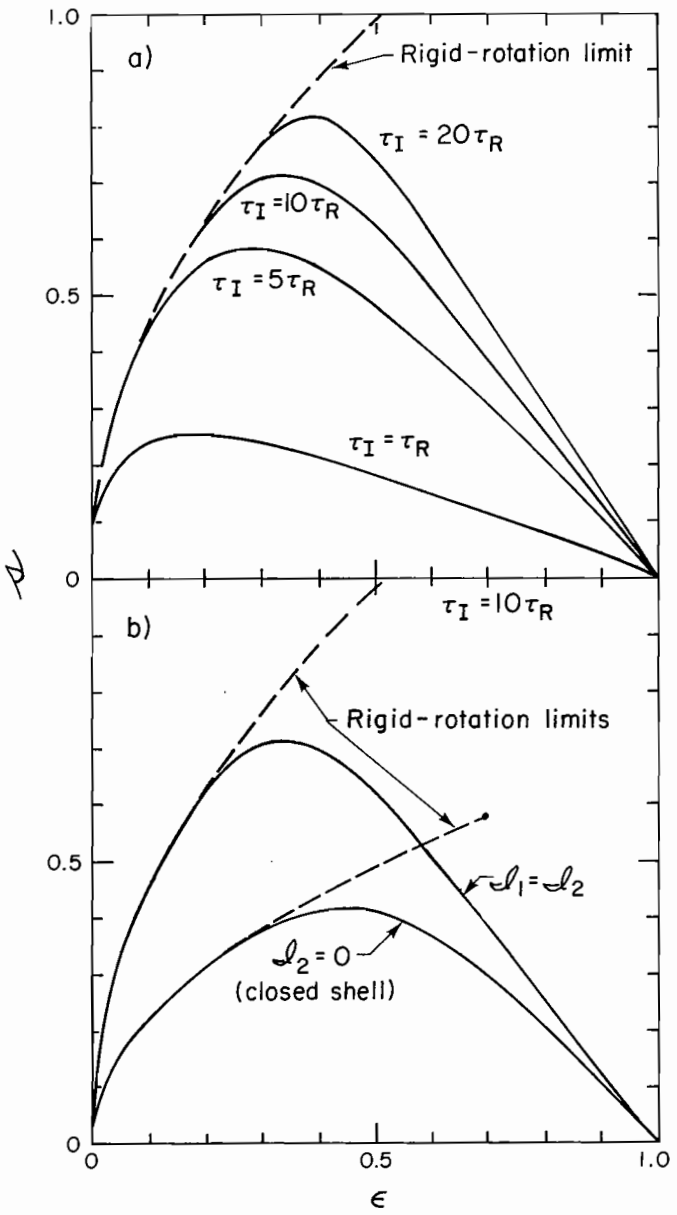

Fig. 1. Reduced orbital kinetic energy vs reduced sum of the spin of a mass-symmetric system, a) for different values of the ratio τ_I/τ_R and b) for two values of ϑ_2/ϑ_1. (XBL 818-2425)

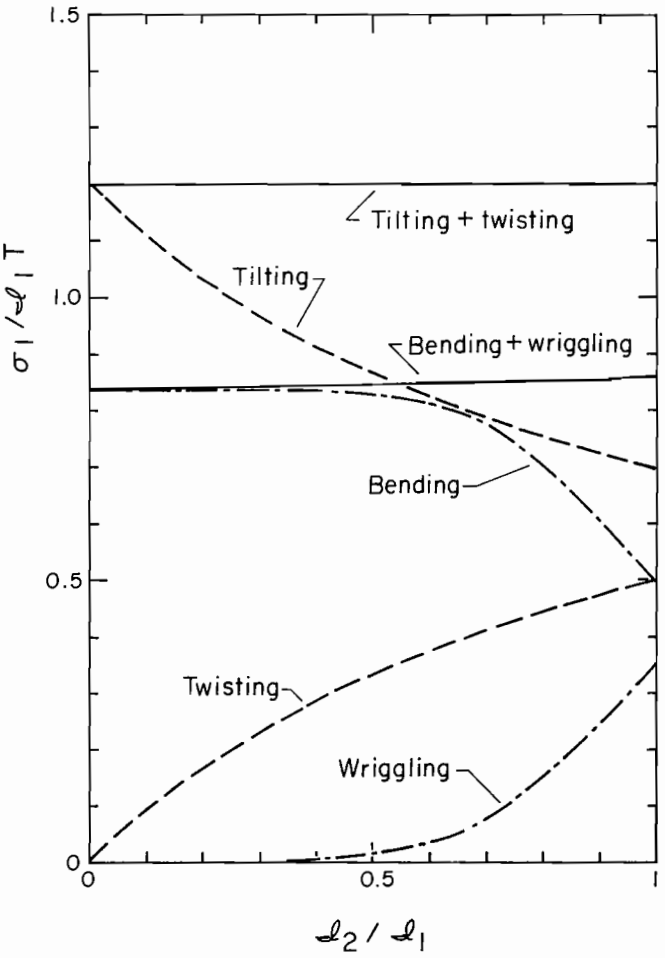

Fig. 2. Reduced variances of the spin distribution of fragment 1 as a function of the moment of inertia of fragment 2 for a mass-symmetric system. (XBL 818-2424)

The Influence Of Fluctuations On The Correlation Between Exit-Channel Kinetic Energy And Entrance-Channel Angular Momentum For Heavy Ion Collisions*

L.G. Moretto and L.G. Sobotka

The role of fluctuations on the relationship between the exit-channel kinetic energy and the entrance-channel angular momentum in deep inelastic heavy ion reactions has been studied in the equilibrium limit. Two sources of fluctuations are considered: first, the coupling of the orbital motion to thermally excited angular-momentum-bearing modes, and the second, the effect of random shape fluctuations at scission.

Let us consider the simple analytical case of two equal touching spheres with one wriggling mode[1] coupled to the orbital motion. Using a 2IdI weight, where I is the entrance channel angular momentum, the distribution function is

$$P(\epsilon,\lambda)\, d\epsilon d\lambda \propto \frac{\lambda}{\sqrt{\epsilon}} \exp -\left[\frac{7}{2}\epsilon - \sqrt{\frac{5}{2}}\lambda\sqrt{\epsilon} + \frac{5}{28}\lambda^2\right] d\epsilon d\lambda \quad . \quad (1)$$

Here ϵ and λ are reduced variables defined by $\epsilon = E/T$ and $\lambda = I/(\vartheta T)^{1/2}$, where E is the exit channel kinetic energy over the Coulomb barrier, T is the nuclear temperature, and ϑ is the moment of inertia of one of the two spheres. The properties of this distribution function can be observed in the two-dimensional plot in Fig. 1, where we see that the one to one correspondence between exit channel energy and entrance channel angular momentum is substantially perturbed.

Shape fluctuations at scission arise because of the reasonably flat dependence of the total potential energy as a function of deformation and of the rather steep dependence of the two-fragment Coulomb interaction.

Therefore, a small (energy-wise) fluctuation at scission, of the order of 1/2 T in the thermal limit, leads to an amplified fluctuation in the final kinetic energy.[2]

As an example, let us consider the system Fe + Fe. The overall features of the probability distribution, $P(E_{TKE},I)$, are shown by the two-dimensional plot in Fig. 2. While the centroid of the energy distribution at fixed ℓ moves towards higher values with increasing ℓ, the width also increases, leading to a dramatic overlap of distributions with widely different ℓ-values. Most interesting are the entrance-channel angular momentum distributions for a variety of exit-channel kinetic energies. These distributions are so broad that at any kinetic energy the whole ℓ-wave spectrum is substantially sampled. Again we see that the correlation between exit-channel kinetic energy and entrance-channel angular momentum is quite problematic.

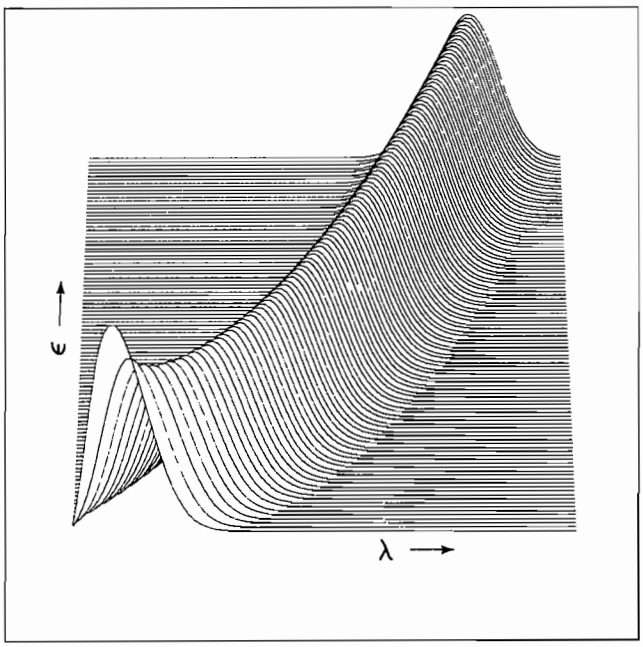

Fig. 1. Two-dimensional plot of the distribution function given in Eq. (1). (XBL 815-2268)

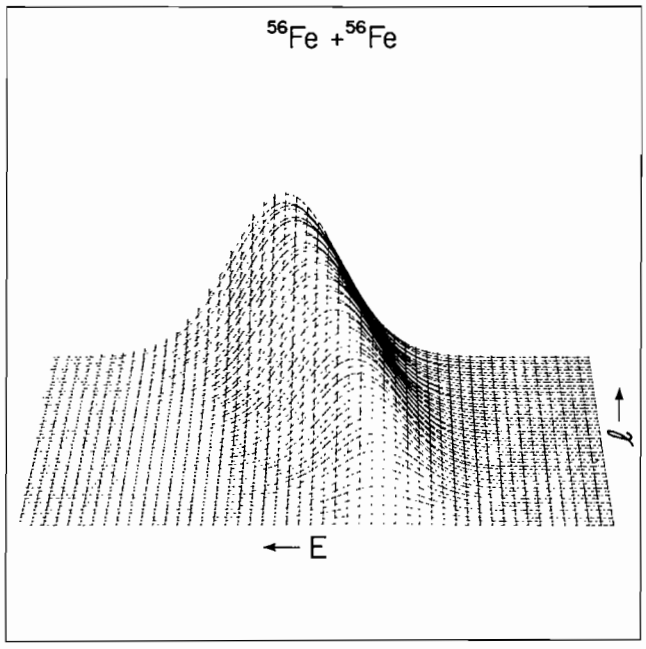

Fig. 2. Two-dimensional plot of the emission probability as a function of entrance-channel angular momentum and exit-channel kinetic energy. (XBL 815-2267)

Footnotes and References

*Condensed from LBL-13007.

1. L.G. Moretto and R.P. Schmitt, Phys. Rev. C **21**, 204 (1980).
2. L.G. Moretto, Nucl. Phys. A **247**, 211 (1975).

On the Use of Isomer Ratios in ^{44}Sc for Predicting Spin Populations in High Energy Heavy Ion Nuclear Reactions

H. Groening, K.J. Moody and G.T. Seaborg*

It has been suggested that isomer ratios can be used to determine the spin distributions in the evaporation chains of different products formed in spallation reactions.[1] By following the methodology described in Ref. 2 to fit the isomer ratio dependence on energy for the reaction ^{29}Si(^{18}O,p2n) ^{44}Sc^{m}, ^{44}Sc^{g}, we have also made a fit of the isomer ratio dependence on energy[3] for the reaction ^{41}K(α,n) ^{44}Sc^{m}, ^{44}Sc^{g}, using the same set of parameters. Figure 1 shows the positions of the calculated ^{44}Sc* population averages in the E-J plane for both reactions, joined by "tie" lines that define regions of equal isomer ratios. Our results show that isomer ratios can be used to predict angular momentum distributions in ^{44}Sc* populations, particularly if such ratios are low. As the ratios become higher, the average energy becomes as important a factor as the average spin, thereby making unique identifications of such properties difficult.

Figure 2 shows in semilog plot the average excitation energy vs average spin for ^{44}Sc* and also for the ^{47}Ti* precursor. Tie line (AB), which joins two points with equal excitation energies gives rise to a common isomer ratio, suggesting that isomer ratios offer little hope in identifying uniquely spin properties of ^{44}Sc precursors, even if the average energies are known. This situation is expected to deteriorate as such average energies increase.

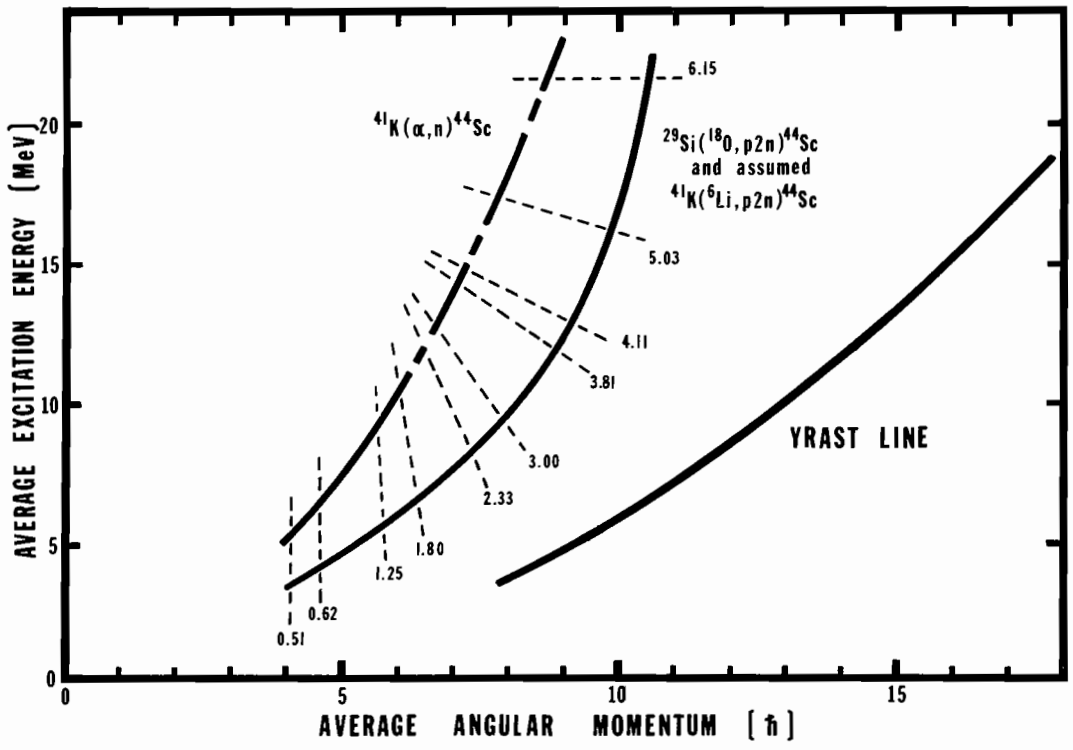

Fig. 1. Calculated centroids of population distributions in ^{44}Sc* for the reactions ^{29}Si(^{18}O,p2n) ^{44}Sc* and ^{41}K(α,n) ^{44}Sc*. Dashed lines join regions of population averages that give rise to equal isomer ratios. (XBL 818-11297)

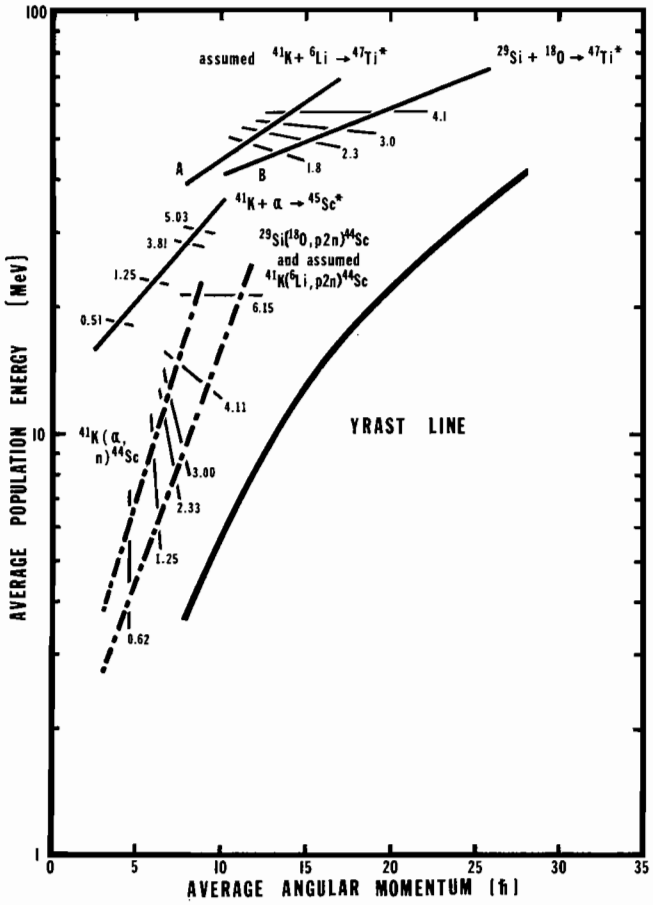

Fig. 2. Same as Fig. 1 except that partial average population regions in $^{47}Ti^*$ that give rise to a common isomer ratio in $^{44}Sc^*$ are also included. Also shown are partial regions in $^{45}Sc^*$ that result in given isomer ratios in $^{44}Sc^*$. (XBL 818-11294)

Footnote and References

*On leave from Universidad Simón Bolívar, Caracas, Venezuela.

1. G. Rudstam, Physica Scripta **20**, 165 (1979).
2. H. Groening, K. Aleklett, K.J. Moody, P.L. McGaughey, W. Loveland and G.T. Seaborg, in this annual report.
3. C. Riley, K. Ueno, and B. Linder, Phys. Rev. **135**, B1340 (1964).

Pre-Equilibrium Nucleon Jets in TDHF Calculations of Medium-Energy, Heavy-Ion Collisions

H. Stöcker, R.Y. Cusson,†‡ J.A. Maruhn,‡ and W. Greiner‡*

Recent experiments with the new 85 MeV/A ^{12}C beam at CERN[1] have further stimulated the current interest in the intermediate bombarding energy range 20 MeV/A $\leq E_{Lab}/A_{proj} \leq$ 200 MeV/A. Our study of the ^{12}C(30 MeV/A) + ^{198}Au reaction shows three interesting regions of impact parameter b (Ref. 2; see Fig. 1): i) deep-inelastic scattering in the grazing region, b $\sim$ 9 fm, ii) complete disintegration of the projectile, which escapes as fast, forward peaked preequilibrium nucleon jet, and PEP's in the full overlap region 0 $\leq$ b $\leq$ 4.25 fm, and iii) the partial overlap region 4.25 $\lesssim$ b $\lesssim$ 9 fm, where several phenomena can occur in varying proportions: a) jet emission at finite angles, b) generally unfocused pre-equilibrium emission, and c) massive transfer, where the remainder of the projectile can orbit around the target. Our results at 85 MeV/A (see Fig. 1) are similar to the 30 MeV/A ones in region i) and ii). However, in the intermediate region iii), one can no longer distinguish three separate processes. Instead, one observes the pieces of a partially broken up projectile at negative angles, and remnants of both jets and unfocused pre-equilibrium emission are found.

The formation of a typical nucleon jet is illustrated in Fig. 1 (b = 1 fm, E_{Lab} = 30 MeV): Once the ^{12}C nucleons have entered the target, they expand inside the

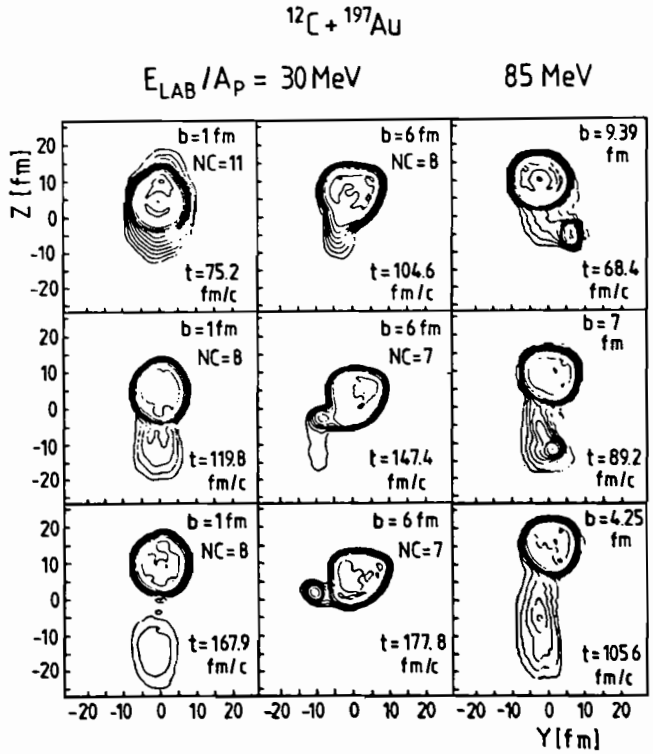

Fig. 1. Contours of constant density in the scattering plane of $^{12}C \rightarrow {}^{197}Au$ collisions. (XBL 8110-12216)

much larger Au nucleus. This is similar to the spreading of a wave packet in free space. By examining the current distributions, one finds that the expansion is accompanied by a strong velocity dispersion, where the various components move apart from each other with $V_{proj} - V_F \lesssim V \lesssim V_{PEP}$, according to their Fermi momenta. First, the fastest particles escape with $V_{PEP} \sim V_{proj} + V_F$ at very low density $p \sim 10^{-3}\ \rho_0$. We find only a very small amount of these quasi-free PEP's. At somewhat later time ($t = 120$ fm/c) strong preequilibrium jet emission of ~ 8 of the projectile nucleons is observed at $\sim 5\%\ \rho_0$ at smaller velocities (see Fig. 1). The jet should be observable as individual nucleons at forward angles and with a broad energy distribution extending above the thermal evaporation range. At the intermediate impact parameters, generally unfocused preequilibrium emission accompanies the jet emission, as well as backward scattered low energy projectile fragments (see Fig. 1).

The target is not destroyed after the emission of the jet, although 15-40% of the incident momentum and all of the incident ^{12}C binding energy are absorbed by the Au target. This is not sufficient to provoke complete spallation but may result in copious evaporation of nucleons before fission.[1] The recoil momenta determined from target fission measurements[1] are larger than the values predicted here. The correct values should come from the including of n-n collisions neglected here. The general picture emerging is thus that complete fusion at low energy gives way gradually to massive transfer and to the jet process reported here and the number of escaping nucleons rises with E_{Lab} until most of the projectile nucleons come out unbound.

Footnotes and References

*LBL and GSI, Darmstadt, West Germany.
†Permanent address: Department of Physics, Duke University, Durham, NC 27706.
‡Institut für Theoretische Physik, Universität Frankfurt and Oak Ridge National Laboratory, Oak Ridge, TN.

1. GSI-Heidelberg-Münster collaboration, U. Lynen et al.; Marburg-Oslo-CERN collaboration, T. Lund et al.,; Grenoble-Lund-CERN collaboration, H. Niefenecker et al. (all to be published).
2. H. Stöcker et al., Phys. Lett. **1018**, 379 (1981).

Explosion-Evaporation Model for Fragment Production in Intermediate-Energy Nuclear Collisions*

George Fái and Jørgen Randrup

The disassembly of a piece of hot (20-200 MeV/nucleon) nuclear matter is described as a two-stage process. In the primary, fast stage (which is referred to as the explosion) the system quickly fragments into free nucleons and composite nuclei according to available phase space. (At higher energies pion creation may also be significant.) The ejectiles produced in the explosion have to be stable on a time scale characteristic of this violent process. In the present work we include all states having a width $\Gamma < 1$ MeV.

The metastable products of the explosion will subsequently decay further on a slower time scale in a relaxation process, first by sequential emission of light particles, later by gamma decay. This secondary stage is referred to as the evaporation.

Following Ref. 1, we assume that the explosion populates phase space statistically. Employing the grand canonical approximation, we calculate the partition function

$$Z = \sum_f e^{-\beta(E_f - \mu A_f - \nu T_f)} \quad . \tag{1}$$

The sum extends over all possible final states f. The Lagrange multipliers, β, μ, ν are adjusted to ensure that the ensemble average of the total energy E_f, baryon number A_f, and isospin T_f are equal to the prescribed values E_o, A_o, and T_o.

For given values of the available excitation energy per nucleon ϵ, the asymmetry $I = (N-Z)/A$, and the available volume at disassembly [in units of the reference volume $(4\pi r_o^3 A_o)/3)$] χ, the Lagrange multipliers β, μ, ν are determined by solving the three constraint equations. Subsequently, the partition function can be constructed, yielding the information on the system immediately after the primary explosion.

In describing the evaporation stage, we include the most frequently emitted light particles: neutrons, protons and alpha particles.

A few instructive results are shown in the figures. In Fig. 1 we compare the relative yields of final fragments (full histogram) to those prior to the evaporation stage (dashed histogram) in one particular example.

The change of the relative abundancies of the various fragment species in the evaporation phase significantly affects the final deuteron-to-proton yield ratio, d/p. This general feature makes it essential to take account of the decay of composite fragments before using d/p as a measure of the entropy of the initial source, as has been attempted in Ref. 2.

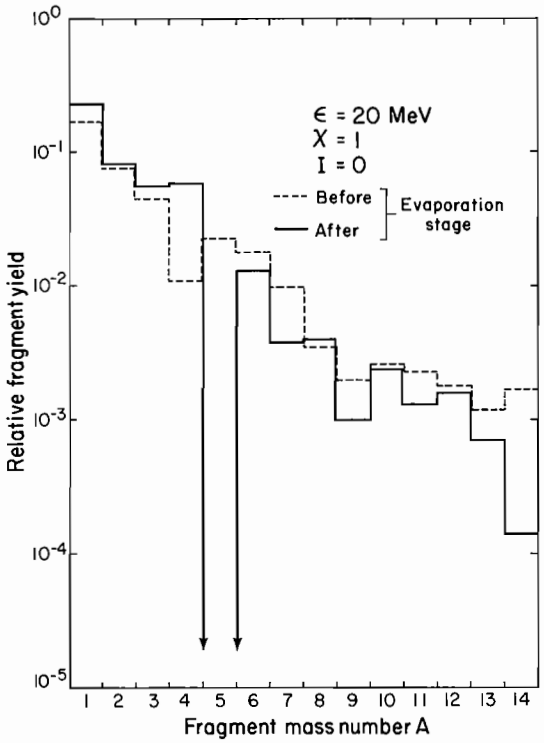

Fig. 1. (XBL 816-3190)

Figure 2 displays the d/p ratio obtained for several values of the parameters χ and I in our model as a function of the available excitation energy per participant nucleon ϵ. The comparison of our results to the experimental data of Nagamiya et al.[3] can only be considered a qualitative one at this point. The source is identified with the participant nucleons and is assumed to consist of projectile and target matter according to the standard sharp sphere geometry; the total center-of-mass energy is assumed to be available for excitation. The data points are included in Fig. 2. The theoretical curves represent expected extreme limits of the parameter range. In our model the final relative abundancies are sensitive to the extension of the primary breakup in space and time, and the measurement of composite fragment yields may therefore elucidate the details of the disassembly process.

While existing dynamical theories, such as the intranuclear cascade and nuclear fluid dynamics, only yield a kind of matter distribution emerging from the nuclear collision, the present model incorporates actual physical fragments. So far we have focused on the relative fragment yields but the spectra can also be obtained in a straightforward manner. The model may thus offer a convenient augmentation of existing dynamical theories for intermediate-energy nuclear collisions.

Footnotes and References

*Condensed from LBL-26261.

1. J. Randrup and S.E. Koonin, Nucl. Phys. A **356**, 223 (1981).

2. P.J. Siemens and J. Kapusta, Phys. Rev. Lett. **43**, 1486 (1979).

3. S. Nagamiya et al., Lawrence Berkeley Laboratory Report LBL-12123 (1981).

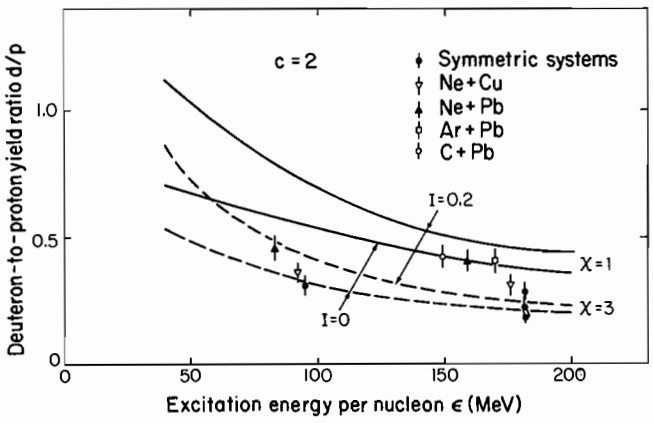

Fig. 2. (XBL 816-3191)

Pion, Light Fragment, and Entropy Production in Nuclear Collisions*

H. Stöcker

The production of pions and light fragments in fast nuclear collisions is calculated in a relativistic fluid dynamical model. We include viscous effects and a chemical equilibrium model of particle production. The linear bombarding energy dependence and, in particular, the absolute values of the calculated pion, production, and deuteron yields are found to be in agreement with the experimental data. The previous discrepancy between the calculated entropy and the measured d/p ratio is resolved.

Footnote

*Based on LBL-12302.

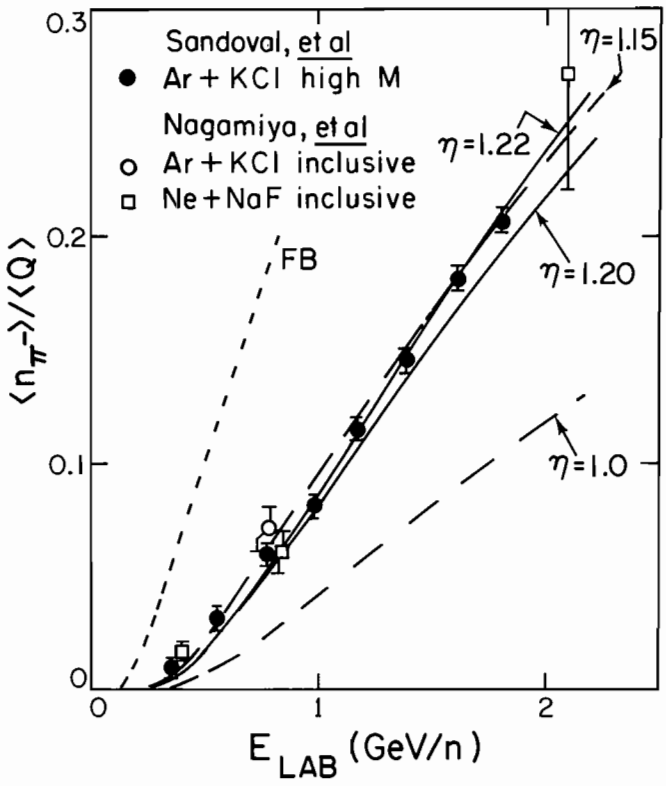

Fig. 1. Bombarding energy dependence of the mean number of pions per nuclear fragment. (XBL 814-652)

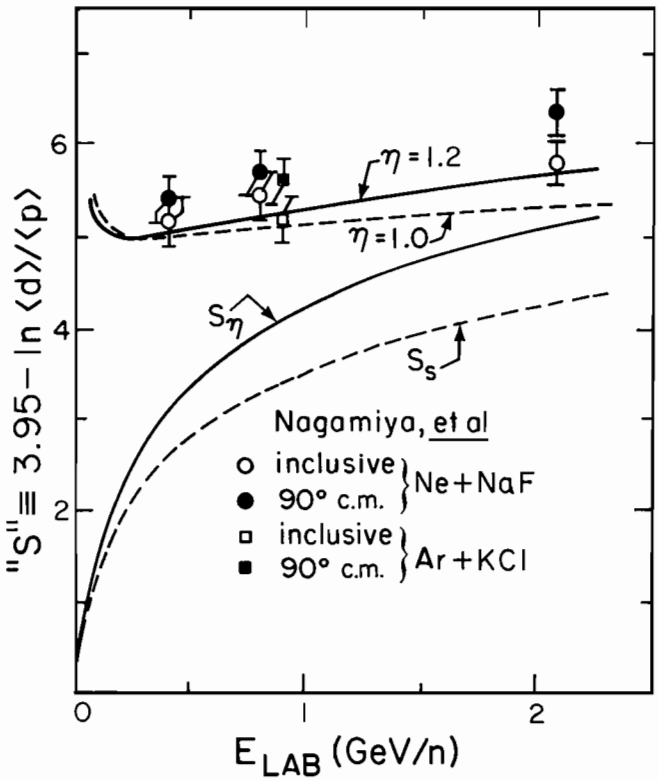

Fig. 2. Connection between the d/p ratio and the entropy. (XBL 814-651)

Pion Production from Heavy Ion Collisions at 90-380 MeV/N*

P. Hecking†

Pion multiplicities and pion spectra from heavy-ion collisions with medium bombarding energies of 90-380 MeV per nucleon are not well understood. The lower the bombarding energy, the worse the thermal model performs, indicating that a nonthermal production mechanism is at work, either exclusively or in addition to a thermal component.

For the nonthermal mechanism, the invariant pion production cross section is given by

$$E\left(\frac{d^3\sigma}{dp^3}\right) = \sigma_{HI} N_{Coll} \sigma_{NN}^{-1} \left(\overline{E\frac{d^3\sigma}{dp^3}}\right)_{NN\pi} \quad (1)$$

Here, σ_{HI} is the (geometrical) heavy-ion cross section and N_{Coll} is the number of initial nucleon-nucleon collisions, taken from a Glauber description.

$$\left(\overline{E\frac{d^3\sigma}{dp^3}}\right)_{NN\pi}$$

is the average pion production cross section per nucleon-nucleon collision (taken from experimental $NN\pi$ data), averaged over the momentum distribution of the initial nucleons.[1]

$$\left(\overline{E\frac{d^3\sigma}{dp^3}}\right)_{NN\pi}$$

as well as the total nucleon-nucleon cross section σ_{NN} are rather different from their vacuum values because of the Pauli-blocking of the final state nucleons. The pion angular distribution of the elementary reaction $NN \rightarrow NN\pi$ as well as the pion reabsorption in both nuclei are included.

No compression phenomena, shock waves, or collective effects of any kind are considered within this model. It is assumed that the nuclei simply overlap in coordinate space, the density is the sum of the local densities, and pion production is homogeneous in the overlap region.

Figure 1 shows the importance of the thermal and the proposed nonthermal production mechanism. At forward angles the nonthermal component is predominant at lowest energies and competes with the thermal component at higher energies, depending on the pion momentum. Pions with large momenta are mostly of nonthermal origin. For pion emission at 90° (not shown in the figure), the nonthermal production rate is an order of magnitude smaller, and hence the spectrum is more thermal. The angular distribution of the combined thermal and nonthermal production mechanism agrees with the result of Ref. 2.

In conclusion, pion emission at 90-380 MeV per article seems to be well described by a combination of the thermal and a nonthermal mechanism.

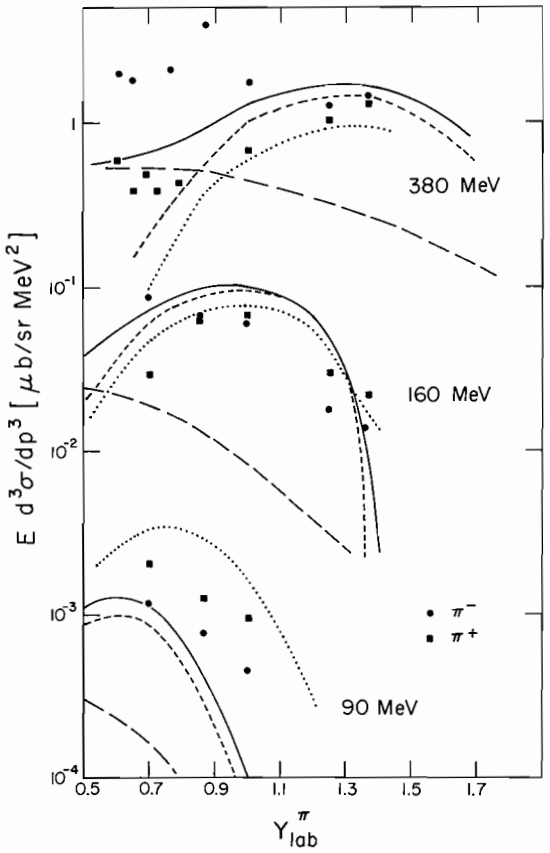

Fig. 1. Triple differential pion production cross section for the reaction Ne → NaF at three bombarding energies as a function of the laboratory pion rapidity at 0° emission angle. The dashed curves are the thermal model, and the full curves are sum of the thermal and nonthermal production rate. (XBL 818-2450)

Footnotes and References

*Condensed from LBL-16271.

†Work supported in part by the Deutsche Forschungsgemeinschaft under Contract He 1155/1.

1. G.F. Bertsch, Phys. Rev. C **15**, 713 (1979).
2. S. Nagamiya et al., LBL-12123.

Microscopic Theory of Deuteron Formation

M. Gyulassy, E. Remler, and K. Frankel

We apply the Wigner density formalism of Remler[1] to the production of deuterons in nuclear collisions. The theory is based on the intranuclear cascade model, which follows the space-momentum trajectories of all particles. The starting point is the transition rate formula

$$\Gamma_{12}(t) = -\frac{1}{\hbar} \mathrm{Tr}\rho_{12}[U_{12},\rho(t)] \quad (1)$$

for particles 1 and 2 to scatter into a bound state characterized by the density matrix, ρ_{12}. In Eq. (1) $\rho(t)$ is the

full A-body density matrix and $U_{12} = \Sigma(V_{1i} + V_{2i})$ for $i \geq 3$ is the interaction potential of particles 1 and 2 with the remainder of the system. As we are interested in the classical limit, we evaluate the trace in the Wigner representation.

In the classical limit,

$$\rho_W(x,p_1,\ldots,x_A\rho_A;t) =$$

$$<\prod_{i=1}^{A} (2\pi\hbar)^3\delta^3[x_i - \bar{x}_i(t)]\ \delta^3[p_i - \bar{p}_i(t)]> \qquad (2)$$

in terms of the classical trajectories $\bar{x}_i(t)$ and $\bar{p}_i(t)$. The Wigner transform of the commutator in Eq. (1) simplifies in the classical limit to

$$\lim_{\hbar\to 0} \frac{-i}{\hbar} [U_{12},\rho]_W =$$

$$\sum_{i=1}^{2}\sum_{j=3}^{A} \nabla_{x_i} V(x_i - x_j)(\nabla p_i - \nabla p_j)\ \rho_W \ . \qquad (3)$$

The final expression for the transition rate is

$$\Gamma_{12_{\hbar\to 0}} =$$

$$<\sum_{j\geq 3} \left\{F_{1j}\cdot\nabla_{p_1} + F_{2j}\cdot\nabla_{p_2}\right\} \rho_{12}^{w}(\bar{x}_1\bar{p}_1,\bar{x}_2\bar{p}_2)> \qquad (4)$$

in terms of the Wigner transform, ρ_{12}^{W}, of the bound density matrix and the classical forces $F_{ij} = -\nabla_{x_i} V(x_i - x_j)$.

Intranuclear cascade provides a particular simple example of Eqs. (2,4). The forces are impulses at discrete times τ_i. The integrated probability for deuteron production is then simply given by[1]

$$P_{12} = <\sum_{i=0}^{N} \frac{(2\pi)^3}{V} \delta^3[\underline{P} - \bar{p}_1(i)$$

$$- \bar{p}_2(i)]\left\{\rho_d[r(i),q(i)] - \rho_d[r(i+1),q(i)]\right\}> \qquad (5)$$

where

$$r(i) = \bar{x}_i(\tau_i) - \bar{x}_2(\tau_i) \ ,$$

$$q(i) = \bar{p}_1(\bar{\tau}_i + \epsilon) - \bar{p}_2(\tau_i + \epsilon) \ ,$$

and

$$\rho_d(r,q) = 8\ \exp(-r^2/d^2 - q^2d^2)$$

for a Gaussian deuteron wave-function ($d \simeq 2.1$ fm).

The brackets $<\ldots>$ denote an ensemble average over many cascade events. We have performed the first calculations based on Eq. (5) using Cugnon's cascade code. The results for Ne + U and Ar + Ar show that the deuteron spectra for lab energies $\geq$ 50 MeV/A are well accounted for. For lower energy deuterons, further calculations are necessary to estimate higher mass composite yields.

An important qualitative result that was obtained is that the free proton inclusive distributions can be strongly modified from the summed charges inclusive yield due to deuteron production. In particular, for central collisions, the cascade code predicts a forward enhancement of the total yield. However, in the forward direction the phase space density is high; and, therefore, most nucleons emerge as bound fragments. This nucleosynthesis process depletes the free proton spectra at forward angles. We are investigating whether the observed forward proton suppression is due to this mechanism as opposed to the hydrodynamic flow mechanism.

References

1. E. Remler, NSF-ITP-81-29, preprint (1981).
2. M. Gyulassy, E. Remler, K. Frankel, preprint in preparation.

Coulomb Final State Interactions

M. Gyulassy and S.K. Kauffmann

Work on Coulomb distortions of inclusive spectra was completed; simple analytical formulas were derived and applied to data. A new analysis of the range of applicability of our formulas was carried out. In terms of the Coulomb parameters, $\eta_{eff} = Z\alpha\omega'/k'$ and $\rho_{eff} = k'R$, with (ω',k') being the thermal averaged energy momentum in the rest frame of a fragment of charge Z, radius R, and temperature T, our generalized Gamow formulas apply when

$$|\eta_{eff}| < \rho_{eff}$$

or

$$2|\eta_{eff}| < (1 - \rho_{eff}^2)/\rho_{eff} \ . \qquad (1)$$

For the Ne + NaF $\to \pi$ data, Eq. (1) is satisfied. However, for reactions with $Z \gtrsim 40$, nonperturbative corrections must be calculated.

In addition, we investigated the impact parameter dependence of the Coulomb effects. We found that the impact parameter b* that contributes most to π^+, π^-, π° yields differ due to Coulomb effects. For example, at the projectile rapidity b* = 3.09, 2.44, 1.47 fm for π^-, π°, π^+ respectively. Therefore, in this kinematic range, the π^- prefer more peripheral collisions because of the large Coulomb enhancement near the projectile. On the other hand, π^+ prefer to come from more central collisions at this rapidity due to the large Coulomb suppression due to projectile remnants in peripheral collisions. The important lesson here is that the inclusive π^+ and π^- yields sample different impact parameters and, therefore, the ratio π^+/π^- mixes different dynamical mechanisms. As shown in Ref. 1, the π^+/π^- ratio depends sensitively on eight physical parameters of the nuclear system. Hence, Coulomb effects cannot be easily disentangled nor effectively used as a diagnostic tool of nuclear collisions.

Reference

1. M. Gyulassy, S.K. Kauffmann, Nucl. Phys. A **362**, 503 (1981).

Formulation Of The Coulomb Effects Of Spectator Fragments On Pions From Heavy Ion Collisions*

Hafez M.A. Radi,† J.O. Rasmussen, J.P. Sullivan, K.A. Frankel, and O. Hashimoto‡

Coulomb effects on heavy-ion pion production cross sections are formulated in terms of weighted averaging over various projectile fragments. Satisfactory fits to zero-degree pion data are found for Ar + C and Ne + C systems. The fragment distributions of excited compound nuclei, before nucleon evaporation, must be used; and the fragment velocity dispersion parameter needed is smaller than that measured for fragments after nucleon evaporation. Average charge Z_{eff} values are determined and compared with those from an experimental paper. In the heavy-ion energy range of the O° pion studies (300 MeV < E/A < 600 MeV), it is inferred that target-projectile factorization for fragmentation cross sections does not hold.

We take the velocity distribution of projectile fragments as Gaussian, with velocity dispersion width α_F given as

$$\alpha_F = \sigma_o c/(m_N c^2)\sqrt{(A_o - A_F)/[A_F(A_o - 1)]} \quad . \qquad (1)$$

In Eq. (1) the constant σ_o has been found to be about 86 MeV/c by experiment; $m_N c^2$ is the nucleon rest mass energy constant; A_o is the projectile mass; and A_F is the mass of fragment under consideration.

Furthermore, the averaging technique requires weighting with respect to the cross section of forming a fragment of mass A_F and charge Z_F, $\sigma(A_F,Z_F)$ before evaporation of protons and neutrons, and also with respect to the differential cross section (before Coulomb correction) of forming a pion simultaneously with a fragment of mass A_F near beam velocity, which is assumed to be proportional to the mass loss $(A_o - A_F)$. $\sigma(A_F,Z_F)$ is calculated by the firestreak computer code of P. McGaughey and D. Morrissey. Figure 1 shows comparison of their code with data.[1]

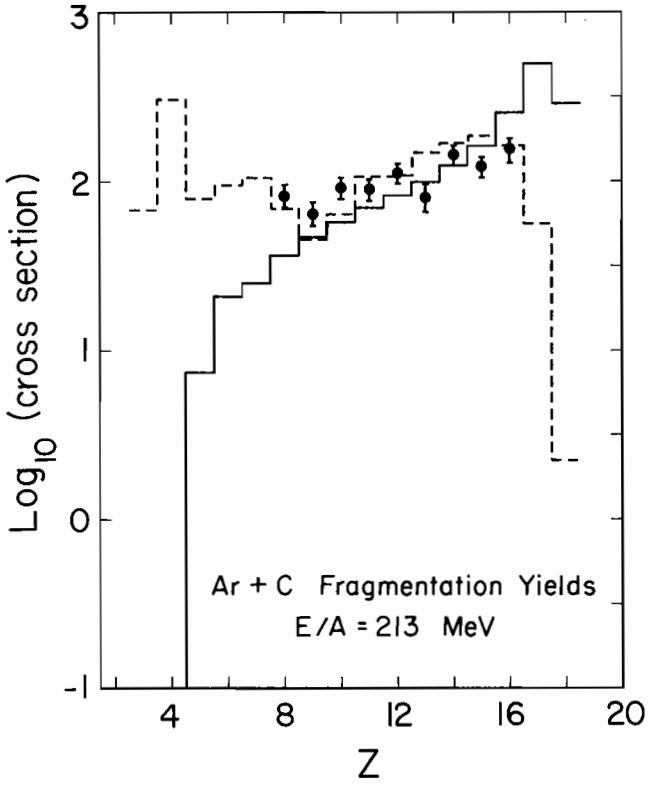

Fig. 1. Comparison of ^{40}Ar fragment yields for given Z between theory and experiment. Data points are from Symons et al.[2] at E/A = 213 MeV on a carbon target. The solid (dashed) histogram is the theoretical distribution before (after) nucleon evaporation according to the firestreak code of McGaughey. The summed cross sections are in millibarns. (XBL 816-10169)

The Sommerfeld parameter is averaged over the velocity dispersion to give

$$\langle \eta_{\pm} \rangle_{\beta_F} = \pm \left(\frac{Z_F e^2}{\hbar c} \right) \frac{\mathrm{erf}[\beta_{\pi\pm}/(\sqrt{2}\,\alpha_F)]}{\beta_{\pi\pm}} \quad . \qquad (2)$$

which replaces the average over β_F in the pion cross section. The grand average of the pion cross section becomes

$$\langle \sigma_{\pi\pm} \rangle = \frac{N_\pi \sum_{A_F,Z_F} N_{A_F} \sigma(A_F,Z_F)(A_0 - A_F)\, G_{\pm}(\langle \eta \rangle_{\beta_F}) \left\{ 1 + \frac{m_\mu r_0 c}{\hbar} \beta_{\pi\pm} \langle \eta_{\pm} \rangle_{\beta_F} A_F^{1/3} \right\}^2}{\sum_{A_F,Z_F} N_{A_F} \sigma(A_F,Z_F)(A_0 - A_F)} \qquad (3)$$

where

$$N_{A_F} = \sqrt{2\pi}\, \alpha_F^3 \ ,$$

and

$$G_{\pm}(x) = 2\pi x [\exp(2\pi x) - 1]^{-1} \ .$$

Since the pions should move out many nuclear diameters during a mean life of compound nuclei, it seems more correct to use the primary fragment distribution rather than the final distribution for our pion Coulomb code. Figure 2 shows the results of our theoretical code compared to ^{40}Ar + C experimental pion data of Sullivan et al. The firestreak code fragment yields at 533 MeV/N, slightly broader than those of Fig. 1, were used as input. Here, we made the simplest assumption for the pion production factor, namely, purely linear dependence on fragment mass loss ($A - A_F$). A momentum dispersion constant of $\sigma_0 = 60$ MeV/c and a radius constant $r_0 = 1.5$ fm were used in Eq. (3). The theoretical curve was corrected by folding in the experimental resolution. The agreement seems quite satisfactory.

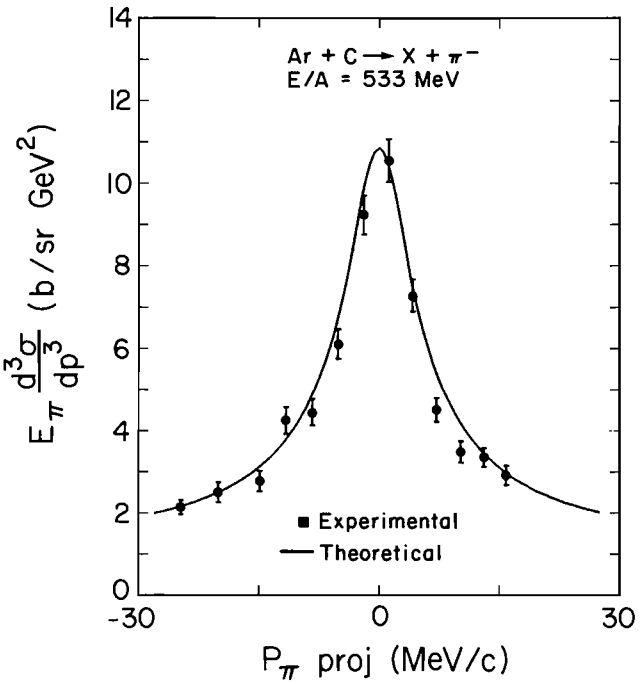

Fig. 2. The π^- spectrum at 0° calculated by Eq. (3) and compared to data of Sullivan et al.[2] The solid curve is the theory after folding with experimental resolution. The abscissa is pion momentum in the projectile frame.
(XBL 816-10170)

Footnotes and References

*Condensed from Lawrence Berkeley Laboratory Report LBL-12591, Phys. Rev. C **25**, (Feb. 1982); and from Proceedings of 5th High Energy Heavy Ion Study, May 18-21, 1981, LBL-12652 (1981).

†Physics Department, Kuwait University, Kuwait.

1. T.J.M. Symons et al., Phys. Rev. Lett. **42**, 40 (1979).
2. J. Sullivan et al., Lawrence Berkeley Laboratory Report LBL-11971 (1980), Phys. Rev. C **25**, (Feb. 1982).

Dynamics vs Symmetrization in Hadron Interferometry

M. Gyulassy

The famous Hanbury-Brown and Twiss effect leads to the expectation that the small angle correlation function R_{12} of identical pions ($\pi^-\pi^-$) should reveal the space-time geometry of the source

$$R_{12} = 1 + |\rho(k_1 - k_2)|^2 \qquad (1)$$

where $\rho(q)$ is the Fourier transform of $\rho(\underline{x},t)$, the pion pro-

duction region. However, in Ref. 1, partially coherent pion fields were shown to modify Eq. (1) as

$$R = 1 + |\rho(k_1 - k_2)|^2 (1 - D_1)(1 - D_2) + 2\rho(k_1 - k_2)[D_1(1 - D_1)D_2(1 - D_2)]^{1/2} \quad (2)$$

where $D_i = D(\underset{\sim}{k}_i)$ is the degree of coherence of the field.

In this work,[2] a new correlation source was found that is specific to hadron interactions. I call these ensemble correlations. The idea is that inclusive cross sections implicitly average over an ensemble of final configurations. If the two particles are correlated dynamically with the unobserved ones, then that ensemble average can induce a large modification of Eq. (2).

Two examples were considered: final state nonisotropic shadowing and coherent jet production. The result is[2]

$$R_{12} = R_{12}^{abs}\{1 + |\rho(k_1 - k_2)|^2 (1 - D_1)(1 - D_2) + 2R_{12}^{I}\rho(k_1 - k_2)[D_1(1 - D_1)\, D_2(1 - D_2)]^{1/2} + (R_{12}^{ch} - 1)\, D_1D_2\}\ , \quad (3)$$

where R^{ch} is the coherent jet ensemble correlation function and R^I is an interference factor due to coherent ensemble effects. R_{12}^{abs} is an absorption factor. Detailed formulas for these Rs are found in Ref. 2. As an illustration of Eq. (3), the form of R_{12} appropriate for an almost chaotic field with $D \ll 1$ was derived

$$R_{12} \simeq 1 + e^{-q^2R^2} + X_{jet}e^{-q^2r_{jet}^2}\ , \quad (4)$$

where x_{jet} specifies the coherent jet ensemble and r_{jet}^2 measures the momentum spread of that jet. For $A \sim 100$, $D \simeq 0.1$ we estimate $X_{jet} \simeq 1$.

Equation (3) liberates us from the bias that the intercept of the correlation function should be less than 2. In particular, $R_{11} = R_{11}^{abs}\ (2 + X_{jet})$, which could be arbitrarily large. It shows that the canonical Hanbury-Brown Twiss form, Eq. (1), cannot be taken for granted. When interesting dynamical correlations exist, these can in general overwhelm the correlations due to Bose or Fermi statistics.

References

1. M. Gyulassy, S.K. Kauffmann, L.W. Wilson, Phys. Rev. C **20**, 2267 (1979).
2. M. Gyulassy, LBL-12389 (1981).

The Quasi-Elastic Component in High-Energy Nuclear Collisions*

Bernd Schürmann† and Jørgen Randrup

The reaction mechanisms acting in high-energy nuclear collisions have been the subject of intensive studies in recent years. Although purely thermal models have been quite successful in explaining early measurements of inclusive spectra, recent, more accurate measurements at forward angles indicate the presence of a strong quasi-elastic component. Simplified multiple-collision models transport theory, micro-canonical, and the two-component model direct-plus-thermal contain the quasi-elastic scattering mechanism in one way or another. The discussion of a nonequilibrated component in the inclusive spectra of high-energy nucleons has been carried to the extreme in Ref. 1, where it was assumed that the *knock-out* mechanism (i.e., a "cold" projectile nucleon collides with a "cold" target nucleon and both subsequently leave the interaction region) is the *dominant* reaction mechanism at forward angles. Meanwhile, it has become clear, however, that such a knock-out process has a quite small cross section, if properly normalized. By contrast, the properly weighted *single-collision* process contributes significantly. In the single-collision mechanism the observed nucleon suffers only one collision, while its collision partner may have undergone previous scatterings. Guided by experiment, it appears a reasonable approximation to replace the momentum-space part of the single-collision contribution by the knock-out distribution. This approximated single-collision contribution is denoted the *direct* component. It is the aim of this note to phrase the notions of a "knock-out," a "single collision," and a "direct" component in a quantitative way and, in particular, to compare the direct and the single-collision components.

The tool for our study is the rows-on-rows model,[2] in which the one-particle inclusive invariant cross section is an incoherent sum of multiple-scattering contributions,

$$E\frac{d\sigma}{d\vec{p}} = \sum_{k=1}^{\infty} E\frac{d\sigma^{(k)}}{d\vec{p}}\ . \quad (1)$$

The contribution from nucleons which have suffered exactly k collisions can be written as

$$E\frac{d\sigma^{(k)}}{d\vec{p}} = \sum_M \sigma_{AB}(M,k) \sum_{m=1}^{M} W^A_{mk}(\vec{p}) + \sum_N \sigma_{AB}(k,N) \sum_{n=1}^{N} W^B_{kn}(\vec{p}) \quad . \tag{2}$$

Here, the indices A and B refer to the projectile and target, respectively. The quantity $\sigma_{AB}(m,n)$ is the cross section for the scattering of a row consisting of m projectile nucleons with a row consisting of n target nucleons. The spectral functions

$$\sum_{m=1}^{M} W^A_{mk} \quad \text{and} \quad \sum_{n=1}^{N} W^B_{kn}$$

are normalized to M and N, respectively. In the rows-on-rows model, the cross sections $\sigma_{AB}(m,n)$ are calculated in the eikonal approximation. From their explicit form (cf, e.g., Ref. 2), one easily derives the sum rules

$$\sum_M M\sigma_{AB}(M,k) = A\,\sigma_B(k)$$

$$\sum_N N\sigma_{AB}(k,N) = B\,\sigma_A(k) \tag{5}$$

with

$$\sigma_A(k) = \frac{1}{k!}\int d\vec{s}\left[\sigma^{tot}_{NN}\tilde{\rho}_A(\vec{s})\right]^k e^{-\sigma^{tot}_{NN}\tilde{\rho}_A(\vec{s})} \tag{6}$$

and analogously for $\sigma_B(k)$. Here σ^{tot}_{NN} is the free nucleon-nucleon total cross section, and $\tilde{\rho}_A$ is the z-integrated nucleon density of nucleus A (normalized to the total nucleon number also denoted by A). It follows that the contribution to the total inclusive cross section from nucleons which have collided k times is given by

$$\sigma^{(k)} = \int E\frac{d\sigma^{(k)}}{d\vec{p}}\frac{d\vec{p}}{E} = A\sigma_B(k) + B\sigma_A(k) \quad . \tag{7}$$

A recent calculation[3] of these quantities in a full three-dimensional cascade model yields results which are nearly identical to those of the rows-on-rows model given in Ref. 2. This fact lends additional support to the utility of the eikonal approximation.

In the following, we focus on the single-collision term of Eq. (4) and its approximations. The direct term in the transport model[4] and the two-component model[5] is obtained from Eqs. (4) and (5) by approximating P^A_{M1} by P^A_{11} and P^B_{1N} by P^B_{11}; i.e.,

$$E\frac{d\sigma^{direct}}{d\vec{p}} = A\,\sigma_B(1)\,P^A_{11}(\vec{p}) + B\,\sigma_A(1)\,P^B_{11}(\vec{p}) \tag{8}$$

The knock-out component is obviously given by

$$E\frac{d\sigma^{ko}}{d\vec{p}} = \sigma_{AB}(1,1)[P^A_{11}(\vec{p}) + P^B_{11}(\vec{p})] \quad . \tag{9}$$

One finds that $\sigma_{AB}(1,1) \ll A\sigma_B(1)$, $B\sigma_A(1)$, (when A,B $\gg 1$, as is usually the case). Therefore, the pure knock-out process is only a small fraction of the total direct component. For the symmetric system Ne on NaF at 800 MeV/N, which we shall use as an illustration, one finds typically $d\sigma^{ko}/d\sigma^{direct} \simeq 0.2$. This is the reason why the knock-out component will not be visible in the inclusive cross section.

After having clarified the relation between the single-collision, the direct, and the knock-out components, it remains to be seen whether

$$E\frac{d\sigma^{direct}}{d\vec{p}}$$

is a good approximation to

$$E\frac{d\sigma^{(1)}}{d\vec{p}} \quad .$$

To elucidate this question we have calculated the corresponding spectra in the rows-on-rows model,[2] using Saxon-Woods nuclear density distributions with the parameters specified in Ref. 2), Gaussian momentum distributions with equivalent Fermi momenta $P_F = 230$ MeV/c, a total nucleon-nucleon cross section $\sigma^{tot}_{NN} = 40$ mb, and differential cross sections $d\sigma/dt \sim \exp(t/2q^2)$ with $q = 350$ MeV/c. Figure 1 shows the results for 800 MeV/N

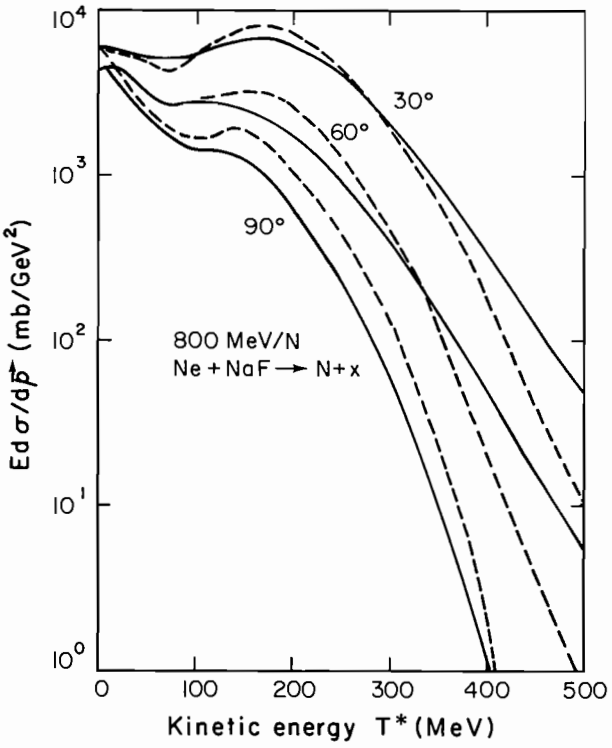

Fig. 1. (XBL 8010-2253)

Ne on NaF. The inclusive nucleon spectra are shown in the mid-rapidity frame at angles 30°, 60°, 90°. The correspondence between the single-collision spectrum (solid curves) and the direct spectrum Eq. (8) (dashed curves) is rather good over a wide kinematical range. (The agreement is better than a factor of two for proton energies between 50 MeV and 450 MeV.) The main reason for this striking result is that the leading corrections P_{21}^{A} and P_{12}^{B} are still rather similar to P_{11}, as can be inferred from the collision kinematics. Although the deviations are larger at the high-energy end, this is of little consequence since the multiple-scattering component of the nucleon inclusive cross section is dominant in this regime.

To summarize, we have elucidated the relation between the notions of a single, direct, and knock-out component in the nucleon inclusive cross section. A significant outcome of our investigation is the good agreement between the single-collision and the direct component over a wide kinematical region. Since the latter has a far simpler structure than the former, it permits an easy and fairly reliable estimate of the single-collision term. As a consequence, given the experimental inclusive cross section, it is relatively easy to disentangle single from multiple scattering contributions and study their competition in various kinematical regions. Such investigations are adding greatly to our general understanding of the reaction mechanism in high-energy nuclear collisions.

Footnotes and References

*Based on Phys. Rev. C **23**, 2766 (1981) (LBL-11964). This work was partially supported by the Bundesministerium für Forschung and Technologie, West Germany.

†Technische Universität München, Physik Department, D-8046 Garching, West Germany.

1. S.E. Koonin, Phys. Rev. Lett. **39**, 680 (1977).
2. J. Knoll and J. Randrup, Nucl. Phys. A **324**, 445 (1979).
3. J. Cugnon, Caltech preprint MAP-15 (1980).
4. H.J. Pirner and B. Schürmann, Nucl. Phys. A **316**, 461 (1979).
5. M. Chemtob and B. Schürmann, Nucl. Phys. A **336**, 508 (1980); Z. Phys. A **294**, 371 (1980).

Consequences of Impact Parameter Restrictions in Relativistic Nuclear Collisions*

Steffen Bohrmann†

The statistical model of high energy nuclear collisions[1] has proven to be a valuable tool for studying the high momentum parts of inclusive spectra. Its main ingredients are:

1. Geometrically defined groups of nucleons interact independently from each other, and
2. Momentum distributions within one group are determined by phase space.

Comparison of predictions of this model with observed spectra of protons from relativistic nuclear collisions at 180° leads to two important conclusions:

1. The two-component structure of the spectra is due to the different decay schemes of participants and spectators; the statistical model, a model for participants only, reproduces the high momentum component only.
2. The shape of the high momentum component is closely related to the average group size (number of nucleons contained in a group).

The model also predicts that restricting the impact parameter to small values (i.e., going over to central collisions) has practically no influence on the spectral shape. This means that the average group size is rather insensitive to impact parameter restrictions. It can be shown that, although the distribution of group sizes changes considerably, the average group size remains practically constant (Fig. 1). This finding is valid for any combination of projectile and target masses and is supported by recent results of three-dimensional cascade calculations.[3] If one assumes that the probability for observing "collective effects" is, in a way, proportional to the number of mutually interacting particles, the above result implies that the restriction to

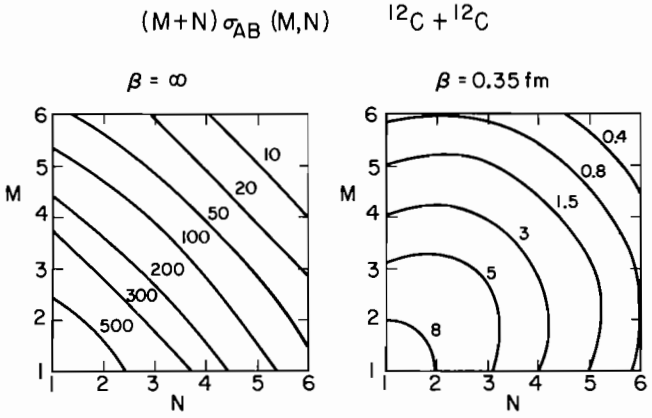

Fig. 1. The weight (M+N) σ_B(M,N) of different combinations of projectile and target nucleon numbers (M and N, respectively) in the inclusive cross section in millibarns. Left: impact parameter averaged; average group size is $\langle M+N \rangle = 3.8$. Right: central collision; $\langle M+N \rangle = 4.2$. The parameter β is the width of a Gaussian weight for the impact parameter. (XBL 814-3757)

central collisions does not necessarily increase the chance for such observations.

Footnotes and References

*Condensed from LBL-12928. Work supported by NATO-fellowship, DAAD, W.-Germany, and by BMFT, W.-Germany.

†Inst. f. Theor. Phys., Philosophenweg 19, 6900 Heidelberg, W.-Germany.

1. J. Knoll, Phys. Rev. C **20**, 773 (1979).
2. J.V. Geaga, et al., Phys. Rev. Lett. **45**, 1993 (1980).
3. J. Cugnon, et al., Nucl. Phys. A **363**, 444 (1981).

Recent Results of Statistical Model Calculations for Relativistic Nuclear Collisions*

Steffen Bohrmann† and Jörn Knoll‡

The applicability of the statistical model of high energy nuclear collisions[1] to a wide range of recent experimental data has been investigated. The main results are:

1. The model gives reliable predictions for the high momentum parts of inclusive spectra over a wide range of projectile energies from $\leqslant$ 100 MeV/A to $\geqslant$ 1000 MeV/A.
2. The model gives reliable predictions for almost any combination of projectile and target masses.
3. The model gives reliable predictions for the shapes of inclusive nucleon as well as pion spectra, but not for pion multiplicities (Ref. 2). The observed slope difference between nucleon and pion spectra from the same reaction is reproduced. It follows from the concept of independently interacting nucleon groups, which is basic to the model; the majority of nucleons comes from ensembles in which no pions have been produced, while the pions come from groups that have been "cooled" by the pion production process.
4. The model predicts the observed "scaling" behavior with respect to beam energy and target mass for inclusive pion spectra at 0° plotted versus the Feynman scaling variable X_F (cf. Ref. 2).
5. Above $\simeq$ 1000 MeV/A, the observed spectra tend to be steeper than the calculated spectra. This indicates that all the available energy and momentum is no longer distributed evenly over the members of a group, as is assumed in the model. One might describe this as an "onset of transparency."

The wide range of applicability of the statistical model with respect to projectile energies, projectile and target masses, and type of the observed particles indicates that any more detailed dynamical model of high energy nuclear collisions must incorporate the ingredients of the statistical model: small numbers of mutually interacting particles and even occupation of the available phase space, especially close to kinematical limits. These are serious restrictions on possible reaction dynamics.

Footnotes and References

*To be published. Work supported by NATO-fellowship, DAAD, West Germany, and by BMFT, West Germany

†Inst. f. Theor. Phys., Philosophenweg 19, 6900 Heidelberg, West Germany.

‡Gesellschaft für Schwerionenforschung, Postfach 110541, 6100 Darmstadt 11, Federal Republic of Germany.

1. J. Knoll, Phys. Rev. C **20**, 773 (1979).
2. S. Bohrmann and J. Knoll, Nucl. Phys. A **356**, 498 (1981).

Cascade Calculations of Relativistic Nuclear Collisions

*J.D. Stevenson**

Cascade calculations have been surprisingly successful in explaining the details of relativistic heavy ion collisions. In my work,[1,2] I have emphasized that cascades predict within experimental errors the inclusive proton and neutron cross sections. I also demonstrated that an apparent anomaly[3] in the neutron-to-proton ratio for $\simeq$ 400 MeV/N (Ne + U) was, in fact, explained by my cascade model when formation of light nuclei was taken into account using the coalescence model.[4] Figure 1 is a comparison of the neutron-to-proton ratio calculations with experimental

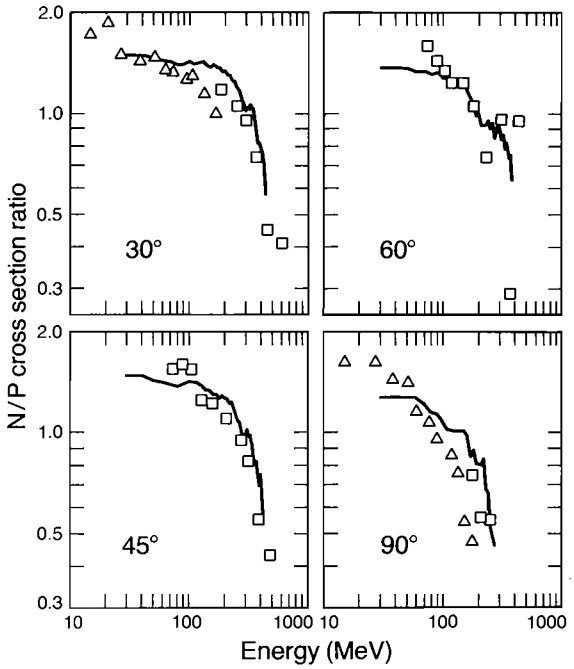

Fig. 1. Neutron-to-proton ratio. Symbols are data from Ref. 3. The solid line is calculated from the cascade model discussed in the text. (XBL 809-11909)

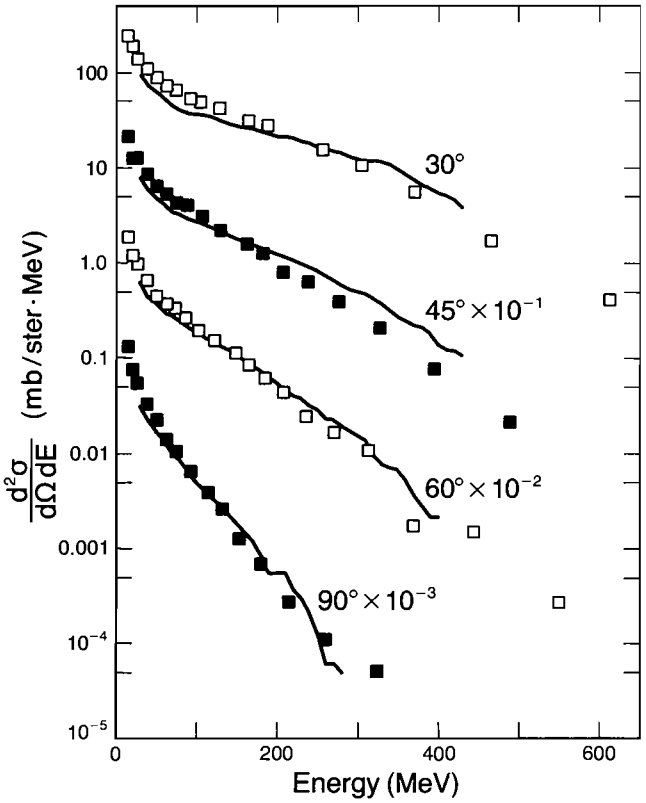

Fig. 2. The square symbols are the experimental neutron cross sections corrected to the time before coalescence. The solid line is calculated from the cascade model. (XBL 809-11910)

results. Figure 2 compares my calculation with the neutron spectra of Ref. 3.

The most important unanswered question regarding cascade calculations concerns their limits of validity: where do they fall? My current plans include comparing cascade results to the data from CERN on 56 and 84 MeV/N ^{12}C-induced reactions. I am also interested in comparing cascades to new, exclusive reaction data from the HISS and Ball-Wall detectors.

Footnotes and References

*Also at Space Sciences Laboratory.

1. J.D. Stevenson, Phys. Rev. Lett. **41**, 1702 (1978).
2. J.D. Stevenson, Phys. Rev. Lett. **45**, 1773 (1980).
3. W. Schimmerling et al., Phys. Rev. Lett. **43**, 1985 (1979).
4. H.H. Gutbrod et al., Phys. Rev. Lett. **37**, 667 (1976).

Kaon Rescattering in Relativistic Nuclear Collisions*

J. Randrup

Inclusive spectra of kaons produced in relativistic nuclear collisions have recently been measured.[1] In conjunction with the experiment, a theoretical study was made of the kaon production.[2] This study pictured the nucleus-nucleus collision as a sequence of elementary baryon-baryon collisions. The corresponding multiple-collision problem was solved in the linear cascade model, "rows on rows."[3] In each elementary collision there is a small, $\sim 10^{-3}$, branching ratio for kaon production which can therefore be included perturbatively. The required differential cross sections were obtained by generalizing the scarce NN data by help of the one-pion exchange model. In this way, the spectra of the produced kaons were calculated for a number of experimentally interesting cases.

Correspondence of this reference calculation with the data should only be expected if the kaons were to propagate through the surrounding matter without suffering any disturbances on their way. Because, in the energy region considered, the average kaon-nucleon cross section, which is

nearly totally elastic, is $\sigma_{KN} \simeq 9$ mb, the kaons do in fact have a fairly good chance of escaping undisturbed. However, simple estimates indicate that the average number of collisions suffered by a produced kaon is around one and rescattering therefore may not be entirely negligible. The purpose of the present work is to elucidate the role that the kaon rescattering mechanism has in bringing the calculation into good agreement with the preliminary and yet unpublished data.

The first step towards understanding the importance of the rescattering mechanism is to estimate the number, κ, of elastic collisions a produced kaon is expected to suffer with the surrounding matter. We arrive at the following rough estimate

$$\kappa \simeq 0.7(R_A + R_B)\, \rho\sigma_{KN} \simeq (A^{1/3} + B^{1/3})/8$$

where A and B are the nuclear mass numbers: we have used 1.15 fm for the nuclear radius constant, $\rho = 0.17/\text{fm}^3$ for the nucleon density, and $\sigma_{KN} = 9$ mb.[4] (Table 1 shows the collision number κ for some cases under experimental investigation.) Therefore, on the average, a produced kaon is expected to suffer, at most, one rescattering. Nevertheless, the appearance of the spectral distribution can be significantly altered.

To elucidate quantitatively the effect of kaon rescattering we have made the following augmentation of the model of Ref. 2: each kaon produced is allowed to suffer isotropic elastic collisions with the baryons before escaping from the interaction zone. The number of actual collisions suffered by a given kaon is governed by a Poisson distribution, $P(k) = \kappa^k \exp(-\kappa)/k!$, characterized by the specified mean value κ. The baryon collision partner (either a nucleon or a delta) is assumed to have a momentum distribution corresponding to the one-particle inclusive cross section. This calculational simplification is not expected to be important for the ensuing conclusions.

To illustrate the effect of rescattering, the resulting observable inclusive kaon cross sections are displayed in Fig. 1 in the form of contour plots in the rapidity plane.

Table 1. The estimated mean kaon collision number κ for a number of experimentally interesting combinations of projectiles and targets.

κ	NaF	KCl	Pb
p	0.46	0.55	0.87
d	0.50	0.58	0.90
Ne	0.68	0.77	1.08
Ar	0.77	0.85	1.17

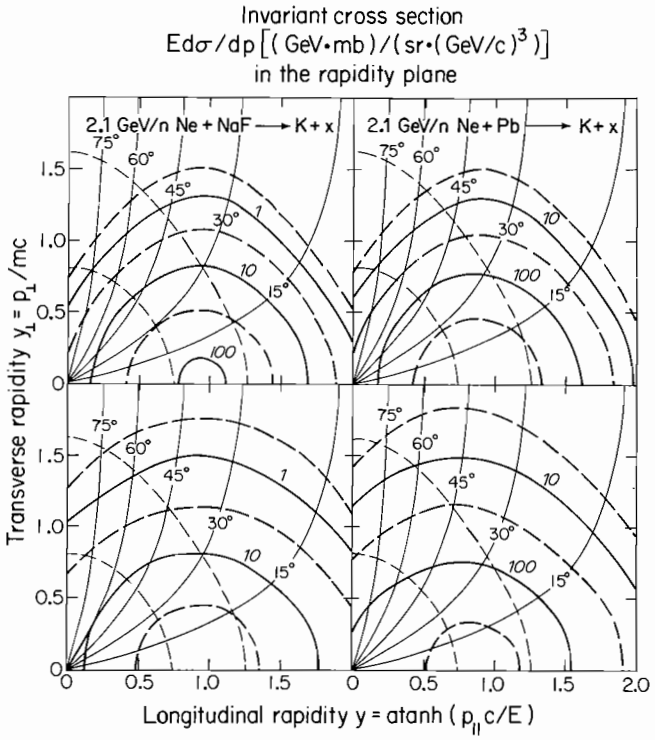

Fig. 1. Contour plot in the rapidity plane of the invariant differential cross section for observing a kaon, whether it be a K^+ or a K°. Upper portion: primary spectra as calculated in Ref. 2; lower portion: final spectra after rescattering using the κ-values in Table 1. Grids of fixed laboratory angles and fixed laboratory momenta (of 400 and 800 MeV/c) are superimposed to aid the comparisons.
(XBL 809-1953)

The cases shown are 2.1 GeV/n Ne on NaF and Pb. The upper portion shows the primary kaon distributions as calculated in Ref. 2. Initially, the kaons are nearly isotopic in the mid-rapidity frame and fall off relatively steeply. Their appearance after the rescattering is shown in the lower portion. The rescattering process spreads the distribution over a wider domain in rapidity space and produces a marked elongation in the beam direction, caused by the predominantly forward-backward directed motion of the baryons. In the asymmetric case, a tilt develops because of the larger abundance of target participants. At large laboratory angles, this evolution significantly alters the differential spectra; they become much larger and fall off considerably gentler. The overall kaon multiplicity is of course unaffected, since the kaons suffer only elastic scattering. The approximate scaling of the primary differential spectra[2] is thus broken and the final distributions appear more like what would result in a thermal calculation.

The effect of rescattering on the angular distributions is only moderate at forward angles, but the effect is dramatic at sidewards angles. In the typical kinematic region around $p_K = 500$ MeV/c, the kaon yield is easily increased by an order of magnitude; and the slopes are halved.

The results demonstrate that the scattering of kaons after their initial creation can substantially affect their spectral distributions. In the presented calculations, we have employed the κ-values given in Table 1 which represent only a rough guess. One should therefore not expect immediate agreement with the data, particularly not in the large-angle region where the dependence on κ is most delicate. Rather, by virtue of this very sensitivity, one may hope that the large angle kaon spectra can eventually be exploited to provide information on the actual number of rescatterings and, therefore, yield new insight into the collision dynamics.

Footnote and References

*Based on LBL-11508: Phys. Lett. B **99**, 9 (1981).

1. S. Schnetzer et al., Proceedings of the International Conference on Nuclear Physics, Berkeley, 24-30 August 1980, p. 619, and to be published.
2. J. Randrup and C.M. Ko, Nucl. Phys. A **343**, 590 (1980).
3. J. Knoll and J. Randrup, Nucl. Phys. A **324**, 445 (1979).

Central Collisions of Heavy Ions – Indication for Fluid Dynamical Behavior?*

*H. Stöcker,† C. Riedel,† G. Buchwald,‡ L.P. Csernai,‡ G. Graebner,‡ W. Greiner,‡ J.A. Maruhn,‡ P. Subramanian,‡ Y. Yariv,¶ K. Frankel, M. Gyulassy, J. Stephenson, D. Strottman,** J.R. Nix,¶‖ B. Schürmann,***

The first detailed comparison of a variety of models with high multiplicity selected proton cross sections is presented. The reaction studied is Ne (393 MeV/n) + U → p + X (high associated multiplicities). The observed preferential sidewards emission of the matter is reproduced by a hydrodynamical calculation with final evaporation of protons, but the intranuclear cascade models and the two component (phase space) model fail in reproducing the data. The results seem to indicate that collective nuclear flow, as described by nuclear fluid dynamics, does occur in nuclear collision. The forward peaking of the protons predicted by the cascade calculations, on the other hand, provides an example of a qualitative failure of such models, which are based on subsequent independent nucleon-nucleon collisions. While previous data in AgCl detectors have also indicated sidewards peaking of α-particles, more precise and detailed data on central collisions will be necessary to extract information on the nuclear equation of state.

Footnotes

*Based on LBL-12634.
†GSI, Darmstadt, West Germany.
‡Universität Frankfurt, West Germany.
¶Weizmann Institute, Israel.
‖Los Alamos National Scientific Laboratory.
**Universität München, West Germany.

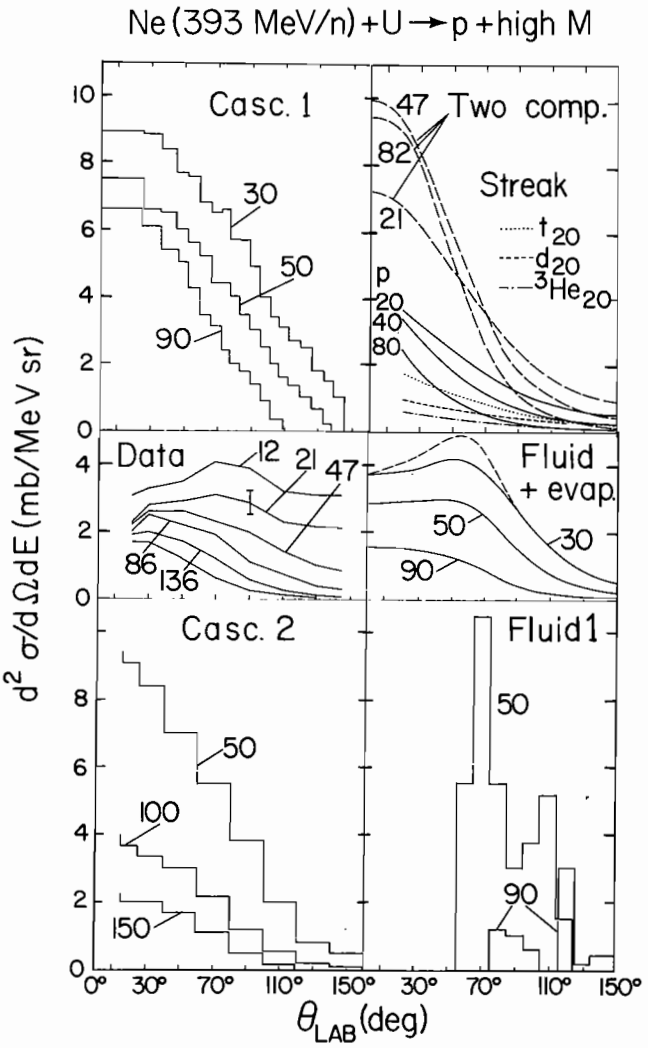

Fig. 1. (XBL 814-772)

Two Particle Correlations Caused by Collective Fluid – Dynamical Flow*

H. Stöcker,† L.P. Csernai,‡ G. Buchwald,‡
G. Graebner,‡ J.A. Maruhn† and W. Greiner‡

Three-dimensional fluid dynamical calculations with the description of final evaporation were performed for Ar + Pb and Ne + U at E_{Lab} = 400 and 800 MeV/n. The triple differential cross sections show the signs of the bounce-off effect, an azimuthal anticorrelation between the projectile and target fragments. The correlation function calculated from this triple differential cross section shows a good agreement with experiments on: (1) correlations between light and heavy fragments (see left side of the figure), and (2) two nucleon correlations (right). Thus, our calculations confirm that correlations in collisions of heavy ions are mainly determined by the collective flow of the nuclear matter and microscopic correlations play only a minor role for collisions of very heavy systems.

The figure shows the azimuthal dependence of the triple differential cross section for the system Ne + U (upper left) at E_{Lab} = 393 MeV/n and the corresponding correlation function for light to heavy fragments (lower left), together with the data. The right hand side of the figure shows the calculated (upper right) and measured two nucleon correlation function (lower right) for the system Ar + Pb at E_{Lab} = 800 MeV/n.

Footnotes

*Based on LBL-12660.
†GSI, Darmstadt, West Germany.
‡Universität Frankfurt, West Germany.

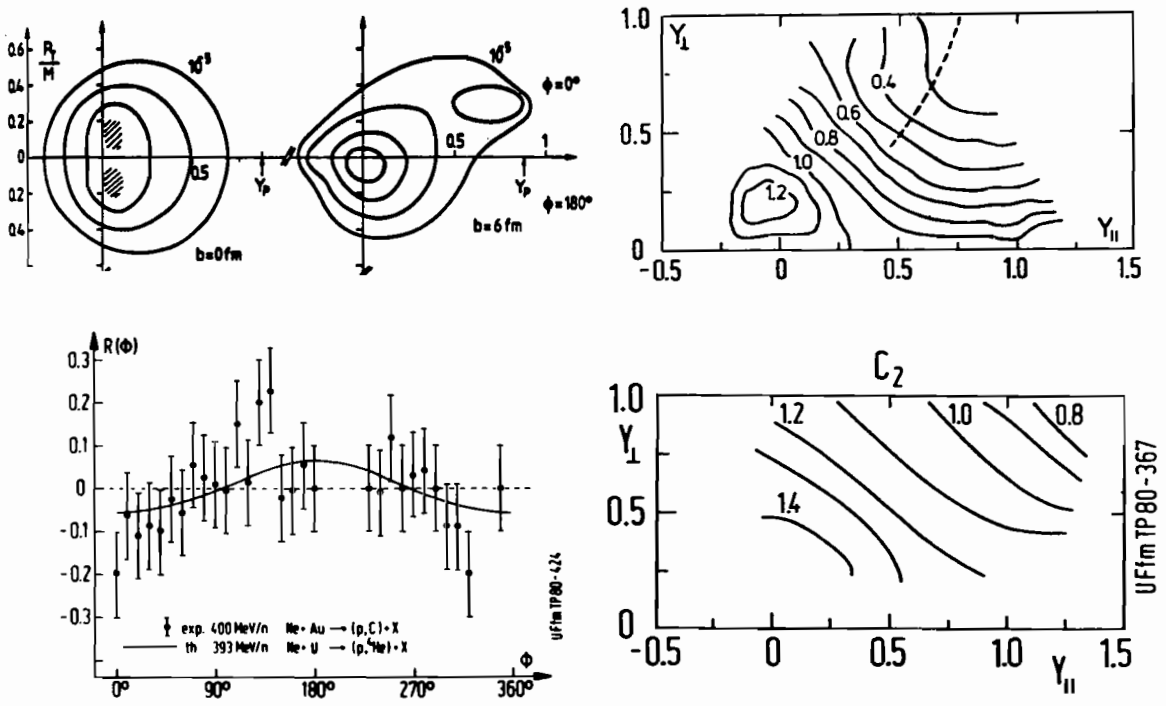

Fig. 1. Data on left from H. Gutbrod et al., on right from I. Tanihata et al.

(XBL 8110-12213)

Jets of Nuclear Matter from High Energy Heavy Ion Collisions*

H. Stöcker,† L.P. Csernai,‡ G. Graebner,‡
G. Buchwald,‡ H. Kruse,‡ R.Y. Cusson,‡ J.A. Maruhn,‡ and W. Greiner‡

The nuclear fluid dynamical model with final thermal breakup is used to study the reaction $^{20}Ne + ^{238}U$ and $^{40}Ar + ^{40}Ca$ at $E_{Lab} = 390$ MeV/n. The calculated double differential cross sections $d^2\sigma/d\Omega dE$ are in agreement with recent experimental data. However, it is shown that the azimuthal dependence of the *triple* differential distributions, $d^3\sigma/dEdcos\theta d\phi$, to be obtained from 4π exclusive experiments with single event analysis, can yield considerably deeper insight into the collision process and allow for snapshots for the reactions. Strongly correlated jets of nuclear matter are predicted. The jet angle, θ_{jet}, relative to the beam axis increases from 0° for peripheral collisions to 90° for central collisions. A transition is predicted from a 180° azimuthally correlated two jet structure at intermediate impact parameters to a doughnut-shaped azimuthally symmetric distribution for central collisions. The figure shows the azimuthal dependence of the triple differential rapidity distribution (left) and the impact parameter dependence of the angle of the jet axis, θ_{jet} relative to the beam axis.

Footnotes

*Based on LBL-11774.
†GSI, Darmstadt, West Germany.
‡Universität Frankfurt, West Germany.

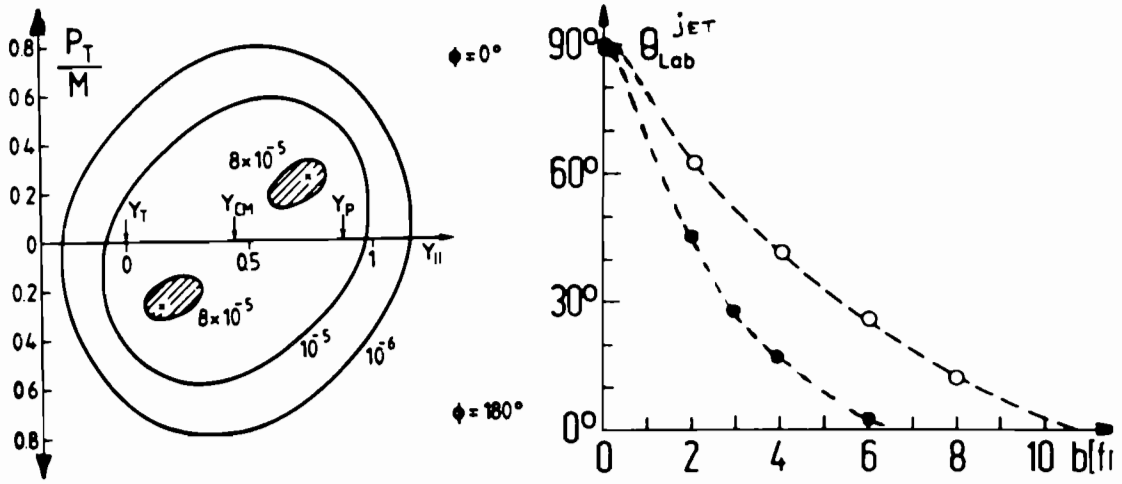

Fig. 1. (XBL 8110-12214)

The Bounce-Off Effect as a Barometer for Hot, Dense Matter in High Energy Nuclear Collisions*

Horst Stöcker and Bernd Müller†

The observed large collective transverse momentum transfer[1] in high energy nuclear collisions is studied in a simple bounce-off model. The calculated momentum transfers are in agreement with the experimental data. The bounce-off process is shown to be sensitive to the nuclear equation of state. The transverse momentum transfer can be estimated via

$$\Delta p_T \simeq P(\rho,T)\ G(b)$$

where $P(\rho,T)$ is the pressure in the high energy, high temperature zone and $G(b)$ is a geometrical function which depends on the impact parameter only. We suggest using this for a systematic experimental investigation of $P(\rho,T)$

in high energy nuclear collisions. Such measurements could provide evidence for phase transitions into abnormal states in dense nuclear matter and into quark matter. Above all, the scattered fragments are direct witnesses of the initial, hot, and dense parts of the reaction and as such they deserve much future attention.

Footnotes and References

*Condensed from LBL-12471.

†Department of Physics and Astronomy, Nuclear Physics Division, Vanderbilt University, Nashville, TN 37203.

1. H.H. Gutbrod, LBL-11123 and A. Warwick, et al., LBL-12180 to be published.

Probing Dense Nuclear Matter via Nuclear Collisions*

H. Stöcker, M. Gyulassy, and J. Boguta

We study the sensitivity of nuclear hydrodynamics to the equation of state of nuclear matter at high densities and temperatures. The relativistic Rankine Hugoniot equation is used to calculate the pressure, P, and entropy, S, generated in nuclear collisions between E_{Lab} = 50 and 200 MeV/n in a variety of models for the equation of state (see Fig. 1). P(E) and S(E) can be directly related to experimental observables. The pressure, as the driving force for the fluid motion, determines the mean collective flow behavior, especially the transverse momentum transfer, while the entropy produced determines the hadron production rates and chemical composition of light nuclear fragments.

We find both P(E) and S(E) to be most sensitive on a $\lesssim$ 50% level to the compression part of the equation of state at intermediate bombarding energies, $E_{Lab} <$ 250 MeV/n. At high energies, $E_{Lab} >$ 1 GeV/n, P(E), and S(E) are sensitive (on a $\lesssim$ 25% level) to the thermal part of the equation of state.

Hence, high precision is required in the combined measurement of P(E) and S(E) via detailed jet analysis and composition analysis, which promises, in fact, the best prospects for determining the equation of state ultimately from nuclear collision data.

Footnote

*Condensed from LBL-12095.

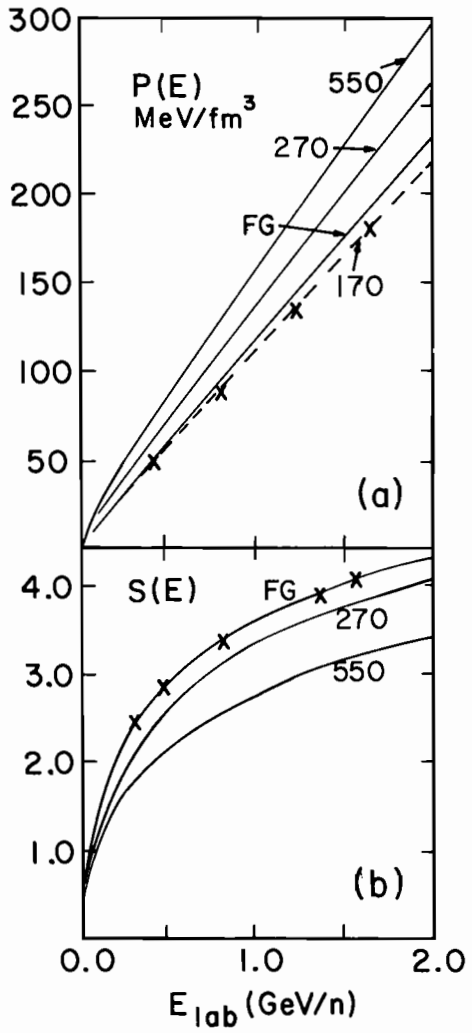

Fig. 1. (a) Total pressure P(E) vs E for Fermi gas (solid line) compared with mean field theory, K = 550, K = 270, and K = 170 (marked with X). (b) Entropy per baryon S(E) vs E for equation of state in (a). S_{FG} is the exact Fermi gas result.

(XBL 813-8436A)

Optical Model Solutions for Pions in Nuclear Matter*

P. Hecking†

Pionic modes and pion propagation in baryonic matter are of considerable interest concerning pion production in nuclei and heavy-ion collisions and more exotic phenomena such as pion condensation. The purpose of this work is to point out the extent that information about propagation and attenuation of the "pionic" branch of the pion spectrum in nuclear matter, in contrast to the Δ-isobar branch or the acoustical branch, can be deduced from optical model parameters which are compiled from scattering and pionic atom data.

The (complex) pion momentum $k = k_1 + ik_2$ in the medium is related to the (also complex) optical potential $U_{opt}(k,\omega)$ by the expression

$$k^2 - k_o^2 = -2\omega U_{opt}(k,\omega) \qquad (1)$$

where $k_o^2 = \omega^2 - m_\pi^2$ is the pion momentum. The optical potential U_{opt} can be parameterized in the usual manner with the complex quantities b_o, c_o, B_o, and C_o and with Landau Fermi-liquid parameter g', which describes the short-range correlation. These five quantities have been determined from pion scattering[1] and pionic atom data.[2]

The imaginary part k_2 (of k) is connected with the pion mean free path by

$$\lambda = \frac{1}{2k_2} = \frac{k_1}{2\omega \,\mathrm{Im}\, U_{opt}} \qquad (2)$$

Table 1 gives the result for the "self-consistent" solution of Eq. (1) with $U_{opt}(k,\omega)$. The mean free path λ is rather flat for $0.8\ m_\pi c^{-1} \lesssim k_o \lesssim 2.4\ m_\pi c^{-1}$, although one should expect a pronounced minimum at the resonance. Also for $\rho = 2\rho_o$ (not shown in Table 1), the mean free path is larger than at $\rho = \rho_o$, which is rather unreasonable. Furthermore, a λ between 0.6 and 1 fm seems extraordinarily small.

A different approach would be the application of the free pion momentum k_o in $U_{opt}(k_o,\omega)$ instead of k. A distinct minimum at the resonance is obtained, fitting well to the estimate ($\lambda \sim \rho^{-1}\sigma_{\pi N}^{-1}$) with $\sigma_{\pi N} = 140$ mb; for $\rho = 2\rho_o$ the mean free path is smaller throughout than for $\rho = \rho_o$; and the result is in good agreement with the Δ-isobar model (in the resonance region). Also the pion spectrum in medium energy heavy-ion collisions is highly nonthermal,

Table 1. The solutions for $U_{opt}(k,\omega)$ and $U_{opt}(k_o,\omega)$ in Eq. (1) for the optical model parameters of Refs. 1 and 2 at $\rho = \rho_o = 0.17$ fm^{-3}.

	$U_{opt}(k,\omega)$		$U_{opt}(k_o,\omega)$	
k_o [$m_\pi c^{-1}$]	k_1 [$m_\pi c^{-1}$]	λ [fm]	k_1 [$m_\pi c^{-1}$]	λ [fm]
0	−0.18	0.68	0.14	1.47
0.4	−0.42	1.09	0.39	2.93
0.8	0.19	0.75	1.06	3.92
1.2	0.76	0.57	1.65	2.59
1.6	1.13	0.61	2.16	1.36
2.0	1.25	0.70	2.60	0.70
2.4	1.60	0.97	2.45	0.51

which advocates a rather large mean free path. The mean free path λ has also been determined[3] for parameters c_o, B_o, and C_o, which had been obtained from nuclear matter calculations.[4] The results agree well with those for empirical values of c_o, B_o, and C_o.

In conclusion, a "self-consistent" solution of the pion momentum k in the medium turns out to be unsatisfactory in comparison with the approximation $k = k_o$ in the optical potential U_{opt}, if the parameters for U_{opt} are deduced from experimental data. The reason for this is not entirely clear; probably the abilities of the optical model are overstressed.

Footnotes and References

*Condensed from LBL-12911.

†Work supported in part by the Deutsche Forschungsgemeinschaft under contract He 1155/1.

1. K. Stricker, H. McManus and J.A. Carr, Phys. Rev. C **19**, 929 (1978).
2. J. Hüfner, Phys. Rep. C **21**, 1 (1975).
3. P. Hecking, Phys. Lett. **103B**, 401 (1981).
4. J. Chai and D.O. Riska, Nucl. Phys. A **329**, 429 (1979).

Finite Temperature Pion Condensation

*N.K. Glendenning and A. Lumbroso**

In a related work, pion condensation in zero temperature matter was investigated in a relativistic field theory solved in the mean field approximation.[1] Unlike earlier work on the subject, the theory was constrained to possess the known saturation properties of nuclear matter. Here, we investigate matter in the same theory at finite temperature. Finite temperatures are interesting because pion condensation is believed to be an important mechanism involved in the cooling of neutron stars. Moreover, nuclear collisions at high energy, if they produce dense matter, certainly produce it at finite temperature.

The properties of the normal state can be used to determine all parameters of the theory except for the effective pion-nucleon coupling, g_π. This is a very important parameter of the theory, one which we take great care in determining. It would be unacceptable to simply use the vacuum value. This would greatly overestimate the importance of the condensate state. Through the derivative coupling in our Lagrangian,[1] the pions interact with nucleons dominantly in the p-wave state as it should be. We can represent this by the diagram

corresponding to a pion absorption on a particle in the Fermi sea exciting a particle-hole state and the subsequent re-emission of the pion. In addition, other processes are believed to be important which are not explicit in our theory. One of these is the absorption of a pion to create a Δ isobar;

where the double line represents the isobar. This process encourages condensation and is very important because it is not inhibited by the Pauli-exclusion principle. Acting in the opposite direction are the repeated scatterings of the particle-hole excitations by the nucleon-nucleon interaction. In the particle-hole state, which has quantum numbers of the pion, this can be discussed in terms of the Landau parameter g'. The above two diagrams should be replaced by the renormalized p-wave interaction defined by[2]

where the particle state can be either nucleon or isobar. While these additional processes would be extremely difficult to incorporate in a theory of the fully developed condensate state such as ours, they are relatively easy to incorporate in the pion self-energy at the pion condensation threshold. The reason is that, at threshold, the infinitesimal pion field does not affect the nucleon states so that the above contributions can be calculated on the unperturbed basis. Such a calculation of the pion condensation threshold has been carried out by many authors, initially by Migdal[2] and Sawyer and Scalapino.[3] The finite temperature propagator was first calculated by Ruck, Gyulassy, and Greiner,[4] and more recently by Hecking, Weise, and Akhoury.[5] We make use of this most recent calculation of the condensate critical density as a function of temperature.

Our strategy in brief is to renormalize the pion-nucleon coupling $g\pi$ in our theory to such a value as to reproduce, at each temperature, the critical density as calculated by Hecking et al.[5] In this way we constrain our theory to the bulk properties of the normal state and the best estimates, to date, of the pion condensation threshold density.

We make a remarkable observation concerning the pion condensed state, which is illustrated in Fig. 1. The binding energy per nucleon as a function of density at various temperatures between 0 and 100 MeV is shown. At low temperature, the condensate makes very little contribution to the energy, when the theory is constrained by the bulk properties of nuclear matter, as was found in our earlier work.[1] But at higher temperatures, although the critical density increases, the condensate makes an increasingly important contribution to the energy. This dramatic softening in the equation of state will strongly influence the hydrodynamical flow of hot dense matter if a transition to the condensed state occurs. This is likely in the region

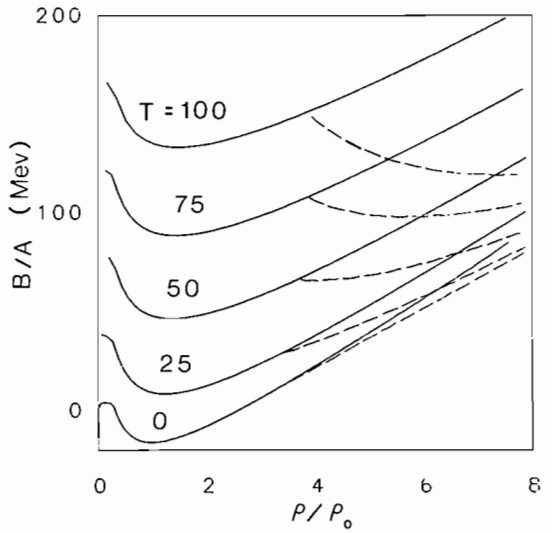

Fig. 1. Binding energy for asymmetric nuclear matter. Solid lines are normal and dashed pion condensate state. The critical density follows the trajectory in the ρ-T plane calculated in Ref. 5 for $g' = 0.6$. (XBL 811-7534)

above the critical density, because the free energy in the pion condensed state is lower than in the normal state at the *same* energy and baryon densities. Moreover, because the temperature is *much* higher in the condensed state, subsequent transition to a quark matter phase may be facilitated, if the density is high enough.

Footnote and References

*On leave from CEN, Saclay, France.

1. B. Banerjee, N.K. Glendenning, M. Gyulassy, LBL-10979 and Nucl. Phys. A, in press.
2. A.B. Migdal, Phys. Rev. Lett. **31**, 247 (1973).
3. R.F. Sawyer and D.J. Scalapino, Phys. Rev. D **7**, 953 (1973).
4. V. Ruck, M. Gyulassy and W. Greiner, Z. Physik A **277**, 391 (1976).
5. P. Hecking, W. Weise and R. Akhoury, Preprint.

Pion Condensation Threshold in Nuclear Matter and Thermal Δ-Isobars*

P. Hecking

Pion condensation in nuclear and neutron matter at zero, as well as finite temperature, has been investigated in recent years with the hope of finding some evidence of it in heavy-ion collisions and/or the properties of neutron stars. Pion condensation occurs at the lowest baryon density, ρ_B, for which a solution of the pion dispersion relation

$$\omega^2 = k^2 + m_\pi^2 + \Pi(k,\omega,\rho_B,T)$$

exists. The (negative) pion self-energy in the medium depends on ρ_B, the pion four-momentum $q = (\omega,k)$, and the temperature T with $\omega = 0$ for isospin-symmetric (N = Z) nuclear matter.

An important part of the pion self-energy Π results from the $\pi N\Delta$ and $\pi\Delta\Delta$ interaction with the Δ(1232)-isobar. At finite temperature, there are already purely thermal Δ-isobars present, even in the absence of a pion condensate. Consequently, the pion self-energy Π results in part from the interaction of the pion with a Fermi-sea of Δ-isobars. The density ρ_Δ is obtained from the chemical equilibrium $\mu_N(T) = \mu_\Delta(T)$ of the reaction $N + N \rightarrow N + \Delta$. The p-wave part of the pion self-energy Π is given by the response of a Fermi-sea of nucleons (or Δ-isobars). Short-range repulsive correlations, given by the Landau Fermi-liquid parameter g′, an effective nucleon mass $m^* < m$ and finite range π-baryon vertices with a cutoff Λ, are taken into account along the lines of Refs. 1 and 2.

The cutoff Λ is rather well determined in the range 1-1.4 GeV and is not very density-dependent. At nuclear density $\rho_0 = 0.17$ fm^{-3}, the Fermi-liquid parameter g′ has values of 0.6-0.7 and the effective mass m^* is ~ 0.8 m; but their values, especially that of m^*, remain uncertain for densities larger than ρ_0. In order to cope with that, several values for g′ are taken; and for m^* two choices are made: a density independent $m^* = 0.8$ m and a density-dependent $m^*(\rho) = m[1 - k_F(\rho)\, k_F^{-1}(\rho_0)\, 0.2]$ with the Fermi-momentum k_F.

Figure 1 shows the result for the critical baryon density ρ_c. One obvious feature is the rather "parallel" behavior of the phase boundaries with increasing temperature for various values of Λ and g'. The Fermi-sea of thermally excited Δ-isobars is of importance only above $k_BT \sim 50$ MeV. Below this temperature, ρ_Δ approaches zero exponentially. Even at $k_BT \sim 100$ MeV, the influence on ρ_c is a (less than) 20% effect. The temperature $k_BT \sim 100$ MeV is obtained in a typical central heavy-ion collision with a bombarding energy of 1 GeV/N, provided complete thermalization is obtained.

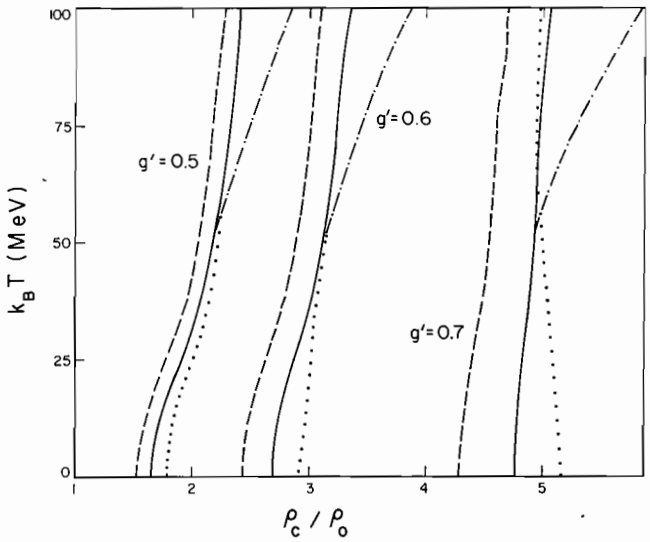

Fig. 1. Critical baryon density $\rho_c(T)$ as function of the temperature and various parameters. The pion-condensed phase is to the right of the curves. Without Δ-Fermi-sea: full curves: Λ = 1.2 GeV and $m^* = 0.8$; dashed curves: Λ = 1.4 GeV and $m^* = 0.8$; dotted curves Λ = 1.2 GeV and $m^* = m(\rho)$. With Δ-Fermi-sea: dashed-dotted curves: Λ = 1.2 GeV and $m^* = 0.8$. (XBL 812-349A)

It turns out that a Fermi-sea of thermally excited Δ-isobars is of equal or less importance for the critical effective nucleon mass m*, and the short-range correlation parameter g'. The latter still remains the most decisive and, unfortunately (especially at densities larger than ρ_o), also the least well known.

Footnotes and References

* Condensed from LBL-12254. This work was supported in part by the Deutsche Forschungsgemeinschaft under contract He 1155/1.

1. P. Hecking, Nucl. Phys. A **348**, 493 (1980).
2. H.J. Pirner, M. Rho, K. Yazaki and D. Bonche, Nucl. Phys. A **329**, 491 (1979).

Test for Pion Condensation in Nuclear Collisions

M. Gyulassy

If pionic instabilities occur in nuclear collisions, a macroscopic spin-isospin current, $\mathfrak{J}_{\mu 5}(x,t)$, would grow in time in the nuclear volume. Since $\mathfrak{J}_{\mu 5}$ is a source of pions

$$(\Box + m_\pi^2)\ \underset{\sim}{\pi}(x) = g\pi\partial^\mu\ \mathfrak{J}_{\mu 5}(x)\ , \tag{1}$$

a time-dependent $\mathfrak{J}_{\mu 5}$ will radiate pions. Furthermore, that radiation is in the form of a coherent state. The idea is therefore to calculate the pion spectrum that would be generated by $\mathfrak{J}_{\mu 5}$ and compare it with data.[1]

Based on mean field calculations,[2] we expect a *large* amplitude spin-isospin wave associated with pion condensation

$$g_\pi\partial^\mu\ \mathfrak{J}_{\mu 5}(x) \underset{t\to\infty}{\to} g_\pi k_c \alpha_5 \rho e^{-i\underset{\sim}{k_c}\underset{\sim}{x}} \tag{2}$$

with

$$g_\pi \simeq m_\pi^{-1}\ ,\ k_c \simeq 2m_\pi\ ,\ \alpha \sim 1/2\ ,\ \rho \simeq m_\pi^3\ .$$

As a guess of the small time behavior, we combine the results of growth rate calculations[3] with Eq. (2) to estimate

$$g_\pi\partial^\mu\ \mathfrak{J}_{\mu 5}(x) =$$

$$\theta(t)\ \gamma(k_c)\ t\ g_\pi k_c \alpha\rho e^{-i\underset{\sim}{k_c}\underset{\sim}{x}} e^{-x_2/2R^2} e^{-t/\Delta t} \tag{3}$$

where the growth rate is $\gamma \simeq 0.2\ m_\pi^{-1}$ and $\gamma(k)$ is peaked for $\underset{\sim}{k}_c \sim 2m_\pi\ \hat{e}_\perp$, i.e., perpendicular to the beam axis. Taking the modulus square of the space-time Fourier transform of Eq. (3) gives the single pion inclusive distribution. That invariant distribution has the form

$$\omega\frac{d_3\sigma}{dk^3} = \sigma_o n_o \frac{\gamma^3(k)}{\langle\gamma\rangle} \tag{4}$$

where

$$\langle\gamma\rangle = \int d^3k\ \gamma(k)/\omega_k\ ,$$

and

$$\frac{n_o}{A} \simeq g_\pi^2 k_c^2 \alpha^2 \rho \gamma^2(k_c)/(\sqrt{2}\ \omega_{kc})^5 \sim 10^{-4} \tag{5}$$

is the average number of coherent pions radiated by $\mathfrak{J}_{\mu 5}$ per nucleon. Note that $n_o/A \ll (n/A)_{exp} \sim 10^{-2}$.

Even though n_o is so small, the important observation is that $\omega d^3\sigma/dk^3$ is peaked at $\theta_{cm} = 90°$, $k_{cm} \sim 2m_\pi$ due to the peculiar dependence[3] of $\gamma(\underset{\sim}{k})$ on $\underset{\sim}{k}$. The chaotic source of pions produces, on the other hand, an approximately thermal spectrum that is peaked at $k_{cm} \sim 0$! For $k_{cm} \sim 2m_\pi$, $\omega d^3\sigma/dk^3)_{chaotic} \propto \exp(-2m_\pi/T)$. For low enough bombarding energies, the slope $T \ll 2m_\pi$ and the chaotic yield are strongly suppressed. Therefore, the small coherent component could even become dominant for $k_{cm} \sim 2m_\pi$, $\theta_{cm} \sim 90°$ when the bombarding energy is low enough. Estimates in Ref. 1 indicate that 200 MeV/A is the ideal bombarding energy to reach for this coherent component. The signature of pionic instabilities would be a break in the 90° slope parameter at $k_{cm} \sim 2m_\pi$.

References

1. M. Gyulassy, Nucl. Phys. A **354**, 395c (1981).
2. B. Banerjee, N.K. Glendenning, M. Gyulassy, Nucl. Phys. A **361**, 326 (1981).
3. M. Gyulassy, W. Greiner, Ann. Phys. **109**, 485 (1977).

Significance of Temperature Measurement in Relativistic Nuclear Collisions*

H. Stöcker, A. A. Ogloblin,† W. Greiner‡

We point out the importance of temperature measurements in fast nuclear collisions. Recent data[1] indicate values for T_0 at 3.6 GeV/n which come close to the limiting temperature $T^{max} \simeq m_\pi C^2$ which has been postulated for a hadronic mass spectrum that increases exponentially. The bombarding energy dependence of the temperature is calculated in the fluid dynamical model for a pure nuclear gas and for an exponentially increasing hadronic mass spectrum and compared to the data (left figure). The spectra of pions, protons, and deuterons are calculated using an isotropic expansion model (right figure). It is interesting to note that the apparent temperatures after the expansion are close to the initial temperatures.

Footnotes and Reference

*Condensed from LBL-12971

†Kurchatov Institute, Moscow

‡Inst. f. Theor. Physik, Frankfurt

1. V. G. Antonenko et al., Pisma Jetp **28**, 609 (1978); and S. Nagamiya, et al., LBL-12123.

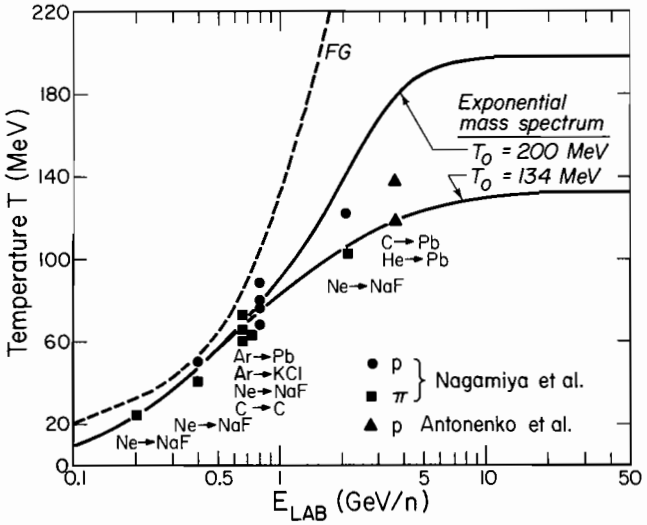

XBL 817-1049

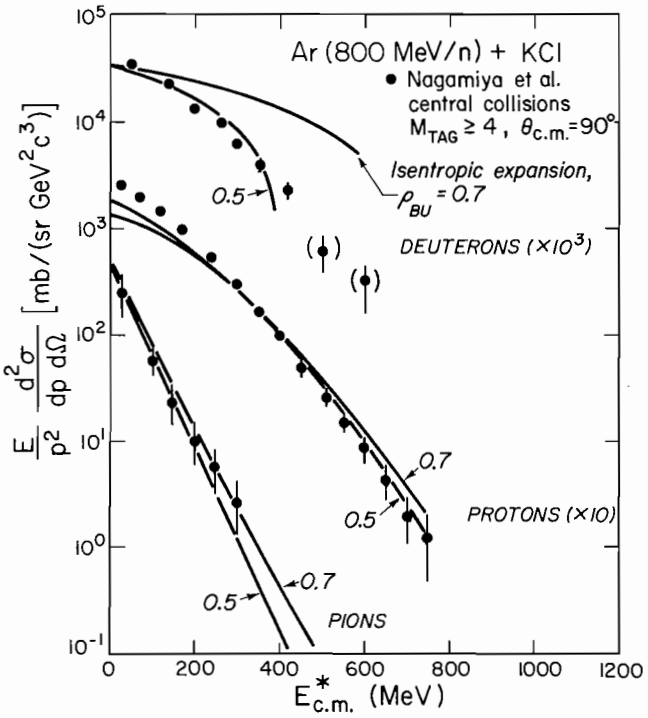

XBL 817-1046

Fig. 1.

On the Significance of Temperature Measurements of Nuclear Fireballs

Norman K. Glendenning

Several experiments, involving the collision of high-energy particles with nuclei and performed over a range of energies, have been interpreted as measuring the temperatures of nuclear fireballs. The extracted temperatures have the appearance of approaching an asymptotic value, and this has given rise to the thought that the ultimate temperature of hadronic matter predicted by Hagadorn[1] has actually been observed. The purpose of this note is to suggest that the interpretation of the data as indicating an asymptotic temperature is probably not correct.

The first remark is that if a dense high energy fireball is formed in a nuclear collision, the fireball subsequently must expand because it is unbound. Depending on the initial density of the fireball, the expansion may entail a manyfold expansion until a freezout density is reached. Although evaporated particles that escape during the expansion carry information about the conditions at the instant of escape, they are indistinguishable from others emitted earlier or later. Meanwhile, the temperature of the fireball falls during the expansion, and the populations of the various hadronic species readjust. The bulk of the observable particles are released at the freezout point in the evolution, and they therefore obscure the information about the hottest stages carried by those particles that were emitted early in the life of the fireball. The conclusion to be drawn from the discussion up to this point is that the spectra of particles emitted by nuclear fireballs are dominated by particles released at the freezout stage[2], and therefore the temperature deduced from the slope of spectra will be the final fireball temperature. To learn about the conditions in the initial fireball requires more elaborate experimentation and analysis than the observation of spectra.[2]

The question remains whether the final fireball temperatures that have been deduced carry interesting information about the underlying mass spectrum of hadrons or the existence of an ultimate temperature. To address this question, we must first admit that we do not know the precise conditions that prevail when thermal contact of the particles is lost. Presumably the hadronic density has fallen to normal nuclear density or less. Adopting as a nominal freezout condition that the *total* hadron density including all baryons, antibaryons, and mesons is 0.17 fm^{-3}, the density of normal nuclei (Fig. 1), shows the fireball temperature at freezout as a function of C.M. energy per net baryon. The thermodynamics of a relativistic free gas of hadrons is assumed.[2] If all of the initial bombarding energy remains in the fireball until freezout, then these two energies are equal. If the spectrum of hadrons is an exponentially increasing function of their mass, the temperature of the fireball is bounded by $T_0 \simeq 134$ MeV. For energies above $\sim$ 5 GeV, the energy is stored in

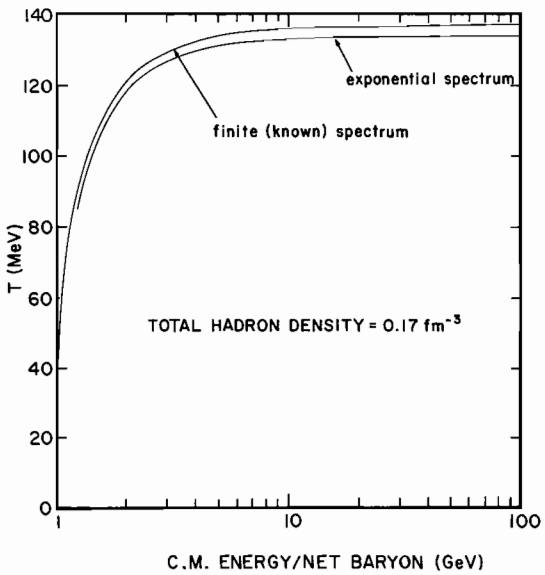

Fig. 1. Fireball temperature at fixed total hadronic density = 0.17 fm^{-3} as a function of total c.m. energy per net baryon for two extreme forms of the hadronic mass spectrum. (XBL 818-11471)

massive resonances to such an extent that the temperature remains saturated near this asymptote down to the freezout density.[2] However, as the other curve indicates, if the spectrum of hadronic resonances is bounded and limited to those already known, the opposite extreme from an exponential spectrum, the temperature rises so slowly with energy above $\sim$ 5 GeV that it appears to be asymptotic even though it is unbounded. Moreover, it is indistinguishably close to the temperature curve corresponding to the exponential hadronic spectrum! Only if T_0 were much less than m_π would the asymptotic temperature of an exponential spectrum be distinguishable from the temperature corresponding to a finite hadronic spectrum. But T_0 is not expected to differ appreciably from m_π.

The reason that the temperature *at* freezout density rises so slowly with energy is that mesons are copiously produced. The flatness of T at a value near m_π is purely coincidental for the finite spectrum. In fact, T is unbounded. Doubling m changes T by only several MeV. The evolution of temperature and particle populations for a 20 GeV/nucleon fireball was shown in Ref. 2, Figs. 5 and 6.

The conclusion is clear. Measurement of the *final* fireball temperature cannot be used to infer the form of the hadronic mass spectrum nor the existence of an asymptotic

temperature unless it is much less than $T \simeq 130$ MeV. This conclusion was reached under the assumption of a freezout density of 0.17 fm^{-3}. It is unreasonable to expect it to be larger than this, but it could be less. In this case, the curves in the figure would be even closer than they are.

References

1. R. Hagadorn, in *Cargese Lectures in Physics,* ed. by E. Schatzman, Gordon and Breach, New York, 1973, Vol. VI.

2. N. K. Glendenning and Y. J. Karant, Phys. Rev. C **21**, 1501, (1980).

Nuclear Physics from Subhadronic Structure–a Toy Model*

Herbert M. Ruck

In a mathematical model in 1+1 dimensions (one time, one space dimension), we mimic some properties related to (1) the structure of single particles (hadrons), (2) two particle interactions (nuclear potential), and (3) multiparticle states (nuclei and nuclear matter), as known from nuclear physics in 3+1 dimensions. The model consists of a set of classical field equations that describe two fermionic fields, "quarks," interacting with two scalar fields, "gluons." The number of fields involved and the structure of the interactions are determined by the internal cyclic symmetry group Z(3). The self-interaction of the scalar fields is cubic and quartic and is essential to the entire calculation.

It can be shown in 1+1 dimensions as well as in 3+1 dimensions, that as long as the internal symmetry Z(3) is preserved the fermions cannot be separated from each other and are therefore confined. Aside from this general result the calculations are done in the special case of 1+1 dimensions, where the soliton solutions of nonlinear equations occur readily, and by neglecting the feedback of the fermions onto the scalar fields. Partial results about lifting this approximation are reported at the end of this note.

1. For *single particles* we obtain a composite-extended structure, with the ground-state of mass $M = 10$, for particular values of the three free parameters in the model. Time oscillations of the fields generate a resonance state with $M^* = 15.56$. If the internal symmetry can be violated in a collision by removing one fermion, a system analog to the colored state in QCD results with the mass $M^c = 21.68$. A system without fermions, "glueball," has the highest mass $M^g = 23.31$.

2. The *two particle interaction* potential between two ground-states has a shallow attraction of −10 percent of M near the touching point of the particles and a hard core repulsion of 185% of M at complete overlap. The interaction between "colored" states or "glueballs" is strongly attractive.

3. The construction of *multiparticle states* shows the saturation phenomenon of multiparticle forces. Converting the data of the binding energy as a function of the distance into a function of the number density, we obtain the equation of state.

Recently, taking the feedback of the fermions onto the scalar fields into account, we solved iteratively the basic field equations. The effect of the new solutions is a shift in the mass spectrum which, for the same parameters as above, is now $M = 17.03$, $M^* = 22.69$, $M^c = 22.04$, and $M^g = 23.31$. The hard core of the interaction potential for two ground-states is no longer present.

Footnote

*Condensed from H. Ruck, Lawrence Berkeley Laboratory Reports LBL-12316, -12479, -12872, and -12852.

Percolation versus Gibbs Equilibrium – the Phase Transition from Hadron Matter to Quark Matter*

Horst Stöcker

The phase transition from hadron matter to quark matter is investigated in two distinct models: the percolation approach and the Gibbs phase equilibrium. We find a strong dependence of the onset of the percolation phase transition on the internal excitation energy E* of the matter; for E* $\simeq$ 3 GeV per baryon, the percolation sets in already at the ground state density of nuclear matter, $\rho_0 \simeq 0.17$ fm^{-3}. The implications of our results for relativistic nuclear collisions are discussed. In the hydrodynamical model, the onset of the hadron-quark matter phase transition is predicted at bombarding energies $E_{Lab} \geq 1$ GeV/n for central collisions of massive nuclei.

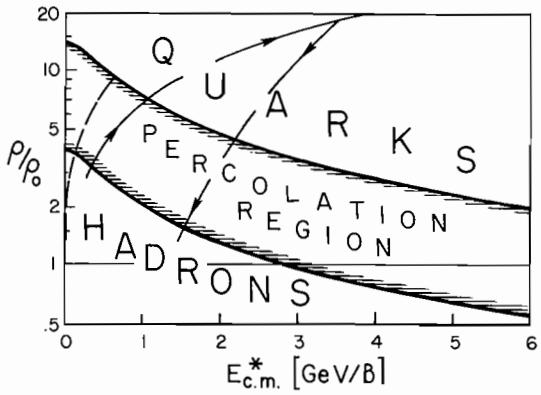

Fig. 1. (XBL 814-764)

Footnote

*Based on LBL-12633.

Strange Baryon Fraction from Quark-Gluon Plasma

N. K. Glendenning, M. Gyulassy, R. Anishetty, P. Koehler, and L. McLerran

We have calculated the fraction, f_s, of baryons that have non-zero strangeness emerging from very high energy nuclear collisions. If a quark-gluon plasma is formed, then that fraction can be calculated perturbatively from QCD. Asymptotically, $f_s \to 1 - (2/3)^3 \simeq 0.7$ because $(2/3)^3$ is the *a priori* probability that all three quarks are non-strange. As a function of energy per baryon, E*/A, in the rest system of the plasma, we found $f_s = 0.45, 0.5, 0.55, 0.6$ for E*/A $\simeq$ 9, 11, 14, 20 GeV/A. Below E*/A $\lesssim$ 7 GeV/A, perturbation theory is unreliable.

In contrast, f_s for a Hagadorn gas of hadrons reaches for E*/A $\gtrsim$ 4 GeV, the asymptotic value $f_s \neq 0.34, 0.35, 0.37, 0.38$, for E*/A $\simeq$ 9, 11, 14, 20 GeV/A.

Therefore, if large enough energy densities $\epsilon = E^*/A\rho \gtrsim 10$ Gev (0.15 fm^{-3}) $\sim$ 1-2 GeV/fm^3 can be equilibrated in a nuclear collision, f_s could possibly serve as a signature of a quark-gluon plasma phase transition.

Non-Linear Vacuum Polarization in Strong Fields

M. Gyulassy

Based on the Wichmann-Kroll formalism, the effect of non-linear $\alpha(Z\alpha)^{n\geq 3}$ vacuum polarization was reviewed for very large Z systems, Z $\to$ 180. The question is whether QED effects could prevent the $1S_{1/2}$ electronic orbitals from reaching a binding energy $B = 2m_e$. Beyond that point, the vacuum decays to a state with two free positrons and two bound electrons. The non-linear vacuum polarization density ρ^{3+} is calculated assuming that the j = 1/2 states dominate. The basic formula is

$$\rho^{3+}(r) \simeq \frac{|e|}{2\pi} \int \frac{d\omega}{2\pi i} \mathrm{Tr}[G_1(r,r;\omega) + G_{-1}(r,r,\omega) - 2Z\alpha G_1^1(r,r;\omega)] \quad (1)$$

in terms of the radial Green's functions G_k and the first order piece G_k^1. The results of these calculations were published in Ref. 1.

The new observation[2] is that an effective screening charge can be defined from the energy shifts due to Eq. (1) as

$$\Delta E3+ = Q_{eff}^{3+} <\alpha/r>_{1S_{1/2}} , \qquad (2)$$

where $<1/r>$ are calculated from the finite radius electron wavefunctions. Similarly the screening charge due to third order $\alpha(Z\alpha)^3$ can be defined. These quantities are convenient because they can be readily compared to the point nucleus screening charged computed by Wichmann and Kroll. The results are shown in Fig. 1. The remarkable result is that $Q_{eff}(Z)$ seems to be just a shifted version of the Wichmann-Kroll charge $Q_{wk}(Z)$ such that

$$Q_{eff}(Z) \simeq Q_{wk}(Z - Z_c + 137) , \qquad (3)$$

where $Z_c \simeq 175$ is the critical charge for a finite radius nucleus. Figure 1 shows directly that $Q_{eff} \ll Z$ even for $Z \to Z_c$ and therefore diving ($B = 2m_e$) is not prevented by vacuum polarization.

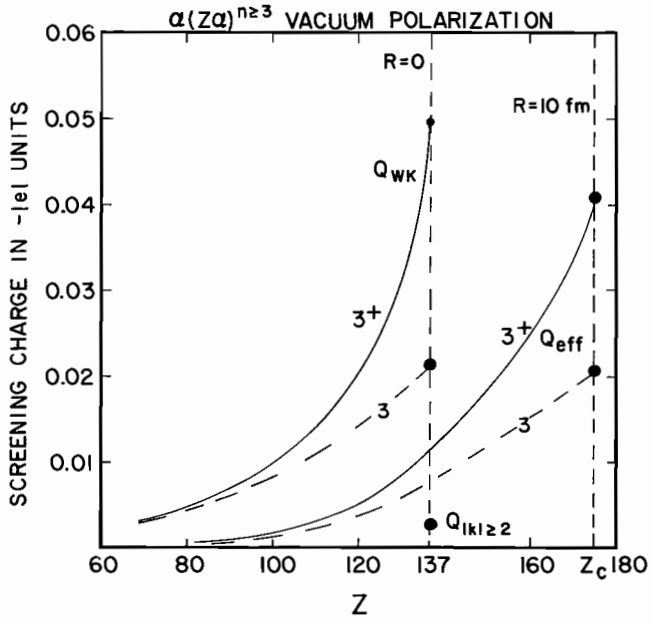

Fig. 1. Effective non-linear screening for orders $\alpha(Z\alpha)^{n>3}$ labeled 3^+ and order $\alpha(Z\alpha)^3$, labeled 3. (XBL 817-10647)

References

1. M. Gyulassy, Nucl. Phys. A **244**, 497 (1975).
2. M. Gyulassy, Lawrence Berkeley Laboratory Report LBL-12972 (1981).

III. INSTRUMENTATION

INSTRUMENTATION

A. Spectrometers

HISS Detector Systems

*Hank Crawford**

Experiments at the HISS facility require analysis of multiple particles from each event to investigate the energy transfer spectrum, the production of very high transverse momentum light and heavy fragments, the role of electromagnetic excitation in nuclear fragmentation, and the size of the interaction region in relativistic nucleus-nucleus reactions. In this report, I describe the detector system which, in conjunction with the HISS dipole, must provide the charge, mass, and momentum of 10 or more fragments from each interaction.

The Phase 1 detector system consists of three major subsystems. To measure rigidity, we use two large (1 × 2 m) drift chambers in conjunction with the HISS magnetic field ($\int Bdl = 75$ kG-m). To measure charge for light fragments ($Zf \leq 6$), we pulse-height analyze both the time-of-flight scintillators and a subset of drift chamber wires. To measure charge for $Zf > 6$, we use a 1 × 1 × 5 m multiple sampling xenon filled ionization chamber. To measure velocity, we use both a scintillator array (30 pieces, each 200 cm × 10 cm × 2 cm) for time of flight and a silica aerogel Cherenkov hodoscope (10 pieces each 100 × 10 × 2 cm). In addition, we will employ two position sensitive detectors to define the incident particle vector. With the system configured as shown in Fig. 1, we expect to attain charge resolution of $dZ < 0.01Z$, mass resolution of < 0.3 amu at $A = 60$, and momentum resolution of $dp < 0.001P$ for each fragment.

The first generation of experiments proposed for the HISS facility required construction of drift chambers for operation 2 m and 3 m downstream of the center of the dipole as shown in Fig. 1.[1] The alternation of anode and cathode wires in successive planes removes left-right ambiguity, improves particle pair resolution, and allows construction of a track vector from a single chamber.

The electronics for these chambers were designed to provide both position and pulse height information for each fragment passing through them. This pulse height is to distinguish charges 1,2, and greater than 2 to augment the charge information attained in the TOF wall and MUSIC detector and to aid in unscrambling multiple fragment events. Each chamber, being ~ 10 cm thick, can provide a rough track vector which will point to the second chamber location. This allows straightforward unscrambling of even high multiplicity events.

Charge for light fragments ($Zf \leq 6$) is determined by pulse-height analysis of the TOF wall scintillators and by pulse-height analysis of a subset of the drift chamber

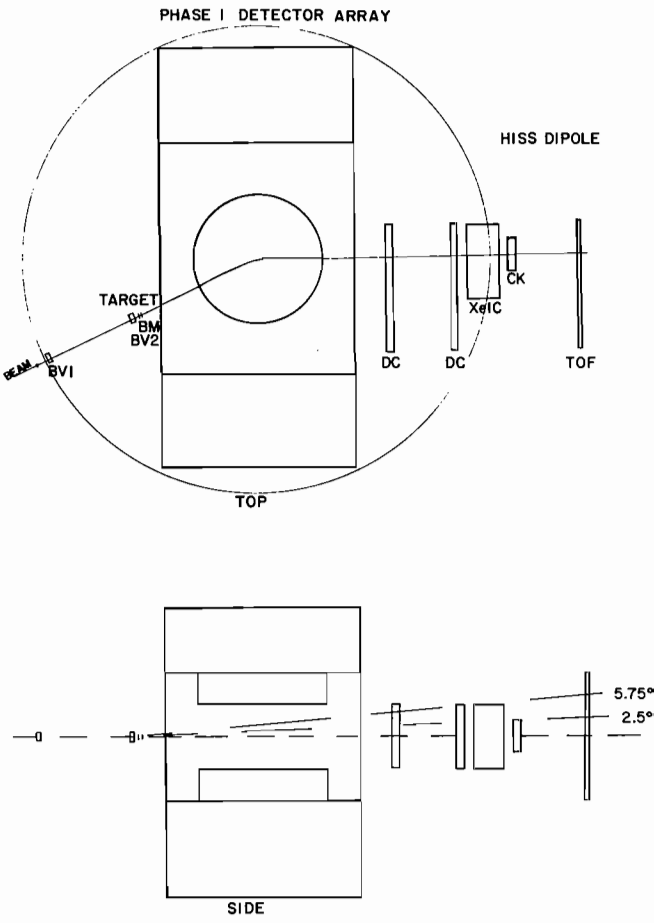

Fig. 1. (XBL 807-10739)

wires. Fragment charge for heavy fragments is determined primarily by a new type of large area high resolution detector, a Multiple Sampling Ionization Chamber (MUSIC). High charge resolution is attained in the MUSIC detector by measuring many samples of the ionization produced along the path of a particle as it traverses 50 cm of Xe gas.[2]

A measurement of fragment velocity is required to convert rigidity and charge measurements to momentum, charge, and mass. Velocities of light fragments will be determined by time of flight from the target to the scintillators of the time-of-flight wall. Velocities of heavy fragments ($Af > 10$) will be determined by their signal levels in a silica aerogel Cherenkov detector array.[3]

As designed, the detector system is modular to accommodate the range of experiments envisioned. The charge, mass, and momentum resolution are sufficient to provide high quality data over a broad range of new physics from high energy heavy ion interactions.

Footnote and References

*UC Space Sciences Laboratory.

1. D.E. Greiner et al., IEEE Trans. Geosci. Elec. **16**, 163 (1978).
2. G. Igo and R.M. Eisberg, Rev. Sci. Instrum. **25**, 450 (1954).
3. M. Cantin et al. Nucl. Instrum. and Methods **118**, 177 (1974).

Monitoring the HISS Magnet

*F. Bieser and C. McParland**

The recently completed HISS superconducting dipole has been outfitted with nearly 100 sensors to provide diagnostic and control feedback information about the electrical, mechanical, and cryogenic systems. Thirty-two strain gages are mounted around the support rings, which must withstand over one million pounds of thrust as the magnet is energized. Measurements are made with a resolution of 1, 2, or 4 microstrain with full scale limits of plus or minus 2000, 4000, or 8000 μstrain. Nineteen thermistors are located on the cryostats and transfer lines to monitor the temperatures of the coil bobbins and helium gas during cool-down. Measurements cover the range of 293 K (room temperature) to 4 K with a resolution of 0.1 K.

Solid state pressure transducers and liquid level sensors monitor the pressure and level of the liquid helium. Isolation amplifiers are used to monitor various voltages while the magnet is energized. Forty-eight channels of relay input registers monitor the power supply and quench protection chains.

All parameters are read into a PDP 11/34 computer via CAMAC once every second. A variety of pictorial displays are available on video monitors for real-time monitoring. The data is compressed and archived on the VAX 11/780 where it can be accessed at any future time for trend analysis, event reconstruction, etc.

Dipole parameters, read once a second, are archived into five separate files. These files contain data from the most current hour, day, week, month, and year. Since all five files are of identical length, each file's time resolution is different. Thus, interesting events (dipole current charges, loss at coolant, etc.) can be examined immediately with one-second resolution between data points. As time passes, this same data propagates through each file, losing some time resolution between each file. The above system, combined with the MULTI analysis program, enables graphics display and analysis of all dipole engineering data.

Footnote

*UC Space Sciences Laboratory.

Program Needs for a High-B Field Facility for Visual Detectors at the Bevalac

Harry H. Heckman

The current trend in Bevalac research requires the use of 4π, high-spatial-resolution, visual track detectors. In addition to nuclear emulsions, such detectors include plastics and AgCl crystals. Future visual-detector experiments of high priority will be those to determine: (1) the properties of "anomalons," i.e., projectile fragments that have anomalously short mean free paths, and (2) the multiplicities, charge, and energy spectra of projectile and target fragments produced in relativistic uranium-nucleus collisions. We cite these two experiments, not only for their scientific interest, but also to demonstrate how the use of nuclear emulsions (in particular), when exposed in a high-intensity magnetic field of 0.3-0.5 megagauss (MG), will enable us to obtain the following *exclusive* charged particle data: (1) the total multiplicity of charged particles and their emission angles, and (2) the rigidity R (hence momenta P = ZR when charge Z is measured) of all charged particles that are emitted within approximately $\pm$ 30° of the plane normal to B (i.e., $\Omega = 2\pi$ sterad). These measurements can be performed under the highest conceiv-

able multiplicities, M, expected from U_{92} + Ag_{47} collisions at 1 A GeV, e.g., M $\simeq$ 150-300. Furthermore, the charge and rigidity measurements can be made to accuracies $\sigma_Z < 0.5$ unit and $\Delta R/R \lesssim \pm 5\%$, respectively, in track lengths of 1 cm, or less, a feature crucial to our planned experiments on anomalons. Measurements of ionization (dE/dx) and rigidity will lead to the mass identification of π, K, and nuclei $Z \lesssim 5$ over a significant range in phase space.

In anticipation of the applicability of a high-B field facility for visual detector to Bevalac research, Heckman and Herlach exposed a small ($\sim$ 1 cm^3) emulsion stack to 19 GeV electrons at SLAC while placed in an exploding single-turn, field-producing coil at B = 0.92 MG.[1] At $\sim$ 1 MG, magnetic deflection dominates multiple scattering and the measurements of rigidity can be made to an accuracy of several percent. It was found that: (1) no deleterious effects occur to nuclear emulsion, physically or photographically, when subjected to pulsed magnetic fields as high as 1 MG, and (2) the < 1 micron spatial resolution of emulsion enables precise curvature measurements of a particle track irrespective of accompanying particle background and/or multiplicities.

As an example of a specific experimental application of a high-B facility, we consider the case of the catastrophic destruction of a 1 A GeV ^{238}U nucleus in a head-on collision with an emulsion nucleus where all the emitted particles have Z = 1 and include π, K, p, d, and t. Figure 1 is a plot of rigidity vs ionization, expressed as grain density relative to minimum grain density, for each particle. The rigidities of the π and K mesons are plotted to arbitrarily high values, whereas the p, d, and t are limited to velocities $\beta \leq \beta_{beam}$. The open rectangles indicate the Fermi widths of projectile fragments. The small bars underneath the rectangles show the errors of rigidity measurement (ℓ = 1 cm, B = 0.5 MG) at beam velocity. The vertical and horizontal error bars drawn on the d-curve of R vs g/g_{min} represent a $\pm$ 5% error in the measurement of g/g_{min} and a $\pm$ 6% error in R, respectively. The obvious conclusion from this figure is that the p, d, and t are fully resolved over all allowed rigidities. With the expectation that the pion spectra are predominantly < 1 GV and the production of kaons will be small, complete mass separation of all Z = 1 particles can be expected in actual practice.

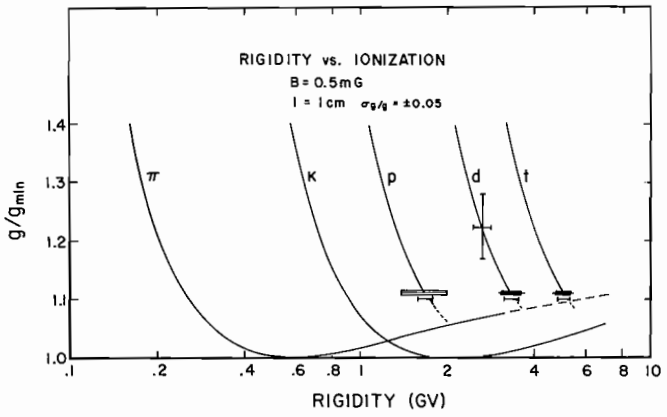

Fig. 1. Rigidity versus normalized grain density for Z=1 mesons and nuclei. (XBL 8111-12618)

Basic guidelines for the design of a high-B field facility for the Bevalac that we propose are:

1. B field = 0.3 to 0.5 MG, normal to plane of detector. Field volume at least 5 cm diameter × 1 cm.
2. Pulse duration should be order of 1-10 msec, with the requirement that the field be maintained to within a few percent of peak field during beam arrival. Compatibility with beam extraction is essential.
3. Pulse rates of the magnet may be as low as 1/min; with coil lifetime $\simeq$ 1000 pulses.
4. The coil design should i) accommodate the entrance (and exit) of the beam ($\sim$ 1 cm diam.) without intercepting the coil or other structures and ii) allow for easy mounting of the detectors in the field volume.
5. The B field over the area of the detector should be uniform to 10%. Field structure (calibration) can be determined by curvature measurements of beam tracks of known rigidity.

Reference

1. H.H. Heckman and F. Herlach, Nucl. Instrum. Meth. **106**, 269 (1973).

TASS – Two-Arm Spectrometer System

G.R. Roche, J.M. Engelage,† J.V. Geaga,‡ J.W. Harris,§ P.N. Kirk†*
R.W. Koontz, H.G. Pugh, C.L. Ruiz,† L.S. Schroeder, and R.N. Treuhaft

The construction of the Two-Arm Spectrometer System (referred to as TASS) was first motivated by a backward-forward particle correlation study in p-nucleus and nucleus-nucleus reactions.[1] The design for TASS was started in 1979, with installation completed by July 1980. Recently, a second-generation experiment to study $\pi^{\pm}$ production with high statistics has been started,[1] and several proposals for future study are being prepared.

TASS consists of two C-magnets mounted on top of separate air pads which allow the independent angular positioning of the arms. Figure 1 shows a diagram of the

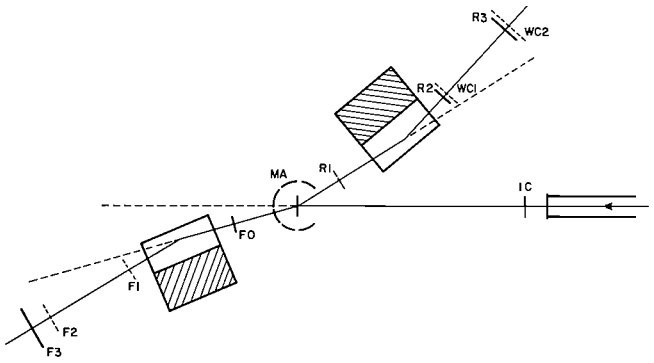

Fig. 1. Diagram of the Two-Arm Spectrometer System.

R1:	3-element scintillator hodoscope
R2,R3:	scintillator gating counters
WC1,WC2:	multiwire proportional chambers
F0,F3:	scintillator gating counters
F1,F2:	16-element scintillator hodoscopes
MA:	16-element multiplicity array
IC:	ion chamber

(XBL 8110-1610)

apparatus. In its present configuration, the rear arm consists of both scintillation counters and wire chambers; these are used with the known magnetic field of the spectrometer to provide the momentum, angle, and identity of a charged particle traversing the system. The forward arm consists primarily of two 16-element scintillation hodoscopes, which allow us to measure the forward particle's momentum, angle, and identity, using the beam center at the target location or the interaction point coordinates given by the rear arm. Extensive wire orbiting of both spectrometer magnets has been done.

Table 1 gives the main characteristics of TASS.

TASS is equipped with electronic circuitry and a PDP-11 computer, which at present enables the following on-line analyses to be made: time-of-flight and amplitude distributions for each scintillation counter, real to random signal for each arm and both arms in coincidence, momentum and angle distributions, and particle identification. The data-taking rate can be of the order of 200 events per spill, with a dead time of about 30%.

As an example of TASS performance, Fig. 2 shows the ability of the system to identify particles. The figure is a scatter-gram of the particle masses determined when the two arms of TASS were operated in a coincidence mode.

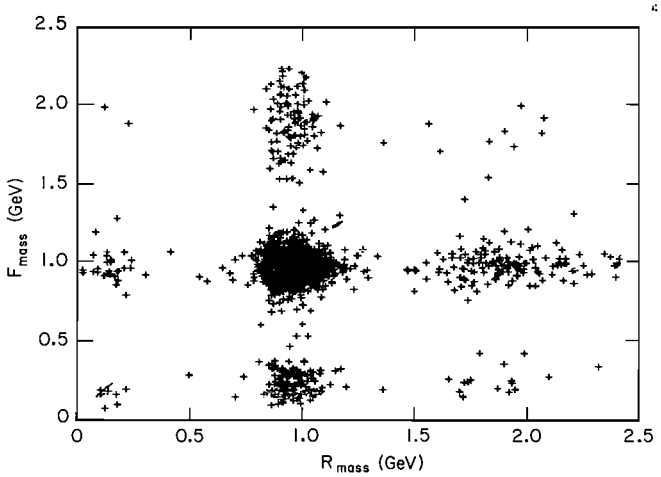

Fig. 2. Scatter-gram of the particle masses determined when the two arms of TASS were operated in a coincidence mode. FMASS and RMASS are the masses of the particles in the forward and rear arms, respectively.

(XBL 8110-1611)

Table 1. Characteristics of TASS.

	Rear arm	Front arm
Central momentum range	0 to 2150 MeV/c	0 to 2150 MeV/c
Momentum acceptance: $\Delta p/p_o$ (% of the central momentum p_o)	−35 to +50%	−35 to +50%
Angular range (minimum angle between both arms = 70°)	60 to 180°	1 to 60
Angular acceptance: $\Delta\Omega$ (steradian)	$3.26 \cdot 10^{-3}$	$2.01 \cdot 10^{-3}$
Horizontal angular acceptance	2.77°	2.71°
Vertical angular acceptance	3.86°	2.43°
$\frac{\Delta p}{p_o} \cdot \Delta\Omega$(steradian)	$2.77 \cdot 10^{-3}$	$1.71 \cdot 10^{-3}$
Momentum resolution	2.0%	4.4%
Angular resolution	0.25°	0.33°

This data sample was taken with the rear arm at $\theta_b = 120°$, $p_b = 400$ MeV/c, and the forward arm at $\theta_f = 45°$, $p_f = 400$ MeV/c for 2.1 GeV protons on carbon. The data are seen to produce a clustering of points at the expected masses for pions, protons, and deuterons. Thus, we observe clear coincidence signals for proton forward/proton backward, pion forward/proton backward, etc.

By early 1982, TASS will be improved by the addition of wire chambers to the front arm, so that both arms will be identically instrumented. The orientation of the rear magnet is also being rotated by 180° to enable both arms to be used in the forward direction; the minimum angle between the arms will then be reduced to 45°. We anticipate a full program on TASS using the up-graded Bevalac in 1982 and beyond.

Footnotes and Reference

*On leave from University of Clermont-Ferrand II, France, supported in part by a NATO grant.
†Department of Physics and Astronomy, Louisiana State University.
‡Department of Physics, University of California-Los Angeles.
§Gesellschaft für Schwerionenforschung, Darmstadt, West Germany.
1. See R.N. Treuhaft et al., "Few Nucleon Interactions and Correlation Studies," this annual report.

Streamer Chamber Instrumentation

R. Brockmann, J.W. Harris,* A. Sandoval,* H. Strobele,* R. Stock,* M. Maier,† R.E. Renfordt,† J. Miller,‡ H.G. Pugh,‡ M. Raff,‡ L.S. Schroeder,‡ F. Riess,§ K. Wolf,‖ A. Dacal,¶ and M.E. Ortiz¶*

During the year, improvements were made in the trigger system, the targets, the image quality, and the data and image acquisition. In the trigger system, the beam defining scintillation counters were replaced by two 150 micrometer 300 mm^2 Si surface barrier detectors with a fast time pickoff. In addition to reducing the overall mass of the trigger system and therefore the probability of interactions in the trigger counters, the energy resolution permitted discrimination between fragmented beams and interactions in the detectors.

Metallic targets were used inside the chamber for the first time. Thin Ca and Pb targets inside 9-μm plastic bags in air or encapsulated in an atmosphere of SF_6 were used. For the low-energy runs a stack of six thin BaI_2 targets (25 mg/cm^2) was constructed and used successfully.

Several changes were made to improve the quality of the streamer chamber photographs. The Sprague solid capacitors were replaced with oil-filled, 0.1 μF Maxwell capacitors in the Marx generator, improving the stability and reliability of the high-voltage system (Fig. 1). A better system for monitoring Marx generator high voltage and time jitter was installed.

The streamer chamber gas mixture was modified by the addition of isobutane in a concentration of several ppm. The result was more condensed flares and brighter, better defined tracks.

The camera system was modified by the addition of image intensifiers, although the utility of these devices was found to be compromised by a still-unresolved problem of ghost images (For details see separate report in this section). A charge coupled device (CCD) TV camera was installed to monitor the events, providing directly digitized images (See separate report in this section). Downstream of the chamber, the two walls of plastic scintillator, used for pulse height and time-of-flight analysis of fragments, were fitted with LEDs for purposes of uniform calibration.

Extensive use of computers was made. An LSI-11/23, running under RT-11, controlled the CCD electronics. A PDP 11/34, running QDA/MULTI under RSX-11M, took data from a CAMAC crate monitoring the scintillator hodoscopes and the beam and trigger counters, providing immediate feedback on the beam tune, the trigger electronics, and the high-voltage pulse.

Footnotes

*GSI, Darmstadt, West Germany.
†Universität Marburg, West Germany.
‡LBL, Berkeley.
§Universität München, West Germany.
‖Argonne National Laboratory.
¶IFUNAM, Mexico.

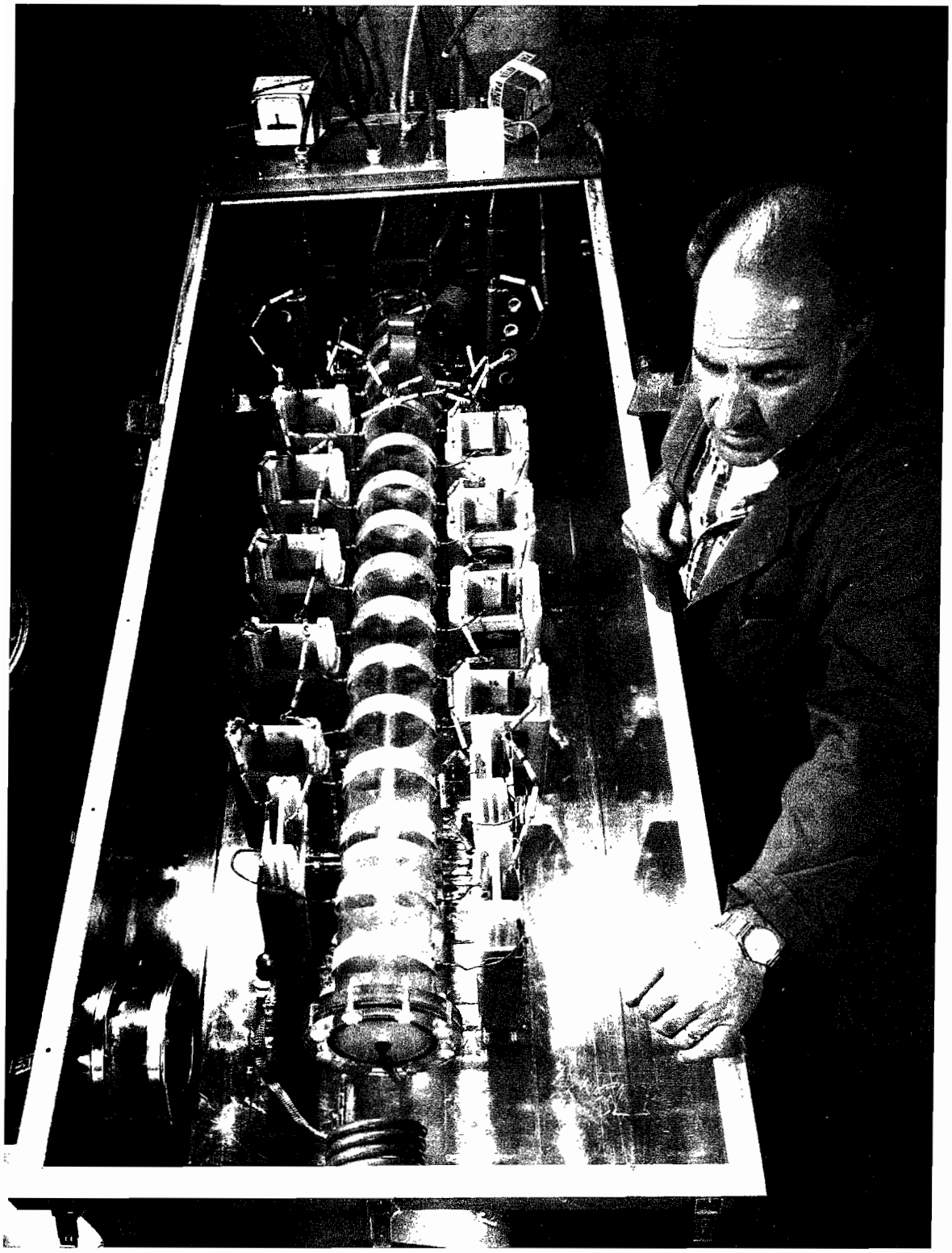

Fig. 1. View of the Marx generator with the new set of capacitors. The capacitors, with a voltage difference of 60 kV, are charged in series and discharged in parallel through the spark gaps in the column, producing a 720 kV pulse that, after shaping, is applied to the streamer chamber. (CBB 817-6558)

Use of a Directly Digitized CCD Camera

R. Brockmann,[*] J.W. Harris,[*] A. Sandoval,[*] H. Strobele,[*] R. Stock,[*]
M. Maier,[†], R.E. Renfordt,[†] J. Miller,[‡] H.G. Pugh,[‡] M. Raff,[‡]
L.S. Schroeder,[‡] F. Riess,[§], K. Wolf,[‖] A. Dacal,[¶] and M.E. Ortiz[¶]

Since the introduction of the streamer chamber in the early 1970s, there have been several studies of the use of directly digitized pictures. These usually employ very sensitive TV tubes[1] or solid state cameras.[2] In the past, technological reasons have made it unfeasible to supplant the film with directly digitized images for data acquisition. The recent availability of large arrays of charge-coupled devices (CCD) with high quantum efficiencies as TV camera sensors, the development of fast (5-20 MHz) ADCs, and the availability of relatively inexpensive large memory modules enable reevaluation of their use for streamer chamber event recording.

We have obtained a CCD camera, digitizer, and memory developed by Lawrence Livermore National Lab, based on an RCA-SID 52501 CCD with 525 by 320 sensitive elements (Fig. 1). Each sensitive element is 30 μm $\times$ 30 μm in size, with a linear response and a quantum efficiency of 56% at 736 nm (color of the streamers in HeNe). With the camera enabled, it can be triggered by an external pulse and the image is read out after 8 ms of integration and digitized pixel by pixel into 8 bit words. The data are stored in a 160K of RAM memory, which can be directly accessed by an LSI 11-23 computer. The digitized data in the memory can also be converted to analog and stored in the CCD for viewing on a TV monitor.

Software has been developed to enable picture hold-and-store replay, obtain slices of the picture or relief maps of the intensity, and do background subtraction and curve fitting. The camera has been tested in several of the recent experiments. In Fig. 2 the interaction of a 2.1 GeV/A Ar on Pb is shown as recorded on film. Fig. 3 shows the intensity contour of the same event recorded by the CCD camera. Depending on the particle emission angle, one obtains between 100 and 300 samples of the light intensity per track giving enough spatial resolution for a track reconstruction equal to that of the film. However, the two track resolution is worse than on film, being about 1.2 cm in streamer chamber space if the whole chamber is imaged onto one CCD compared to 0.5 cm if film is used. This can be improved by using larger or multiple CCDs. At present the main problem is the enormous amount of information that must be processed and stored. With the LSI-11, one frame can be written onto a 1600 bpi magnetic

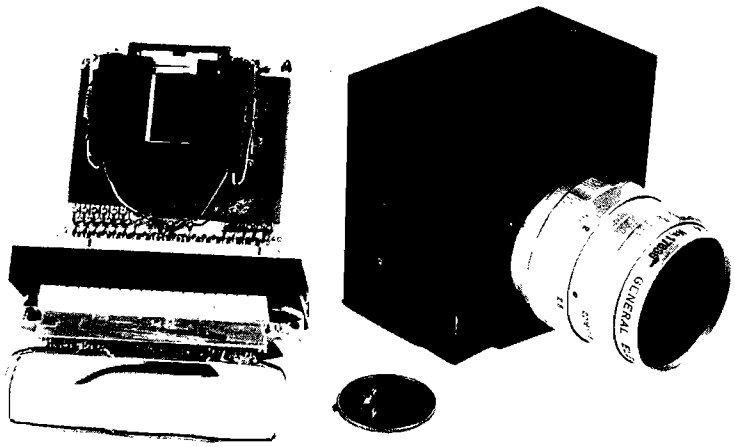

Fig. 1. CCD camera head. The 7.3 $\times$ 9.8 mm^2 image sensor, mounted on the board at the left of the picture contains an array of 320 $\times$ 525 light sensitive elements. A 25-cm CCTV lens was used to image the streamer chamber on the array.
(CBB 817-6556)

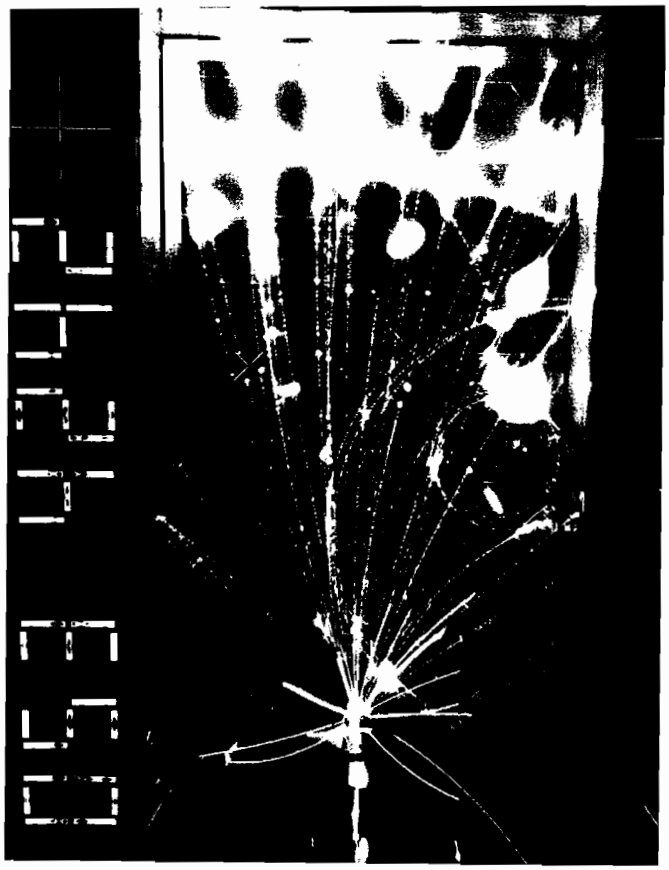

Fig. 2. Interaction of a 2.1 GeV/A ^{40}Ca on Pb recorded on film. This picture was selected for comparison with the directly digitized CCD picture (Fig. 3) because of its large multiplicity and large range of brightness between the beam, flare, and sparking tracks on one side and minimum ionizing pions and electrons on the other. In this case the beam enters from below. (XBB 818-8061)

tape in 4 seconds; a tape can hold only 100 frames. Data comparison and use of faster and larger storage devices are being investigated.

Footnotes and References

*GSI, Darmstadt, West Germany.
†Universität Marburg, West Germany.
‡LBL, Berkeley.
§Universität München, West Germany.
‖Argonne National Laboratory.
¶IFUNAM, Mexico.

1. M. Sevei, Proceedings of the Frascati Conference on Instrumentation 1973.
2. F. Villa and L.C. Wang, Nucl. Instrum. & Methods **144**, 533 (1977).

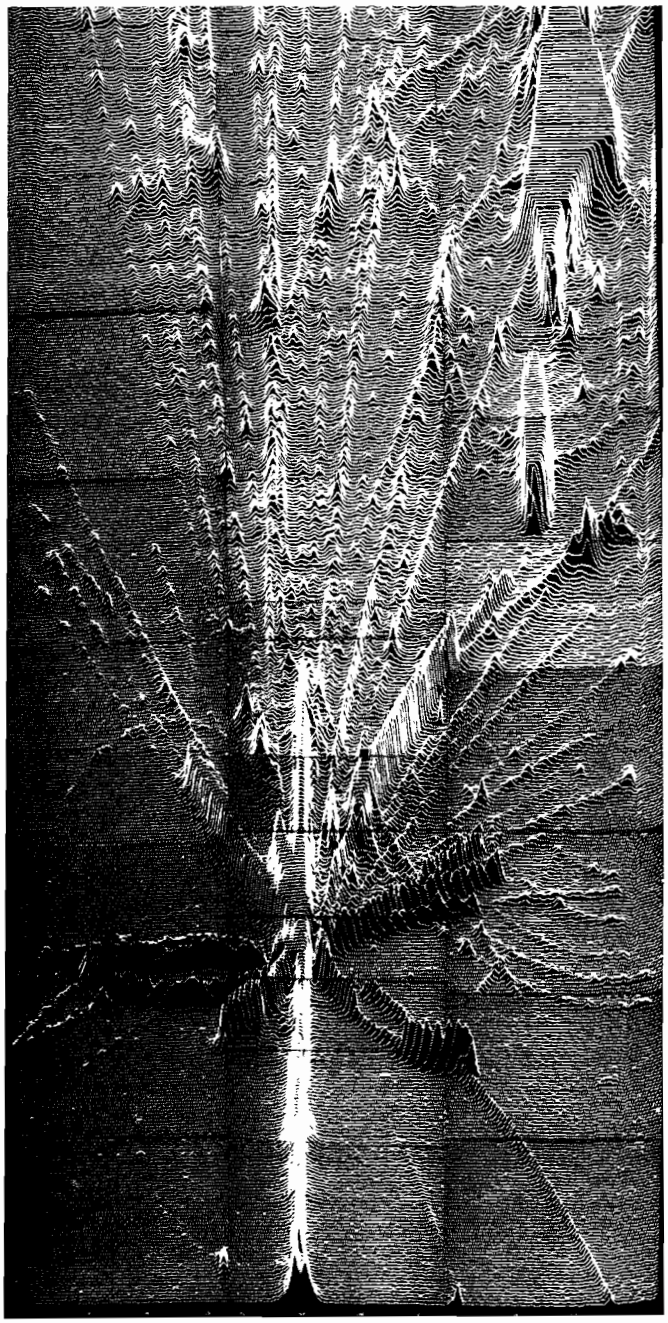

Fig. 3. Intensity contours of the directly digitized CCD image of the same event as Fig. 2. Each CCD pixel has been digitized into eight bits and shown here as linear spectra. The minimum ionizing tracks are just above background. Tracks well separated from each other are perfectly resolved. In the high track density regions, as for example, just downstream of the target, one sees that the minimum distance for two track resolutions is a factor of 2 to 3 larger than on film. (XBB 817-6698)

Image Intensifier Cameras for Event Recording at the Streamer Chamber

R. Brockmann,[*] J.W. Harris,[*] A. Sandoval,[*] H. Strobele,[*] R. Stock,[*] M. Maier,[†] R.E. Renfordt,[†] J. Miller,[‡] H.G. Pugh,[‡] M. Raff,[‡] L.S. Schroeder,[‡] F. Riess,[§] K. Wolf,[‖] A. Dacal,[¶] and M.E. Ortiz[¶]

To directly photograph streamer chamber events, the primary ionization produced by charged particles in the gas has to be amplified by at least a factor of 10^8. This is done by applying an electric field with a strength of $\sim$ 30 kV/cm for about 15 ns. In the Bevalac Streamer Chamber, a 400 kV pulse at the central electrode is required to generate this field strength. It is desirable to run the chamber at lower field gradients, which provides better stability and longer lifetime for the high-voltage Marx generator. This can be accomplished by photographing the fainter tracks with image-intensified cameras.

We have acquired four single stage, electrostatically focused Varo image intensifiers (Model 1248-1) with a 1/2-inch optical-fiber output coupling to the film. The image intensifiers have an S-20 photocathode and a P-20 phosphor with a gain of 140 at 15 kV and a resolution of 30 line pairs/mm. There is an inherent pincushion distortion on the intensified image that must be corrected in addition to the usual lens distortions.

The lens support on the flight research cameras were modified to accommodate the image intensifiers. The imaging on film is done by pressing the film with air against the optical fiber output of the proximity-focused image intensifiers. The stray magnetic field of the streamer chamber was reduced from 200 gauss to 1 gauss to enable the image intensifiers to operate properly. This was accomplished by using a Helmholtz coil to cancel the field.

The blooming of extremely bright tracks was reduced due to proximity focusing of the image intensifiers. This will be useful in the particle identification project that is being implemented at ANL for the analysis of these data.

An unexpected problem arose for sparking tracks which are about 1000 times brighter than the streamers. The slow component of the P20 phosphor produces a ghost image of sparking tracks in the next frame after the film has advanced (approximately 300 msec later). Fortunately, in this run, because such sparks were rare and also because the use of a 7-target stack greatly reduced the probability of successive interactions in the same target, there was very little confusion. Nevertheless, for high energy runs with a single target, the use of these image intensifiers is severely compromised due to the ghost images in the P2O phosphor. The use of faster phosphors is being investigated.

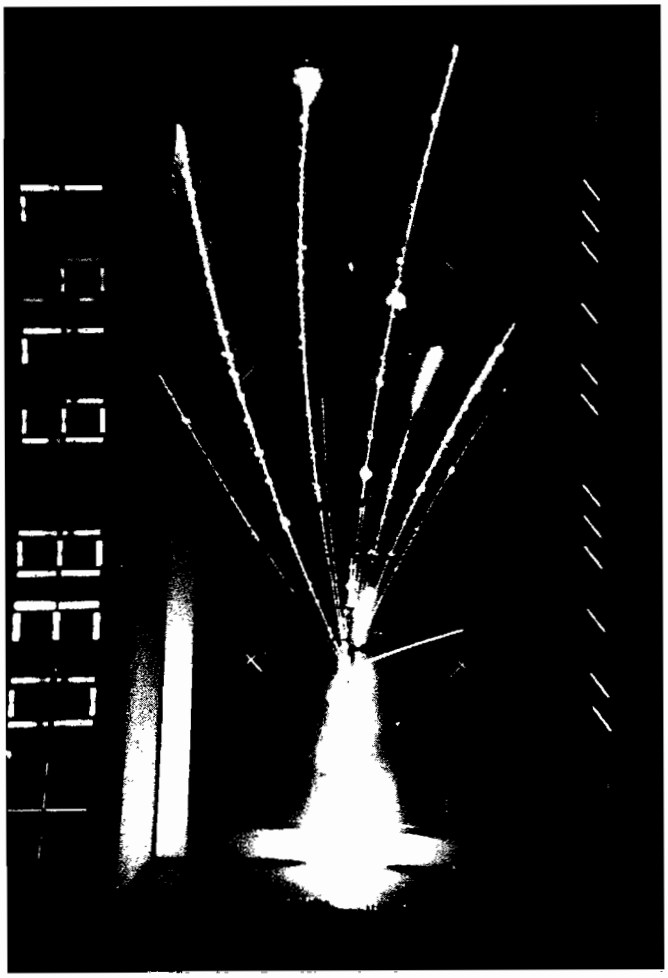

Fig. 1. Streamer chamber picture of the interaction of a 50 MeV/u ^{40}Ar on BaI_2 taken with the image intensifier equipped cameras. Several of the particles stop in the gas, producing a Bragg peak. One sees differences in ionization densities for different tracks.

(XBB 814-3521)

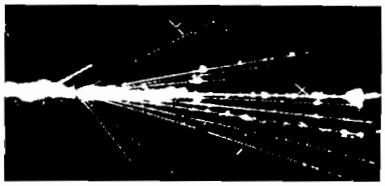

Fig. 2. Interaction of a 90 MeV/u ^{40}Ar on KCl with a ghost track produced by a very bright track of the previous event. (XBL 812-8062)

Footnotes

*GSI, Darmstadt, West Germany.
†Universität Marburg, West Germany.
‡LBL, Berkeley.
§Universität München, West Germany.
‖Argonne National Laboratory.
¶IFUNAM, Mexico.

The Plastic Ball Spectrometer

A. Baden, H.H. Gutbrod, H. Löhner, M.R. Maier, A.M. Poskanzer, H. Riedesel, H.G. Ritter, H. Spieler, A.I. Warwick, F. Weik, H. Wieman, and K.L. Wolf

The Plastic Ball was constructed for the study of relativistic nuclear reactions at the Bevalac.[1] It consists of 815 ΔE-E detectors covering a solid angle of 96% of 4π. Each module is capable of identifying the hydrogen and helium isotopes and the positive pions. The low energy pion channel (LEP) at LAMPF was used to determine the energy response and efficiency of several prototype modules for positive pions and protons at various energies.[2] Resolution and efficiency were found to be independent of the point at which the particle entered the detector. Scattered out particle events could be reconstructed by including neighboring detectors in the analysis.

After assembly of the modules, each counter was tested and calibrated at the 184 Inch Cyclotron with α-particles of 400 and 800 MeV. In this procedure, the voltage of the photomultiplier tube was first adjusted in order to obtain approximately the same pulse height for all modules. This measurement yielded calibration factors to take into account differences in the E and ΔE response. For 36 modules (2 of each type), the dependence of the pulse height on the energy of the incident hydrogen and helium isotopes was obtained by looking at the fragmentation products emitted by a thick target in the 800 MeV α-beam and by measuring the time of flight of those products.

After the measurement with the beam, each module was calibrated with a standard light source (xenon flash monitored by a photodiode) that was coupled to the module via a light fiber cable. During the experiment, this light source is regularly fired and serves to survey the stability of the detectors.

After assembly the Plastic Ball was installed on the Bevatron floor and operated successfully during two weekends in June. A total of two million events (minimum bias and central trigger) were taken in this first experiment for the following projectile-target combinations: 400 and 1000 MeV/u calcium on calcium, 400 and 1000 MeV/u argon on lead, and 800 MeV/u neon on lead.

Analysis of the data is in progress, and preliminary results show that, after applying known correction factors, the response of all modules is identical. The quality of the p,d,t-separation for 20 modules added is shown in Fig. 1. The x-axis represents the projection of a band in the ΔE-E plane on an axis perpendicular to the particle identification lines and the y-axis the number of events.

References

1. M.R. Maier, H.G. Ritter, and H.H. Gutbrod, IEEE Trans. Nucl. Sci. **NS-27** No. 1 (1980).
2. H.H. Gutbrod et al., IEEE Trans. Nucl. Sci. **NS-28** No. 1 (1981).

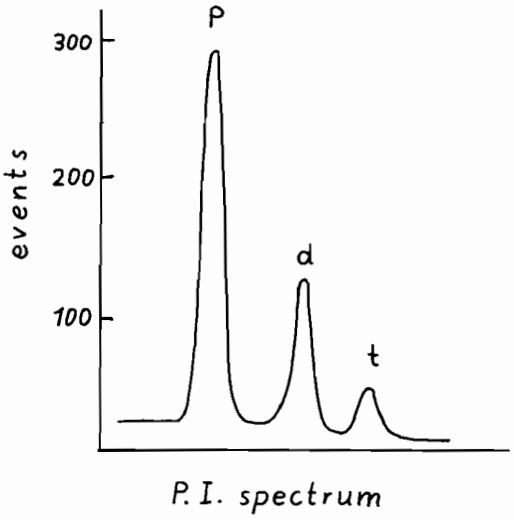

Fig. 1. The proton, deuteron, and triton separation achieved with the Plastic Ball modules. (XBL 818-11300)

New Developments at OASIS

J.M. Nitschke and J.D. Molitoris

Several new developments and improvements of the On-line Apparatus for SuperHILAC Isotope Separation (OASIS) occurred during the last year. Major changes in the target/ion-source region will be covered in a separate section of this annual report. The ion source is being operated in the electron bombardment/plasma and surface ionization modes. As has been reported previously, several rare earth elements, as well as Na, Fr, Ra, and Ac, have been separated using surface ionization. In addition, we have now obtained In isotopes from ^{107}In to ^{104}In. Plasma ionization has been used for Cd, Ag, Se, and Br. All these nuclei were produced in compound nucleus reactions, mostly with parasitic ^{20}Ne beams), with the target located about 4 cm from the ion source.

A modification of the ion source, however, enables us to now produce neutron-rich isotopes via deep inelastic reactions. The Ta target in this case is located about 1 mm from the ionization region and an acceptance angle of nearly 2π sr for the target recoils is achieved. With ^{40}Ar beams on ^{181}Ta, the following isotopes were identified: ^{39}Cl, ^{34}Si, ^{36}P, and ^{39}S. With ^{20,22}Ne beams on ^{181}Ta, we have separated $^{19, 20, 21}$O and $^{20, 21, 22}$F. The oxygen isotopes were also separated as carbon monoxides to avoid contamination from fluorine.

For the identification of neutron-rich light β-emitters, a cooled (80°K) Si ΔE-E β-telescope was built which permits on-line counting inside the cave. Because of severe background problems, highest priority at the moment is given to an isotope beam transport line which will guide isotopically pure beams to a shielded room located above the separator. Ion optical calculations (Fig. 1) show that this can be accomplished with an electrostatic mirror and two quadrupole triplets, Q_2 and Q_3. The transport line terminates in a tape system which will permit conduct of low background studies of isotopes far from the line of β stability. The tape system, which is presently under development, is based on an IBM 729 tape drive with a tape speed of 3 m/s. Assuming a distance of 10 cm between collection and counting position, half-lives below 100 ms can be studied if the release time of the ion source is of this order of magnitude. The detection equipment initially associated with the tape system will consist of a large volume, high efficiency Ge γ-detector, a Si ΔE, and a high-purity Ge detector for β particles.

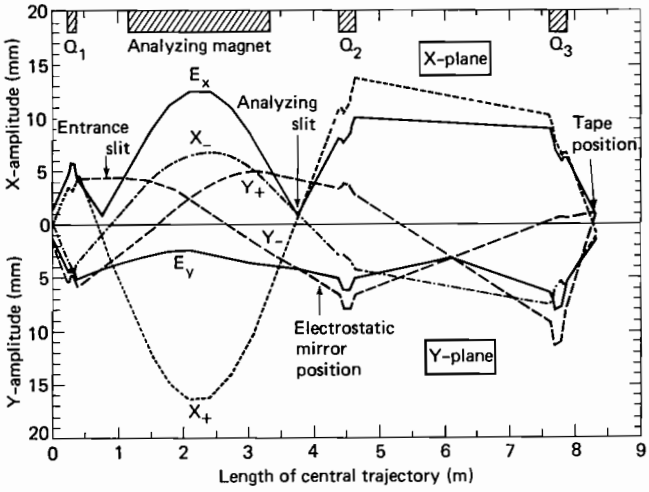

Fig. 1. First order ion optics for the on-line isotope separator OASIS including the isotope transport line. The analyzing magnet is an 180°, n = 1/2 dipole, Q_1, Q_2, and Q_3 are electrostatic quadrupole triplets, and $x_\pm$, $y_\pm$ are positive and negative x and y particle vectors, respectively. E_x and E_y represent the beam envelope along the central trajectory. (XBL 818-1192)

The entire separator is monitored by a PDP-11/10 process control computer which displays and prints out all major parameters, calculates masses from NMR measurements, and stabilizes the main high-voltage power supply. In the future, it will also be used to stabilize critical ion source parameters which are important in maintaining high ionization efficiencies during prolonged on-line runs.

A Versatile, High Temperature, High Efficiency Ion Source for the On-Line Isotope Separator OASIS

J.M. Nitschke

The heart of any on-line isotope separator is the ion source. Considerable effort was therefore put into the development of a source for the On-line Apparatus for SuperHILAC Isotope Separation facility (OASIS) which would meet the following requirements:

a. high efficiency,
b. short delay time,
c. good beam quality,
d. versatility, and
e. long life time.

Most of these goals have been achieved with the design shown in Fig. 1.

The operating principle of the source can be described as follows: target recoils are embedded in the anode end plate (catcher) and, because of its high temperature, diffuse rapidly into the ionization plasma region which is surrounded by the anode grid. This grid extracts electrons from a concentric cathode which, in turn, is heated by electron bombardment. The electrons oscillate on radial paths through the ionization volume, creating positive ions with the highest density on the axis of the ion source where the ions are extracted and accelerated towards the isotope separator.

The above-mentioned design goals are accomplished in the following ways.

a. High efficiency (η) is achieved due to the oscillation of the electrons and a high electron temperature and density ($\eta_{Kr} \simeq 34\%$).

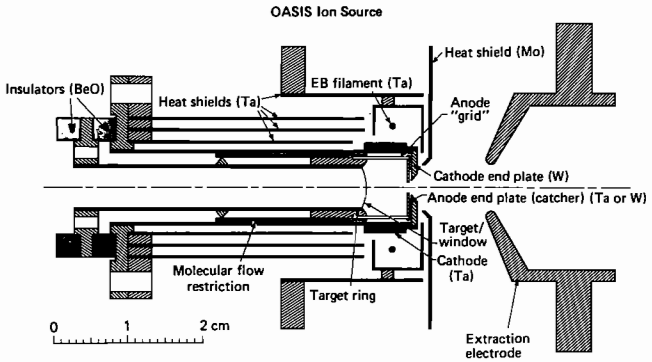

Fig. 1. Schematic representation of the OASIS ion source in its DIC version for the study of nuclei produced in deep inelastic reactions. (XBL 818-1193)

b. Short delay times are obtained because of the high catcher temperature (2800°C for Ta), the small volume of the source (typically 0.26 cm^3), and the large exit opening (typically 1.5 mm diameter).

c. The resolution of the separator is better than 1000 ($m/\Delta m$) for $\geq$ 90% transmission, which indicates a good beam quality. This can be attributed to the fact that there is no magnetic field present in the ion source (the field of the filament cancels on the axis), and that the total extracted ion current is low (typically $\leq$ 20 μA).

d. The source is quite versatile and, apart from the DIC version shown in Fig. 1, can be converted for the study of CN reactions and operated in the surface ionization mode.

e. The lifetime of the source (typically 10 to $>$ 100 hours) is limited by the evaporation of the tantalum or tungsten anode end plate. The usual insulation problems of high temperature ion sources are absent because all insulators are at low temperature ($\leq$ 1500°C).

The source is sealed by small gaps (typically 0.25 mm) which act as molecular flow restrictions, and the entire ionization region is kept at a temperature of $\sim$ 2500°C which avoids condensation of most elements. The operating parameters are usually kept within the following ranges:

anode potential:	120 to 160 V
anode current:	0.6 to 1.5 A
electron bombardment power:	400 to 600 W
extraction and acceleration potential:	50 kV

B. Detectors

A Glow Memory Chamber for Use in the Measurement of High Multiplicity Events*

M.A. Elola, T.A. Mulera, V. Perez-Mendez, and P.E. Wiedenbeck

One characteristic of relativistic heavy ion collisions is the high multiplicity (50-100 secondary particles) of a "typical" event. Information regarding the multiplicity, both its magnitude and any directional information, is desirable as an indicator of the violence of the collision and in the study of such phenomena as jet formation, hydrodynamic splash or other forms of collective behavior. We have continued our development of a detector capable of providing such information for use as a target area detector in the Heavy Ion Spectrometer System (HISS) at the Bevalac.

Conventional wire chamber readout techniques are plagued by x-y correlation ambiguities when more than one particle is registered in the chamber. In fact, to completely resolve all such ambiguities for n particles requires the reading out of n + 1 separate coordinates. Clearly, resolution of the ambiguities involved in an event of multiplicity 50, say, would be prohibitively expensive by this method. The reading out of each separate x-y coordinate in the detector via charge coupled devices, for example, is likewise an expensive solution to the problem. In our scheme, the x-y ambiguities are resolved in an inexpensive fashion by employing the detector itself as a correlated event memory, a method first suggested by Neumann and Sherrard.[1]

The passage of a charged particle through our apparatus is used to ignite a glow discharge at the point of passage. This ignition may be achieved through the use of pulsed spark chamber techniques or by some less cataclysmic avalanche method. Once ignited, the glow discharge may be maintained by a DC potential of several hundred volts for an indefinite period of time. This "memorization" of the position of the event allows the x-y correlation ambiguity to be resolved as follows. Each wire of one coordinate, say x, which registers a hit, is successively interrogated by the superposition of a voltage pulse over the DC glow maintenance voltage. The wires of the y-coordinate are then examined for the transmission of this pulse through the conductive glow. In this way, the x-y positions of the glows, and thus of the hits, are determined in an unambiguous way.

A large effort has been expended in studying the glow discharge mechanism and in prototyping glow discharge memory gaps. A "honeycomb" cell structure has been developed which gives good glow stability and multiple hit efficiency, and which also prevents the ignition of spurious glows in cells neighboring the location of the desired glow. Development of a readout system to locate these glows is being carried out with the help of the Physics Instrument Systems Group.

Ignition of glow discharges may be achieved by placing a conventional spark chamber gap atop the glow memory gap. Residual ions and ultraviolet light from the spark serve to ignite a glow discharge in the cell nearest the spark. Because of the traditional problems of long dead times and high radiofrequency noise levels associated with the use of spark chambers, alternative ignition methods are being investigated. Two such methods are ignition by ultraviolet light produced in gas scintillations, and ignition by the production and multiplication of electron-ion pairs in an avalanche less cataclysmic than a spark discharge, i.e., an avalanche taking place in the proportional or Geiger-Muller regime.

The final version of the multiplicity detector will surround the HISS target and will have an active area subtending as much of 4π steradians as is compatible with construction requirements.

A prototype device including a readout system (developed with the help of the Physics Instrument Systems Group) is being assembled. A novel feature is the ignition scheme, which consists of a multi-step avalanche chamber operating with pulsed high voltage.[2] Tests performed with this device will determine its single and multiple track efficiency, spatial and temporal resolution, and count rate capability. If the performance of this chamber proves satisfactory, it may be employed as an end cap in the HISS target area detector.

Footnote and References

*Condensed from a paper in preparation for the IEEE 1981 Nuclear Science Symposium.

1. M.J. Neumann and T.H. Sherrard, IEEE **NS-12**, 379 (1965). An elaboration of this idea may be found in H. Kobayakawa and T. Yamaki, International Conference on Instrumentation for High Energy Physics, Frascati (1973).

2. G. Roux et al., IEEE **NS-15**, 67 (1968).

Development of a Calorimeter for Relativistic Heavy Ions

J.D. Stevenson, J. Martinis* and P.B. Price*

Calorimeters have been used extensively in high-energy physics. They provide a relatively compact, low-cost detector with a large dynamic range.

We have built a small calorimeter and tested its response[1] to heavy ions at the Bevalac. Figure 1 shows the average pulse height in the calorimeter for various 2.1 GeV/N ions with charge-to-mass ratio of 1/2. The response of the calorimeter is quite linear.

Our primary interest in using the calorimeter was originally to search for exotic, high-mass, neutral particles such as polyneutron nuclei or hyperstrange nuclei among projectile fragments. We have recently found another interesting application[2] of the calorimeter. We have measured the total mass of the projectile residue on an event-by-event basis for 2.1 GeV/N ^{20}Ne + C and ^{20}Ne + Mo. Unlike previous measurements of cross sections for individual projectile fragments, the measurements are quite sensitive to the size of the target nucleus. The carbon target data (Fig. 2) are depleted of low-mass projectile residues by about a factor of 20 as predicted from a simple geometrical abrasion model (solid curve). The results provide the first conclusive evidence for the validity of the abrasion model. The portion of the curve at masses higher than that of the beam is due to the finite instrumental resolution of the calorimeter.

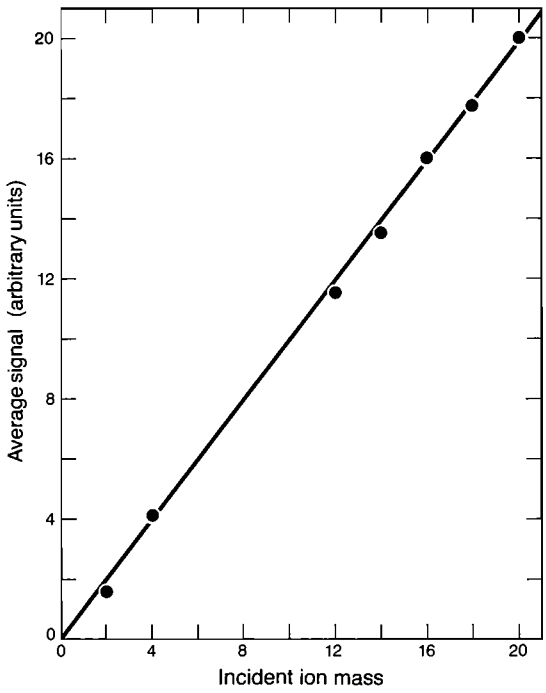

Fig. 1. Plot of the average signal in the calorimeter for various 2.1 GeV/nucleon ions as a function of ion mass.
(XBL 811-7694)

Footnote and References

*Also at Space Sciences Laboratory.

1. J. Stevenson, J. Martinis and P.B. Price, Nucl. Instrum. and Meth. (1981) in press; also LBL-12264.
2. J. Stevenson, J. Martinis and P.B. Price, submitted to Phys. Rev. Lett. (1981).

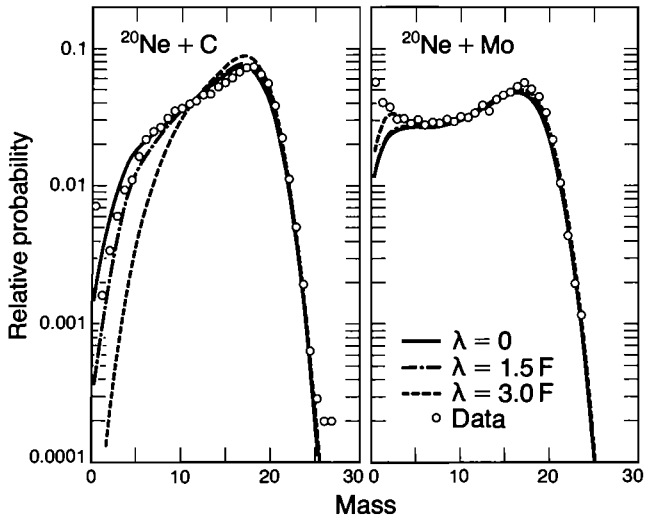

Fig. 2. Plots of the distribution of summed projectile masses for 2.1 GeV/nucleon ^{20}Ne + C and ^{20}Ne + Mo. Masses beyond 20 are due to spreading of instrumental resolution. The curves are based on abrasion calculations.
(XBL 8110-12205)

A Lead-Glass Gamma-Ray Detector for Relativistic Heavy Ion Collisions*

M.P. Budiansky, S.P. Ahlen,† and G. Tarlé†

We have developed a lead-glass detector for high-energy ($\sim$ 20-400 MeV) gamma rays resulting from relativistic heavy ion collisions. This detector has achieved an energy resolution significantly superior to any previously reported for lead glass.

Our detector has been used in an experiment at the LBL Bevalac. Our interest has been in measuring gamma rays from such sources as nucleus-nucleus bremsstrahlung, π° decay, and decay of the excited nucleon state $\Delta(1236)$. For this purpose we required a detector sensitive to gamma rays of energy $\gtrsim$ 20 MeV, and preferably insensitive to lower-energy gamma rays from deexcitation of nuclear levels. In addition, the detector had to be able to reject the large number of neutrons produced by high-energy ($\sim$ 1.8 GeV/nucleon) collisions of ions as heavy as argon.

The basic detector scheme has been used by others[1,2] and is shown in the right half of Fig. 1. The photon to be detected interacts in lead sheet C, where it converts to an electron-positron pair. These two particles produce signals in scintillator S and plastic Cerenkov detector Ck and then deposit the rest of their energy in the array of lead-glass blocks (30 × 30 × 30 cm of SF5 lead glass). A valid photon event is determined by the presence in S and Ck of signals corresponding to two relativistic singly-charged particles. We have calibrated our detector in a series of experiments at the electron linac at the Lawrence Livermore National Laboratory. We obtained electrons of energy 30, 50, 70, and 94 MeV, and we obtained calibration photons from the electron beam by using the method[3] shown in Fig. 1.[3] S2, S1, and A are scintillator paddles, and T is a lead target; the detectors to the right of the dashed line comprise the gamma-ray detector to be tested. An electron passing through the target has a certain probability of stopping in the target and transferring almost all of its kinetic energy to a single bremsstrahlung photon. The production of such a bremsstrahlung photon is identified by having signals in S1 and S2, and no signal in A.

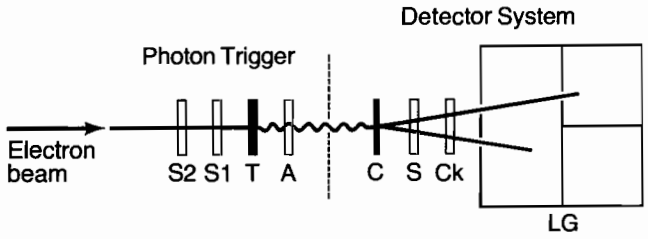

Fig. 1. Left half of figure shows scheme used at LLNL to obtain calibration photons. Right half shows main components of photon detector. (XBL 8011-12206)

By using RCA's "teacup dynode" phototubes and good light collection, we have achieved excellent energy resolution. Figure 2 shows the full width at half-maximum for Gaussian curves fitted to the lead-glass signal distributions for electrons of various energies. The FWHM is fit approximately by the relationship:

$$\text{FWHM} \simeq 5.7\% \,/\, \sqrt{\text{E(GeV)}} \ .$$

This is a factor of 2 better than the typical values given in the Particle Properties Data Booklet.

Footnotes and References

*Condensed from paper submitted to Nucl. Instrum. and Methods.

†also at Space Sciences Laboratory.

1. A.F. Dunaitsev and Yu.D. Prokoshkin, Nucl. Phys. **56**, 300 (1964).
2. G. Neuhofer et al., Phys. Letts. B **37**, 438 (1971).
3. D.J. Thompson, J. Geophys. Res. **79**, 1309 (1974).
4. Particle Data Group, Kelly et al., Rev. Mod. Phys. **52**, S1 (1980).

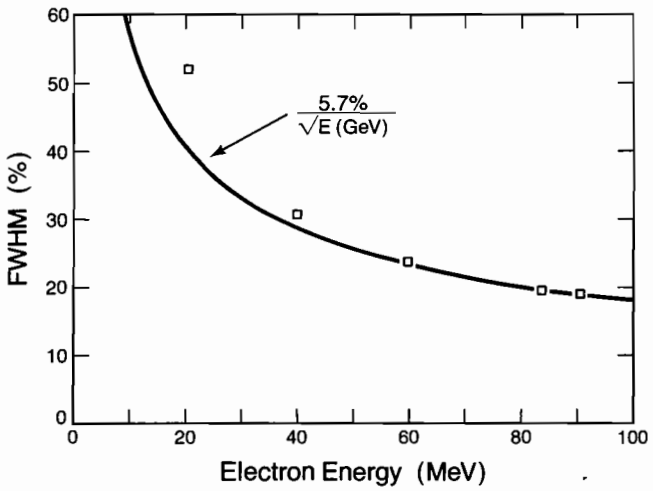

Fig. 2. Lead-glass energy resolution for electrons of various energies. (XBL 8010-12207)

Response of Organic and Inorganic Scintillators to Relativistic Heavy Ions*

M.H. Salamon and S.P. Ahlen†

We have studied the response of inorganic [NaI(Tl)][1] and organic (Pilot Y, Pilot B, Pilot F and NE110) scintillators[2] to the ions ^{20}Ne, ^{40}Ar and ^{56}Fe from 50 to 500 MeV/amu. Scintillator response is most conveniently characterized as the scintillation efficiency, dL/dE (light output per unit energy deposited) as a function of stopping power, dE/dx. Data for NaI(Tl) are shown in Fig. 1, while those for Pilot Y are in Fig. 2 (similar results were found for the other plastic scintillators).

Also shown in the figures are the results of calculations of response based on different scintillation mechanisms. For NaI(Tl) we adopted a diffusion model whereby deposited energy is free to migrate in the form of excitons. The saturation of scintillation light (observed as a reduction in dL/dE with increased dE/dx) is accounted for in the model by allowing for a bimolecular exciton-exciton quenching mechanism. The separation of efficiency curves of different ions for a given dE/dx reflects the dependence of dose profile on projectile velocity. Our model for NaI explains a-posteriori, for the first time, why there is no observed dependence of relative saturation behavior as a function of Tl concentration. Rather than depleting the fluorescent Tl sites, high energy densities are effectively reduced due to intense non-radiative exciton-exciton annihilations. Thus, the quenching process is a property of the NaI host itself.

A very simple model has been used to account for the Pilot Y data. Because of the inefficient molecular energy migration processes in plastic, as compared with NaI scintillators, there is a much stronger *delta-ray* effect, which enhances the separation of efficiency curves for Pilot Y compared to NaI. It is adequate to consider two distinct physical regions: the core, which is the region quite close to the trajectory, and the halo, which is outside the core. Quenching of scintillation light occurs within the core according to the Birks model:[2] $dL/dE \propto 1/(1 + B_s(dE/dx)_c)$, where $(dE/dx)_c$ is the energy deposited per unit length in the core and B_s is the quenching parameter. Energy deposited outside the core by delta rays is not subject to saturation. By incorporating higher-order corrections, the core and halo stopping powers can be calculated. The distinction is provided by the parameter T_o, which is the minimum delta-ray energy corresponding to the halo. The calculated points in Fig. 2 were obtained by determining the overall normalization from the muon point and the B_s parameter from low-energy alpha data. The best-fit value of T_o was 11.5 keV. The strong dependence of plastic scintillators on delta-ray energies makes these detectors ideal for the task of searching for antimatter in cosmic rays by taking advantage of the charge sign asymmetry of the Mott cross section.

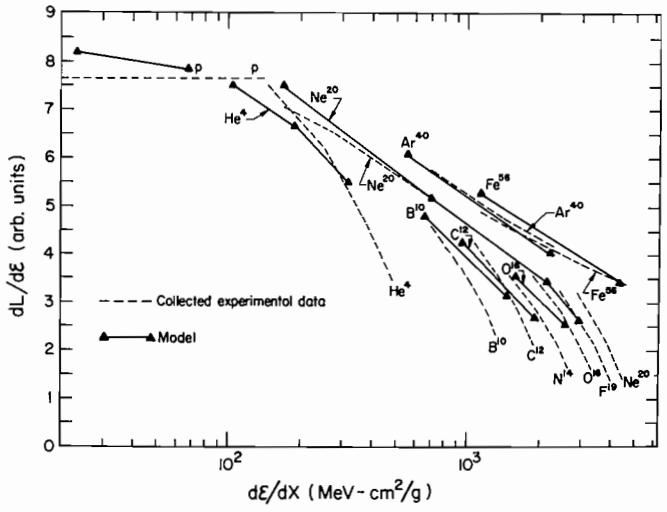

Fig. 1. NaI data and results of calculations from model. (XBL 8011-12802)

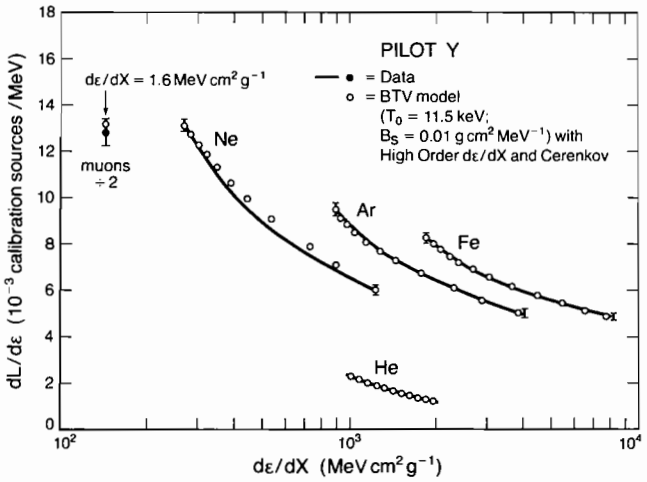

Fig. 2. Pilot Y data and results of calculation from model. Contributions due to Cerenkov radiation have been included. (XBL 8010-12208)

Footnotes and References

*Condensed from Refs. 1 and 2.

†Also at Space Sciences Laboratory.

1. M.H. Salamon and S.P. Ahlen, Phys. Rev. B (1981), to be published.

2. M.H. Salamon and S.P. Ahlen, submitted to Nucl. Instrum. and Methods (1981).

Calculation of the Relativistic Bloch Correlation to Stopping Power*

S.P. Ahlen†

Previous work[1] done at the Bevalac with relativistic ^{20}Ne, ^{40}Ar and ^{56}Fe ions in Al, Ca and Pb absorbers has clearly demonstrated the existence of a substantial deviation of particle stopping power from that predicted by the standard Bethe theory. Although much of the discrepancy could be accounted for by inclusion of Mott cross section corrections and Bloch's nonrelativistic wave packet correction, there was a slight residual discrepancy. It was suspected that the discrepancy was due to the inadequacy of Bloch's nonrelativistic treatment. Recently,[2] this calculation has been extended to arbitrary particle velocity by the incorporation of the third-order Born approximation to the Dirac wavefunction of an electron scattering off of a heavy nucleus. By summing over momentum states, a relativistic wave packet was constructed which was then allowed to scatter off the nucleus. In this manner, the close-collision energy loss of a heavy nucleus passing through matter could be calculated. Comparison of the results of this calculation with particle range data and with the Bethe theory is shown in Fig. 1. The abscissa is the charge of 600 MeV/amu ions utilized and the ordinate is the discrepancy of calculated entrance energies with those obtained from time-of-flight (TOF) measurements. The dashed lines correspond to standard deviations in the TOF measurement, while error bars include uncertainties in range measurements and in the values of the adjusted mean ionization potential. It is seen that the calculations which include all corrections are in excellent agreement with data. The same is clearly not the case for the Bethe theory.

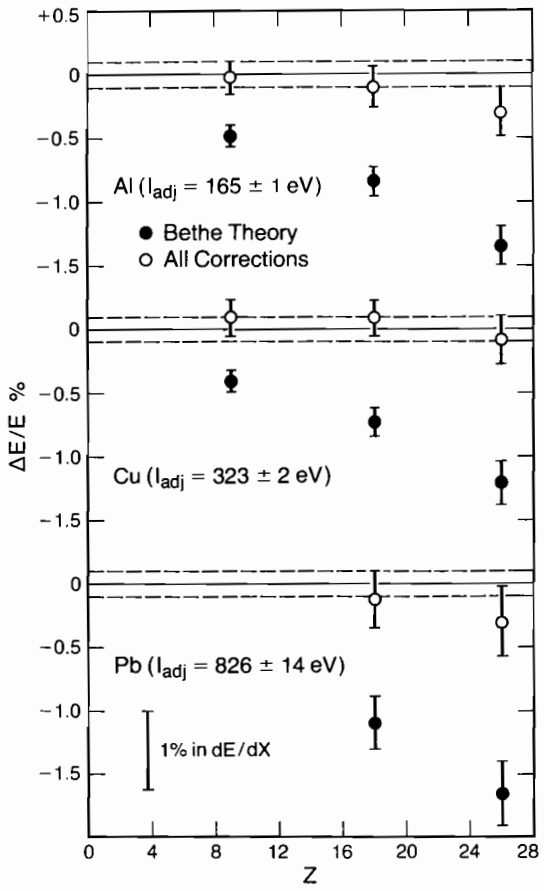

Fig. 1. Comparison of the Bethe theory with particle range data and with calculations which include all corrections. (XBL 8110-12209)

Footnotes and References

*Condensed from Ref. 2.

†Also at Space Sciences Laboratory.

1. M.H. Salamon, S.P. Ahlen, G. Tarlé and K.C. Crebbin, Phys. Rev. A **23**, 73 (1981).

2. S.P. Ahlen, submitted to Phys. Rev. A (1981).

A Search for New Nuclei Far from the Valley of Stability

J.D. Stevenson, P.B. Price* and J. Musser*

Fragmentation of relativistic heavy ions has proved to be a powerful technique[1,2] for studying nuclei far from the valley of stability.

In our previous work with a beam of 213 MeV/n ^{48}Ca we observed ^{20}C and ^{27}F for the first time (see Fig. 1). We are now building a new detector which will allow fragments with energies from 300 to 600 MeV/n to be isotope-identified. Using these higher energies will result in factors of ~ 20 to 50 improvement in sensitivity for rare isotopes. This improvement is primarily due to use of

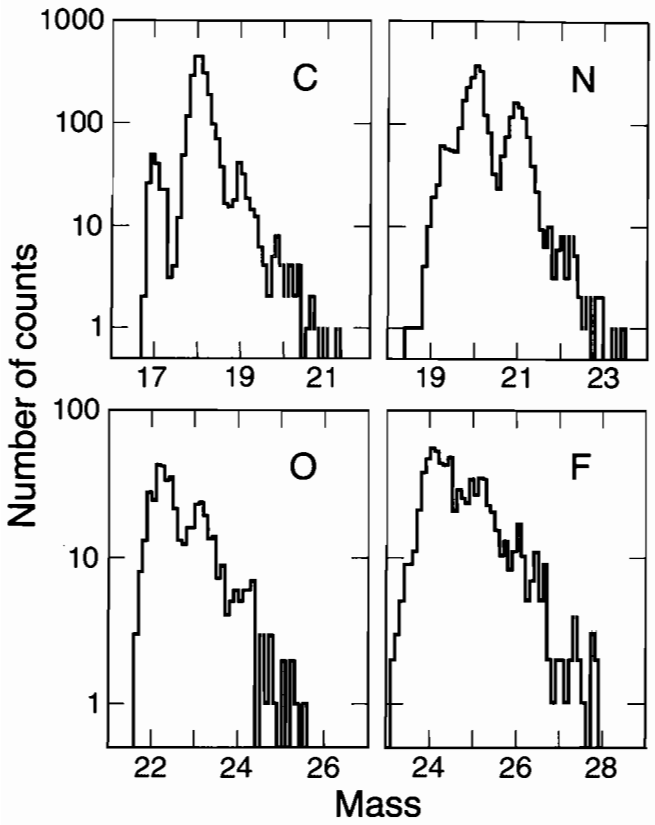

Fig. 1. Mass histograms for carbon, nitrogen, oxygen, and fluorine fragments from 213 MeV/nucleon ^{48}Ca projectiles. The isotopes ^{20}C and ^{27}F are clearly observed.
(XBL 8110-12210)

thicker targets and improved transport efficiency through the beam-40 spectrometer. With the higher beam intensities and heavier ions soon to become available, it should be possible, with this system, to determine the limits of particle stability at least up to neon.

The detector uses velocity vs rigidity to separate isotopes. The velocity measurement is done with a Cerenkov detector rather than time of flight. A Cerenkov detector provides a much better velocity measurement for heavy ions in this energy range than any practical time-of-flight system. The mass resolution is expected to be in the range $\sigma_m = 0.2$ to 0.3 for masses less than about 50.

Footnote and References

*Also at Space Sciences Laboratory.

1. G.D. Westfall et al., Phys. Rev. Lett. **43**, 1859 (1979).
2. J.D. Stevenson and P.B. Price, LBL-11737 and Phys. Rev. C (1981), in press.

Radiation Damage in Si(Au) Surface Barrier Detectors Produced by Energetic Heavy Ions

L.G. Sobotka, G.J. Wozniak, R.J. McDonald, and L.G. Moretto

During the past year we have done experiments at the SuperHILAC using beams of ^{40}Ar, ^{84}Kr, ^{136}Xe, and ^{165}Ho. Typically the beam-like particle (after elastic, quasi-elastic, or deeply inelastic scattering) was detected in a partially depleted Ortec detector of type A-023-150-300. In the course of an experiment these detectors are generally exposed to approximately 10^8 particles/cm^2.

While no significant radiation damage was observed in the Ar runs, the heavier ions produced significant damage in the Si detectors. One of the most obvious signs of this damage is the loss of pulse height as a function of dose. This correlation for a representative sample of detectors exposed to Kr, Xe and Ho ions is shown in Fig. 1. If the applied voltages are similar, an increase in the rate of pulse height loss is observed as the mass of the ion increases.

Perhaps more interesting is the correlation of the rate of pulse height loss with applied voltage. This correlation is shown in Table 1 for seven detectors exposed to Xe ions. In fact, it seems that the signs of damage (pulse height loss) diminish as the applied bias is increased. This is probably the result of an increase in charge collection efficiency in the damaged regions as the field strength increases.

These results indicate that large energy corrections as a function of dose are required for experiments where partially depleted Si detectors are exposed to $> 10^7$ very heavy ions. These corrections are likely to become prohibitively large for experiments using the intense beams of very heavy ions that will shortly become available at the SuperHILAC. Totally depleted Si detectors with large overbiases may be an acceptable alternative due to the high field strength throughout the bulk of the detector. In addition, p-type Si has been reported to be more resistant to radiation damage than n-type.[1] Therefore, for experiments involving very heavy ions it may be preferable to use p-type Si, even though the dead layers are larger.

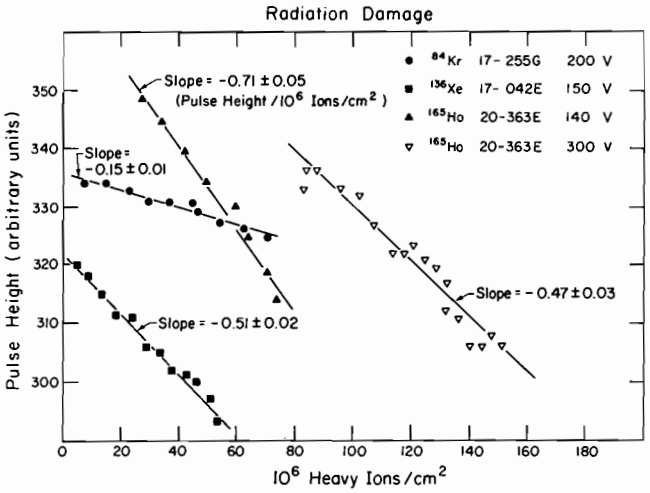

Fig. 1. Radiation damage in Si(Au) detectors produced by various heavy ions. Detector number, voltage and least squares fit of rate of pulse height loss is indicated in (pulse height/10^6 ions/cm^2). (XBL 818-2453)

Table 1. Correlation of rate of pulse height loss with applied voltage.

Detector	Beam	Bias (V)	Slope $\frac{\text{Pulse height}}{10^6\ \text{HI/cm}^2}$
15-450C	Xe	105	−0.64 ± 0.02
15-441J	Xe	105	−0.57 ± 0.03
15-329D	Xe	125	−0.61 ± 0.05
17-042E	Xe	150	−0.51 ± 0.02
15-596C	Xe	225	−0.32 ± 0.02
15-596B	Xe	250	−0.29 ± 0.02
15-248G	Xe	265	−0.25 ± 0.02

Reference

1. V.V. Avdeichikov, Nucl. Instrum. and Methods **155**, 125 (1978).

Development of a Beta Detector and Computer Analysis System for the On-Line Mass Separator, RAMA

J.M. Wouters, H.M. Thierens, M.D. Cable, R.F. Parry, and Joseph Cerny*

The RAMA on-line mass separator has, until recently, been used predominantly for studies of β-delayed proton emitters. A system consisting of a fast tape drive, a plastic scintillator telescope, a Ge(Li) detector, and a computer analysis program, has now been added to permit the determination of β-endpoints to $\sim$ 120 keV accuracy via β-γ coincidence spectroscopy. Our first results using this system, the β-endpoint measurements of $^{103\text{-}105}$In, are discussed elsewhere in this annual report.

The first component of this system, a fast tape drive, transports the activity collected on the focal plane of RAMA 18 cm to the detector station. Since the tape drive's initial development,[1] the detector station has been repositioned (see Fig. 1) and a newer capstan motor has been added to reduce the transport time of radioactive sources to 120 milliseconds. Recently, an automatic tape rewind feature has been included for short-lived activities that require rapid cycling of the tape. This feature allows the MODACS III computer, which monitors RAMA, to rewind the tape with minimum downtime.

The β-telescope consists of a 10-mm diameter and 1-mm thick NE102 plastic scintillator as a ΔE detector (for γ-ray rejection) and a large cylindrical NE102 plastic scintillator, 11.4 cm in both diameter and length as an E detector. The γ-ray detector is located on the opposite side of the tape in close proximity to the ΔE scintillator for β-γ coincidence spectroscopy. Standard fast-slow coincidence

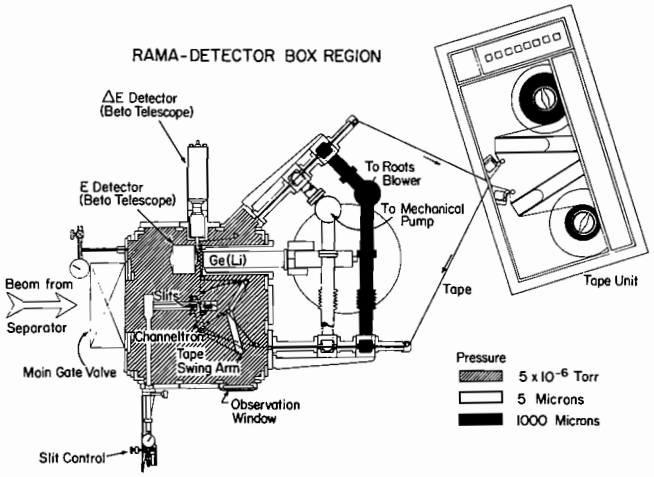

Fig. 1. Schematic view of the detector box region of the on-line mass separator RAMA.

(XBL 817-1034)

networks are used between all three detectors with a coincidence timing of 5 ns (FWHM) between the two scintillators and 20 ns (FWHM) between the β-E scintillator and the Ge(Li) detector.

The final spectra obtained with the above system need to be corrected for the finite energy resolution of the E

scintillator.[2] The program SPECTR performs this correction by assuming a theoretical shape, T(E), for the β-spectrum with endpoint energy E_o and distorting it using a semi-empirically derived response function, R(E,E') for the E detector. This procedure yields an energy-dependent correction factor, K(E), by which the measured β-spectrum is multiplied. A Gaussian response function is employed with a $\sqrt{E}$ dependence for the FWHM:

$$K(E) = T(E) \left[\int_0^{E_o} T(E')\, R(E,E')\, \partial E' \right],$$

where

$$R(E,E') = \frac{1}{\sigma_1 \sqrt{2\pi E'}}\, e^{-(E-E')^2/2\sigma_1^2 E'}$$

The endpoint is then calculated by SPECTR, which performs a weighted linear least squares fit on a Fermi-Kurie plot of the data. Finally, the error is calculated in a two-step procedure. First, the statistical error associated with the linear least squares fit, weighted by $\sigma_i^2 = 4p_iF_iE_i$, is determined:[3]

$$\sigma_{E_o}^2 = \frac{1}{A^2\Delta} \sum_i \frac{(E_i - E_o)^2}{\sigma_i^2},$$

with

$$\Delta = \sum_i \frac{1}{\sigma_i^2} \sum_i \frac{E_i^2}{\sigma_i^2} - \left(\sum_i \frac{E_i}{\sigma_i^2} \right)^2 .$$

In this expression A is the slope of the Fermi-Kurie plot, F_i is the Fermi function, E_o is the endpoint, and the energy corresponding to channel i, E_i, is summed over the energy limits of the fit. This statistical error is then added quadratically to the error due to the energy calibration:

$$\sigma_{E_{\text{calibration}}}^2 =$$

$$\sum_i^N \left[\sigma_{\text{Lit}_i}^2 \left(X_o \frac{\delta f_A}{\delta E_i} + \frac{\delta f_B}{\delta E_i} \right)^2 + \sigma_{FK}^2 \left(X_o \frac{\delta f_A}{\delta x_i} + \frac{\delta f_B}{\delta x_i} \right)^2 \right],$$

where the slope f_A and the intercept f_B of the calibration function depend on the literature values for the endpoints of the calibration nuclei E_i with uncertainties σ_{Lit_i} and the corresponding measured channel number X_i with errors σ_{FK_i}.

Five known endpoints were measured to calibrate the spectrometer and as an overall test of the system. The linearity of the final energy calibration (see Fig. 2) demonstrates the accuracy of this approach.

Footnote and References

*On leave from the University of Gent, Belgium.

1. Nuclear Science Annual Report for 1978-1979, LBL-9711, p. 227.
2. P.C. Rogers and G.E. Gordon, Nucl. Instrum. and Methods **37**, 259 (1965).
3. David M. Rehfield, Nucl. Instrum. and Methods **157**, 351 (1978).

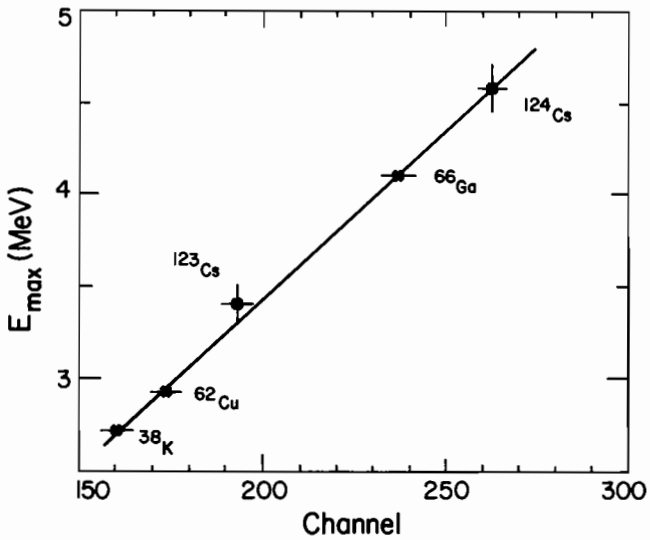

Fig. 2. Energy calibration of the β spectrometer using the nuclei ^{38}K, ^{62}Cu, ^{66}Ga, ^{123}Cs, and ^{124}Cs.

(XBL 815-820)

C. Emulsions and Plastic Track Detectors

Demonstration of a Detector with Unprecedented Charge Resolution*

S.P. Ahlen,† P.B. Price,† G. Tarlé,† and M. Tincknell†

The most fundamental limitation of detectors of all types used in the transmission mode is the fluctuation of deposited energy. By deliberately modifying the polymerization procedure of the commercial plastic, CR-39, we have produced a material which, when used as a nuclear track detector, has a charge resolution better than would be predicted on the basis of fluctuations in total deposited energy.[1] This is demonstrated in Fig. 1. As illustrated in the inset, 1.86 GeV/amu ^{56}Fe nuclei were incident on a slab of polyethylene. The outgoing particles penetrated a stack of ten sheets of the modified CR-39, two of which were used in the analysis of the charge of the emerging particles. The analysis involved the measurement of the minor axes of four consecutive tracks of each particle. The average value of the minor axis was then tabulated in the histogram. The resulting charge resolution at Fe is 0.12e. For comparison, the charge resolution at a 3 mm Si detector in a similar configuration has been measured to be 0.17e.[2] Since the effective thickness of the CR-39 detectors used to obtain the data in Fig. 1 was only 190 μm, it is apparent that track detectors have a substantially enhanced intrinsic resolution compared to total energy loss detectors such as silicon semi-conductor diodes. This is due to the complete insensitivity of track detectors to delta rays which are chiefly responsible for energy straggling.

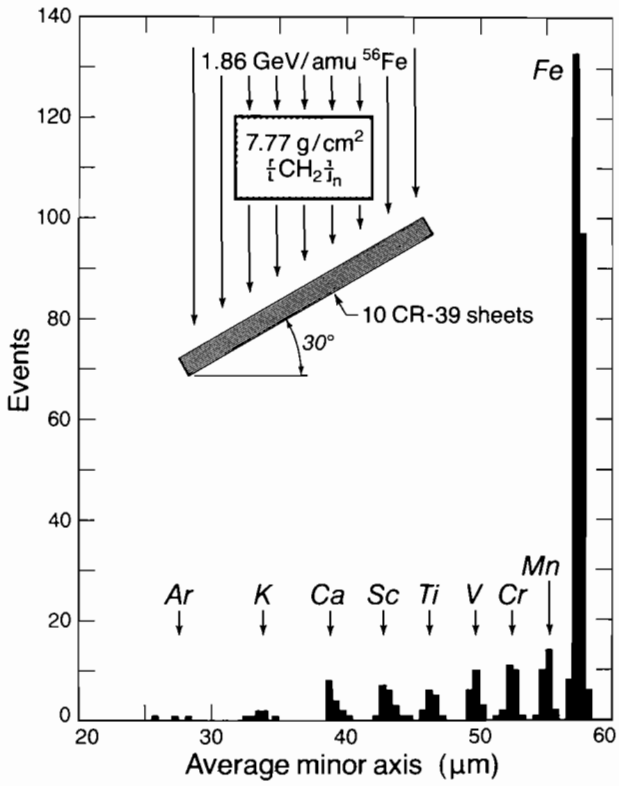

Fig. 1. Histogram of the average of the minor axes of four track mouths for the particles emerging from the polyethylene indicated in the inset.

(XBL 8110-12262)

As one particularly suitable application of these new detectors, we have recently exposed several stacks of pure CR-39 and of alternating CR-39/lead assemblies to 1.8 GeV/amu ^{40}Ar in the hopes of furthering the understanding of the so-called "anomalons." With the use of a semi-automated measuring system currently under construction, we will be able to measure the charge of a million particle tracks in the space of one year. Thus, statistically meaningful information will be obtained in a shorter period of time than is possible with nuclear emulsion. In addition, the use of the track detectors allows for greater flexibility in target choice.

Footnotes and References

*Condensed from Ref. 1.

†Also at Space Sciences Laboratory

1. G. Tarlé, S.P. Ahlen and P.B. Price, Nature (1981), in press.

2. G.D. Westfall, et al., Phys. Rev. C **19**, 1309 (1979).

Identification and Imaging of Nuclear Particles Using Etched Solids*

S.P. Ahlen,† P.B. Price,† and G. Tarlé†

Although media capable of recording visible light images were developed only within the last century, it is a fascinating fact, with widespread consequences, that media capable of recording permanent nuclear track images are as old as the solar system. In fact, when a highly charged particle penetrates *any* nonconducting solid, it creates a submicroscopic trail of radiation-damaged material that can be chemically amplified, by the so-called track-etch process, into a track large enough in diameter to be measured in an optical microscope.

This article reviews track production mechanisms and the track-etch technique and then discusses several recent advances, especially in high-resolution particle identification and imaging. The major topics are extraterrestrial tracks; fission track dating; space physics; nuclear physics; technological uses; the CR-39 polymeric detector; the use of dopants to improve the resolution and image quality of the CR-39 detector; the high charge resolution of doped CR-39; applications of doped CR-39 to cosmic rays, antimatter searches, searches for nonintegrally charged nuclei and monopoles; and advances in nuclear imaging with CR-39, including heavy-ion radiography, microscopic mapping of trace element distributions, lensless heavy-ion microscopy, and coded imaging of laser fusion reactions.

Footnotes

*Condensed from a paper in the September, 1981 issue of Physics Today.

†Also at Space Sciences Laboratory.

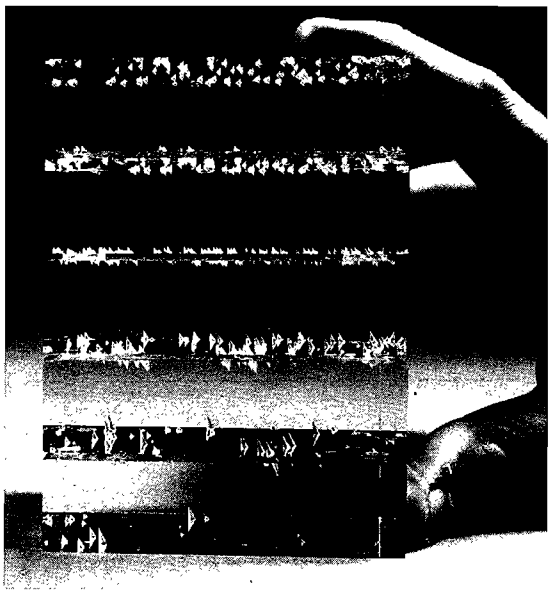

Fig. 1. Macroscopic etched tracks of a 100 GeV beam of ^{56}Fe nuclei brought to rest in a stack of five slabs of CR-39 doped with 1% of dioctyl phthalate. Careful examination of the actual slabs shows numerous examples of nuclear fragmentations. Etching for 1 month in 6.25 normal sodium hydroxide solution at 70° C has removed ~ 0.75 mm of material from the surfaces and caused the cone-shaped track etch pits to develop.

(CBB 813-2393)

Applications of Nuclear Track-Recording Solids to High-Energy Phenomena*

P.B. Price†

As part of a Festschrift for Nicolas Cabrera, this paper introduces solid state physicists to some of the ways in which the track-etch process enables problems in cosmic ray astrophysics, particle physics, and relativistic heavy ion physics to be studied.

The density of defects along the track left by a nuclear particle in a nonconducting solid provides a permanent record of the particle's velocity, charge, and mass. The record can be deciphered by etching the solid in a suitable reagent and measuring the sizes of the etch pits at points of intersection of the track with the surfaces. Useful solids include minerals and glasses, which are sensitive only to particles with charge/velocity ratio $Z/\beta > 150$, and to polymers, the most sensitive of which detects particles with Z/β as low as 6.

After a discussion of the mechanisms of track formation in inorganic solids (via a so-called ion-explosion spike) and in polymers (via scission of long-chain molecules), I summarize the present status of the track-etch technique by which our group has obtained charge-resolution unequalled by any other transmission detectors of equivalent thickness. I then describe briefly a few applications.

1. Relativistic Nucleus-Nucleus Collisions

a. Negative results of searches for products with charge greater than projectile charge by more than 2e in reactions such as 1.8 GeV/N ^{40}Ar + Pb. New experiments in 1982 will use ions having $Z \geq 36$ in the hope of seeing density isomers.

b. Evidence for nonthermal emission of fragments with $Z = 3$ to 12 in such reactions as 0.5 GeV/N ^{40}Ar + Au.

c. Production of new nuclides ^{20}C and ^{27}F in projectile fragmentation.

d. An experiment with high statistics ($> 10^5$ secondary interactions) to characterize the properties of anomalons. Three stacks with different combinations of CR-39 detectors and targets were successfully exposed to 1.86 GeV/N ^{40}Ar ions in June 1981. Among the results we should be able to obtain will be a rigorous determination of the fraction of secondary interaction products with nonintegral charge.

2. Particle Physics

a. A search for highly ionizing particles produced at PEP in 15 GeV e^+ + 15 GeV e^- collisions. Our present limit (95% CL) on the cross section for production of monopoles with $M \lesssim 14$ GeV/c^2 and $\beta > 0.01$ is $\sigma < 1$ pb. The same limit applies to electrically charged particles with $Z/\beta > 16$ and a range greater than ~ 0.5 mm of plastic.

b. A search for highly ionizing particles that survive traversal through 600 g/cm^2 of air to reach large arrays of plastic (CR-39) at the summit of White Mountain, California. Two specific classes of particles are being sought: Grand-Unification Monopoles with mass $\sim 10^{15\pm1}$ GeV/c^2 and quark globs (the possible precursors of Centauro-type interactions). Despite negative results to date (flux < 0.4 m^{-2} y^{-1} at 95% CL), we have succeeded in measuring, for the first time, the energy spectra of He and Li at mountain altitude, and we have detected nuclei with Z up to ~ 15 at an altitude of 41,000 feet, in accord with our calculated fluxes of surviving cosmic ray fragments.

3. High-Energy Particles in Space

a. Discovery of preferential emission of heavy nuclei in solar flares.

b. Measurement of charge distribution of ultraheavy cosmic rays, up to $Z \simeq 96$, in a 250-day exposure of 1.2 m^2 plastic stack on Skylab.

c. Discovery of intense fluxes of heavy (Z up to 26), multi-MeV/N ions in the inner magnetosphere, using a detector outside the Skylab.

d. Collaborative experiment with the University of Chicago, using transition-radiation detectors plus CR-39 to measure accurately charge distributions of cosmic rays at Lorentz factors up to ~ 2000. This experiment is scheduled for the second Spacelab flight, some time in 1984.

e. A planned experiment using CR-39, plastic scintillators, and plastic Cerenkov detectors, to search for an anti-iron/iron ratio as low as 3×10^{-7} in the cosmic rays. The experiment could be flown either in a balloon or on the shuttle and could also study anomalons at energies well above those attainable at the Bevalac.

Needless to say, this work was and is being done in collaboration with senior colleagues, graduate students and undergraduates.

Footnotes

*Condensed from paper to appear in January, 1982 issue of Philosophical Magazine.

†Also at UC Space Sciences Laboratory.

On the Possibility of Detecting Fractionally Charged Relativistic Projectile Fragments in Nuclear Emulsion

Harry H. Heckman

One of the speculations on the "anomalon" effect observed in emulsion studies on the interaction properties of projectile fragments in RHI collisions is that they may indicate the existence of fractionally charged projectile fragments. With this speculation in mind, I have shown that charge measurements on relativistic nuclei can be made in nuclear emulsion to an accuracy $\lesssim \pm 0.05e$, provided: (1) the lacunarity ($L = \sum_n$ gap lengths/track length) is $L > 0.10$, and (2) track length $\ell \gtrsim 2$ mm.

As discussed by Barkas[1], the experimental observation that the distribution of gap lengths in an ionization track is exponentially distributed leads to the following expression which relates the lacunarity to the grain density g of the track:

$$L = e^{-\alpha g} , \qquad (1)$$

where α is the average developed grain size in the emulsion. Assuming g is proportional to $DE/dx \simeq Z^2F(\beta)$, we have at relativistic energies, e.g., T = 2 A GeV, the elementary result that $Z^2 = -k\,\ell nL$, where k is a constant determined by calibration with beam nuclei of known

charge. A measurement of L of a relativistic track thus leads to an estimate of its charge:

$$Z = \sqrt{k\,\ell n L}\ , \tag{2}$$

with an error in Z

$$\sigma_Z = \frac{k}{2Z}\,\frac{\sigma_L}{L}\ . \tag{3}$$

A good approximation of the fractional error in L is given by

$$\frac{\sigma_L}{L} = \left[\frac{2\alpha}{\ell}\left(\frac{1-L}{L\,\ell n L^{-1}} - 1\right)\right]^{1/2}\ , \tag{4}$$

where ℓ is the track length over which the lacunarity L is measured.

From Eqs. (3 and 4) one finds, quite astonishingly, that one needs only to measure L over distances ℓ = 1-3 mm of track length to obtain a measure of Z to an accuracy of ± 0.05 units. Taking a value of k = 9.62 (appropriate to our emulsions currently being scanned), Table 1 gives the predicted values of ℓ necessary to obtain a σ_Z = 0.05.

We have experimentally verified the predicted accuracies of charge measurement by the lacunarity method for charges Z = 1, 2 and 3. The measurements on Z = 2 nuclei over a 1 mm track length are shown in Fig. 1. Figure 1a shows the measurements on ^{3}He beam nuclei (1.9 A GeV) and Fig. 1b shows the measurements of Z = 2 projectile fragments from 1.9 A GeV ^{56}Fe interaction in emulsion.

The observed rms widths of the distributions of 0.04-0.05 charge units are in agreement with the simple theoretical model of track structure described above. With the demonstrated ability to measure the charges of RHI to accuracies ~ 0.05 e, one clearly has the capability of searching for fractionally charged ions in multiples as small as 1/3e.

Reference

1. W.H. Barkas, *Nuclear Research Emulsions,* Academic Press, New York (1963).

Table 1. Track length ℓ necessary to determine charge to σ_Z = ± 0.05. L is the lacunarity of RHI tracks, charge Z, at energy ~ 2 A GeV. Saturation effects will limit applications to Z ≤ 4.

Z	L	(mm)
1	0.912	0.73
2	0.693	0.79
3	0.438	0.94
4	0.231	1.18

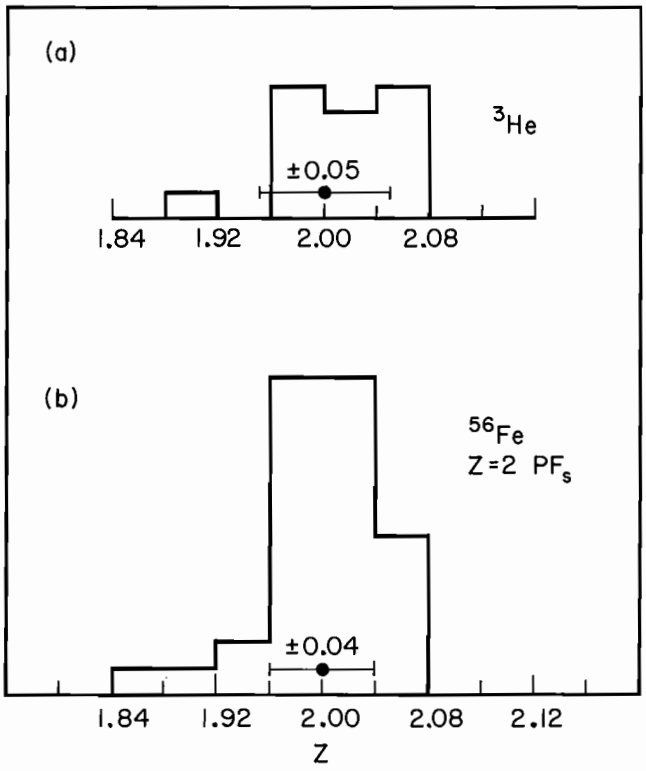

Fig. 1. Measured values of charge Z for (a) ^{3}He beam nuclei and (b) Z = 2 projectile fragments of ^{56}Fe. Beam energies are 1.9 A GeV. Measurements were made over 1 mm track length.

(XBL 8111-1609)

ICAMS: A System for Computer Assisted Nuclear Microscopy

E.M. Friedlander, H.H. Heckman, Y.J. Karant

We are in the process of installing the first prototype of a new system for emulsion data analysis and reduction, the ICAMS (Interactive Computer Assisted Measurement System). ICAMS is composed of two basic parts: a central computer and individual ODS (Optical Data Stations). The central computer (PDP-11) is responsible for overall system control and data reduction for physics interpretation. The system operates under the standard multi-task RSX-11M operating environment, to which has been added an additional package, ICMON (ICams MONitor system), to perform ODS control on a system basis.

Each ODS has a local microprocessor (6502) with a 9611 arithmetic processor. This combination enables local rapid computation for the control of the actual stage motion, thereby permitting each ODS to respond quickly to the individual operator. Each ODS independently:

1. Prompts the operator to perform measurement functions.
2. Responds to operator data entry commands.
3. Automatically records (x,y,z) position information to 1 micron accuracy.
4. Upon command, automatically follows a given trajectory and automatically returns to any vertex in the emulsion.
5. Verifies certain track parameters (such as fit of a trajectory to a specified hypothesis) to provide on-line data quality control. Figure 1 is a block diagram of the basic components of the ICAMS.

Since the data are immediately available in the central computer, we can fully eliminate many of the traditional slow steps of visual data reduction, such as scan sheets, computer data entry forms, and handwritten computer data validation forms. Instead, all of the information important to an operator appears on the individual ODS consoles, while data from all the ODS also is accessible to the physicist for immediate review.

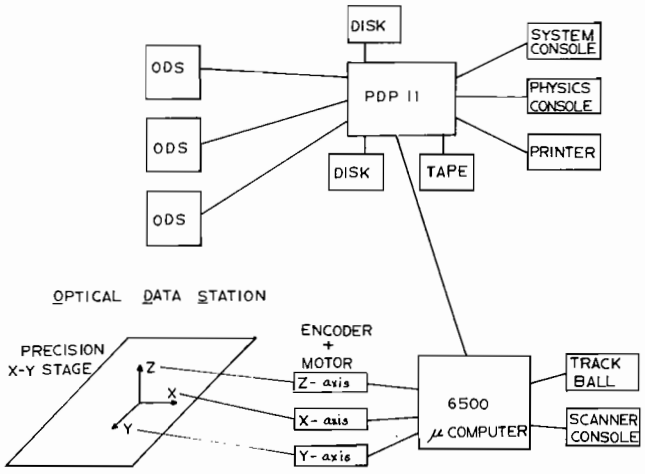

Fig. 1. System layout of ICAMS, illustrating the central PDP 11 computer and peripherals, and one of the ODS attached to ICAMS. Each ODS has its own microcomputer with its own peripherals. The link between each ODS and ICAMS is directly on the PDP 11 UNIBUS.

(XBL 8110-11749)

Study of Highly Ionizing Particles at Mountain Altitude*

K. Kinoshita and P.B. Price†

The inspiration for this experiment was the widely acknowledged peculiar nature of the "Centauro" class of ultrahigh-energy interactions discovered at Mt. Chacaltaya about a decade ago by a Brazil-Japan collaboration. The rate of Centauro events is quite low, $\sim 0.02\ m^{-2}\ yr^{-1}$. Among the proposed explanations is the possibility that they might be initiated by a highly charged primary particle. To look for such particles, we deployed a series of CR-39 plastic track detectors with large collecting power at the summit of White Mountain, California (603 g/cm^2). Two experiments have been completed and analyzed: a single layer with a 10 m^2 yr exposure and three coincident layers with a 0.025 m^2 yr exposure. In the first experiment, the single layer was adopted to maximize the collecting area at some sacrifice in velocity information. The results demonstrate the superiority of CR-39 as a detector of highly ionizing particles ($Z/\beta \gtrsim 30$) and its particular suitability as a collector of very rare particles. The performance of the plastic was evaluated by examining the high density of tracks due to slow, light ions. The low-energy spectra of nuclei with $Z < 3$ have been measured and are found to be consistent with spectra calculated from a model

where the source of ions is atmospheric collisions of energetic hadrons. This is the first time that energetic Li has been identified at mountain altitude and that enough He has been seen to permit measurements of its energy spectrum. A density $\sim 10\ m^{-2}$ of fast particles with $Z \geq 4$ found in individual layers is consistent with the exposure received in a 10-hour commercial jet flight. A fast scanning method was used to examine the entire single-layer array. In the interval $30 \lesssim Z/\beta \lesssim 100$ no events were found, from which we infer an upper limit of $0.4\ m^{-2}\ yr^{-1}$ (95% CL) on the flux of electrically charged particles with $Z/\beta \simeq 30$ to 100 and on the flux of superheavy magnetic monopoles with $\beta > 0.02$. Two objects were located which, if they are indeed tracks, would correspond to particles with $Z/\beta > 100$, with abundance $\sim 0.2\ m^{-2}\ yr^{-1}$. Without sheets in coincidence, it is impossible to distinguish these objects from certain flaws in the plastic. A new detector, with three layers interleaved with absorbers and with an area of 20 m^2, will correct this shortcoming and be able to measure the spectra of light elements to higher energies as well.

Footnotes

*Abstract of paper in Phys. Rev. D.

†Also at UC Space Sciences Laboratory.

D. Computers

The Design of MIDAS–A Modular Interactive Data Analysis System*

Creve Maples, William Rathbun, Daniel Weaver, and John Meng

A specialized, multi-user computer facility utilizing a parallel processor architecture to achieve high-speed, interactive reduction and analysis of experimental data is currently under development.[1] Data analysis is currently restricted to either a large central computer system (with the advantage of high computational speed and large mass storage capacity but typically batch-oriented and with limited interactive graphics capability) or to a smaller and more dedicated computer system (often offering a highly developed interactive graphics capability and permitting more flexible user control of the hardware environment but with slower calculational speed). Because of the high level of interactive graphics required, the necessity of continuously dealing with large data bases (from 200 to 5000 Mbytes per user), and the potentially significant amount of processing required per data packet (event), neither typical small nor large computer environments appear ideally suited to the requirements of data analysis.

The design objective is an environment that permits the user to interact with and guide the analysis process and to optimize conditions in order to best utilize the user's time. To be an effective interactive tool, the proposed system must be able to operate on large amounts of data and produce results, in terms of graphic displays within human time frames of seconds to minutes. The two main difficulties which must be addressed to achieve the desired performance are CPU and I/O bandwidth limitations.

Assuming that the data to be analyzed consist of relatively discrete and independent packets of information, the process of data analysis lends itself extremely well to the techniques of parallel processing. By creating an environment where data packets may flow through the system in parallel rather than serially, as is currently required, considerable improvement in processing speed and throughput is possible. The proposed system, although possessing all the attributes of a conventional mid-range computer, is not designed as a general purpose computational facility, but instead is to specifically handle problems associated with high-speed, interactive data analysis. To this end, certain very general assumptions are made concerning the structure of data and the process of analysis. These assumptions are:

1. The data base pre-exits.
2. The data base consists of packets of information (events).
3. Each event packet is essentially independent of other events.
4. Processing for each event packet is well defined and essentially repetitive for a given event type.

The general architecture of the system, shown in Fig. 1, consists of five subsystems, which are described below.

1. The Primary Computer System is designed to handle user requests and to allocate resources of the system. It is the only processor that directly deals with user's requests, and it has absolute control in allocating physical resources and determining system priorities. It is designed to respond to requests within human or interactive time scales and, therefore, will not directly handle CPU intensive problems such as analysis. The design is a distributed environment, not a network, operating as a master-slave hierarchy in which the Primary Computer functions as the master.

2. The Interactive System consists of the processors and associated hardware necessary to support the interactive needs of the users. These elements provide communication only with the Primary Computer. Basically, each

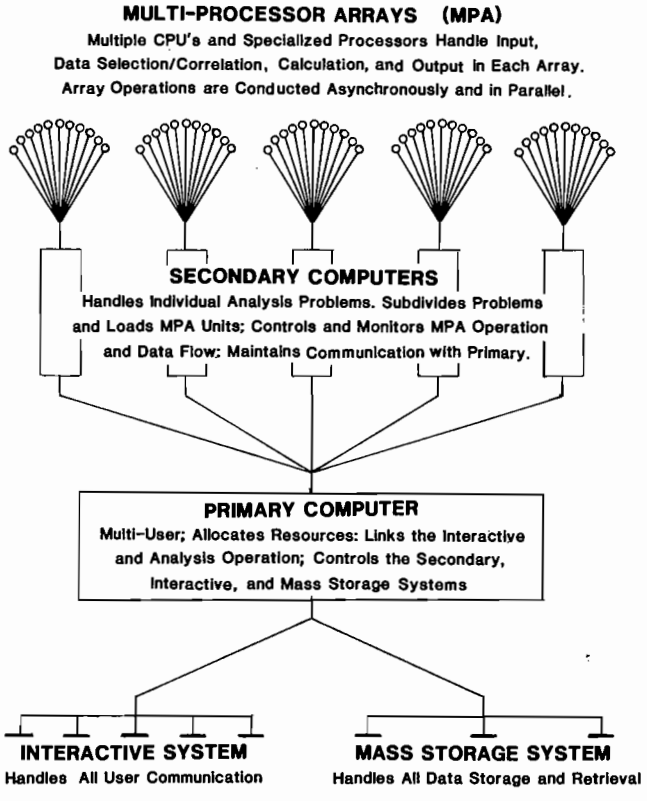

Fig. 1. General architectural design of the MIDAS system. (XBL 815-9786)

section of the Interactive System consists of a high-speed, high-resolution graphics terminal and a dedicated hardcopy device capable of providing a copy of the graphics screen and functioning as a printer and rough plotter. The terminals are a very important aspect of the system since they provide the interactive communication channel between the user and the entire system. Each would be equipped with a processor to handle simple graphics manipulation and screen updates and also with special interactive devices such as programmable switches, track balls, touch panels, etc.

3. *The Mass Storage System* is involved with the storage and retrieval of experimental data or results. Separate disc and tape drives are maintained by the Primary Computer for the storage and handling of user programs, files, etc. The Mass Storage System is controlled directly and solely by the Primary Computer and is functionally divided into three sections: magnetic tape control, disc control, and random-access bulk memory control, each of which is governed by Multi-ported Programmable Controllers (MPC). These controllers are specialized CPUs whose function is to control data flow to and from the specific device. Utilization of such devices permits the complete overlapping of data retrieval and transmission with analysis and processing. The magnetic tape and disc systems provide high-speed sequential access to stored information, typically raw or transformed data. High-speed, random-access storage, for which discs are not suitable, is supplied by external bulk memory. Each memory unit will have two addressing modes: Direct Memory Access (DMA) and Direct Memory Incrementation (DMI). The DMA mode gives standard read or write access to any memory location, and the DMI capability is useful in the creation of large multi-dimensional histogram arrays from analyzed data.

4. *The Secondary Computer System* will handle CPU-intensive problems delegated to it by the Primary (e.g., the analysis of data according to some specified criteria). The Secondary communicates with, and is controlled by, the Primary Computer and, in turn, communicates with and controls a Multi-Processor Array which is described below. Although the Secondary Computer is a general purpose CPU and is potentially capable of devoting all its resources to the solution of a particular problem, it is, in general, too slow to be directly effective. Its normal function is thus to prepare the high-speed, parallel units of the Multi-Processor Array to handle the particular analysis problem specified by the user. Once the setup and initialization is complete, the Secondary Computer allows the data to flow into the parallel system and continuously monitors the processing of the data. Although the Secondary is not directly involved in the analysis or data transfer through the system, it can control all active elements of the Multi-Processor Array.

5. *A Multi-Processor Array (MPA)* is associated with and controlled by each Secondary Computer. An MPA consists of an input port, an output port, and a number of CPUs and specialized devices to permit high-speed, asynchronous, parallel operations on the incoming data stream. The general function of each of these devices and their interrelationship are as follows:

a) The *Input Formatter* is a parallel pipelined device that receives raw data from the input port. Its function is to "read" and unpack the data according to information supplied by the Secondary, for example, separating non-data information (such as header records, directories, or end-of-files) from data, recognizing a separate event or data packet, uncompressing events if necessary, and performing simple logical operations on the data stream. Since the Input Formatter is a pipeline processor, data passes through it at I/O bus speeds and each pipeline stage operates in parallel on a different data word. Its ultimate objective is to place a formatted event (or multiple events) into a Data Stack.

b) Each MPA contains a number of independent Data or Memory Stacks (currently 16). Each memory stack contains its own 32-bit I/O bus, 16 Kbytes or 200 ns solid state memory, and special memory zeroing hardware. The stacks are designed to hold formatted data or events and each stack may be dynamically switched to any processor in the MPA.

c) The *Programmable Arithmetic Modules (PAM)* are, in effect, commercial, high-level CPU and EAU (Extended Arithmetic Unit) boards. Each PAM contains integer and floating point hardware, multiple register banks, hardware mapping, and will support pipeline mode operation. In order to maximize throughput, these CPUs do not "read" or transfer data into memory; instead, any Data Stack, containing data to be processed, may be switched to any PAM unit. The attached Memory Stack, from the perspective of the associated PAM, is operationally indistinguishable from dedicated memory. Multiple PAMs may thus process data asynchronously and in parallel. PAM units are initially down-loaded with user-specified analysis code by the Secondary. The analysis code obtains data from a dedicated common block. This common block (actually a Memory Stack) may also be used to store analysis results. At the completion of the analysis of one data block, the program exits, a new block is switched in, and the analysis restarts on new data. The entire switching process should require, at the most, a few microseconds.

d) The *Conductor* is the hardware unit that controls the dynamic switching of Data Stack buses to appropriate active processors. The Conductor is initialized by the Secondary with a preselected switching sequence. This specifies which processors will be utilized in the subsequent analysis and the order in which the data will be presented to the processors. When an active processor signals completion, its current Data Stack is switched to the next available class of processor in the sequence. The next unattached Data Stack, which is available for that class processor, is switched in and the processor restarted. Iterative operations between processors are also permitted within this framework. It is important to emphasize that data itself is *not* being transferred in these operations, but rather that memory blocks containing data are being

switched. When all processing of the data in a stack is completed, the Conductor can activate stack hardware that will automatically zero the memory. At this point, the stack is available for new data and the switching sequence is restarted.

e) The *Programmable Sorting Module (PSM)* is a rather simple processor which was designed to permit a Data Stack to be examined rapidly for user-specified patterns or correlations (loaded into it by the Secondary Computer). The module utilizes special hardware to perform masking, gating and logical tests at very high speeds. The information generated can then be transferred to a Data Stack (for use by any other processor), to the Storage Memory, or to the Output Port. Although a PAM could be programmed to carry out similar operations, this type of data examination is sufficiently common and time consuming to warrant a specialized hardware unit.

f) The *Output Formatter* is essentially the inverse of the Input Formatter. It is a pipelined processor designed to take selected information from a Data Stack, format, compress it if desired, and transmit the results either to the local Storage Memory or the Output Port. Information in a Data Stack may be utilized to determine the exact processing necessary.

g) The *Storage Memory* is a dual-ported bulk memory unit designed for local storage of analysis results. One port provides standard DMA read/write access and is connected directly to the Secondary Computer. This link can supply interim as well as final results to the Secondary (for transmission to the Primary) independent of the operation of the MPA. The second port may be utilized for either sequential or incremental memory access. In the latter case, the content of the transmitted memory address is incremented. The initial design specifies that this unit contains at least 128K of 32-bit memory, with a maximum storage capacity of 8 Mbytes. There is one such storage memory in each MPA.

The fundamental objectives of the MIDAS facility are to provide:

1. high-speed data processing,
2. optimized data transmission rates,
3. high interactive capability,
4. modular construction, and
5. ease of usage.

The architecture described here provides a framework in which these goals appear achievable. The basic design was presented to and approved by a special workshop consisting of hardware and software representatives from various National Laboratories, universities, and private industry. The construction and development is planned in four stages, each leading to a viable and stable configuration, as well as serving to test certain basic architectural aspects.

Footnote and Reference

*Condensed from LBL-12504.

1. Creve Maples et al., IEEE Trans. Nucl. Sci. **NS-3764**, (1981).

Development of a MIDAS Prototype*

Creve Maples, William Rathbun, Daniel Weaver, and John Meng

In 1979, a proposal[1] was made to develop a Modular Interactive Data Analysis System (MIDAS), that utilized a parallel processor architecture to achieve high-speed, interactive reduction and analysis of experimental data. In February 1980, after the completion of a detailed design document, a workshop (attended by scientists, electronic engineers and designers, computer scientists, and software systems specialists from several universities and National Laboratories) was held to discuss and dissect the detailed proposal. A number of design modifications and enhancements resulting from this workshop were subsequently incorporated into the basic architecture of the system. Software models, emulating the architecture of the system, were constructed to predict the effect of various hardware design considerations on the overall system throughput. Theoretical determinations of the critical paths and operational performance constraints are, however, very difficult in such a highly parallel and asynchronous environment.

The development of the proposed architecture into a working facility, MIDAS, was planned in four separate phases: 1) a prototype, 2) a working model, 3) a complete system (3 to 5 users), and 4) future extensions. Each phase was designed to provide particular capabilities and to test the viability of different aspects of the architecture. These discrete development phases would, furthermore, permit detailed evaluation of the project with respect to estimated cost, manpower, development time, and performance. The goals of each phase are well defined and each represents a working system. This report deals with the first or prototype phase, a schematic outline of which is shown in Fig. 1.

Hardware construction of the basic prototype began in May 1980. In terms of the previously defined architecture,[2] the prototype is an abbreviated version of a single Distributed System—a Secondary Computer and a simplified Multi-Processor Array (MPA)—plus one element of the Mass Storage System, a disc with a Multi-ported Programmable Controller (MPC). The purpose of Phase 1 is to test the performance and control of the MPA. This unit contains all of the high-performance design features

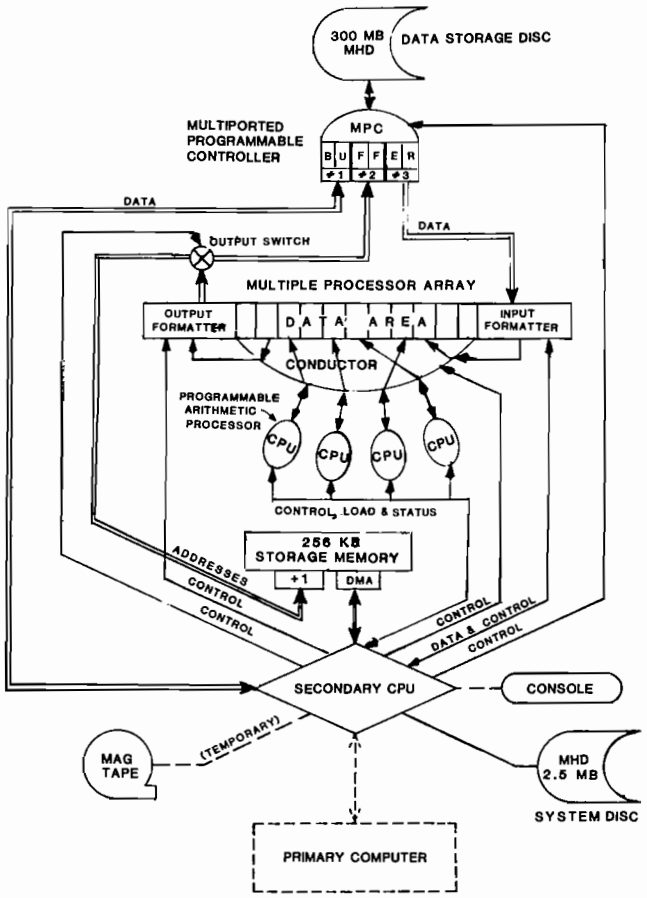

Fig. 1. Schematic Layout of MIDAS Phase 1 Prototype. (XBL 815-9787)

that are essential to the architecture: asynchronous parallel processors and parallel multi-bus operation. Due to the absence of a Primary Computer in this development phase, the Secondary has been given more capability (memory, peripherals, etc.) and responsibility than would normally be required. For example, in this prototype it is responsible for loading data onto the disc through the MPC, and for directly controlling the MPC. Such direct connections between a Secondary Computer and the Mass Storage System will not exist in the general design.

The Phase 1 prototype of the Multi-Processor Array contains: two I/O processors (the Input and Output Formatters); four general purpose, parallel CPUs (Programmable Arithmetic Modules, each with 128 Kbytes of memory); the high-speed bus switching controller (the Conductor); eight Data Stacks (each with independent buses and 16 Kbytes of memory); and a dual-ported Storage Memory (with 512 Kbytes of memory). The development of a PSM^2 (intended to perform masking, gating, and logical tests at very high speeds) is not essential to the basic design or operation, and it is therefore not included in the Phase 1 development. The goal of high-speed data processing is achieved by utilizing multiple, high-level CPUs operating asynchronously and in parallel on the data stream. The transmission of data, or I/O throughput, is optimized by utilizing multiple I/O buses operating in parallel, by minimizing the actual movement of data, and by completely overlapping I/O and CPU operations. Both of these objectives are tested in the Phase 1 development.

This prototype is scheduled for completion in summer 1981. At this time, benchmark tests will be run on the model to compare processing capability, both with current computers and with the performance predicted by our software models. The latter is an important comparison since knowing the accuracy of the software architectural model makes possible more precise predictions of the capabilities of the future development stages. The comparison tests will be performed as far as possible, by analyzing real experimental data, which utilizes identical software on both the Phase 1 prototype and existing computers. Because performance is potentially sensitive to the dependence of a particular analysis on I/O versus CPU utilization, tests will be conducted on both CPU- and I/O-intensive problems. Although generalized predictions are difficult, the results of model calculations suggest that the Phase 1 prototype should give a factor of 6 to 12 increase in throughput compared to our current (ModComp IV-25) computers. The hardware cost of the Phase 1 system is expected to be approximately $110K and is estimated to require 4 man-years of hardware effort and 2 of software effort.

Footnote and References

*Condensed from LBL-12504.

1. Creve C. Maples, IEEE Trans. Nucl. Sci. **NS-26**, 4580 (1979).

2. Creve Maples et al., IEEE Trans. in Nucl. Sci. **NS-28**, 3746 (1981).

The Utilization of Parallel Processors in a Data Analysis Environment

Creve Maples, Daniel Weaver, William Rathbun, and John Meng

In many research environments, data are accumulated as a series of information packets or events. These events consist of discrete pieces of information, or parameters, which are associated with the detection of the event. Recording these events as they occur in real-time permits later reconstruction of the data off-line and allows more detailed examination and evaluation of the information. In nuclear and particle physics, the past decade has witnessed an explosion in the volume and complexity of recorded experimental data. The complexity of modern experiments is, in large part, caused by the increasing rarity or subtlety of the physical processes under examination. This in turn leads to an increasing complexity in the data reduction and analysis. It is not uncommon for basic data analysis to require many days of computer processing, in some cases as much as 10 times longer than the data collection process.

In 1979, a proposal[1] was made to develop a specialized computer facility specifically designed to deal with the rapidly escalating problems associated with interactive data reduction and analysis. This proposed design utilized a hierarchy of multiple, high-level processors to permit high-speed parallel analysis of data. The basic structure of data (discrete event packets) makes its analysis ideally suited to parallel processing. In this framework, events are analyzed asynchronously and in parallel by multiple CPUs as opposed to the serial one-event-at-a-time approach of conventional computers. Such a design is now practical because high-level CPUs are commercially available at a relatively modest cost. Construction of the proposed Modular Interactive Data Analysis System (MIDAS) was begun in May 1980.

Essentially all the processors employed in the MIDAS design are full, mid-range computers, not microprocessors. This level of processor is necessary to maintain overall flexibility, provide the necessary computing power, and permit parallel utilization of standard user code. Although MIDAS is generally designed to deal with problems associated with interactive data processing, the actual analysis programs typically will be user generated and will vary widely in terms of their application and the demands placed on the facility. It is therefore essential that the system be capable of employing code written in essentially standard high-level languages (e.g., FORTRAN), in the multiple-processor environment and in a manner basically transparent to the user.

The architecture adopted for MIDAS is a distributed processor environment organized in a "vertical tree" structure. This structure utilizes a master-slave hierarchy for control and communication. In this environment, processors at each level of the "tree" control the processors in the branch directly above and report to the processor directly below. There is essentially no direct communication between processors at the same level. Such an architecture greatly simplifies operation and communication in a highly parallel, asynchronous environment and avoids many difficulties encountered in more traditional computer networks. Detailed information on the MIDAS architecture, design considerations, and development plans are presented elsewhere.[2,3]

The processors are organized into three functionally distinct systems controlled by a central computer referred to as the "Primary." Each system consists of a number of processors with specific responsibilities. The following is an outline of the control structure:

- Primary Computer
  - Interactive System
  - Mass Storage System
    - Multiported Programmable Controllers (MPC)
  - Distributed Processing System
    - Secondary Computers
      - Multi-Processor Array (MPA)
        - Input Formatter
        - Programmable Arithmetic Module (PAM)
        - Data Stacks
        - Conductor
        - Programmable Sorting Module (PSM)
        - Output Formatter
        - Storage Memory

A schematic illustration of the organization of the major processing elements is provided in Fig. 1. A rather high degree of parallel operation is inherent in this structure. The Primary Computer and the three systems it controls — Interactive, Mass Storage, and Distributed — all operate in parallel. The Interactive System in Fig. 1 consists of five independent processors while the Mass Storage System utilizes three classes of processing units (for disc, tape and bulk memory) involving five Multiported Programmable Controllers. The Distributed Processing System consists of five Distributed Subsystems, also illustrated in Fig. 1. Each Subsystem (a Secondary Computer and Multi-Processing Array) operates in parallel, both externally, with respect to other Subsystems, and internally with respect to the Secondary Computer and the Multi-Processor Array. The Multi-Processor Array consists of multiple processing units which operate asynchronously and in parallel.

High-speed data processing is the specific responsibility of the Distributed Subsystems. Each of these consists of two processing levels, a Secondary Computer and a Multi-Processor Array. The Secondary is responsible for the particular single analysis problem delegated to it by the Primary; and it, in turn, controls a Multi-Processor Array. Although the actual configuration of this array is flexible, for the purpose of discussion it will be assumed to consist of 11 programmable processors, two logic units associated

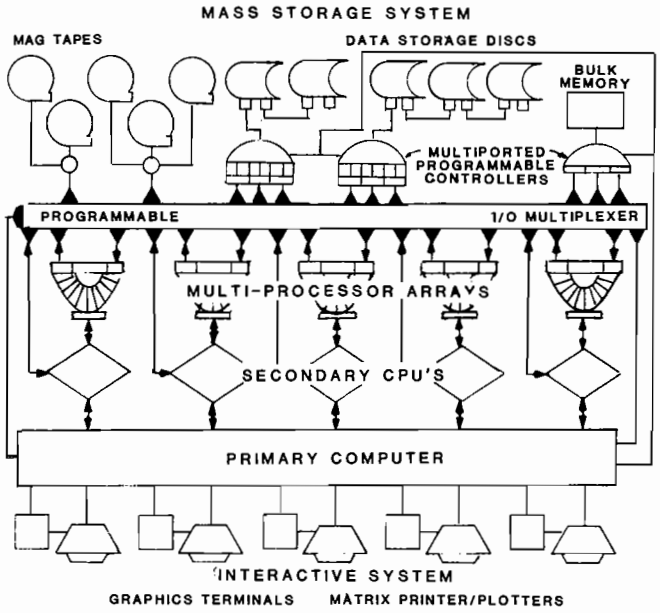

Fig. 1. Organization of major processing elements in the MIDAS design. (XBL 818-11277)

with memory (or bus) switching, and a local memory for storing results. The 11 processors include 8 general purpose CPUs and three specialized units. Two of the specialized units are pipelined I/O processors and the third is designed for high-speed data pattern recognition. The function, operation, and control of the various processors, utilized within the MIDAS design to achieve high-speed data analysis, are reviewed in Ref. 2.

The process of analysis may be divided into four general stages:

1. problem definition,
2. setup and initialization,
3. data reduction and analysis, and
4. presentation of results.

The general application of parallel processing to each of these stages is outlined below (more detailed information is contained in Ref. 4). In defining the problem, a user would typically be involved with two processors, a dedicated unit of the Interactive System and the Primary Computer. At this stage of operation, the functions of the Primary Computer are to respond to user requests for information and to store information from the user pertaining to specific analysis requirements. Once the problem is specified, the Primary will initialize the necessary units in the Mass Storage System and will allocate a Distributed Subsystem to perform the actual analysis. During initialization, the Primary would use the I/O Multiplexer to connect the input and output channels of the selected Multi-Processor Array with the appropriate Mass Storage ports. The analysis specifications are then transmitted by the Primary Computer to the selected Secondary. These specifications might consist of a list of data transformations or actual analysis code, an array defining sets of sorting conditions or logical correlations which are of interest, an array describing the desired formatting of the results, and information on the structure of raw data. The analysis code will be compiled and linked, if necessary, to form an analysis task. This task will typically then be loaded by the Secondary into each of the PAM (Programmable Arithmetic Module) CPUs. Each PAM unit is a high level commercial computer, stripped of everything but processor and memory. These modules will execute the down-loaded tasks directly with essentially no operating system, but with certain error traps operational.

The actual analysis operation is carried out in a Multi-Processor Array under the supervision and control of a Secondary Computer. After the Secondary Computer has completed initialization of the MPA it begins the analysis operation by starting the Input Formatter which is directly connected to a port in the I/O Multiplexer. The Distributed Subsystem need not know what device will be transmitting information to this port because all transmissions across the I/O Multiplexer follow the same protocol. A virtual disc port could, for example, be supplying data to the Input Formatter. Since the disc MPC was initially supplied with a list of the requisite data, the first 32 Kbytes of information have been retrieved from disc and are stored in memory buffers of the virtual port. When the Input Formatter acknowledges the data-ready flag, a direct-memory transfer of data begins.

The presentation of analysis results to the user should be considered in two time frames, preliminary results during analysis and final results at the conclusion of analysis. During the analysis process, a user may wish to receive various information on its progress. Specific requests for information are received by the Primary Computer which normally transfers them to the Secondary. The Storage Memory, where local results are stored, has a direct DMA connection to the Secondary Computer. At appropriate times the Secondary, if requested, will obtain a copy of the current results from this memory and transfer them to the Primary. Once in the Primary, this preliminary information may be manipulated and examined at will by the user through the Interactive System. In this manner, continuously updated results may be supplied to the user without interfering in the analysis process. If these preliminary results are not satisfactory, a user may immediately abort the analysis rather than waiting for its completion.

The goal of the MIDAS design is to provide an individual user with high-speed analysis capability. Sixteen processors, operating asynchronously and in parallel, are dedicated to each user during analysis. This utilizes only one Distributed Subsystem of the five shown in the basic design. The MIDAS structure shown in Fig. 1 has 71 processors and can handle five simultaneous analysis problems. Because of the architecture, these independent analysis problems can be run at the same time and with essentially no interference; that is, each analysis will be carried out at the same speed whether or not the others are present.

The operating structure of MIDAS supports a considerable number of processing units, independent I/O buses, mass storage devices, and a substantial amount of memory and is reasonably tolerant of hardware failures. The functional segregation of operations, the duplication of

hardware, and the dynamic ability to allocate resources should greatly reduce the seriousness of most hardware failures and generally permit quick recovery and continued operation. The flexible, modular framework of the MIDAS system permits the simultaneous execution of different analysis problems, each of which utilizes multiple processors. The structure further permits the dynamic allocation of resources according to the particular needs of each problem. Finally, the modular nature of the design and the independent asynchronous operation of each processor should permit the relatively simple incorporation of new technology in the future.

Footnote and References

*Condensed from LBL-12505.

1. Creve C. Maples, IEEE Trans. Nucl. Sci. **NS-26**, 4580 (1979).
2. Creve Maples et al., IEEE Trans. Nucl. Sci. **NS-28**, 3746 (1981).
3. W. Rathbun et al., IEEE Trans. Nucl. Sci. **NS-28**, 3875 (1981).
4. C. Maples et al. IEEE Trans. Nucl. Sci. **NS-28**, 3880 (1981).

A Fast, Time-Sliced, Multiple Data Bus Structure for Overlapping I/O and CPU Operations*

W. Rathbun, C. Maples, J. Meng, and D. Weaver

Within the Nuclear Science Division of LBL, a specialized Modular Interactive Data Analysis System (MIDAS), designed specifically to reduce the time required for interactive data analysis, is being constructed. The general architecture of this system has been discussed in detail elsewhere.[1-3] Basically, analysis time is reduced by minimizing the movement of data and maximizing the use of parallel operations in both data transfer (I/O) and data processing. Through the multiple data bus structure described in the following paragraphs, several independent processors operate asynchronously and in parallel on large blocks of event-structured data loaded into sixteen independent memories or data stacks. This structure allows large blocks of data to be rapidly switched among various processors, in contrast to conventional word-by-word bus movement of data.

The Data Stacks provide a key element in the MIDAS system's high-speed parallel operation. Various processors comprising the Multi-Processor Array can be electronically connected to the Data Stacks in a predetermined sequence. One of these processors, the Input Formatter, is a specialized hardware device developed to unpack an input stream of event-structured data and fill any stack requesting new data. A second type of processor consists of a stripped-down version of a commercially-produced CPU with a fast arithmetic processor. As many as eight of these CPU-type processors, Programmable Arithmetic Modules, can operate in parallel on data in a given user's data stacks. A third type of processor, the Output Formatter, unpacks results stored in the data stacks and passes them to another processor, ultimately to be graphically communicated to the user. Other processors have been conceived and can be added to the parallel system as the application may dictate. When one processor has completed its work on a given stack, another processor can be rapidly connected to the stack to perform additional operations as required. These operations may include calculations or data transformations, may serve to create an augmented data base upon which future calculations can be performed, or may provide for the tabulation of results for ultimate presentation in a manner selected by the user. The following sections detail the switching and control logic which manages the communication with the Data Stacks.

Event-structured data loaded into the Data Stacks can be accessed by any of several classes of processors in a programmable manner. These processors, discussed in detail elsewhere,[2,3] can operate simultaneously and asynchronously in a sequence determined by the user or the analysis program. Hardware logic known as the Conductor handles this dynamic interconnection sequence.

Current hardware permits as many as eight CPU's and four other processors to be simultaneously connected to separate Data Stacks. Each processor operates on its currently assigned stack asynchronously and in parallel with all other system operations. Each Data Stack appears as a dedicated memory block to the currently-attached processor. When a processor has completed working on a given set of data, it signals the Conductor to switch the associated Data Stack to the next processor type in a user-determined sequence. Several types of processors can be sequentially mapped to a given stack.

The key to this switching process is a simple Connect Module illustrated in Fig. 1. Each device capable of passing data into and out of the Data Stacks has a dedicated Connect Module consisting of an Input FIFO, a Connect Register, and an Output FIFO. The Input FIFO holds up to sixteen 4-bit stack numbers, specifying the list of Data Stacks to be worked on by the processor. The Connect Register holds the current 4-bit stack number (connect code), which serves to gate the data bus of the associated processor into its currently dedicated Data Stack. The Output FIFO holds the connect code of the stack just processed so that it can be passed into the Input FIFO of the

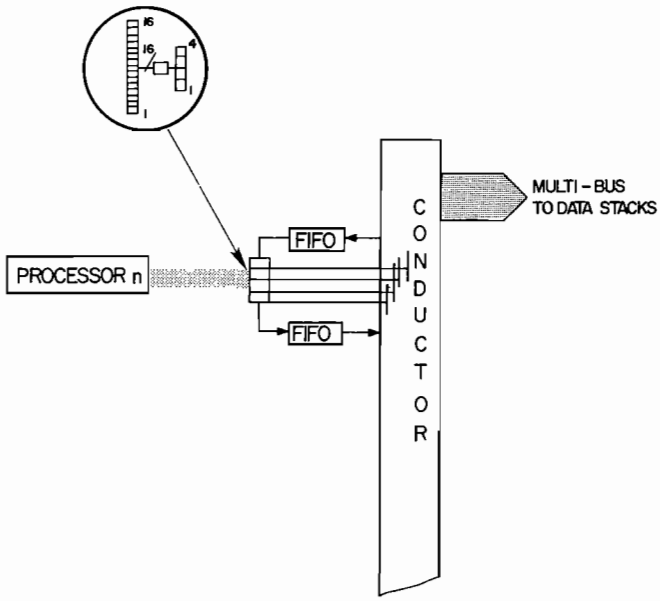

Fig. 1. Details of a Connect Module, which interfaces a Data Stack to a selected processor. The inset illustrates how a four-bit connect code is decoded to enable one of sixteen sets of gates. (XBL 816-10208)

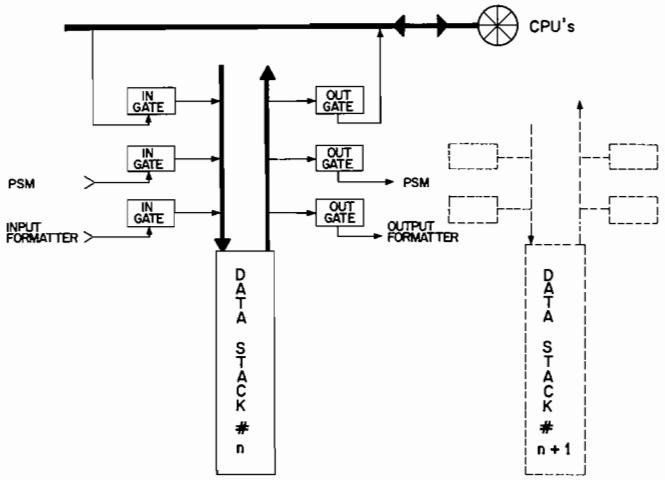

Fig. 2. The Stack Gates which connect all processors of the Multi-Processor Array with all Data Stacks. (XBL 816-10207)

next processor of the pre-loaded sequence. Associated with each Data Stack is a control block, which contains the order in which the processors are to be attached to that stack. This sequence is initially downloaded by a Secondary Computer that oversees the operation of the parallel processors.

To reduce the large number of interconnections potentially possible in the Multi-Processor Array (up to 12 active processors connected to any of 16 Data Stacks), two classes of data buses have been implemented: (a) a time-sliced bus through which CPU-type processors can access their respective Data Stacks and (b) standard I/O buses that are connected to all other processors of the Multi-Processor Array. Figure 2 shows how all processors are connected to the read and write gates of all stacks through Stack Gates. When a processor has completed its operations on a given stack, it signals "done" to the Conductor; this causes the next connect code in the processor's Input FIFO to be shifted into the Connect Register, enabling the set of gates connecting this processor with the desired stack. These gates stay enabled until the current processor has signaled that it has finished with the stack, except for the time-sliced gates connecting the CPUs to the Data Stacks. These time-sliced gates are reloaded at each phase of the time-slice, as determined by the contents of the Connect Register of the associated CPU. This gate switching can be accomplished in approximately thirteen nanoseconds. In the time-sliced environment, the eight CPU-type processors of the Multi-Processor Array share a common set of gates into the Data Stacks. A time-slicer scans all CPUs every 100 nanoseconds. Any CPU requesting a data transfer into or out of a stack is allocated an extended cycle of approximately 50 nanoseconds. A write operation can be accomplished in a single cycle, but a read operation requires two cycles: the first cycle strobes the address and the data requested are available by the next cycle. At each phase of the time-slice, the Connect Register of the associated CPU, if active, is decoded into appropriate stack-enable gates which connect the processor to the associated stack. When a CPU has finished processing a stack, it generates a signal that causes the next stack number (connect code) in the associated Input FIFO to be shifted into the Connect Register, enabling the read and write gates that connect the processor to the proper stack.

The goal of the MIDAS system is to provide a highly effective tool for the interactive analysis of experimental data. The huge volume of data to be processed necessitates a high degree of parallelism, both in I/O and CPU-intensive operations. The use of multiple data buses that connect independent Data Stacks to selected parallel processors provides the framework to attain the desired throughput. While the MIDAS system is designed specifically to facilitate the analysis of data from experimental physics, the architecture should adapt well to a wide variety of analysis problems, including medical and geophysical applications. Additionally, the modular structure allows processors or peripherals to be upgraded or replaced as advancing technology dictates.

Footnote and References

*Condensed from LBL-12498.

1. Creve C. Maples, IEEE Trans. Nucl. Sci. **NS-26**, 4580 (1979).

2. Creve Maples et al., IEEE Trans. Nucl. Sci. **NS-28**, 3746 (1981).

3. Creve Maples et al., IEEE Trans. Nucl. Sci. **NS-28**, 3880 (1981).

Multidimensional Numerical Integration*

R.W. Koontz

Computer models of experimental apparatus and of particle interactions are an essential part of modern nuclear science. For many applications, this modeling process reduces, at least in part, to numerical evaluation of multidimensional integrals. Numerical evaluation of such integrals, however, is generally not a simple task and often involves months of program design and testing. Therefore, there is considerable opportunity for resource saving by constructing a general purpose program that does multidimensional integration in an arbitrary number of dimensions.

I have constructed a multidimensional numerical integration program called "INTGRL" that has been tested on integrals with dimensions up to ten with good accuracy. An 8-point Gauss quadrature rule, exact up to polynomials of order 17 in one dimension, is used as the basic panel rule. A complete description of the program may be found in Ref. 1.

Footnote and Reference

*In preparation for publication in Nuclear Instruments and Methods.

1. R.W. Koontz, Lawrence Berkeley Laboratory Report LBL-12892 (1981).

DATACQ, A New Data Acquisition Program

*Friedemann Weik**

Most data acquisition installations at the Bevalac use QDA[1] to transfer the data from CAMAC via a micro programmed branchdriver (MBD) into a DEC PDP-11/34 (or 11/45) and from there to magtape. However, if the size of an event is of the same order as the buffersize, as can be the case at the Plasticball[2] or HISS,[3] the restriction to fixed size buffers and a synchronous communication with the MBD may waste a lot of memory and lead to increased deadtime.

To handle those data more efficiently, a new data acquisition program DATACQ, was developed. Since its overall structure is not too different from QDA, modifications to the user-part of existing MBD-code are minimal. The use of conditional assembly directives can make them run in both systems.

.The handling of variable size buffers is done in the following way. Initially, DATACQ hands as much contiguous memory to the MBD as possible, plus a value indicating the "wanted buffer size." On an interrupt from CAMAC (LAM), the MBD obtains from a specific user-entry the length of the new event and checks if this (pending) event fits into the remaining memory and if the current buffer size plus the length of this event are smaller than the "wanted buffer size." If both checks are valid, the event is stored in the buffer. If the second condition fails, the current buffer is marked as a complete buffer by interrupting the computer and sending the correlated control information. Since the pending event would fit into the remaining memory, the beginning of a new buffer is marked by inserting a 6-word header, and the event is stored in the new buffer without waiting for the acknowledgment of the interrupt. A wait is only imposed if there is not enough memory for the pending event. As soon as at least the memory needed for the pending event is available, the MBD continues. If, on the other hand, a memory block, which is contiguous to the one known by MBD, becomes available, it is handed to the MBD and is seen there with the next event.

DATACQ handles the end of buffer interrupt from the MBD by updating, appending, or inserting into its table of the currently defined buffers. At that time, the new buffer is marked for transfer to magtape, to disk, or into another much larger buffer area. The transfer of the variable size buffer is asynchronous and is handled on a first-in first-out mode.

A preliminary version of DATACQ, with parallel transfer to disk and magtape but without the transfer to a larger buffer, has been successfully used with HISS.

Footnote and References

*Gesellschaft fuer Schwerionenforschung D-6100 Darmstadt, West Germany.

1. E. Harvey, IEEE Trans. Nucl. Sci. **NS-26**, 4633 (1979).
2. A. Baden et al., contribution to this annual report.
3. C. McParland et al., contribution to this annual report.

An X-Y Histogramming Package Added to MULTI

*Friedemann Weik**

The current version of MULTI[1] in use at the Bevalac data acquisition computers (PDP 11/34 or 11/45) normally utilizes only one graphics display (Tektronix 4012) at a time. To get X-Y information, one has to tie up this graphics display with a scatterplot; the storage screen of the display is the only medium that can hold this information.

To improve this situation, a package to create, store, and display two-dimensional histograms was added to MULTI. The package itself consists of several programs, which reside in 3-9 tasks outside of MULTI, which has the ability to control those tasks and send data to them for storage. Many of the programs are written in MACRO-assembler to optimize speed and minimize the memory needs. Communication relies heavily on the SEND/RECEIVE DATA and the mapping facilities of the RSX11M operating system.

Instead of reserving one place for each possible X-Y combination, only the points with actual counts are stored in an "ordered" way. This will be explained in the following example: A ΔE-E histogram for the Plastic Ball module #586 was defined to accept for E (DA803) and ΔE (DA1811) the channel range from 10 - 2000 with every 10 channels contracted to 1. The storage area should not exceed 8192 words and the histogram was named M0D586. The definition command in MULTI (written as one line) for that was:

```
H2 DA803 DA1811 MOD586 8192 10
 2000 10 10 2000 10
```

To store the "used" points in 8192 words instead of 40,000, the following scheme was used. For each Y-row with at least one count, there is a word with the Y-value of that row plus another word to tell how many X-points of that row contain counts. There is one word for each of these X-points with the (contracted) X-coordinate information stored in their lower bits. The remaining bits give the number of counts in the bin. Higher X-resolution means fewer bits available for counting contents before overflow is reached. In this example, X ranges from 1 to 200, requiring 8 bits. This leaves 7 bits (= 127) for contents and one bit for the sign indicating a bin overflow.

Every new point has to be inserted by moving all higher points one place up in memory until all available space is used. In case of a space overflow a message is printed and no new points are inserted after that printout.

The display of the histograms is done by another task, which gets its commands from MULTI and which maps to the selected data area. There are three display modes: a simple isometric display (Fig. 1), a scatterplot with randomization around the contracted area to show the intensity (Fig. 2), and a contour plot (Fig. 3). The randomization can be switched off to speed up the display and to show the actual location.

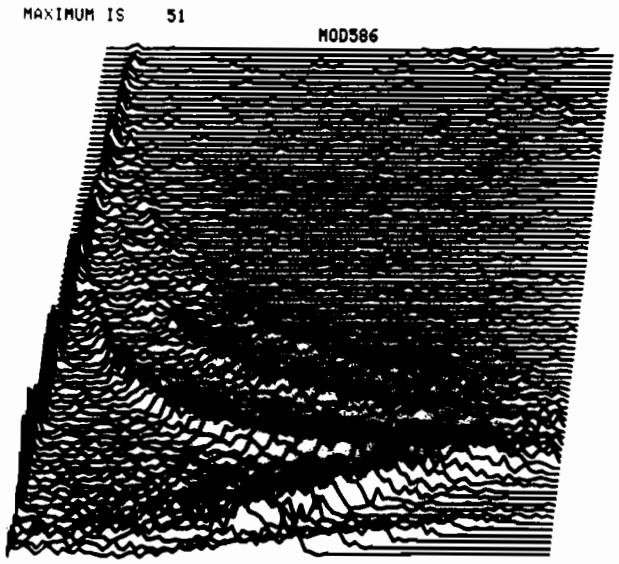

Fig. 1. Isometric display. (XBB 818-7793)

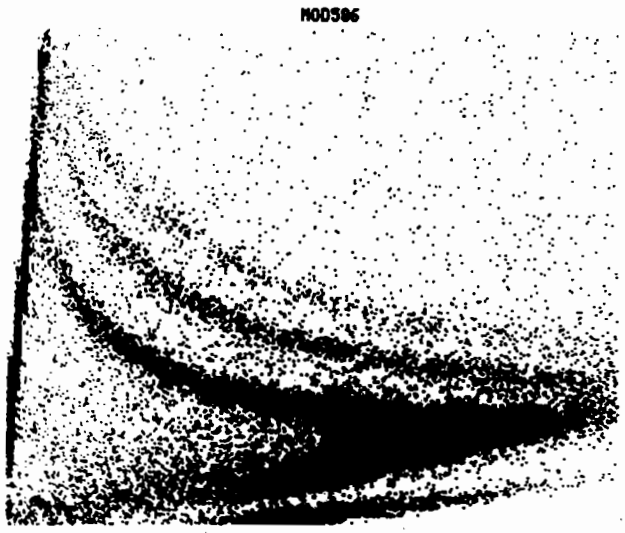

Fig. 2. Scatter plot. (XBB 818-7792)

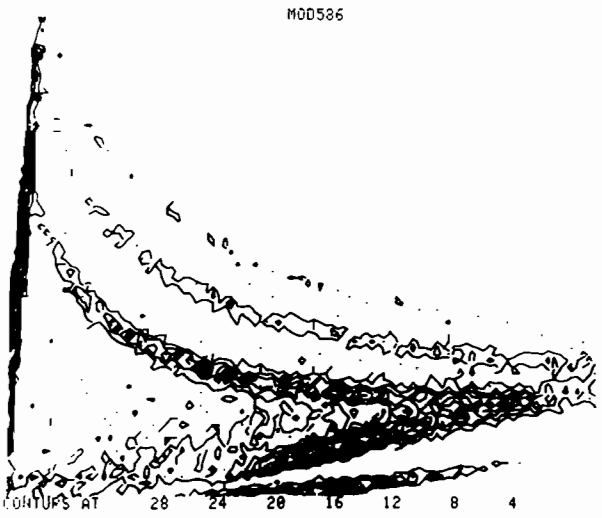

Fig. 3. Contour plot. (XBB 818-7794)

Footnote and Reference

*Gesellschaft fuer Schwerionenforschung D-6100 Darmstadt, West Germany.

1. J.F. Bartlett et al., FERMILAB Report PN-97.4.

Data Acquisition at the HISS Facility

*Charles McParland**

Experimental data at the HISS facility has been acquired and analyzed with a system of loosely coupled computers connected by a shared mass storage disk. Data from various detector systems are routed via CAMAC and an intelligent branch driver (MBD) to one of three front-end PDP-11 computers. These machines acquire variable length data events and log them to local magnetic tape.[1] Displays of spill-by-spill diagnostic information as well as current data set statistics are compiled and displayed in the experimental area.

In addition to tape logging, data are written to a shared 80-megabyte disk system. This disk contains three large data files, one for each front-end computer. These files are organized as circular buffers and always contain the "most recent" experimental data. Each front-end computer has write access to its data file; all other accesses are read only. Thus, each front-end data file on the shared disk appears similar in both content and format to the most recent section of experimental data tape (about 20 megabytes).

Coupled to this shared disk system is a VAX 780 computer. Although this general purpose machine is not directly involved in experimental data acquisition, it does have access to the "most recent" experimental data.

A collection of subroutines provides a simple user interface to data files. Users can connect to any front-end data file and access data from any location within these files.

One unique feature of this user interface is the ability to access any source of experimental data, either current "live" data or previously recorded data residing on disk or tape. Users can easily select any source of data for their analysis programs. This enables one set of programs to be developed for both on-line data analysis and off-line data reduction. This feature is expected to reduce the development time for future on-line analysis programs and greatly improve the quality of experimental diagnostic tools.

Footnote and Reference

*Also Space Science Laboratory.

1. See contribution of F. Weik in this annual report.

Data Acquisition Setup for the Plastic Ball (488H)

*Friedemann Weik**

Since a previous experiment (489H)[1] of moderate size with 455 datawords/event touched the limits of the standard data acquisition system in use at the Bevalac,[2] a more powerful system had to be used for the Plastic Ball experiment (488H)[3] which is capable of generating up to 3673 data-words/event. Since an improvement in memory size and in computing power was needed, a solution with more than one computer was sought. To keep the additional effort for system development and management to a minimum, a second computer of DEC's PDP 11-series (11/44), which uses the same operating system as the existing 11/50, was selected.

The resulting layout of the data acquisition setup is shown in Fig. 1. The experimental data are collected in CAMAC ADCs and TDCs. Each ADC-crate has its own processor (LeCroy 2280) to subtract pedestal values of the ADCs and to suppress empty channels. An equivalent system (LeCroy 4290) is used for the long range (10 us) TDCs. Since standard eight-fold TDCs had to be used for the TOF-measurement in the Plastic Ball, the data compression is done by the micro programmed branch driver (MBD) during the transfer from CAMAC into the memory of the PDP 11/50.

The layout for the PDP 11/50 follows the general rules for the Bevalac data acquisition system (248 kB memory, MBD, 2 magtape drives, 10 MB disk capacity, RSX11M operating system) with which an adjusted version of the QDA / MULTI system could be used. The QDA / MULTI system has a clear cut between data acquisition (QDA) and monitoring (MULTI). This cut was used for the implementation into a two-computer system, having the PDP 11/50 to deal only with data-taking and the PDP 11/44 with monitoring using its increased power.

The original transfer task between QDA and MULTI (MULQDA) was broken up into two tasks, one for each machine. A relative fast link (DA11B) supported by the operating system couples the two computers. The PDP 11/44 with an 80 MB disk, a cache memory, and 248 kB memory is connected to three Tektronix graphics terminals, all of which can be used simultaneously by MULTI. Additional standard terminals and the line-printer are used during program development. The 80 MB disk is dual-ported (SI9400 controller, DM980 drive) and can be accessed by the PDP 11/50. This connection, however, should only be used to transfer files to the PDP 11/50 and to backup the disk to magtape.

To supplement the hardware improvements, a new data acquisition program is developed with variable blocksize and follow-up buffering (DATACQ).[4] A preliminary version of this program (including disk-spooling) has successfully been used during HISS-experiments.[4] MULTI has been broken into about 20 tasks to overcome the size-limitations and to implement new features.[6] Further specialized monitors and display programs are planned.

Footnote and References

*Gesellschaft fuer Schwerionenforschung D-6100 Darmstadt, West Germany.

1. A. Baden et al., contribution to this annual report.
2. C. McParland, Lawrence Berkeley Laboratory Nuclear Physics Division Annual Report 1979-1980, LBL-11588, p. 200.
3. A. Baden et al., see "DATACQ, a New Data Acquisition," in this annual report.
4. F. Weik, contribution to this annual report.
5. C. McParland et al., contribution to this annual report.
6. F. Weik, see "An X-Y Histogramming Package Added to MULTI," in this annual report.

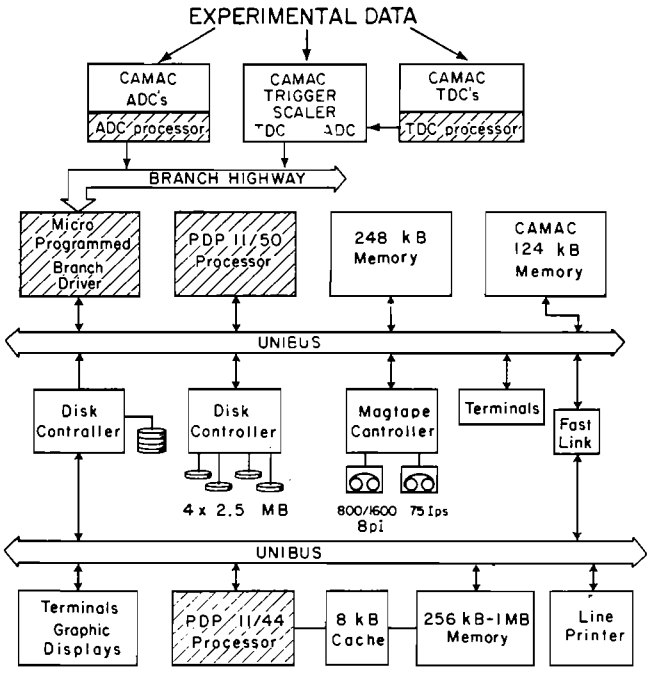

Fig. 1. (XBL 809-1959)

IV. ACCELERATORS

Accelerators

88-Inch Cyclotron Operation

D.J. Clark, C.M. Lyneis, D. Elo, L. Glasgow, R. Lam, T. Mast, R. Muller, P. Tans, and J. Welch

The 88-Inch Cyclotron, operated by the Nuclear Science Division, provides a large fraction of the beam time that is used by Division scientists. Variable energy, high-resolution beams from hydrogen through argon are produced and used for studies of nuclear structure and nuclear reaction mechanisms. The 88-Inch Cyclotron is also the Laboratory's major source of medical isotopes and its only source of polarized proton and deuteron beams.

The large energy constant, K, recently increased to 160, permits the acceleration of ions as heavy as ^{40}Ar to energies useful for nuclear physics. The lighter heavy ions reach energies up to 30 MeV/u. This cyclotron is one of the few sources in the world of variable energy heavy ions in the important transition region between low and high energies: 10-30 MeV/u.

These beams, as well as the polarized proton beams, are extensively used by outside groups from many institutions in the U.S. and abroad. In recent years, about 25% of the operating time has been taken up by outside users. Proposals are made by letter and are informally reviewed by two outside consultants. Approval can be made within two weeks, and the experiment can be scheduled within two weeks thereafter. This economical and flexible system is much appreciated by the users.

Operations

In the year ending June 30, 1981, the 88-Inch Cyclotron was scheduled for 20 eight-hour shifts per week for experiments in nuclear science, isotope production, and machine development. One eight-hour period per week was scheduled for routine maintenance. In addition, there were five weeks of shutdown for general maintenance and machine improvements, and because of budgetary restrictions. Accelerator time distribution is shown in Table 1. The list of beams available is shown in Table 2, while Fig. 1 shows the particle distribution of light and heavy ion beams over the past 13 years. The ratio of heavy-ion to light-ion beam time has stabilized at 2:1 in the last several years.

Upgrading the cyclotron is an ongoing process. Some modifications are directed at immediately improving the efficiency and reliability of the cyclotron. Longer-range improvement projects are directed toward extending the capabilities of the cyclotron into new regions such as development of new beams, higher energies, or increased currents. Both immediate and long-range improvements are crucial to the continued successful operation of the cyclotron.

During the past year a number of modifications were made on the magnet power supplies and the rf system. A new regulator was installed on the M41, M42 analyzer magnets, raising the maximum current from 1000 μA to 1160 μA, and we expect to increase the current to 1250 μA by a minor modification of the linear transformer. This will allow the magnets to be used on the high-energy α-particle and heavy-ion beams resulting from the new higher K operation. A new regulator was added to the switching magnet power supply for the high resolution beam line. Regulation was added to the valley coil no. 5 power supply to improve the stability of beam extraction from the cyclotron. To reduce power usage and tube replacement costs, two new 300 W wide-band amplifiers are now ready for installation in place of the final rf driver tube. A new fault detector for the modulator was installed, which will better protect the final rf amplifier tube from inadvertent damage.

Extensive modifications were done on the components used in the polarized source and axial injection system. A new ionizer was installed on the polarized source and will be ready for testing in late 1981; it is expected to improve the output of polarized ions by a factor of 10. The installation of the new ionizer required modification of the axial injection system because of physical size changes. While the system was disassembled, the high-voltage vacuum feedthroughs, which had been a source of vacuum leaks, were replaced. A cryopumping head was added to replace

Table 1. Operating and maintenance time distribution of the 88-Inch Cyclotron, including total calendar time except holidays (7/80-6/81).

	Hours	%
Operating Time		
Experimental program	6,312	74.9
Beam development	340	4.1
Subtotal:	6,652	79.0
Maintenance Time		
Routine	512	6.0
Scheduled shutdown	818	9.8
Unscheduled shutdown	442	5.2
Subtotal:	1,772	21.0
Grand Total:	8,424	100.0

Table 2. 88-Inch Cyclotron beam list.

Ion	Energy[a] (MeV)	Ext. Beam Intensity (euA[b])
p	0.2- 55	100 - 20
p (polarized)	6 - 55	0.3
d	0.5- 65	100 - 20
	65 - 70	~0.5
d (polarized)	10 - 70	0.3
$^{3}He^{1+}$ (d)	2 - 47	>20
$^{3}He^{2+}$ (d)	4 - 140	100 - 10
$^{4}He^{2+}$	3 - 130	100 - 10
	130 - 140	~0.5
$^{6}Li^{1+}$ (d)	2 - 23	10
$^{6}Li^{2+}$ (d)	23 - 93	5
$^{6}Li^{3+}$ (d)	93 - 195	0.5
$^{7}Li^{2+}$	20 - 80	5
$^{7}Li^{3+}$	80 - 180	0.5
$^{9}Be^{2+}$	15 - 62	5
$^{9}Be^{3+}$	62 - 140	2
$^{9}Be^{4+}$	140 - 249	0.05
$^{10}B^{2+}$ (d)	14 - 56	10
$^{10}B^{3+}$ (d)	56 - 126	50
$^{10}B^{4+}$ (d)	126 - 224	0.3
$^{10}B^{5+}$ (d)	224 - 320	0.001
$^{11}B^{2+}$	12 - 51	10
$^{11}B^{3+}$	51 - 115	50
$^{11}B^{4+}$	115 - 204	0.3
$^{12}C^{2+}$	12 - 47	>20
$^{12}C^{3+}$	47 - 105	30
$^{12}C^{4+}$	105 - 212	5 - .5
$^{12}C^{5+}$	187 - 306	0.01-.001
$^{12}C^{6+}$	292 - 384	10^{5} p/sec
$^{13}C^{3+}$ (d)	43 - 97	>20
$^{14}N^{2+}$	10 - 40	20
$^{14}N^{3+}$	40 - 90	15
$^{14}N^{4+}$	90 - 160	15
$^{14}N^{5+}$	160 - 250	2
$^{14}N^{6+}$	250 - 360	10^{6} p/sec
$^{14}N^{7+}$	360 - 448	100 p/sec
$^{15}N^{4+}$ (d)	84 - 150	15
$^{16}O^{1+}$	9	1
$^{16}O^{2+}$	9 - 35	>5
$^{16}O^{3+}$	35 - 79	20
$^{16}O^{4+}$	79 - 155	30-.2
$^{16}O^{5+}$	140 - 219	5
$^{16}O^{6+}$	219 - 315	0.3
$^{16}O^{7+}$	315 - 429	10^{7} p/sec
$^{16}O^{8+}$	429 - 512	0.2 p/sec
$^{18}O^{3+}$ (d)	31 - 70	20
$^{18}O^{4+}$ (d)	70 - 124	>10
$^{18}O^{5+}$ (d)	124 - 194	5
$^{19}F^{3+}$	30 - 66	5
$^{19}F^{4+}$	66 - 118	10
$^{19}F^{5+}$	118 - 184	2
$^{20}Ne^{3+}$	28 - 63	>10
$^{20}Ne^{4+}$	63 - 112	10
$^{20}Ne^{5+}$	112 - 175	5
$^{20}Ne^{6+}$	175 - 252	1
$^{20}Ne^{7+}$	252 - 343	0.01
$^{20}Ne^{8+}$	343 - 448	~50 epA
$^{22}Ne^{5+}$(d)	102 - 159	>5
$^{22}Ne^{6+}$(d)	159 - 229	1
$^{24}Mg^{4+}$	50 - 93	2
$^{24}Mg^{5+}$	93 - 146	0.2
$^{25}Mg^{4+}$(d)	50 - 90	2
$^{26}Mg^{4+}$(d)	48 - 86	2
$^{28}Si^{5+}$	80 - 125	1
$^{28}Si^{6+}$	125 - 180	0.2
$^{28}Si^{7+}$	180 - 245	0.05
$^{32}S^{6+}$	100 - 158	2
$^{32}S^{7+}$	158 - 214	0.2
$^{35}Cl^{7+}$	144 - 196	0.5
$^{35}Cl^{8+}$	196 - 256	0.05
$^{37}Cl^{6+}$	95 - 136	0.3
$^{37}Cl^{7+}$	136 - 185	0.08
$^{40}Ar^{2+}$	3.5- 14	0.4
$^{40}Ar^{6+}$	87 - 126	4
$^{40}Ar^{7+}$	126 - 172	2
$^{40}Ar^{8+}$	172 - 224	0.5
$^{40}Ar^{9+}$	224 - 280	10^{5}p/sec
$^{40}Ar^{10+}$	280 - 350	10^{3}p/sec
$^{40}Ca^{6+}$	87 - 126	1
$^{40}Ca^{7+}$	126 - 172	0.2
$^{56}Fe^{10+}$	180 - 250	1 p/sec
$^{63}Cu^{9+}$	142 - 180	5 enA
$^{63}Cu^{10+}$	180 - 222	0.1 enA
$^{63}Cu^{11+}$	222 - 269	$5x10^{3}$p/sec
$^{84}Kr^{2+}$(c)	1.6- 6.6	0.001
$^{84}Kr^{8+}$	82 - 107	0.250
$^{84}Kr^{9+}$	107 - 135	0.120
$^{84}Kr^{10+}$	135 - 167	0.030
$^{84}Kr^{11+}$	167 - 202	0.003
$^{197}Au^{13+}$	102 - 120	2 p/sec
$^{197}Au^{14+}$	120 - 140	0.1 p/sec

a) Heavy ion energy range shows nominal maximum energy for a particular charge state down to the energy which can be reached by the next lowest charge state. Beams can also be run at energies below 1 Mev/nucleon.

b) Electrical microamperes except as noted.

c) 15th harmonic

d) Isotopically enriched source feed

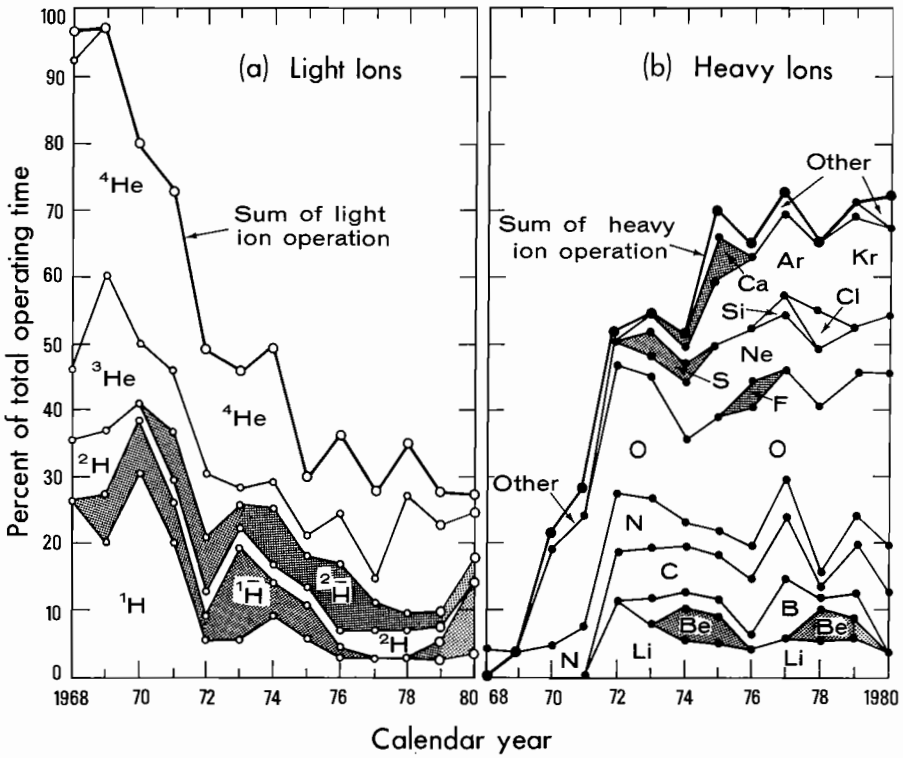

Fig. 1. Distribution of light and heavy ion beams, as percent of cyclotron operating time, 1968-1980.

(XBL 809-1999A)

a diffusion pump. The improved vacuum should benefit both polarized and heavy ion beams.

The external heavy-ion PIG source and its beam line to the axial injection beam line were completed, tested, and used during this report period. Ions from the new source are transported horizontally before being deflected vertically into the existing axial injection column that is also used for polarized protons. The final assembly and testing of the new heavy ion facility were done in collaboration with the Muller astrophysics group, which proposes to use the source for sample injection in their radioisotope detection program. Initial tests of the source emphasized injection of $^{12}C^{3+}$ and $^{14}N^{3+}$ at energies of about 7 kV with acceleration to about 40 MeV. A series of tests made steady improvement in the ion source output, transport efficiency, and extracted current from the machine. The best transmission from source to cyclotron external beam was 2% at 12 kV injection, with a first harmonic buncher being used. Losses include charge exchange in the injection line and cyclotron phase acceptance and emittance matching. The addition of cryopumps in the injection line and the cyclotron is expected to improve the transmission. Typical currents at the exit of the cyclotron were about 1 μA. A source specifically designed for sputtering has been built and will be tested soon.

The south port cryopump was installed and tested. The tests showed that a modification to allow temperature control of the cold head is required. Without a temperature control, the device can cause the hydrogen coolant to freeze, which in turn decouples the refrigerator from the cryopanels. A temperature controller will be installed shortly, allowing the south port cryopump to become operational. This additional pumping will improve the vacuum in the tank and thus the heavy ion performance of the machine.

The passive magnetic deflection channel will provide radial focusing and greater deflection strength for all cyclotron beams. The radial focusing will increase the beam transmission to experimental targets. The greater deflection strength will provide efficient extraction of the high-energy α-particle and heavy ion beams accelerated, using the new higher K operation. The magnetic channel will replace the third element of the electrostatic deflector. The magnetic design is complete. Final orbit calculations of phase space ellipses through the channel will be done as a joint project with the Cyclotron Institute, Texas A&M University. Mechanical design and fabrication will then be completed.

Planning is underway for an advanced heavy ion source for the cyclotron. The goal is to provide useful beam intensities of 10^9-10^{10} particles/sec on target with energies of 2 to 3 times those of present heavy ion beams with masses between nitrogen and xenon. The energy would be up to 40 MeV/u for the lower masses. The charge states would be, for example, N^{7+} and $Ar^{14\text{-}18+}$. The two leading candidates for sources are the Electron Beam Ion Source (EBIS) and the Electron Cyclotron Resonance (ECR) source.

Research and development to build a test bench EBIS

were begun in January 1980, under the direction of the plasma group in the LBL Accelerator Division. The goal is to reproduce the high electron-beam densities observed by the Orsay group. This requires careful alignment of the electron gun and magnet system, and high-vacuum technology. The progress during the past year includes the successful production of an extremely well-aligned magnetic field and electron beam—both straight to within 0.05 mm along the 60-cm solenoid length. Detailed measurements have been made on the relation of electron beam profile to magnetic field and injection voltage. Study of the ion beam is now underway. This test bench will give valuable information on the requirements for high-charge-state production. If the tests indicate that the intensity, charge state, and duty factor requirements can be met, a full-scale EBIS will be built for installation on the axial injection system of the cyclotron.

SuperHILAC Operations and Research

M.S. Zisman and R.M. Diamond

The SuperHILAC furnishes beams from ^{4}He to ^{208}Pb (and soon ^{238}U) with energies variable from 1.2 to 8.5 MeV/nucleon. It is the only accelerator in the United States currently able to provide very-heavy-ion beams at energies above the Coulomb barrier, and will continue to be the prime source of such projectiles in this country for the next several years.

As a result of its unique capabilities, the SuperHILAC has been made a national facility available to qualified scientists in nuclear and atomic physics throughout the United States, and to collaborating groups in Canada and Europe. At present, more than half of the operating time is given to user groups from outside the Laboratory. Proposals are submitted twice a year, and beam time is allocated by a Program Advisory Committee made up of experts in heavy-ion physics who may be involved in experiments at the SuperHILAC, but are not major users there. In addition, a User's Executive Committee, made up principally of major users elected by the whole user community, helps advise the Nuclear Science and the Accelerator and Fusion Research Divisions on the operation of the machine and the needs of the users. The SuperHILAC runs 20 shifts a week, 7 to 8 months a year.

On the whole, machine performance has been quite smooth and reliable during the past year; experimenters have had beam available to them about 75% of the scheduled time. Improvement of the accelerator is an ongoing process, and the major development of the past few years is the construction and bringing into operation of the third injector, ABEL. This is an injector for relatively high-intensity, very heavy-ion beams. It consists of a twin high-power PIG source, a 750-kV Cockcroft-Walton accelerator, and a Wideroe linac. Between the Cockcroft-Walton and the Wideroe, a 90° bending magnet provides isotope separation with a resolution of 1 part in 300. This new injector was brought into service in June, just before the annual budgetary shutdown, and should now provide the users with more reliable and more intense beams of rare-earth ions on up to uranium. Anticipated ions from the ABEL injector, for fall of FY 1982, along with hoped-for intensities, are given in Table 1.

A feature necessary for the simultaneous operation of the SuperHILAC and the Bevalac was the development of timesharing the beam. The macrostructure of the beam out of the SuperHILAC is 36 pulses/sec of variable width, 1 to 9 msec long. These pulses may be divided between different beams from the injectors, at different energies, in almost any manner desired. A typical operation is 32 pulses/sec of a very heavy ion to the main SuperHILAC user, 2 pulses/sec of a lighter ion to the Bevalac, and 2 pulses/sec of either beam (at a different energy if so desired) to the next SuperHILAC user to test his equipment or to do a parasitic experiment. This scheme has been very successful. Work is continuing in order to increase the duty cycle from the present 25% for "light" heavy ions and 10% for Pb to ~ 35% and 20%, respectively, and to construct a buncher cavity of a new design to provide beam bunches in a particular beam line of less than 500 psec FWHM.

The construction of an on-line isotope separator, mentioned in last year's report, has been completed, and this instrument has been successfully used. Efforts are now underway to provide a laboratory above the separator along with a tape transport system to allow low-background β- and γ-spectroscopic studies on the separated products.

Table 1. ABEL Ions Available In FY 1982.

	Post-exit pnA (avg. at 36 pps)
^{84}Kr (22^{+})	~ 75
^{129}Xe (29^{+})	~ 40
^{197}Au (37^{+})	~ 5
^{208}Pb (39^{+})	~ 5
^{238}U (42^{+})[a]	~ 5

[a]Not expected before beginning of FY 1982.

The research program at the SuperHILAC is varied, but can be grouped into four main categories. Roughly 50% of the beam time is devoted to the study of heavy-ion reaction mechanisms, with five outside groups and one from LBL participating. A second topic is nuclear structure studies; these are carried out primarily by an LBL group that collaborates with three major outside groups. A third category is the study of exotic nuclei—the production of new isotopes of known elements and of new chemical elements. Two LBL groups and one from outside carry on the bulk of these studies; they have largely focused on the very heavy elements, but with the availability of the new isotope separator, more work will take place over the whole periodic table. The fourth type of study is heavy-ion atomic physics, which is carried out by two LBL groups (outside the Nuclear Science Division) and three outside groups.

The studies at the SuperHILAC by groups in the Nuclear Science Division are described in the various group reports in this annual report.

PART 3. APPENDICES

Thesis Abstract

Effects of Particle Evaporation on the Angular Momentum of the Emitting Nucleus for Deep Inelastic and Compound Nuclear Reactions

S.K. Blau

A model is developed which allows one to calculate analytically the angular momentum removed, and the angular momentum misalignment created by the evaporation of light particles from an excited nucleus. The mass, temperature, and angular momentum of the emitting nucleus are explicitly considered. The formalism applies equally well to heavy ion and compound nuclear reactions.

Nuclear Science Division Seminars

July 24, 1980	Dr. Hans Sann	Symmetric Mass Yields and the Reaction U + Ca
Aug. 11, 1980	J. de Swart Nijmegen, Holland	Dibaryon Resonances and Multiquark States
Aug. 14, 1980	Itshalk Tserruya Weizmann Institute Israel	Neutron Emission from 12 MeV/n Kr + Er − a Nonequilibrium Component?
Aug. 19, 1980	Gabi Goldring Weizmann Institute Israel	Tilted Foil Hyperfine Interactions
Aug. 29, 1980	Yuri T.S. Oganessian	Transuranium Element Research at Dubna
Sept. 8, 1980	Uli Lynen GSI, Darmstadt West Germany	Reactions with 86-MeV/n Carbon Beams
Sept. 15, 1980	W.J. Swiatecki LBL	The Dynamics of Nuclear Coalescence or Reseparation and Dynamical Limits on Superheavy Element Formation
Sept. 29, 1980	John O. Newton Australian National University, Canberra	Limits to Evaporation Residue Cross Sections from Fission and Particle Decay at High Angular Momentum

Oct. 20, 1980	Grant J. Mathews Kellogg Radiation Laboratory, Caltech	Current Topics in Nuclear Synthesis
Nov. 3, 1980	Kurt Kilian MPI, Heidelberg West Germany	Anti-Protons at LEAR
Nov. 10, 1980	Ken Moody LBL	Actinide Production in the Reaction of ^{136}Xe and ^{86}Kr with ^{248}Cm
Dec. 1, 1980	Ed Ludwig University of North Carolina and TUNL	The Interesting Systematics Observed in Studies of Isospin Forbidden Resonances
Dec. 8, 1980	Gerhard Soff Frankfurt West Germany	Atomic Clock for Nuclear Collisions
Dec. 15, 1980	R.J. McDonald LBL	Fragment Spin Orientation in Deep Inelastic Reaction from Anisotropy Measurements of Continuum γ-Rays
Dec. 22, 1980	Sigurd Köhler University of Arizona	Heavy Ion Collisions with Two-Body Dissipation
Jan. 12, 1981	R.W. Koontz LBL	Fragmentation of ^{4}He at 35 MeV/n: Correlated Fragments and "Impulsive Absorption"
Jan. 19, 1981	H. Zankel University of Graz Austria	Approximate Coulomb Corrections in Light Nuclear Systems
Jan. 26, 1981	Achim Weiguny LASL and Münster University West Germany	Quasi-Molecular and Surface Wave Resonances in Heavy-Ion Scattering
Feb. 17, 1981	James Symons LBL	$\alpha\alpha$ and Pα Collisions in the CERN Intersecting Storage Rings
Feb. 23, 1981	Georg Leander Lund University Sweden	Theoretical Description of Quasi-Continuum Gamma Rays
Mar. 2, 1981	Al Stetz Oregon State University	Double Charge Exchange Reactions on Helium Isotopes

Mar. 9, 1981	John Calarco Stanford University	Excitation and Decay of Giant Resonances
Mar. 16, 1981	Phil J. Siemens Texas A&M University	Matter at 10^{12} K: Theory versus Experiment
Mar. 23, 1981	Arturo Menchaca-Rocha University of Mexico	On the Time Evolution of ^{16}O-Induced Direct Reactions
Mar. 30, 1981	Hiroski Toki Michigan State University	Pionic Mode of Excitation in Nuclei
Apr. 3, 1981	Günther Rosner Max Planck Institut Heidelberg West Germany	Deep Inelastic and Fusion Processes in the Reactions $^{32}S + {}^{27}Al$ at $E/A \leq 10$ MeV
Apr. 6, 1981	Norman K. Glendenning LBL	Pion Condensation Gravitational Waves and the Evolution of Neutron Stars
Apr. 13, 1981	Thomas Døssing NORDITA Copenhagen	Angular Correlations and Spin Alignment in Deep Inelastic Nuclear Reactions
Apr. 27, 1981	Charles R. Gruhn LBL	Bragg Curve Spectroscopy
May 4, 1981	Rudolph C. Hwa University of Oregon	From Parton to Nuclei
May 11, 1981	Rosemarie McFarland LBL Jan Wouters LBL	Heavy Ion Direct Transfer Reactions in the Actinide Region Mass Measurements of the Neutron Deficient Indium Isotopes
June 1, 1981	Sam Austin Michigan State University	The Giant Isovector Resonances —A Hadronic View
June 15, 1981	L.G. Arnold Ohio State University	Relativistic Nuclear Optical Model: Nucleons on Nuclei or Bags on Pokes
June 17, 1981	Bo Jakobsson University of Lund Sweden	Production of Light Particles and Beam Fragmentation in 58 and 86 MeV A Heavy Ion Reactions
June 29, 1981	Leon Van Hove CERN and ITP, Santa Barbara	What Happens to Quarks and Gluons in Hadronic Collisions?

Nuclear Theory Meetings

July 23, 1980	Eugene Marshalek Notre Dame University	Review of Microscopic Boson Expansion
July 30, 1980	Alan Goodman Tulane University	Finite Temperature HFB Theory
July 31, 1980	Igal Talmi Weizmann Institute Israel	Interacting Boson Model for Nuclei
Aug. 7, 1980	Robert Vinh Mau Paris	Recent Progress with the Paris Nucleon-Nucleon Potential
Aug. 21, 1980	Sven Bjornholm Niels Bohr Institute Copenhagen	On the Dividing Line Between Heavy Ion Scattering and Capture Reactions
Sept. 3, 1980	L. Csernai	Realistic Two and Three Dimensional Fluid Dynamical Calculations with a Description of Final Evaporation
Sept. 10, 1980	B.R. Mottelson NORDITA Copenhagen	Alignment Effects for Particles and Pairs (Analysis of Some Features of the Interacting Boson Model)
Oct. 22, 1980	J. Boguta LBL	Relativity and Nuclear Structure
Oct. 29, 1980	Herbert Ruck LBL	Polynomial Quantum Chromodynamics
Nov. 12, 1980	T. Matsui Stanford University	Structure of Pion Condensation
Jan. 14, 1981	P. Hecking LBL	Abnormal Matter and Pion Condensation
Feb. 4, 1981	Berndt Müller Frankfurt University West Germany	Hot Color Phase Transitions of the QCD Vacuum at High Temperatures
Mar. 11, 1981	Dr. H. Orland Saclay, France	Functional Integral Methods
Mar. 18, 1981	E.A. Remler Institute for Theoretical Physics Santa Barbara	Composite Particle Production in Heavy Ion Collisions
Mar. 25, 1981	Herbert Ruck LBL	From Quarks to Nuclear Matter
Apr. 1, 1981	Hiroski Toki Michigan State University	Short-Range Part of NN Interaction within the Non-Relativistic Quark Model

May 13, 1981	Kei-Fei Liu University of Kentucky	Quarks in Nuclei
May 27, 1981	W. Norenberg GSI	Memory Effects in the Energy Dissipation for Slow Collective Motion
July 22, 1981	Peter Moller Lund University, Sweden	Nuclear Shapes
July 27, 1981	J.P. Blaizot CEN, Saclay, France	Time Dependent Variational Principles and Semiclassical Bound States
July 29, 1981	Xin-Hua Yang	Many Body Theory of Confined Quarks and Gluons and the Calculation of the Exchange and Self-Energy

Papers Published And LBL Reports Issued

1980-81

ALBRECHT, K. (See DIEBEL, M., LBL-11522)

ALEKLETT, K., D.J. Morrissey, W. Loveland, P.L. McGuaghey, and G.T. Seaborg
The Energy Dependence of ^{209}Bi Fragmentation in Relativistic Nuclear Collisions, LBL-11273, July 1980, Phys. Rev. C **23**, 1044 (1981).

ALEKLETT, K. (See LOVELAND, W., LBL-10010)

ARYAEINEJAD, R., R.B. Firestone, W.H. Bentley and William C. McHarris
In-Beam γ-Ray Spectroscopy of Excited States in ^{143}Eu Phys. Rev. C **23**, 194 (1981).

AWES, T.C. (See BACK, B.B., LBL-11852)

ÄYSTÖ, J., M.D. Cable, R.F. Parry, J.M. Wouters, D.M. Moltz, and Joseph Cerny
Decays of the $T_Z = -2$ Nuclei ^{20}Mg, ^{24}Si and ^{36}Ca, LBL-11193, June 1980, Phys. Rev. C **23**, 879 (1981).

ÄYSTÖ, J. (See CERNY, J., LBL-12853)

ÄYSTÖ, J. (See MOLTZ, D.M., LBL-11427)

BACK, B.B., A.C. Shotter, T.J.M. Symons, A. Bice, C.K. Gelbke, T.C. Awes, and D.K. Scott
Fission of ^{238}U Induced by Inelastic Scattering of 120 MeV α-Particles, LBL-11852, September 1980, Phys. Rev. C **23**, 1105 (1981).

BAER, H.W. (See MARTOFF, C.J., LBL-11914)

BANERJEE, B., N.K. Glendenning and M. Gyulassy
Pion Condensation in a Field Theory Consistent with Bulk Properties of Nuclear Matter, LBL-10979, May 1980, Nucl. Phys. A **361**, 326 (1981).

BEMIS, C.E., Jr. (See NITSCHKE, J.M., LBL-10173)

BENTLEY, W.H. (See ARYAEINEJAD, R.)

BENTLEY W. H. (See WALKER, P.M.)

BERMAN, B.L. (See OLSON, D.L., LBL-12292)

BICE, A.N., A.C. Shotter, D.P. Stahel and Joseph Cerny
Investigation of the (^{10}B, ^{6}Li* (3^+, 2.18 MeV)) Reaction as a Method for α-Cluster Transfer Studies, LBL-11194, July 1980, Phys. Letts. B **101**, 27 (1981).

BICE, A. (See BACK, B.B., LBL-11852)

BICE, A.N. (See SHOTTER, A.C., LBL-11375)

BICE, A.N. (See SHOTTER, A.C., LBL-11376)

BICE, A.N. (See SHOTTER, A.C., LBL-11458)

BIRCHALL, J., W.T.H. van Oers, H.E. Conzett, P. von Rossen, R.M. Larimer, J. Watson, and R.E. Brown
Analyzing Powers of ^{3}He(p,p)^{3}He Elastic Scattering between 30 and 50 MeV, LBL-11121, June 1980, presented at the 5th International Symposium on Polarization in Nucl. Phys., Santa Fe, NM, August 11-15, 1980.

BISTIRLICH, J.A. (See MARTOFF, C.J., LBL-11914)

BLAU, S.K., L.G. Moretto
Effects of Particle Evaporation on the Angular Momentum of the Emitting Nucleus for Deep Inelastic and Compound Nuclear Reactions, LBL-10926, September 1980, Nucl. Phys. A **359**, 477 (1981).

BLAU, S. (See MORETTO, L.G., LBL-10805)

BLOCKI, J., W.J. Swiatecki
A Generalization of the Proximity Force Theorem, LBL-9574, Annals of Physics **132**, 53 (1981).

BOGUTA, J.
Remarks on the Beta Stability in Neutron Stars, LBL-11465, August 1980, submitted to Phys. Letts. B.

BOGUTA, J.
Nucleon-Nucleus Optical Potential in a Relativistic Theory of Nuclear Matter, LBL-11466, August 1980, submitted to Phys. Letts. B.

BOGUTA, J.
Relativistic Quantum Field Theory of Finite Nuclei, LBL-11467, August 1980, submitted to Phys. Letts. B.

BOGUTA, J.
Properties of $T \neq 0$ Nuclei in a Relativistic Field Theory of Nuclear Matter, LBL-11468, August 1980, submitted to Phys. Letts. B.

BOGUTA, J.
Ground State Properties of 0^{16} Ca^{40} and Ca^{48} In a Relativistic Hartree Theory of Nuclear Matter, LBL-11894, December 1980, submitted to Nucl. Phys. A.

BOGUTA, J.
A New Mechanism Leading to Density Isomers, LBL-12333, April 1981, submitted to Phys. Letts.

BOGUTA, J.
Density Dependence of the Single Particle Potential in Nuclear Matter, LBL-12628, April 1981, submitted to Phys. Letts.

BOGUTA, J., S. Bohrmann
Relativistic Quantum Field Theory of a Hypernuclei, LBL-11670, October 1980, submitted to Phys. Letts. B.

BOGUTA, J. (See STÖCKER, H., LBL-12095)

BOHRMAN, S. and Jörn Knoll
Finite Particle Number Effects in High-Energy Nuclear Collisions: Implications on Pion Spectra, LBL-10970, May 1980, Nucl. Phys. A **356**, 498 (1981).

BOHRMANN, S. (See LBL-11670, BOGUTA, J.)

BOHRMANN, S. (See KO, Che Ming, LBL-11041)

BOLOTIN, H.H. (See McDONALD, R.J., LBL-11608)

BROWN, R.E. (See J. BIRCHALL, LBL-11121)

BUCHWALD, G. (See STÖCKER, H., LBL-11774)

CABLE, M.D. (See ÄYSTÖ, J., LBL-11193)

CABLE, M.D. (See CERNY, JOSEPH, LBL-12853)

CABLE, M.D. (See MOLTZ, D.M., LBL-11427)

CERNY, J., J. Äystö, M.D. Cable, P.E. Haustein, R.F. Parry, H.M. Thierens, and J.M. Wouters
A Study of the Beta-Decay Energies of Highly Neutron-Deficient Indium Isotopes, LBL-12853, June 1981, presented at the Fourth International Conference on Nuclei Far from Stability, Helsingør, Denmark, July 7-13, 1981.

CERNY, J. (See ÄYSTÖ, J., LBL-11193)

CERNY, J. (See BICE, A.N., LBL-11194)

CERNY, J. (See MOLTZ, D.M., LBL-11427)

CERNY, J. (See SHOTTER, A.C., LBL-11375)

CERNY, J. (See SHOTTER, A.C., LBL-11376)

CERNY, JOSEPH (See SHOTTER, A.C., LBL-11458)

CHESSIN, S.A. (See GEAGA, J.V., LBL-10265)

CHIOU, J.H. (See MA, A.Y., LBL-9689)

CHO, Y.C. (See MA, A.Y., LBL-9689)

COLE, A.J. (See RAE, W.D., LBL-12568)

CONZETT, H. E.
Concerning Tests of Time Reversal Invariance Via the Polarization-Analyzing Power Equality, LBL-11087, June 1980, presented at the International Conference on Polarization Phenomena in Nuclear Physics, Santa Fe, NM, August 11-15, 1980.

CONZETT, H.E.
Polarization Effects in Light Nuclei, LBL-11545, September 1980, Rapporteur's Report, presented at the Fifth International Symposium on Polarization Phenomena in Nuclear Physics, Santa Fe, NM, August 11-15, 1980.

CONZETT, H.E.
Large Deviations from the Polarization-Analyzing Power Equality and Implied Breakdown of Time Reversal Invariance, LBL-11546, September 1980, Invited paper presented at the Fifth International Symposium on Polarization Phenomena in Nuclear Physics, Santa Fe, NM, August 11-15, 1980.

CONZETT, H.E., P. von Rossen, F. Hinterberger, R.J. Slobodrian, C. Rioux, and R. Roy
Large Deviations from the Polarization-Analyzing Power Equality and Implied Breakdown of Time Reversal Invariance, LBL-11576, September 1980, Invited paper presented at the 1980 International Symposium on High Energy Physics with Polarized Beams and Polarized Targets, Lausanne, Switzerland, September 25 — October 1, 1980.

CONZETT, H.E. (See BIRCHALL, J., LBL-11121)

CONZETT, H.E. (See SLOBODRIAN, R.J., LBL-11372)

CRAMER, J.G. (See ZISMAN, M.S., LBL-10204)

CRAWFORD, H.J. (See OLSON, D.L., LBL-12292)

CROWE, K.M. (See MARTOFF, C.J., LBL-11914)

CSERNAI, L.P. (See STÖCKER, H., LBL-11774)

CUGNON, J., J. Knoll, and J. Randrup
Participant Intimacy - A Cluster Analysis of the Intranuclear Cascade, LBL-11301, August 1980, Nucl. Phys. A **360**, 444 (1981).

CUMMING, J.B. (See LOVELAND, W., LBL-10010)

CUSSON, R.Y. (See STÖCKER, H., LBL-11774)

DACAL, A. (See HARRIS, J.W., LBL-12334)

DACAL, A. (See RAE, W.D., LBL-11135)

DACAL, A. (See RAE, W.D., LBL-12568)

DEVRIES, R.M. (See ZISMAN, M.S., LBL-10204)

DIAMOND, R.M. and F.S. STEPHENS
Nuclei at High Angular Momentum, LBl-10325, June 1980, Ann. Rev. Nucl. Part. Sci. 1980 30:85-157.

DIAMOND, R.M.
Nuclear States and Shapes at High Spin, LBL-11436, August 1980, presented at the XII Summer School in Nuclear Physics, Mikolajki, Poland, September 1-13, 1980.

DIAMOND, R.M.
Continuum Gamma-Ray Spectroscopy, LBL-12792, June 1981, presented at the Divisional Conference of the European Physics Society on Nuclear and Atomic Physics with Heavy Ions, Bucharest, Romania, June 9-12, 1981.

DIAMOND, R.M. (See McDONALD, R.J., LBL-11608)

DIAMOND, R.M. (See NEWTON, J.O., LBL-12261)

DIAMOND, R.M. (See SIE, S.H., LBL-11352)

DIAMOND, R.M. (See WOZNIAK, G.J., LBL-11196)

DIEBEL, M., Klaus Albrecht and Rainer W. Hasse
Microscopic Calculations of Fission Barriers and Critical Angular Momenta for Excited Heavy Nuclear Systems, LBL-11522, September 1980, submitted to Nucl. Phys.

DINES, E.L. (See NEWTON, J.O., LBL-12261)

DRAPER, J.E. (See NEWTON, J.O., LBL-12261)

EGGERS, R.C., L.P. Somerville
The Maximum Likelihood Method Applied to the Problem of the Multi-Component Decay, LBL-12060, January 1981, submitted to Nucl. Inst. Meth.

ESKOLA, P. (See NITSCHKE, J.M., LBL-10173)

FABER, S.R. (See WALKER, P.M.)

FIRESTONE, R.B., R.C. Pardo, R.A. Warner, Wm.C. McHarris, and W.H. Kelly
The ϵ/β^+ Decay of ^{145}Gd: Resolution of ϵ/β^+ Decay Branching Ratio Anomalies and Evidence for Pronounced Structures in the β-Decay Strength, LBL-12424, March 1981, submitted to Physical Review C.

FIRESTONE, R.B. (See ARYAEINEJAD, R.)

FIRESTONE, R.B. (See MATSUSHITA, N.)

FIRESTONE, R.B. (See SCHUBERT, K.R.)

FIRESTONE, R.B. (See WALKER, P.M.)

FOWLER, M. (See NITSCHKE, J.M., LBL-10173)

FRIEDLANDER, E.M., R.W. Gimpel, H.H. Heckman, Y.J. Karant, B. Judek, and E. Ganssauge
Evidence for Anomalous Nuclei among Relativistic Projectile Fragments from Heavy Ion Collisions at Bevalac Energies, LBL-11136, June 1980, Phys. Rev. Lett. **45**, 1084 (1980).

GANSSAUGE, E. (See FRIEDLANDER, E.M., LBL-11136)

GEAGA, J.V., S.A. Chessin, J.Y. Grossiord, J.W. Harris, D.L. Hendrie, L.S. Schroeder, R.N. Treuhaft and K. Van Bibber
Observation of High Momentum Protons From Limiting Target Fragmentation, LBL-10265, April 1980, Phys. Rev. Letts. **45**, 1993 (1981).

GEAGA, J.V. (See HARRIS, J.W., LBL-12334)

GELBKE, C.K. (See BACK, B.B., LBL-11852)

GHIORSO, A. (See LEINO, M.E., LBL-12816)

GHIORSO, A. (See NITSCHKE, J.M., LBL-10173)

GIMPEL, R.W. (See FRIEDLANDER, E.M., LBL-11136)

GLENDENNING, N.K.
Hyper-Strange Hadronic Matter, LBL-11538, November 1980, Phys. Rev. C **23**, 2757 (1981).

GLENDENNING, N.K.
Pion Condensation and the Evolution of Neutron Stars, LBL-12427, March 1981, submitted to Phys. Rev. Letts.

GLENDENNING, N.K., A. Lumbroso
Pion Condensation, Density Isomers and Anisotropic Pressures, LBL-12108, January 1981, Reported at the International Workshop IX on Gross Properties of Nuclei and Nuclear Excitations, Hirschegg, Austria, January 1981.

GLENDENNING, N.K. (See BANERJEE, B., LBL-10979)

GOLDBERG, D.A. (See ZISMAN, M.S., LBL-10204)

GOODMAN, A.L.
Finite-Temperature HFB Theory, LBL-11151, July 1980, submitted to Phys. Rev. C.

GOODMAN, A.L.
The Two-Level Model at Finite-Temperature, LBL-11171, July 1980, submitted to Nucl. Phys. A.

GRAEBNER, G. (See STÖCKER, H., LBL-11774)

GREINER, W. (See STÖCKER, H., LBL-11774)

GREINER, D.
The HISS Spectrometer at LBL, LBL-11818, November 1980, Invited speaker at the Workshop on "Future Relativistic Heavy Ion Experiments," GSI Darmstadt, West Germany, October 7-10, 1980.

GREINER, D.E. (See OLSON, D.L., LBL-12292)

GROSSIORD, J.Y. (See GEAGA, J.V., LBL-10265)

GRUHN, C.R.
Bragg Curve Spectroscopy, LBL-12678, May 1981, Invited talk presented at the INS International Conference on Radiation Detectors, Tokyo, Japan, March 23-28, 1981.

GUTBROD, H.H., M.R. Maier, H.G. Ritter, A.I. Warwick, F. Weik, H. Wieman, and K.L. Wolf
Charged Particle Identification with Modules of the Plastic Ball, presented at the IEEE Nuclear Science Symposium, Orlando, Florida, November 5-7, 1980, LBL-11797, October 1980, IEEE Transactions on Nucl. Science **NS-28**, 451 (1981).

GYULASSY, M.
Relativistic Nuclear Collisions: Theory, LBL-11040, July 1980, Invited lecture presented at the INS Kikuchi Summer School on Nuclear Physics at High Energies, Fiji-Yoshida, Japan, July 1-4, 1980.

GYULASSY, M.
Current Topics in Relativistic Nuclear Collisions, LBL-11556, August 1980, presented at the International Conference on Nuclear Physics, Lawrence Berkeley Laboratory, Berkeley, CA, August 24-30, 1980; and published in the Proceedings.

GYULASSY, M.
Relativistic Nuclear Collisions in Perspective, LBL-11790, November 1980, submitted to Comments on Particle & Nuclear Physics.

GYULASSY, M. and S.K. Kauffmann
Coulomb Effects in Relativistic Nuclear Collisions, LBL-10279, March 1980, Nucl. Phys. A **362**, 503 (1981).

GYULASSY, M. (See BANERJEE, B., LBL-10979.

GYULASSY, M. (See NOACK, C.C., LBL-11053)

GYULASSY, M. (See STÖCKER, H., LBL-12095)

HARRIS, J.W., A. Sandoval, R. Stock, H. Stroebele, R.E. Renfordt, J.V. Geaga, H.G. Pugh, L.S. Schroeder, K.L. Wolf, and A. Dacal
Production Near Threshold in Central Nucleus-Nucleus Collisions, LBL-12334, April 1981, submitted to Phys. Rev. Letts.

HARRIS, J.W. (See GEAGA, J.V., LBL-10265)

HARVEY B.G.
Small Momentum Widths in Heavy-Ion Fragmentation at 20 MeV/amu and Below, LBL-12787, May 1981, submitted for publication in Phys. Rev. Letts.: Comments.

HARVEY, B.G. (See RAE, W.D., LBL-11135)

HARVEY, B.G. (See RAE, W.D., LBL-12568)

HASSE, R.W. (See DIEBEL, M., LBL-11522)

HAUSTEIN, P.E. (See CERNY, J., LBL-12853)

HAUSTEIN, P.E. (See LOVELAND, W., LBL-10010)

HAUSTEIN, P.E. (See MOLTZ, D.M., LBL-11427)

HECKING, P.
Pion Condensation Threshold in Nuclear Matter and Thermal Δ-Isobars, LBL-12254, February 1981, submitted to Physical Review C.

HECKMAN, H.H.
Evidence for Anomalous Nuclei Among Relativistic Projectile Fragments at Bevalac Energies, LBL-12120, January 1981, presented at the Workshop on Future Relativistic Heavy Ion Experiments Gesellschaft für Schwerionenforschung, Darmstadt, W. Germany, October 7-10, 1980.

HECKMAN, H.H.
Experiments with Relativistic Heavy Ions: A Potpourri of Chemistry, Canis Majoris and Grains of Silver, LBL-21656, May 1981, presented at the Third Adriatic Europhysics Study Conference on the Dynamics of Heavy-ion Collisions, Hvar, Croatia, Yugoslavia, May 25-30, 1981.

HECKMAN, H.H. (See FRIEDLANDER, E.M., LBL-11136)

HECKMAN, H.H. (See OLSON, D.L., LBL-12292)

HENDRIE, D.L. (See GEAGA, J.V., LBL-10265)

HERNANDEZ, E.S., G. Mantzouranis
Markovian and Non-Markovian Effects in Heavy-Ion Reactions at 10-200 MeV per Nucleon, LBL-9568, August 1979, Phys. Rev. C **22**, 575 (1980).

HERNANDEZ, E.S., W.D. Myers, J. Randrup, and B. Remaud
Quantal Dynamics of Charge Equilibration in Damped Nuclear Collisions, LBL-9761, October 1979, Nucl. Phys. A **361**, 483 (1981).

HERSKIND, B. (See NEWTON, J.O, LBL-12261)

HINTERBERGER, F. (See CONZETT, H.E., LBL-11576)

HINTERBERGER, F. (See SLOBODRIAN, R.J., LBL-11372)

HSEUH, H.C. (See LOVELAND, W., LBL-10010)

HSU, C.C. (See MORRISSEY, D.J., LBL-12181)

HSU, C.C. (See SOBOTKA, L.G., LBL-11148)

HSU, C.C. (See SOBOTKA, L.G., LBL-11840)

HSU, C.C. (See WOZNIAK, G.J., LBL-11196)

HULET, E.K. (See NITSCHKE, J.M., LBL-10173)

JING-SHANG, Zhang, (See ZHONG-YU, MA, LBL-11893)

JUDEK, B. (See FRIEDLANDER, E.M., LBL-11136)

KARANT, Y.J. (See FRIEDLANDER, E.M., LBL-11136)

KASAGI, J. (See MATSUSHITA, N.)

KAUFFMANN, S.K. (See GYULASSY, M., LBL-10279)

KAUFFMANN, S.K. (See NOACK, C.C., LBL-11053)

KAUFMAN, S.B. (See LOVELAND, W., LBL-10010)

KELLY, W.H. (See FIRESTONE, R.B., LBL-12424)

KELLY, W.H. (See MATSUSHITA, N.)

KLUGE, H. (See WOZNIAK, G.J., LBL-11196)

KNOLL, J., J. Randrup
Proton-Proton Correlations in High-Energy Nuclear Collisions, LBL-11418, August 1980, submitted to Phys. Letts.

KNOLL, J. (See BOHRMAN, S., LBL-10970)

KNOLL, J. (See CUGNON, J., LBL-11301)

KO, Che Ming, and S. Bohrmann
A Model for Pion Absorption in Nuclei, LBL-11041, June 1980, Phys. Letts. B **97**, 188 (1980).

KOIKE, M. (See MARTOFF, C.J., LBL-11914)

KOKER, G.T. (See SCHUBERT, K.R.)

KOONIN, S.E. (See RANDRUP, J., LBL-10959)

KRUSE, H. (See STÖCKER, H., LBL-11774)

LANDRUM, J.H. (See NITSCHKE, J.M., LBL-10173)

LARIMER, R.M. (See BIRCHALL, J., LBL-11121)

LEBER, R.E. (See NITSCHKE, J.M., LBL-10173)

LEDERER, C. M.
Isotopes, LBL-10124, October 1980, an abridged version of this report will be published in the Encyclopedia of Chemical Technology, eds. M. Grayson and D. Eckroth, John Wiley and Sons, Inc., New York (to be published in 1981).

LEDERER, C. M.
El Transition Probabilities from $K^{\pi} = 0^{-}$ and $K^{\pi} = 1^{-}$ States of ^{238}Pu, LBL-12075, January 1981, submitted to Phys. Rev. C.

LEGRAIN, R. (See RAE, W.D., LBL-11135)

LEGRAIN, R. (See RAE, W.D., LBL-12568)

LEIGH, J.R. (See SIE, S.H., LBL-11352)

LEINO, M.E., S. Yashita, and A. Ghiorso
Alpha Decay of Neutron Deficient Polonium and Bismuth Isotopes, LBL-12816, May 1981, submitted to Phys. Rev. C.

LEMAIRE, M.-C. (See NAGAMIYA, S., LBL-12123)

LINDENBERGER, K.H. (See NEWTON, J.O., LBL-12261)

LINDSTROM, P.J. (See OLSON, D.L., LBL-12292)

LIU, Yuan-fang, Cheng Luo, Hans R. von Guten, and Glenn T. Seaborg
A Procedure for a Fast Separation of Berkelium and Cerium, LBL-12909, April 1981, to be published in Inorganic and Nucl. Chem. Letts.

LOUGHEED, R.W. (See NITSCHKE, J.M., LBL-10173).

LOVELAND, W., Cheng Luo, P.L. McGaughey, D.J. Morrissey and G.T. Seaborg
Target Fragment Energies and Momenta in the Reaction of 4.8 GeV ^{12}C and 5.0 GeV ^{20}Ne with ^{238}U, LBL-11658, October 1980, submitted to Phys. Rev. C.

LOVELAND, W., D.J. Morrissey, K. Aleklett, G.T. Seaborg, S.B. Kaufman, E.P. Steinberg, B.D. Wilkins, J.B. Cumming, P.E. Haustein, and H.C. Hseuh
Target Residue Recoil Properties in the Interaction of 8.0 GeV ^{20}Ne with ^{181}Ta, LBL-10010, May 1980, Phys. Rev. C. **23**, 253 (1981).

LOVELAND, W. (See ALEKLETT, K., LBL-11273)

LUMBROSO, A. (See GLENDENNING, N.K., LBL-12108)

LUO, C. (See LIU, YUAN-FANG, LBL-12909)

LUO, C. (See LOVELAND, W., LBL-11658

MA, A.Y., X.Z. Wu, G.S. Zhang, Y.C. Cho, Y.S. Wang, J.H. Chiou, S.T. Sen, F.C. Yang, and J.O. Rasmussen

Calculation of Muon Final State Probabilities After Muon-Induced Fission, LBL-9689, August 1979, Nucl. Phys. A **348**, 446 (1980).

MAHONEY, J. (See RAE, W.D., LBL-11135)

MAHONEY, J. (See RAE, W.D., LBL-12568)

MAIER, M.R. (See GUTBROD, H.H., LBL-11797)

MAIER, M.R. (See RICHARDSON, L.W., LBL-10146)

MAIER, M.R. (See WOZNIAK, G.J., LBL-11493)

MANTZOURANIS, G. (See HERNANDEZ, E.S., LBL-9568)

MANTZOURANIS, G. (See MYERS, W.D., LBL-11542)

MARTINIS, J. (See STEVENSON, J., LBL-12264)

MARTOFF, C.J., J.A. Bistirlich, K.M. Crowe, M. Koike, J.P. Miller, S.S. Rosenblum, W.A. Zajc, H.W. Baer, A.H. Wapstra, G. Strassner, and P. Truol
Orbital Recoupling Dominance in the A = 20 Isovector Giant M1 Transition, LBL-11914, December 1980, submitted for publication.

MARUHN, J.A. (See STÖCKER, H., LBL-11774)

MAST, T.S. (See MULLER, R.M., LBL-12797)

MATHEWS, G.J. (See SCHMITT, R.P., LBL-9512)

McHARRIS, W.C. (See ARYAEINEJAD, R.)

McHARRIS, W.C. (See MATSUSHITA, N.)

MATSUSHITA, N., W.C. McHarris, R.B. Firestone, J. Kasagi, and W.H. Kelly
On Improving Ge Detector Energy Resolution and Peak-to-Compton Ratios by Pulse-Shape Discrimination, Nucl. Instr. Meth. **179**, 119 (1980).

McDONALD, R.J., A.J. Pacheco, G.J. Wozniak, H.H. Bolotin, L.G. Moretto, C. Schück, S. Shih, R.M. Diamond, and F.S. Stephens
Evidence for Spin Fluctuations in the Deep Inelastic Reaction ^{165}Ho + ^{165}Ho at 8.5 MeV/amu, LBL-11608, May 1981, submitted to Nuclear Physics.

McDONALD, R.J. (See MORRISSEY, D.J., LBL-12181).

McDONALD, R.J. (See SOBOTKA, L.G., LBL-11148).

McDONALD, R.J. (See WOZNIAK, G.J., LBL-11196).

McGAUGHEY, P.L. (See ALEKLETT, K., LBL-11273).

McGAUGHEY, P.L. (See LOVELAND, W., LBL-11658).

McHARRIS, Wm. C. (See FIRESTONE, R.B., LBL-12424)

MILLER, J.P. (See MARTOFF, C.J., LBL-11914)

MOELLER, E. (See NAGAMIYA, S., LBL-12123)

MOLITORIS, J.D., J.M. Nitschke
Evaluation of Thin Metal Foils as Targets and Windows for Heavy-Ion Experiments, LBL-9725, January 1981, submitted to Nuclear Instruments and Methods.

MOLTZ, D.M., J. Äystö, M.D. Cable, R.F. Parry, P.E. Haustein, J.M. Wouters, and J. Cerny
Advances in the Helium-Jet Coupled On-Line Mass Separator RAMA, LBL-11427, September 1980, presented at the Electromagnetic Isotope Separator-10 Conference, Zinal, Switzerland, September 1-6, 1980, Nuclear Instruments and Methods **186**, 141 (1981).

MOLTZ, D.M. (See ÄYSTÖ, J., LBL-11193)

MORETTO, L.G.
Spin and Isospin Fluctuations in Heavy Ion Collisions and Their Dependence Upon the Shape of the Dinuclear Complex, LBL-11428, August 1980, Lectures given at the XIII Masurian School of Nuclear Physics, "Nuclear Structure Study by Means of Nuclear Reactions," Mikolajki, Poland, September 1-13, 1980.

MORETTO, L.G.
Angular Distributions of Sequentially Emitted Particles and Gamma Rays in Deep Inelastic Processes, LBL-11975, January 1981, presented at the Fourth Oaxtepec Symposium in Nuclear Physics, Oaxtepec, Mexico, January 1981.

MORETTO, L.G., S. Blau, and A. Pacheco
Angular Momentum Misalignment in Deep Inelastic Processes and Angular Distribution of Sequentially Emitted Particles and Gamma Rays, LBL-10805, December 1980, Nucl. Phys. A **364**, 125 (1981).

MORETTO, L.G.
Experimental Evidence and Theoretical Implications of Fluctuations in Deep Inelastic Heavy Ion Collisions, LBL-12596, April 1981, presented at the Europhysics Conf. on Nucl. Physics, Hvar, Croatia, Yugoslavia, June 29-July 3 1981.

MORETTO, L.G. (See BLAU, S.K., LBL-10926)

MORETTO, L.G. (See McDONALD, R.J., LBL-11608)

MORETTO, L.G. (See MORRISSEY, D.J., LBL-11491)

MORETTO, L.G. (See MORRISSEY, D.J., LBL-12181)

MORETTO, L.G. (See RICHARDSON, L.W., LBL-10146)

MORETTO, L.G. (See SCHMITT, R.P., LBL-9512)

MORETTO, L.G. (See SOBOTKA, L.G., LBL-11148)

MORETTO, L.G. (See SOBOTKA, L.G., LBL-11840)

MORETTO, L.G. (See WOZNIAK, G.J., LBL-11196)

MORRISSEY, D.J., L.G. Moretto
Manifestations of Excitation Energy Equilibrium in Deep-Inelastic Collisions, LBL-11491, September 1980, Phys. Rev. C **23**, 1835 (1981).

MORRISSEY, D.J., G.J. Wozniak, L.G. Sobotka, A.J. Pacheco, C.C. Hsu, R.J. McDonald, and L.G. Moretto
Angular Momentum, Statistical Equilibrium and Sequential Fission in Very Asymmetric Systems, LBL-12181, March 1981, submitted to Phys. Rev. Letts.

MORRISSEY, D.J. (See ALEKLETT, K., LBL-11273)

MORRISSEY, D.J. (See LOVELAND, W., LBL-10010)

MORRISSEY, D.J. (See LOVELAND, W., LBL-11658)

MORRISSEY, D.J. (See SOBOTKA, L.G., LBL-11840)

MORRISSEY, D.J. (See WOZNIAK, G.J., LBL-11196)

MULLER, B. (See STÖCKER, H., LBL-12471)

MULLER, R.M., P.P. Tans, T.S. Mast, and J.J. Welch
Mass Spectrometry with a Very Small Cyclotron, LBL-12797, May 1981, presented at the Argonne Symposium on High Energy Spectrometry, Argonne National Lab., Argonne, IL, May 11-13, 1981.

MURPHY, M.J. (See RAE, W.D., LBL-11135)

MURPHY, M.J. (See RAE, W.D., LBL-12568)

MYERS, W.D.
The Width of the Charge Distribution in Fission, LBL-12072, January 1981, to be presented at the Conference on Gross Properties of Nuclei and Nuclear Matter, Hirschegg, Austria, January 19-23, 1981.

MYERS, W.D.
The Dependence of RMS Charge Radii on the Neutron Skin and on Deformation, LBL-12073, January 1981, presented at the Bormio Winter Meeting, Bormio, Italy, January 26-30, 1981.

MYERS, W.D., G. Mantzouranis, J. Randrup
Adiabaticity Criterion for Charge Equilibration with Application to Fission, LBL-11542, September 1980, Phys. Letts. B **98**, 1 (1981).

MYERS, W.D., K.-H. Schmidt
The Effect of Deformation and the Neutron Skin on RMS Charge Radii, LBL-12790, May 1981, presented at the Fourth International Conference on Nuclei Far From Stability, Helsingør, Denmark.

MYERS, W.D. (See HERNANDEZ, E.S., LBL-9761)

NAGAMIYA, S., M.-C. Lemaire, E. Moeller, S. Schnetzer, G. Shapiro, H. Steiner, and I. Tanihata
Production of Pions and Light Fragments at Large Angles in High-Energy Nuclear Collisions, LBL-12123, March 1981, submitted to Phys. Rev. C.

NAGAMIYA, S. (See TANIHATA, I., LBL-11488)

NEIMAN, M.
SUSIE: A Program For Analysis of 1 Dimensional Spectra; Version: 20 February 1981, PUB 3014, February 1981.

NEWTON, J.O., B. Herskind, R.M. Diamond, E.L. Dines, J.E. Draper, K.H. Lindenberger, S. Shih, C. Schück, F.S. Stephens.
Observation of Giant Dipole Resonances Built on States of High Energy and Spin, LBL-12261, February 1981, Phys. Rev. Letts. **46**, 1383 (1981).

NEWTON, J.O. (See SIE, S.H., LBL-11352)

NITSCHKE, J.M.
Synthesis and Investigation of Neutron-Rich Transuranium Isotopes, LBL-11712, September 1980, Presented at the International Symposium on the Synthesis and Properties of New Elements, Dubna, U.S.S.R.

NITSCHKE, J.M., M. Fowler, A. Ghiorso, R.E. Leber, M.J. Nurmia, L.P. Somerville, K.E. Williams, E.K. Hulet, J.H. Landrum, R.W. Lougheed, J.F. Wild, C.E. Bemis, Jr., R.J. Silva, and P. Eskola
Search for an 80-ms Spontaneous Fission Activity in Bombardments of ^{249}Bk with ^{15}N, LBL-10173, January 1980, Nucl. Phys. A **352**, 138-146 (1981).

NITSCHKE, J.M. (See MOLITORIS, J.D., LBL-9725)

NOACK, C.C., M. Gyulassy, and S.K. Kauffmann
Test of Square Law for Deuteron Formation in Relativistic Nuclear Collisions, LBL-11053, August 1980, submitted to Phys. Rev. C.

NUCLEAR SCIENCE DIVISION
Nuclear Science Division Annual Report 1979-1980, LBL-11588, UC-34, March 1981.

NURMIA, M.J. (See NITSCHKE, J.M., LBL-10173)

OLSON, D.L., B.L. Berman, D.E. Greiner, H.H. Heckman, P.J. Lindstrom, G.D. Westfall, and H.J. Crawford
Electromagnetic Dissociation of Relativistic ^{18}0 Nuclei, LBL-12292, February 1981, submitted to Phys. Rev. C.

PACHECO, A.J. (See McDONALD, R.J., LBL-11608)

PACHECO, A.J. (See MORETTO, L.G., LBL-10805)

PACHECO, A.J. (See MORRISSEY, D.J., LBL-12181)

PACHECO, A.J. (See SOBOTKA, L.G., LBL-11148)

PACHECO, A.J. (See WOZNIAK, G.J., LBL-11196)

PARDO, R.C. (See FIRESTONE, R.B., LBL-12424)

PARRY, R.F. (See ÄYSTÖ, J., LBL-11193)

PARRY, R.F. (See CERNY, J., LBL-12853)

PARRY, R.F. (See MOLTZ, D.M., LBL-11427)

PRICE, P.B. (See STEVENSON, J.D., LBL-11737)

PRICE, P.B. (See STEVENSON, J., LBL-12264)

PUGH, H.G.
Future Relativistic Heavy Ion Experiments, LBL-11974, December 1980, Introductory Remarks presented at the Workshop held at Gesellschaft für Schwerionenforschung, Darmstadt, West Germany, October 7-10, 1980.

PUGH, H.G.
Ultrarelativistic Heavy Ions, LBL-12053, December 1980, Presented at the Fourteenth Los Alamos Meson Physics Facility Users Group Meeting, Los Alamos, NM, October 27-28, 1980.

PUGH, H.G. (See HARRIS, J.W., LBL-12334)

RAE, W.D., A.J. Cole, A. Dacal, R. Legrain, B.G. Harvey, J. Mahoney, M.J. Murphy, R.G. Stokstad, and I. Tserruya,
Coherent and Incoherent Processes in Projectile Fragmentation, LBL-12568, April 1981, submitted to Phys. Rev. Letts.

RAE, W.D., R.G. Stokstad, B.G. Harvey, A. Dacal, R. LeGrain, J. Mahoney, M.J. Murphy, and T.J.M. Symons
Molecular Resonances and the Production of Fast α-Particles in the Reaction of ^{16}O with $^{12,13}C$ Nuclei, LBL-11135, June 1980, Phys. Rev. Letts. **45**, 884 (1981).

RAE, W.D. (See SHOTTER, A.C., LBL-11458)

RANDRUP, J.
Kaon Rescattering in Relativistic Nuclear Collisions, LBL-11508, September 1980, Phys. Letts. B **99**, 9 (1981).

RANDRUP, J., and S.E. Koonin
The Disassembly of Nuclear Matter, LBL-10959, August 1980, Nuclear Physics A **356**, 223 (1981).

RANDRUP, J. (See HERMANDEZ, E.S., LBL-9761)

RANDRUP, J. (See KNOLL, J. LBL-11418)

RANDRUP, J. (See MYERS, W.D., LBL-11542)

RANDRUP, J. (See CUGNON, J., LBL-11301)

RANDRUP, J. (See SCHURMANN, B., LBL-11964)

RASMUSSEN, J.O. (See MA, A.Y., LBL-9689)

RASMUSSEN, J.O. (See ZHONG-YU, MA, LBL-11893)

RATTAZZI, G.U. (See SOBOTKA, L.G., LBL-11148)

RATTAZZI, G.U. (See SCHMITT, R.P., LBL-9512)

REGIMBART, R. (See SCHMITT, R.P., LBL-9512)

REMAUD, B. (See HERNANDEZ, E.S., LBL-9761)

RENFORDT, R.E. (See HARRIS, J.W., LBL-12334)

RICHARDSON, L.W., G.J. Wozniak, M.R. Maier and L.G. Moretto
Neutron-Gamma Discrimination Using NaI(Tl) Scintillators with Application for Measurement of the Gamma-Ray Multiplicity Distribution in Heavy-Ion Reactions, LBL-10146, November 1979, Nucl. Inst. and Meth. **173** (1980).

RICHARDSON, L.W. (See WOZNIAK, G.J., LBL-11493)

RIOUX, C. (See CONZETT, H.E., LBL-11576)

RIOUX, C. (See SLOBODRIAN, R.J., LBL-11372)

RITTER, H.G. (See GUTBROD, H.H., LBL-11797)

RONNINGEN, R.M. (See WALKER, P.M.)

ROSENBLUM, S.S. (See MARTOFF, C.J., LBL-11914)

ROY, R. (See CONZETT, H.E., LBL-11576)

ROY, R. (See SLOBODRIAN, R.J., LBL-11372)

RUCK, H.M.
Polynomial Chromodynamics in 1 + 1 Dimension I. Confinement of Quarks and the Structure of Composite Particles, LBL-12316, February 1981, submitted to Nucl. Phys.

RUCK, H.M.
Polynomial Chromodynamics in 1 + 1 Dimensions, LBL-12479, January 1981, submitted for publication.

SANDOVAL, A. (See HARRIS, J.W., LBL-12334)

SCHMIDT, K.-H. (See MYERS, W.D., LBL-12790)

SCHMITT, R.P., G.J. Wozniak, G.U. Rattazzi, G.J. Mathews, R. Regimbart and L.G. Moretto
Fast Particle Emission in the Deep Inelastic Reaction $^{nat}Cu + ^{20}Ne$ at 12.6 MeV/Nucleon, LBL-9512, January 1980, Phys. Rev. Letts. **46**, 522 (1981).

SCHNETZER, S. (See NAGAMIYA, S., LBL-12123)

SCHNETZER, S. (See TANIHATA, I., LBL-11488)

SCHROEDER, L.S.
Pion Production in Nucleus-Nucleus Collisions Below A Few GeV/Nucleon – Past, Present and Future, LBL-10899, July 1980, Presented at the Seminar on High Energy Nuclear Interactions and Properties of Very Dense Matter, Hakone, Japan, July 7-11, 1980.

SCHROEDER, L.S.
High Energy Nuclear Collisions in the Few GeV/Nucleon Region – Projectile and Target Fragmentation
LBL-11102, June 1980, invited talk presented at the 1980 Institute for Nuclear Studies, Kikuchi Summer School on Nuclear Physics at High Energies, Fuji-Yoshida, Japan, July 1-4, 1980.

SCHROEDER, L.S. (See GEAGA, J.V., LBL-10265)

SCHROEDER, L.S. (See HARRIS, J.W., LBL-12334)

SCHUBERT, K.R., G.T. Koker and R.B. Firestone
Alnus Glutinosa and *Glycine Max*: Short-term Studies Using [^{13}N] Ammonium, Plant Physiology **67**, 662 (1981).

SCHÜCK, C. (See McDONALD, R.J., LBL-11608)

SCHÜCK, C. (See NEWTON, J.O., LBL-12261)

SCHÜCK, C. (See WOZNIAK, G.J., LBL-11196)

SCHURMANN, B., J. Randrup
The Quasi-Elastic Component in High-Energy Nuclear Collisions, December 1980, LBL-11964, submitted to Phys. Rev. C.

SCOTT, D.K. (See BACK, B.B., LBL-11852)

SEABORG, G.T. (Scientific Editor)
Proceedings of the Symposium Commemorating the 25th Anniversary of the Discovery of Mendelevium, LBL-11599, March 28, 1980.

SEABORG, G.T.
Charting the New Elements, LBL-11610 (1980), SCI-QUEST, 1980, **53**, 7(1980).

SEABORG, G.T. (See ALEKLETT, K., LBL-11273)

SEABORG, G.T. (See LIU, Yuan-Fang, LBL-12909)

SEABORG, G.T. (See LOVELAND W., LBL-10010)

SEABORG, G.T. (See LOVELAND W., LBL-11658)

SEN, S.T. (See MA, A.Y., LBL-9689)

SHIPIRO, G. (See NAGAMIYA, S., LBL-12123)

SHIH, S. (See McDONALD, R.J., LBL-11608)

SHIH, S. (See NEWTON, J.O., LBL-12261)

SHIH, S. (See WOZNIAK, G.J., LBL-11196)

SHOTTER, A.C., A.N. Bice and J. Cerny
An Analytical Expression for the Effective Solid Angle of a Rectangular Collimator for the Passage of Fragments from Breakup Projectiles, LBL-11375, August 1980, Nucl. Inst. and Methods. **180**, 201-203 (1981).

SHOTTER, A.C., A.N. Bice, D.P. Stahel, and J. Cerny
The Quasielastic Breakup of 187 MeV ^{12}C Ions on ^{208}Pb, LBL-11376, July 1980, submitted to Phys. Letts.

SHOTTER, A.C., A.N. Bice, J.M. Wouters, W.D. Rae, and J. Cerny
Observation of the Direct and Sequential Breakup of ^{7}Li from ^{12}C and ^{208}Pb Targets at 70 MeV, LBL-11458, September 1980, Phys. Rev. Letts. **46**, 12 (1981).

SHOTTER, A.C. (See BACK, B.B., LBL-11852)

SHOTTER, A.C. (See BICE, A.N., LBL-11194)

SIE, S.H., J.O. Newton, J.R. Leigh, and R.M. Diamond
Multiplicity of the Statistical γ-Rays Following (HI,xn) Reactions, LBL-11352, August 1980, Phys. Rev. Letts. **46**, 405 (1981).

SILVA, R.J. (See NITSCHKE, J.M., LBL-10173)

SLOBODRIAN, R.J., C. Rioux, R. Roy, H.E. Conzett, P. von Rossen, and F. Hinterberger
Breakdown of Time Reversal Invariance in the Interaction of Nuclear Particles, LBL-11372, August 1980, submitted to Phys. Rev. Letts.

SLOBODRIAN, R.J. (See CONZETT, H.E., LBL-11576)

SOBOTKA, L.G., C.C. Hsu, G.J. Wozniak, D.J. Morrissey and L.G. Moretto
Angular Momentum Transfer and Partition in the Deep-Inelastic Reaction: 664 MeV ^{84}Kr + ^{Nat}Ag, LBL-11840, April 1981, submitted to Nucl. Phys.

SOBOTKA, L.G., C.C. Hsu, G.J. Wozniak, G.U. Rattazzi, R.J. McDonald, A.J. Pacheco and L.G. Moretto
Evidence for Rigid Rotation and Large Deformations in the Deep Inelastic Reaction: 664 MeV ^{84}Kr + ^{nat}Ag, LBL-11148, August 1980, Phys. Rev. Letts. **46**, 887 (1981).

SOBOTKA, L.G. (See MORRISSEY, D.J., LBL-12181).

SOBOTKA, L.G. (See WOZNIAK, G.J., LBL-11196).

SOMERVILLE, L.P. (See EGGERS, R.C., LBL-12060)

SOMERVILLE, L.P. (See NITSCHKE, J.M., LBL-10173)

STAHEL, D.P. (See BICE, A.N., LBL-11194)

STAHEL, D.P. (See SHOTTER, A.C., LBL-11376)

STEINBERG, E.P. (See LOVELAND, W., LBL-10010)

STEINER, H. (See NAGAMIYA, S., LBL-12123)

STEINER, H. (See TANIHATA, I., LBL-11488)

STELZER, H.
Some Recent Developments in Nuclear Charged Particle Detectors, LBL-11366, August 1980, presented at the International Conference on Nuclear Physics Lawrence Berkeley Laboratory, Berkeley CA, August 24-30, 1980.

STEPHENS, F.S.
Phenomena at Very High Spins, LBL-10645, March 1980, presented at the Conference on Band Structure and Nuclear Dynamics, New Orleans, LA, February 27 - March 1, 1980, Nucl. Phys. A **347** (1980) 275-286.

STEPHENS, F.S.
Properties of Nuclei at Very High Spin, presented at the International Conference on Nuclear Physics, Lawrence Berkeley Laboratory, Berkeley, CA, August 24-30, 1980. LBL-11620, September 1980.

STEPHENS, F.S. (See DIAMOND, R.M., LBL-10325)

STEPHENS, F.S. (See McDONALD, R.J., LBL-11608)

STEPHENS, F.S. (See NEWTON, J.O., LBL-12261)

STEPHENS, F.S. (See WOZNIAK, G.J., LBL-11196)

STEVENSON, J.D.
Neutron Emission in Relativistic Nuclear Collisions, LBL-11736, December 1980, submitted to Phys. Rev. Lett.

STEVENSON, J., J. Martinis, and P.B. Price
A Calorimeter for High-Energy Heavy Ions, LBL-12264, January 1981, submitted to Nucl. Instr. & Meth.

STEVENSON, J.D., P.B. Price
Production of the Neutron-Rich Nuclides ^{20}C and ^{27}F by Fragmentation of 213 MeV/Nucleon ^{48}Ca, LBL-11737, December 1980, submitted to Phys. Rev. lett.

STOCK, R. (See HARRIS, J.W., LBL-12334)

STÖCKER, H.
Pion, Light Fragment and Entropy Production in Nuclear Collisions, LBL-12302, April 1981, submitted to Phys. Rev. Letts.

STÖCKER, H., L.P. Csernai, G. Graebner, G. Buchwald, H. Kruse, R.Y. Cusson, J.A. Maruhn, and W. Greiner
Jets of Nuclear Matter from High Energy Heavy Ion Collisions, LBL-11774, November 1980, (LBL-11774 revised February 1981), submitted to Phys. Rev. Letts.

STÖCKER, H., M. Gyulassy, and J. Boguta
Probing Dense Nuclear Matter Via Nuclear Collisions, LBL-12095, January 1981, submitted to Phys. Letts.

STÖCKER, H., and B. Müller
The Bounce off Effect as a Barometer for Hot, Dense Matter in Fast Nuclear Collisions, LBL-12471, March 1981, submitted to Phys. Letts.

STOKSTAD, R.G.
Nuclear Structure and Heavy-Ion Fusion, LBL-11664, October 1980, presented at the XIII International Summer School in Nuclear Physics, Mikolajki, Poland, September 1-13, 1980; and to be published in Nukleonika.

STOKSTAD, R.G. (See RAE, W.D., LBL-11135)

STOKSTAD, R.G. (See RAE, W.D., LBL-12568)

STRASSNER, G. (See MARTOFF, C.J., LBL-11914)

STROEBELE, H. (See HARRIS, J.W., LBL-12334)

SWIATECKI, W.J.
The Dynamics of the Fusion of Two Nuclei, LBL-12642, April 1981, submitted to Nucl. Phys. A.

SWIATECKI, W.J.
Fusion Cross-Sections and the New Dynamics, LBL-12708, May 1981, presented at the 4th International Conference on Nuclei Far from Stability, Helsingør, Denmark, June 7-13, 1981.

SWIATECKI, W.J. (See BLOCKI, J., LBL-9574)

SYMONS, T.J.M. (See BACK, B.B., LBL-11852)

SYMONS, T.J.M. (See RAE, W.D., LBL-11135)

TANIHATA, I.
Two-Particle Correlations in Nuclear Collisions, LBL-11320, July 1980, presented at the INS Kukuchi Summer School on Nuclear Physics at High Energies, Fuji-Yoshida, Japan, July 1-4, and the Hakone Seminar on High Energy Nuclear Interactions and Properties of Dense Nuclear Matter, Hakone, Japan, July 7-11, 1980.

TANIHATA, I., S. Nagamiya, S. Schnetzer, and H. Steiner
One- and Two-Proton Inclusive Spectra in 800 MeV Proton-Nucleus Collisions and the Mean Free Path of Protons in Nuclei, LBL-11488, October 1980, submitted to Phys. Letts. B.

TANIHATA, I. (See NAGAMIYA, LBL-12123)

TANS, P.P. (See MULLER, R.M., LBL-12797)

THIERENS, H.M. (See CERNY, J., LBL-12853)

TREUHAFT, R.N. (See GEAGA, J.V., LBL-10265)

TRUOL, P. (See MARTOFF, C.J., LBL-11914)

TSERRUYA, I. (See RAE, W.D., LBL-12568)

VAN BIBBER, K. (See GEAGA, J.V., LBL-10265)

VAN OERS, W.T.H. (See J. BIRCHALL, LBL-11121)

VON ROSSEN, P. (See J. BIRCHALL, LBL-11121)

VON GUNTEN, H.R. (See LIU, YUAN-FAN, LBL-12909)

VON ROSSEN, P. (See CONZETT, H.E., LBL-11576)

VON ROSSEN, P. (See SLOBODRIAN, R.J., LBL-11372)

WALKER, P.M., S.R. Faber, W.H. Bentley, R.M. Ronningen, and R.B. Firestone
A Study of ^{172}Yb Following the ^{170}Er (α,2n) Reaction, Nucl. Phys. A **343**, 45 (1980).

WANG, Y.S. (See MA, A.Y., LBL-9689)

WAPSTRA, A.H. (See MARTOFF, C.J., LBL-11914)

WARNER, R.A. (See FIRESTONE, R.B., LBL-12424)

WARWICK, A.I. (See GUTBROD, H.H., LBL-11797)

WATSON, J. (See BIRCHALL, J., LBL-11121)

WATSON, J.W. (See ZISMAN, M.S., LBL-10204)

WEIK, F. (See GUTBROD, H.H., LBL-11797)

WELCH, J.J. (See MULLER, R.M., LBL-12797)

WESTFALL, G.D. (See OLSON, B.L., LBL-12292)

WEIMAN, H. (See GUTBROD, H.H., LBL-11797)

WILD, J.F. (See NITSCHKE, J.M., LBL-10173)

WILKINS, B.D. (See LOVELAND, W., LBL-10010)

WILLIAMS, K.E. (See NITSCHKE, J.M., LBL-10173)

WOLF, K.K. (See GUTBROD, H.H., LBL-11797)

WOLF, K.L. (See HARRIS, J.W., LBL-12334)

WOUTERS, J.M. (See ÄYSTÖ, J., LBL-11193)

WOUTERS, J.M. (See CERNY, J., LBL-12853)

WOUTERS, J.M. (See MOLTZ, D.M., LBL-11427)

WOUTERS, J.M. (See SHOTTER, A.C., LBL-11458)

WOZNIAK, G.J., R.J. McDonald, A.J. Pacheco, C.C. Hsu, D.J. Morrissey, L.G. Sobotka, L.G. Moretto, S. Shih, C. Schuck, R.M. Diamond, H. Kluge, and F.S. Stephens
The Rise and Fall of the Spin Alignment in Deep-Inelastic Reactions, LBL-11196, July 1980, Phys. Rev. Letts. **45**, 1081 (1980).

WOZNIAK, G.J., L.W. Richardson and M.R. Maier
Time-Walk Characteristics of an Improved Constant Fraction Discriminator
LBL-11493, September 1980, Nucl. Instr. and Meth. **180**, 509 (1981).

WOZNIAK, G.J. (See McDONALD, R.J., LBL-11608)

WOZNIAK, G.J. (See MORRISSEY, D.J., LBL-12181)

WOZNIAK, G.J. (See RICHARDSON, L.W., LBL-10146)

WOZNIAK, G.J. (See SCHMITT, R.P., LBL-9512)

WOZNIAK, G.J. (See SOBOTKA, L.G., LBL-11148)

WOZNIAK, G.J. (See SOBOTKA, L.G., LBL-11840)

WU, X.Z. (See MA, A.Y., LBL-9689)

XI-ZHEN, Wu (See ZHONG-YU, MA, LBL-11893)

YANG, F.C. (See MA, A.Y., LBL-9689)

YASHITA, S. (See LEINO, M.E., LBL-12816)

Yi-ZHONG, Zhuo (See ZHONG-YU, MA, LBL-11893)

ZAJC, W.A. (See MARTOFF, C.J., LBL-11914)

ZHANG, G.S. (See MA, A.Y., LBL-9689)

ZHONG-YU, MA, Wu Xi-zhen, Zhang Jing-Shang, Zhuo Yi-zhong, and J.O. Rasmussen
Calculation of Muon Final Probabilities After Muon-Induced Fission in Four-State Basis, LBL-11983, May 1981, submitted to Phys. Letts.

ZISMAN, M.S., J.G. Cramer, D.A. Goldberg, J.W. Watson, and R.M. Devries
Dominance of Strong Absorption in ^{9}Be + ^{28}Si Elastic Scattering. LBL-10204, December 1979, Phys. Rev. C **21**, 2398 (1980).

Author Index

Abachi, S. 140
Ahlen, S.P. 233, 234, 235, 239, 240
Aleklett, K. 101, 112, 113, 114
Alexander, J.M. 77, 80, 82
Anderson, L. 127
Anderson, O. 59
Andrews, H.R. 57
Anishetty, R. 215
Awes, T.C. 84, 90
Aysto, J. 38
Azuma, R.E. 34
Baden, A. 228
Banerjee, B. 170
Baumgardt, H.G. 122
Benenson, W. 130, 131
Bice, A.N. 107, 108, 110, 111
Biesser, F. 219
Bistirlich, J.A. 130, 131, 146
Bjornstad, T. 31, 32, 34, 119
Blair, J.S. 162
Blann, M. 181
Blau, S.K. 267
Bleszynski, M. 125
Blocki, J. 157
Boguta, J. 207
Bohrmann, S. 168, 173, 200, 201,
Bonner, B.E. 66
Bonner, W.A. 69
Bossingham, R. 130, 131, 146
Bowman, H.R. 130, 131, 146
Brady, F.P. 66
Brandan, M.E. 99
Britt, H.C. 181
Brochard, F. 145
Brockmann, R. 133, 134, 141, 150, 223, 225, 227,
Browne, E. 73
Bruckner, W. 127
Buchwald, G. 204, 205, 206
Budiansky, M.P. 233
Buguta, J. 167, 168, 169
Butler, P.A. 57
Buttke, T. 130
Cable, M.D. 38, 107, 110, 237
Carroll, J.B. 125, 129, 140, 145
Cerny, J. 107, 108, 110, 111, 237
Christensen, P.R. 181
Clark, D.J. 259
Clawson, C.W. 146
Cline, D. 57
Cole, A.J. 99, 105
Colombani, P. 57
Conzett, H.E. 63, 65, 66, 68, 69
Cork, B. 149
Crawford, H.J. 37, 149, 219
Crawley, G.M. 130, 131
Crowe, K.M. 130, 131, 146
Csernai, L.P. 204, 205, 206
Cusson, R.Y. 177, 190, 206
Dacal, A. 99, 105, 133, 134, 141, 150, 223, 225, 227
Davis, J. 129
de Saint-Simon, M. 35
Deleplanque, M.A. 59
Detraz, C. 35
Diamond, R.M. 53, 57, 59, 61, 94, 97, 262
Dines, E.L. 53, 61
Donangelo, R. 165
Draper, J.E. 53, 61
Duek, E. 77, 82
Eichler, E. 57
Ellegaard, C. 59
Ellis-Akovali, Y.A. 71
Elo, D. 259
Elola. M.A. 231
Engelage, J.M. 144, 221
Epherre, M. 35
Erkkila, B.H. 181
Fai, G. 191
Fawcett, J. 129
Ferguson, R.L. 181
Firestone, R.B. 39, 40, 72
Fowler, G.N. 137
Frankel, K.A. 130, 131, 146, 194, 196, 204
Freedman. M.S. 152,
Friedlander, E.M. 120, 121, 122, 137, 243
Galonsky, A. 84,
Ganezer, K.S. 125, 140, 145
Gaussauge, E. 121
Gavron, A. 181
Geaga, J.V. 140, 144, 221
Gelbke, C.K. 84, 87, 90
Ghiorso, A. 44, 46, 48, 50
Gimpel, R.W. 121
Glasgow, L. 259
Glendenning, N.K. 170, 209, 213, 215
Gobbi, A. 177
Graebner, G. 204, 205, 206
Gregorich, K.E. 4l
Greiner, W. 177, 190, 204, 205, 206, 212
Groening, H. 101, 189
Guerreau, D. 80, 82
Guidry, M.W. 57, 165
Guillemaud, D. 35
Gunten, H.V. 49, 52
Gustafsson, H.A. 31, 32, 34, 119
Gutbrot, H.H. 118, 152, 228
Gyulassy, M. 170, 194, 195, 197, 204, 207, 211, 215
Hagebo, E. 113
Hahn, J. 177
Haldorsen, I. 113
Hamagaki, H. 143
Hamilton, J.H. 57, 161
Hansen, O. 181
Hanson, P.G. 32, 34, 35

Harris, J.W. 133, 134, 141, 144, 150, 221, 223, 225, 227
Harvey, B.G. 99, 103, 104, 105
Hashimoto, O. 130, 131, 146, 196
Hausser, O. 57
Haustein, P.E. 38
Hecking, P. 193, 208, 210
Heckman, H.H. 121, 124, 220, 241, 243
Henderson, D.J. 152
Hendrie, D.L. 103
Herskind, B. 59, 61
Hichwa, R.D. 57
Hinterberger, F. 65
Hoang, T.F. 149
Hoffman, D.C. 49
Hogen, J.J. 42
Hsu, C.C. 96, 97, 184
Huizenga, J.R. 179
Hulet, E.K. 46
Igo, G.J. 125, 140, 145
Ingersoll, J.G. 146
Johnson, N.R. 57
Johnson, P. 112
Jonson, B. 31, 32, 34, 35, 119
Jonsson, O.C. 119
Judek, B. 121
Kadota, S. 143
Kahler, A.C. 57,
Kallne, J. 129
Kaplan, M. 77, 80, 82
Karant, Y.J. 120, 121, 243
Kasagi, J. 84,
Kashy, E. 130, 131
Kauffmann, S.K. 195
Kaufman, S.B. 118, 152
Keinonen, J. 57
Kelly, W.H. 39
Kildir, M. 80
King, N.S.P. 66
Kinoshita, K. 243
Kirk, P.N. 144, 221
Klapisch, R. 35
Kluge, H. 59
Knoll, J. 201
Koehler, P. 215
Koike, M. 130, 131, 146
Koontz, R.W. 144, 221, 253
Kraus, Jr., R.H. 113, 114
Kruse, H. 206
Kurck, J.P. 146
Lam, R. 259
Langevin, M. 35
Larsson, P.O. 31, 32
Lederer, C.M. 74
Lee, D. 49
Lee, I.Y. 57
Legrain, R.L. 84, 90, 99, 105
Leino, M. 44
Lemaire, M.-C. 127, 137
Lemmon, R.M. 69
Lindenberger, K.H. 53, 61, 94
Lindfors, V 31, 32, 119
Lindstrom, P. 140
Liu, Y.-F. 49, 52
Logan, D. 77, 80, 82
Lohner, H. 228
Lombard, R. 137, 143
Lougheed, R. 46
Loveland, W. 101, 112, 113, 114, 116, 117
Lumbroso, A. 209
Lund, T. 113
Luo, Cheng 52
Lustig, H.J. 177
Lynch, W.G. 87
Lyneis, C.M. 259
Ma, Z.-y. 164,
Mahoney, J. 103, 105
Maier, M. 118, 133, 134, 141, 150, 152, 223, 225, 227, 228
Mantzouranis, G. 178
Maples. C. 245, 247, 249, 251
Martinis, J. 232
Martoff, C.J. 130, 131, 146
Maruhn, J.A. 177, 190, 204, 205, 206
Mast, T. 259
Mattsson, S. 31, 32, 34, 35, 118
McClelland, J.B. 125, 129
McDonald, R.J. 53, 76, 94, 96, 97, 236
MacDonald, W.J. 146
McFarland, R.M. 46, 50, 114
McGaughey, P.L. 101, 112, 113, 114, 116, 117
McHarris, Wm. C. 39
McLerran, L. 215
McNaughton, M.W. 66
McParland, C. 220, 255
Meng, J. 246, 247, 249, 251
Miake, Y. 143
Miller, J. 130, 131, 133, 134, 141, 146, 150, 233, 225, 227
Minehart 129
Moeller, E. 127, 127, 137, 143
Molitoris, J.D. 229
Molzahn, D. 113
Moody, K.J. 41, 42, 101, 112, 114, 189
Moretto, L.G. 53, 76, 94, 96, 97, 183, 184, 186, 188, 236
Morita, Y. 113, 117
Morrissey, D.J. 53, 76, 94, 96, 97, 116, 184
Mulera, T.A. 140, 145, 231
Muller, B. 206
Muller, K.-H. 171, 172, 173
Muller, R. 259
Murphy, D.L. 37, 99, 103, 105, 130, 131, 146
Musser, J. 235
Myers, W.D. 158, 178
Nagamiya, S. 127, 137, 143
Naulin, F. 35
Neese, R.E. 165
Neiman, M. 57
Newton, J.O. 53, 61, 94
Nichols, T.L. 165
Nissen-Meyer, S. 127

Nitschke, J.M. 48, 229
Nix, J.R. 204
Nolen, Jr., J.A. 130, 131
Nunnelley, L.L. 93, 116
Nurmia, M.J. 45, 48, 49, 50
Nyman, G. 31, 34, 35
Oertel, C. 116
Ogloblin, A.A. 212
Oliveira, L.F. 165
Oliveira, Z.M. 160
Oostens, J. 145
Ortiz, M.E. 133, 134, 141, 150, 223, 225, 227,
Pacheco, A.J. 53, 76, 94, 96, 97, 183, 186
Pang, W. 103
Pardo, R.C. 39
Parry, R.F. 38, 237
Patin, Y. 181
Peker, L.K. 161
Perez-Mendez, V. 125, 129, 140, 145, 231
Peter, J. 118, 130, 131, 152
Plasil, F. 181
Poggi, G. 84, 90
Pontoppidan, S. 181
Poskanzer, A.M. 31, 32, 34, 35, 119, 228
Price, P.B. 232, 235, 239, 240, 243
Prussin, S.G. 160
Pugh, H.G. 133, 134, 141, 144, 150, 221, 223, 225, 227
Puigh, R.J. 93
Qiu, X.J. 162
Quebert, J. 131
Radi, H.M.A. 196
Rae, W.D.M. 99, 105, 108
Raff, M. 133, 134, 141, 150, 223, 225, 227,
Randrup, J. 160, 178, 179, 181, 182, 191, 198, 202
Rasmussen, J.O. 130, 131, 146, 161, 162, 164, 165, 196
Rathbun, W. 245, 247, 249, 251
Ravn, H.L. 31, 32, 34, 35, 119
Remler, E. 194
Renfordt, R.E. 133, 134, 141, 150, 223, 225, 227,
Richardson, L.W. 87, 184
Riedel, C. 204
Riedesel, H. 228
Riedinger, L.L. 57
Riess, F. 133, 134, 141, 150, 223, 225, 227
Rioux, C. 65
Ritter, H.G. 118, 152, 228
Rivet, M.F. 77
Robinson, E.L. 57
Roche, G.R. 144, 221
Romero, J.L. 66
Ronningen, R.M. 57
Roy, R. 65
Ruck, H.M. 214
Rud, N. 57
Ruiz, C.L. 144, 221
Sagle, A.L. 66, 125, 129, 140, 145
Saini, S. 84, 90
Salamon, M.H. 234
Sandoval, A. 133, 134, 141, 150, 223, 225, 227
Schardt, D. 31, 119
Schmidt, K.-H. 158
Schmitt, R.P. 183
Schnetzer, S. 127, 137, 143
Schopper, E. 122
Schroder, W.U. 179
Schroeder, L.S. 127, 133, 134, 141, 144, 150, 221, 223, 225, 227
Schuck, C. 53, 59, 61, 94
Schurmann, B. 198, 204
Scott, D.K. 84
Seaborg, G.T. 41, 49, 52, 101, 112, 113, 114, 116, 117, 127, 189
Shapiro, G. 127, 137
Shida, Y. 143
Shih, S. 53, 59, 61, 94, 97
Shirley, V.S. 71
Shor, A. 140
Shotter, A.C. 107, 108, 110, 111
Simon, R.S. 57
Singh, B. 72
Slobodrian, R.J. 65
Sobotka, L.G. 53, 76, 94, 96, 97, 188, 236
Somerville, L.P. 45, 46, 48, 50
Spieler, H. 228
Steinberg, E.P. 118, 152
Steiner, H. 127, 137, 143
Stelzer, H. 118, 152,
Stephens, F.S. 53, 54, 55, 57, 59, 61, 94, 97
Stephenson, J. 204
Stetz, A. 129
Stevenson, J.D. 201, 232, 235,
Stock, R. 133, 134, 141, 150, 223, 225, 227
Stocker, H. 177, 190, 193, 204, 206, 207, 212, 215
Stokes, R.H. 181
Stokstad, R.G. 99, 105
Strobele, H. 133, 134, 141, 150, 223, 225, 227
Strottman, D. 204
Subramanian, P. 204
Sullivan, J.P. 130, 131, 146, 196
Sutter, R. 145
Swenson, L.W. 129
Swiatecki, W.J. 157, 159, 174
Symons, T.J.M. 37
Takahashi, K. 35
Talaga, R.L. 125, 145
Tanihata, I. 127, 137, 143, 145
Tans, P. 259
Taras, P. 57
Tarle, G. 233, 239, 240
Thibault, C. 35
Thierens, H.M. 38, 237

Thomas, T.D. 93
Tincknell, M. 239
Toke, J. 159
Touchard, F. 35
Treuhaft, R.N. 144, 221
Truol, P. 146
Tsang, M.B. 87
Tserruya, I. 105
Van Bibber, K. 103
Vandenbosch, R. 93
Vaz, L.C. 80
Videbaek, F. 181
Viggars, D. 72
von Rossen, P. 65
Ward, D. 57
Warner, R.A. 39
Warner, R.E. 87
Warwick, A.I. 118, 152, 228
Weaver, D. 245, 247, 249, 251
Webb, M.P. 181
Weik, F. 118, 152, 228, 253, 254, 256
Weiman, H. 152
Weiner, R.M. 137
Welch, J. 259
Westfall, G.D. 37, 90
Whipple, E.T. 125
Whitney, R.R. 129
Wiedenbeck, P.E. 231
Wieman, H. 118, 228
Wilkins, B.D. 118, 152
Wolf, K. 84, 133, 134, 141, 150, 223, 225, 227, 228
Woodward, D. 140, 145
Wouters, J.M. 38, 108, 237
Wozniak, G.J. 53, 76, 94, 96, 97, 184, 236
Wu, X.-z. 164
Yariv, Y. 204
Yashita, S 44
Yates, S.W. 57
Yoo, E. 146
Young, G.R. 181
Zajc, W.A. 130, 131, 146
Zarbakhsh, F. 125, 140, 145
Zhang, J.-s. 164
Zhuo, Y.-z. 164
Zisman, M.S. 77, 80, 82, 93, 262

GPO 587-122 / 1